

Rulemaking Comments

From: elling@torium.se
Sent: Thursday, July 03, 2008 11:46 AM
To: Rulemaking Comments
Subject: DCThMSR 1/3
Attachments: US_NRC_DCThMSR_v1.pdf

DOCKETED
USNRC

July 7, 2008 (2:35pm)

OFFICE OF SECRETARY
RULEMAKINGS AND
ADJUDICATIONS STAFF

Dear Sir,

referring to the NRC-2008-0237, Thorium ElectroNuclear AB, based in Stockholm Sweden, submits comments for the Double Cylinder Thorium Molten Salt Reactor.

The DCThMSR is protected by Patent Pending. The patent text is not enclosed but scientific publications would describe it adequately.

Two zip packs of references follow in emails DCThMSR 2/3 and 3/3.

Pls acknowledge.

Kind regards
Elling Disen
elling@torium.se
Founder
Thorium ElectroNuclear AB
www.torium.se

Received: from mail2.nrc.gov (148.184.176.43) by OWMS01.nrc.gov
(148.184.100.43) with Microsoft SMTP Server id 8.0.751.0; Thu, 3 Jul 2008
11:47:03 -0400

X-Ironport-ID: mail2

X-SBRS: 1.9

X-MID: 17634858

X-IronPort-AV: E=Sophos;i="4.27,742,1204520400";
d="pdf?scan'208";a="17634858"

Received: from pne-smtpout2-sn1.fre.skanova.net ([81.228.11.159]) by
mail2.nrc.gov with ESMTP; 03 Jul 2008 11:46:28 -0400

Received: from [192.168.1.113] (81.233.0.25) by
pne-smtpout2-sn1.fre.skanova.net (7.3.129) id 4843FAEB0062FFA9 for
Rulemaking.Comments@nrc.gov; Thu, 3 Jul 2008 17:46:24 +0200

Message-ID: <486CF43B.6080005@torium.se>

Date: Thu, 3 Jul 2008 17:46:03 +0200

From: "elling@torium.se" <elling@torium.se>

User-Agent: Thunderbird 2.0.0.14 (Windows/20080421)

MIME-Version: 1.0

To: Rulemaking.Comments@nrc.gov

Subject: DCThMSR 1/3

Content-Type: multipart/mixed;
boundary="-----080004020504080305030900"

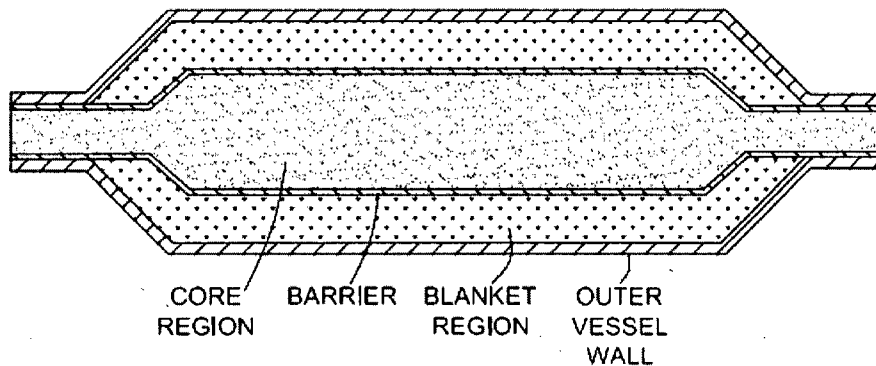
Return-Path: elling@torium.se

Comments to U.S. NUCLEAR REGULATORY COMMISSION

10 CFR Part 50 [NRC-2008-0237]

Regulation of Advanced Nuclear Power Plants; Draft Statement of Policy

Double Cylinder Thorium Molten Salt Reactor – DCThMSR



Figur 1 : DCThMSR vessel

Thorium ElectroNuclear AB

Stockholm, Sweden

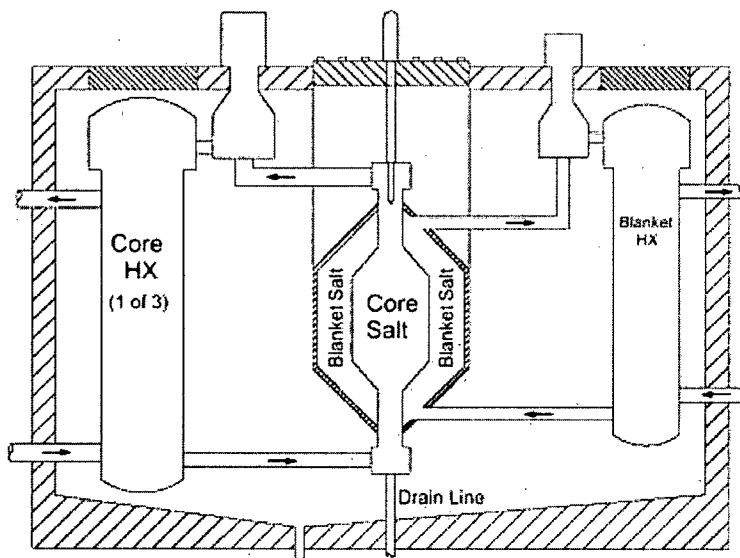
+46 (0)70 8968 715 www.torium.se thorium@telia.com

July 7th, 2008

ACTION : This document is in request to NRC-2008-0237, [1]. The purpose is to “provide for more timely and effective regulation of advanced reactors” ([1], p.8, s.2, l:1).

PUBLIC DOMAIN : The Double Cylinder Th Molten Salt Reactor, “ DCThMSR”, is an invention protected by Patent Pending, [2].

BACKGROUND : The Norwegian Government ordered a report on the country’s thorium resources that was rendered on Feb 15th 2008. There will be an open hearing in the Norwegian Parliament in the autumn of 2008. Political circumstances would be favorable to a pilot project from Sept 2009. Thorium ElectroNuclear AB aims to introduce the DCThMSR credibly into this chain of opportunities. Norway is a country with sparse nuclear engineering expertise; a crucial reference would be an preliminary evaluation from the US NRC.



Figur 2 : Reactor room outline

SUMMARY : The DCThMSR design rests firmly on the proven legacy from the Molten Salt Reactor Experiment, “MSRE”. The original so-called “plumbing problem”, the difficulty of combining mechanical strength and neutron economy in graphite walls separating the fertile

and fissile molten salt loops, has been solved by evolving from a spheric "nest" of salt channels to concentric cylinders of hastelloy.

The GenIV reference design, Molten Salt Breeder Reactor, MSBR, is one-region with fertile and fissile reactions in the same salt loop. A variant TMSR is the working model of the SUMO project, started in April 2008 and hosted by EURATOM.

The DCThMSR will have superior performance on all key metrics as well as unique properties. It is a wellknown fact that MSRs are unconditionally stable. In absence of graphite the reactivity coefficient and the void coefficient are strongly negative. At loss of flow or loss of pump operation, the temperature transient stays below the melting point of the hastelloy.

Absence of graphite would all but eliminate the risk of fire.

The melt can be drained gravitationally to tanks with non-critical geometry and good decay heat removal properties. MSRs have passive, intamperable and inherent safety.

The vapour pressure above the melt is insufficient for a radiotoxic release to a wider area. The MSRE had the unintended consequence of providing insight into the longterm behaviour of the salt melt with fissile material left insitu : After two decades, radiolysis led to release of toxic F₂, HF and UF₆. In contrast, during the MSRE itself, the melt was cleansed of uranium by fluorination down to natural levels in a matter of hours.

Consequences of a leak of fissile salt through the cylindric separation into the fertile loop of the DCThMSR need to be canvassed. The prediction is that the higher pressure in the fertile loop would make this event unlikely and that eventual consequences would be minor.

Fast boron injection methods should be investigated. The energy production in the fissile loop and the breeding in the fertile loop could be permanently quenched by boron neutronic poison activated as a function of reactor state diagnostics and control.

At a diagnosed threat of loss of containment or loss of vessel, boron fluorides would spray into both fissile and fertile salt volumes by way of instant pyrochemical actuation analogue to a car inflatable cushion before the impact. The drain pans and containment wall could be boronated either from coating or from the hastelloy makeup.

The DCThMSR plant could be 30m underground so that a large commercial airplane impact would have minor consequences. A secondary salt loop could interface to the energy conversion system positioned on ground in free air.

[2] outlines a fleet system where standard DCThMSR's only would need nuclear grade work orders for fissile transfer, waste removal, wear inspection and parts replacement every 6 – 24 months, as well as at startup and decommissioning. This maintenance shedule could be served by inspectors travelling in a convoy of specialised tank truckers.

Daily operation could be supervised and controled remotely with sparse non-expert operators on site.

Polls show that anti-nuclear sentiment stems from seeing tall buildings on the horizon, the fear of the bomb and the perception of radiotoxic eternity and inevitability ; pychological factors that would be diminished with the DCThMSR fact sheet marketed properly.

All fissile material, in particular reactor grade Pu waste, could activate the thorium fuel cycle, incinerating itself in the process. The Yucca Mountain debacle, also replicated in most nuclear energy states, could turn into one a focus on temporary storage of HLW forms suitable for DCThMSR incineration.

After all, 1 million year corrosion guarantees for HLW encapsulation are hard to justify scientifically. In Sweden, a row has erupted over copper as a corrosion barrier in moist environments, holding up the final and long overdue decision for a geological repository.

Proliferation resistance would be in-depth 4-fold. A terrorist would have to divert dripping hot salt melt, let it cool, separate out bomb material, transform the fluorides, survive the penetrating U232 gammas, survive IR surveillance of the hot melt, survive U232 gamma surveillance from a relevant quantity of bomb material, isotopically enrich U233 from below the IAEA 12% weapons definition limit – all in a time window of a few months at most. A hijack scenario where the reactor structure is diverted to breeding Pu from uranium fuel, needs to be investigated further but could be detected by antineutrino instruments.

A DCTHMSR infrastructure opens up the promise of perennial, global thorium energy; a realistic candidate for the GNEP. The deliverable conversions could be to nuclear H₂/NH₃, to cool pipes as well as to heat pipes, desalination and electrical power. The decommissioned weapons stocks and waste piles should be earmarked for DCTHMSR startup charges.

A “straightforward development program” holds the promise of proof of concept, demonstration of enabling technologies, simplified regulatory compliance and commercial license.

The MSR concept is more intuitively comprehensible than LWR operation with all its complex and dynamic parameters that all need to be constantly eagle-eyed.

The MSR concept and the DCTHMSR design is pedagogic and the components few, robust, unsophisticated and cheap. Draining the fissile salt into the dump tanks followed by a cleansing flush would be routine in order to undertake wear inspection and parts replacement.

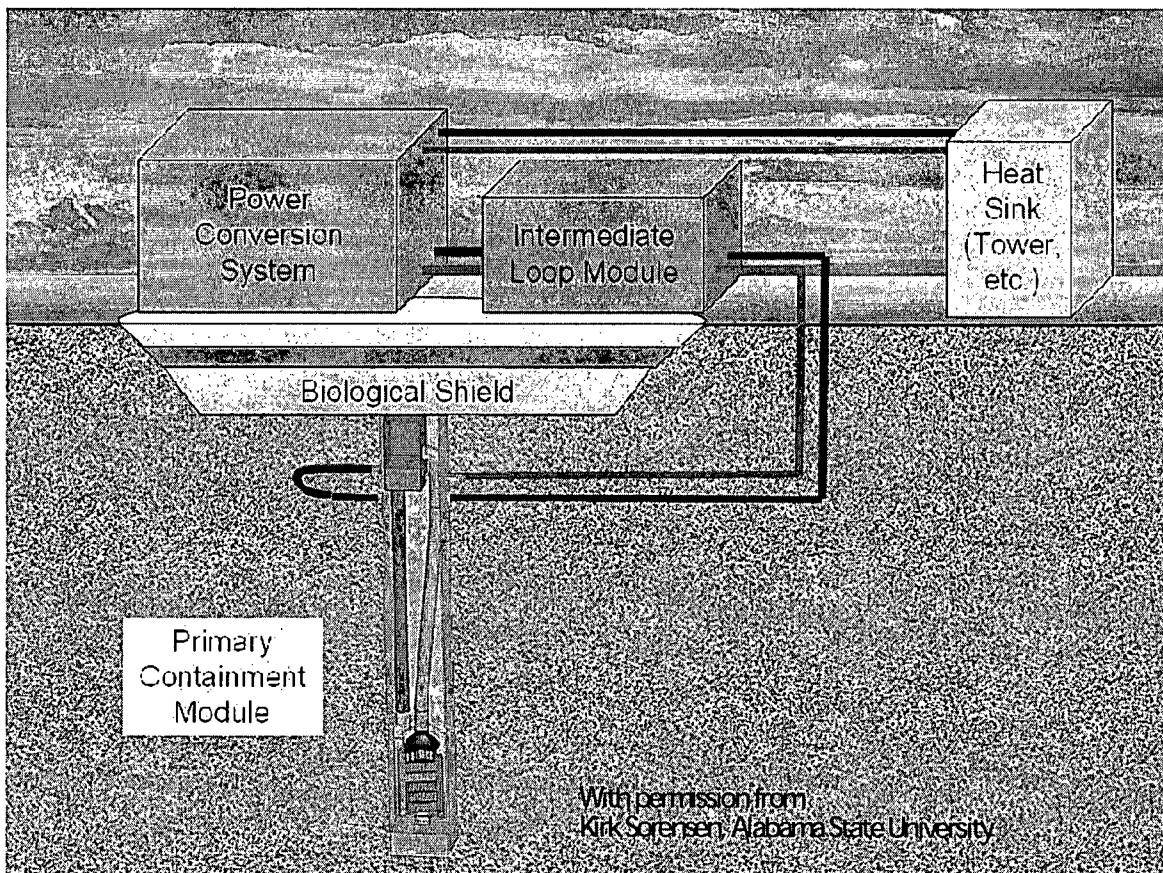
Biological shields to contain salt spills from entering the water table and the environment would be the last barrier to yield in the worst accident scenario of a direct hit by clusterbombs or an insider terrorist attack.

DcThMSR design is far from finalised, detailed, reviewed by experts and audited by industry. The US NRC evaluation would be a guideline to narrow down the options' list and set up milestones for a proof of concept.

A PRELIMINARY EVALUATION of the DcThMSR using the existing framework of regulatory documents intended for water or pressurised type reactors with externally controlled conditional stability and severe accident scenarios could be less useful. The DcThMSR is so radically different that a preliminary evaluation maybe should start out with generic considerations above comments referring to existing rulemaking.

- 1) Is unconditional stability deemed a proven fact from MSRE and validated models or does it have to be revalidated in DcThMSR experiments ?
- 2) What are the simplifications from unconditional stability and absence of severe accident consequences on the containment, on the regulatory burden and on onsite nuclear grade work orders?
- 3) Would small reactor size and denaturation further ease compliance ?
- 4) Is there a watershed difference in protection requirements between reactor grade Pu waste and LEU ?
- 5) How can long term corrosion be predicted ?
- 6) How must the characterisation of mixed salts' exposure to open air be carried out ?
- 7) Is a pure thorium-U233 fuel cycle realistically acceptable to regulators and shouldn't it even be desirable as a differentiator to business as usual?
- 8) Wouldn't 1000ppm U232 be sufficient for selfprotection and detection?
- 9) Isn't a solution to the Yucca mountain problem alone worth a push for a DcThMSR fleet ?
- 10) Wouldn't Pu and TRU from denaturation add more concerns than advantages ?

- 11) Could the current debate over MSRE salts' disposal,exaggerate melt decommission issues ?
- 12) Is there something this bird's eye view has missed ?
- 13) Isn't the DCThMSR the obvious answer for GNEP ?
- 14) Is fast injection technology a necessity given the set of redundant safeguards ?
- 15) Shouldn't uncertain uranium supplies favour a shift to thorium for the Nuclear Renaissance?
- 16) What could a flow chart linking diagnostics to safeguard actions look like ?
- 17) Is a type approval within reach ?



Figur 3 : Underground site

TABLE OF CONTENTS :

1.	DCThMSR DESIGN DESCRIPTION	9
2.	ENUMERATED : ENGINEERING ISSUES.....	9
2.1.	ISSUE # 1 : CORROSION	9
2.2.	ISSUE # 2 : TRITIUM CONTROL	9
2.3.	ISSUE # 3 : NEUTRON LIFETIME	10
2.4.	ISSUE # 4 : FLOW PATTERN	10
2.5.	ISSUE # 5 : FISSION PRODUCT MAKEUP.....	10
2.6.	ISSUE # 6 : START CHARGE REGIME.....	11
2.7.	ISSUE # 7 : MELT DECOMMISSION	11
3.	ENUMERATED : CORE SAFETY FEATURES.....	11
3.1.	CORE SAFETY FEATURE # 1 : UNCONDITIONAL STABILITY.....	11
3.2.	CORE SAFETY FEATURE # 2 : FAST GRAVITATIONAL DRAIN	12
3.3.	CORE SAFETY FEATURE # 3 : FAST POISON INJECTION	12
4.	ENUMERATED : SECURITY FEATURES.....	12
4.1.	SECURITY FEATURE # 1 : UNDERGROUND SITE.....	12
4.2.	SECURITY FEATURE # 2 : REGULAR INSPECTION OF SEPARATION WALL	13
4.3.	SECURITY FEATURE # 3 : REMOTE CONTROL AND COMMAND.....	13
4.4.	SECURITY FEATURE # 4 : OVERLAPPING SURVEILLANCE.....	13
4.5.	SECURITY FEATURE # 5 : ONSITE ANTI-NEUTRINO DETECTION.....	13
4.6.	SECURITY FEATURE # 6 : GLOBAL U232 DETECTION - SELFPROTECTION.....	13
4.7.	SECURITY FEATURE # 7 : LETHAL SELF-PROTECTION	14
5.	ENUMERATED : DESIGN OPTIONS.....	14
5.1.	OPTION # 1 : PURE THORIUM-U233 FUEL CYCLE	14
5.2.	OPTION # 2 : HYBRID THORIUM-U33 FUEL CYCLE.....	15
5.3.	OPTION # 3 : DENATURATION	16
5.4.	OPTION # 4 : THORIUM IN FUEL SALT	16
	Neutron economy would permit adding thorium to the fuel salt	16
5.5.	OPTION # 5 : ABSENCE OF ONSITE FLUORINATORS.....	17
5.6.	OPTION # 6 : GRAPHITE MODERATION.....	17
6.	ENUMERATED : ACCIDENT SCENARIOS.....	19
6.1.	ACCIDENT SCENARIO # 1 : LOSS OF PUMPING POWER.....	19
6.2.	ACCIDENT SCENARIO # 2 : LEAKAGE THROUGH SEPARATION WALL	19
6.3.	ACCIDENT SCENARIO # 3 : DETECTION OF SHOCK, VIBRATION	19
6.4.	ACCIDENT SCENARIO # 4 : LOSS OF VESSEL	19
6.5.	ACCIDENT SCENARIO # 5 : LOSS OF CONTAINMENT	19
7.	BALANCE OF PLANT.....	20
8.	A DCThMSR 100MWe BRAYTON CYCLE (He) PILOT.....	20
8.1.	PILOT OPERATION # 1 : TRITIUM CAPTURE.....	20
8.2.	PILOT OPERATION # 2 : COMPACT HEAT EXCHANGERS	20
8.3.	PILOT OPERATION # 3 : PRACTICAL CORE ACCESS	20
8.4.	PILOT OPERATION # 4 : NOBLE METAL FISSION PRODUCT FILTER.....	21
8.5.	PILOT OPERATION # 5 : FISSION TRANSFER	21
8.6.	PILOT OPERATION # 6 : FISSION PRODUCT REMOVAL.....	21
8.7.	PILOT VERIFICATION # 1 : NEUTRONICS - SERVICING SCHEDULE.....	21
8.8.	PILOT VERIFICATION # 2 : CORROSION RATE	21
8.9.	PILOT VERIFICATION # 3 : COMPLETE CHEMICAL ANALYSIS	21
8.10.	PILOT VERIFICATION # 4 : MELT BULK PROPERTIES.....	22
8.11.	PILOT DEMONSTRATION # 1 : FAST POISON INJECTION.....	22
8.12.	PILOT DEMONSTRATION # 2 : FULL SALT MIX INTO AIR	22
8.13.	PILOT DEMONSTRATION # 3 : MELT TRU LEVEL AT DECOMMISSION	22
9.	LIST OF REFERENCES	23
10.	LIST OF FIGURES.....	24

1. DCTHMSR DESIGN DESCRIPTION

[3] provides an introduction to the double cylinder design. The MSRE history and the differences from the GenIV MSBR and the EURATOM TMSR are included.

2. ENUMERATED : ENGINEERING ISSUES

This section aims to enumerate the primary issues for preliminary regulatory evaluation.

2.1. ISSUE # 1 : CORROSION

Corrosion in the MSRE, resulting from the presence of the fission product Tellurium, was later resolved. At least two improved hastelloys are promising candidates, coming out of Kurchatov, Russia [4] and Kharkov, Ukraine [5]. Additions of Molybdenum, Vanadium, Niobium and Yttrium to the original hastelloy seem to eliminate the cracking mechanism. Full scale neutron flux testing over 1000s of hours and electron beam diagnostics would be adequate to extrapolate for structural components' lifetimes.

DCVTHMSR fission product makeup from the chosen fuel and waste regime would have to be analysed for unidentified corrosion mechanisms such as the MSRE Tellurium cracking.

A regulatory criteria on corrosion without waiting a reactor life time of 30-60 years TBD should be defined. If cracking and brittling are non-existent in diagnostics over a pilot run, a rate in terms of μm per year should suffice. The corrosion is crucial for the thickness of the separation wall. Since the core would be easily accessible, the wall could be surface monitored regularly with xray and ultrasound techniques, as the case with airplane structures.

2.2. ISSUE # 2 : TRITIUM CONTROL

MSRE identified tritium in quantities that would need to be captured in a 2500MWth design.

Tritium circuits are established technology except for the escape into the heat exchanger load and secondary salt loops.

A Brayton cycle turbine on Helium could solve this problem. Tritium separation from He is established technology ([6], p4).

For secondary loops to capture tritium when the conversion is other than electrical Brayton power, a salt formulation should be found that also is a good heat transport medium.

2.3. ISSUE # 3 : NEUTRON LIFETIME

Reactor control characteristics and load follow responses can be predicted from the average neutron lifetime. The MSRE proved to be a practical machine for start, stop and regulation – properties that would not change with the DCThMSR. The fuel options would have an impact. Neutron lifetimes can be estimated from neutronics codes.

2.4. ISSUE # 4 : FLOW PATTERN

Risk of turbulent or laminar flow would be estimated with thermohydraulic codes. Chemistry inhomogenities and material transport would be included. The French TMSR research, now the SUMO project with EURATOM, lists startup flow patterns as an issue to be investigated. Since the molten salts resembles water for fluid dynamics, design recommendations for smooth flow geometries in pumps, corners, bends, drains, joints would be amply accessible.

2.5. ISSUE # 5 : FISSION PRODUCT MAKEUP

([6], p6) lists fission product makeup as the most unknown crucial issue. Fission product removal would be accomplished by helium bubbling for noble gases, a metal sponge for noble metals and vacuum distillation. Chemical reactions, complex formations and valence for several fission products are uncertain or unknown. Reductive bismuth extraction, as planned with the French TMSR, would imply complicated equipment on site and proliferation risks to be avoided.

The actual prediction is that noble metal plateout with its associated decay heat would be handled. How to replace the metal filter sponge and capture the vacuum distillation fission products to a mobile convoy should be straightforward since core access would be routine.

2.6. ISSUE # 6 : START CHARGE REGIME

Peace meal start charge administered over weeks at startup ([7], p5) implies enhanced proliferation risk by diversion. The ideal startup is instant dissolve into the fuel salt. A regulatory issue would be the sensitive period before the start charge is transferred completely in situ.

2.7. ISSUE # 7 : MELT DECOMMISSION

The MSRE clean up problem has put focus on the melt properties, [8]. The clean up problem stemmed from radiolysis in the crystallised and uncleaned melt from U233 content releasing toxic HF, F2 and UF6. Freeze protection ([6], p4) would eliminate the onset of radiolysis. The MSRE melt was cleansed of U233 by fluorination to natural levels in a matter of hours ([8], p3). TRU fluorination is 70x more intensive in F2 and could pose serious corrosion issues. Melt decommission could be carried out at a central site. Prediction of TRU and radiotoxic level of melt at decommission would be a regulatory criteria. Dilution and vitrification for geological repository, if indeed necessary, would be easier than for the waste of fission products, in turn easier than for today's HLW. Several methods could be developed ([9], p4), [10].

3. ENUMERATED : CORE SAFETY FEATURES

3.1. CORE SAFETY FEATURE # 1 : UNCONDITIONAL STABILITY

The MSRE was verified practically for the physical impossibility of runaway and meltdown scenarios. Even better, MSRE was considered a safe machine despite the fact that it probably had a slightly positive reactivity coefficient [11], due to the presence of graphite. The stability includes containment of transients by natural circulation even in case of loss of forced power and in the case of loss of gravitational drain, [12]. A central question for evaluation would be simplifications to be gained compared with current LWR regulation.

3.2. CORE SAFETY FEATURE # 2 : FAST GRAVITATIONAL DRAIN

Dump tanks would have geometry that evacuates decay heat passively as demonstrated for MSRE. Valves closing upon completed dump could seal the dumped salts from mixing, the whole operation taking a few seconds.

3.3. CORE SAFETY FEATURE # 3 : FAST POISON INJECTION

Fast boron injection into both into blanket and fuel salt would be an even faster method to quench reactivity and radiolysis onset and minimise decay heat. The system FABIS described in [13] should be investigated for adaption to MSR conditions. BF₃ could be a poison candidate. Fast injection could be activated by shock and vibration sensors. In the fractions of seconds prior to potential loss of reactor structure and salt mixing, both salt volumes would have their neutronics permanently turned off. Fast injection nozzles could be present both in multifunctional brackets with the double cylinder core as well as in the containment walls and the dump tanks.

4. ENUMERATED : SECURITY FEATURES

4.1. SECURITY FEATURE # 1 : UNDERGROUND SITE

Integrity of reactor room containment, biological shield, dump tanks, offgas system, nuclear, radiotoxic and chemically toxic inventories in case of plane impact would be secured 30m below ground surface. Suspension for protection against earthquake could be envisaged if desirable. The case of bunker buster bombs and terrorists bypassing the reactor room containment are probably the hardest cases, against which the fast injection system would be benchmarked. A destruction of conversion facility on the ground over the site connected by the secondary salt loop, would not present a major risk to the reactor.

4.2. SECURITY FEATURE # 2 : REGULAR INSPECTION OF SEPARATION WALL

The separation wall between blanket and fuel salt would be easily accessed for inspection of microcracks by xray or ultrasound instruments. Easy access is accomplished by dumping and subsequent flushing by non-radioactive salts as practised with the MSRE. The separation wall thickness would be influenced by inspection intervals and corrosion rate.

4.3. SECURITY FEATURE # 3 : REMOTE CONTROL AND COMMAND

Remote shutdown commands, sealed reactor room during operation, sparse onsite manpower, real time log file upload, secure redundant telecomm links and biometric access controls would provide margins for human factor engineering. The reactor room would not be accessible during operation, reducing the risk for access to the neutron source for parasite breeding. Failed actuation of dump, flush, valves and pumps from remote or outside containment would in last resort result in gravitational drain or fast injection spraying from the containment walls. The loss of operation due to failure in safety and security systems would not be catastrophic neither in terms of investment, radiotoxicity and chemical toxicity.

4.4. SECURITY FEATURE # 4 : OVERLAPPING SURVEILLANCE

The log file including flow patterns, temperature distribution, pressure distribution, vessel stress, neutronic cartography, tight mass balance and complete chemical analysis would be uploaded realtime.

4.5. SECURITY FEATURE # 5 : ONSITE ANTI-NEUTRINO DETECTION

New technology could detect illicit fuel cycles and parasite breeding, [14] and [16].

4.6. SECURITY FEATURE # 6 : GLOBAL U232 DETECTION - SELFPROTECTION

1000ppm U232 content would open up the possibility of global U233 surveillance, [22].

4.7. SECURITY FEATURE # 7 : LETHAL SELF-PROTECTION

1000ppm U232 content would present serious risks to unprotected bombmakers health ([23], p10).

5. ENUMERATED : DESIGN OPTIONS

This section aims to enumerate the design options for preliminary regulatory evaluation. Pilot priorities and design choices would be made partly on the basis of this feedback. The options are embedded in [3] but taken apart and spelled out for clarity.

5.1. OPTION # 1 : PURE THORIUM-U233 FUEL CYCLE

The IAEA defines weapons grade U233 in larger concentration than 12%. A pure Th fuel cycle would breed U233 from Th232 in the fertile blanket. U233 would be present in both the fissile and fertile loops.

Removal and separate decay tanks for protactinium would not be needed.

IAEA U233 selfprotection levels would not be reached but gamma intensity ([8], p3) would be a severe proliferation barrier.

Illicit access to U233 could be onsite parasite fluorination below the precision of the materials flow log file or diversion of loop salts volumes.

U232level would be around 1000ppm.

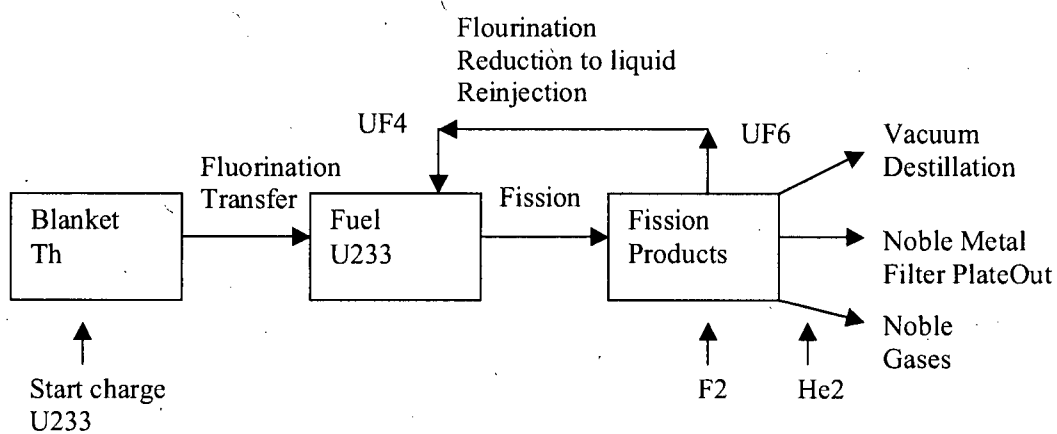
5.1.1. OPTION # 1 : PROs

A) TRU levels would be orders of magnitudes lower than for current LWRs, probably so low as not to have engineering consequences.

B) Global U233 accounting would start from zero, enabling a clean separation to the current uranium industry.

5.1.2. OPTION # 1 : CONS

- A) Startup charges are not available for the first generation DCThMSRs that would have to be started on other U-Pu materials.
- B) Proliferation regulation on U233 would need to be established from zero.



Figur 4 : Pure Th-cycle material flow

5.2. OPTION # 2 : HYBRID THORIUM-U33 FUEL CYCLE

DCThMSRs started on reactor grade Pu, decommissioned weapons Pu, HEU or LEU would have a fertile mix of Th and U fertile and a fissile mix of U233, U235, Pu239, their isotopes and TRUs ([7], p5).

A hybrid fuel cycle would imply fissile proliferation concerns roughly on par with current LWRs.

5.2.1. OPTION # 2 : PROs

- A) Reactor grade Pu and LEU would today nor be perceived the same proliferation risk as U233.

5.2.2. OPTION # 2 : CONS

- A) Criticality risks of the complex fissile mixes must be assessed.

B) Pu and TRUs must be fluorinated out upstream of waste tap and reinjected into the fuel salt. 70x the amount of F2 would be needed for Pu fluorination as per quantity of U and could be highly corrosive.

5.3. OPTION # 3 : DENATURATION

Neutron economy would permit dilution with U238 below the IAEA weapons definition levels.

Denaturation flush could be implemented as a fast injection in combination with fast poison injection.

5.3.1. OPTION # 3 : PROs

A) Proliferation risk reduced.

B) Service convoys not carrying weapon grade fissiles

5.3.2. OPTION # 3 : CONs

A) Higher Pu and TRUs inventory must be fluorinated out upstream of waste tap and reinjected into the fuel salt.

B) Larger start charge.

5.4. OPTION # 4 : THORIUM IN FUEL SALT

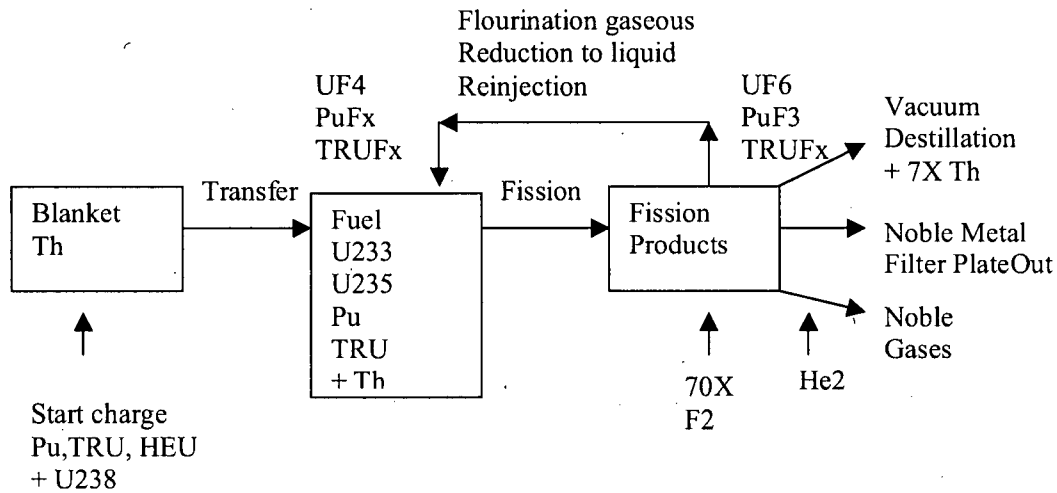
Neutron economy would permit adding thorium to the fuel salt.

5.4.1. OPTION # 4 : PROs

A) Longer service intervals

5.4.2. OPTION # 4 : CONs

A) 7x more thorium wasted during fission product removal.



Figur 5 : Hybrid fuel cycles with denaturation and Th in fuel

5.5. OPTION # 5 : ABSENCE OF ONSITE FLUORINATORS

Fuel makeup and neutron economy would permit batchwise transfer of fissile from the blanket to the fuel loop.

Batchwise fluorination could be serviced by mobile equipment with unique access codes.

Unserviced site would power down. Fissile and waste inventories would be out of control for mobile inspectors if denied access.

5.5.1. OPTION # 5 : PROs

A) Proliferation risk reduced.

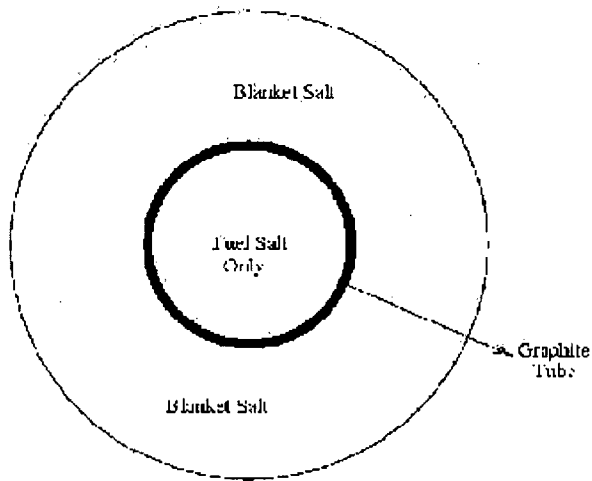
5.5.2. OPTION # 5 : CONS

A) Site owner could claim interrupted service and power down to be a blackmail situation.

ION # 6 : GRAPHITE MODERAT

The inner cylinder would preferably be made in hastelloy only. Graphite moderation yields different performance. Graphite could be layered within the separation wall structure resulting with less risk of fire and lesser consequences when brittling from neutronic wear. Graphite walls and control rods would be replaced every few years but this could be feasible given easy access to core.

Graphite Tube Molten Salt Cylindrical Reactor



Figur 6 : Graphite separation wall

5.5.3. OPTION # 6 : PROs

- A) The reactor would operate closer to the point of max reactivity.
- B) Lower specific energy production would permit smaller output power and smaller form factors.
- C) Lower fissile inventory

5.5.4. OPTION # 6 : CONs

- A) Thermal neutron spectrum creates more wear in hastelloys.
- B) Waste routines for brittle radiotoxic graphite must be established.

6. ENUMERATED : ACCIDENT SCENARIOS

6.1. ACCIDENT SCENARIO # 1 : LOSS OF PUMPING POWER

Loss of pumping power would have the same core scenario [12] as the following accident conditions : loss of flow, loss of load heat evacuation, overload fuel injection.

6.2. ACCIDENT SCENARIO # 2 : LEAKAGE THROUGH SEPARATION WALL

Loss of blanket pressure would set up for the fuel salt to leak into the blanket salt in the case of wall leakage. Criticality, vapor pressure and decay heat characterisations are lacking for a complete mix and or an inhomogenous uncomplete mix. The predictions are that these characterisations would be benign : the negative reactivity coefficients of both salts in the DCThMSR would combine to an overall negative coefficient for the mix ([3], p8, s5)

6.3. ACCIDENT SCENARIO # 3 : DETECTION OF SHOCK, VIBRATION

Incoming shock waves from external impacts could be sensed as a risk to vessel integrity.

6.4. ACCIDENT SCENARIO # 4 : LOSS OF VESSEL

Mix of fertile and fissile salts inside containment would be the consequence if fast injection fails.

6.5. ACCIDENT SCENARIO # 5 : LOSS OF CONTAINMENT

A bunker bomb impact or a terrorist bypassing containment would rip the containment open to air. Mixed salts could be exposed to the water table and radiotoxic vapours would be released. The longer term impact could be radiolysis from crystallised drops. The full characterisation of this worst case scenario needs to be carried out full scale. The effect of on accidental reactivity from moderator material like graphite and water must be described. The prediction is benign with limited consequences in a small perimeter.

7. BALANCE OF PLANT

The redundancy of security options in addition to the inherent core safety properties would allow for a new standard in nuclear engineering. Activation of security features and human engineering would have ample margins for different risk assessments and national regulations.

8. A DCThMSR 100MWe BRAYTON CYCLE (He) PILOT

Scaling up the MSRE from 8 MWth to 250 MWth is conservative since other reference designs are 2500 MWth. Finding a government willing to host and guarantee a pilot reactor is far easier when the installation would be a full reference plant producing power. Given the benign and unique properties and established enabling technology, this radical idea of a full plant might be worth the risk given time saved during an uncertain situation for global energy supply. Assembling a Great Group of MSR experts around a crash project in a Skunkworks would not back an inch from top notch security standards. The demonstrator would include monitoring and verification technologies to be removed, simplified and cost-balanced for a first version commercial offering.

8.1. PILOT OPERATION # 1 : TRITIUM CAPTURE

Tritium diffusing through the heat exchangers and the second salt loop into He working gas of the Brayton turbine would be captured using established technology, fex [15], p10.

8.2. PILOT OPERATION # 2 : COMPACT HEAT EXCHANGERS

UC Berkeley has developed relevant materials, models and geometries, [17]. Joint technologies would be included.

8.3. PILOT OPERATION # 3 : PRACTICAL CORE ACCESS

Already the MSRE could operate and service the core from outside the containment barrier, [18]. Gravitational dump, valves, flush cleansing, vessel inspection and wall replacement would be even safer and easier with today's robot technology.

8.4. PILOT OPERATION # 4 : NOBLE METAL FISSION PRODUCT FILTER

The thermal load from decay heat, the radiotoxicity and chemical toxicity are partly unknown parameters, even given the MSRE [19].

8.5. PILOT OPERATION # 5 : FISSILE TRANSFER

Fluorinators including converters gaseous – liquid, for all U, Pu and TRU are established technology, [21]. [21] refers to a continuous salt stream for the MSBR but would the system would be adaptable to a schedule where the fluorinator is brought onsite with a mobile service.

8.6. PILOT OPERATION # 6 : FISSION PRODUCT REMOVAL

Processing procedures for the full plateout filter needs to be detailed. The offgas system and the vacuum distillation waste components would be stored in containers. A dirty bomb scenario for the mobile service could justify vitrification onsite before transportation.

8.7. PILOT VERIFICATION # 1 : NEUTRONICS - SERVICING SCHEDULE

The main unknown parameter of the DCThMSR is the frequency of servicing set by the neutronics of the core. Estimates are between 6 and 24 months depending on reactor size and fuel options. Continuous onsite fluorination is available if non-proliferation permits.

8.8. PILOT VERIFICATION # 2 : CORROSION RATE

The partly uncertain valences and chemistry of fission product could result in discovery of new corrosion mechanisms. Aided by complete chemical analysis, the only way to check for subtle trace levels electrochemistry and validate the design would be a full scale pilot. Possible fixes like adjustment of redox potentials melt – filter – structure could be implemented.

8.9. PILOT VERIFICATION # 3 : COMPLETE CHEMICAL ANALYSIS

The PBMR has a complete fission product release model, [20]. A corresponding model must be validated for the DCThMSR. A pilot would have all analysis instrumentation necessary to establish a complete flow of materials and mapping of chemistry.

8.10. PILOT VERIFICATION # 4 : MELT BULK PROPERTIES

Reactivity coefficients, temperature gradients, pressure profiles, flow patterns, load time change constants, neutron lifetimes, melt homogeneity, out-of-core neutron flux and thermohydraulic properties could be verified before addition of fuel and fissiles.

8.11. PILOT DEMONSTRATION # 1 : FAST POISON INJECTION

This system is not established technology.

8.12. PILOT DEMONSTRATION # 2 : FULL SALT MIX INTO AIR

Toxicity would spread as crystallised drops of salts or concentrations of vapourised salt. The behaviour and perimeter of worst case release must be evaluated.

8.13. PILOT DEMONSTRATION # 3 : MELT TRU LEVEL AT DECOMMISSION

Analogue to determination of corrosion rate and complete chemistry, TRU level in melt could be predicted by accurate measurements.

9. LIST OF REFERENCES

- [1] : NRC-2008-0237
- [2] : USPTO Serial # 12/118,118, International PCT Application # PCT/CA2008/000895
- [3] : "Molten Salt Reactors : A New Vision for a GenIV Concept", Leblanc, 2008
- [4] : "Progress in Development of Li,Be,Na/F Molten Salt Actide Recycler & Transmuter Concept", Ignatiev & al, 2007
- [5] : "Combined effect of molten salt fluoride salt and irradiation on Ni-based alloys" , Bakai, 2008
- [6] : "Molten Salt Reactor Technology Gaps", Forsberg, 2006
- [7] : "Optimized Transition from the Reactors of Second and Third Generations to the Thorium Molten Salt Reactor", Merle-Lucotte & al, 2007
- [8] : "Waste stream generated and waste disposal plans for molten salt reactor experiment at Oak Ridge National Laboratory", Haghighi & al, 2002
- [9] : "Thorium-fueled underground power plant based on molten salt technology", Moir & Teller, 2004.
- [10] : "Direct conversion of spent fuel to HLW glass", Forsberg & al, 1994.
- [11] : "Moving on from the MSBR", Mathieu & al, 2005.
- [12] : "Neutronics development of SIMMER for Molten Salt Reactors", Wang & al
- [13] : "Fast-Acting Boron Injection System", Tuunanen & al, 2003
- [14] : "Monitoring the Thermal Power of Nuclear Reactors with a Prototype Cubic Meter Antineutrino Detector", Bernstein & al, 2008

- [15] : "Tritium Handling during LLEs Cryogenic Target Filling Operation", Janezic, 2007
- [16] : "How to spot states making secret plutonium"
 Link : <http://technology.newscientist.com/article/mg18925366.300>
- [17] : "Global thermal model for an off-set strip fin intermediate heat exchanger"
 Link : <http://eugenieurquiza.googlepages.com/kenoresearch>
- [18] : "MSRE design and operations report", ORNL-TM-0728
 Link : <http://www.energyfromthorium.com/pdf/ORNL-4728.pdf>
- [19] : "Processing of the MSRE flush and fuel salts" , ORNL-TM-2578
 Link : <http://www.energyfromthorium.com/pdf/ORNL-2578.pdf>
- [20] : "Development and validation of fission product release models and software at PBMR",
 van der Merwe, 2004
- [21] : "Conceptual design of a continuous fluorinator experimental facility", ORNL-TM-5253
- [22] : "Nuclear detection", Srikrishna & al, 2005
- [23] : "U232 and the proliferation resistance of U233 in spent fuel", Kang & al, 2001

10. LIST OF FIGURES

Figur 1 : DCThMSR vessel	1
Figur 2 : Reactor room outline	2
Figur 3 : Underground site	7
Figur 4 : Pure Th-cycle material flow	15
Figur 5 : Hybrid fuel cycles with denaturation and Th in fuel.....	17
Figur 6 : Graphite separation wall	18

Molten Salt Reactors: A New Vision for a Generation IV Concept

David LeBlanc

Physics Department, Carleton University, Ottawa Ontario
dleblanc@physics.carleton.ca

Abstract

Molten Salt Reactors were developed at Oak Ridge (ORNL) from the late 1940s to the early 1970s, highlighted by two successful test reactors. The Molten Salt Breeder Reactor (MSBR) evolved into a single fluid, graphite moderated design. Until very recently, this 1970s design version has been taken to be the starting point for any resurgence of the Molten Salt concept. This paper will show that a Molten Salt Reactor can in fact take many different forms. Through new solutions and applying new technology, it is hoped that an improved design can be brought to such a level that it can no longer be ignored as a practical ally in the resurgence of nuclear power.

1. Introduction

A Molten Salt Reactor (MSR) is one in which fluorides of fissile and/or fertile elements such as UF_4 , PuF_3 and/or ThF_4 are combined with carrier salts to form a fluid. Single Fluid designs have both fertile and fissile combined in one salt, whereas the lesser known 2 Fluid design has separate salts for fissile ($^{233}\text{UF}_4$) and fertile (ThF_4). Typical operation sees salt flowing between a critical core and an external intermediate heat exchanger. A secondary coolant salt then transfers heat to steam or closed gas cycle. The vast majority of work has involved fluoride salts as corrosion resistant alloys have been shown to be compatible with these salts. Chloride based salts have also been proposed, especially for fast breeder designs, but have unique problems and no operational experience to draw upon. Designs specifically for the thorium- ^{233}U cycle using fluoride salts have also been termed Liquid Fluoride Thorium Reactors (LFTR).

Fluid fuel reactors and MSR in particular have numerous operational and safety advantages over solid fuel designs. A detailed review is beyond the scope of this presentation but briefly:

- Fluid nature of the fuel means meltdown is an irrelevant term and allows the fuel salt to be automatically drained to passively cooled, critically safe dump tanks.

- Most fission products quickly form stable fluorides that will stay within the salt during any leak or accident. The volatile fission products such as the noble gases and noble metals come out of the salt as produced. Noble gases simply bubble out and are stored outside the reactor loop. Noble and semi noble metals will plate out on metal surfaces and can be collected by replaceable high surface area metal sponges within the loop.

- The continuous removal of the noble gas Xenon means that there is no "deadtime" of the reactor after shutdown or a power decrease that solid fueled reactors must deal with due to the production of ^{135}Xe from the decay of ^{135}I . As well, no excess reactivity need be in place to deal with such events.

- Most MSR designs have very strong negative temperature and void coefficients which act instantly, aiding safety and allowing automatic load following operation.

-No pressure vessel is needed as the salts run at atmospheric pressure. No water or sodium means no possible steam explosion or hydrogen production within the containment. In designs without graphite moderator, there is not even combustible material present.

- Fuel concentrations are easily adjusted on a continuous basis meaning no excess reactivity and no need for control rods or burnable poisons. Shutdown rods are often included but even these are not necessary given the ability to drain fuel out of the core to storage tanks.

-Utilization of the thorium to ^{233}U cycle produces several orders of magnitude less transuranic wastes than a conventional once through cycle and about one order of magnitude less than a U-Pu fast breeder (based on 0.1% losses during fuel processing). This leads to waste radiotoxicity being less than equivalent uranium ore levels within a few hundred years.

-Fuel processing and utilization of thorium permits break even breeding with ease and ability to reach a breeding ratio of 1.06 or even up to 1.13. Adding ^{238}U to denature the uranium content and still break even is also possible.

-Break even operation requires approximately 800 kg of thorium per GW(e) year added simply as ThF_4 . Startup fissile requirements can be as low as 200 kg/GW(e) or as high as 5.5 tonnes in harder spectrum designs, with 700 to 1500 kg more common. Thorium startup inventory varies from 50 to 200 tonnes.

-Thorium is 3 times as abundant as uranium. Proven reserves are large even with the small current industrial use of thorium and lack of prospecting. As example, a single new deposit in Lemhi Pass Idaho has added 600,000 tonnes to the world's proven reserves of 1.2 million tonnes. The USGS quotes a price of 27\$/kg for thorium nitrate and 80\$ to 100\$ for high purity thorium oxide.

-Without fuel processing, MSR's can run as simple converters with excellent uranium utilization.

-Offer many advantages for the destruction of transuranic wastes from traditional once through reactors. TRUs may also be used as startup fissile inventory for the thorium to ^{233}U cycle in many designs.

2. Background

Molten salt reactors were developed primarily at Oak Ridge National Laboratories beginning in the late 1940s. Almost 30 years of funded research and development followed a design evolution leading to the adoption in the late 1960s of what is known as the Single Fluid, graphite moderated Molten Salt Breeder Reactor (MSBR). What is important to realize however, is that this evolution was guided by goals and limitations that are far different than would now exist. In particular, the overwhelming priority given to the MSBR program was a minimization of the doubling time, the time to breed the startup inventory of the next reactor. The two routes for this are decreasing the startup fissile inventory and increasing the breeding ratio. This mandated priority was due to the early belief that nuclear power would follow an exponential growth and that uranium supplies were severely limited. Another fact was that MSBR's main competition was the heavily funded liquid sodium cooled fast breeder whose potential doubling time has always been impressive.

In order to properly evaluate potential molten salt reactors designs, it is important to first re-establish priorities. Given the ability of these reactors to start up on wide variety of fissile material, the doubling time is no longer of any real importance. Reaching a break even breeding ratio of 1.0 and

not beyond should be a high priority as this allows extremely low fuelling costs and no fissile material need enter or exit a plant after start up. This simple change alone gives great leeway to reconsider options that may be more practical but neutronically inferior, such simplifying fission product removal. An examination of molten salt design from first principles can lead to novel new solutions to unsolved problems which may further improve the prospects of this unique reactor.

Proliferation and long term waste concerns are also a more prevalent concern today. Transuranic waste production (Pu, Am, Cm etc) from the Th-²³³U cycle is several orders of magnitude lower¹ than for a LWR and will remain one its greatest advantages. Proliferation concerns¹ of a Th-²³³U cycle, while beyond the scope of this paper, might be considered roughly on par with other commercial reactors. Almost no plutonium is produced and it is of far lower fissile/fertile ratio than for LWR once through cycles. Weapons useable ²³³U is however produced but is always contaminated by significant amounts of ²³²U whose decay chain emits an extremely energetic 2.6 MeV gamma ray. This would aid detection and make handling nearly impossible. If deemed necessary though, a combination of depleted uranium and thorium can be used as fertile makeup to keep all uranium denatured. This complicates reactor operation somewhat but would result in designs with very high proliferation resistance.

2.1 The “traditional” MSBR

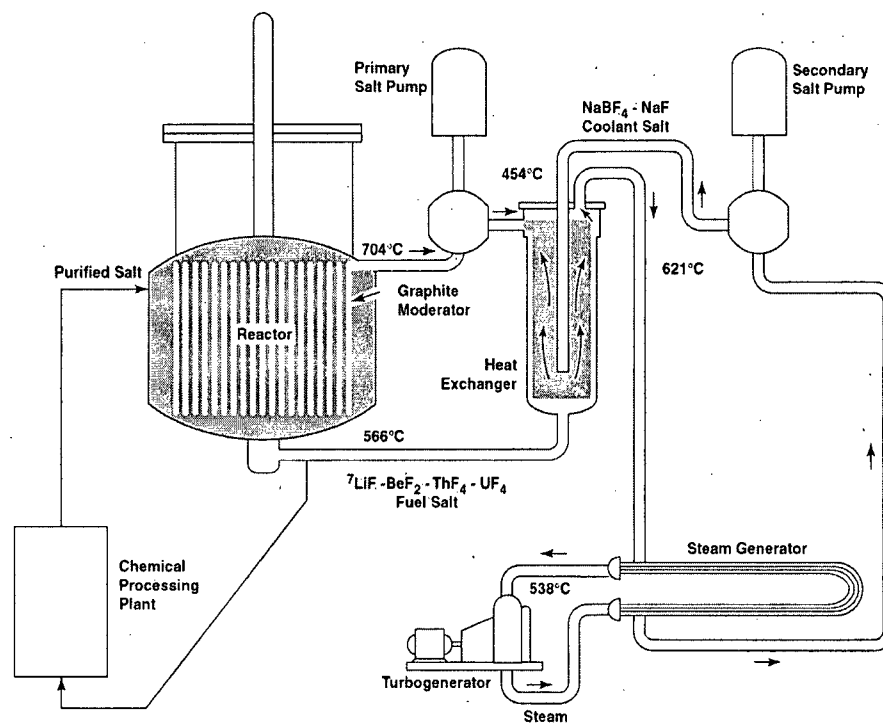


Figure 1 The 1970s Single Fluid, graphite moderated Molten Salt Breeder Reactor. 1000 MWe with a specific fissile inventory of 1500 kg. Reproduced from ORNL 4812.

Before a review of newly discovered and re-discovered molten salt designs it is useful to examine what might be viewed as the “traditional” MSBR which is the 1970s, graphite moderated, Single Fluid design^{2,3}. Both thorium and uranium are combined in a single fluid with a carrier salt (²⁷LiF-BeF₂). The core consists of graphite blocks with small channels through which the salt flows. The

salt is pumped between the core and an intermediate heat exchanger where it transfers heat to a secondary coolant. In the original design, the secondary loop then transfers heat to a steam Rankine cycle but a Brayton closed gas cycle⁴ is now considered a better fit to the salts high temperature. Another newly proposed modification of the traditional system is to employ carbon based, compact heat exchangers^{4,5} which can dramatically lower the out of core salt volume. The nickel alloy Hastelloy N is used for all piping and is rated for upwards of 750 Celsius with very good corrosion behaviour. The processing of fission products was to be by the liquid bismuth reductive extraction method which is briefly reviewed in the next section.

Potentially the largest drawback of this design is in terms of the significant processing needs for the salt. In a Single Fluid design, the thorium within the salt behaves very much like the rare earth fission products. This rules out the use of many simpler potential processing methods and greatly increases the complexity of the proposed liquid bismuth reductive extraction method.

Another requirement that is particular to this Single Fluid design is protactinium removal. ^{233}Pa is the 27 day half-life intermediate between ^{232}Th and fissile ^{233}U . The moderately high neutron flux of this design would result in too high a neutron loss to ^{233}Pa if it were not removed from the salt with a fast cycle time, 3 to 10 days being typical. The removed ^{233}Pa is stored for several months to allow it to decay to ^{233}U which is then reinjected into the salt. This rapid removal of ^{233}Pa is both costly and complex. As well, it adds a significant proliferation risk as the ^{233}U produced in decay tanks outside the core flux can be relatively free of ^{232}U . As will be shown however, many other molten salt designs can omit this entire procedure.

In order to evaluate new or even abandoned molten salt designs, a review of basic principles and a historical background is of benefit.

2.2 Salt processing methods

There are 2 types of fuel processing commonly used to increase the conversion or breeding ratio in molten salt reactors. Protactinium removal is also sometimes needed but is costly and introduces proliferation concerns and should be avoided if at all possible.

The first process is to remove uranium from the fuel salt. This is typically done before the salt is further processed for fission products. This is known as the fluoride volatility⁶ process and has been well known since the 1950s. It is one of the main advantages of working with these salts is that by simply bubbling first HF then F_2 gas through the salt, the uranium content in the salt will convert from UF_4 to UF_6 which comes out of the salt as a gas. This UF_6 can be later converted back to UF_4 and re-injected into the reactor as needed. Fluorination of higher actinides such as PuF_3 to gaseous PuF_6 is technically possible but much more problematic due to corrosion issues⁷.

Fission product removal is the main need and many methods were investigated at ORNL and elsewhere. Before 1964, there were various methods proposed with perhaps the most simple and attractive being salt replacement. In this, the fissile ^{233}U is first removed and transferred to clean new carrier salt. The used salt with fission products can be sent to long term storage or further treatment to concentrate the fission products. The drawbacks are that any contained thorium would be lost and that the best carrier salt (2^7LiF-BeF_2) is quite expensive as the lithium requires isotopic enrichment.

In 1964 a breakthrough was made called Vacuum Distillation⁶. In this method ^{233}U is first removed from the salt followed by distillation at low pressure to recover the carrier salt and leaving the majority

of fission products in the still bottoms. This process would leave behind any thorium contained in the carrier salt.

In 1968 a new method was developed that could allow processing for fission products for salts with both uranium and thorium (i.e. Single Fluids). Known as liquid bismuth reductive extraction, this involved contacting a side stream of molten salt with liquid bismuth and a reducing agent such as lithium. The lithium trades places with various fission products which then entrain with the bismuth. While the process can function in the presence of thorium it is far simpler to employ if it is absent.

2.3 The evolution of the MSBR program

The very first molten salt reactor project was the overly ambitious Aircraft Reactor Program for the U.S. Air Force to design a nuclear powered bomber using heat transferred from a molten salt reactor to replace combustion heat in a jet engine. While the practicality of such a concept remained far from proven, the significant funding and manpower assigned to it allowed great progress to be made in terms of molten salt reactors in general. The highlight of this project was the Aircraft Reactor Experiment which was a low power test reactor but which demonstrated operation at salt temperatures up to 860 C. It used highly enriched $^{235}\text{UF}_4$ in a NaF-ZrF₄ carrier salt with canned beryllium oxide for added moderation.

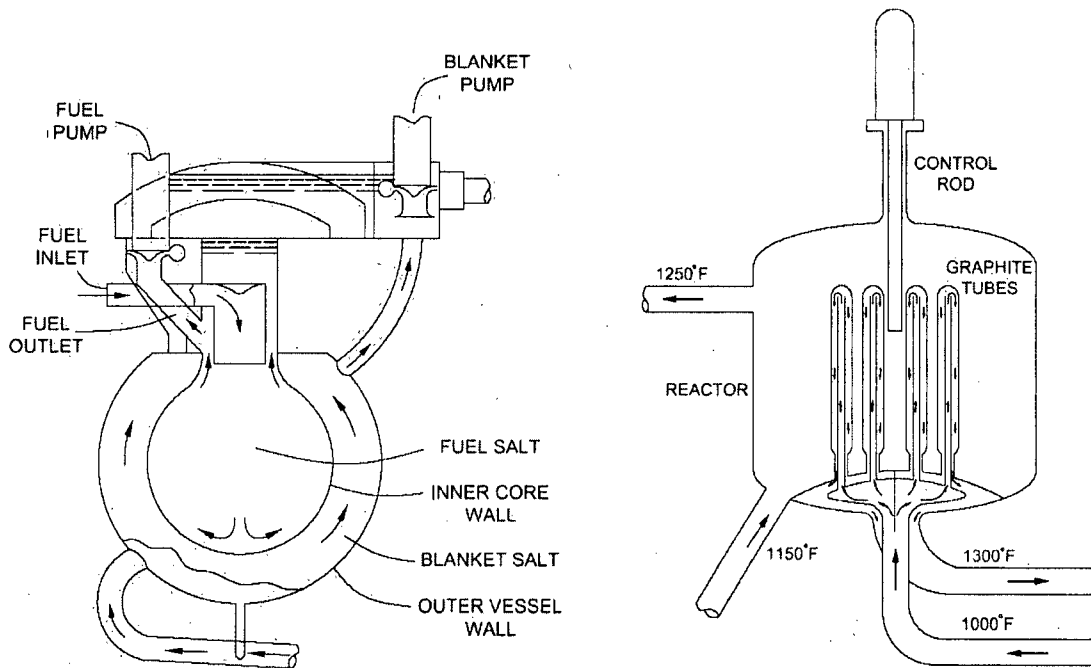


Figure 2. (Left) Depicts the 1950s graphite free, two-region concept. Reproduced from ORNL 2474. (Right) Depicts the 1960s intermixed 2 Fluid MSBR design using internal graphite plumbing. Reproduced from ORNL 4528.

In the mid 1950s a true Molten Salt Breeder Reactor program got underway at ORNL. A very simple homogeneous design was proposed⁸ as either a ^{235}U burner reactor or a thorium breeder on the Th- ^{233}U cycle. It was a two zone system as shown in the left side of Figure 2. A central spherical core contains fuel salt and was separated from an outer thorium blanket salt by a 1/3 inch Hastelloy N barrier. The fuel salt contained a mix of both fissile (PuF_3 , $^{235}\text{UF}_4$ or $^{233}\text{UF}_4$) and fertile ThF_4 in a carrier salt while the blanket salt contained ThF_4 in a carrier. In some studies, if the central core was very small, the fuel salt might lack any ThF_4 and would then qualify as a true 2 Fluid design.

While the simplicity of such a design was extremely attractive, in 1959 it was decided to switch focus to employing graphite moderation in order to improve the potential doubling time. It was recognized that a true 2 Fluid system can improve the neutron economy and simplifies fuel processing. The simplest 2 Fluid design would be a central core zone with fissile salt plus graphite surrounded by the fertile blanket salt (with or without graphite). The problem is such an arrangement has little power producing volume as the critical diameter would be small. ORNL workers concluded that blanket salt must also be intermixed within the central core region to allow a larger diameter core. This led to a design⁹ with complex graphite plumbing that ran fuel salt up and back down graphite tubes with blanket salt in the space between tubes and around the whole core to catch leakage neutrons. The right side of Figure 2 depicts the core with just a few of the hundreds of graphite tubes depicted.

This design proved highly complex, especially due to the fact that graphite will first shrink and then expand under neutron irradiation. This led to what was termed the "plumbing problem" that was never solved to satisfaction. This basic design remained the focus for nearly a decade however, which gives testament to the advantages seen in separate fissile and fertile salt streams. It should be noted that while graphite swelling is an issue, there is no safety concern of stored Wigner energy since the graphite operates at high temperature.

Also during the 1960s, the highly successful test reactor, the Molten Salt Reactor Experiment was constructed and operated. It was an 8 Mw(th) design chosen to be a single fluid for simplicity. Almost 5 years of operation saw very few operational difficulties. Two unknown issues with Hastelloy N did surface, one was corrosion induced by the fission product tellurium and the other was irradiation damage caused by (n,alpha) reactions in nickel. Both these issues were addressed by modifying the alloy makeup of the Hastelloy but it is now recognized that Hastelloy N may have a limited lifetime if used within the full neutron flux of the core. Outer vessel and piping use should pose no problems.

In 1968 the liquid bismuth technique was brought to light that could potentially process a fuel salt that also contained thorium. Even given the great complexity of this new process, the "plumbing problem" was just too great an issue and ORNL switched focus to the Single Fluid graphite moderated design of Figure 1. In the early 1970s however, for reasons many would argue more political than technical, the MSBR program was terminated by the AEC. The Single Fluid design became the textbook design and little mention of alternatives has appeared until very recent years.

2.4 A resurgence of interest

The late 1970s until the late 1990s saw only modest activity worldwide. Several voices attempted to keep the concept relevant including Charles Forsberg at ORNL and Kazuo Furukawa in Japan. In

recent years though there has been a resurgence of interest as the many advantages of the general design are recognized and the limited potential for improvement of other reactors has become evident.

The selection of molten salt reactors as one of the six Generation IV reactors in 2002 reactors has certainly contributed to the increase in interest. Much recent activity has also been based on molten salt reactors acting as transuranic waste burners. Most initial TRU burner work looked to modify graphite moderated designs and/or employ subcritical accelerator driven concepts. The latest work¹⁰ points to graphite free systems being the optimal route. A technical issue in TRU burning designs is the fact the PuF_3 is much less soluble in most carrier salts compared to UF_4 or ThF_4 . The carrier salt NaF-LiF-BeF_2 has recently been shown to be more than adequate and forms the basis of the MOSART¹¹ design out of Russia.

The most intensive new efforts have been from a group in France, centred in Grenoble which have undertaken a major modelling, design and salt chemistry program. This work has included discovery of a reactivity problem with the traditional Single Fluid MSBR. While the temperature coefficient has the needed fast acting negative term, as graphite heats up the overall temperature coefficient becomes positive. They have proposed remedies to this but they too have reached the conclusion that moving away from graphite moderation will attain the best results. Their latest design offering utilizes a 78%LiF-22%(Th+U) F_4 fuel salt as core, surrounded by radial blanket of LiF-Th F_4 in a graphite matrix. Termed the Thorium Molten Salt Reactor¹² (TMSR), the combination of high fissile concentration (5.5 tonnes $^{233}\text{U/GWe}$) and at least a partial blanket results in a high breeding ratio of 1.13 with a 6 month fission product removal rate and the ability to extend this processing time to 20 years and still break even.

Work involving molten salts has also increased in the U.S. but in a rather different way. Charles Forsberg and others are promoting the use of molten salts as simple coolants for high temperature solid fuel reactors. These designs are termed a Molten Salt Cooled Reactors¹³ (MSCR) as opposed to molten salt fuelled designs. Molten salts have high heat capacity and other excellent heat transfer qualities. This lowers pumping requirements, results in smaller heat exchangers and allows large cores to have adequate decay heat removal by natural circulation of the salt. The major design constriction this work faces is assuring a negative coolant void coefficient which has proved challenging but attainable. This work could entail much engineering development that would also be relevant to molten salt fuelled designs but has undoubtedly meant a diversion of expertise and attention away from thorium fuelled MSBR designs.

3. Solving the 2 Fluid “plumbing problem”

All original fluid fuel reactor designs involved utilizing two zones, a central core or seed zone surrounded by a fertile blanket (i.e. thorium). For the $^{233}\text{U-Th}$ cycle, the core might contain a mix of fissile and fertile in a carrier medium or in some cases only fissile. Molten salt work differentiated between these two cases by the terms “2 Fluid” for only fissile in the core and “1 and ½ Fluid” designs if the core contained thorium as well.

Early in development, the advantages of a 2 Fluid design became evident. If the core salt lacked thorium, it would be far easier to process for fission products. However a core without thorium will have a quite small critical diameter if the fissile concentration is kept high enough to limit losses to the carrier salt and/or graphite. The critical diameter is on the order of 1 meter for both pure salt

cores or heterogeneous cores with graphite. ORNLs solution was to use plumbing to intermix the 2 fluids within the core zone which as previously reviewed, proved unmanageable.

A solution to this dilemma may in fact be surprisingly simple. Traditionally reactor cores are spherical or short cylinder primarily to minimize neutron leakage. With an encompassing outer fertile blanket in a 2 Fluid design, leakage is not an issue. The simple solution thus proposed is core geometry switch to increase volume while maintaining the relatively small critical diameter.

As a first approximation the critical diameter will be the ratio of the Buckling constants between the given geometries. Thus, for the same graphite and/or fuel salt combination, an infinite cylinder will have a critical diameter approximately 76.6% that of a sphere. If a specific combination of fissile concentration, graphite percentage and carrier salt gives a critical diameter of 1 meter for a sphere, then for comparison, a 5 meter long cylinder would have critical diameter of 0.77 m and a 4m by 4m slab would be 0.51 m thick.

Side View of Reactor Core and Surrounding Blanket Salt
 Core is Graphite + Fuel Salt or 100% Fuel Salt
 Typical Diameter of 1 meter

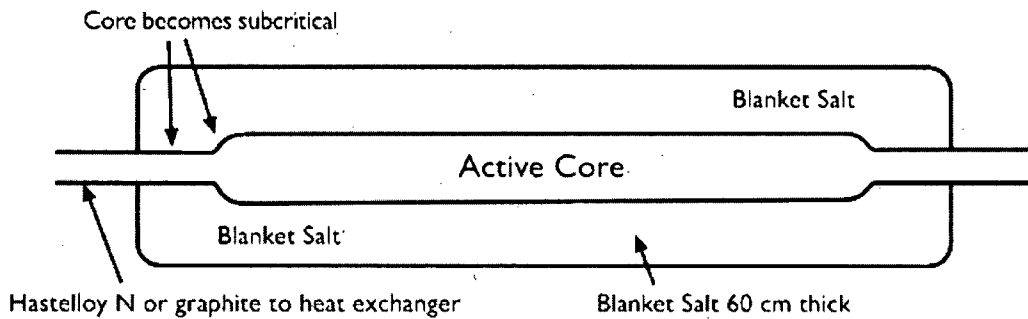


Figure 3 Generalized depiction of an elongated cylindrical 2 Fluid core with encompassing blanket salt. Inlet/outlet for blanket salt cooling are not shown.

The great advantage of going to an elongated cylinder or slab is the fact that a practical total power can now be obtained without intermixing but by simply extending the length of the core. While a barrier needs to be maintained between the core and blanket regions, this will be far less complex than the intimate intermixing of fuel and blanket salts in ORNL 2 Fluid designs. In terms of end plenums on these cylindrical cores, the simplest arrangement would be to taper the ends to a sub critical diameter while still surrounded by the blanket salt (see Figure 3). This should all but eliminate leakage of neutrons. While modelling efforts are ongoing, previous calculations from ORNL work of homogeneous designs of the late 1950s and 2 Fluid graphite work of the 1960s can be used to a significant degree to predict characteristics.

Such a design will have a strongly negative temperature and void coefficient for the fuel salt which is true for any 2 Fluid design. A major improvement over ORNLs intermixed 2 Fluid design is that the blanket should also have negative coefficients. This is due to the fact that the outer blanket acts as a very weak neutron reflector, thus lowering its density decreases this reflective quality and lowers reactivity in the core.

As with any fluid fuelled, two zone design, the leakage of core fluid into the blanket must be guarded against. The simplest method, proposed for all ORNL designs is to run the blanket fluid at a slightly higher pressure. As the blanket salt is far denser than the core salt, hydrostatic pressure accomplishes this automatically. Thus any leak through the barrier will add fertile to the core and lowers reactivity.

3.1 Graphite moderated version

There are some advantages to employing graphite moderation including very low fissile specific inventories and providing a built in structure to aid in the barrier between core and blanket. The much lower overall power density of graphite designs results in the need for much greater overall core volumes to attain power plant levels. This may mean multiple units per plant but this fact also brings other operation advantages. The limited lifetime of graphite due to fast neutron damage would also entail periodic replacement as is true of most MSBR designs. The small dimension and multiple units should assist in this aspect.

Using ORNL studies¹⁴ leads to an estimate of a 100 cm diameter for a long cylinder with 0.3%²³³UF₄ in fuel salt and a 20% salt/graphite ratio. Other parameters based on ORNL work are a salt power density of 400 kW/L (80 kW/L core) and an inlet of 565 C and outlet temperature of 705 C. Using the volumetric heat capacity of the salt, $\rho C_p = 4.69 \text{ J/cm}^3\text{K}$ and a choice of a 4.5 m/sec in core salt velocity results in a 464 MW(th) power production and a core length of 7.4 meters. Connection to steam cycle at the 44.4% efficiency ORNL predicted yields a 206 MW(e) output. The Brayton gas cycle is projected to produce an even higher efficiency. Graphite lifetime would be on the order of 2 to 5 years depending upon whether flux flattening methods are employed. It is proposed that core arrangement would be horizontal for this design. The 1 meter diameter graphite core would be surrounded by a 60 to 100 cm of a 27%ThF₄-73%LiF blanket salt. This blanket will result in extremely low neutron flux reaching the outer vessel wall.

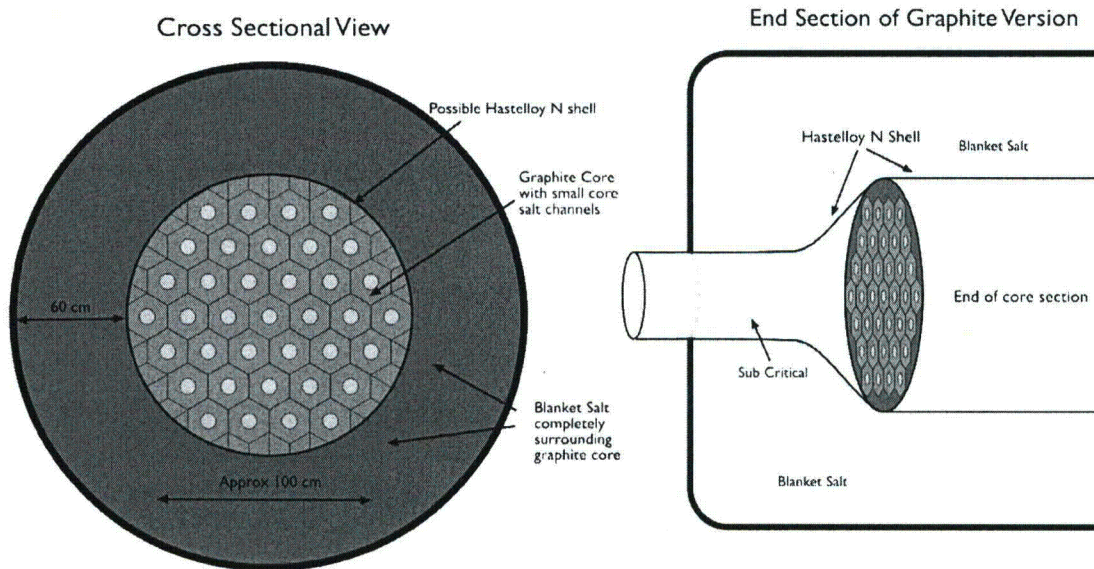


Figure 4 Cross sectional and end view of the 2 Fluid reactor using graphite moderator.

The total volume of salt and the fissile molar concentration dictate the specific inventory. For a graphite moderated design it should be possible to reach 0.15% ²³³UF₄ or even 0.1% or lower and

still break even. Taking into account salt volume needed out of core leads to a conservative estimate of 20 m^3 as adopted in French studies with a lower limit of perhaps 10 m^3 given the use of new compact heat exchangers. These estimates give a potential lower limit of start up fissile inventory of a mere 130 kg/GW(e) with 400 kg/GW(e) being a more conservative goal. For comparison ORNL 2 Fluid work was about 700 kg/GW(e) , ORNL Single Fluid 1500 kg/GW(e) , an LWR is 3 to 5 tonnes/GW(e) and liquid metal cooled fast breeders about 10 to 20 tonnes/GW(e).

3.2 Homogeneous, graphite free versions

Perhaps more impressive are the possibilities with homogenous designs lacking graphite moderator. With the entire volume of the core producing power, the needed volume is far less. Single cores for 1000 MW(e) are readily attainable although there are still advantages to smaller unit sizes. Without graphite moderation the assumption is often made that this means a much higher specific inventory and a quite hard spectrum. However, the carrier salt itself is a modest moderator and a wide variety of fissile concentration and neutron spectrum are in fact attainable. Recent French work requires a high specific inventory of 5.5 tonnes/GW(e) partly due to the fact that they choose to remove BeF_2 from the carrier salt due to toxicity concerns. In order keep the melting point low enough, the combined $\text{ThF}_4 + \text{UF}_4$ content needs to be 22% (about 2% $^{233}\text{UF}_4$). As well, with only a radial blanket in the TMSR design, attempting a much lower concentration would see a significant increase in neutron losses to the top and bottom reflectors.

Graphite Free Molten Salt Cylindrical Reactor

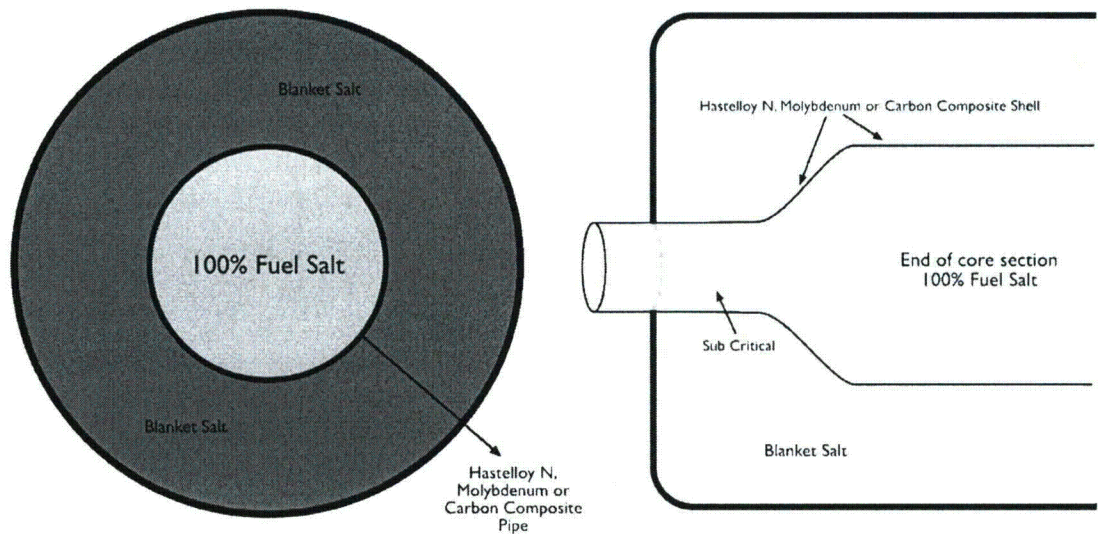


Figure 5 (Left) Cross sectional view of graphite free version (Right) End section showing tapering to a sub-critical while still within the blanket salt

ORNL calculations¹⁵ from the spherical cores of the 1950s design provide an excellent tool for estimation. While the accuracy of such early data must of course remain suspect, it is hoped adequate for at least cursory investigations. This study assumed a 1/3 inch (8.5 mm) thick Hastelloy N barrier for cores up to 12 feet (3.7 m) diameter, thus for much smaller cylinders a thinner wall should suffice. The study also assumed a 2 foot (60 cm) blanket which allowed significant leakage in some cases, expanding this to 100 cm should convert most of those losses to thorium absorptions.

The values of Table 1 give the initial breeding ratios, thus no losses to fission products or protactinium. ORNL also projected¹⁶ long term breeding ratios for the 8 foot core case in detail. Even with a relatively long 1 year processing time for fission product removal and no protactinium separation, the breeding ratio only dropped from 1.078 to 1.044.

TABLE I. Initial State Nuclear Characteristics of Spherical Two Region, Homogeneous, Molten Fluoride Salt Reactor with ²³³U ORNL 2751 (1959). Values in italics are projected by the author

Inner Core Diameter	3 feet	4 feet	4 feet	6 feet	8 feet
Thorium in Fuel Salt	0 %	0 %	0.25 %	0 %	7%
²³³ UF ₄ in Fuel Salt	0.592%	0.158%	0.233%	0.048%	0.603%
Neutrons per absorption in ²³³ U					
Be, Li and F in Fuel Salt	0.0639	0.1051	0.0860	0.318	0.078
Hastelloy N Core Wall	0.0902	0.1401	0.1093	0.1983	0.025
Li and F in Blanket Salt	0.0233	0.0234	0.0203	0.0215	0.009
Leakage	0.0477	0.0310	0.0306	0.016	0.009
Neutron Yield	2.1973	2.1853	2.1750	2.2124	2.200
Median Fission Energy	174 ev	14.2 ev	19.1 ev	0.33 ev	243 ev
Initial Breeding Ratio	0.9722	0.8856	0.9288	0.6586	1.078
<i>Projected B.R. Thinner Wall*</i>	<i>1.060</i>	<i>0.9836</i>	<i>1.011</i>	<i>0.7722</i>	<i>1.099</i>
<i>Projected B.R. Carbon Wall**</i>	<i>1.105</i>	<i>1.054</i>	<i>1.066</i>	<i>0.8714</i>	<i>1.112</i>

* Projected assuming a thinner Hastelloy core wall of 1/6 inch (4.2 mm) and 90% leakage reduction by using a thicker blanket

** Projected assuming a Graphite or Carbon-Carbon core wall and 90% leakage reduction by using a thicker blanket salt

Taking the 3 foot (91 cm) case as example, this would equate to a 70 cm wide cylindrical. Going to a more modest power density of 200 kW/L still gives impressive results. Using the same 140 K temperature change and a much slower salt speed of 2 m/s gives a 505 MW(th) output from a 6.6 meter long core. At 44.4% for steam cycle, this is 224 MW(e). Even including a meter thick blanket and outer vessel wall still results in an extremely simple to manufacture design that can fit within a tractor trailer for transport.

It must be noted that Hastelloy N at the time of these early studies was thought to be good for 10 to 20 years in core. Thermal neutron induced damage discovered in the MSRE means that Hastelloy N might not have a very long lifetime in the full flux of the core. ORNL had success in limiting this damage by modifying the alloy makeup, this trend could perhaps be continued with further study. As well, maintaining a harder spectrum at the barrier might actually improve lifetime as it is predominately thermal neutrons that contribute to the damaging (n,alpha) reactions. Potentially a much superior metal barrier is a high molybdenum alloy. Molybdenum is known have a much greater tolerance to neutron damage. It has been suggested for use not only in molten salt fission designs but also for the barrier between plasma and a 2LiF-BeF₂ coolant salt in fusion studies. As well, less expensive iron alloys including the common stainless steels 304 and 316 have also shown promise at somewhat lower operating temperatures. Given the simplicity of the core wall and outer vessel combination it is also not unreasonable to assume that periodic replacement even as short as annually could be still quite economical.

Carbon based material or a simple graphite tube would be ideal if their usability can be assured. The limited lifetime of graphite is well documented and would require periodic replacement. The irradiation tolerance of carbon based materials such as silicon impregnated carbon-carbon composites is an important question. There are thus several choices for a barrier material but it should be highlighted that this issue is of central importance to the proposed design.

3.3 Adding fertile, the 1 and ½ fluid or denatured options

While the pure 2 Fluid system has many advantages, adding a limited amount of thorium to the fuel salt does not necessarily detract from the fission product processing advantages. This is true if the thorium present in the fuel salt is allowed to be removed with the fission products. Traditionally this option would not be considered, for example in the Single Fluid 1970s design with 68 tonnes of thorium in the salt and a 20 day cycle time would mean wasting 1241 tonnes of thorium per GW-year. However for homogenous designs, a lower thorium concentration and more importantly much longer processing times afforded by the harder spectrum can result in new options. As an example the 8 foot (244 cm) example with 7% ThF₄ and 0.6% ²³³UF₄ would contain roughly 14 tonnes of thorium if the fuel salt volume was 15 m³. The processing time could easily be extended to 2 years or more for this version and still break even on breeding. Thus with a thorium discard option, only 7 tonnes per year would be wasted. With the low cost and abundance of thorium the added expense is practically negligible and there would still a roughly 30 fold improvement over LWR once through for resource utilization. Furthermore, thorium is far more abundant than uranium.

Adding thorium to the fuel salt also results in wider critical diameters for similar fissile concentrations. For example 0.6% ²³³UF has a 3 foot (91cm) critical diameter without thorium but an 8 foot (244 cm) diameter with 7% ThF₄. Thus a return to near spherical geometry for larger volumes is possible by the addition of fertile into to the core salt.

A similar result of wider, shorter cores is also be attained by adding fertile ²³⁸U to the fuel salt to run a denatured cycle that keeps ²³³U at less than 12% of uranium content. Thus uranium in all stages of operation will remain unfit for weapons use and allow easier compliance to existing regulations and the Nuclear Non-Proliferation Treaty. It is hoped that a pure Th-²³³U cycle can be shown to be equally proliferation resistant but it is obviously prudent to plan for both options. In practice running denatured would entail having both thorium and depleted uranium in the blanket salt such that the uranium remains denatured in the blanket as ²³³U is produced. Running a denatured cycle entails significantly increased production of plutonium and other transuranics which would need to be recovered and re-injected to the core during processing for fission products. This adds to complexity but if the processing cycle time is greatly lengthened compared to the traditional 20 day cycle, this results in very small daily processing needs. Running a break even denatured cycle was calculated to be possible for a graphite moderated Single Fluid design¹⁷ in the late 1970s so it should be little problem to break even for a 2 Fluid graphite moderated version. For homogeneous versions, there will undoubtedly be a lower limit on the fissile molar concentration and thus spectrum hardness to overcome ²³⁸U resonant absorptions. This would mean a larger starting fissile load is required, but this is easy to provide as low enriched uranium is ideal for startup in this case.

As a final reactor example, the 8 foot (244 cm) core case of ORNL can be examined. This had 7% ThF₄ and 0.6% ²³³UF₄ which represents approximately a 1200 kg/GW(e) starting fissile load for a total salt volume of 15 m³. In cylindrical geometry this would be a core close to 2 m in diameter.

Again assuming a modest power density of 200 kw/L, and in this case a salt velocity of 1.3 m/s gives an output of about 1000 MW(e) with a core length of only 4.2 meters.

Going to higher fissile plus fertile molar concentrations in the core salt and the resultant harder neutron spectrum has many advantages. Losses to fission products and protactinium are significantly lowered as their cross sections drop off faster than for fissile elements. This results in far less fuel processing requirements. Improving the neutron economy gives the ability to employ other carrier salts that do not contain ^7Li or Be as these elements are expensive and produce tritium. Disadvantages include a shortening of the prompt neutron lifetime which can complicate reactor control. The very strong negative reactivity coefficients aids in this respect. Also, the issue of accidental criticality if salt spills can reach moderator has been raised. Proper design with boronated leak pans guards against this and any potential energy release of a spill reaching criticality should be small given that the salt would simply flash to vapor.

A potential plant layout for the above example is shown in Figure 6. Vertical core orientation is thought best for a shorter core. The thick blanket salt means almost no neutron flux reaches the outer vessel wall. Thus it need not be very thick or contain reflective material. A drain line activated by a freeze plug, drains the core to critically safe dump tanks should the salt temperature rise for any reason. A spill drain to dump tanks is also shown at the low point of the containment structure.

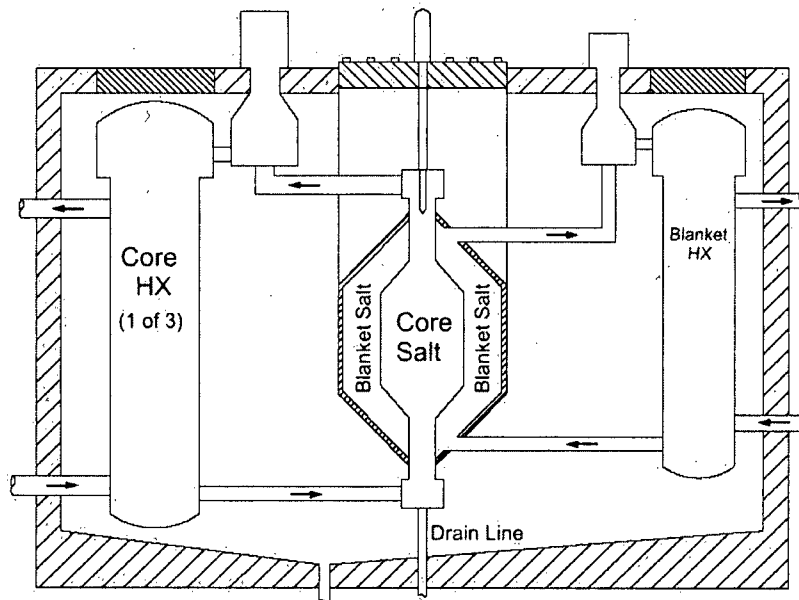


Figure 6. Potential plant layout within containment for an inner core of about 2 meter diameter. Secondary coolant salt transfers heat out of containment to drive a steam or closed gas cycle.

4. Conclusions

As the advantages of employing thorium have become widely recognized, it is time to formally reexamine the reactor specifically designed for its use. As is hopefully now evident, molten salt reactor designs offer great flexibility and advantages in almost all operational aspects. Costs of the traditional Single Fluid design have been estimated to be roughly on par with LWR costs, such that the great simplifications in design and fuel processing proposed here and elsewhere offer great saving potential. Overall safety sees a multitude of advantages over other reactor designs and denatured operation can be employed if even greater proliferation resistance is desired. Design and modeling work is ongoing on these presented designs and numerous others giving the versatility to adapt to design obstacles. For example, if a barrier between core and blanket proves unfeasible, barrier free alternative designs are already being modeled.

While at present, government and industry support is sorely lacking worldwide, the research and development needs¹⁸ are far less than many may imagine. Perhaps ORNLs greatest legacy in this respect has been their dedication to fully document all aspects of their work and this wealth of information is now readily accessible. While the lack of after sale profits (enrichment, solid fuel fabrication etc) may require a different business model to attract corporate interest, the potential rewards are indeed great for any government, corporation or agency willing to take a leading role in this vital effort.

5. Acknowledgements

If wish to thank Bruce Hoglund for numerous production discussions and Kirk Sorensen for his work in enhancing public awareness and the creation of an extensive open data base of material at <http://thoriumenergy.blogspot.com>

6. References

- [1] Le Brun, C., "Impact of the MSBR concept technology on long-lived radio-toxicity and proliferation resistance", Technical Meeting on Fissile Material Management Strategies for Sustainable Nuclear Energy, Vienna 2005
- [2] Bettis E.S. et al., "The Design and Performance Features of a Single-Fluid Molten-Salt Breeder Reactor ", Nuclear Applications and Technology, Vol 8 1970, pp 190-207
- [3] Rosenthal M.W. et al., "Molten Salt Reactor Program, The Development Status of Molten Salt Breeder Reactors", ORNL 4812, August 1972
- [4] Forsberg, C.W. et al., "Advanced Molten Salt Reactors using High Temperature Reactor Technology", 2004 International Conference on Advances in Nuclear Power Plants, ICAPP '04
- [5] Peterson, P.F. et al., "Advanced CSiC composites for high temperature nuclear heat transport with helium, molten salts and sulfur-iodine thermochemical hydrogen process fluids" Second Information Exchange Meeting on Nuclear Production of Hydrogen, Oct 2-3, 2003
- [6] Scott, C.D. et al., "Preliminary design study of a continuous fluorination-vacuum distillation system", ORNL 3791 Jan 1966

- [7] Cathers, G.I. et al., "Recovery of PuF₆ by Fluorination of Fused Fluoride Salts", ORNL 3298, Sept 1962
- [8] MacPherson H.G "Molten Salt Program Quarterly Progress Report" ORNL 2551, 1958
- [9] Kasten P.R. "Design Studies of 1000 Mw(e) Molten Salt Breeder Reactors" ORNL 3996 1966
- [10] Greenspan E. et al., "Transmutation performance of Molten Salt versus solid fuel reactors" 15th Int. Conf on Nuclear Engineering, Nagoya Japan 2007 ICONE15
- [11] Ignatiev, V. et al., "Progress in Development of Li, Be, Na/F Molten Salt Actinide Recycler and Transmuter Concept", Proceedings of the ICAPP 2007
- [12] Merle-Lucotte, E. et al., "Optimized transition from the reactors of second and third generation to the Thorium Molten Salt Reactor", Proceedings of the ICAPP 2007
- [13] Forsberg, C.W. "Developments in Molten Salt and Liquid Salt Cooled Reactors", Proceedings of the ICAPP 2006
- [14] Briggs, R.B. "Summary of the Objectives, the Design, and a Program of Development of Molten Salt Breeder Reactors", ORNL TM 1851, June 1967 (*Table 21*)
- [15] Alexander, L.G. et al., "Nuclear Characteristics of Spherical, Homogeneous, Two-Region, Molten-Fluoride-Salt Reactors" ORNL 2751, 1959
- [16] MacPherson, H.G. "Molten Salt Quarterly Report" ORNL 2626 period ending Oct 1958
- [17] Engel, J.R. et al., "Molten Salt Reactors for the Efficient Nuclear Fuel Utilization without Plutonium Separation", ORNL TM 6413, Aug 1978
- [18] Forsberg, C.W., "Molten Salt Reactor Technology Gaps" Proceeding of ICAPP 2006

Progress in Development of Li,Be,Na/F Molten Salt Actinide Recycler & Transmuter Concept

Victor Ignatiev, Olga Feynberg, Ivan Gnidoi, Aleksandr Merzlyakov, Vladimir Smirnov,
Aleksandr Surenkov, Igor Tretiakov, Raul Zakirov
Russian Research Center – Kurchatov Institute, Moscow, RF
Valery Afonichkin, Andrei Bovet
Institute of High Temperature Electrochemistry, Ekaterinburg, RF
Vladimir Subbotin, Aleksandr Panov, Andrei Toropov, Alexei Zherebtsov
Institute of Technical Physics, Snezhinsk, RF
Tel. +7-495-196-71-30, Fax. +7-495-196-86-79, E-mail: ignatiev@quest.net.kiae.su

Abstract –To examine and demonstrate the feasibility of molten salt reactors to reduce long lived waste toxicity and to produce efficiently electricity in closed fuel cycle some national and international studies were initiated last years. In this paper main focus is placed on experimental and theoretical evaluation of single stream MOlten Salt Actinide Recycler & Transmuter (MOSART) system fuelled with compositions of plutonium plus minor actinide trifluorides (AnF_3) from PWR spent fuel without U-Th support. The paper summarizes the most current status of the MOSART design data received within ISTC#1606 phase 2.

I. INTRODUCTION

Recent years have demonstrated a growing interest in the nuclear energy systems employing the technology of molten salt fluorides. Among the systems selected in GIF Generation IV, Molten Salt Reactors (MSR) presents a promising flexible option in response to the goals and criteria assigned to future nuclear systems: fuel cycle sustainability, safety, environmental impact, proliferation resistance, diversity of applications and economics.

A study is underway within ISTC#1606 phase 2 to examine and demonstrate the feasibility of MOlten Salt Actinide Recycler & Transmuter (MOSART) system to reduce long lived waste toxicity and to produce efficiently electricity in closed cycle.^{1,3} Focus is placed on the experimental and theoretical evaluation of single stream MOSART concept fuelled with different compositions of plutonium and minor actinides from LWR spent fuel without U-Th support.

These studies are performed in the following main work packages:

1. Study on system's neutronic, thermal hydraulic and fuel cycle properties, accounting for technology constrains.

2. Experimental consideration of fuel salt key physical & chemical properties
3. Experimental verification of Ni-Mo alloys for fuel circuit in corrosion facilities with redox measurement

As result of ISTC#1606 Phase 1 studies claim was made, that the solvent system selected appear to resolve main reactor physics, thermal hydraulics, fuel salt clean up and safety problems as applied to the Li,Be,Na/F MOSART concept¹.

This paper summarizes the most current status of the MOSART design data received within ISTC#1606 phase 2.

II. DESIGN CONSIDERATION

Design basic objective for MOSART concept is to provide the fissile concentration and geometry of the fuel salt to obtain heat release of about 2400 MWt at conditions affording the effective transmutation of plutonium and minor actinides from LWR spent fuel without U-Th support.

The fuel and coolant salts, graphite and Ni-Mo alloy are special materials for MOSART, which have been studied and developed at first in ORNL^{4,5}, later RRC-Kurchatov Institute and now under consideration within ISTC#1606^{4,5}. Principal design data for MOSART fuel

circuit received in our study are given in Tables I and II. Plan view of MOSART fuel circuit is shown on Fig. 1.

There is, of course, not one possible arrangement of MOSART unit. Fig. 1 shows the preliminary primary system design configuration that is used to evaluate its neutronics and thermal hydraulics feasibility. As in well-established MSBR⁴ design the fluoride fuel salt mixture is circulated through the reactor core by four pumps operating in parallel. Pumps circulate salt through heat exchangers and return it to a common plenum at the bottom of the reactor vessel. Each circuit contains a 1 m³/s single stage centrifugal pump and a shell-and-tube heat exchanger.

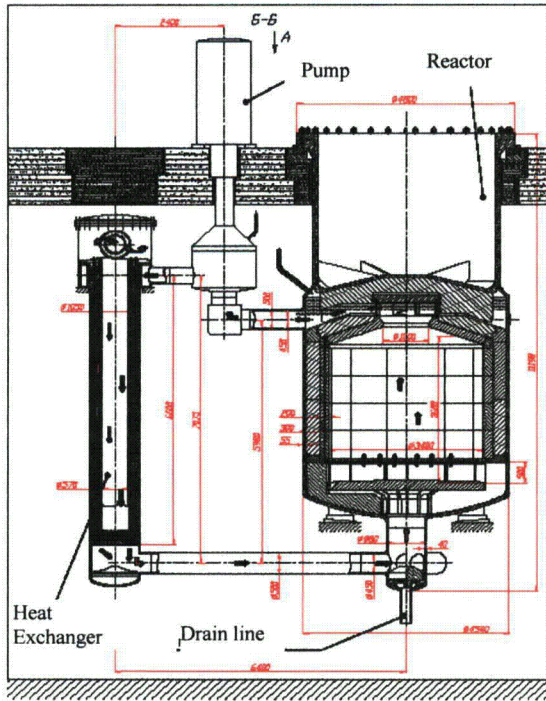


Fig. 1: MOSART Fuel Circuit

Heat is transferred from the primary salt to secondary fluid NaF-NaBF₄ having composition 8-92 mole % and liquidus temperature 384°C. Each of the four secondary circuits has a 1.3 m³/s centrifugal pump with variable-speed drive. In addition to its primary functions of isolating the highly radioactive primary circuit from the steam system and serving as an intermediate heat transfer fluid, the molten NaF-NaBF₄ mixture would play a major role in limiting the release of tritium from MOSART system.

Tritium, xenon and krypton are sparged from circulating fuel salt by helium introduced in a side stream

by a bubble generator and subsequently removed by a gas separator. Provisions are made for maintaining soluble fission products at low required level by fuel salt processing. To minimize actinide losses in reprocessing we considered removal time about 300 edpf for soluble fission products (rare-earth trifluorides). The reactor is capable of being drained essentially free of salt and afterheat following shutdown can be safely dissipated.

TABLE I
 Principal Design Data

	MOSART	MSBR
Thermal capacity, MWt	2400	2250
Reactor vessel ID, m	4.54	4.43
Vessel wall thickness, cm	5.5	5.1
Vessel design pressure, N/m ²	5.2 · 10 ⁵	5.2 · 10 ⁵
Core height, m	3.6	3.96
Radial thickness of reflector, cm	20	76.2
Volume fraction of salt in core, %	100	13/37
Average core power density, MW/m ³	75.0	22.2
Peak core power density, MW/m ³	163	70.4
Average neutron flux, n cm ⁻² s ⁻¹	10 ¹⁵	2.6 · 10 ¹⁴
Max graphite damage flux, n cm ⁻² s ⁻¹	1.45 · 10 ¹⁴	3.3 · 10 ¹⁴
	>180keV	>50keV
Graphite temperature at max graphite damage region, K	1084	982
Estimated useful life of graphite, yrs	4	4
Total weight of graphite, t	20	304
Average salt velocity in core, m/s	0.5	1.3
Total fuel salt in reactor vessel, m ³	40.4	30.4
Total fuel salt in primary system, m ³	56.2	48.7
Cycle time for salt inventory, efpd	300	30

The start up and feed fuel material scenarios for MOSART critical core are following: 1) TRU from UOX spent fuel of a commercial PWR (60 GWd/tU - 4.9% ²³⁵U/U; after 1 year cooling); 2) 4.9% ²³⁵U/U irradiated in PWR up to 60 GWd/tHM (Stage 1); after 7 years cooling the Pu from the spent fuel it is used for MOX fuel production with natural uranium and 7% Pu; after 3 additional years of MOX fuel production, this fuel also irradiated in PWR up to 60 GWd/tHM (Stage 2). Remained Pu and minor actinides from Stage 1 irradiation, after 10 years cooling are the fuel for MOSART.

Fuel salt is molten 15LiF-27BeF₂-58NaF (in mole%) mixture with 479°C melting temperature fuelled by trifluorides of actinides with mass proportion at equilibrium for chosen fuel cycle scenario. Lithium is enriched to 99.99% ⁷Li. In the design of the MOSART, the material that is specified for nearly all metal surfaces contacting the fuel and coolant salts is an alloy, which is modification of the present commercial Hastelloy N (see Section III). The only exception is part of the chemical

processing system, which are made of molybdenum, and the infrequently used fuel storage tank, which is of stainless steel.

2400MWt MOSART system has the cylindrical core having an intermediate to fast energy spectrum of neutrons. No solid material is present in the core of this reactor as moderator. The salt inlet temperature in core is assumed as 600°C. The diameter / height of the cylindrical core is about 3.4 m / 3.6 m. The effective flux of such system is near $1 \cdot 10^{15}$ n cm⁻² s⁻¹. Fuel salt specific power is about 43 W/cm³. The core salt mass flow rate is 10000 kg/s. Average axial velocity of stream in core is equal about 0.5m/s. The fuel salt enters the core through inlet radial window at the bottom of core and the salt flow is upward through the core to promote natural circulation. The fuel salt leaves the reactor vessel through outlet pipe attached to the top reflector. Out core circulation time is about 4 s.

TABLE II
 Characteristics of Heat Exchangers

	MOSART	MSBR ²
Inlet/outlet fuel salt temperature, K	873/988	839/978
Fuel salt mass flow rate, kg/s	10000	11820
Secondary salt mass flow rate, kg/s	9400	8872
Fuel salt velocity, m/s	5	3
Tube spacing in heat exchanger on pitch circle, mm	12.2	18.8
ID of central tube in heat exchanger, m	0.57	0.51
Shell ID, m	1.05	1.73
Tube OD, mm	10	9.5
Total number of tubes in four heat exchangers	18591	23584
Length of one heat exchanger, m	6.6	6.8
Total volume of fuel salt in heat exchangers tubes, m ³	6.2	7.6
Heat transfer coefficient, primary side, W/m ²	17100	-
Heat transfer coefficient, secondary side, W/m ²	17656	-
Overall heat transfer coefficient, W/m ²	5700	4820
Pressure drop in heat exchanger, primary side, kPa	660	890

For MOSART graphite reflector there is no strong requirement on gas permeability (10^{-8} cm²/s), but molten salt should be excluded from the open pore volume (pore structure < 10^{-6} m). Last requirement can be met by currently available commercial graphite. Optimal thickness for removable radial and axial graphite reflectors accounts for 0.2 m. Cooling was provided for the reactor vessel and other parts of design to keep temperatures within the tolerances imposed by neutron fluence and stress conditions. About 1% of the reflector volume is the fuel salt. Owing to relative power in graphite reflectors the total

fuel salt flow rate through reflectors was chosen 275 kg /s (2.75 % from the total flow). Neutron fluences and maximum graphite temperatures are kept low enough to provide an estimated reflector graphite life of about four years. Thermal conductivity and density of the graphite reflectors was accepted equal to the following values: $\lambda_C = 57W \cdot m^{-1} \cdot K^{-1}$ and $\rho_C = 1800kg/m^3$.

Between reflector and reactor vessel, 30 cm width steel blocks with 1% of fuel salt are installed to reduce the damage flux arriving at surface of the 5cm reactor vessel wall made of Ni- Mo alloy. To minimize the reactor vessel wall temperature the 5mm fuel salt annulus is assumed between iron blocks and reactor vessel.

The reactor vessel is about 4.54m in diameter and 11.2 m high. It has 55mm thick walls and 75 mm -thick dished heads at the top and bottom. The 15 cm diameter fuel salt drain line connects to the bottom of the reactor vessel inlet manifold. The reactor vessel is expected to last of the life of the plant. The reactor is capable of being drained essentially free of salt and afterheat following shutdown can be safely dissipated.

III. CORE NEUTRONICS, THERMAL HYDRAULICS AND FUEL CYCLE

The equilibrium fuel salt composition was obtained with the help of MCNP-4B+ORIGEN2.1 code (with library received on the basis of ENDF/B-V,VI) calculation of transition to equilibrium of 2400MWt MOSART core with soluble fission product removal time equal 300 efpd.

For 2400MWt homogeneous cylindrical core with 20cm nickel and graphite reflectors at equilibrium critical loading 3D power distribution maps have been obtained. Differ from Ni reflector for graphite one there is the power growth (up to 60% from the maximal value in the core centre) on the boundary of the fuel salt and graphite reflector due to thermal neutrons return to the core. The total power outputs due to n+ γ radiation for the graphite and nickel reflectors have been obtained. The relative power in graphite and nickel reflectors are 2.2% and 1.7% of total core power respectively.

On the basis of 3D power distributions received in neutronics calculations for cores with reflectors the thermal hydraulic calculations have been carried out. Calculations were executed by Russian commercial code Flow Vision. Various possibilities of fuel salt inlet / outlet for core cylindrical geometry with fuel salt cooled reflectors have been analyzed. The expediency of use of reflectors of porous type was shown.

Calculations of the coupled thermal hydraulics task (fluid convection in core with thermal conductivity in reflectors) have allowed (1) due to increase of height of radial fuel salt inlet window from 0.1 m up to 0.5 m and (2) using top conic reflector, instead of a flat one, to carry out alignment of core velocity distribution. Alignment of a velocity distribution has resulted in significant reduction of the maximal fuel salt temperature in core from 1385K down to 1107K. The peak temperature of a radial reflector has made 1142K, in the bottom and top reflector - accordingly 1098K and 1085K. However in the bottom part on periphery of core small recirculation area was kept.

Introduction of the distribution plate at core inlet with porosity of 32 % has allowed completely to avoid recirculation areas of flow and to lower the maximal temperature of fuel salt to a level 1034K, that only 46K higher than average fuel salt temperature at core outlet. The maximal temperature of radial nickel reflector has made 1119K, of bottom and top reflectors - accordingly 1096K and 1063K.

Transition to graphite reflector for given power distributions essentially has not changed significantly the characteristic (velocity and temperature distributions of fuel salt) in core and reflectors. The maximal temperature in core has increased on 2K and has made 1036K. The temperature of a radial reflector has decreased in comparison with similar variant with a nickel reflector from 1119K down to 1087K, temperatures of the bottom and top reflectors have decreased on 10K and 20K accordingly.

The optimized MOSART core configuration satisfies the two most important thermal hydraulic considerations: (1) the maximum temperature of solid reflectors is low enough to allow it use for suitable time and (2) regions of reverse or stagnant flow are avoided.

Further specification of thermal hydraulics characteristics of core and reflectors may be received by use of two-temperature model of a porous body. Also it will be necessary to take into account reactor vessel protection required, by e.g. 30 cm width iron blocks with 1% of fuel salt installed to reduce the damage flux arriving at surface of the reactor vessel wall made of Ni-Mo based alloy. To minimize the reactor vessel wall temperature the 5mm fuel salt annulus would be assumed between iron blocks and reactor vessel.

Received on a thermal hydraulic stage of calculation the improvement of MOSART core design and 3D temperatures distributions of the core and reflectors were used for specification of system neutronic characteristics (see Fig. 2 and 3). As can see from Fig. 2 for last core

configuration the required AnF_3 concentrations in fuel salt for equilibrium critical loadings, as for the scenario 1 (1.03 mole%, compared to 0.6 mole% for infinite core) and for the scenario 2 (1.30 mole% compared to 0.8 mole% for infinite core), remain truly less than trifluorides solubility limit (2 mole%) for chosen carrier salt at minimal temperature in primary circuit 600 °C, even in view of probable uncertainties in the neutron cross-sections of minor actinides. Contribution to the system's neutron balance of the nuclides up to ^{251}Cf was considered. Note, that at equilibrium, AnF_3 concentration (in mole%) is about one order of magnitude higher than that of LnF_3 in fuel salt. Transient to equilibrium in 2400MWt MOSART core needs about ten years. Masses of plutonium and minor actinides in primary circuit at equilibrium according MCNP calculation for scenario 1 and scenario 2 are respectively 7320 kg and 9346 kg.

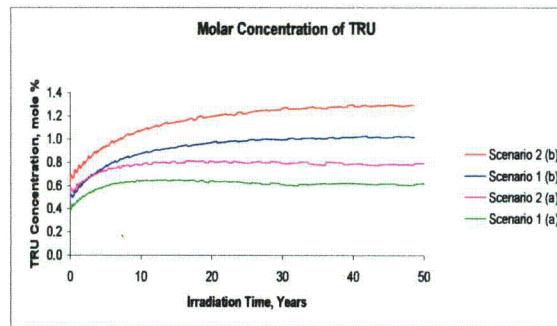


Fig. 2 Fissile AnF_3 concentrations for different MOSART start-up and feed fuel salt compositions at transient to equilibrium: a-infinite in radial direction core, b-finite core.

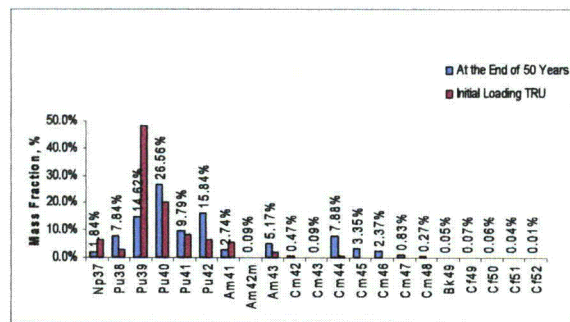


Fig. 3. Actinides mass fraction in MOSART: Scenario 2

Data obtained as a result of the burn up calculations permit to determine integral parameter, characterizing system efficiency for plutonium and minor actinides transmutation:

$$K_G(t) = \frac{N_F^{TRU}(t)}{N^{TRU}(t)},$$

where $N^{TRU}(t)$, and $N_F^{TRU}(t)$ - full amount, respectively, loaded and burned plutonium plus minor actinides during period t (this parameter is proportional to the core thermal power and reaches its maximum in critical system of MOSART type fuelled by only plutonium and minor actinides).

If we deal with the critical system loaded by only plutonium and minor actinides with relatively small transition to equilibrium time:

$$\frac{1}{K_G(T)} = 1 + \frac{M_E}{P} E_f \left(\frac{z}{\tau} + \frac{1}{T} \right),$$

where T -lifetime of the fuel loading, M_E -equilibrium plutonium and minor actinides loading, P - thermal power of the system, E_f - fission energy, $1/\tau$ - soluble fission product removal rate; z - losses to waste.

As can see K_G aspires to maximal meaning for the systems with long lifetime T , minimal possible equilibrium specific loading (M_E/P) and minimal losses to waste in fission products removal process (z/τ). For the case of actinides losses to waste stream in single pass $z=10^{-3}$ and $T=50$ yrs K_G factor responsible for transmutation efficiency and equal 0.95 for the infinite in radial direction core loaded by scenario 1 is decreased for the case of 3D finite core down to 0.83. For scenario 2 last value is equal 0.80.

The experimental data on fuel salt density obtained (see next Section) have been used for calculation of temperature reactivity coefficients in 2400MWt MOSART core with 0.2m graphite reflector for the equilibrium critical fuel loading in the temperature range 900 - 1600K. Calculations have been done in assumption of core isothermal fuel salt temperature and on base of 3D temperature distributions for core operating at nominal power, received in thermal hydraulic calculation. The account of temperatures distribution in the core operating at nominal power, make temperature reactivity coefficients more negative, compared to isothermal core. For last case they are equal to -4.125 pcm/K and -6.625 pcm/K for the first and the second scenarios of the equilibrium critical loading, respectively.

Within IAEA coordinated research "Studies of Innovative Reactor Technology Options for Effective Incineration of Radioactive Waste" the comparison of 2400MWt MOSART core neutronic characteristics (for scenario 1) by different calculation schemes was carried out³. The received results have confirmed essential

distinction in cross-sections of minor actinides used in different libraries. At the same time the results obtained with the help of different codes, but with the use of the same nuclear data coincide rather well. The disorder in values of K_{eff} is near 2.5 %. Thus the maximal value gives JEFF3.1, and minimal ENDF6.8.

Work on comparison of neutronic, thermal hydraulic and safety related parameters of MOSART core, obtained by different calculation schemes with attraction of new results will be continued.

Fig. 4 shows preliminary conceptual flow sheet for MOSART fission products clean up unit. Most important processing operations consist in recycling of actinides for transmutation and removal of lanthanides in order to hold actinides plus lanthanides concentration in the fuel salt below the solubility limit and neutron absorption in lanthanides to acceptable level.

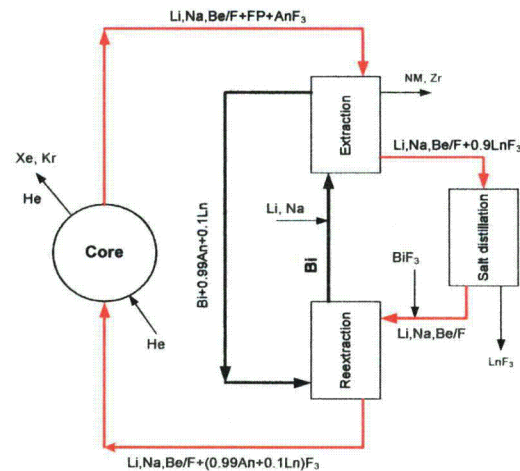


Fig. 4. Conceptual scheme of MOSART fuel salt clean up

At the first stage of the fuel salt clean up all actinides and some of fission products (noble metals, zirconium) are co-extracted into liquid bismuth. At the second stage lanthanides are separated from the $Li, Be, Na/F$ solvent by method of salt distillation. This method of lanthanides removal is under consideration, because our last experiments indicate that in lanthanides extraction process the large amount of sodium is removed into liquid bismuth from $Li, Be, Na/F$ system. Further, the actinides are re-extracted and recycled to the core for transmutation. Sodium extraction could be sufficiently decreased by sodium addition into liquid bismuth.

The $Li, Be, Na/F$ salt distillation process could produce some problems, because of high temperatures (1200-1300°C) needed to achieve necessary distillation capacity

(about 0.2 m³ per day). However, these difficulties would be managed. For example, the amount of salt distilled could be sufficiently decreased by preliminary crystallization of the main part of lanthanides in cold traps.

IV. PHYSICAL END ELECTROCHEMICAL PROPERTIES OF FUEL SALT.

IV.A. Physical Properties

Below are listed the main physical properties of molten 15LiF-27BeF₂-58NaF (mole %) and 17LiF-58NaF-25BeF₂ (mole%) mixtures received to be used in the design calculation:

Composition 15LiF-27BeF₂-58NaF (mole %) corresponds to ternary eutectic with liquidus temperature 479±2°C. Liquidus temperature was determined using curves of heating and for composition 17LiF-25BeF₂-58NaF (mole%) is equal to 486±2°C.

PuF₃ solubility in the melt was measured by original technique of local γ -spectrometry. It provides reliable determination of equilibrium in system melt-solid state and measurement with relative error less than 9%. For molten 17LiF-25BeF₂-58NaF and 15LiF-27BeF₂-58NaF mixtures (in mole %), the data appear to follow a linear relationship within the experimental accuracy of the measurements when plotted as $\ln P$ of molar concentration of PuF₃ vs. $1/T(K)$, respectively:

$$\ln P = -0,6334 \cdot \frac{10^4}{T} + 8,38$$

$$\ln P = -0,5936 \cdot \frac{10^4}{T} + 7,49$$

For molten 15LiF-58NaF-27BeF₂ and 17LiF-58NaF-25BeF₂ (mole%) mixtures the following solubility of PuF₃ was obtained in our study: 1.33 and 1.94 mole % at 550°C and 1.94 and 3.00 mole % at 600°C. The effect of NdF₃ on the solubility of PuF₃ in molten 17LiF-25BeF₂-58NaF (mole %) mixture was determined. Presence of EuF₂ up to 0.3 mole % in solvent did not affect PuF₃ solubility in molten 17LiF-25BeF₂-58NaF (mole %) mixture.

Density of the melts has been measured by hydrostatic weighting method in temperature range 482 - 770 °C. The mistake of measurement is estimated as 0.9 %. The following correlation of density on temperature of molten 15LiF-58NaF-27BeF₂ and 17LiF-58NaF-25BeF₂ (mole%) mixtures are obtained respectively:

$$\rho [g/cm^3] = 2.163 \pm 0.0023 - (4.06 \pm 0.29) 10^{-4} (t[^\circ C] - 601.4)$$

$$\rho [g/cm^3] = 2.150 \pm 0.0029 - (3.34 \pm 0.44) 10^{-4} (t[^\circ C] - 678.5)$$

Analysis of experimental data shows, that for molten 15LiF-27BeF₂-58NaF (mole%) mixture value (-4.06±0.29) 10⁻⁴ [g/(cm³K)] can be recommended for factor $d\rho/dt$. Processing of experimental data for 17LiF-58NaF-25BeF₂ gives value $d\rho/dt = (-3.34 \pm 0.44) 10^{-4}$ [g/(cm³K)].

Thermal conductivity of molten Li,Be,Na/F system has been measured by monotonous heating technique in temperatures range 500-750°C. Total dispersion of measurements is determined by accuracy of calibration and estimated as 15 %. The following correlation are obtained by least squares method:

$$\lambda (W/(m K)) = 0.838 + 0.0009 [t (^\circ C) - 610.3]$$

Viscosity of different molten Li,Be,Na/F mixtures have been measured by method of attenuation torsional oscillations of the cylinder with melt under study in a temperature range from freezing up to 800°C. Accuracy of measurement is 4-6 % (dispersion). Dependence of 15LiF-27BeF₂-58NaF (mole %) mixture kinematic viscosity vs temperature in the temperature range 480 - 800 °C is represented as:

$$\nu (m^2/s) = 0.1360 \exp\{2914/T(K)\}$$

Addition to molten 15LiF-27BeF₂-58NaF (mole %) mixture of 1 mole % CeF₃ (as PuF₃ proxy) leads to some decrease of kinematic viscosity. This effect is negligible at high temperatures, and grows up to 25-30% at temperature decreasing down to 550°C.

Heat capacity for temperature range from 700 to 1000 K was evaluated basing on data molten for binary systems and individual components: $C_p = 2090 J \cdot kg^{-1} \cdot K^{-1}$.

Vapor pressure (in Pa) was evaluated by ideal mixture method basing on data molten for binary systems and individual components:

$$\ln p = 18.920 - 1.469 \cdot 10^{-4} T(K) - 25283/T + 0.9819 \ln(T).$$

IV.B. Electrochemical Properties

The electrochemical behavior of PuF₃, NdF₃ and ZrF₄ solutions in 15LiF-58NaF-27BeF₂ and 60LiF-40NaF (mole %) melts were studied by cyclic voltammetry (CV) with linear potential sweep and chronopotentiometry methods. 60LiF-40NaF (in mole %) melt was investigated as possible alternative solute for electrochemical separation of actinides and lanthanides. The concentration of PuF₃ in fluoride melts investigated was equal (0.3-1)·10⁻³ mole/cm³.

The main results of the experiments carried out:

- In 15LiF-58NaF-27BeF₂ melt plutonium is deposited on molybdenum cathode earlier than beryllium;
- Difference of deposition potentials of plutonium and beryllium in 15LiF-58NaF-27BeF₂ melt is equal $\Delta E_{\text{Pu-Be}} = 0.15 \pm 0.02$ V (913K) and for plutonium and neodymium this value is estimated as $\Delta E_{\text{Pu-Nd}} \approx 0.3$ V;
- Difference of deposition potentials of Pu and Na in 60LiF-40NaF is equal $\Delta E_{\text{Pu-Na}} = 0.30 \pm 0.02$ V (1023K);
- Deposition potentials of Nd in 60LiF-40NaF melt containing NdF₃ is more negative than deposition potential of sodium; therefore Na is deposited on solid Mo working electrode (WE).

CVs of 15LiF-58NaF-27BeF₂ and 60LiF-40NaF (mole %) melts with PuF₃ addition are presented in Fig. 5 and 6.

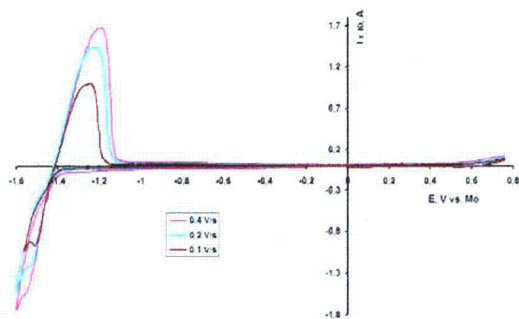


Fig. 5. CV of PuF₃ ($5 \cdot 10^{-5}$ mole/cm³) in 15LiF-27BeF₂-58NaF melt for various scan rate. WE - Mo ($S \approx 0.5$ cm²), RE - Mo. T=853K.

Equilibrium electrode potentials of Pu³⁺/Pu⁰ and Be²⁺/Be⁰ couples in 15LiF-27BeF₂-58NaF and Pu³⁺/Pu⁰ and Na⁺/Na⁰ couples in 60LiF-40NaF (mole%) melts are equal:

$$E_{\text{Pu}^{3+}/\text{Pu}^0} \approx -1.75 \pm 0.05 \text{ V (Na, Li, Be/F; 893K)}$$

$$E_{\text{Be}^{2+}/\text{Be}^0} = -1.90 \pm 0.01 \text{ V (Na, Li, Be/F; 893K)}$$

$$E_{\text{Pu}^{3+}/\text{Pu}^0} \approx -1.63 \pm 0.02 \text{ V (Na, Li/F; 1023K)}$$

$$E_{\text{Nd}^{3+}/\text{Nd}} < E_{\text{Na}^+/\text{Na}} = -1.93 \pm 0.01 \text{ V (Na, Li/F; 1023K)}$$

Equilibrium electrode potentials were measured with respect to reference electrode (RE) based on Ni/NiF₂ (redox couple Ni²⁺/Ni⁰, 1 mole % NiF₂ in fluoride melts). The behavior of the reference electrode used was not stable. For this reason it is necessary to regard these equilibrium electrode potential values as assessed values. A value of the diffusion coefficient of Pu³⁺ ions in the 15LiF-58NaF-27BeF₂ melt with addition of PuF₃ ($9 \cdot 10^{-5}$ mole/cm³) calculated using the Randles-Sevcik equation is equal $D_{\text{Pu}^{3+}} \approx 5 \cdot 10^{-5}$ cm²/s (T=893K).

An assumption was made concerning the alloying of plutonium with Be and Ni in the process of plutonium ions electrochemical reduction in fluoride melts under investigation. Based on the experimental results received it is possible to assert, that electrowinning on solid cathodes could be used for fuel salt clean up from corrosion products and for An/Ln separation. Further studies are necessary in order to determine the nature of Pu-Ni alloying and its utilization in the process of plutonium recovering from fuel salt.

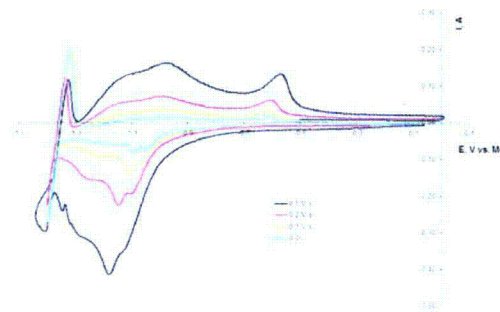


Fig. 6. CV of PuF₃ ($3.1 \cdot 10^{-5}$ mole/cm³) in LiF-NaF melt for $v = 0.05, 0.1, 0.2, 0.5$ V/s. WE - Mo ($S \approx 0.4$ cm²), RE - Mo. T=1023K.

IV.C. Validation of Ni|NiF₂ Reference Electrode

The emf method and cyclic voltammetry were used to study different electrochemical cells with a nickel RE placed in a graphite container having an insulating PBN coating. A bridge of the salt melt in a capillary 0.1 mm diameter provided the ionic conduction. The conditional standard potentials of sodium and beryllium were evaluated at temperatures of 800 to 1000 K. The thermodynamic functions ΔH^* , ΔS^* and ΔG^* of oxidation reactions of sodium and beryllium by NiF₂ solutions in the 17LiF-25BeF₂-58NaF (mole%) melt were calculated.

It was found that NiF₂ solutions in molten 60LiF-40NaF and 17LiF-25BeF₂-58NaF mixtures were very sensitive to changes of the composition and redox potential of the environment (the gaseous atmosphere, the test melt). As a result, a nickel powder or nickel films were formed on the container walls, in the bulk and on the surface of the melt during long-term experiments. The decrease in the NiF₂ concentration of the RE standard melt led to an uncontrolled drift of the RE potential and erroneous measurement of the emf. Precipitation of metallic nickel from the melt caused plating of the RE capillary and appearance of the electron conduction on the walls of the salt bridge. Ultimately, a short circuit occurred between the half-elements of the electrochemical cell.

The thermodynamic simulation of the reactions taking place in the systems under study suggested that at the experimental temperatures PBN interacted with NiF_2 solutions by an endothermic reaction, which was followed by the formation of nickel, NaBF_4 and nitrogen (Fig.7). As a result, the PBN insulator lifetime on the surface of RE graphite container is limited and decreases with growing temperature.

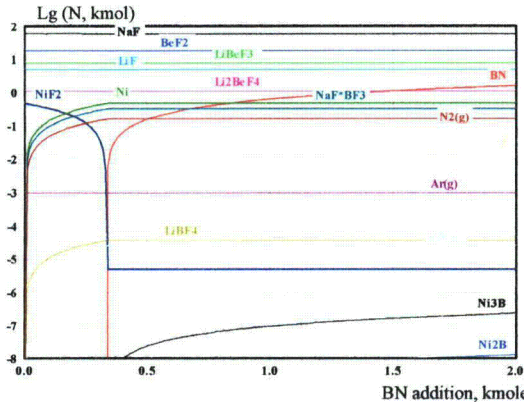


Fig. 7. Variation of the assigned equilibrium composition of the initial reaction mixture ($17\text{LiF}-25\text{BeF}_2-58\text{NaF}$) + 0.5 mole % NiF_2 when additions of boron nitride were introduced in sequence at 500°C .

Advances in the development of a simple reliable nickel RE are possible, if following R&D will be performed:

- Development of designs providing isolation of the nickel RE from the cell atmosphere and preventing the direct contact of salt melts with the NiF_2 solution in the RE half-element;
- Selection of up-to-date solid electrolytes and inert insulating materials for solid ion conducting membranes, which would preserve their properties over a wide interval of the redox potential of the fluoride salt melt;
- Development of reliable methods for protection of the container and membrane materials against corrosive salt melts; the use of up-to-date coating deposition technologies for this purpose;
- Standardization of methods for production of containers with ion conducting diaphragms (membranes)

V. MATERIALS COMPATIBILITY

ISTC#1606 corrosion task include following stages:

- Compatibility test between Ni-Mo alloys and molten $15\text{LiF}-27\text{BeF}_2-58\text{NaF}$ salt in natural convection loop.
- Study on PuF_3 addition effect in molten $15\text{LiF}-27\text{BeF}_2-58\text{NaF}$ salt on compatibility with Ni - Mo alloys.

- Te corrosion study for molten $15\text{LiF}-27\text{BeF}_2-58\text{NaF}$ salt and Ni-Mo alloys in stressed and unloaded conditions.

Material specimens of three Hastelloy N type modified alloys, particularly: RF HN80M-VI with 1% of Nb, RF HN80MTY with 1% of Al and MONICR (Scoda, Chez Republic) we chosen for our study in corrosion facilities⁴.

The design provides tests of the materials specimens in loop at molten salt heat up about 100°C and its flow rate up to 5 cm/s ($\text{Re} > 3000$). This loop includes the system for redox potential measurement during corrosion studies. It is installed inside the hot cell for operations with actinides.

Results of 1200 hrs loop corrosion experiment with on-line redox potential measurement demonstrated that high temperature operations with Li,Be,Na/F salt are feasible using carefully purified molten salts and loop internals. In established interval of salt redox potential $1.25-1.33\text{ V}$ relative to Be reference electrode, corrosion is characterized by uniform loss of weight from a surface of samples with low rate. Under such exposure salt contained respectively less than (in mass %): Ni - 0.004; Fe -0.002; Cr- 0.002. Specimens of HN80M-VI and HN80MTY from hot leg of loop exposed at temperatures from 620°C till to 695°C showed uniform corrosion rate from $2\text{ }\mu\text{m/ year}$ to $5\text{ }\mu\text{m/ year}$. For MONICR alloy this value was in the range of $9 - 19\text{ }\mu\text{m/ year}$.

It was not found any significant change in corrosion behavior of materials samples in melt due to the presence of 0.5 mole % PuF_3 addition in Li,Be,Na/F salt. Specimens of HN80M-VI from the loop exposed during 400 hrs at temperature 650°C showed uniform corrosion rate of about $6\text{ }\mu\text{m/ year}$. Under such exposure salt contained respectively about (in mass %): Ni - 0.008; Fe -0.002; Cr- 0.002. It was not found any traces of intergranular cracking for all specimens after loop tests even in the melt with PuF_3 addition. Data of chemical analysis of specimen's surface layer showed decrease of the chromium contents by the $10-20\text{ }\mu\text{m}$.

As first step of Te corrosion study ampoule tests with Cr_3Te_4 source were done. The alloy resistance to intergranular cracking was estimated by parameter "K", which is value equal to product of cracks number on 1 cm length of longitudinal section of specimen subjected to tensile strain, multiplied by average cracks depth in μm .

The first set was made for unloaded conditions with well-purified salt reduced by metallic beryllium, and the second one - with addition of nickel difluoride. In the first set of ampoules after 100hr exposition at 650°C in $15\text{LiF}-58\text{NaF}-27\text{BeF}_2$ melt containing (in mass.%) respectively: $\text{Te} < 0.01$; Ni - 0.008; Fe -0.02; Cr < 0.001 the traces of

intergranular cracking were found only on MONICR samples ($K = 30 \text{ pc}\cdot\mu\text{m}/\text{cm}$). For the second set with melt containing (in mass.%): Te<0.01; Ni-0.26; Fe-0.0095; Cr-0.39 microphotographs showed that the surfaces of all alloys are full of cracks along the grain boundaries to the depth from $30 \mu\text{m}$ up to $60 \mu\text{m}$: MONICR ($K = 7920 \text{ pc}\cdot\mu\text{m}/\text{cm}$), HN80M-VI ($K = 3420 \text{ pc}\cdot\mu\text{m}/\text{cm}$) и HN80MTY ($K = 1040 \text{ pc}\cdot\mu\text{m}/\text{cm}$).

Studies on Te addition effects in molten $15\text{LiF}\cdot 27\text{BeF}_2\cdot 58\text{NaF}$ salt (mole%) on compatibility with Ni-based alloys both in stressed and unloaded conditions in corrosion test facility with redox potential measurement are underway now within ISTC#1606 and more new experimental results coming soon.

IV. SPECIAL MATERIALS INVENTORIES

As can see from Table III total inventory of $\text{LiF}\cdot\text{NaF}\cdot\text{BeF}_2$ in the primary system will make, approximately, 120 t (from them the reactor vessel will contain approximately 86 t of salt). Thus, for primary system is required 71.4 t NaF, 11.4 t ${}^7\text{LiF}$ (3.1t of ${}^7\text{Li}$ metal) and 37.2t BeF_2 . In case of enrichment ${}^7\text{Li}$ up to 99.99 % the cost of the salt solvent inventory will make 3 000 000 \$ at the price 170 \$/kg on ${}^7\text{LiF}$ and will increase up to 10 700 000 \$ at cost 800 \$/kg on ${}^7\text{Li}$. We shall remind, that only initial inventory of fuel salt in MSBR² demanded more than 50 t ${}^7\text{LiF}$, respectively. Thus, transition from the ${}^7\text{LiF}\cdot\text{BeF}_2$ -based salt used in MSBR, to ${}^7\text{LiF}\cdot\text{NaF}\cdot\text{BeF}_2$ mixture used in MOSART, allows essentially to decrease the cost of initial solvent inventory due to minimization of expensive ${}^7\text{Li}$ amount. Cost of the secondary coolant is accepted equal 5\$/kg. At total volume of the secondary coolant in the system 240m^3 , its cost will make near 2 300 000 \$.

MOSART reactor vessel will contain up to 20 t of the graphite reflector demanding replacement of each 4 years, and about 175t of steel shielding. For comparison, the graphite initial inventory in MSBR makes 304 t, and the central part of core is subject to replacement each 4 years. It demands the additional charge of graphite 44 t/year. Thus, after 30 years of MSBR operation at NPP will be collect about 1200 t of irradiated graphite, in comparison with 160 t for MOSART system. The total cost of graphite (at specific cost 30 \$ / kg) required 30 years MOSART operation will not exceed 5 000 000 \$.

The carried out estimations of capital making cost of MSBR included significant uncertainty because of uncertainties in design. From them, in particular, followed, that cost of primary and secondary salt carriers was insignificant compared to the total capital investments in the plant, whereas expenses for components made from Hastelloy NM (29 %) and graphite (6 %) made about 35 % from the total capital investments. In cost of

components made of Hastelloy NM cost of an alloy itself made about 33 %, and 67 % of cost concern to expenses for manufacturing of the main components of primary system. Already it is now obvious, that relative cost of a graphite reflector in MOSART capital making cost will make less than 1 % valid essentially smaller amount of a used material and less strict requirements to its gas permeability.

TABLE III
 Materials inventories MOSART and MSBR systems

	MOSART, t	MSBR, t
Fuel inventory	7.32 (9.35)*	(1.47 +68)**
${}^7\text{LiF}\cdot\text{NaF}\cdot\text{BeF}_2$	120	162
$\text{NaF}\cdot\text{NaBF}_4$	456	456
Graphite	20	304
Hastelloy NM	1280	1377
Steel	3028	2840

* Pu and minor actinides for scenarios 1 (2), ** U+Th

The basic contribution to capital cost of MOSART, as well as in project MSBR, will bring the equipment made of alloy Hastelloy NM. As the weight and sizes of the main circulation pumps (hence, and their cost) not so strongly depend on capacity, transition from MSBR to MOSART conditions will change a situation insignificantly. Transition from the $\text{LiF}\cdot\text{BeF}_2\cdot\text{ThF}_4$ fuel salt used in MSBR to $\text{LiF}\cdot\text{NaF}\cdot\text{BeF}_2$ system, used in MOSART, will allow due to the better transport properties of last a little to improve specific heat removal (to lower metal consumption) in intermediate heat exchanger by 10 %.

The analysis allows planning a actions directed on reduction of cost for MOSART primary and secondary systems equipment. First of all, it is represented expedient instead of shell-tube heat exchanger to use plate type heat exchanger, made of fofered sheets with 1mm thickness. In such heat exchangers higher specific heat removal and cheaper sheet material allow to decrease cost considerably.

2400MWt MOSART system will demand 1280 t of Hastelloy NM for components of the primary and secondary circuits, that approximately on 100t lower, than in the MSBR. Consumption of Hastelloy NM in the primary and secondary circuits of MOSART is approximately equal. If to accept specific cost of Ni-Mo alloy chosen for MOSART 50 \$ / kg (it is in 6-8 times is higher than cost of products made of stainless steel) at mass 1280t, cost of a material of components of the primary and secondary circuits in 2400MWt MOSART system will make about 64 000 000 \$. The price of this alloy was determined roughly on the basis of ratio between the average cost of sheet and high-quality hire from Hastelloy N in conditions of US manufacture of in 1969-

1970, making then for a sheet of 22 \$ / kg, 55 \$/ kg for nozzles and covers, and 66 \$/ kg for heat exchanger tubes.²

V. CONCLUSIONS

In study main attention has been paid to single fluid Li,Be,Na/F MOSART system with design objective to provide the fissile concentration and geometry of the fuel salt to obtain heat release of about 2400 MWt at conditions affording the effective transmutation of plutonium and minor actinides s from LWR spent fuel without U-Th support.

It is important that, as result our studies for molten Li,Be,Na/F system, was found quite wide range with minimal of LiF (17-15 mole%) and of BeF₂ (27-25mole%) content in the ternary composition, which provide fuel salt able to get PuF₃ solubility of 2 and 3 mole%, respectively, at 600°C, to keep adequate melting point (<500°C) and very low vapour pressure, to have good nuclear properties, low activation, suitable transport properties, to be well compatible with the materials in the system and moderately expensive.

2400MWt MOSART system has homogeneous core with intermediate - to- fast spectrum of neutrons. The fuel salt specific power is about 43 W/cm³. The effective flux of such system is near 1×10^{15} n cm⁻² s⁻¹. At equilibrium state for both scenarios of start up and feed actinides compositions and the soluble fission product removal cycle 300 epdf for cores with different reflector parameters considered, the AnF₃+LnF₃ concentration in fuel salt is truly within the solubility limit for molten 15LiF-27BeF₂-58NaF (mole %) at minimum fuel salt temperature in primary circuit of 600°C. Minimal AnF₃+LnF₃ critical concentrations at equilibrium were received for core with 0.2m graphite reflector.

2400MWt MOSART core of homogeneous configuration can satisfy most important neutronic and thermal-hydraulic considerations: (1) AnF₃+LnF₃ concentration in fuel salt is truly within the solubility limit of AnF₃+LnF₃ for molten 15LiF-27BeF₂-58NaF (mole %) at minimum fuel salt temperature in primary circuit of 600°C for both fuel cycle scenarios under consideration; (2) core with 0.2m graphite reflector in the temperature range 900-1600K has strong negative temperature reactivity coefficients (- 4.125 pcm/K and - 6.625 pcm/K for the first and the second scenarios of the equilibrium critical loading, respectively); (3) regions of reverse, stagnant or laminar flow are avoided and (4) the maximum temperature of solid reflectors is low enough to allow it use for suitable time.

Preliminary calculations of kinetic and dynamic characteristics of the MOSART system indicate that it would exhibit high levels of controllability and safety³. System would also posses inherent dynamic stability and would require only modest amounts of reactivity control capability.

Preliminary consideration of environment effects indicate that MOSART system could have attracted performance and actinides transmutation efficiency features while providing lower total materials inventories and waste compared to prior MSR designs, including MSBR (e.g., it allows significantly reduce to the order mass flows of graphite and ⁷Li enriched of 99.99 % in the design).

While a substantial R&D effort would be required to commercialize MOSART, there are no killing unresolved issues in the needed technology. The major technical uncertainties in the conceptual design are in the area of tritium confinement, fuel salt processing and behavior of some fission products.

ACKNOWLEDGMENTS

This effort is done by RRC-Kurchatov Institute (Moscow), VNIITF (Snezhinsk) and IHTE (Ekaterinburg) within ISTC#1606 Phase 2 supported by EU.

REFERENCES

1. V. V. Ignatiev e.a., "Integrated Study of Molten Li,Be,Na/F Salts for LWR Waste Burning in Accelerator Driven and Critical Systems", *Proc. of the GLOBAL'05*, Tsukuba, Japan, October, 9-13, 2005
2. R. S. Robertson, "Conceptual Design Study of a Single Fluid Molten Salt Breeder Reactor", ORNL-4541, 1971
3. V. V. Ignatiev et. al., "Progress in Integrated Study of Molten Salt Actinide Recycler & Transmuter System", *Proc. of 9th OECD/NEA IEM on Partitioning & Transmutation*, Nimes, France, September, 2006
4. V. V. Ignatiev e.a., "Experience with Alloys Compatibility with Fuel and Coolant Salts and their Application to MOSART concept", *Proc. of ICAPP'06*, Reno, USA, June, 2006
5. J.R. Engel e.a., "Conceptual Design Characteristics of DMSR with Once-through Fueling", ORNL/TM-7207, USA, 1980

Molten-Salt-Reactor Technology Gaps

Charles W. Forsberg
Oak Ridge National Laboratory*
P.O. Box 2008; Oak Ridge, TN 37831-6165
Tel: (865) 574-6783; Fax: (865) 574-0382
E-mail: forsbergcw@ornl.gov

File Name: MSR Publish: MSRGap.ICAPP06.Paper
Final Paper Due Date: March 15, 2006
Manuscript Date: February 10, 2006

Manuscript Number: 6295

Session: 3.09 Liquid-Salt-Cooled High-Temperature Reactors-III
2006 International Congress on the Advances in Nuclear Power Plants (ICAPP '06)
Embedded Topical in the 2006 American Nuclear Society Annual Meeting
American Nuclear Society
June 4-8, 2006
Reno, Nevada

The submitted manuscript has been authored by a contractor of the U.S. Government under contract DE-AC05-00OR22725. Accordingly, the U.S. Government retains a nonexclusive, royalty-free license to publish or reproduce the published form of this contribution, or allow others to do so, for U.S. Government purposes.

*Oak Ridge National Laboratory, managed by UT-Battelle, LLC, for the U.S. Department of Energy under contract DE-AC05-00OR22725.

Molten-Salt-Reactor Technology Gaps

Charles W. Forsberg

Oak Ridge National Laboratory, P.O. Box 2008, Oak Ridge, Tennessee
Tel: (865) 574-6783; Email: forsbergcw@ornl.gov

Abstract — Molten salt reactors (MSRs) are liquid-fuel reactors that can be used for producing electricity or hydrogen as well as burning actinides and producing fissile fuels (breeding). Fissile, fertile, and fission products are dissolved in a high-temperature molten fluoride salt with a very high boiling temperature (~1400°C). The fuel salt flows through a reactor core, where fission occurs within the flowing salt; through an intermediate heat exchanger; and back to the reactor core. An intermediate heat-transfer loop transports the heat to a turbine hall or to a hydrogen production facility. Two experimental reactors were successfully built in the 1950s and 1960s. MSRs are being reexamined today because of their unique fuel cycle capabilities and safety characteristics. A technology gap analysis has been initiated to understand technological challenges for development and deployment. Some technology challenges have been resolved by new technologies that did not exist in the early 1970s when the program was shut down. Other technological challenges remain. Six areas (power cycles, fuel inventories, noble metal plate-out, fuel storage, high-level waste forms, and peak reactor temperatures) were examined. The results of the analysis are summarized.

I. INTRODUCTION

Between 1950 and 1976^{1,2} a large Molten Salt Reactor (MSR) development program was conducted in the United States, two test reactors were successfully operated, a design of a 1000-MW(e) reactor was completed, and plans were developed to construct a demonstration reactor. Since then, little research and development (R&D) has been done on MSRs. This paper summarizes recent work³ that identified technology gaps for deployment of MSRs and general technical advances that have either eliminated specific technology gaps or shown pathways to potentially more economically viable solutions.

The MSR was originally developed for the aircraft nuclear propulsion program, where a very high power density was required to minimize the reactor size and hence the weight of the reactor shielding. It was then developed as a breeder reactor and was the backup option to the sodium-cooled fast reactor. Ultimately, it was decided to concentrate efforts on the development of a single breeder reactor concept—the sodium-cooled fast reactor. These billion-dollar programs created the base MSR technology. The relatively trouble-free 8-MW(t)

Molten Salt Reactor Experiment (MSRE) provided an effective demonstration of many aspects of the reactor technology.

The MSR was chosen as one of the six Generation IV reactor concepts because it uses liquid fuel; that is, the fuel is dissolved in the coolant. All of the other reactors use solid fuel. The liquid fuel creates major advantages and some unique challenges. In the three decades since the large-scale MSR development program was undertaken, major changes have occurred.

- *Technology.* Advances in technology have partly or fully addressed several of the technical challenges that would be associated with full-scale development of an MSR. Technological advances have created the potential more capable MSRs, such as a very-high-temperature MSR for hydrogen production and other new missions.
- *Goals.* The original goal of the MSR was to serve as a breeder reactor that produces electricity. Current goals include hydrogen production and a variety of different fuel cycle missions including burning of actinides from other reactors.

- *Requirements.* The safety, environmental, and nonproliferation requirements for all power reactors have changed.

These changes imply that an MSR developed for today's market may have significantly different features than would have been required 30 years ago. This paper reports on studies of six technological challenges for a commercial MSR. The six areas were chosen because they have significant impact on commercial viability (economics and developmental cost) and are generally applicable to all MSRs. For specific missions, such as burning actinides from other reactors, other mission-specific technical challenges may exist. This paper reports on work completed to date and is not a comprehensive examination of all technical issues.

II. GENERAL DESCRIPTION OF THE MSR

In an MSR (Fig. 1), the molten fluoride salt with dissolved fissile, fertile, and fission isotopes flows

through a reactor core moderated by unclad graphite. In the core, fission occurs within the flowing fuel salt, which then flows into a primary heat exchanger, where the heat is transferred to a secondary molten-salt coolant. The fuel salt then flows back to the reactor core. The graphite-to-fuel ratio is adjusted to provide the optimal neutron balance, an epithermal neutron spectrum. In the preconceptual 1000-MW(e) designs developed in the early 1970s, the liquid fuel salt typically enters the reactor vessel at 565°C and exits at 705°C and ~1 atmosphere (coolant boiling point: ~1400°C). Volatile fission products (e.g., krypton and xenon) are continuously removed from the fuel salt. The secondary coolant loop with a liquid salt transfers the heat to the Brayton power cycle to produce electricity or a hydrogen production facility. The term *liquid salt* denotes a clean fluoride salt that does not contain fissile materials, fertile materials, or fission products.

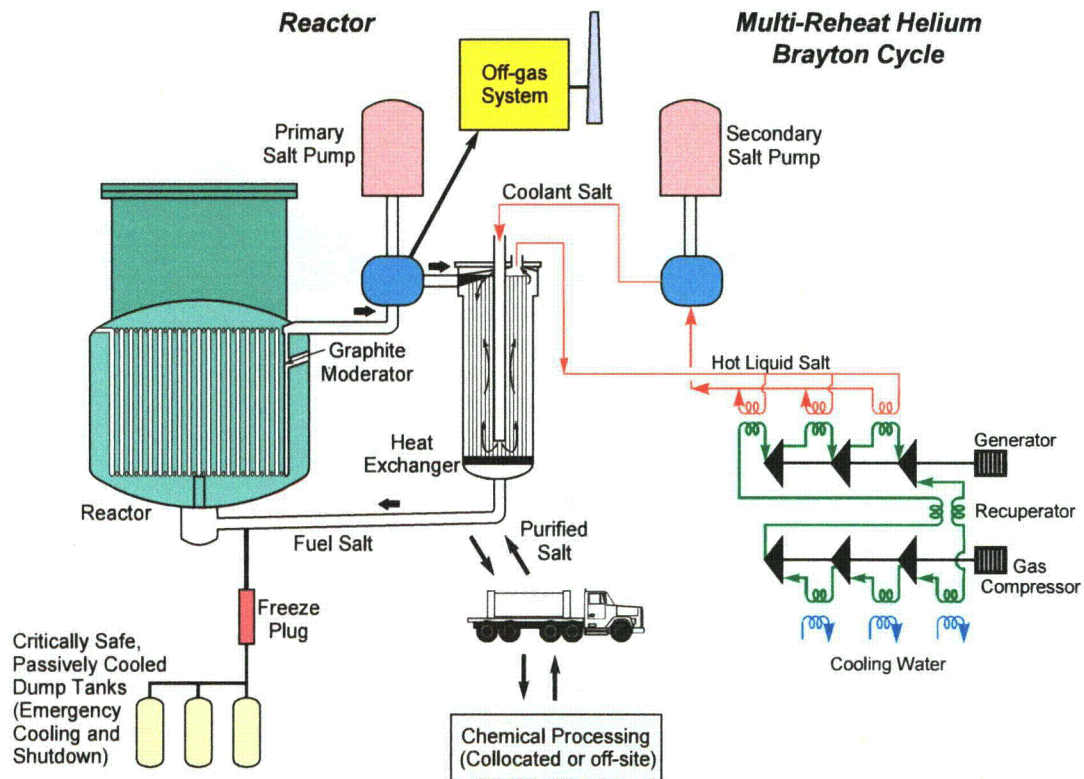


Fig. 1. MSR with multi-reheat helium Brayton cycle.

As a liquid-fuel reactor, the MSR has two sets of unique characteristics relative to solid-fuel reactors.

- *Safety.* Under emergency conditions, the liquid fuel is drained to passively cooled critically safe dump tanks. By the use of freeze valves (cooled sections of piping) and other techniques, this safety system can be passively initiated upon overheating of the coolant salt. MSR's operate at steady-state conditions, with no change in the nuclear reactivity of the fuel as a function of time. Last, the option exists to remove fission products online and then solidify those radionuclides into a stable waste form. This minimizes the radioactive inventory (accident source term) in the reactor core and potential accident consequences.
- *Fuel cycles.* The liquid fuel allows online refueling and a wide choice of fuel cycle options: burning of actinides from other reactors, a once-through fuel cycle, a thorium-²³³U breeder cycle, and a denatured thorium-²³³U breeder cycle. Some of the options, such as a thermal-neutron-spectrum thorium-²³³U breeder cycle require online refueling and thus can not be practically achieved using solid fuels. The use of a liquid fuel also avoids the need to develop fuel or fabricate fuel.

III. ANALYSIS OF TECHNOLOGY GAPS

A series of issues in the 1970s designs of MSR's were identified, analyzed, and evaluated in terms of technical solutions available today. Many² but not all of these issues were identified in evaluation and closeout reports of the MSR projects in the 1970s.

III.A. Power Cycles

When MSR's were being developed in the 1960s, the only demonstrated power cycle for the large-scale conversion of heat to electricity was the steam (Rankine) cycle; thus, early MSR's (and liquid metal fast reactors) were designed with steam power cycles. The coupling of an MSR with a steam cycle resulted in a series of technical challenges. Since that time, gas Brayton power cycles have been developed by the aircraft industry and are now widely used in the utility industry, with natural gas as the preferred fuel. Direct and indirect Brayton cycles are also being developed for various high-temperature reactors. Indirect multi-reheat nitrogen or helium Brayton^{4,5}

cycles offer major economic and technical advantages relative to steam cycles for electricity production using MSR's.

- *Efficiency.* MSR's are naturally high-temperature reactors. Depending upon the choice of salt, the freezing points are between 320 and 500°C. The heat transfer properties (viscosity, thermal conductivity, etc.) improve rapidly with increasing temperature. Consequently, the detailed 1000-MW(e) conceptual design of the MSR had a reactor-core fuel-coolant exit temperature of 705°C. However, because of corrosion and other constraints in steam cycles, peak steam cycle temperatures are between 500 and 550°C. In the 1960s designs, high-temperature heat was inefficiently dumped to lower temperatures to match what the steam cycle could tolerate. This process reduces heat exchanger sizes but has a large penalty in terms of efficiency. In contrast, many Brayton cycles operate above 1000°C. The adoption of closed helium or nitrogen Brayton power cycles enables the power cycle to efficiently use the high-temperature heat generated by the MSR. *This capability allows a 15% improvement in electrical power output without changing the temperatures of the fuel salt exiting the reactor core.*
- *Freeze protection.* Salt coolants must be kept sufficiently hot to ensure good heat transport and avoid freezing of the molten fuel salt and the liquid salt in the intermediate heat-transport loop. With a steam cycle and the lower temperatures, special design features must be used so that feed water does not freeze the salt. With the higher-temperature Brayton cycle, freeze protection is greatly simplified.
- *Tritium control.* In an MSR, tritium is generated as a fission product and may be generated by coolant activation. Unlike solid-fuel reactors, the tritium in an MSR is highly mobile in the salt and tends to diffuse through the high-temperature heat exchangers into the working fluid of the power cycle. At the time the MSR program was cancelled, tritium control was considered the largest remaining engineering development challenge, because any tritium that entered the steam cycle resulted in tritiated water. Isotopically separating tritiated water from nontritiated water in the steam cycle is difficult and expensive. The MSR program partly developed the use of a fluoroborate

coolant salts in the secondary heat transfer system to trap the tritium. While technically workable, such systems are potentially complex and expensive for high levels of tritium trapping. Adoption of a Brayton cycle provides an alternative tritium trapping option where the tritium is removed from the helium in the Brayton power cycle. This is potentially a high-performance low-cost option based on demonstrated inexpensive methods to remove tritium gas or tritiated water from helium. Helium-cooled high-temperature reactors produce tritium from nuclear reactions with ^3He and from leaking fuel; consequently, these reactors are equipped with systems to remove the tritium from the helium.

- *Chemical reactions.* Molten salts do not chemically react with nitrogen or helium. However, these molten salts will slowly react with steam over time. The reaction rate is many orders of magnitude slower than for sodium and water. Changing from a steam cycle to a gas Brayton cycle eliminates this class of challenges.

Closed Brayton power cycles using helium are being developed for the modular high-temperature gas-cooled reactors (MHTGRs) for which helium is the coolant gas. A prototype helium-cooled MHTGR is being constructed in South Africa with a helium Brayton power cycle. Additional technology development would be required for an MSR; however, the closed Brayton cycle technology is transitioning to a commercial technology.

III.B. Fuel Inventory

In an MSR, the fuel salt circulates from the reactor core to the intermediate-loop heat exchangers and back to the reactor core. Heat is produced in the core and subsequently dumped in the heat exchangers. Thus, a significant fraction of the fuel salt is outside the reactor core in the heat exchangers. Historically, MSRs have been designed with various tube-and-shell heat exchangers. In the last decade, compact plate-fin and printed circuit high-temperature heat exchangers have been developed for the aircraft, chemical, and offshore-oil industries. The adoption of compact heat exchangers drastically reduces the molten fuel salt inventory in the heat exchangers and may reduce the inventory of fuel salt in the reactor by up to 50%. There are major benefits in using such heat exchangers.

- *Fuel salt inventory.* Reducing the fuel inventory reduces both fuel salt costs and nonproliferation risks, because the total fissile inventory in the nuclear system is decreased.
- *Fuel salt processing.* In an MSR, volatile fission products (including xenon) are removed continuously, which creates a large parasitic neutron sink in solid-fuel reactors. For nonvolatile fission products, the fuel salt is processed online or off-line, depending upon design goals. Reducing the salt inventory reduces the quantities of salt to be processed.
- *Heat exchanger size.* The size of the heat exchangers is reduced by a factor of 3 or more. This reduction has major economic implications because the primary heat exchangers have fuel salt flowing through them on one side and clean salt flowing through on the second side. The fuel salt, which contains the fission products and actinides, is highly radioactive. In an MSR, the reactor vessel and primary heat exchangers are located in a hot cell. Reducing the size of the heat exchanger significantly reduces the size of the hot cell, its support equipment, and the reactor building.
- *Tritium control.* The aircraft and other industries have developed compact heat exchangers with buffer gas zones to separate different fluids that may react explosively—such as hot gases vaporizing fuels in aircraft. The same technologies enable trapping of tritium from the primary system in the heat exchanger. While this may not be important for electricity production when using Brayton cycles that allow trapping of tritium, it is another option for tritium trapping if the MSR is used for hydrogen production where high temperature heat is required for the thermochemical hydrogen production cycles.

The advanced heat exchangers are commercial products used in industry. These heat exchangers are being considered for use in high-temperature helium-cooled reactors⁶ and in the transport of heat⁷ from high-temperature gas-cooled reactors to hydrogen production plants using liquid-fluoride-salt heat-transport systems. Additional work is required to fully evaluate their use in MSRs.

III.C. Noble Metal Plate-Out

In an MSR, fission products are generated in the molten salt. Most of the fission products form stable fluorides that dissolve in the salt. Noble and seminoble metals (e.g., Nb, Mo, Tc, Ru, Rh, Pd, Ag, etc.)³ form multi-atom clusters in the molten salt and ultimately plate out on metal surfaces such as those of heat exchangers or are vented to the off-gas system. The noble metals produce significant decay heat. If the plate-out is excessive, the decay heat from the noble metals may damage the heat exchangers via overheating should a loss of cooling occur. At the end of the MSR projects in the United States in the early 1970s, the assessments indicated that plate-out was not likely to be a major safety issue (potential for noble metals to escape to the environment). However, it had the potential to be a significant design and operational issue. In the last decade there have been major advances in this area.

- *Better understanding of the physical processes.* The R&D challenges are to understand the plate-out mechanisms and to test methods for removal of the metal atoms. A major problem has been the difficulty in generating a molten salt with noble metal atoms that can be used to study plate-out and removal mechanisms. Generating molten salts with noble metal atoms using a molten salt test reactor or an irradiation loop is extremely expensive and involves highly radioactive systems. Recently the French have successfully developed laboratory methods to generate molten salts with noble metal atoms in nonradioactive systems. This development should enable more rapid progress in understanding and development of technologies to remove noble metal atoms from molten salts.
- *New materials.* Plate-out depend upon the surface characteristics. Earlier work showed that noble metals preferentially plated out on metal surfaces relative to carbon surfaces. The potential use of carbon-carbon composite heat exchangers, rather than metal heat exchangers, may significantly reduce noble-metal plate-out on the heat exchangers—the thin-walled reactor component with most of the reactor surface area and most sensitive to decay heat when cooling systems are not operating. Slowing noble-metal plate-out in the primary system provides the time for the salt cleanup systems to remove a larger fraction of the noble metals from the salt.

- *Improved separation methods.* There are several potential methods to remove noble metal from molten salts. The molten salts can be purged with inert gases, with the noble metals preferentially forming aerosols that can be filtered from the gas stream. Newer options include ultra-high-surface-area metal or coated carbon-foam matrixes designed to preferentially encourage plate-out of noble metals in the salt cleanup system.

These developments may allow successful resolution of issues regarding noble metal plate-out issues within several years and help determine (1) whether a significant challenge exists and (2) what the preferred options are for control of noble metal fission products.

III.D. Fuel Storage

The use of MSRs will require the storage and transport of MSR fuel salts with and without uranium. The MSR projects in the 1960s did not identify any issues with long-term storage of the fuel salts; however, no long-term tests were conducted. Since that time, events⁸ have revealed challenges in the long-term storage of highly radioactive fuel salts in solid form. The MSRE, an 8-MW(t) test reactor, was shut down and placed in storage in 1969, with the fuel salt (including its uranium) dumped to drain tanks. The fuel salt was stored as a solid at ambient temperatures. In 1994, a gas sample taken from the MSRE off-gas system (which remained connected to the fuel and flush-salt drain tanks) showed the generation of fluorine from the fuel salt and the partial transport of uranium (in the form of UF_6) from the salt into the off-gas system.

Molten fuel salts in high radiation fields do not release fluorine, because the fuel salt is an ionic solution with very rapid recombination rates. However, it is now known⁹ that if the fluoride fuel salt is a *solid at a temperature significantly below its melting point*, radiation can cause the partial decomposition of the salt, release free fluorine, and result in the formation of UF_6 . The 30-year storage of MSR fuel salt (an unintended large-scale long-term experiment in fuel-salt storage) and the subsequent remediation program now provide the basis to understand (1) what happens when frozen fuel salts are stored for multi-decade periods of time, (2) the requirements for safe long-term storage, and (3) alternative methods to ensure safe storage.

III.E. High-Level Waste (HLW) Form

In an MSR, the fuel is a fluoride salt. Ultimately, the fission products must be removed and disposed of as HLW, while the fissile materials are recycled. This process requires the chemical conversion of the fission products from a fluoride chemical form chosen for in-reactor operations to a repository-acceptable waste form. In the 1960s, no significant work was done to develop such an HLW form.

Since the 1960s, however, a variety of other nuclear processing facilities have generated fluoride waste forms. Laboratory studies have been conducted on how to produce high-quality waste forms from many of these fluoride waste streams. Radioactive fluoride waste streams have been generated from (1) processing of spent nuclear fuel (SNF) in the Idaho Chemical Processing Plant, (2) plutonium processing in the weapons complex, (3) development and use of fluoride volatility processing to recover uranium from SNF, and (4) molten salt processing.

Two approaches have been partly developed to convert fluoride waste forms to an acceptable form for repository disposal. Either approach potentially provides a basis for development of an MSR waste conversion and solidification process.

- *Conversion to nonfluoride waste forms.* Several processes have been partially developed to convert fluoride waste forms to traditional nonfluoride waste forms. The glass material oxidation and dissolution system (GMODS)^{3, 10} converts fluoride wastes into non-fluoride-containing borosilicate glass—the traditional HLW glass. Other processes produce phosphate waste forms.
- *Fluoride HLW form.* Several potential waste forms contain significant fluorides and may meet the requirements for a repository-acceptable waste form. Borosilicate glasses containing fluorides are a leading candidate for processing the fluoride HLW at the Idaho site¹¹; however, the viability of a fluoride-containing borosilicate glass is strongly dependent upon the chemical composition of the initial HLW form. Other researchers¹² are examining fluorapatites as a waste form. Examples of fluorapatites include $\text{Sr}_{10}(\text{PO}_4)_6\text{F}_2$ and $\text{Sr}_8\text{CsNd}(\text{PO}_4)_6\text{F}_{2.3}$.

A fully developed process to convert fluoride HLWs into repository-acceptable waste forms does not currently exist. However, several candidate processes and waste forms have been partly developed in the last 30 years.

III.F. Peak Reactor Temperature

The peak temperature of an MSR is limited by the materials of construction. The developmental work on MSRs resulted in the development of a modified Hastelloy-N, a high-nickel code-qualified alloy suitable for MSR service that allows peak temperatures to $\sim 750^\circ\text{C}$. In the longer term, higher temperatures are highly desirable to (1) improve efficiency in the production of electricity, (2) provide the high-temperature heat required for hydrogen production, and (3) allow the use of higher-melting-point fuel salts that may provide major fuel cycle advantages. While there are many higher-temperature alloy options for systems with clean fluoride salts, an MSR with dissolved uranium and other species presents special challenges. It is the uranium and certain fission products (not the fluoride salt itself) that primarily determine corrosion rates. In these systems, the corrosion rates are very low with the use of high nickel alloys; however, such alloys lose strength at higher temperatures.

Long-term experience shows carbon-based materials to be compatible with molten salts at temperatures of 1000°C . Short-term tests have shown graphite to be compatible with molten salts at temperatures to 1400°C . Carbon-carbon composites are presently being developed for many industrial applications (pumps, heat exchangers, etc.) and have already been developed for use in high-temperature reactors, particularly for in-core high-temperature applications (control rods, core support structures, etc.). Carbon-carbon composites¹³ are potentially an enabling technology for very high temperature MSRs. However, there are major technical uncertainties including joining technologies. If these uncertainties can be overcome, large-scale development work and demonstrations would be required before these materials can be considered for major safety-related components such as reactor vessels. This is a new long-term materials option that did not exist 30 years ago.

IV. CONCLUSIONS

MSRs were developed in the 1950s and 1960s. The large-scale R&D efforts yielded a workable reactor concept but a reactor with significant

operational and other challenges. In the last three decades, there have been major advances in technology. A technology gap analysis has identified potential solutions for many of the technological challenges that were identified in the 1970s and that may significantly lower the capital cost of the MSR. The commercial viability of the MSR has improved both in absolute terms and in comparison with other reactor concepts. However, significant work is required before definitive conclusions can be made about the economics, advantages, and disadvantages of the MSR relative to those of other advanced reactor concepts.

REFERENCES

1. *Nuclear Applications and Technology*, **8**, 2 (Entire issue), (February 1970).
2. U.S. ATOMIC ENERGY COMMISSION, *An Evaluation of the Molten Salt Breeder Reactor*, Wash-1222, Washington, D.C. (September 1972).
3. C. W. FORSBERG, *Molten Salt Reactor Critical Systems Evaluations: Control of Noble Metals, Acceptable Waste Forms, and Fuel-Salt Storage*, ORNL/GEN4/LTR-05-005, Oak Ridge National Laboratory, Oak Ridge, Tennessee (2006).
4. H. ZHAO and P. F. Peterson, *A Reference 2400 MW(t) Power Conversion System Point Design for Molten-Salt-Cooled Fission and Fusion Energy Systems*, UCBTH-03-002, University of California at Berkeley (2004).
5. P. F. PETERSON, "Multiple-Reheat Brayton Cycles for Nuclear Power Conversion with Molten Coolants," *Nuclear Technology*, **144**, 3, 279–288 (2003).
6. C. F. McDONALD, "Compact Buffer Zone Plate-Fin IHX—The Key Component for High-Temperature Nuclear Process Heat Realization with Advanced MHR," *Applied Thermal Engineering*, **16**, 1, 3–32 (1996).
7. W. E. KIRST, W. M. NAGLE, and J. B. CASTNER, "A New Heat Transfer Medium for High Temperatures," *Transactions of the American Institute of Chemical Engineers* **36**, 371–394 (1940).
8. G. D. DEL CUL, A. S. Icenhour, D. W. Simmons, L. D. Trowbridge, D. F. Williams, L. M. Toth, and S. Dai, "Overview of the Recovery and Processing of ^{233}U from the Oak Ridge Molten Salt Reactor Experiment (MSRE) Remediation Activities," *Proc. of Global 2001, Paris, France, September 9–13, 2001*.
9. L. M. TOTH and L. K. Felker, "Fluorine Generation by Gamma Radiolysis of a Fluoride Salt Mixture," *Radiation Effects and Defects in Solids*, **112**, 201–210 (1990).
10. C. W. FORSBERG, E. C. Beahm, and J. C. Rudolph, "Direct Conversion of Halogen-Containing Wastes to Borosilicate Glass," *Symp. Proc. Scientific Basis for Nuclear Waste Management XX, December 2–6, 1996, Boston, Massachusetts*, **465**, 131–137, Materials Research Society (1997).
11. K. VINJAMURI, *Candidate Glass-Ceramic Waste Forms for Immobilization of the Calcines Stored at the Idaho Chemical Processing Plants*, INEL-94/00026, Idaho National Engineering Laboratory, Idaho Falls, Idaho (1994).
12. O. HEMMERS and B. E. Burakov, Transmutation Research Program, Task 16: "Evaluation of Fluorapatite as a Waste-Form Material," <http://aaa.nevada.edu/task16.html>, (2005).
13. P. F. PETERSON, C. W. Forsberg, and P. Pickard, "Advanced CSiC Composites for High-Temperature Nuclear Heat Transport with Helium, Molten Salts, and Sulfur-Iodine Thermochemical Hydrogen Process Fluids," *Proc. of Second Information Exchange Meeting on Nuclear Production of Hydrogen, Argonne National Laboratory, Illinois, USA, October 2–3, 2003*.

Optimized Transition from the Reactors of Second and Third Generations to the Thorium Molten Salt Reactor

E. Merle-Lucotte, D. Heuer, M. Allibert, V. Ghetta, C. Le Brun, L. Mathieu*, R. Brissot, E. Liatard
LPSC/IN2P3/CNRS, 53, avenue des Martyrs, F-38026 Grenoble Cedex, France
Tel: (33)-4-76-28-41-50, Fax: (33)-4-76-28-40-04, Email:merle@lpsc.in2p3.fr

Abstract – Molten salt reactors, in the configuration presented here and called Thorium Molten Salt Reactor (TMSR), are particularly well suited to fulfil the criteria chosen by the Generation IV forum, and may be operated in simplified and safe conditions in the Th/²³³U fuel cycle with fluoride salts. Amongst all MSR configurations in the thorium cycle, many studies have highlighted the configurations with no moderator in the core as simple and very promising. Since ²³³U does not exist on earth and is not being produced today, we aim at designing a critical MSR able to burn the Plutonium and the Minor Actinides produced in the current operating reactors, and consequently to convert this Plutonium into ²³³U. This leads to closing the current fuel cycle thanks to TMSRs started with transuranic elements on a Thorium base, i.e. started in the Th/Pu fuel cycle, similarly to fast neutron reactors operated in the U/Pu fuel cycle. We will detail optimizations of this transition between the reactors of second and third generations to the Thorium cycle. Such a transition is based on a fleet of TMSRs with no moderator in the core, including TMSRs started with Plutonium and TMSRs directly started with ²³³U. We developed parametric studies to optimize these TMSRs, amongst which the study presented here, based on one of the main TMSR parameters: the percentage of heavy nuclei in the fuel salt of the TMSR configuration, which modifies the moderation ratio of the reactor and thus influences both the initial fissile inventory and the spectrum of the reactor. We analyze the characteristics of each reactor configuration, in terms of deterministic safety parameters, fissile matter inventory, salt reprocessing, radiotoxicity and waste production, and finally deployment capacities.

I. INTRODUCTION

Molten Salt Reactors (MSRs), one of the systems selected by the Generation IV forum, may be operated in simplified and safe conditions in the Th/²³³U fuel cycle and with fluoride salts, whether in a thermal or a fast neutron spectrum^{1,2,3,4}. These MSRs are called Thorium Molten Salt Reactors (TMSRs). More precisely, we consider in this study TMSRs with no moderator in the core, the moderation ratio depending only on the salt composition. It has been demonstrated⁵ that such reactors can operate with the relevant properties, in terms of breeding ratio, feedback coefficients, production of transuranic nuclei and material steadiness to irradiation.

In Section II, we introduce the TMSR concept with no moderator in the core, also the called non-moderated TMSR. We state the main criteria used to optimize these reactors, such as safety level, radiotoxicity and waste production, and deployment capacities. Regarding these criteria, we present some parametric studies of this TMSR concept: TMSR configurations are evaluated in section III

by varying the reprocessing constraints and the proportion of heavy nuclei contained in the fuel salt.

One of the pending questions concerning TMSRs is the supply of the fissile matter, and as a consequence the deployment possibilities of a fleet of TMSRs, since ²³³U does not exist on earth and is not yet produced in the current operating reactors. In order to optimize the transition between second and third generation reactors and TMSRs, we choose to produce ²³³U directly in non-moderated TMSRs started with Plutonium as fissile matter on a Thorium basis, and then operated in the Th/²³³U cycle⁵. We aimed at designing a reactor able to burn the Plutonium and the minor actinides produced in currently operating reactors to close their fuel cycle, and consequently to convert this Plutonium into ²³³U. Such Pu-started TMSRs are studied and evaluated in section IV.

Finally, the full transition between the second and third generation reactors to the Thorium cycle is optimized in the second and third sections by considering the deployment capacities of each TMSR considered, both Pu-started and ²³³U-started configurations. The main constraint of a sustainable power deployment is the saving

of resources, i.e. in our case the best conversion of Plutonium in ^{233}U and the configurations allowing the shortest doubling times, as detailed in section V.

This work is based on the coupling of a neutron transport code called MCNP⁶ with the materials evolution code REM^{3,7}. The former calculates the neutron flux and the reaction rates in all the cells while the latter solves the Bateman equations for the evolution of the materials composition within the cells. These calculations take into account the input parameters (power released, criticality level, chemistry ...), by adjusting the neutron flux or the materials composition of the core on a regular basis. Our calculations rest on a precise description of the geometry and consider several hundreds of nuclei with their interactions and radioactive decay; they allow a thorough interpretation of the results.

II. GENERAL DESCRIPTION OF THE REACTORS, PARAMETERS AND CRITERIA

II.A. Description of the non-moderated MSR concept

The general concept of the Thorium Molten Salt Reactor (TMSR) is a 2500 MWth (1 GWe) reactor operated in the $^{232}\text{Th}/^{233}\text{U}$ fuel cycle. In this article, TMSRs may be started directly with ^{233}U or with Plutonium and minor actinides, mixed with Thorium. The reactor is composed of a single large fuel salt channel, 1.25m radius and 2.60m height, as shown on Fig. 1. One third of the 20 m³ of fuel salt circulates in external circuits and, as a consequence, outside of the neutron flux (Fig. 2).

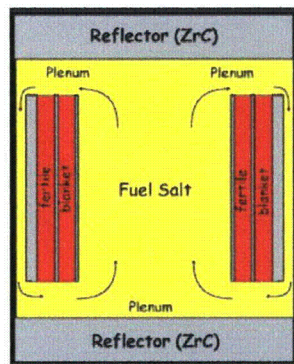


Fig.1. Vertical section of the non-moderated TMSR simulated core

A fertile radial blanket surrounds the core. It contains a binary fluoride salt $\text{LiF} - \text{ThF}_4$, with 28 mole % of ^{232}Th . This blanket has been designed such that it stops approximately 80 % of the neutrons, thus protecting external structures from irradiation while improving the system's breeding. The salt channel is also surrounded by

two axial reflectors. These reflectors are made of ZrC in order to avoid the use of a moderator material.

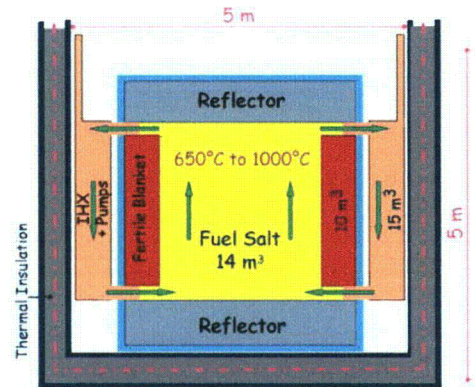


Fig.2. Vertical schematic section of the whole TMSR, including pumps and heat exchangers

We assume that helium bubbling in the salt circuit is able to extract the gaseous Fission Products (FP) and the noble metals within 30 seconds^{1,3}. We also consider an off-line reprocessing of the total salt volume in a separate chemical unit, with a complete extraction of the FPs. In this reprocessing, the TRUs are not extracted but are reinserted in the core to insure their self-burning in the TMSR. This off-line reprocessing will be discussed in paragraph III.A. We also assume that the ^{233}U produced in the blanket is extracted within a 6 month period.

II.B. Reactor parameters considered: Proportion of heavy nuclei in the fuel salt and Reprocessing

In this section, we aim at optimizing this TMSR concept by varying two reactor parameters:

- the composition of the fuel salt, more precisely the proportion of heavy nuclei in the fuel salt;
- the reprocessing, which modifies the salt composition while modifying the reactor's poisoning by FPs.

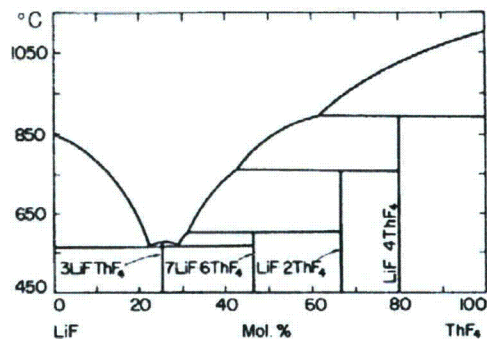


Fig.3. $\text{LiF} - \text{ThF}_4$ phase diagram

The modification of the fuel salt consists in varying the proportion of heavy nuclei in the fuel salt; this has an influence both on the initial fissile inventory and on the spectrum of the reactor. For HN proportions ranging from 20 mole % to 30 mole %, the salt used is a binary fluoride salt LiF-(HN)F₄, whose melting temperature is around 570°C (Fig. 3). We thus choose an operating temperature of 630°C, with a corresponding ²³³U proportion in heavy nuclei of about 3 %, a thermodynamic efficiency of 40 %, and a salt density around 4.3 with a dilatation coefficient⁸ of 10⁻³/°C. For lower proportions of HN, this binary salt is no longer liquid at the operating temperature of 630°C previously selected. Two alternatives can be considered:

- Introducing Beryllium in the fuel salt to lower its eutectic point. The salt is then LiF-BeF₂-(HN)F₄ at the same operating temperature as before.
- Operating at a higher temperature (around 1000°C), still using a binary fluoride salt LiF-(HN)F₄.

The first solution, Beryllium addition, has been chosen in this study to avoid some problems due to much higher operating temperatures, in particular with materials. This choice, in turn, raises new issues such as Plutonium solubility, which we discuss in Paragraph IV.D.

Regarding the second parameter, the off-line reprocessing, the amount of FPs produced in the reactor, and thus to be extracted by the reprocessing, depends only on the power produced. It may be difficult, even impossible, to extract the main FPs (lanthanides) in the presence of HN. As a consequence, and in order to have equivalent reprocessing in every reactor configuration, it is necessary to have the same amount of HN reprocessed per day whatever the HN proportion in the fuel salt. We will first study the influence of this parameter in paragraph III.A. Then, for all TMSRs considered in this article we fix a delayed reprocessing of a salt volume containing 200 kg of HN per day. This choice is detailed in paragraph III.A.

II.C. Criteria used for the TMSR evaluation

Our TMSR optimization is based on three main criteria detailed in this paragraph: the safety level, the radiotoxicity and waste production, and the deployment capacities.

II. C. 1. Safety level

The feedback coefficient is traditionally broken down into three sub-coefficients related to the different components of the core presented above:

$$\left(\frac{dk}{dT}\right)_{total} = \left(\frac{dk}{dT}\right)_{salt_heating} + \left(\frac{dk}{dT}\right)_{salt_dilatation} + \left(\frac{dk}{dT}\right)_{graphite_heating}$$

The third sub-coefficient is negligible in our case since there is no graphite moderator in core.

The uncertainties indicated in this article are a quadratic combination of the statistical and systematic uncertainties on the determination of the sub-coefficients. The statistical errors are precisely estimated by simulation, the quantification of the systematic errors is more difficult. More precisely, concerning the systematic uncertainties on the contribution of salt heating, the cross-sections concerned are well known, inducing only negligible uncertainties. The uncertainties on the salt density and its dilatation lead to systematic errors lower than 20% on the contribution of salt dilatation, a value used for the estimation of uncertainties in the next sections.

II. C. 2. Waste production and radiotoxicity

Wastes result both from leakages occurring during the reprocessing and from the final transuranic elements inventories. These transuranic elements inventories present at the end of a reactor's lifespan may be re-injected in a new reactor and are usually not considered as waste, as long as such reactors are operating. But these actinides inventories have to be taken into account for a sustainable waste management, where the entire life of a fleet of reactors, from launching to shutdown, has to be considered. Leakages are proportional to the integral of the transuranic elements inventories and to the amount of HN reprocessed per day (equivalent for all our TMSRs). Leakages occurring all along a reactor's lifespan are negligible compared to the final inventories. Only these final inventories of transuranic elements are thus given for each TMSR, at equilibrium. For Pu-started TMSRs, more precisely here for TMSRs started with the transuranic elements produced in current operating reactors and then operated in the thorium cycle, we estimate the reduction of radiotoxicity reached thanks to these TMSRs at equilibrium, one of our goals being to close the current fuel cycle.

II. C. 3. Deployment capacities

This has to be evaluated both for each reactor configuration and for a combination of Pu-started TMSRs producing ²³³U and of ²³³U-started TMSRs, as presented in section V. We first compare the ²³³U production in a TMSR configuration with its own initial fissile (²³³U), by considering the reactor doubling time. Then we compare the ²³³U production by a Pu-started TMSR configuration with the initial ²³³U inventory necessary to launch the corresponding ²³³U-started TMSR.

III. THORIUM MOLTEN SALT REACTORS STARTED WITH ^{233}U

III.A. Study as a function of the off-line reprocessing

For each proportion of heavy nuclei in the salt, ranging from 6 mole % to 27.5 mole %, we evaluate by simulation the breeding ratio of each reactor configuration as a function of the amount of heavy nuclei reprocessed per day. The result of this study is displayed on Fig. 4, allowing the visualization of many parameters of interest of the non-moderated TMSR: reprocessing design, reactor deployment and breeding capacities.

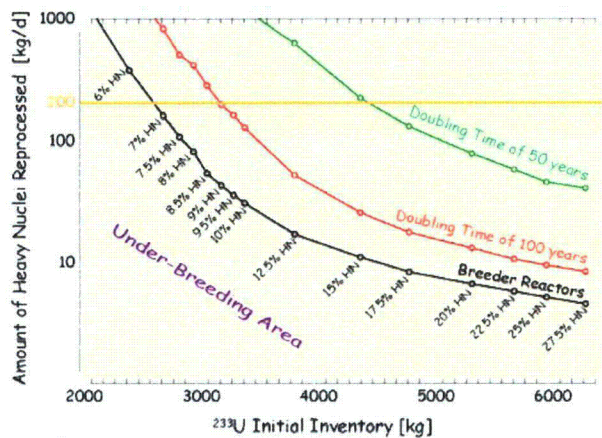


Fig.4. Amount of heavy nuclei reprocessed per day versus initial fissile (^{233}U) inventory, for different heavy nuclei proportions in the fuel

In Fig. 4, the dark line represents breeder reactors, the red one the reactors producing their initial ^{233}U inventory in 100 years (i.e. what is called a doubling time of the reactor of 100 years), and finally the green line stands for reactors producing their initial ^{233}U inventory in 50 years (or a reactor doubling time of 50 years). Under-breeder reactor configurations, which are located under the black line (bottom of the figure), will not be considered in the following since they do not allow any sustainable reactor deployment.

The ^{233}U initial inventory ranges from 2400 kg for a HN proportion in the salt of 6 mole % to 6300 kg for a HN proportion of 27.5 mole %. This corresponds to a variation of the neutron spectrum from an epithermal to a fast spectrum, as shown on Fig. 5.

We chose a reasonable reprocessing rate of 200 kg of HN per day, indicated by the orange horizontal line on Fig. 4. This choice disqualifies TMSRs with HN proportions lower than 7%, since they cannot then be breeder reactors (see Fig. 4).

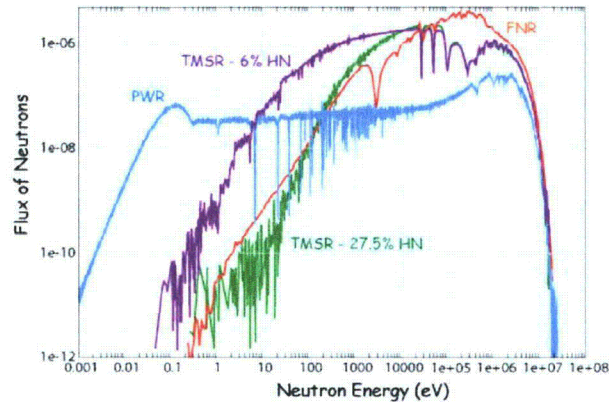


Fig.5. Neutron spectrum of two TMSR configurations (6% and 27.5% of heavy nuclei in the salt) compared to the neutron spectrum in a pressurized water reactor (PWR) and in a fast neutron reactor (FNR)

III.B. Safety level

The total feedback coefficient at equilibrium is displayed on Fig. 6, together with its components, the contributions of the salt heating and salt dilatation, as a function of the HN proportion in the salt. All these safety coefficients are significantly negative for all HN proportions, including the density coefficient which can be viewed as a void coefficient. The total feedback coefficient ranging from -10 pcm/K to -5 pcm/K and thus insuring a very good level of deterministic safety⁹ in all these ^{233}U -started TMSR configurations, safety is not a discriminating factor in our case to choose the optimal salt composition.

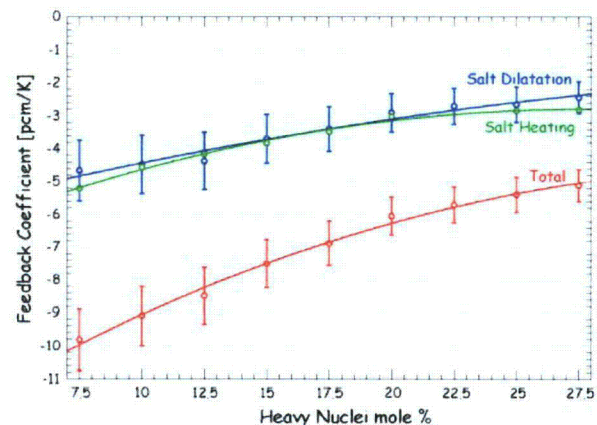


Fig.6. Feedback Coefficients of ^{233}U -started TMSRs at equilibrium as a function of the HN proportion

III.C. Production of transuranic elements

TMSRs are supposed to be at equilibrium after 200 years of operation. The inventories of transuranic elements

obtained are displayed on Fig. 7, for different HN proportions.

The Pu inventory equal to around 300 kg and the Am inventory equal to 7 kg only slightly depend upon the HN proportion. The Np inventory ranges from 100 to 200 kg, and the Pa inventory from 70 to 100 kg. Note that the Cm inventory displayed on Fig. 7, equal to some kilograms, is not correctly evaluated for the higher HN proportions since this inventory does not yet reach equilibrium in these cases. The global behavior of this Cm inventory, however, is coherent with the results presented on Fig. 7.

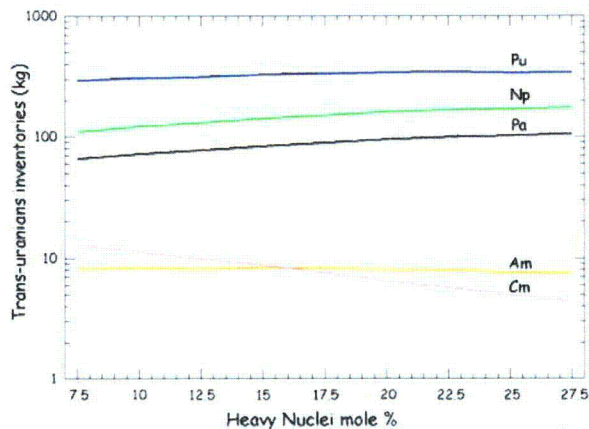


Fig.7. Inventory of the transuranic elements of the ^{233}U -started TMSRs at equilibrium, as a function of the proportion of heavy nuclei in the salt

One tends traditionally to consider that the faster the neutron spectrum is (here the larger the HN proportion is), the lower the amounts of TRU are in a reactor at equilibrium, since the TRU burning is better. We do not observe such a behavior on Fig. 7 because the heavy nuclei inventories are significantly larger for large HN proportions.

Finally the TRU inventories do not really depend upon the HN proportion in the fuel salt, so that this parameter is not discriminating either.

IV. THORIUM MOLTEN SALT REACTORS STARTED WITH PLUTONIUM

The idea in this section is to design a TMSR able to burn Pu while producing ^{233}U , without losing the advantages of the $^{232}\text{Th}/^{233}\text{U}$ fuel cycle. We have thus simulated TMSRs started with Plutonium and Thorium, and then operated in the $^{232}\text{Th}/^{233}\text{U}$ fuel cycle, i.e. fed with Thorium. More precisely, to be more realistic, these TMSRs are started with the mix of Pu, Np, Am and Cm listed in Table I corresponding to the transuranic elements

of an UOX fuel after one use in a standard PWR and five years of storage^[ref].

TABLE I

Proportions of transuranic nuclei in UOX fuel after one use in PWR without multi-recycling (burnup of 60 GWd/ton) and after five years of storage¹⁰

Element	Proportion in the mix
Np 237	6.3 %
Pu 238	2.7 %
Pu 239	45.9 %
Pu 240	21.5 %
Pu 241	10.7 %
Pu 242	6.7 %
Am 241	3.4 %
Am 243	1.9 %
Cm 244	0.8 %
Cm 245	0.1 %

Note that these reactors and their fuel salt are completely equivalent to the TMSRs presented in the previous section, except for the initial fuel load.

IV.A. Safety level

The feedback coefficients for Pu-started TMSRs have been evaluated after one year of operation and at equilibrium.

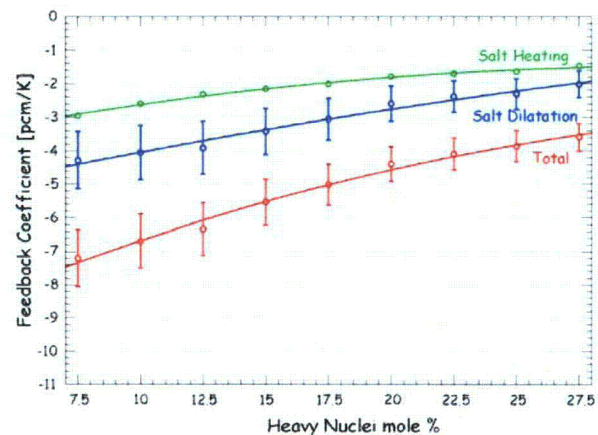


Fig.8. Feedback Coefficients of Pu-started TMSRs after one year of operation as a function of the HN proportion

The total feedback coefficients after one year of operation are displayed on Fig. 11 as a function of the HN proportion, together with their components, the contributions of salt heating and salt dilatation. They correspond to the initial safety behavior of the reactor, since the inventories after one year of operation are quite

identical to the initial inventories, but we also take into account the effects of the fission products which are not present in the initial load of the core.

All these initial safety coefficients are still largely negative for any HN proportion, even if less negative (~25%) than for the ^{233}U -started TMSRs (see Fig. 6). The salt density contribution is equivalent, while the salt heating contribution is less negative because of the presence of Pu instead of ^{233}U .

The feedback coefficients evaluated at equilibrium are equivalent to the results presented on Fig.6 for the ^{233}U -started TMSRs, since these reactors are identical at equilibrium (see paragraph IV.B).

IV.B. Inventories and Waste reduction

Table II. Initial inventories (kilograms) of Th and fissile matter for the Pu-started TMSRs and for the ^{233}U -started TMSRs

HN proportion	^{233}U started TMSR		Pu-started TMSR	
	Th	^{233}U	Th	$^{239}\text{Pu} + ^{241}\text{Pu}$
7.5%	19760	2550	13850	4887
10%	24050	3105	17560	5524
12.5%	27790	3575	20890	6022
15%	33060	4140	25380	6786
17.5%	37230	4650	29150	7297
20%	42380	5170	33640	7968
22.5%	46100	5580	37040	8378
25%	48640	5820	39320	8668
27.5%	52190	6180	42570	9037

As detailed in Table II, the initial fissile inventories are higher for the Pu-started TMSR than for the ^{233}U -started TMSR, from 20% for the larger HN proportions to 40% for the lower HN proportions. Only the amount of fissile Pu is indicated for the Pu-started TMSRs, the amounts of other transuranic elements used to start the reactor being proportional according to the percentages given in Table I.

The initial inventory in fissile Pu necessary for a Pu-started TMSR ranges from 4 to 8 metric tons, and the Thorium initial inventory from 14 to 42 metric tons.

These reactors being studied to close the current fuel cycle, we have to estimate the reduction of radiotoxicity reached thanks to these TMSRs at equilibrium. We aim at burning all TRUs introduced to start the reactor, so as to have TRU inventories at equilibrium identical to the TRU inventories of ^{233}U -started TMSRs, and this is verified.

Fig.9 shows the burning rate obtained for all the transuranic elements after 25, 50, 100 and 200 years of operation. Operation times greater than 60 years (a reactor

lifespan) are obtained by transferring the salt contained in the ending TMSR in a new TMSR. This is made easier thanks to the fact that the fuel is liquid.

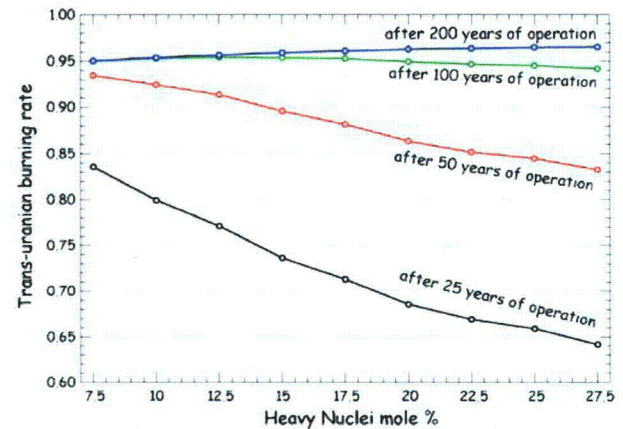


Fig.9. Burning rate of all the transuranic elements after different operation times, as a function of the HN proportion

The lower HN proportion configurations allow faster reductions, since more than 80% of the TRUs are burned after only 25 years of operation, and nearly 95% after 50 years of operation. The larger HN proportion configurations allow higher burning rates, up to 97%, but on the longer run, after more than around 100 years of operation.

Finally, in terms of transuranic inventory, the TMSRs started with Plutonium become equivalent to TMSRs directly started and operated with ^{233}U after around forty years, where more than 85% of the initial TRU inventories are burned, the assets of the Thorium fuel cycle being then recovered.

IV.D. Plutonium Solubility

Pu having a lower solubility limit in a fluoride salt, compared to Uranium for example, this issue has to be examined for the Pu-started TMSRs. Fig. 10 presents the initial mole proportion in the different Pu-started configurations (red line), proportion ranging from 2.5% for the lower HN proportions to 6.5% for the larger HN proportions. According to many studies among which the MSBR studies, it is well attested that the Pu maximum solubility limit in a fluoride salt decreases as the Th proportion increases, deteriorates even faster as Be is added, and is improved if the temperature is increased.

The maximum solubility limit for Pu indicated on Fig. 10 together with its uncertainty (yellow area) give an idea of the typical shape of the solubility limit in a fluoride salt. The lowering of this limit for the smaller HN proportions

is due to the addition of Beryllium in the salt. In our simulations, the maximal Pu solubility limit is reached for the TMSR with 20% of HN in the salt, with no Be added and with the minimal amount of Th in the salt. The reactor configurations with larger HN proportions may encounter Pu solubility problems.

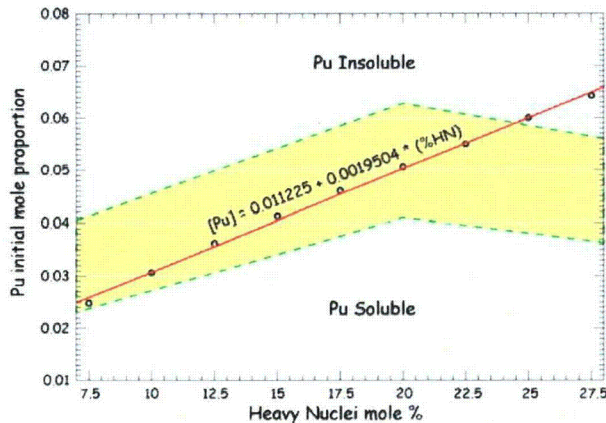


Fig.10. Initial Pu mole proportions in the fuel salt for the different HN proportion configurations (dark dots and red line). The yellow area states for the Pu solubility limit with its uncertainties.

While taking into account the uncertainties on the evaluation of the solubility limit and to be sure not to overshoot this limit, a good compromise could be to slightly increase the reactor operating temperature by around 100 degrees. This allows the use of a fuel salt with no Beryllium and with a lower proportion of HN, and thus a good solubility of Pu.

V. DEPLOYMENT CAPACITIES AND RESOURCES MANAGEMENT

Concerning ^{233}U -started TMSRs, the deployment capacities are based on the amount of ^{233}U produced compared to the initial fissile (^{233}U) inventory necessary to start such a reactor. An example of the amount of ^{233}U produced and extracted all along a TMSR lifespan is presented on Fig. 11 (red line) for a TMSR with 10% of HN in the fuel salt, other TMSR configurations with different HN proportions behaving identically: for TMSRs directly started with ^{233}U , the ^{233}U extraction follows a linear growth, of 37 kg per year in the case shown. This production is directly related to the breeding ratio of the configuration.

Pu-started TMSRs allow the extraction of significantly larger amounts of ^{233}U during the first 20 years of operation (Fig. 11, black line), thanks to the burning of TRUs which saves a part of the ^{233}U produced in the core.

This production reaches 100 kg per year in the example shown, i.e. 60% more than in the corresponding ^{233}U -started TMSR. After the first 20 years, the ^{233}U extraction rate is equivalent to that of the ^{233}U -started TMSR.

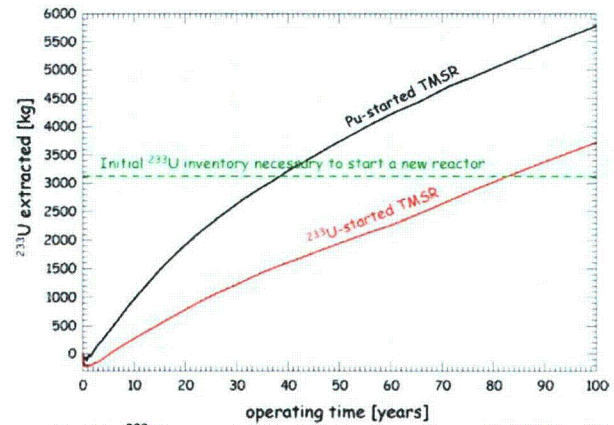


Fig.11. ^{233}U extracted during the operation of TMSR with 10% of HN in the fuel salt

The operating time necessary to produce one initial fissile inventory is called the reactor doubling time. On Fig. 11, the reactor doubling time of a ^{233}U -started TMSR is equal to 83 years and corresponds to the crossing of the ^{233}U production line (red line) with the initial ^{233}U inventory (green dashed line). This reactor doubling time is reduced to 40 years when using Pu in the first load (Fig. 12, dashed line).

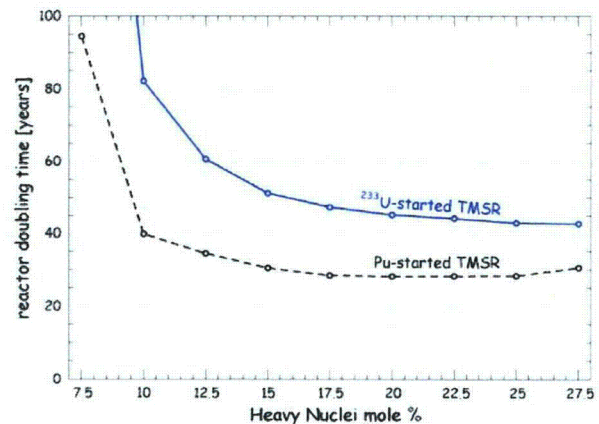


Fig.12. Reactor doubling time of ^{233}U -started (solid line) and Pu-started TMSRs for different HN proportion configurations

To optimize the deployment capacities of a reactor, it first seems logical to minimize the initial fissile inventory, especially in our case where the fissile matter used is not currently available. This means choosing preferably the lower HN proportions. As previously mentioned, a more complete parameter to consider is the reactor doubling

time, which combines this initial fissile inventory constraint with the breeding capacities of the system, i.e. its own capacity to start itself. By generalizing the procedure illustrated on Fig. 11, we thus calculate the reactor doubling times for all HN proportions considered (see Fig. 12). We see again the result detailed on Fig. 11 of a reactor doubling time of 83 years for an HN proportion of 10%.

The higher deployment capacities allowed by the use of TRUs in the Pu-started TMSR are also visible on the reactor doubling times, displayed on Fig. 12 (dashed line), where the configurations with HN proportions larger than 15% have the lower reactor doubling times, around 30 years, to be compared with the doubling times of 45 years reached for the ^{235}U -started TMSRs.

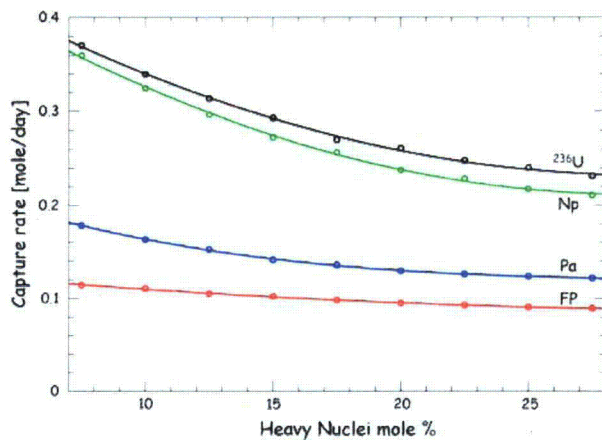


Fig.13. Examples of parasitic capture rates for different components of the fuel salt as a function of the HN proportion

Finally, these configurations with HN proportions larger than 15% have the lowest reactor doubling times and consequently have the best deployment capacities.

These findings that the TMSR configurations with large HN proportions have higher deployment capacities come into conflict with the simple analysis based only on the minimization of the initial fissile inventory, considered at the beginning of this section. Some neutronic behaviors of the core have indeed to be taken into account. For example, for an identical reprocessing, the poisoning of the core by the fission products is relatively more significant for a configuration with a lower HN proportion, as shown on Fig. 13 which presents the values of some parasitic capture rates for different HN proportions. This leads to a reduction of the breeding ratio during reactor operation and finally to smaller deployment capacities for the lower HN proportion configurations.

To conclude this paragraph, the use of Pu and minor actinides to start TMSRs not only allows closing the current fuel cycle but also improves the deployment of such reactors.

VI. CONCLUSIONS

We have presented here a very promising, simple and feasible concept of Molten Salt Reactor with no moderator in the core, operated in the Th/ ^{233}U fuel cycle, and called non-moderated Thorium Molten Salt Reactor (TMSR).

We have detailed in this article some parametric studies, related to the system reprocessing constraints, and the heavy nuclei composition of the salt which modifies the neutron spectrum of the reactor. We have thus demonstrated the very good characteristics of such reactors, in terms of deterministic safety parameters, waste production, deployment capacities...

Since ^{233}U does not exist on earth and is not being produced today, we have examined a new way to produce ^{233}U directly in standard TMSRs started with the Plutonium and transuranic nuclei produced in the currently operating reactors as fissile matter on a Thorium base, and then operated in the Th/ ^{233}U cycle. We aimed at designing a critical reactor able to burn the Plutonium and the Minor Actinides produced in the currently operating reactors, and consequently to convert this Plutonium into ^{233}U . This leads to closing the current fuel cycle thanks to these Pu-started TMSRs, i.e. TMSRs started in the Th/Pu fuel cycle, similarly to fast neutron reactors operated in the U/Pu fuel cycle. The burning of transuranic elements in these Pu-started TMSRs results in high waste reduction rates, up to 95-97% for all TMSR configurations evaluated.

We particularly point out in our analyses the excellent level of deterministic safety of all the TMSR configurations studied, for the ^{233}U -started TMSRs as well as for the Pu-started TMSRs.

Finally, to optimize the transition from the second and third generation reactors to the Thorium cycle, we have considered the deployment capacities of each TMSR configuration, combining Pu-started and ^{233}U -started reactors. The main constraint of a sustainable power deployment was the saving of resources, i.e. in our case the higher breeding ratio and the best conversion of Plutonium in ^{233}U . This results in short reactor doubling times, around 30 years, especially for the TMSR configurations containing the proportions of heavy nuclei larger than 15%, i.e. with the faster neutron spectra. Crossing this criterion with the constraint of the Pu solubility, which leads to a preference for TMSR configurations with less than around 20% of heavy nuclei in the salt, the most

promising TMSRs turn out to be the configurations with heavy nuclei proportions ranging from , 15% to 20%, typically 17.5% of heavy nuclei in the fuel salt.

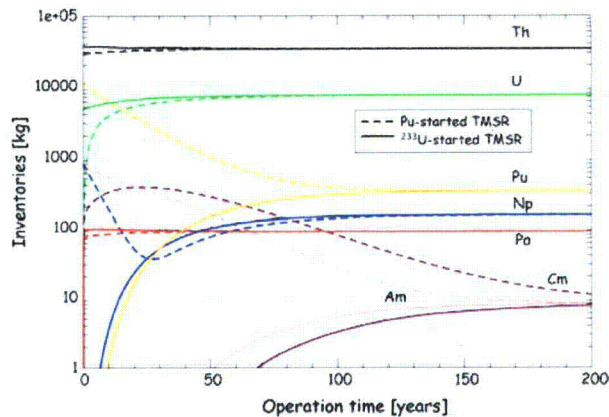


Fig.14. Heavy nuclei inventory for the ^{233}U -started TMSR (solid lines) and for the Pu-started TMSR (dashed lines)

This typical TMSR configuration contains 4.5 mole % of Plutonium to launch the Pu-started version, with a reactor doubling time of 30 years and a feedback coefficient at equilibrium equal to -7 pcm/K both for the ^{233}U -started and the Pu-started reactors, allowing a high level of deterministic safety. Fig. 14 illustrates the evolution of the fuel salt composition all along the operation of this reactor, for the ^{233}U -started (solid lines) and for the Pu-started (dashed lines) TMSR.

ACKNOWLEDGMENTS

We are thankful to Elisabeth Huffer for her help during the translation of this paper.

REFERENCES

1. L. Mathieu et al, "Proposition for a Very Simple Thorium Molten Salt Reactor", *Global Conference*, Tsukuba, Japan (2005).
2. L. Mathieu, D. Heuer et al, "The Thorium Molten Salt Reactor: Moving on from the MSBR", *Prog. in Nucl. En.*, vol 48, pp. 664-679 (doi:10.1016 / j.pnucene.2006.07.005) (2006)
3. L. Mathieu, "Cycle Thorium et Réacteurs à Sel Fondu : Exploration du champ des Paramètres et des Contraintes définissant le Thorium Molten Salt Reactor", PhD thesis, Institut National Polytechnique de Grenoble, France (2005) (in French).
4. A. Nuttin et al, "Potential of Thorium Molten Salt Reactors", *Prog. in Nucl. En.*, vol 46, p. 77-99 (2005).
5. E. Merle-Lucotte, D. Heuer C. Le Brun, L. Mathieu, R. Brissot, E. Liatard, O. Meplan, A. Nuttin, "Fast Thorium Molten Salt Reactors started with Plutonium", *Proceedings of the International Congress on Advances in Nuclear Power Plants (ICAPP)*, Reno, USA (2006).
6. J.F. Briesmeister, "MCNP4B-A General Monte Carlo N Particle Transport Code", Los Alamos Lab. report LA-12625-M (1997).
7. A. Nuttin, "Potentialités du concept de réacteur à sels fondus pour une production durable d'énergie nucléaire basée sur le cycle thorium en spectre épithermique", PhD thesis, Institut National Polytechnique de Grenoble, France (2002) (in French).
8. V. Ignatiev, E. Walle et al, "Density of Molten Salt Reactor Fuel Salts", *Nureth Conference*, Avignon, France (2005).
9. E. Merle-Lucotte, D. Heuer, L. Mathieu, C. Le Brun, "Molten Salt Reactor: Deterministic Safety Evaluation", *Proceedings of the European Nuclear Conference*, Versailles, France (2005).
10. C. de Saint Jean, M. Delpech, J. Tommasi, G. Youinou, P. Bourdot, "Scénarios CNE : réacteurs classiques, caractérisation à l'équilibre", CEA report DER/SPRC/LEDC/99-448 (2000) (in French).

**WASTE STREAM GENERATED AND WASTE DISPOSAL PLANS
FOR MOLTEN SALT REACTOR EXPERIMENT
AT OAK RIDGE NATIONAL LABORATORY**

Mahmoud H Haghghi Ph.D., Mark K Ford,
Bechtel Jacobs Company. LLC
P. O. Box 2008, Oak Ridge, TN 37831-6427

Robert M Szozda
Operational Management Services, Inc.
1723 James Ferry Road, Kingston, TN 37763

Michael R Jugan
Department of Energy (DOE)
55 Jefferson Avenue, Oak Ridge, TN 37830

ABSTRACT

The Molten Salt Reactor Experiment (MSRE) site is located in Tennessee, on the U.S. Department of Energy (DOE) Oak Ridge Reservation (ORR), south of the Oak Ridge National Laboratory (ORNL) main plant across Haw Ridge in Melton Valley. The MSRE was run by ORNL to demonstrate the desirable features of the molten-salt concept in a practical reactor that could be operated safely and reliably. It introduced the idea of a homogeneous reactor using fuel salt media and graphite moderation for power and breeder reactors. The MSRE reactor and associated components are located in cells beneath the floor in the high-bay area of Building 7503 (Figure 1).

The reactor was operated from June 1965 to December 1969. When the reactor was shut down, fuel salt was drained from the reactor circuit to two drain tanks. A "clean" salt was then circulated through the reactor as a decontamination measure and drained to a third drain tank. When operations ceased, the fuel and flush salts were allowed to cool and solidify in the drain tanks. At shutdown, the MSRE facility complex was placed in a surveillance and maintenance program.

As a result of the S&M program, it was discovered in 1994 that gaseous uranium ($^{233}\text{U}/^{232}\text{U}$) hexafluoride (UF_6) had moved throughout the MSRE process systems. The UF_6 was generated when radiolysis of the fluorine salts caused the individual constituents to dissociate to their component atoms, including free fluorine. Some of the free fluorine combined with uranium fluorides (UF_4) in the salt to form UF_6 . UF_6 is gaseous at slightly above ambient temperatures; thus, periodic heating of the fuel salts (which was intended to remedy the radiolysis problems) and simple diffusion had allowed the UF_6 to move out of the salt and into the process systems of MSRE.

Currently, MSRE is undergoing the D&D process to remove the fuel and salt from fuel drain tanks and fuel flush tank. During the D&D activities the uranium will be separated and recovered from the salts and residual salts containing fission products, other uranium daughter radionuclides, and residual uranium in the salts will be disposed of as waste. Recently, the majority of the uranium-laden charcoal material residing with in the auxiliary charcoal bed (ACB) has been removed and is currently awaiting process and disposal. In addition, the Reactive Gas Removal System (RGRS) has been deployed at MSRE since 1996 to remove reactive gases containing uranium material (i.e., UF_6) and other reactive gases (i.e., F_2 , MoF_6 , HF , etc.) from the MSRE off gas systems and capturing them on sodium fluoride (NaF) and alumina traps, respectively. The uranium material in these NaF traps will be recovered and the residual

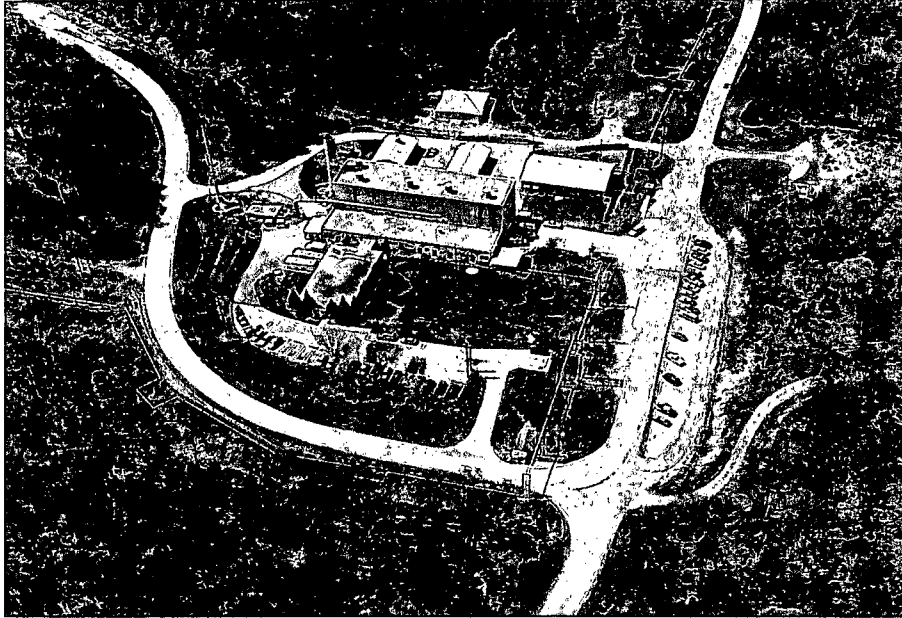


Fig. 1 Aerial view of the MSRE facility

NaF traps that contain the $^{233}\text{U}/^{232}\text{U}$ daughters will be disposed of as waste. Due to these D&D activities at MSRE, a variety of waste streams are generated (aside from the routine operation low level radioactive waste), and each encompasses its own waste management and disposal issues. Plans are being developed at MSRE for safe final disposal of these different waste streams at different off-site disposal facilities.

INTRODUCTION/BACKGROUND

The MSRE is an 8 MW reactor that was operated at Oak Ridge National Laboratory (ORNL) from 1965 through 1969 as a demonstration of the technology needed to develop a large scale Molten Salt Breeder Reactor. The reactor used a unique liquid fuel, formed by dissolving UF_4 fuel in a carrier salt composed of a mixture of LiF, BeF, and ZrF. The fuel salt circulated through a reactor vessel, a fuel salt pump, and a primary heat exchanger at temperatures above 600°C (1112°F). In the reactor, the salt was forced through channels of graphite to provide the geometry and moderation necessary for a nuclear chain reaction. Heat was transferred from the fuel salt to the secondary coolant salt in the primary heat exchanger. The coolant salt is similar to the fuel salt, except that it contains only LiF (66%) and BeF (34%). The coolant salt passed from the primary heat exchanger to an air-cooled radiator, a coolant salt pump, and then returned to the primary heat exchanger. Each of the salt loops was provided with drain tanks, located such that the salt could be drained out of either circuit by gravity. A single drain tank was provided for the nonradioactive coolant salt. Two drain tanks were provided for the fuel salt. The fuel salt drain tanks were provided with a system to remove the intense heat generated by radioactive decay immediately after an emergency reactor shutdown and fuel salt drain. A third drain tank connected to the fuel salt loop was provided for storing a batch of flush salt. This batch of salt, similar in composition to the coolant salt, was used to condition the fuel salt loop after it had been exposed to air and to flush the fuel salt loop of residual fuel salt and contaminants before accessing the reactor circuit for maintenance or experimental activities. All three tanks are located in the drain tank cell, a stainless steel lined below grade cell that could be covered by two layer of concrete shield blocks.

The MSRE was originally fueled by adding ~218 kg of uranium, consisting of 30% ^{235}U and 70% ^{238}U , to the carrier salt. In 1968 this initial charge of uranium was stripped from the salt using a fluoride volatility process wherein the molten salt was sparged with fluorine gas to convert UF_4 to the volatile UF_6 which was subsequently recovered by chemisorption on sodium fluoride (NaF). The reactor was refueled with ~37 kg of uranium, consisting of ~83% ^{233}U (with ~250 ppm of ^{232}U). When reactor operations were terminated in December 1969, the fuel, flush, and coolant salts were drained into their respective drain tanks. The fuel salt was divided between the two fuel-salt drain tanks.

The ^{233}U isotope makes for a particularly difficult fuel to handle because high levels of gamma radiation are associated with it. A small percentage of ^{232}U is included in ^{233}U as an impurity. The decay chain of ^{232}U includes ^{208}Tl , which is a strong gamma radiation emitter (2.6 MeV gamma energy and 100% emission rate). This daughter product builds up rapidly, causing exposure rates of up to approximately ~37 R/hour per gram of salt. Because of the high exposure rates (as well as fission and activation products in the plant), much of the work at MSRE and in subsequent processing steps is done remotely or in hot cells.

Following reactor shutdown, several activities were performed to evaluate the performance of the materials of construction and to improve containment of the stored salts. Prior to reactor operation, it had been discovered that irradiation of the solid salt produced fluorine gas, presumably by providing the energy to release fluorine radicals (or atomic fluorine) from the salt molecules. This atomic fluorine could then combine to form F_2 . Experiments indicated that at sufficiently high temperatures the effects of radiolysis were reversed. An annual annealing process was instituted in which the salt was heated to temperatures above 149°C (300°F), but below the melting point, for periods of about two weeks so that radiolytic fluorine would recombine with the lithium or beryllium in the salt. This procedure was carried out through December 1989. After this time annealing procedures were halted in part because a high radiation area in a remote section of the facility was postulated to be caused by the migration of radioactive material and this migration may have been caused by the annealing procedure.

In 1994, a gas sample was withdrawn from the off-gas system. It was found that the gas sample contained UF_6 near its saturation pressure, smaller but significant quantities of MoF_6 , and about 50% fluorine. A review was promptly undertaken to assess the extent of uranium migration, and a deposit of uranium (~2 to ~3 kg) was identified on the auxiliary charcoal bed (ACB). (In 2001, after the removal of the ACB uranium and a reduction in the radiation field in the area, less than 1 kg of uranium was also found in the four other main charcoal beds, which were connected to the drain tank off-gas piping.) Since the identification of these findings a Remediation project was undertaken to remove the uranium material from the off-gas system; remove the highly contaminated fuel and flush salts from fuel drain tanks and fuel flush tank; and uranium material from ACB.

Since 1996 the MSRE has been undergoing the D&D process using the Reactive Gas Removal System (RGRS) to remove reactive gases containing uranium material (i.e., UF_6) and other reactive gases (i.e., F_2 , MoF_6 , HF, etc.) from the MSRE off gas systems and capturing them on sodium fluoride (NaF) and alumina traps, respectively. Recently, the majority of the uranium-laden charcoal material residing within the auxiliary charcoal bed (ACB) has been safely and successfully removed using the uranium deposit removal system, remote equipment, and long-handled tools. This material is awaiting processing and disposal by a down-blending process. In addition, salt removal equipment has been designed and installed at MSRE to remove and dispose of the fuel and salt from fuel drain tanks and fuel flush tank after recovering the uranium from these tanks. During the salt removal activity the uranium will be separated as UF_6 from the salt and will be recovered on NaF traps using the MSRE RGRS system.

Reactive Gas Removal System (RGRS)

The reactive gas removal system is connected to the MSRE off-gas system via sampler-enricher hardware, which was used during reactor operation to withdraw salt samples for analysis or to add enriching salt to a well-mixed location in the pump bowl. In addition it provides an enclosed access point to one of the MSRE off-gas system lines. The RGRS (Figure 2) consists of a glove box, which houses the RGRS system valves and piping that allows the system to withdrawal reactive gases (including UF_6) from the MSRE off-gas system. The RGRS system uses a NaF trap for uranium (UF_6) removal from the MSRE gases, followed by an alumina trap for removal of the fluorine. Beyond the alumina trap a molecular sieve trap is used to absorb residual moisture, which possibly contains HF generated from the alumina trap. This prevents the corrosion of the other system components. Gas coming out of the last trap is sent to a holdup tank and after allowance for the decay of ^{220}Rn (one of the ^{232}U daughters) it is discharged via the MSRE ventilation system through F_2 -resistance HEPA filters. The RGRS is also equipped with a Fourier-transform infrared spectrometer system that monitors UF_6 concentration at various locations between the traps.

To date approximately 23 kg of the 37 kg of ^{233}U have been removed from the salts by purging the off-gas piping and trapping the gaseous UF_6 on 26 NaF traps using the RGRS system. The recovered materials have been transported to their interim storage facility at ORNL, awaiting conversion to a stable form.

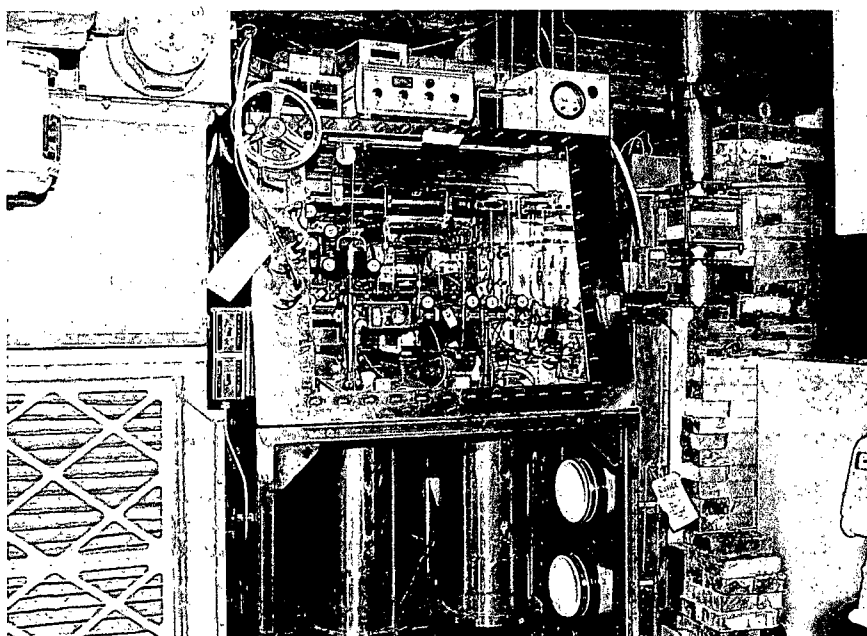


Fig. 2. The MSRE RGRS System

Uranium Deposit Removal (UDR)

As mentioned earlier due to radiolysis process in the fuel salt it is estimated that ~2-3 Kg of the UF_6 migrated to the MSRE ACB and another ~1 Kg migrated to the other four charcoal beds via MSRE off-gas system. The majority of the uranium in the ACB was identified to reside in the top ~14 in of the bed. To remove the uranium-laden charcoal material in the ACB, an elaborate remote-handled charcoal removal system was designed, fabricated, tested, and installed at MSRE ACB (Figure 3). Using this

system and remote equipment, the ACB top was removed. Then the diffuser residing top of the charcoal was removed to gain access to the uranium-laden charcoal within the ACB and the top ~14 in of the uranium-laden charcoal was vacuumed into the shielded charcoal canister. As mentioned in the case of the salt, this material is highly radioactive with exposure rates of ~500 R/h at the side of the collection canister. This material could contain as much as ~30 Ci of ^{137}Cs - ^{137m}Ba as well. This material is planned to be down-blended with urinal nitrate and disposed of as waste.

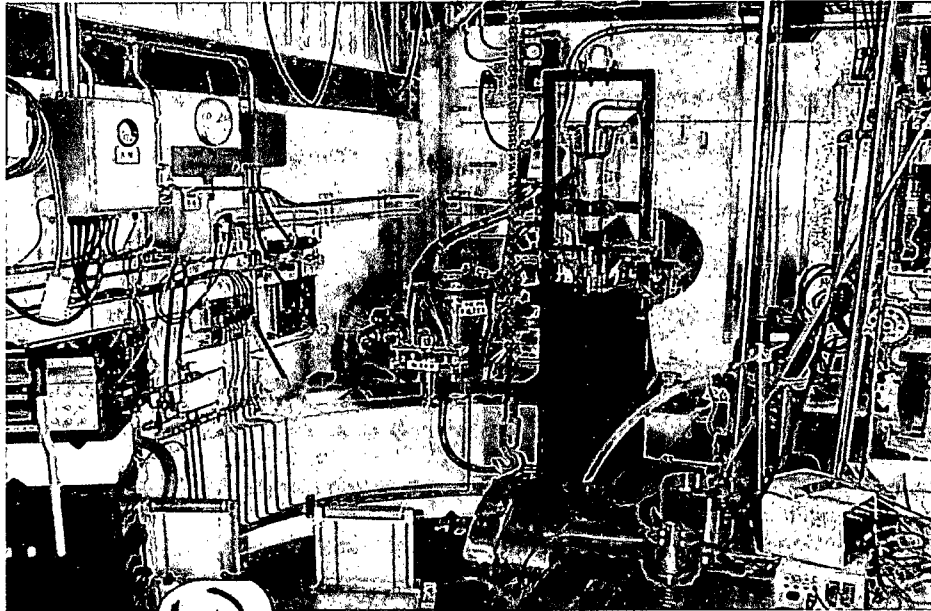


Fig. 5. UDR charcoal removal equipment at ACB

Uranium Recovery from Salts and residual Salts Removal

The fuel salt in the two fuel drain tanks and flush salt in the flush tank will be melted for removal using a process known as "pool melt." A heated probe, which melts the salt and supplies gases for sparging, will be lowered onto the middle of the salt block. A pool of liquid salt will be created at the point of contact between the probe and the salt. While the pool of salt is melting and slowly expanding, it will be sparged with a mixture of hydrogen fluoride (HF), hydrogen (H_2) and helium (He). This hydrofluorination process restores the chemical balance in the salt and ensures that the uranium is in the form of UF_4 . Without this chemistry adjustment, the reduced uranium could precipitate, preventing its recovery. The melting and chemical processing will continue as the probe is lowered into the salt. The pool of melted salt will expand and become deeper until all of the salt is molten.

After all of the salt has reached a liquid form, the molten salt will be sparged with a fluorine-helium mixture, which oxidizes the dissolved UF_4 to form volatile UF_6 . The gaseous UF_6 will escape the salt and be carried away by the circulating helium and excess fluorine. These gases will then move into a refrigerated collection vessel (cold trap) where the UF_6 will be trapped as a frozen solid. Afterward, the cold traps will be warmed to ambient temperature to render the solid UF_6 back to a gaseous state. The gaseous UF_6 will then be collected on NaF traps using the RGRS and packaged for transportation to an interim storage area or to the conversion facility at ORNL. Approximately 1 kg of UF_6 will be collected

on each NaF trap. This operation will continue until all of the UF_6 from a specific drain tank has been recovered on the NaF traps.

Once uranium is separated from the salts, the residual salts will be transferred into storage containers (~10 canister with a total of 8 metric tons of residual salts from flush and fuel salt tanks). A chemically active "getter" will be added to the salt packages to capture any fluorine gas that may be generated. Currently, these cans are planned to be loaded into a shielded container and staged at an interim storage area at ORNL pending final disposal off-site. The majority of the salt removal equipment has been designed, fabricated and installed at MSRE facility and equipment check out and integrated testing are on-going (Figure 4).

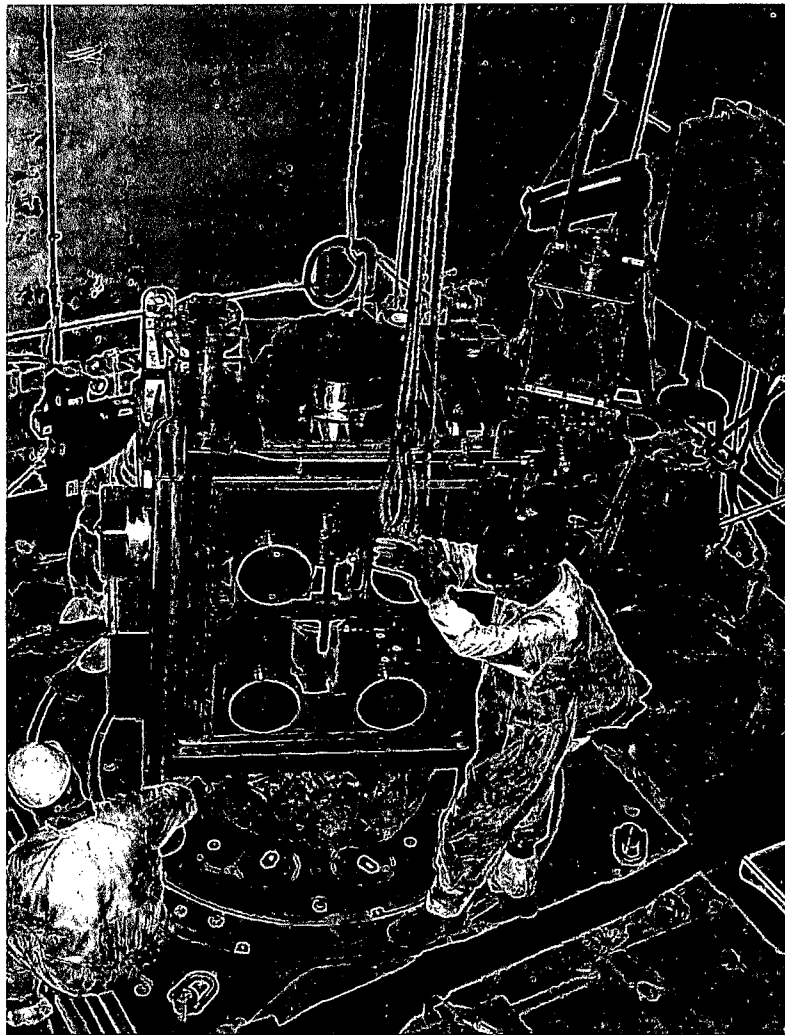


Fig. 4. Salt removal equipment, installation of pool melt probe glove box in the drain tank cell

Conversion and Disposition of Uranium

The uranium hexafluoride collected in the NaF traps is not in a stable form suitable for long-term storage. Unless preventive action is taken, radiolysis will continue to separate free fluorine from the UF_6 , generating gas pressure and reducing the uranium. A process will therefore be employed to convert the UF_6 to the more stable U_3O_8 form. Although this conversion process is common in the uranium industry, a modification tailored to a small-scale remote chemical operation will be applied in this case. The ^{233}U will be processed in a hot-cell at ORNL.

The conversion process for the NaF traps consists of a recovery scheme interconnected with the oxide conversion unit. Most of the equipment is common to the two steps. The first step of the conversion process is to transfer the uranium hexafluoride from the NaF traps to a conversion reaction vessel. In the second step, the resulting solid UF_6 is step-heated and subsequently exposed to pressurized steam, which allows the hydrolysis reaction to take place. The reaction steps are repeated until the temperature of the system reaches as high as $850^\circ C$ as necessary. Moist air is introduced at the end of the hydrolysis process to complete the conversion to an oxide. The vessel is then heated to up to $950^\circ C$ to produce a good quality U_3O_8 (<0.5% moisture content). At the completion of conversion, the vessel containing the U_3O_8 is allowed to cool. The lines are evacuated and filled with an inert gas, and the vessel is disconnected, capped, placed into an overpack, removed from the hot cell, and transported to a permanent storage area. The residual NaF traps containing all of the $^{233}U/^{232}U$ and possibly other radionuclides (i.e. $^{137}Cs/^{137m}Ba$) will be transported to an interim storage location at ORNL for staging and shipping to an off site disposal facility.

MSRE Wastes Generated during D&D Activities

Important waste streams generated by the MSRE D&D project include the spent NaF traps, the uranium-laden charcoal, and the residual salt.

The main waste stream generated during the conversion operation is the spent NaF trap. Less than 1% of the original uranium content is expected to be present after processing. The residual content will be determined for each trap by weight loss in the trap, on-line instrumentation, and weight gained in the conversion vessel. Essentially all of the uranium daughters produced by radioactive decay and most transuranium species will remain in the NaF trap. For this reason, the level of radiation emanating from the trap will remain very high (~ 100s of R/h at contact) for several years. These radiation levels will decline as ^{228}Th , along with its associated daughters, decays with a half-life of 1.9 years. Current plans are to transport the residual NaF traps using a shielded carrier to a temporary storage facility where radioactive decay will occur, and then to a final disposal site. The current selected off-site facility for these traps is the Nevada Test Site. Plans and documentation are being prepared to achieve this goal.

The HF produced during the transformation of the UF_6 into U_3O_8 will be trapped as a solid. Several HF trapping materials have been tested; the one found to be the most effective is a granulated grout made with blast furnace slag and lime. The spent HF trapping material, which is contained in plastic cartridges, will be removed and discarded as solid low-level waste (SLLW). The spent trapping material consists of a mixture of highly insoluble calcium, aluminum, and silicon fluorides and is not a hazardous waste.

The exhaust gases are filtered by a combination of solid traps in series. A NaF trap placed before the off-gas system will trap traces of UF_6 that could migrate to the plant off-gas system. This trap will be treated at the end of the conversion campaign to recover any accumulated traces of uranium. Alumina or soda lime traps follow in series to trap reactive gases such as F_2 or HF. Alumina or soda lime will also trap UF_6 ; hence, they offer redundant protection. A hold up volume is also present to ensure a residence time for the exhaust gases of about 10 minutes to allow for radon decay. The spent alumina or soda lime traps

will be discarded as SLLW. They may be sent as a unit, including the stainless steel container, or emptied to allow for reuse of the trap.

The uranium-laden charcoal currently stored in the charcoal canister in a shielded container is planned to be chemically processed, down blended, and pH-adjusted to an acceptable level to be added to the Melton Valley storage tanks (MVST). The second alternative is to solidify the material after chemical processing and dispose of the material in the Nevada Test Site as a monolith. MSRE has conducted preliminary work on the process and proof of principle and successfully adjusted the pH to the MVST requirement in order to keep the material in a uniform liquid form once introduced to the tanks. At the same time experiments were conducted to show that the same material can successfully and safely be solidified into a monolith appropriate for waste transport.

The end-point location for disposal of the stripped salts or components of the salts will be the Waste Isolation Pilot Plant (WIPP) in New Mexico. Currently MSRE has developed a white paper and an acceptable knowledge package to characterize the waste for WIPP disposal. The waste is considered to be a defense-related transuranic (TRU) waste. Evaluation and selection of WIPP for disposal of the MSRE residual salts will be documented upon completion of the necessary documentation/requirement and negotiation among MSRE, DOE and WIPP site. Therefore, decisions about waste acceptance criteria cannot be made yet. As a result, the WIPP alternatives developed can not be fully implemented at this time. Selection of a disposal of residual salts at WIPP must wait until WIPP questions about the acceptance of MSRE salts for disposal can be evaluated. In the interim, fuel and flush salts will be removed from the MSRE facility and placed in interim storage at another ORNL facility. The salt remaining after the uranium removal process will be stored until it is shipped to a disposal location.

THORIUM-FUELED UNDERGROUND POWER PLANT BASED ON MOLTEN SALT TECHNOLOGY

RALPH W. MOIR* and EDWARD TELLER†

Lawrence Livermore National Laboratory, P.O. Box 808, L-637
Livermore, California 94551

Received August 9, 2004

Accepted for Publication December 30, 2004

FISSION REACTORS

TECHNICAL NOTE

KEYWORDS: molten salt reactor, thorium, underground

This paper addresses the problems posed by running out of oil and gas supplies and the environmental problems that are due to greenhouse gases by suggesting the use of the energy available in the resource thorium, which is much more plentiful than the conventional nuclear fuel uranium. We propose the burning of this thorium dissolved as a fluoride in molten salt in the minimum viscosity mixture of LiF and BeF₂ together with a small amount of ²³⁵U or plutonium fluoride to initiate the process to be located at least 10 m underground. The fission products could be stored at the same underground location. With graphite replacement or new cores and with the liquid fuel transferred to the new cores periodically, the power plant could operate for up to 200 yr with no transport of fissile material to the reactor or of wastes from the reactor during this period. Advantages that include utilization of an abundant fuel, inaccessibility of that fuel to terrorists or for diversion to weapons use, together with good economics and safety features such as an underground location will diminish public concerns. We call for the construction of a small prototype thorium-burning reactor.

I. POWER PLANT DESIGN

This paper brings together many known ideas for nuclear power plants. We propose a new combination including non-proliferation features, undergrounding, limited separations, and long-term, but temporary, storage of reactor products also underground. All these ideas are intended to make the plant economical, resistant to terrorist activities, and conserve resources in order to be available to greatly expand nuclear power if needed as envisioned by Generation IV reactor requirements.

We propose the adoption of the molten salt thorium reactor that uses flowing molten salt both as the fuel carrier and as

a coolant. The inventors of the molten salt reactor were E. S. Bettis and R. C. Briant, and the development was carried out by many people under the direction of A. Weinberg at Oak Ridge National Laboratory.¹ The present version of this reactor is based on the Molten Salt Reactor Experiment²⁻⁴ that operated between 1965 and 1969 at Oak Ridge National Laboratory at 7-MW(thermal) power level and is shown in Fig. 1. The solvent molten salt is lithium fluoride (LiF, ~70 mol%) mixed with beryllium fluoride (BeF₂, 20%), in which thorium fluoride (ThF₄, 8%) and uranium fluorides are dissolved (1% as ²³⁸U and 0.2% as ²³⁵U in the form of UF₄ and UF₃. UF₃/UF₄ ≥ 0.025).^a This mixture is pumped into the reactor at a temperature of ~560°C and is heated up by fission reactions to 700°C by the time it leaves the reactor core, always near or at atmospheric pressure. The materials for the vessel, piping, pumps, and heat exchangers are made of a nickel alloy.^{5,6} The vapor pressure of the molten salt at the temperatures of interest is very low (<10⁻⁴ atm), and the projected boiling point at atmospheric pressure is very high (~1400°C). This heat is transferred by a heat exchanger to a nonradioactive molten fluoride salt coolant^c with an inlet temperature of 450°C and the outlet liquid temperature of 620°C that is pumped to the conventional electricity-producing part of the power plant located above-ground. This heat is converted to electricity in a modern steam power plant at an efficiency of ~43%.

The fluid circulates at a moderate speed of 0.5 m/s in 5-cm-diam channels amounting to between 10 and 20% of the volume within graphite blocks of a total height of a few meters.

^aInstead of the Be and Li combination, we might consider sodium and zirconium fluorides in some applications to reduce hazards of Be and tritium production from lithium.

^bIt seems likely all these components could be made of composite carbon-based materials instead of nickel alloy that would allow raising the operating temperature so that a direct cycle helium turbine could be used rather than a steam cycle (~900°C) and hydrogen could be made in a thermochemical cycle (~1050°C). A modest size research and development program should be able to establish the feasibility of these high-temperature applications.

^cA secondary coolant option is the molten salt, sodium fluoroborate, which is a mixture of NaBF₄ and NaF. Other coolants are possible depending on design requirements such as low melting temperature to avoid freeze-up.

*E-mail: Moir1@llnl.gov

†We are sorry to inform our readers that Edward Teller is deceased September 9, 2003.

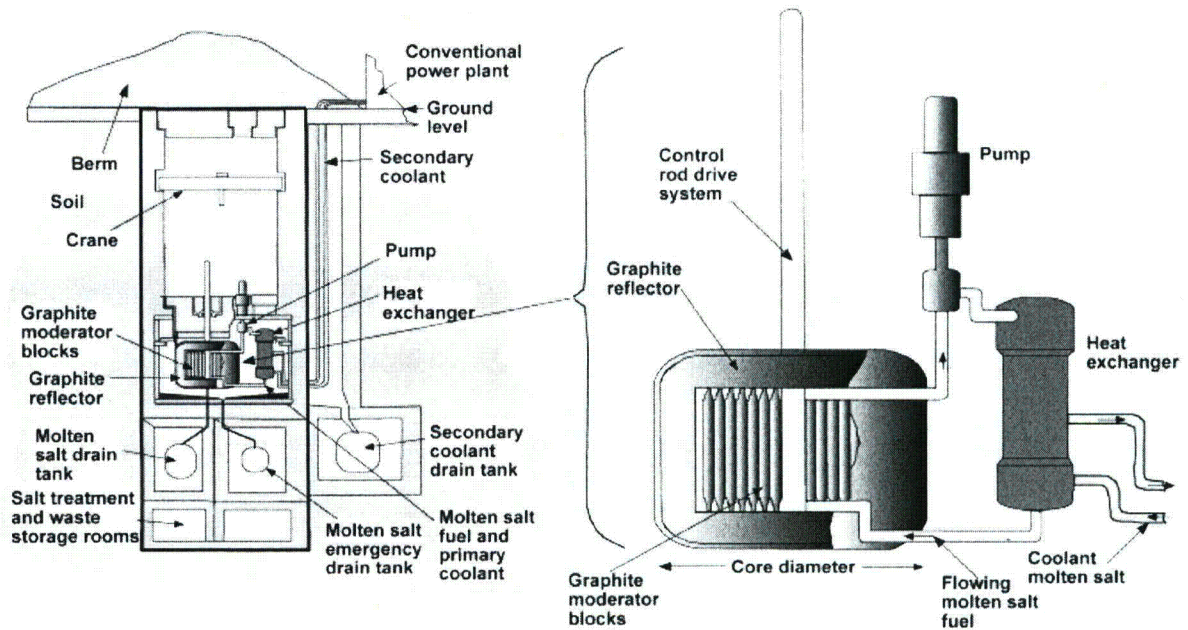


Fig. 1. The nuclear part of the molten salt power plant⁷ is illustrated belowground with the nonradioactive conventional part aboveground; many rooms and components are not shown. New cores would be installed after each continuous operating period of possibly 30 yr or the graphite in the cores can be replaced.

Of all these components, only graphite can burn and then slowly. Leakage of air or water into the molten salt is to be minimized to limit corrosion, as oxidation rates are low. In case of an accident, the fuel would be isolated from the graphite by passively draining the molten salt to the drain tank thus removing the decay heat source making the graphite hot.

The graphite slows down the fast neutrons produced by the fission reaction. The slowed neutrons produce fission and another generation of neutrons to sustain the chain reaction.

One of the slowed neutrons is absorbed in ^{232}Th producing ^{233}Th , which undergoes a 22-min beta decay to ^{233}Pa . The ^{233}Pa undergoes a month-long beta decay into ^{233}U , which with a further neutron produces fission and repeats the cycle. The reactions are illustrated in Fig. 2. Note that the cycle does not include ^{235}U , which is used only to initiate the process. The result is a drastic reduction of the need for mined uranium.

The initial fuel to start up the reactor can be mined and enriched ^{235}U [~ 3500 kg for 1000 MW(electric)]. An alternative

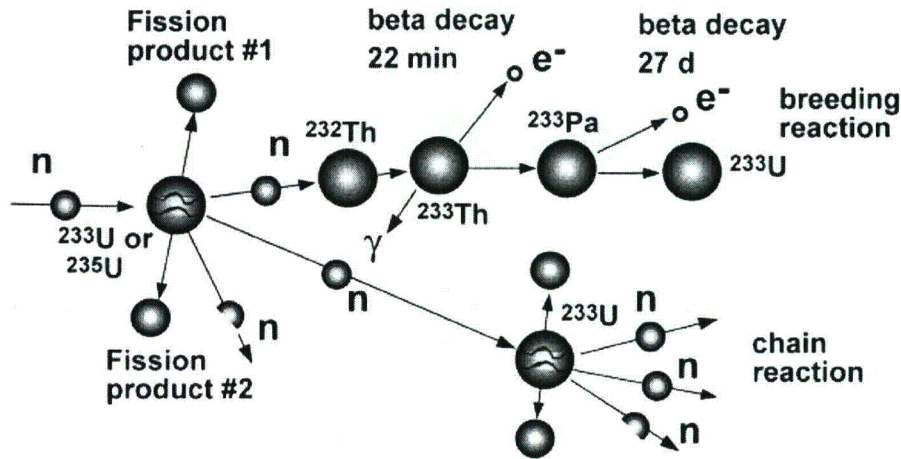


Fig. 2. Illustration of the process of breeding or producing new fuel, ^{233}U , from neutron capture in ^{232}Th as a part of the chain reaction. Each fission reaction produces two or three neutrons (about 2.5 on average as illustrated by the "half neutron" above).

might be to start up on discharged light water reactor (LWR) spent fuel, particularly ^{239}Pu . Actually, ^{239}Pu is contained in a waste of transuranium elements that people might actually pay to give this fuel away. As the plant operates, the plutonium and higher actinides and ^{235}U would be fissioned and replaced with ^{233}U produced from thorium, which is even a better fuel than ^{235}U , because nonfission thermal neutron captures are about half as likely.

An important feature of our proposal is to locate everything that is radioactive at least 10 m underground—where all fissions occur—while the electric generators are located in the open, being fed by hot, nonradioactive liquids. The reactor's heat-producing core is constructed to operate with a minimum of human interaction and limited fuel additions for decades. Of the three underground options,⁸ excavation into mountains with tunnel or vertical access or surface excavation with a berm covering, we prefer the berm as illustrated in Fig. 1. Undergrounding will preclude the possibility of radioactive contamination in case of airplane disasters. A combination of 10 m of concrete and soil is enough mass to stop most objects. It would eliminate tornado hazards and, most particularly, contribute to defense against terrorist activities. In case of accidents, undergrounding, in addition to the usual containment structures, enhances containment of radioactive material. The 10-m figure is a compromise between safety and plant construction expense. We anticipate the cost to construct underground with only 10 m of overburden using the berm technique will add <10% to the cost.

The molten salt reactor that operated in the 1960s had a big advantage in the removal of many fission products without much effort. Gases (Kr and Xe) simply bubble off aided by helium gas bubbling, where these gases are separated from the helium and stored in sealed tanks to decay. Noble and semionoble metals^d precipitated. In the planned reactor, the old method of removing the gases may be repeated. The precipitation process might conceivably be enhanced by using a centrifuge and filtering rather than the old uncontrolled method of precipitation. In this way, the need to remove the remaining fission products, e.g., the rare-earth elements (Sm, Pm, Nd, Pr, Eu, and Ce) and alkali-earth elements with valence two and three fluoride formers, is reduced and may be postponed to intervals, perhaps as long as once every 30 yr. The accumulation of these elements has a small effect on neutron economy and on chemistry such as corrosion. Experience is needed on these long-term effects.

Most fission products have half-lives of ~30 yr or less. These "short-lived" fission products can be stored and monitored at the plant site for hundreds of years, while their hazard decreases by three orders of magnitude or more by the natural process of radioactive decay. Three elements are notable because they need to be separated for special treatment because of their extra long lives: ^{99}Tc , ^{129}I , and ^{135}Cs [with half-lives of 210 000 yr, 1.6 million yr, and 2.3 million yr; capture cross sections of 20, 30, and 9 b (10^{-24} cm²); and production rates of 23, 3.8, and 34 kg/GW(electric)·yr, respectively]. New ways should be found for separating these long-lived products ($\gg 30$ -yr half-life) from short-lived products (≤ 30 -yr half-life).

^dNoble and semionoble metals are Zn, Ga, Ge, As, Nb, Mo, Tc, Ru, Rh, Pd, Ag, Cd, In, Sn, and Sb. Semionoble here means they do not form fluorides but rather precipitate in elemental form.

After a period of operation, perhaps as long as 30 yr, the reactor is shut down, owing to the swelling of the graphite blocks as shown in Fig. 3. The criterion^{4,9} used here is 30 yr for a 10-m-diam core at 1000 MW(electric), for a neutron dose of $<3 \times 10^{26}$ n/m² for $E > 50$ keV and a swelling of 3 vol% at 750°C for a capacity factor of 85%. Robotic technology is developing so rapidly that graphite replacement might be a quick and a low-cost operation. Another process that might be life limiting is corrosion. At the time that a new or refurbished power-generating graphite core is put into operation and the corroded parts are replaced, the fuel dissolved in the molten salt is transferred to the new core in a liquid state. This fuel transfer and core refurbishment allows the power station to continue operating for several more decades. At this time, the remaining fission products in solution can be removed by the chemical process known as *reductive extraction* to limit the neutron loss to absorption. The bulk of materials (lithium, beryllium, and thorium fluorides) may last for several hundred years before they are transmuted to other elements by nuclear reactions.

This process might conceivably be continued as long as we operate the power station, perhaps even hundreds of years, making operations and ownership similar to a dam but with less impact. The fission products will be separated and stored at the power plant site in a suitable form under careful supervision or they will be transported to a permanent disposal site. We propose the twofold argument for the safe interim storage of radioactive material: first, that the location will be underground, and second, that the storage will be at the site of operating reactors, which require carefully planned defense anyway.

When the site with its collection of reactors is to be shut down, careful considerations will have to be used in the choice between whether the accumulated radioactivity should be transported to a permanent storage site or whether continuation of established supervision is safer and less expensive. The idea is to transport only mildly radioactive fuel to the power plant but have a minimum of transport of highly radioactive fission products and fuel away from the plant, thus minimizing the chance of accidents or terrorist activities. One conclusion is obvious: It

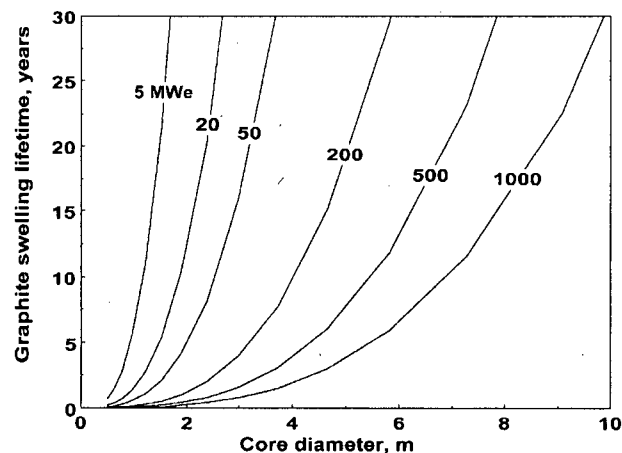
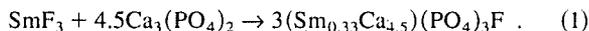


Fig. 3. The core lifetime versus diameter (see Fig. 1) limited by graphite swelling is shown for a wide range of output power.

will become important to find useful applications of radioactivity such as radioactive tracers, thereby converting a serious worry into a potential asset.

II. WASTE FORM: SUBSTITUTED FLUORAPATITE

A possible waste form for the molten salt reactor might be based on the naturally occurring mineral that has been found to contain ancient actinides in the natural reactor in Africa in mineral deposits called fluorapatite^{10,11} $\text{Ca}_5(\text{PO}_4)_3\text{F}$. This low solubility mineral is much like fluoridated tooth enamel. If we substitute the fission product ions, for example, Sm, for the Ca ions, we call this substituted fluorapatite



The result of this reaction is a ceramic powder that can be melted into bricks for long-term storage either at the power plant site or at a repository.

It might be preferable to transport it in a more compact fluoride form and produce the more stable but larger mass and volume form of material at the permanent repository site. The stored fluoride wastes could be melted and transferred in liquid form to a shipping container much like that used for sulfur shipping except more massive and shipped to a permanent storage site where again they are transferred in liquid form to be made into substituted fluorapatite bricks. If permanent storage is decided upon, we estimate the space needed in a Yucca Mountain-like repository for molten salt wastes to be ten and maybe closer to 100 times less than for once-through LWR spent fuel based on the heat generation rate of the wastes.

III. SAFETY

The molten salt reactor is designed to have a negative temperature coefficient of reactivity. This means the reactor's power quickly drops if its temperature rises above the operating point, which is an important and necessary safety feature. The molten salt reactor is especially good in this respect—it has little excess reactivity because it is refueled frequently online and has a high conversion rate that automatically replaces fuel consumed. Failure to provide makeup fuel is fail-safe as the reactivity is self-limiting by the burnup of available fuel. A small amount of excess reactivity would be compensated by a temporary interruption of adding makeup fuel online. Present reactors have ~20% excess reactivity. Control rods and burnable poisons are used not only in accident control but also to barely maintain criticality. In the molten salt reactor, control rods are used to control excess reactivity of perhaps only 2%, which is necessary to warm the salt from the cooler start-up temperature to the operating temperature (i.e., overcome the negative temperature coefficient). That is, only enough fissile fuel is in the core to maintain a chain reaction and little more.

Gaseous fission products are continually removed and stored separately from the reactor in pressurized storage tanks. By contrast, in conventional reactors the gaseous fission products build up in the Zr-clad fuel tubes to a high pressure that presents a hazard and can cause trouble. If an unforeseen ac-

cident were to occur, the constant fission-product removal means the molten salt reactor has much less radioactivity to potentially spread.

The usual requirement of containing fission products within three barriers is enhanced by adding a fourth barrier. The primary vessel and piping boundary, including drain tanks, constitute one barrier. These components are located in a room that is lined with a second barrier, including an emergency drain or storage tank for spills. The third barrier is achieved by surrounding the entire reactor building in a confinement vessel. A fourth safety measure is locating the reactor underground, which itself is one extra "gravity barrier" aiding confinement. A leakage of material would have to move against gravity for 10 m before reaching the atmosphere.

In case of accidents or spills of radioactive material, the rooms underground would remain isolated. However, the residual decay heat that continues to be generated at a low rate would be transferred through heat exchangers that passively carry the heat to the environment aboveground, while retaining the radioactive material belowground. This passive heat removal concept perhaps using heat pipes will be used to cool the stored fission products as well.

The initial fuel needed including the amount circulating outside the core is considerably less than half that of other breeding reactors such as the liquid metal-cooled fast reactor. This is a consequence of fast reactors having much larger critical mass than thermal reactors and for the molten salt case, avoiding the need for extra fuel at beginning of life to account for burnup of fuel.

IV. FUEL CYCLE WITHOUT FUEL PROCESSING AND WITHOUT WEAPONS-USABLE MATERIAL

When the 1000-MW(electric) reactor is started up, the initial fissile fuel is 20% enriched uranium (20% ²³⁵U and 80% ²³⁸U) along with thorium, actually 3.5 tons of ²³⁵U, 14 tons of ²³⁸U, and 110 tons of thorium. This low enrichment makes the uranium undesirable as weapons material without isotope separation, and therefore it does not have to be guarded so vigorously. An important side product is a small amount of ²³²U produced by (*n*,2*n*) and (*γ*,*n*) reactions on ²³³U producing ²³²U. Uranium-232 is highly radioactive and has unusually strong and penetrating gamma radiation (2.6 MeV), making diversion of this fuel for misuse extra difficult and easier to detect if stolen; the resulting weapons would be highly radioactive and therefore dangerous to those nearby as well as making detection easier.

The uranium in the core starts at 20% fissile and drops so it is never weapons usable.^e The plutonium produced from neutron capture in ²³⁸U rather quickly develops higher isotopes of plutonium, making it a poor material for weapons.^f Safeguarding is still necessary but less important. The advantage of this fuel cycle is that 80% of its fuel is made in the

^eFor example after 15 yr of operation, the isotopes of the uranium in the molten salt are ~0.02% ²³²U; 8% ²³³U; 2% ²³⁴U; 4% ²³⁵U; 3% ²³⁶U; and 83% ²³⁸U.

^fAfter operation for 15 yr, the plutonium in the molten salt has the following isotopes: 7% ²³⁸Pu; 36% ²³⁹Pu; 21% ²⁴⁰Pu; 15% ²⁴¹Pu; and 20% ²⁴²Pu.

reactor, and the fuel shipments to the plant during its operation are nonweapons usable.

$$\text{Conversion ratio} = \frac{{}^{233}\text{U and fissile Pu production rate}}{\text{all fissile consumption rate}} \quad (2)$$

The conversion ratio starts out at 0.8, and after 30 yr of operation drops to 0.77 (Ref. 4). Today's LWRs^g each require 5700 tons of mined uranium in 30 yr. Our molten salt reactor example also at 1000-MW(electric) size, in 30 yr of operation at 75% capacity factor would consume by fissioning, 17 tons of thorium, 3.8 tons of ²³⁸U, and 6.7 tons of ²³⁵U. This requires 1500 tons of mined uranium.^h Our worries about the consumption of uranium are reduced by a factor of 4 relative to today's reactors while the depletion of thorium remains entirely negligible.

In our example, 14% of the heavy atoms that have been transported to the reactor are burned up or fissioned in 30 yr of operation.ⁱ If we include the 1500 tons of mined uranium that went into the depletion process and was not used in the reactor, then the percentage of burnup is 1.3%. This compares to our present-day reactor example with once-through fueling of 0.5% burnup of mined uranium with the assumptions in footnote g.

V. ALTERNATIVE FUEL CYCLE

If we decide in future versions of the molten salt reactor to move toward the pure thorium-²³³U cycle with fuel processing,

then the conversion ratio approaches unity and the use of mined uranium will drop by over an order of magnitude or be eliminated once started up. This cycle would start up the reactor with only ²³⁵U and thorium dissolved in the molten salt.^j Neutrons absorbed in thorium would produce ²³³U. Although this fuel is highly radioactive, after chemical separation it is directly usable in nuclear weapons and therefore poses a danger that would have to be guarded against with extra measures. We should avoid designs that permit separation of protactinium because it decays into ²³³U without the highly radioactive ²³²U "spike" previously mentioned.

The strong advantage of this fuel cycle is that it breeds essentially all of its own fuel, thus removing the need for transportation of weapons-usable material to the reactor site once it is started up. Also it makes no further demands for mined uranium for several hundred years although the graphite had to be changed a number of times.⁴ For example, a present-day reactor would use 38 000 tons of mined uranium over 200 yr, while the molten salt reactor once started up on ²³⁵U and thorium would need only 600 tons of mined uranium and could operate for 200 yr (see footnote g again). One hundred thirty-seven tons of thorium would be fissioned.^k The burnup of the 600 tons of uranium and 137 tons of thorium would be ~18%.

Even a small amount of fissile material removed from the reactor would cause it to cease operation, and this mitigates the danger of diversion from the plant site. Diversion of the material for weapons use would be an interruption of normal procedures, which could be carried out only by insiders. It is clear

^gThe assumption on LWR fuel usage can be seen:

$$\frac{1000 \text{ MW(electric)} \cdot 0.75 \cdot 365 \text{ day/yr} \cdot 30 \text{ yr} \cdot 5\%}{0.32 \frac{\text{MW(electric)}}{\text{MW}} \cdot 50\,000 \text{ MWd/T} \cdot 0.45\%} = 5700 \text{ tons}$$

of mined uranium in 30 yr with tails of 0.25%. (5700 tons · 200 yr) / 30 yr = 38 000 tons in 200 yr.

$$\begin{aligned} \text{Burnup of heavy atoms} &= \frac{1000 \text{ MW(electric)} \cdot 235 \text{ amu} \cdot 1.67 \cdot 10^{-27} \text{ kg/amu} \cdot 365 \text{ days/yr} \cdot 24 \text{ h/day} \cdot 3600 \text{ s/h}}{0.32 \text{ MW(electric)/MW} \cdot 195 \text{ MeV} \cdot 1.6 \cdot 10^{-19} \text{ J/eV}} \\ &= 1240 \text{ kg/full power year} \end{aligned}$$

$$\text{Burnup fraction} = 1.24 \text{ tons} \times 30 \text{ yr} \times 0.75 / 5700 \text{ tons} = 0.49\%$$

Mined uranium for the molten salt reactor to start up is 3.5 tons ²³⁵U / 0.0045 = 780 tons of mined uranium. For the alternative fuel cycle, the start-up is 2.8 tons ²³⁵U / 0.0045 = 620 tons of mined uranium.

^h6.7 tons of ²³⁵U / 0.0045 = 1500 tons of mined uranium where we assume the ²³⁵U content of 0.7% of uranium can be used with tails of 0.25%.

$$\begin{aligned} \text{Burnup of heavy atoms} &= \frac{1000 \text{ MW(electric)} \cdot 233 \text{ amu} \cdot 1.67 \cdot 10^{-27} \text{ kg/amu} \cdot 365 \text{ days/yr} \cdot 24 \text{ h/day} \cdot 3600 \text{ s/h}}{0.43 \text{ MW(electric)/MW} \cdot 195 \text{ MeV} \cdot 1.6 \cdot 10^{-19} \text{ J/eV}} \\ &= 915 \text{ kg per full power year} \end{aligned}$$

Burnup fraction = atoms burned (fissioned) in 30 yr / all heavy atoms

$$= \frac{915 \text{ kg} \cdot 0.75 \cdot 30 \text{ yr}}{110\,000 \text{ kg Th} + 32\,400 \text{ kg } {}^{238}\text{U} + 7900 \text{ kg } {}^{235}\text{U}} = \frac{20\,600 \text{ kg}}{150\,300 \text{ kg}} = 13.7\%$$

We use 30-yr period and 75% capacity factor consistently for all cases, so that relative comparisons are unaffected by this assumption. The fissile consumption is then 0.75 × 915 = 690 kg/yr.

^jUranium-233 for start-up fuel could be produced externally from accelerator or thermonuclear fusion produced neutrons absorbed in thorium if these technologies become developed successfully. This fissile source or use of discharge fuel from current fission reactor designs would virtually eliminate the need for further uranium mining but would introduce proliferation issues that could and would have to be dealt with.

^kBurnup of heavy atoms in 200 yr = 0.915 tons/yr per full power year × 0.75 capacity factor × 200 yr = 137 tons in 200 yr. Burnup in 200 yr = (137 tons Th) / (620 tons mined U + 137 tons Th) = 18%.

that continuous operation would be needed. Thus, it should be easily noticed unless carried out by separating small amounts for a long period.

We advocate full compliance and even strengthened international safeguard agreements including inspection regimes and technical means for monitoring the reactor and all its operations. Monitoring devices including cameras and transceivers possibly in miniature or even subgram sizes might aid monitoring systems to find out whether all components in the system are in place and operating normally. It is difficult to exclude the possibility that considerable quantities of components of nuclear explosives might be produced in reactors, and therefore information on the production of these materials should be readily available. This requirement should be considered a crucial part of a policy of openness (to be introduced gradually), which, in a general sense, will be necessary to insure the stability of the world. Openness is not an easy condition to fulfill but perhaps better than any obvious alternative.

VI. ECONOMIC COMPETITIVENESS

Our economic goal is to achieve a cost of electrical energy averaged over the life of the power station to be no more than that from burning fossil fuels at the same location. Past studies have shown a potential for the molten salt reactor to be somewhat lower in cost of electricity than both coal and LWRs (Refs. 4 and 12). There are several reasons for substantial cost savings: low pressure operation, low operations and maintenance costs, lack of fuel fabrication, easy fuel handling, low fissile inventory, use of multiple plants at one site allowing sharing of facilities, and building large plant sizes. The cost of undergrounding the nuclear part of the plant obviously needs to be determined and will likely not offset the cost advantages of a liquid-fueled low-pressure reactor.

VII. WHY HAS THE MOLTEN SALT REACTOR NOT ALREADY BEEN DEVELOPED?

If the molten salt reactor appears to meet our criteria so well, why has it not already been developed since the molten salt reactor experiment operated over 30 yr ago?

Several decades ago an intense development was undertaken to address the problem of rapid expansion of reactors to meet a high growth rate of electricity while the known uranium resources were low. The competition came down to a liquid-metal fast breeder reactor (LMFBR) on the uranium-plutonium cycle and a thermal reactor on the thorium-²³³U cycle, the molten salt breeder reactor. The LMFBR had a larger breeding rate, a property of fast reactors having more neutrons per fission and less loss of neutrons by parasitic capture, and won the competition. This fact and the plan to reduce the number of candidate reactors being developed were used as arguments to stop the development of the molten salt reactor rather than keep an effort going as a backup option. In our opinion, this was an excusable mistake.

As a result there has been little work done on the molten salt reactor during the last 30 yr. As it turned out, a far larger amount of uranium was found than was thought to exist, and the electricity growth rate has turned out to be much smaller

than predicted. High excess breeding rates have turned out not to be essential. A reactor is advantageous that once started up needs no other fuel except thorium because it makes most or all its own fuel.

Studies of possible next-generation reactors, called Generation IV, have included the molten salt reactor among six reactor types recommended for further development. In addition the program called Advanced Fuel Cycle Initiative has the goal of separating fission products and recycling for further fissioning.

VIII. DEVELOPMENT REQUIREMENTS AND CONCLUSIONS

In conclusion, we believe a small prototype plant should be built to provide experience in all aspects of a commercial plant. The liquid nature of the molten salt reactor permits an unusually small plant that could serve the role just so that the temperatures, power densities, and flow speeds are similar to that in larger plants. A test reactor, e.g., 10 MW(electric) or maybe even as small as 1 MW(electric) would suffice and still have full commercial plant power density and therefore the same graphite damage or corrosion limited lifetime. Supporting research and development would be needed on corrosion of materials, process development, and waste forms, all of which, however, are not needed for the first prototype.

We give some examples of development needs. We need to show adequate long corrosion lifetime for nickel alloy resistant to the tellurium cracking observed after the past reactor ran for only 4 yr. If carbon composites are successful, corrosion will likely become less important. We want to prove feasible extraction of valence two and three fluorides, especially rare-earth elements, which will then allow the fuel to burn far longer than 30 yr (200 yr). We need to study and demonstrate an interim waste form suggested to be solid and liquid fluorides and substitute fluorapatite for the permanent waste form of fission products with minimal carryover of actinides during the separation process. This solution holds the promise to diminish the need for repository space by up to two orders of magnitude based on waste heat generation rate. We need a study to show the feasibility of passive heat removal from the reactor after-heat and stored fission products to the atmosphere without material leakage and at reasonable cost. Another study needs to show that all aspects of the molten salt reactor can be done competitively with fossil fuel. The cost for such a program would likely be well under \$1 billion with operation costs likely on the order of \$100 million per year. In this way a very large-scale nuclear power plant could be established, including even the developing nations, in a decade.

ACKNOWLEDGMENT

This work was performed under the auspices of the U.S. Department of Energy by University of California Lawrence Livermore National Laboratory under contract W-7405-Eng-48.

REFERENCES

1. H. G. MacPHERSON, "The Molten Salt Reactor Adventure," *Nucl. Sci. Eng.*, **90**, 374 (1985).
2. P. N. HAUBENREICH and J. R. ENGEL, "Experience with the Molten-Salt Reactor Experiment," *Nucl. Appl. Technol.*, **8**, 118 (1970).

3. M. PERRY, "Molten-Salt Converter Reactors," *Ann. Nucl. Energy*, **2**, 809 (1975).
4. J. R. ENGEL, H. F. BAUMAN, J. F. DEARING, W. R. GRIMES, E. H. McCOY, and W. A. RHOADES, "Conceptual Design Characteristics of a Denatured Molten-Salt Reactor with Once-Through Fueling." ORNL/TM-7207, Oak Ridge National Laboratory (July 1980).
5. C. W. FORSBERG, P. F. PETERSON, and P. S. PICKARD, "Molten-Salt-Cooled Advanced High-Temperature Reactor for Production of Hydrogen and Electricity," *Nucl. Technol.*, **144**, 289 (2003).
6. P. F. PETERSON, "Multiple-Reheat Brayton Cycles for Nuclear Power Conversion with Molten Coolants," *Nucl. Technol.*, **144**, 279 (2003).
7. K. FURUKAWA, K. MITACHI, and Y. KATO, "Small MSR with a Rational Th Fuel Cycle," *Nucl. Eng. Des.*, **136**, 157 (1992).
8. F. C. FINLAYSON, W. A. KRAMMER, and J. BENVENISTE, "Evaluation of the Feasibility, Economic Impact, and Effectiveness of Underground Nuclear Power Plants," ATR-78 (7652-14)-1, The Aerospace Corporation, Energy and Transportation Division, Aerospace (May 1978).
9. R. C. ROBERTSON et al., "Conceptual Design Study of a Single-Fluid Molten-Salt Breeder Reactor," ORNL-454, Oak Ridge National Laboratory (1971).
10. S. M. McDEAVITT, Argonne National Laboratory. Private Communications (2002).
11. D. LEXA, "Preparation and Physical Characteristics of a Lithium-Beryllium Substituted Fluorapatite," *Metall. Mat. Trans. A*, **30A**, 147 (1999).
12. R. W. MOIR, "Cost of Electricity from Molten Salt Reactors," *Nucl. Technol.*, **138**, 93 (2002).

DIRECT CONVERSION OF SPENT FUEL TO HIGH-LEVEL-WASTE (HLW) GLASS

C. W. Forsberg
E. C. Beahm
G. W. Parker
J. Rudolph

Chemical Technology Division
105 Mitchell Road
P.O. Box 2008
Oak Ridge National Laboratory*
Oak Ridge, Tennessee 37831-6495

Tel: (615) 574-6783
Fax: (615) 574-3431

September 20, 1994

for

American Nuclear Society Conference
DOE Spent Nuclear Fuel: Challenges and Initiatives
Session: Processing and Conditioning Options
Salt Lake City, Utah
December 13-16, 1994

DISCLAIMER

This report was prepared as an account of work sponsored by an agency of the United States Government. Neither the United States Government nor any agency thereof, nor any of their employees, makes any warranty, express or implied, or assumes any legal liability or responsibility for the accuracy, completeness, or usefulness of any information, apparatus, product, or process disclosed, or represents that its use would not infringe privately owned rights. Reference herein to any specific commercial product, process, or service by trade name, trademark, manufacturer, or otherwise does not necessarily constitute or imply its endorsement, recommendation, or favoring by the United States Government or any agency thereof. The views and opinions of authors expressed herein do not necessarily state or reflect those of the United States Government or any agency thereof.

The submitted manuscript has been authored by a contractor of the U.S. Government under contract No. DE-AC05-84OR21400. Accordingly, the U.S. Government retains a nonexclusive, royalty-free license to publish or reproduce the published form of this contribution, or allow others to do so, for U.S. Government purposes.

*Managed by Martin Marietta Energy Systems, Inc. under contract DE-AC05-84OR21400 for the U.S. Department of Energy.

MASTER

DISTRIBUTION OF THIS DOCUMENT IS UNLIMITED

DISCLAIMER

Portions of this document may be illegible in electronic image products. Images are produced from the best available original document.

DIRECT CONVERSION OF SPENT FUEL TO HIGH-LEVEL-WASTE (HLW) GLASS

C. W. Forsberg, E. C. Beahm, G. W. Parker, and J. Rudolph

ABSTRACT

The Glass Material Oxidation and Dissolution System (GMODS) is a recently invented process for the direct, single-step conversion of spent nuclear fuel (SNF) to high-level waste (HLW) glass. GMODS converts metals, ceramics, organics, and amorphous solids to glass in a single step. Conventional vitrification technology can not accept feeds containing metals or carbon. The GMODS has the potential to solve several issues associated with the disposal of various U.S. Department of Energy (DOE) miscellaneous SNFs: (1) chemical forms unacceptable for repository disposal, (2) high cost of qualifying small quantities of particular SNFs for disposal, (3) limitations imposed by high-enriched SNF in a repository because of criticality and safeguards issues, and (4) classified design information. Conversion of such SNFs to glass eliminates these concerns. A description of the GMODS, "strawman" product criteria, experimental work to date, and product characteristics are included herein.

1. INTRODUCTION

The disposal of miscellaneous SNF creates unique waste management issues. Miscellaneous SNFs are all SNFs except commercial, high-volume light-water reactor (LWR) SNF. Historically, there have been two waste management options: (a) direct disposal and (b) reprocessing with conversion of the HLW to glass. However, each approach presents difficulties for those handling miscellaneous SNF.

There are major difficulties with direct disposal of miscellaneous SNF because of the characteristics of the materials:

- Some types of miscellaneous SNFs may not be in chemical forms acceptable for repository disposal.
- The current estimated cost to qualify a single SNF type for the repository is estimated to exceed \$60 million dollars¹. There are dozens of miscellaneous SNF types. Total costs to qualify all SNF types will be very expensive.

- Much of the miscellaneous SNF is highly enriched in U-235; this creates unique criticality and safeguards concerns. Repositories are being designed for low-enriched LWR SNFs.
- Some types of miscellaneous SNFs, such as SNF from nuclear submarines, have classified design information. For repository licensing and safeguards, it is desirable to have no classified information associated with the repository.

There are technical, economic, and policy difficulties in reprocessing these materials to recover uranium and plutonium. Many of these SNFs were not reprocessed in the past because the small quantities of such SNFs and their unique characteristics made reprocessing uneconomic. In addition, U.S. nonproliferation policy discourages reprocessing of SNF.

A new approach, a third option, for management of miscellaneous SNF has been invented.²³ It is direct, single-step conversion of miscellaneous SNF to glass. This report describes a strawman criteria for the HLW glass product, the GMODS process, the equipment, a product glass, and presents the results of preliminary laboratory experiments.

Conventional vitrification processes accept only oxide feeds. If SNF with metal fuel or metal/carbon cladding is to be converted to glass with current vitrification processes, a separate process is first required to oxidize the metals to oxides before the SNF can be fed to a glass melter. This type of oxidation process is very difficult using current technology when processing zirconium, aluminum, stainless steel, or carbon clad SNF. For this reason, vitrification has not been previously considered for processing miscellaneous SNF. GMODS may eliminate these barriers and create a practical way to convert SNF to glass.

2. STRAWMAN CRITERIA

If miscellaneous SNF is to be converted to glass, a set of waste-form performance criteria are required to define goals. The simplest approach is for GMODS to match the waste acceptance criteria defined for the two waste types (HLW glass and LWR SNF) accepted for repository disposal. The criteria are:

- (1) mechanical (package dimensions, handling mechanisms, etc),
- (2) repository waste form performance (chemical behavior), and
- (3) nuclear criticality.

Mechanical and chemical waste form performance criteria have been developed⁴ for acceptance of HLW glass for the proposed Yucca Mountain repository. These criteria provide a basis to define appropriate mechanical and chemical criteria for a HLW glass.

There are also criticality criteria. Current repository designs and licensing approaches are based on disposal of LWR spent fuel with < 2 wt.% fissile content in the uranium. Much of the DOE miscellaneous SNF is high-enriched SNF (enrichments exceeding 90%) that create new criticality issues for the repository.^{5,6}

In a repository, selective dissolution and precipitation of uranium in groundwater, over geological time, creates the potential of concentrating uranium and initiating criticality events if the original uranium is highly enriched. Geological evidence⁷ shows that naturally occurring nuclear reactors have been created in the past by these mechanisms when the uranium enrichment levels exceeded several weight percent U-235. In contrast, no evidence exists of naturally occurring reactors at lower enrichment levels.

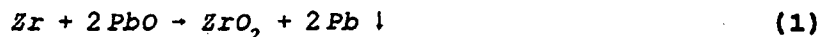
The licensing, safety, and environmental nuclear criticality questions concerning disposal of high-enriched SNF can be avoided by adding miscellaneous SNF and depleted uranium simultaneously to GMODS to create a HLW glass with low-enriched uranium.

A conservative criticality criteria is that the uranium enrichment level of SNF glass should not exceed the average fissile content of LWR SNF going directly to the repository. The fissile content of typical LWR SNF (burnup = 33,000 Mwd/ton) is about 1.4%. LWR SNF contains both U-235 and Pu-239. In time, the Pu-239 decays to U-235 and contributes to the U-235 content. A nuclear criticality criterion of 1.4 wt.% fissile content for the uranium in the glass is used herein. This is consistent with geological evidence that at such enrichments, criticality is unlikely under realistic geological conditions and assures that the glass product fits within the repository licensing and design envelope for LWR SNF.

3. PROCESS DESCRIPTION

The basic concept of GMODS (Fig. 1) is to add miscellaneous SNF, depleted uranium (if required), glass frit, and a sacrificial oxide directly to a glass melter. The characteristic of molten glass systems is that they dissolve oxides—but not metals or organics. The addition of a sacrificial oxide to the molten glass provides a method to oxidize in situ (1) metals to metal oxides and (2) organics to carbon dioxide gas and steam. The metal oxides dissolve into the glass. The carbon dioxide gas and steam exit the melter. The feasibility of GMODS depends upon the selection of the sacrificial oxide and the glass formulation.

The preferred sacrificial oxide is lead oxide (PbO) in a lead borate glass. Lead oxide, which is a component in many glasses, reacts with metals in glass to yield metal oxides and metallic lead (Pb):



The molten lead, the reaction product, sinks to the bottom of the melter. The lead at the bottom of the melter is removed, reoxidized back to lead oxide, and recycled back to the glass melter as new sacrificial oxide. Hence, lead, an oxygen carrier, does not leave the system. The lead oxidation reaction is



The mixture of lead oxide and boron oxide is efficient in oxidizing metals in glass. Lead oxide is a powerful oxidant in this system. Many metals form protective surface oxides that limit chemical reaction rates. In a lead-borate glass, the boron oxide rapidly dissolves oxide protective layers into the glass; this thus allows efficient oxidation of bare metal by the lead oxide.

GLASS-CONVERSION FURNACE

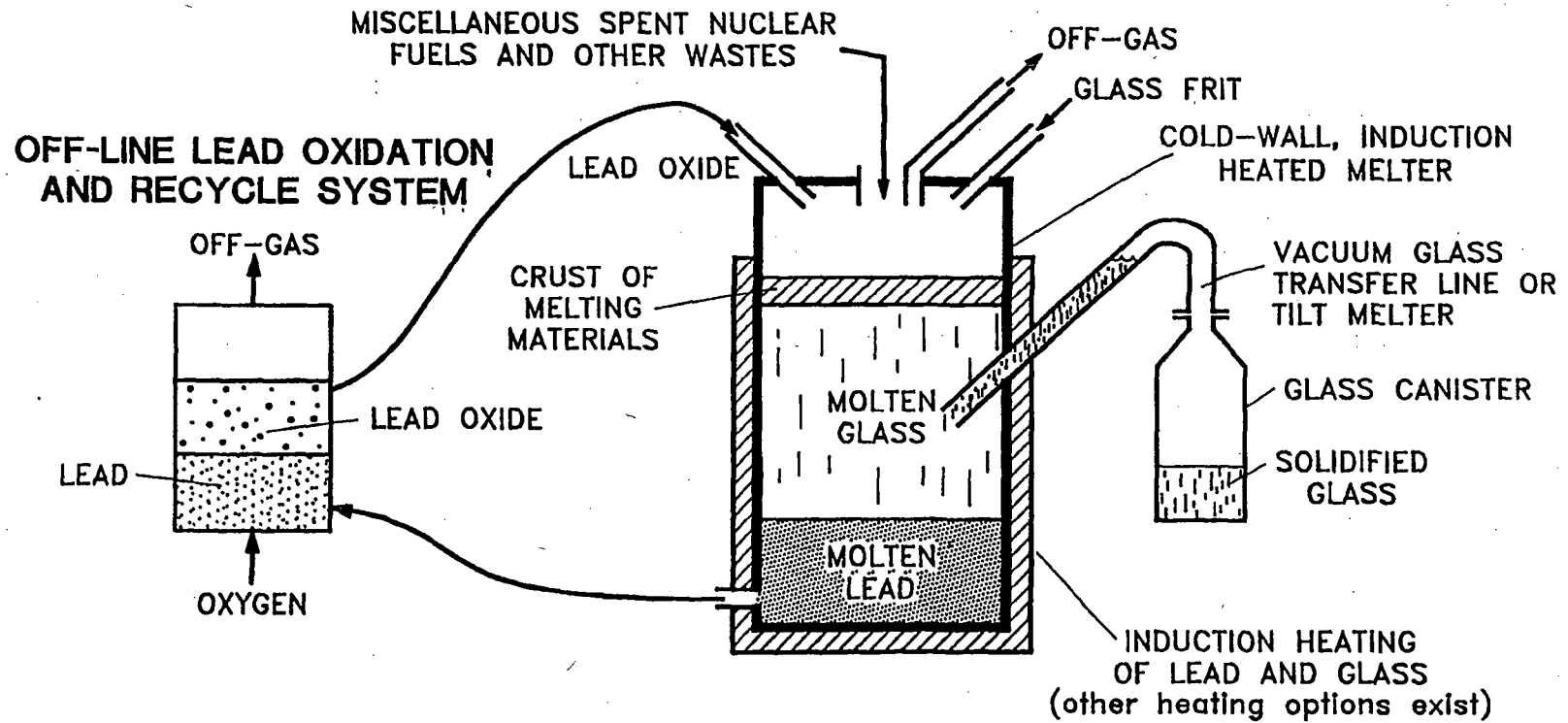


Fig. 1. Glass Material Oxidation and Dissolution System (GMODS) for Direct Conversion of Miscellaneous Spent Nuclear Fuels (SNFs) to Glass.

After dissolution of the SNF, additional glass additives (SiO_2 , etc.) are added to improve the glass quality before the mixture is poured into containers or sent to "marble" production machines for solidification. Optimum glasses for rapid oxidation-dissolution of SNF are different in composition than are glasses for long-term durability; thus, glass additives used to create a more durable glass are introduced after SNF oxidation-dissolution is completed.

If required, the lead oxide may be removed from the final glass before solidification by the addition of carbon, which reduces the lead oxide to lead metal while producing gaseous carbon dioxide [Eq. (5)]. The lead oxide may be removed from the dissolution glass for multiple reasons: (1) better final HLW glass, (2) reduction of the volume of the glass, and (3) avoidance of the costs to provide added sacrificial lead oxide.

GMODS produces limited off-gas because solid lead oxide is the oxidizer. The primary off-gases are volatile fission products and carbon dioxide, which results from the reduction of excess lead oxide using carbon.

4. EQUIPMENT DESCRIPTION

Conceptually, the GMODS consists of three process steps: (1) simultaneous oxidation-dissolution of the SNF into glass, (2) glass refining (adding glass additives, etc.) to obtain the appropriate durable glass, and (3) conversion of lead metal back to lead oxide. These steps may be performed sequentially in a single melter or in multiple melters in series. The choice of option depends upon feed composition, final waste-performance requirements, and throughput.

GMODS requires an induction-heated melter such as those used for the processing of scrap metal and for certain specialty glass-making operations. Induction furnaces with capabilities up to 20 tons are currently used to melt radioactive scrap into shielding blocks and waste packages.

Cold-wall, induction-heated melters may be preferred. In a cold-wall melter, a thin layer of frozen glass separates the molten glass from the melter wall. This separation prevents glass corrosion of the furnace

lining. The higher temperatures (1400° C) possible with such melters allow the use of glass formulations with higher waste loadings and/or the production of more durable glasses. The high waste loading per unit volume minimizes cost.

Cold-wall, induction-heated melters are used industrially to melt titanium and superalloys. They are also being developed too, for radioactive waste processing in France^{8,9} and Russia.¹⁰ The French have an operating melter with a throughput of 50 kg/h and are developing a 200 kg/h melter. The French melters have also been used to melt Zircalloy hulls and hardware into ingots.

5. PRODUCT DESCRIPTION

The final product will be a high-uranium borosilicate glass or glassy slag. Work is ongoing at Savannah River Laboratories¹¹ and elsewhere on developing high actinide loaded glasses. The results of work on glassy slags¹² suggests that they may also be a candidate waste form because of the advantage of higher waste loadings; particularly for materials such as ZrO_2 .

For low-enriched miscellaneous SNF (Hanford-N reactor SNF and the Three Mile Island-2 core debris) high loadings of uranium in the final glass are desirable. The limited data¹¹ show glasses with up to 20% uranium make acceptable waste forms. Higher uranium loadings in waste glasses have not been investigated. Other non-waste management reports in the literature suggest uranium loadings up to 50% may be practical. As the uranium loading in weight percent is increased, the glass density increases. Doubling the uranium loading more than doubles the quantity of uranium per unit volume of glass.

For high enriched SNF, depleted uranium can be added to the glass for criticality control. The addition of depleted uranium to the HLW glass for criticality control may allow reductions in the volume and number of waste packages to the repository. Consider, as an example, the disposal of High Flux Isotope Reactor (HFIR) SNF. The HFIR is the main research reactor at Oak Ridge National Laboratory. This SNF is high-enriched U_3O_8 with aluminum cladding. Its geometry is an upright cylinder (height = 79.1 cm, diam. = 43.5 cm.). The chemical composition is shown in Table 1 for (1) a fresh fuel assembly, (2) the SNF and, (3) after the SNF is converted to oxide form.

Table 1. HFIR New Fuel, SNF and Oxidized SNF Compositions on a per Assembly Basis

	U	Al	O ₂	Fission ^(a)	Total
New Fuel					
Kg	10.1	127.99	1.85	0	139.94
Moles	42.978	4740.4	57.8	0	4841.18
SNF					
Kg	7.9	127.99	1.85	2.2	139.94
Moles	33.617	4740	57.8	18.722	4850.139
Wt. %	5.64	91.46	1.322	1.57	100.
Mole %	0.693	97.73	1.192	0.386	100
In Glass	(b)				
Kg	565.4	127.99	215.712	2.2	911.302
Moles	2376.	4740.	6741	18.722	13875.2
Wt. %	62.04	14.04	23.67	0.24	100.
Mole %	17.124	34.2	48.58	0.135	100.

^(a)Assume 2 moles of fission products per mole of uranium fissioned; uranium enrichment levels: fresh fuel: 93%, SNF: 86.1%, and glass input: 1.4%.

^(b)Input of HFIR SNF into final HLW glass composition after GMODS oxidation-dissolution step. Uranium as U₃O₈, fission products as FO₂

Let us consider 3 treatment options: a theoretical case of direct SNF disposal where criticality is ignored, direct disposal with criticality considered, and direct conversion of HFIR SNF to HLW glass. Assume that the Savannah River Site (SRS) or West Valley HLW canister is used (height = 120 in. diam = 24 in., effective waste volume = 0.625–0.8 m³).

If direct disposal is considered without consideration of nuclear criticality, each HFIR assembly occupies about a fifth of a waste canister.

Using direct disposal with consideration of some criticality effects, about 10 waste packages are required per HFIR SNF assembly. Current estimates are that the criticality limit⁵ for a waste package for high-enriched uranium is 700 g/pkg assuming that there is no interaction between uranium in different waste packages over geological time. *A Caution: there are significant uncertainties about this assumption and what it implies in terms of package separation within a repository over geological time.*

If a HFIR SNF assembly is converted to glass with GMODS, the glass may occupy from about one-fourth to a full waste canister depending upon assumptions. A conservative set of assumptions result in 0.6 m³ of glass per SNF assembly. This assumes that the high-enriched uranium is diluted with 0.2 wt.% depleted uranium to a final uranium assay of 1.4 wt.%. It also assumes a glass that is 20 wt% uranium with a density of 4.8 g/cm³. The loading may be increased by several mechanisms.

- The 20 wt% uranium loading in glass is based on existing data but much higher loading may be possible (see above).
- It is assumed that the entire fuel assembly will be converted to glass. Glass volumes can be reduced if some of the SNF structural material (hardware etc.) is removed from the SNF assembly before conversion to glass.
- There are different estimates of the volume fraction of the waste package that can be loaded with glass for given external package size. For canisters with the same external dimensions, SRS assumes 0.625 m³ of glass, while West Valley assumes 0.8 m³.

There are 3 reasons why the volume of repository waste from conversion of high-enriched SNF to low-enriched uranium glass does not cause large increases in volume compared to the volume of high-enriched SNF in waste packages when criticality is not considered.

- High-enriched SNF is primarily structural material and coolant void space. The volume or mass fraction of the SNF assemblies that is high-enriched uranium is small. Dilution with depleted uranium does not make uranium the dominate component in the glass when measured in moles, the basis of glass formulation and volume.
- Uranium glasses have high densities.

- Glass efficiently fills a waste package. SNF assemblies do not efficiently fit into standard waste packages.

It is noted that the cold-wall, induction-heated melter proposed for GMODS is the same technology developed in France and elsewhere for conversion of hulls and hardware from spent fuel reprocessing into solid ingots to minimize final volumes. An optimum miscellaneous SNF strategy for high enriched SNF might include GMODS and separate melting of SNF hardware that can be removed without release of uranium or fission products.

6. EXPERIMENTAL RESULTS

Thermodynamic calculations and preliminary scoping experiments¹³ were conducted to demonstrate key steps of GMODS. The solubility of various oxides in lead borate glasses with molar compositions from $\text{PbO}:\text{B}_2\text{O}_3$ to $4\text{PbO}:\text{B}_2\text{O}_3$ was investigated. High solubility is required for high waste loadings in the glass and rapid dissolution of oxide layers on SNF. For uranium oxide, the highest solubilities in the lead borate dissolution glass were with an initial glass molar composition of $2\text{PbO}:\text{B}_2\text{O}_3$. This particular lead borate-glass when heated to 1020°C dissolves in excess of 20 wt.% UO_2 + 20 wt.% ZrO_2 . Other experiments showed similar solubility for Al_2O_3 .

Chemical reaction tests demonstrated the conversion of uranium dioxide, Zircalloy-2, aluminum, cerium, and stainless steel to dissolved oxides in the dissolution glass with production of lead metal. Figure 2 shows the reaction of Zircalloy-2 cladding in glass partway through the process. Separated lead is shown in globular form. Experiments have also demonstrated oxidation of carbon with production of metallic lead and gaseous carbon oxide release.

Measurements made of the viscosities of lead-borate glasses and lead-borate glasses with uranium (Table 2) show low glass viscosity in the range of 700 to 800°C , suggesting that the glass oxidation-dissolution process step may operate below 1000°C . High loadings of aluminum and zirconium oxide may raise these viscosities.

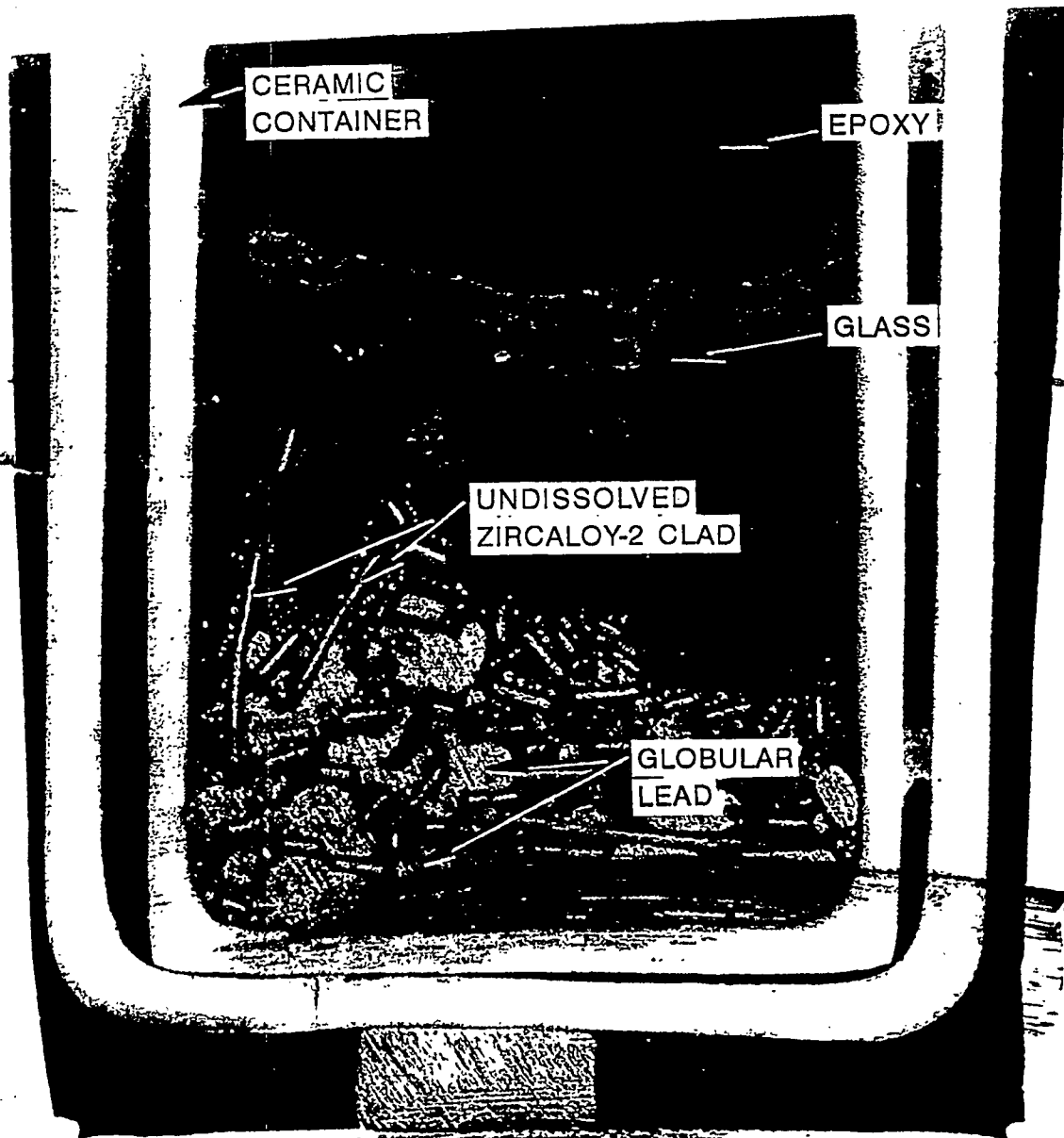


Fig. 2. Dissolution of Zircaloy-2 in Lead-Borate Glass at Half-way Point.

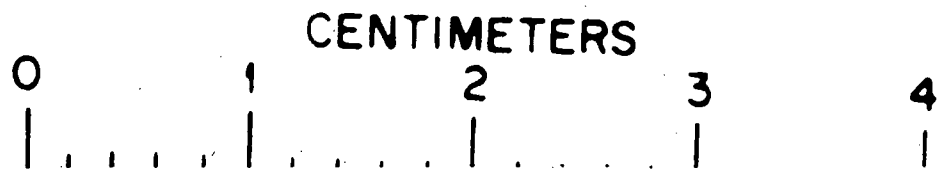


Table 2. Temperature ($^{\circ}\text{C}$) and Viscosity (centipoise) For Different Molar Ratios (R) of Lead Borate Glass and Weight Percent Uranium Oxide in Glass*

R = 1	R = 2	R = 3	R = 4	R = 2
U = 0 wt. %	U = 0 wt. %	U = wt. 0%	U = wt. 0%	U = 20 wt. %
706/263	620/200	603/104	615/75.9	626/1970
750/101	710/47.4	665/59.1	705/57.5	768/116
810/51.6	820/21.8	713/42.3	822/21.3	905/22.2
		803/28.6		

*Example: at 706°C , the glass viscosity is 263 cp for a glass with 1 mol PbO per mole of B_2O_3 ($R = 1$) and 0 wt. % U_3O_8 .

Note: For comparison, antifreeze has a viscosity of 20 cp, while light machine oil has a viscosity of 110 cp.

Added experiments are planned to measure glass physical properties (viscosity, density, thermal conductivity, and heat capacity) and chemical reaction rates for various materials as a function of glass compositions and temperature.

7. CONCLUSIONS

A new process for the direct conversion of SNF to glass has been invented. GMODS may convert SNF that may not be acceptable for the repository because of chemical, mechanical, or nuclear characteristics into a HLW glass suitable for repository disposal.

Thermodynamic calculations indicate process feasibility. Initial proof-of-principle experiments have shown the feasibility of some key chemical reactions. However, significant additional work is required before engineering feasibility could be demonstrated.

REFERENCES

1. J. D. Christian, T. R. Thomas, and G. F. Kessinger, "A Dry Chloride Volatility Process For Processing Spent Nuclear Fuel," *Proc. Spectrum '94: Nuclear and Hazardous Waste Management International Topical Meeting*, Atlanta, Georgia, August 14-18, 1994, p. 1745, American Nuclear Society, La Grange Park, Illinois (1994).
2. C. W. Forsberg, E. C. Beahm, and G. W. Parker, *Patent application to U.S. Patent and Trademark Office: Radioactive Waste Material Disposal*, (1994).
3. C. W. Forsberg, E. C. Beahm, and G. W. Parker, "Direct Conversion of Radioactive and Chemical Waste Containing Metals, Ceramics, Amorphous Solids, and Organics to Glass," *Proc. Spectrum '94: Nuclear and Hazardous Waste Management International Topical Meeting*, Atlanta, Georgia, August 14-18, 1994, p. 1268, American Nuclear Society, La Grange Park, Illinois (1994).
4. U.S. Department of Energy, *Waste Acceptance Systems Requirements Document, Revision 0*, DOE/RW-0351P, Washington D.C., (January 1993).
5. R. P. Rechard et. al., *Initial Performance Assessment of the Disposal of Spent Nuclear Fuel and High-Level Waste Stored at Idaho National Engineering Laboratory*, SAND93-2330, Sandia National Laboratory, Albuquerque, New Mexico (1993).
6. D. Evans and B. Palmer, "Repository Criticality Safety for the DOE Spent Nuclear Fuel Program," *Proc. Fifth Annual Int. Conf. on High-Level Radioactive Waste Management*, Las Vegas, Nevada, May 22-25, 1994, American Nuclear Society, La Grange, Illinois, May 1994.
7. W. G. Culbreth and P. R. Zielinski, "Long Term Effects of Neutron Absorbers and Fuel Matrix Corrosion on Criticality," *Proc. of the Fifth Annual International Conference on High-Level Radioactive Waste Management*, Las Vegas, Nevada, May 22-26, 1994, American Nuclear Society, La Grange Park, Illinois (1994)
8. J. P. Monconyoux and C. G. Sombret, "French High-Level Waste Management Research and Development Program," *Proc. Third International Conference High-Level Radioactive Waste Management*, Las Vegas, Nevada, p. 2406, American Nuclear Society, La Grange Park, Illinois, April 1992.
9. J. P. Monconyoux, R. Boen, M. Puyou, and A. Jouan, "New Vitrification Techniques," *Proc. Third International Conference on Nuclear Fuel Reprocessing and Waste Management*, Sandai, Japan, April 14-18, 1991, American Nuclear Society, La Grange Park, Illinois.
10. I. A. Sobolev et. al., "Vitrification of Radioactive Wastes by Coreless Induction Melting in Cold Crucible," *Proc. Spectrum '94: Nuclear and Hazardous Waste Management International Topical Meeting*, Atlanta, Georgia, August 14-18, 1994, p. 2250, American Nuclear Society, La Grange Park, Illinois (1994).

11. W. G. Ramsey, "Innovative Glass Compositions for Immobilizing Actinide Elements," *Proc. Spectrum '94: Nuclear and Hazardous Waste Management International Topical Meeting*, August 14-18, 1994, Atlanta, Georgia, American Nuclear Society, La Grange Park, Illinois (1994).
12. X. Feng, G. Ordaz, and P. Krumrine, "Glassy Slag—A Complimentary Waste Form to Homogeneous Glass for the Implementation of MAWS in Treating DOE Low-Level/Mixed Waste," *Proc. Spectrum '94: Nuclear and Hazardous Waste Management International Topical Meeting*, Atlanta, Georgia, August 14-18, 1994, American Nuclear Society, La Grange Park, Illinois (1994).
13. C. W. Forsberg et. al., *Glass Material Oxidation and Dissolution System (GMODS) for Direct Conversion of Plutonium Containing Materials to Glass*, ORNL-6825, Oak Ridge National Laboratory, Oak Ridge, Tennessee (In Preparation).

The Thorium Molten Salt Reactor : Moving On from the MSBR

L. Mathieu, D. Heuer, R. Brissot, C. Le Brun, E. Liatard, J.-M. Loiseaux,
O. Méplan, E. Merle-Lucotte, A. Nuttin and J. Wilson,
Laboratoire de Physique Subatomique et de Cosmologie ,
53, avenue des Martyrs, F-38026 Grenoble Cedex, France

C. Garzenne, D. Lecarpentier, E. Walle,
EDF-R&D, Département SINETICS,
1 av du Général De Gaulle, 92140 Clamart, France

Abstract

A re-evaluation of the Molten Salt Breeder Reactor concept has revealed problems related to its safety and to the complexity of the reprocessing considered. A reflection is carried out anew in view of finding innovative solutions leading to the Thorium Molten Salt Reactor concept. Several main constraints are established and serve as guides to parametric evaluations. These then give an understanding of the influence of important core parameters on the reactor's operation. The aim of this paper is to discuss this vast research domain and to single out the Molten Salt Reactor configurations that deserve further evaluation.

Introduction

In order to reduce CO₂ emissions in the coming decades, and, as a result, to mitigate global warming, it appears necessary to stabilize or, better, to reduce the use of fossil fuels. Resorting to a sustainable version of nuclear power may help replace classical energy production partially and thus satisfy an increasing world energy demand while conserving the climate and natural resources. The Generation IV International Forum for the development of new nuclear energy systems [1] has established a set of goals as research directions for nuclear systems: enhanced safety and reliability, reduced waste generation, effective use of uranium or thorium ores, resistance to proliferation, improved economic competitiveness. Molten Salt Reactors (MSR) are one of the systems retained by Generation IV. MSRs are based on a liquid fuel, so that their technology is fundamentally different from the solid fuel technologies currently in use. Some of the advantages specific to MSRs (in terms of safety/reliability, for example) originate directly from this characteristic [2]. Furthermore, this type of reactor is particularly well adapted to the thorium fuel cycle (Th-²³³U) which has the advantage of producing less minor actinides than the uranium-plutonium fuel cycle (²³⁸U-²³⁹Pu) [3, 4]. Moreover, while breeding or regeneration in the U-Pu cycle can be obtained only with a fast neutron spectrum, in the Th-²³³U fuel

cycle it can, in principle, be obtained with a more or less moderated neutron spectrum. In a thermal neutron spectrum, poisoning due to the Fission Products (FP) being worse than in a fast neutron spectrum, the rate at which fuel reprocessing is performed can become a major issue. Because, in an MSR, the fuel is liquid, continuous extraction of the FPs is a possibility. Although MSRs can be operated as incinerators they will be discussed in this paper only as electricity producing critical systems.

In 1964, the Molten Salt Reactor Experiment (MSRE) was initiated at the Oak Ridge National Laboratory (ORNL). Generating 8 MWth of power, the reactor was operated without problems and with different fuels (²³⁵U then ²³³U) over several years. The expertise gained during this experiment led, in the 1970s, to the elaboration of a power reactor project, the Molten Salt Breeder Reactor (MSBR [5]). The studies demonstrated that fuel regeneration is possible with the thorium fuel cycle in an epithermal spectrum, provided very efficient and, as a consequence, constraining, on-line chemical reprocessing of the salt is achieved. Over the past few years, the MSBR has been reassessed in the light of new calculating methods [3, 4] so as to elaborate a new reactor concept that we call the Thorium Molten Salt Reactor (TMSR).

The MSBR suffered from several major drawbacks and was discontinued. The goal being, at the time, to obtain as high a breeding ratio as possible, the on-line chemical reprocessing unit considered had to process the entire salt volume within 10 days and this was very complex [6]. Because of this complexity, the project is often considered unfeasible. In addition, recent calculations have shown that the global feedback coefficient for this system is slightly positive. This contradicts the results that had been presented. The difference is probably due to the fact that, at the time, the compositions were handled in a homogeneous way while they are handled heterogeneously today. This critical issue makes the MSBR a potentially unstable system in some situations.

The aim of this paper is to present solutions to these problems. In our search for better reactor configurations, we have identified several constraints that are discussed in the first part of this work. We then discuss the impact of the various reac-

tor parameters on these constraints, i.e. chemical reprocessing, channel size, fuel volume and the proportion of heavy nuclei (HN) in the salt. A synthesis of these studies is set forth in the last section.

This work is based on the coupling of a neutron transport code (MCNP [7]) with a materials evolution code. The former calculates the neutron flux and the reaction rates in all the cells while the latter solves the Bateman equations for the evolution of the materials composition in the cells. These calculations take into account the input parameters (power released, criticality level, chemistry,...), by adjusting the neutron flux or the materials composition of the core on a regular basis. Our calculations are based on a precise description of the geometry and consider several hundreds of nuclei with their interactions and radioactive decay; they allow fine interpretation of the results. All the data discussed in this paper result from the evolution of the reactor over 100 years.

1 Constraints

We identify five major constraints in this study: safety, chemical reprocessing feasibility, fuel regeneration capability, materials life span, and initial inventory. Other constraints could be considered, such as waste minimization, thermal-hydraulics, or proliferation resistance but we concentrate essentially on the above five major constraints. We seek to understand the impact of the reactor's defining parameters on these constraints. In so doing, we can single out the best reactor configurations according to the weight assigned to each of the constraints.

1.1 Safety

In the work we present here this constraint concerns essentially the evolution of the feedback coefficients that should be negative. The more kinetic aspects of the reactor's safety properties are not considered here. Additionally, the ways in which we change the concept do not modify the other MSR safety properties, such as fuel dumping and the fact that MSRs are free of high pressure areas.

The feedback coefficients, $\frac{dk}{dT}$, are a measure of the variation of the multiplication factor (dk) with the temperature of the core or of a portion of the core (dT). The global feedback coefficient can be broken up into several strongly uncorrelated partial coefficients, each of which characterizes the variation of a specific parameter: the effects due to the expansion of the salt¹, and the purely thermal effects of the salt and of the graphite. This reads:

$$\left(\frac{dk}{dT}\right)_{total} = \left(\frac{dk}{dT}\right)_{density} + \left(\frac{dk}{dT}\right)_{Doppler} + \left(\frac{dk}{dT}\right)_{graphite}$$

In order for the reactor to be intrinsically safe, a temperature increase must not induce an increase of the reactivity and, as

¹ The heating of the salt induces a widening of the resonances due to the Doppler effect and a change in the neutron spectrum moderation due to the salt. Both of these effects are considered together, under the term "Doppler".

a consequence, of the power released by fissions. For this reason, the $\left(\frac{dk}{dT}\right)_{total}$ coefficient must be negative. The thermal kinetics of the graphite, which is heated by gamma radiation and cooled by the salt, is much slower than that of the salt. Making allowance for this delay between the heating of the salt and the heating of the graphite, the coefficient for the salt alone, that is the sum $\left(\frac{dk}{dT}\right)_{density} + \left(\frac{dk}{dT}\right)_{Doppler}$ must also be negative. The degree of safety can be further increased if the density coefficient is made negative. This implies that any local loss of density, e.g. because of a bubble, decreases the reactivity of the system.

The uncertainties on these values are related to statistical errors that are well identified and can be reduced, but also to systematic errors that are not quantified and are related, for example, to uncertainties in cross section evaluations. For this reason, the feedback coefficients must be sufficiently negative to ensure unambiguous stability.

1.2 Feasibility of the Chemical Reprocessing

The term feasibility reflects the complexity associated to the chemical reprocessing. Indeed, some of the separation processes are considered too difficult to be implemented. This can have several causes: the processes considered are not well understood or mastered, the flow of materials to be processed is too large, the reprocessing implies direct coupling to the reactor core,...

The objective is to devise the simplest possible system that is compatible with the other constraints. In particular, it will be important to avoid excessive deterioration of the system's fuel regeneration capability.

1.3 Fuel Regeneration Capability

The breeding ratio expresses the balance between the creation of ²³³U through neutron capture on ²³²Th and the destruction of ²³³U through fission or neutron capture. The breeding ratio in a critical reactor can thus be written:

$$BR = \frac{r_{c,232Th} - r_{c,233U}}{r_{f,233U} + r_{c,233U}}$$

With r_c and r_f respectively the capture rate and the fission rate of the different isotopes.

A breeding ratio less than 1 implies that ²³³U is consumed so that fissile matter must be fed into the core on a regular basis. This inevitably increases both the volume and the frequency of transfer of these dangerous materials. Similarly, a breeding ratio larger than 1 implies that the excess ²³³U produced be placed in storage and/or transported. Because, in all cases, the initial fissile matter inventory has to be produced by other means (e.g. in pressurized water reactors or fast neutron reactors) the highest possible breeding ratio does not necessarily have to be sought.

In order to satisfy the regeneration constraint, we try to achieve a breeding ratio at least equal to 1, knowing that any excess neutrons can always be put to use (improved safety, transmutation capabilities, ...).

1.4 Materials Life Span

This concerns in particular how the graphite reacts to irradiation exposure. Beyond a certain degree of damage, it becomes the seat of swelling. Graphite's life span is determined by the time it takes to reach a fluence limit, that we will set to 2.10^{22} n/cm² at a temperature of 630 °C [8]. In our calculation, we consider only the neutrons whose energy is larger than 50 keV, i.e. those that create real damage in the graphite.

The goal, with this constraint, is to obtain a life span that is not too short so as to avoid replacing the core graphite too frequently.

1.5 Initial Inventory

The inventory, here, is the amount of ²³³U needed to start a 1 GWe power reactor. The smaller the inventory, the faster the deployment of a fleet of such reactors can be achieved [9, 10].

Without excluding configurations with a large inventory, its minimization will be sought.

These constraints are not all equivalent; a weighting factor can be assigned to each of them. This factor depends on the technologies available and the goals that guide reactor choices. As the performance of a system depends on how the constraints are weighted and on how difficult it is to satisfy them, it is not possible to specify the "best" solution. The only possibility is to identify a number of interesting trends. This yields a better understanding of the system and can lead to the definition of a power reactor (stringent constraints) or of a demonstration unit (less stringent constraints).

2 Impact of the Parameters on the Constraints

In this section, we examine how various reactor parameters impact the five constraints discussed above. In order to be able to compare the systems studied, we found it useful to define a standard system from which the different studies could stem.

Our standard system is a 1 GWe graphite moderated reactor. Its operating temperature is 630 °C and its thermodynamic efficiency is 40 %. The graphite matrix comprises a lattice of hexagonal elements with 15 cm sides. The total diameter of the matrix is 3.20 m. Its height is also 3.20 m. The density of this nuclear grade graphite is set to 1.86. The salt runs through the middle of each of the elements, in a channel whose radius is 8.5 cm. One third of the 20 m³ of fuel salt circulates in external circuits and, as a consequence, outside of the neutron flux. A thorium and graphite radial blanket surrounds the core so as to improve the system's regeneration capability. The properties of the blanket are such that it stops approximately 80 % of the neutrons, thus protecting external structures from irradiation while improving regeneration. We assume that the ²³³U produced in the blanket is extracted within a 6 month period.

The salt used is a binary salt, LiF - (HN)F₄, whose (HN)F₄ proportion is set at 22 % (eutectic point), corresponding to a melting temperature of 565 °C. The salt density at 630 °C is

set at 4.3 with a dilatation coefficient of $10^{-3}/^{\circ}\text{C}$ [11]. We assume that helium bubbling in the salt circuit is able to extract the gaseous fission products and the noble metals within 30 seconds. The standard reprocessing we consider is the delayed reprocessing of the total salt volume over a 6 month period with external storage of the Pa and complete extraction of the FPs and the TRansUranians (TRU) (Figure 1).

2.1 Influence of the Reprocessing

2.1.1 How Slow Delayed Reprocessing Works

As previously stated, the MSBR reprocessing is considered too complex to be feasible in the next few decades. The effectiveness of this reprocessing rested mainly on the extraction and storage of the protactinium away from the neutron flux so as to avoid, insofar as possible, the production of ²³⁴U by neutron capture. The half-life of ²³³Pa is 27 days and its extraction has to be markedly faster if it is to be efficient. That is why the reprocessing of the total core volume in 10 days was contemplated.

The difficult part of the reprocessing is Fission Product extraction in the presence of thorium. The idea, with slow reprocessing, is to first extract the thorium, so as to avoid being handicapped by its presence in the FP extraction process. This method could not be applied in the MSBR because of the large thorium flow involved, reaching several tons per day while it is only a few hundreds of kilograms per day in the case of a six month reprocessing time.

In addition, with slow reprocessing, the nuclear core can be disconnected from the processing unit, small amounts of the salt being processed individually, instead of resorting to continuous on-line reprocessing, as in the MSBR. This is a source of simplification, it allows easier control of the procedure while making the core less sensitive to possible problems in the reprocessing unit.

Figure 1 gives a general view of what slow reprocessing could entail. Some of the stages shown in this general schematic, such as protactinium storage, can be eliminated while maintaining the primary assets of the reprocessing. Likewise, the neptunium extracted in the course of the first fluorination, and the other TRansUranians can be either reinjected in the core or managed separately. The advantage, in the first option, is that an "incinerating" configuration is obtained, insofar as all the TRUs are kept in the core. With the second option, the production of americium, curium, and other heavier elements is significantly reduced.

The time allocated to cleaning the salt and reinjecting it can be extended considerably. Indeed, if the time needed to reprocess the core volume is equal to the time before reinjecting the salt, there is as much salt outside the core as inside it. Thus, up to 6 months can separate the extraction of the fuel salt and its reinjection in the core, after removal of the FPs. The fissile matter inventory is not increased, however, thanks to the possibility of extracting the uranium during a preliminary fluorination stage. In the case of slow reprocessing, we assume very good extraction efficiencies (they are set to 1 in the calculations) because plenty of time is available.

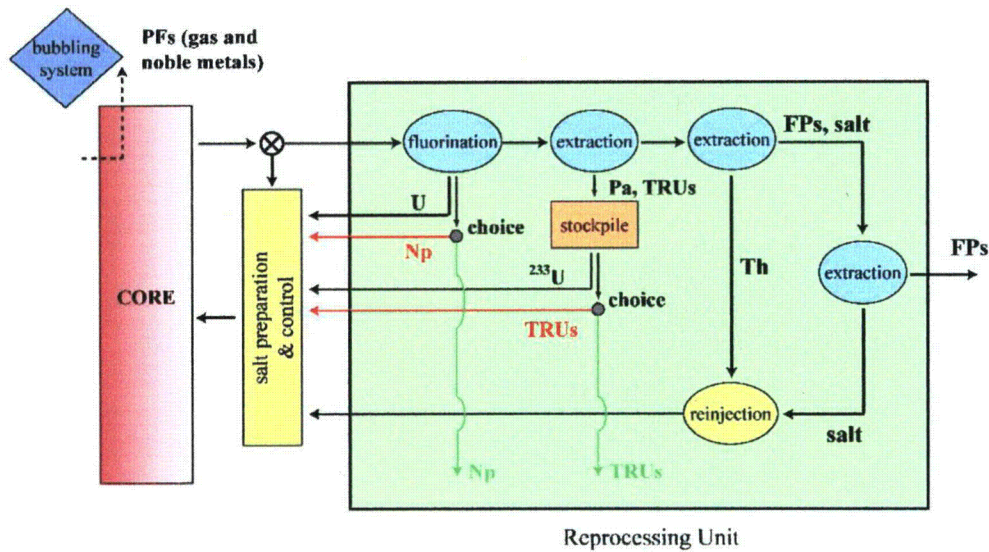


Figure 1: Slow reprocessing overview

It is too early to say that such a reprocessing scheme solves the feasibility issues; it is, however, possible to assert that the simplification of the system improves its feasibility. The impact of this reprocessing on the other constraints, in particular those of regeneration and the feedback coefficients has to be assessed.

2.1.2 Impact of the Reprocessing Time

In Table 1, the breeding ratios obtained at equilibrium are given for various reprocessing options as applied to the reactor configuration described previously. The best breeding ratio is obtained with the MSBR reprocessing and the worst with no reprocessing other than helium bubbling in the core, and ^{233}U recovery in the blanket.

In the table, the MSBR reprocessing is labeled “fast (10 days)” because of the rate at which the protactinium is to be extracted. However, the extraction of the FPs is partial, making the real reprocessing rate longer (equivalent to 50 days for the FPs that capture the most). The option labeled “bubbling only” is set apart because it is dramatically different from the other configurations, making any comparison with them tricky (no equilibrium state).

Varying the reprocessing time from 3 months to 2 years induces about a 0.06 loss in the breeding ratio. For these four configurations, the proportion of protactinium stored outside of the neutron flux is, respectively, 30 %, 20 %, 10 % and 5 %. However, the change in the breeding ratio is due mainly to the change in the capture rate of the FPs and, to a lesser degree, of the TRUs. On the contrary, with fast reprocessing, 80 % of the protactinium is stored outside of the neutron flux and that is the direct cause of the system’s good breeding ratio, way before the FPs and the TRUs. Thus, unless it is extracted rapidly, the Pa’s incidence on regeneration is minor.

We now know the leeway afforded by the reprocessing, since a doubling of the reprocessing time induces a breeding ratio

Reprocessing time	Breeding ratio	dk/dT (pcm/°C)
Fast (10 days)	1.062	-2.25
Slow (3 months)	1.024	-2.37
Slow (6 months)	1.000	-2.36
Slow (1 year)	0.986	-2.39
Slow (2 years)	0.961	-2.50
Bubbling only	0.562	-2.2

Table 1: Breeding ratio and feedback coefficient for several reprocessing options. The statistical error on the feedback coefficient is less than 0.05 pcm/°C.

loss of about 0.02. To be precise, we should add that the degradation of the breeding ratio is three times smaller in configurations with a fast neutron spectrum, where the proportion of graphite in the core is reduced.

It is important to note that the reprocessing option chosen has a moderate impact on the feedback coefficients, as shown in the table. This means that reprocessing time and safety can, in a first approximation, be considered to be independent.

2.1.3 Destination of the TRansUranians

As previously stated, the TRUs can either be fed back into the core or they can be managed separately (incinerated in sub-critical reactors, incinerated in fast neutron reactors, or placed in storage). The choice has an impact on the regeneration capabilities, as shown in Table 2. Indeed, even if some of the TRUs fission, they impair the neutron balance because of their high capture rates. In the auto-incinerating configuration, the most capturing TRUs reach equilibrium within about 30 years and contribute to the deterioration of the neutron balance.

Reprocessing	Breeding ratio	dk/dT (pcm/°C)
TRUs extracted	1.000	-2.36
TRUs reinjected	0.987	-3.12

Table 2: Breeding ratio and feedback coefficient according to TRU management. The statistical error on the feedback coefficients is less than 0.05 pcm/°C.

In the same table, the influence of the TRUs on the feedback coefficients is also shown. This coefficient is slightly improved if the TRUs are kept in the core. This is because the TRUs harden the spectrum, as will be discussed further in Section 2.2. Note that, in a fast neutron spectrum configuration, the impact of TRU reinjection on both the breeding ratio and the feedback coefficients is reduced.

TRU extraction, however, is advantageous in terms of waste production. When they are submitted to a neutron flux, TRUs form, progressively, significant amounts of very heavy elements such as curium. The ratio of capture to fission cross sections is not favorable to incineration in this type of reactor because of its epithermal neutron spectrum. If these elements are removed from the reactor core, larger amounts of neptunium, formed constantly by captures on ^{236}U , are extracted, but the production rate of the other actinides is reduced, as shown in Table 3. The goal, then, is to obtain TRUs that are more manageable in view of incorporating them in the fuel of Fast Neutron Reactors. If such an outlet for TRUs is not available, this option is of no interest.

	TRUs reinjected (inventory)	TRUs extracted (inventory) (output flow)	
Np	105 kg	15 kg	4.3 kg / TWh
Pu	265 kg	2.7 kg	770 g / TWh
Am	7.2 kg	0.5 g	0.14 g / TWh
Cm	17.5 kg	0.1 g	30 mg / TWh

Table 3: TRU production and in core inventory at the end of the time period covered by this study (100 years) for two TRU destinations; reprocessing time is 6 months. The output flow calculation is based on 7 TWh per year energy produced.

2.2 Influence of the Size of the Channels

The size of the channels in which the salt circulates is a fundamental parameter of the reactor. Since the size of the hexagons is kept constant in all of our studies, the size of the channels determines the moderation ratio. Changing the radius of the channels modifies the behavior of the core, placing it anywhere between a very thermalized neutron spectrum and a relatively fast spectrum.

The two extreme possibilities correspond respectively to a large number of very small channels and a single big salt channel. In the latter configuration, there is no graphite in the

hexagons and the core consists in a single channel. In order to allow a comparison of the results with those of the other configurations, in this case, the hexagons are treated as salt channels with an equivalent area (channel radius: 13.6 cm.).

For the configurations in which the channel radius is equal to or larger than 10 cm, it is essential that the graphite of the axial reflectors be replaced with less moderating materials (e.g. zirconium carbide). Otherwise, the fissions occur massively in the vicinity of the reflectors instead of within the core.

As shown in Figure 2, the radius of the channels has a strong impact on most of the constraints².

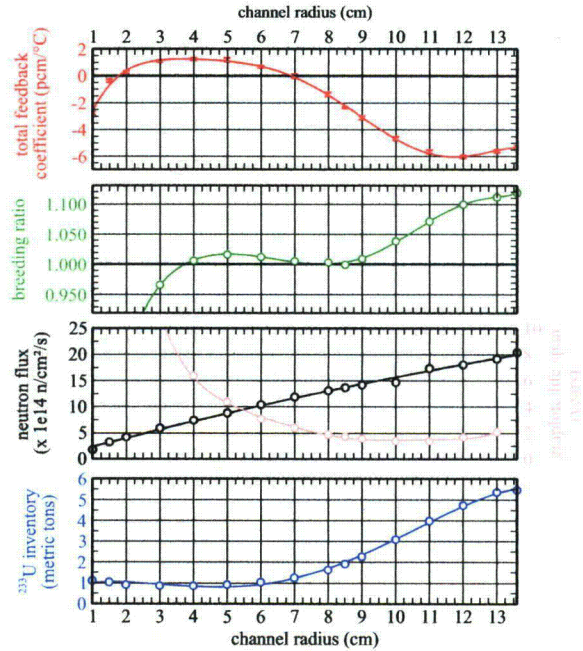


Figure 2: Influence of the channel radius on four of the five constraints (configuration: variable radius, 20 m³ salt, 630°C, 22% (HN)F₄)

2.2.1 Safety Constraint

The study of the feedback coefficients requires a fine analysis of the neutron spectra involved. These are shown in Figure 3 for different channel sizes up to the single channel configuration. The cross section resonances of the materials present in the core have a strong impact on the neutronic behavior of the reactor. The main resonances are visible: fission of ^{233}U at about 2 eV, ^{234}U capture at 5 eV, ^{232}Th capture near 22 eV, and diffusion on ^{19}F near 25, 50 and 100 keV.

As shown in Figure 2, the total feedback coefficient becomes rather strongly negative as the spectrum hardens. This

² The moderation ratio can seem to be a more universal parameter but, like the radius of the channels, it is also influenced by other parameters. An identical moderation ratio can yield very different results according to the density of the materials involved or the size of the hexagons.

evolution is due to the conjoined variation of the three sub-coefficients, Doppler, density and graphite, as illustrated in Figure 4.

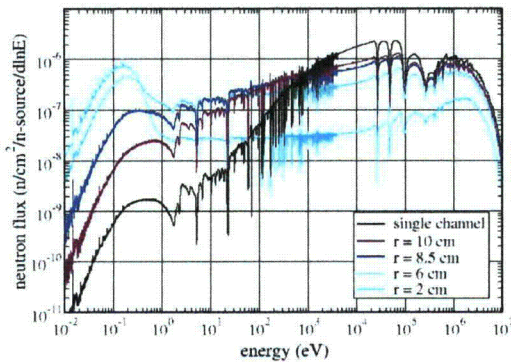


Figure 3: Neutron spectrum for several channel radii (configuration: variable radius, 20 m³ salt, 630 °C, 22% (HN)F₄)

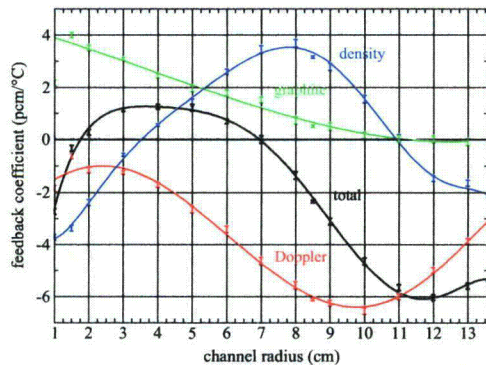


Figure 4: Total feedback coefficient and feedback coefficient components versus channel radius (configuration: variable radius, 20 m³ salt, 630 °C, 22% (HN)F₄)

The Doppler coefficient is linked to the ²³³U fission resonance and the ²³²Th capture resonance (and, to a lesser degree, to the ²³⁴U capture resonance). These two elements have opposite effects on the feedback coefficient: ²³³U worsens it whereas ²³²Th improves it. The thermal agitation of the salt nuclei induces a widening of these resonances so that their influence is increased. The value of the Doppler coefficient depends on how intense the flux is at these resonance values. When the spectrum hardens, the flux is more intense for high energies and less so for low energies, the thorium resonances are favored (main resonance located at 22 eV while that of ²³³U is at 2 eV). The Doppler coefficient then becomes more negative. Beyond a certain degree of spectrum hardening, the large resonances of both thorium and uranium lie in a zone where the flux has

a low intensity and their importance is reduced. This explains the worsening of the Doppler coefficient for large radii.

The density coefficient is related to the expansion of the salt which pushes a fraction of the fuel outside of the moderated zone. The consequence is spectrum softening because the proportion of graphite to salt is larger, thus increasing the fission rate. The effect is small for small radii where thermalization is already very efficient and where it is counterbalanced by captures in the graphite. For large radii, the thermal part of the spectrum contributes practically nothing in the neutron balance and the effects of neutron escape are felt more strongly. The density coefficient can become negative when the effects of captures in the graphite (small radius, large proportion of graphite) or of neutron escapes (large radius, fast neutron spectrum) dominate over the effects of thermalization.

The graphite coefficient comes from an energy shift of the thermal part of the neutron spectrum (around 0.2 eV), due to heating of the moderator. This shift increases the fission rate because of a small low energy (0.3 eV) resonance in the fission cross section of ²³³U [4]. Its impact on the stability decreases as the amount of graphite in the core decreases and as the influence of the thermal portion of the spectrum weakens.

2.2.2 Regeneration Constraint

The capacity to regenerate the fuel varies a great deal with the size of the channels. This can be explained on one hand by the number of neutrons available and, on the other hand, by the increased neutron losses in configurations with small channel radii. The number of neutrons available represents the number of leftover neutrons once both the chain reaction and the regeneration are ensured. This is defined by:

$$N_a = \nu - 2(1 + \alpha)$$

Where α is the mean capture to the mean fission cross section ratio of ²³³U. These available neutrons are distributed mainly between sterile captures and supplementary captures in thorium (breeding). N_a reaches a minimum at about $r = 8.5$ cm because of the variations of α with the neutron spectrum. For small radii, the strong dip in the breeding ratio is due to neutron losses in the graphite because there is so much of it.

2.2.3 Materials Life Span Constraint

The mean cross sections decrease dramatically with the hardening of the neutron spectrum. As increasing the inventory does not compensate for this loss, the neutron flux has to be increased in order to keep the power constant.

While this phenomenon is linear, this is not true of the core graphite's life span, as shown in Figure 2. A few items have to be stressed:

- The graphite in the center undergoes a flux that is more intense than in the periphery. The life span we provide is averaged over the entire core.
- The maximum fluence in the graphite decreases when the temperature increases and the temperature is not uniform. Since the graphite is heated by gamma radiation

and cooled by the salt, the temperature is higher between channels and lower on the channel surface. The temperature difference increases as the channels are further apart. This means that configurations with a smaller channel radius should have a smaller maximum authorized fluence than those with a larger channel radius.

Generally, the flux in the graphite is directly related to the flux in the salt so that increasing the flux in the salt reduces the graphite's life span. It is thus considerably shorter with larger channel radii than with smaller ones.

As can be noticed, the graphite life span curve does not extend all the way to the single channel configuration since, in that configuration, there is no graphite inside the core (except that of the blanket). This configuration then has an asset in that it almost completely solves the issue of the graphite's life span.

2.2.4 In Core Inventory Constraint

For the reactor to be critical, the fissile matter inventory has to be adjusted when the neutron spectrum hardens. Indeed, the mean ^{233}U fission cross section and the mean ^{232}Th capture cross section decrease as the energy of the neutrons increases but the evolution is not identical for the two isotopes. Two different operating regimes can be singled out as shown in Figure 2.

- For small channel radii, the cross section decreases practically in the same way for the two isotopes and the inventory required does not change much.
- For larger radii, beyond 7 cm, the mean fission cross section of ^{233}U decreases faster than the capture cross section of ^{232}Th so that the inventory has to be increased significantly.

2.3 Influence of the Salt Volume

The power per unit volume of salt (specific power) is a determining parameter in a reactor's behavior. In the reference configuration, it amounts to about 250 W/cm^3 for the salt in the core. This parameter can be modified in two ways: by changing the fuel volume at fixed power or by changing the total reactor power at fixed salt volume. These two options yield similar results and only the first one is discussed in this paper.

Since the flow of Heavy Nuclei is considered to be a key factor for the feasibility of the chemical reprocessing, the reprocessing time is adjusted so as to keep this flow constant from one system to the other. Thus, doubling the salt volume implies that core reprocessing takes twice as long. The incidence of the salt volume on the various constraints is rather simple, as shown in Figure 5.

The size does not have a significant impact on the feedback coefficients because the neutron spectrum changes very little with the size. The slight evolution of the coefficient is due to the difference in neutron escapes, which are more likely in smaller reactors.

The evolution of the breeding ratio as the salt volume increases has two main causes: the difference in neutron escapes, and the change in specific power, losses due to the Pa being

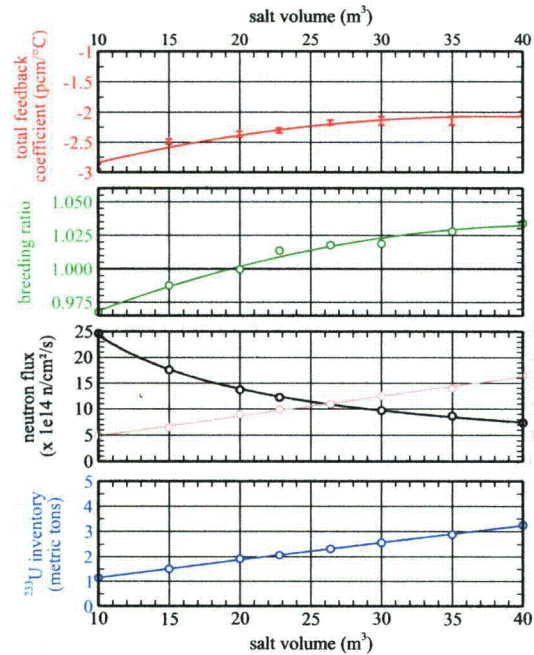


Figure 5: Influence of the salt volume on four of the five constraints (configuration: $r = 8.5 \text{ cm}$, variable salt volume, 630°C , 22% (HN)F₄)

a direct function of the specific power. FP capture rates do not play a significant role in this evolution. Unlike Pa, whose inventory is determined mainly by its rapid radioactive decay, their concentration at equilibrium depends on the reprocessing time. The longer reprocessing time exactly compensates the effect due to the smaller specific power.

The neutron flux in the core is directly related to the specific power and the graphite's life span varies accordingly. Similarly, the inventory in the core depends on the volume but the effect is not directly proportional, because neutron escapes are different.

One last important aspect is the thermal hydraulic constraint. The thermal power is evacuated by the fuel which thus has to circulate in the exchangers. A limit has to be set on the out of core salt volume so as to allow reactor control: the delayed neutrons precursors migrate away from the neutron flux along with the salt. In our studies, the external salt volume is 1/3 of the total volume. Heat evacuation becomes more difficult as the specific power increases. Small sized or high power reactors are at a disadvantage in this respect.

2.4 Influence of the Salt Composition

2.4.1 Elimination of the Be

By definition, the salt plays a central role in MSR. Serving as the solvent for the fuel, as the moderator and as the coolant, it has to have many characteristics specific to the neutronic as well as the chemical, hydraulic, or thermal aspects. Like the

MSRE, the MSBR was based on a fluoride salt, because of its good neutronic properties (capture rate and moderating capability) in a thermal spectrum. Lithium was chosen for the same reasons and beryllium because it brought the melting temperature down to 490 °C. The salt composition was 71.7% LiF - 16% BeF₂ - 12.3% (HN)F₄³.

Our first step in studying the influence of the salt composition was to eliminate beryllium from the salt bringing it to the eutectic point 78% LiF - 22% (HN)F₄. All the studies discussed up to now were done with this composition. The reasons for eliminating beryllium are based mainly on problems with its chemistry, its toxicity, and its availability. The proportion of heavy nuclei in the eutectic changes drastically and its melting point increases from 490 °C to 565 °C⁴. This temperature increase remains moderate and it seems manageable with the commonly used structure materials. Because the significantly higher proportion of Heavy Nuclei has a strong impact on the in core inventory and on the breeding ratio, we have decided to reduce the salt volume from 40 m³ (MSBR) to 20 m³ (reference configuration for these studies) so as to keep the same amount of Heavy Nuclei in the reactor and, as a result, similar neutronic behavior.

The elimination of the beryllium impacts all five constraints. The presence of a ternary component in the salt seems to complicate the reprocessing chemistry, the risk being that this element be extracted instead of the target elements. Thus, using the LiF - (HN)F₄ salt could simplify fuel reprocessing and, as a result, bring it closer to feasibility. The impact on the other constraints is shown in Table 4. The spectrum is harder with the binary salt because of the larger proportion of HN. This translates directly into an improvement of the feedback coefficient and a larger inventory. The change in the breeding ratio is due jointly to the increased proportion of HN (positive action) and to the increased specific power (negative action). The latter also implies a neutron flux increase which, combined with the faster neutron spectrum, leads to a significant deterioration of the graphite's life span.

	LiF - BeF ₂ (40 m ³)	LiF (20 m ³)
Feedback coeff. (pcm/°C)	-1.57	-2.36
Breeding ratio	1.009	1.000
Neutron flux (x10 ¹⁴ n/cm ² /s)	8.6	13.7
Graphite life span (years)	3.3	1.8
²³⁵ U inventory (kg)	1650	1925

Table 4: Constraints according to the type of salt used to dissolve the fuel. The statistical error on the feedback coefficients is less than 0.05 pcm/°C (configuration: r = 8.5 cm, variable salt volume, 630 °C, variable (HN)F₄ proportion).

The elimination of beryllium has an additional and signif-

³ The composition that we really used in our tests with this type of salt [4] is: 70% LiF - 17.5% BeF₂ - 12.5% (HN)F₄.

⁴ In order to make comparisons easier and because the temperature difference is not large, the studies with the 78% LiF - 22% (HN)F₄ salt were done at the same temperature as in previous studies [3, 4], i.e. 630 °C.

icant advantage, that is not related to the constraints that we have identified in this paper. Tritium is produced, in a system like the MSBR, by the (n,nt) reaction on ⁷Li and the (n,t) reaction on ⁶Li, producing 2/3 and 1/3 respectively of the tritium [4]. The lithium used is 99.995 % enriched with ⁷Li; the ⁶Li is rapidly consumed, unless it is regenerated by an (n,α) reaction on ⁹Be. With the elimination of beryllium, this reaction cannot occur and, as a result, the production of tritium is reduced.

2.4.2 Evaluation of the LiF - (HN)F₄

Temperature increase : The proportion of Heavy Nuclei in the binary salt can be adjusted. As it is reduced, the melting point increases, reaching 845 °C with pure LiF. Common structure materials cannot withstand such a temperature increase. However, new promising solutions based on carbon (carbon-carbon, carbon fiber, carbides,...) could help solve this problem [12]. If this technology can be implemented, then the HN proportion parameter can be modified.

	630°C	1030°C
Feedback coeff. (pcm/°C)	-2.36	-1.00
Breeding ratio	1.000	1.026
Neutron flux (x10 ¹⁴ n/cm ² /s)	13.7	9.6
Graphite life span (years)	1.8	1.2
²³⁵ U inventory (kg)	1925	1630

Table 5: Constraints according to the mean temperature of the fuel salt. The statistical error on the feedback coefficients is less than 0.05 pcm/°C (configuration: r = 8.5 cm, 20 m³ salt, variable temperature, 22% (HN)F₄)

The temperature increase due to the change of salt leads us to set the operating temperature at 1030 °C for all the configurations. We will first study the influence of this temperature hike on the standard configuration before studying the influence of the HN proportion in the salt at 1030 °C.

At this temperature, the thermodynamic efficiency is assumed to increase from 40 % to 60 % and this has an incidence on the thermal power of the reactor: 1666 MWth instead of 2500 MWth are needed to produce 1000 MWe. Similarly, the salt density decreases from 4.3 to 3.89 because of the temperature related expansion effect. The impact on the constraints of this temperature increase is detailed in Table 5.

The change in salt density has a direct influence on the moderation ratio, resulting in a better thermalization of the neutron spectrum. This induces, for a channel radius of 8.5 cm, a worsening of the feedback coefficient (a behavior similar to that shown in Figure 4). Similarly, this slight thermalization leads to a larger ²³⁵U fission cross section and, combined with the lower salt density, a smaller necessary inventory. As for the breeding ratio, it is improved because of the reduced specific power, which has a direct incidence on parasitic captures (mainly those of FPs and Pa). The lower specific power has an incidence also on the neutron flux and, thus, on the graphite's life span. However, at such a temperature, the fluence limit that the graphite can withstand is reduced from 2.10²² n/cm² to

10^{22} n/cm² [8]. As a result, the graphite's life span is reduced in spite of the smaller neutron flux.

Influence of the proportion of Heavy Nuclei: Now that the effect of the temperature change from 630 °C to 1030 °C is known, the impact of the proportion of Heavy Nuclei can be explored. It is useful to keep the total amount of Heavy Nuclei constant, as we did when we changed the salt composition. As a consequence, salts with a smaller proportion of HN will have a larger volume. This makes these new configurations potentially interesting from the point of view of thermal power extraction. The core reprocessing time is kept at 6 months since, in that case, the flow of HN to be reprocessed is the same for all the configurations. The salt of the thorium blanket is not modified. The density and expansion coefficient of the fuel salt are crucial parameters, they are given in Table 6 [11].

Since the graphite's life span is directly related to the specific power and since the inventory is kept constant, these constraints are not very interesting in this part of our study. We will thus concentrate our attention on the safety and the regeneration constraints. Rather than presenting the impact of the proportion of HN for a reference configuration ($r = 8.5$ cm, salt volume = 20 m³) as was done previously, we will look at the impact of the channel radii for different HN proportions. This view point will allow a better understanding of the phenomena at play. The results are shown in Figures 6 and 7.

	22%	10%	5%	2%
Salt volume (m ³)	20	36.8	67.2	155
Density	3.89	2.85	2.33	1.98
Expansion coeff. (x10 ⁻⁴ /°C)	10	10	9	8

Table 6: System properties according to the percentage of (HN)F₄

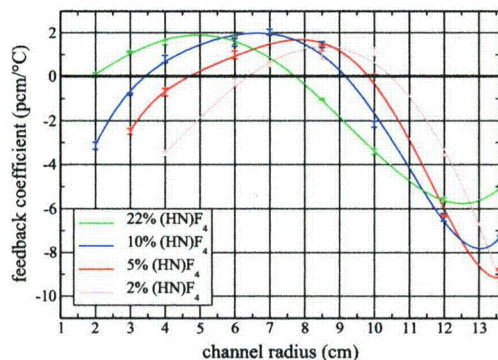


Figure 6: Feedback coefficient versus channel radius for several proportions of (HN)F₄ (configuration: variable radius, variable salt volume, 1030 °C, variable proportion of (HN)F₄).

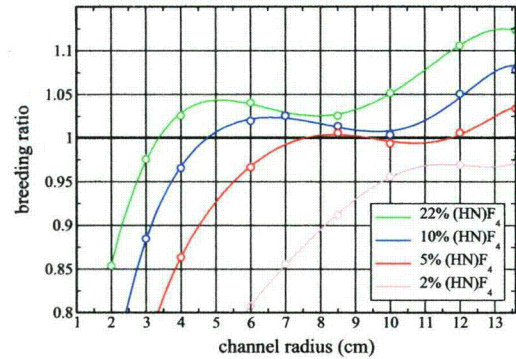


Figure 7: Breeding ratio versus channel radius for several proportions of (HN)F₄ (configuration: variable radius, variable salt volume, 1030 °C, variable proportion of (HN)F₄).

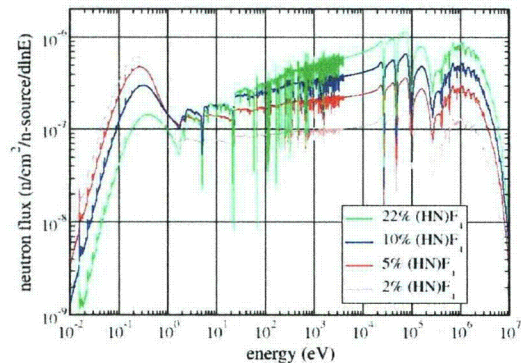


Figure 8: Neutron spectra for several proportions of (HN)F₄ (configuration: $r = 8.5$ cm, variable salt volume, 1030 °C, variable proportion of (HN)F₄).

During the reprocessing outlined in Figure 1, the thorium is extracted in order to allow the extraction of the FPs from the salt. This step is a key point in the reprocessing and it is made easier if the proportion of HN in the salt is small.

Moreover, when this proportion is decreased, the neutrons are scattered for a longer time before they encounter a fissile or fertile element (those that dominate neutron absorptions). This leads directly to a more thermalized neutron spectrum, as shown on Figure 8. Thus, the behavior of configurations with a small proportion of HN is similar to that of configurations with a 22% (HN)F₄ proportion but with smaller channels.

This additional thermalization is the main cause of the evolution of the feedback coefficients. And the visible difference for the configurations with a single salt channel seems to be due mainly to the improvement of the Doppler sub-coefficient. Likewise, the breeding ratio curves are similar from one salt to the other but two effects are observed. The first effect is related

to the thermalization change and the second to a deterioration of the breeding ratio when the HN proportion is decreased. This is due to an increased capture rate in the light elements of the salt on which the neutrons scatter for a longer time.

3 General Discussion

The various studies that have been carried out lead to a better understanding of the way an MSR works. The search for reactor configurations, be it a demonstrator or a power generator, requires that a certain number of constraints be satisfied. To do so, the different studies discussed in this paper have to be combined and the results extrapolated. Since the parameters are not mutually independent, one has to be circumspect in this approach.

Let us try to explore the possible reactor configurations. For the sake of simplicity, the parameter concerning the salt composition will not be considered in a first approach. The salt, then, is 78% LiF - 22% (HN)F₄ and the mean temperature is 630 °C.

Since the safety aspect cannot be circumvented in the design process of a nuclear reactor, we consider that this constraint is necessarily satisfied. Moreover, we consider only those configurations whose total feedback coefficient, not just the salt feedback coefficient, is negative. Except in the case where the size of the reactor is reduced dramatically, leading to a significantly increased neutron flux, the total feedback coefficient is negative only for either very thermalized or fast neutron spectra.

The first option implies a small fissile matter inventory and a weak neutron flux. When submitted to such a flux, the graphite undergoes little damage and its life span is reasonably long. On the other hand, captures in the moderator deteriorate the breeding ratio significantly. If a reactor system does not need to regenerate its fuel, then this very thermalized configuration may be suitable.

The faster neutron spectrum option introduces a real difficulty concerning the graphite, whose life span is then on the order of one year. There are several solutions to this problem.

- Decreasing the specific power of the reactor (by increasing its size and/or decreasing the total power generated) leads directly to a decreased flux intensity and, as a consequence, extends the graphite's life span. This, however, increases in the same proportion the per GWe fissile matter inventory, without providing a very satisfactory solution.
- The absence of moderating graphite in the single salt channel configuration solves this problem, the graphite in the periphery of the core being much less irradiated. However, this option leads to the fastest neutron spectrum and, as a result, the largest fissile matter inventory (5 to 6 metric tons of ²³³U). The specific power can be increased, though, in order to reduce the per GWe inventory.
- It may be possible to use a material whose structure is much less sensitive to irradiation than graphite. Then the configuration space for channel radii lying between 6 and 13 cm would no longer be forbidden.

Finally, the high breeding ratio obtained thanks to the fast neutron spectrum provides more leeway for the reprocessing. In particular, the time for full core reprocessing can be significantly extended. The single salt channel configuration discussed earlier can even do without any reprocessing (except for the bubbling process and uranium retrieval in the blanket) and still regenerate its fuel during the first 20 years of operation. The salt could conceivably be replaced, or entirely reprocessed after this time has elapsed. If a 6 month reprocessing time is kept, it becomes possible to do without a thorium blanket while still regenerating the fuel. This would substantially simplify the reactor design. Finally, we should note that, with a fast spectrum, re-injecting the Transurans in the core would be interesting, both in terms of regeneration (small neutron losses) and in terms of waste production (good incineration capability).

If it proves possible, increasing the temperature to above 1000 °C has many positive repercussions on the constraints, in particular thanks to the increased thermodynamic efficiency. However, it induces better thermalization by the salt and this has to be taken into account.

This opens the way to salt compositions containing small amounts of Heavy Nuclei. The way these reactors behave is practically the same with such compositions as with 22% (HN)F₄. In particular, the neutron spectra have to be either very thermalized or fast to ensure negative feedback coefficients. However, this corresponds to different reactor configurations because of the increased thermalization due to the salt's light nuclei. The capture rate of these light elements deteriorates the breeding ratio and leaves less leeway than with compositions containing more HN. The fundamental importance of this parameter lies elsewhere. Indeed, it is possible either to keep the size constant, thus reducing the inventory but not the specific power, or to increase the size, thus decreasing the specific power but not the inventory. A compromise between these two extremes can be found since decreasing the specific power facilitates the evacuation of the thermal power, a constraint that must not be neglected.

Conclusion

While our studies were, at first, close to the MSBR configuration, they prompted us to diversify our investigations. We analyzed the impact on the behavior of the core of such parameters as the reprocessing, the moderation ratio, the core size, and the proportion of heavy nuclei in the salt.

Our results confirm that there is a problem with the feedback coefficients in the MSBR. In a thermal spectrum, it would be possible to reach an acceptable concept only after in depth investigations taking into account the effect of the salt (negative feedback coefficient) and of the graphite (which makes the global feedback coefficient positive) separately. For very thermalized spectra, the global coefficients are negative thanks to the large neutron losses in the moderator but this leads also to a very poor breeding ratio. Epithermal or fast neutron spectra thus seem more favorable since they combine good feedback coefficients with satisfactory breeding ratio. However they lead to severe problems with the graphite's ability to withstand the

irradiation. As a result, the solution that removes the moderating block seems especially attractive.

Our studies have uncovered a wider range of possibilities than anticipated. Thus, many options remain to be explored. In particular, the evaluation of new materials, be it to obtain a moderator that has better irradiation resistance properties or to allow high temperature operation is crucial for an even more interesting development of the concept. How to extract the thermal power from the core is another issue of major interest since it impacts the behavior of the core through the specific power aspect. In order to ease heat recovery, the salt composition can also be modified so as to dissolve the fissile matter in a larger salt volume. In general, it is possible to change the type of salt, the MSR concept being adaptable to such a change.

As many parameters remain to be studied, other acceptable solutions could be found. In particular, parameters such as the type of salt, the moderating material, the size of the lattice hexagons, the definition of several different areas in the core, could be studied more specifically. In view of the results already obtained, it is clear that many configurations remain to be explored, requiring research on the salt and the materials as well as on the neutronics and the geometry.

Acknowledgements

The paper took benefit from the works made with M.Allibert and discussions during the european contract MOST (MOLten SaLT : FIKW-CT-2001-20183). We would like to thank Elisabeth Huffer for her translation (from French to English) of this paper.

References

- [1] Generation-IV : <http://energy.inel.gov/gen-iv/>
- [2] M.W.Rosenthal et al., "Molten Salt Reactors - History, Status, and Potential", Nuclear Applications and Technology, vol. 8 (1970)
- [3] D.Lecarpentier : "Le concept AMSTER, aspects physiques et sûreté", PhD thesis, Conservatoire National des Arts et Métiers, Paris (2001)
- [4] A.Nuttin et al. : "Potential of Thorium Molten Salt Reactors : Detailed Calculations and Concept Evolution With a View to Large Scale Energy Production", Progress in Nuclear Energy, Vol. 46, No.1, pp. 77-79 (2005)
- [5] EDF/DER : "Analyse critique du projet MSBR", HT-12/24/77
- [6] E.Walle, J.Finne, G.Picard, S.Sanchez, O.Conocar, J.Lacquement : "Molten Salt Reactors : Chemistry of Fuel Salt and Fuel Salt Cleanup", Global, New Orleans, USA (2003)
- [7] J.F.Briesmeister : "MCNP4B-A General Monte Carlo N Particle Transport Code", Los Alamos Laboratory report LA-12625-M (1997)
- [8] P.A.Platonov et al. : "Radiation damage and life-time evaluation of RBMK graphite stack", Kurchatov Institute
- [9] E.Merle-Lucotte et al. : "Etude des scénarios de déploiement mondial de l'électronucléaire", LPSC Internal Note 04-68, Grenoble, France (2004)
- [10] E.Merle-Lucotte, L.Mathieu et al : "Molten Salt Reactors and Possible Scenarios for Future Nuclear Power Deployment", Physor, Chicago, USA (2004)
- [11] I.Victor, E.Walle et al. : "Density of Molten Salt Reactor Fuel Salts", Nureth, Avignon, France (2005)
- [12] B.Tahon, Sgl Carbon Group, private communication (2004)

Neutronics Development of SIMMER for Molten Salt Reactors and its Application for a Molten Salt Transmuter

S. Wang, A. Rineiski, W. Maschek,
Forschungszentrum Karlsruhe, Institute for Nuclear and Energy Technologies
Postfach 3640, D-76021 Karlsruhe, Germany

INTRODUCTION

Molten salt reactors (MSRs) were first proposed by Bettis and Briant of ORNL in the later 1940's attempt to design a nuclear-powered aircraft [1]. The active development program aimed at such an aircraft reactor was carried out from about 1950 to 1956, which operated successfully in 1954 in a 'proof-of-principle' short-term test at a power level of 2.5 MW(th) and at temperature up to 860°C. Following the aircraft reactor experiment, a further Molten Salt Reactor Experiment (MSRE) was built and operated successfully at a power level of 7.3 MW(th) during 1960's by ORNL [2]. The reactor was operated at first using ^{235}U as fissile fuel, after which the ^{235}U was removed from the fuel salt and later replaced with ^{233}U . At the end of the experiment, a portion of ^{239}Pu was added in the fuel. Those experiments demonstrated well that the molten salt reactors were very flexible. The same design can handle a variety of fissile materials and additives in the liquid fuel. So the molten salt reactors in principle can readily be adapted to transmutation and burning of nuclear waste such as plutonium, minor actinide and long lived fission products. Recently, in the European Union, the molten salt reactor technology is revisited, because of its safety advantages and the potential to transmute the minor actinides [3]. In close cooperation with MOST project, in Russia a new MSR concept, MOlten Salt Advanced Reactor Transmuter (MOSART), has been developed for burning TRUs (Pu and MAs) [4]. Compared with the MSRE, there are no graphite bars as structure elements in the core. In MSRs, the liquid fuel flows through the core and as a result, the delayed neutron precursors are redistributed in the core with respect to the flow pattern, furthermore, a portion of the delayed neutron is emitted outside of the core. As a consequence, the delayed neutrons play a significant role and can have important effects on the dynamic response of the systems. To perform this type of molten salt reactor characters, the neutronics module of the SIMMER-III code suitable to deal with movable neutron precursors must be extended. In this paper those extensions and a transient simulation for MOSART concept reactor with the extended SIMMER code are presented.

Safety Analysis Code SIMMER-III

The SIMMER-III code is developed by JAEA (Japan Atom Energy Agency) in cooperation with Forschungszentrum Karlsruhe and CEA (Commissariat à l'Energie Atomique, CEN Grenoble and CE Cadarache) and applied also by IRSN (France), ENEA (Italy), and other partners. This code is a two-dimensional, multi-velocity-field, multi-phase, multi-component, Eulerian, fluid-dynamics code coupled with a structure model (fuel pins etc.) and a space-, time- and energy-dependent neutron dynamics model. It was originally developed for simulating mainly LMFRB and LWR systems under severe accident conditions [5]. Currently, this code is also applied for molten salt transmuters by FZK. To comply with the new demands of MSRs [6], the neutronic part is extended by FZK, which accounts for the particular characterises of MSR – the movement of delayed precursors.

SIMMER III Neutronics Model for Molten Salt Reactors

The neutron kinetics model of SIMMER is based on the improved quasistatic schema which is used to solve the time-dependent multigroup neutron equation [7] (in the following presentation, only one group of delayed neutrons is considered for simplicity, x denotes a space-angular position, Φ , Q , v , χ_p , χ_d are "multigroup" vectors, at steady-state $\chi = (1 - \beta)\chi_p + \beta\chi_d$, $M(t)$ and $F(t)$ are neutron disappearance and production operators, respectively). The neutron flux is presented as a product of amplitude, $N(t)$, and flux shape, $\psi(x, t)$, while imposing a certain constraint:

$$\Phi(x, t) = N(t) \cdot \psi(x, t) \quad (1)$$

$$\langle W(x), \frac{1}{v} \psi(x, t) \rangle = \gamma = const. \quad (2)$$

where $\langle . \rangle$ means phase-space integration, $W(x)$ is the weight function, the flux amplitude, $N(t)$, usually takes into account major flux variations, therefore, the flux shape is recalculated less frequently than the amplitude. The "shape" equations ($U(x, t)$ means the delayed neutron precursor flow velocity):

$$\frac{1}{v} \frac{\partial \psi(x, t)}{\partial t} + \frac{1}{vN(t)} \frac{dN(t)}{dt} \psi(x, t) + M(t)\psi(x, t) = (1 - \beta)\chi_p F(t)\psi(x, t) + \frac{1}{N(t)} \chi_d \lambda C(x, t) \quad (3)$$

$$\frac{\partial C(x, t)}{\partial t} + \nabla[U(x, t)C(x, t)] = -\lambda C(x, t) + \beta F(t)\Phi(x, t) \quad (4)$$

are solved at every „shape“ step. Each "shape" time step consists of one or more "reactivity" steps. At each reactivity step, point-kinetics parameters, (reactivity neutron generation time, etc.) are calculated and the amplitude is computed. The point-kinetics parameters – employed in amplitude computations – depend on the flux shape (assumed to be linear within a shape step), while the flux shape (see Eqs. 3, 4) depends on the amplitude. Therefore, the flux shape, point-kinetics parameters, and the amplitude are usually recalculated several times at each shape step.

In the MSR case, the precursor term is split into two components: (1) the "standard" term (the only one that exists in reactors with solid fuel, and (2) the "moveable" one (that takes into account the precursor movement):

$$C(x, t) = C_s(x, t) + C_m(x, t) \quad (5)$$

$$\frac{\partial C_s(x, t)}{\partial t} = N\beta F\psi - \lambda C_s(x, t) \quad (6)$$

$$\frac{\partial C_m(x, t)}{\partial t} + \nabla[U(x, t)C_m(x, t)] = -\lambda C_m(x, t) - \nabla[U(x, t)C_s(x, t)] \quad (7)$$

the standard precursor term is computed at steady state conditions by assuming that at $t=0$ the left-hand parts of Eqs. 3, 4 are zero and $U(x, t)=0$ (as solid fuel). This term is employed in the thermal hydraulics parts of SIMMER to solve Eq. 7 and to obtain the "movable" precursor term. Then Eqs. 3, 4 are solved again at $t=0$ with modified (the ratio of the movable term to

the standard one is assumed to be constant mesh-wise) precursor terms, and the flux, "standard" and "movable" precursor concentrations are normalized so that the initial reactor power is equal to a certain value specified by the user.

During the transient, the movable precursor term is recomputed at each thermal hydraulics time step (the finest time scale in SIMMER) with an explicit schema used for the time and space discretization. Generally, only few iterations are needed to get the convergence results. The "previous" standard precursor concentrations (which usually vary rather slowly) are employed for computing the movable precursor term during the transient. This is a reasonable approximation since the reactivity step is rather short. The delayed neutrons emitted outside of the core region and into the loop being ignored in the flux shape and amplitude calculations.

The point kinetics model – employed in the quasistatic schema – is based on the following equations:

$$\frac{dN(t)}{dt} = \left(\frac{\rho(t)}{\Lambda} - \frac{\beta_{eff}}{\Lambda} \right) N(t) + \lambda \hat{c}_s(t) + \lambda \hat{c}_m(t) \quad (8)$$

$$\frac{d\hat{c}_s(t)}{dt} = \frac{\beta_{eff}}{\Lambda} N(t) - \lambda \hat{c}_s(t) \quad (9)$$

$$\rho(t) = \frac{1}{\langle W(x), \chi F(t) \psi(x, t) \rangle} \langle W(x), [\chi F(t) - M(t)] \psi(x, t) \rangle \quad (10)$$

$$\hat{c}_m(t) = \frac{1}{\Lambda \langle W(x), \chi F(t) \psi(x, t) \rangle} \langle W(x), \chi_d C_m(x, t) \rangle \quad (11)$$

The reactivity, $\rho(t)$, effective delayed neutron fraction, and other point kinetics parameters (except $\hat{c}_m(t)$) are defined in the conventional manner (therefore, the corresponding expression is given only for the reactivity) formally independent upon the fuel flow rate. The effective movable precursor concentration, $\hat{c}_m(t)$, is computed following Eq. 11. Then the $\lambda \hat{c}_m(t)$ term is added to the effective source, Eq. 8.

LOF Calculations for MOSART

The above described extension of neutronics module of SIMMER coupled with the thermal hydraulic part was applied for the transient calculations of a loss of flow (LOF) in the MOSART concept reactor. The SIMMER model for MOSART is shown in Fig. 1. The RZ fluid-dynamics mesh is 20×30 , the neutronics mesh is 60×90 .

Fig. 2 shows the relative flow rate of the fuel pump coast-down. The calculation was first performed with keeping the total fuel flow rate constant until the steady condition was obtained. Then, the LOF was performed from the steady state (in this calculation the pump coast-down begins from $t=26s$). Those pump coast-down data were taken from ORNL-4233 [8].

Fig.3 gives the molten salt temperature and velocity distribution of the steady state at $t=26s$, immediately before the pump coast-down. The maximal fuel temperature region is near the

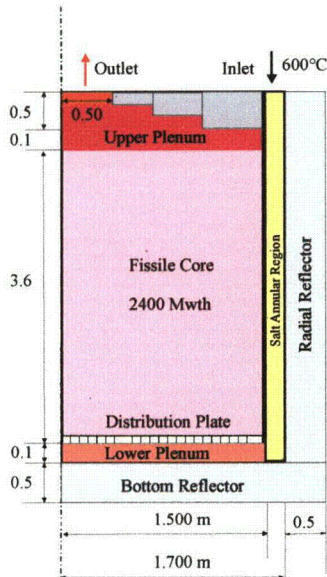


Fig. 1. Sectional view of MOSART geometric model

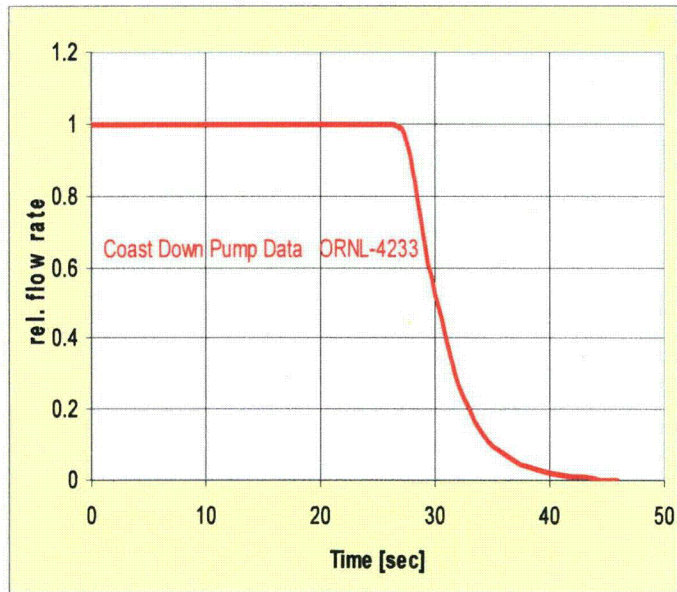


Fig. 2 Pump and Fuel Coast Down Transient

reactor axis and in the reactor midplane, and furthermore, the maximal molten salt temperature is about 1090 K. The pump coast-down begins immediately after $t=26s$, and relative pump power goes to zero until $t=46s$, then the calculation was continually performed until $t=60s$. Fig. 4 gives the salt temperature and velocity distribution at $t=60s$, it can be seen that a recirculation flow is building up in the reactor upper-right corner. The highest liquid fuel temperatures can also be observed in this region. Though there is no pump power to drive the liquid fuel, the fuel flows continually because of the natural convection.

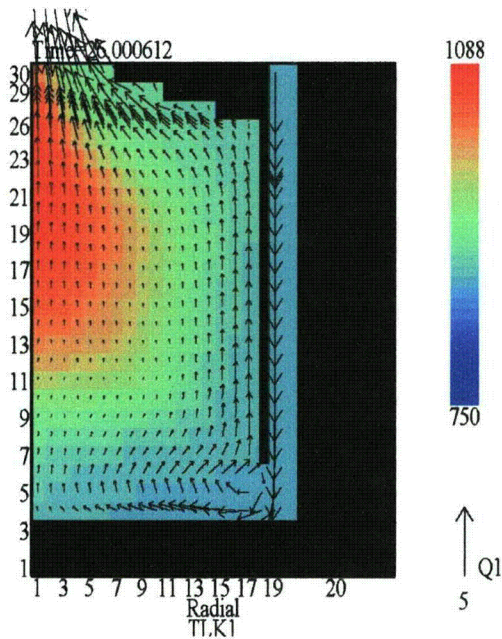


Fig. 3. Velocity vector and Temperature distribution at steady state, Vector scale 5 (m/s).

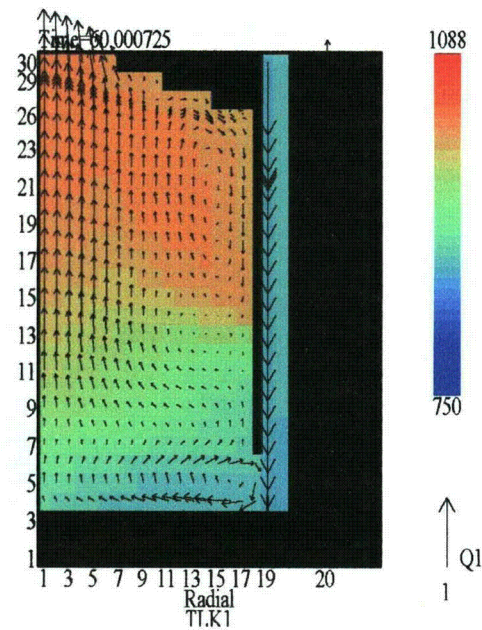


Fig. 4. Velocity vector and Temperature distribution at end of LOF, Vector scale 1 (m/s).

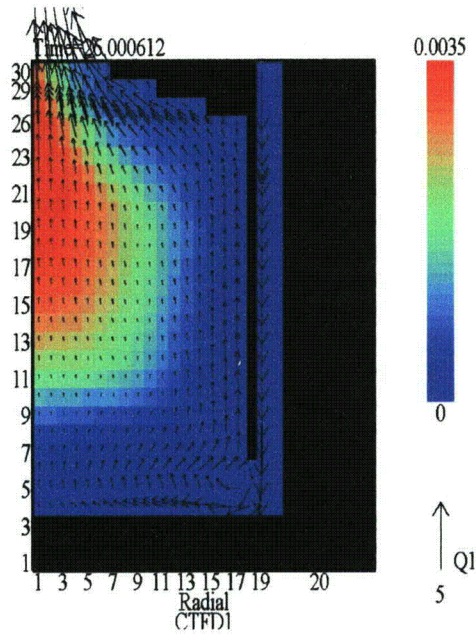


Fig. 5. First group precursor concentration distribution at steady state, (atom/barn-m).

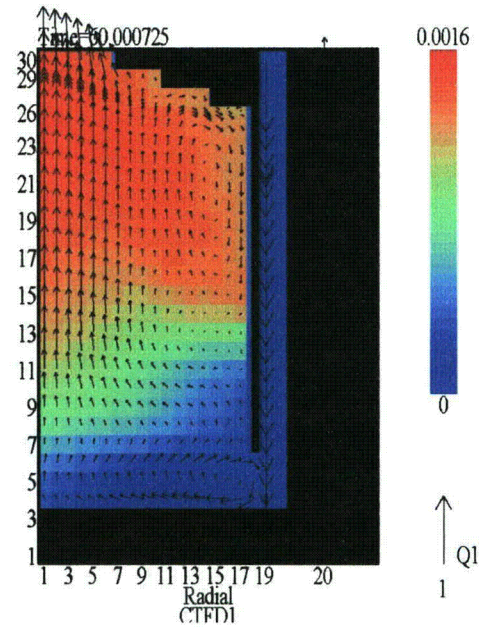


Fig. 6. First group precursor concentration distribution at end of Calculation, $t=60s$, (atom/barn-m).

The 2D precursor concentration distribution of first group at the steady state of $t=26s$ is given in Fig. 5. The unit of precursor concentration is atom/(barn-m). The decay constant of first group in this calculation is assumed as $\lambda_1=0.0126$ (1/s). It can be seen that most of the precursors at steady state are convected into the core axis region near the reactor outlet. The maximal precursor concentration is about 0.0035 atom/(barn-m).

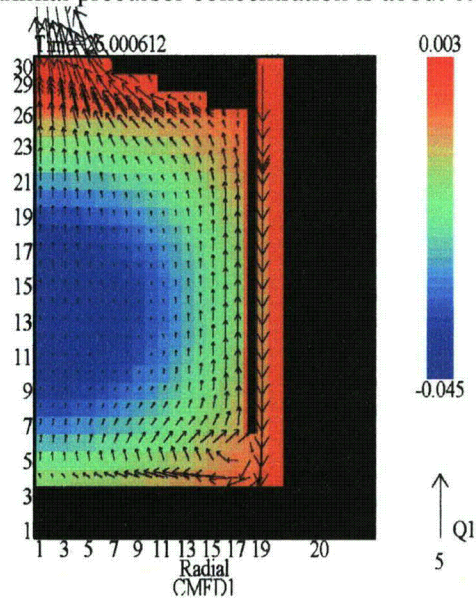


Fig. 7. First group "movable" precursor concentration distribution at steady state

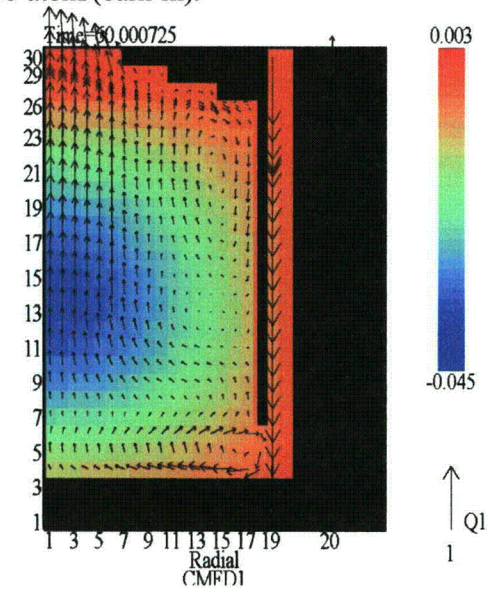


Fig. 8. First group "movable" precursor concentration distribution at end of the calculation, $t=60s$.

Fig. 6 gives the first group precursor concentration at $t=60s$, from this figure it can be recognized that the precursor concentration distribution is quite different from steady state. In fact, because of the natural convection effect, the fuel builds up a recirculation region, a significant part of precursors is convected into this recirculation region in the upper-right corner and can not immediately be transported out of the core. As a result, the fuel temperature in this region is higher than other region and the whole reactor temperature is reduced very slowly, as is indicated in Fig. 4.

Fig. 7 shows the above described so-called “movable” precursor concentration distribution of steady state at $t=26s$. In a large part of the reactor the “movable” precursor concentration is negative with a maximum at the core center. It is about -0.045 atom/(barn-m), while in the reactor outlet region the “movable” precursors are positive.

Fig. 8 gives the “movable” precursor 2D distribution at the transient calculation end of $t=60s$. The distribution configuration is roughly unchanged and only the negative “movable” precursor region shrinks slightly.

Conclusions

The SIMMER code is under development and extended for the molten salt application. Additional terms – for taking into account the delayed neutron precursor movement – are introduced into the time-dependent neutron transport equation solved in the code framework. The moving precursor part is computed in the thermo-hydraulic module of SIMMER and transferred into the neutronics module. The described schema is applied for MOSART calculations for the transient of loss of flow (LOF). The calculation results show that during transient of molten salt reactor, the precursor distribution changes with the flow pattern and redistributes in core. After the pump totally stops, because of the natural convection effect, a recirculation region is built up in the core, and a part of precursor can not directly emitted out of the core, but rather re-circulates in the core, as the result, the fuel temperature reduces very slowly.

References

1. Briant, R., et al., “Collection of Papers on The Aircraft Reactor Experiment”, Nuclear Science and Engineering, Vol. 2, pp 797~853, 1957.
2. Weinberg, A. M., et al., “Collection of Papers on the Molten Salt Reactor Experiment”, Nuc. Appl. Technol. Vol. 8, 1970.
3. MOST PROJECT, “Molten Salt Reactor Technology Phase 1”, 5th Framework Programme of European Commission, October 2001 ~ December 2003, 2004,
4. Ignatiev, V., et al. 2003, “Neutronic Properties and Possible Fuel Cycle of a Molten Salt Transmuter”, Proc. 2003 ANS/ENS International Winter Meeting (GLOBAL 2003), Hyatt Regency, New Orleans, LA, USA, November, 16-20, 2003.
5. Kondo, Sa., et al., “Current Status and Validation of the SIMMER-III LMFR Safety Analysis Code”, Proc. ICONE-7, Tokyo, Japan, 1999.
6. Wang, S, Rineiski, A, and Maschek, W., “thermal Hydraulic Investigations of a Molten Salt Burner Reactor”, Proc. ICONE-13, Beijing, China, 2005.
7. Ott, K. O. and Neuhold, R. J., “Introductory Nuclear Reactor Dynamics”, ANS, La Grange Park, USA, 1986.
8. Prince, B. E., et al., “Zero-Power Physics Experiments on the Molten Salt Reactor Experiment”, ORNL-4233, February, 1968.

EUROPEAN COMMISSION

nuclear science and technology

Fast-Acting Boron Injection System (FABIS)

Contract No: FIKS-CT-2001-00195

Final report
(short version)

Work performed as part of the European Atomic Energy Community's R&T Specific Programme "Nuclear Energy, key action Nuclear Fission Safety 1998-2002"
Area: Operational Safety of Existing Installations

2003

Directorate-General for Research
Euratom

PROJECT PARTNERS

J. Tuunanen (1), A. Daavittila (1), H. Purhonen (3), J. Laine (3), J. Meseth (2), K-F. Freudenstein (2), E. Bielor (2), H. Schmidt (2), and I. Ganzmann (2)

- 1) VTT Processes (FI)
- 2) Framatome ANP (DE)
- 3) Lappeenranta Univ. of Technology (FI)

OBJECTIVES

The objective of the FABIS project was to show that a fast shutdown of the reactor is feasible in the existing and future BWRs with a fast-acting boron injection system (FABIS). FABIS is needed since there is a risk in the existing BWRs that the nuclear fission process can't be stopped by the active fine motion control rod drives or by the passive scram system if there is a common cause failure in the control rod drive system. To reduce this risk, a diverse fast-acting boron injection system (FABIS) is proposed which injects sodium pentaborate into the Reactor Pressure Vessel (RPV). See Figure 1 for the principle flow diagram of the system.

FABIS takes boron from a large tank where it is heated to 250 °C. Heating ensures the densities of the boron solution and water in RPV is the same. With a second set of heaters, the upper 20 % of the water are heated to 331-335 °C (130-140 bar). About 10 % of the boron tank is filled with saturated steam. After activation of FABIS, steam expands and more steam is produced from saturated boron solution due to the pressure reduction. The boron solution flows through pipes inside RPV up to the upper side of the lower core plate. There the boron solution flows through smaller pipes adjacent to the lower core plate into the core bypass through about 100 small nozzles. This guarantees a homogeneous distribution of boron in RPV.

THE RESEARCH PERFORMED AND METHODS ADOPTED

The FABIS project included five work packages (WP1-WP5). The project aimed at answering to the following four questions:

1. How much time is needed for the injected boron solution to be spread both axially and radially over the core in such a way that the fission process stops completely?

The first two work packages (WP1 and WP2) answered to this question with PHOENICS¹ calculations and mixing experiments. Framatome ANP was responsible of WP1 and WP2. The main parameters in the calculations were the mass flow of the core bypass, diameter, flow velocity and direction of the local ejection nozzles and the pulse of the entrance flow to the core bypass. Calculations gave the optimum combination of the parameters leading to fast mixing. The experiments of WP2 verified the calculational results. The test rig was built of perspex in 1:1 scale and colored water simulated the boron solution. In the rig, it was possible to observe the mixing process by optical means and to use video to record the process.

¹ PHOENICS Version 3.4, 2002, Cham UK, Wimbledon.

2. Is there boron in the core entrance flow when the injection is stopped?

A series of TRAB-3D² analyses of WP3 answered to this question. VTT was responsible of WP3. TRAB-3D is a lumped parameter code, which includes 1D or 3D neutronics core models and 1D or node models for RPV hydraulics. The analyses were needed since recriticality of the core could take place if the mixing is insufficient. If the internal recirculation flow in RPV decreases with decreasing steam production and with decreasing speed of the main circulation pumps, the recirculation period will become longer. If the injection of boron solution ends earlier than this recirculation period, pure water may enter the core bypass and the boron solution could be washed out of the core.

3. What are the forces acting onto the lines between the boron solution tank and the RPV due to thermal shocks and pressure waves inside the lines?

In WP4, experiments at Lappeenranta University of Technology (LUT) studied the flow between the boron tank and RPV (see Figure 2). The volumetric scale of the test rig was 1:6 and the maximum pressure 80 bar. The experiments started with high pressure in the boron tank and low pressure in RPV. The valves in the connecting line between the tanks were opened and water from the boron tank was injected to RPV. The second aim of the tests was to find out which part of the inventory of the boron tank must be heated to the saturation temperature and pressure to reach the desired pressure level at the end of the test.

4. How can the results be transformed from the laboratory to the full scale?

The experiments of WP2 and WP4 used different temperatures, pressures and dimensions of the components than in the full-scale FABIS. The purpose of WP5 was to check, using dimensional analysis and engineering judgement, whether the results of the tests must be transformed due to the scale effects. WP5 ended with a system description, with detailed flow diagram and data sheets for the main components so that the realization of the system in a real BWR plant could be done. Framatome ANP was responsible of WP5.

MAIN ACHIEVEMENTS

Calculation of Mixing Process

WP1 included mixing calculations with the PHOENICS code with different jet and bypass flow rates, bore openings and injection angles and with 1 or 2 jets in representative section models. The calculated concentration profile in the gap between the fuel assemblies was sufficiently homogeneous along the core active zone for the optimal parameter combination. Figure 3 shows the calculated values across the core height for the injection/by-pass flow ratio of 4 % and for injection velocity and angle of 20 m/s and 20°. Although the bypass design and distribution is important it arose that small modification to the bypass did not affect the results, since most of the boron mixes already below the fuel assemblies. Hence, if the design is changed, the mixing in the bottom part must be studied carefully keeping the minimum boron concentration deviations as close as possible to the mean. Rather uniform boron distributions with the mean values of 4 % could be achieved with relative low injection rates

² A. Daavittila and H. Rätty. Validation of TRAB-3D. In: FINNUS Final Report, VTT Research Notes 2164. Espoo, Finland, 2002 (<http://www.vtt.fi/pro/tutkimus/finnus/index.html>), pp. 127-133.

of about 0.25 kg/s, being 4 % of the bypass flow rate. Because of this a rather low boron storage volume is needed.

Mixture Tests

The main components of the test rig of WP 2 were

- model of scale 1:1, made of acrylic plastic (perspex),
- 6 control rod guide tube heads with upper part of the control rods and bypass slots,
- 24 full length FAs with foot and bypass holes, and
- separate water circuits for FA bypass flow, control rod bypass flow and boron injection.

The test rig was built to include 2 different sections of the injection positions, one with converging and one with diverging jets. In 1:1 scale, the tests were performed with original mass flows and flow velocities and no further scaling was needed. WP2 started with pretests to check the performance of the rig, to adjust the flow rates of the injection system and the bypass flow pumping units, and to check the measurements. In the second phase, LASER light slit tests were performed at different model cross-sections and recorded on video to observe mixing of boron (simulated by particle seeded water) and coolant at three elevations. A series of tests with colored water was also run and recorded on video to observe the overall mixing behavior.

Mixture Calculations

A CASMO-4 study of the effects of the inter-assembly bypass boron distribution showed the homogeneity achieved with the planned boron injection was satisfactory. With the maximum boron density variation of factor of 2, the required additional boron to compensate the remaining heterogeneity was less than 5 %. Figure 4 shows the boron heterogeneity weight factor for a 3 cm long boron slug of 600 and 800 ppm in the bypass. The TRAB-3D steady-state calculation at the beginning of an equilibrium cycle resulted in an initial bypass boron concentration of 0.04 w-%, if the core should remain subcritical also during the second recirculation, when the boron is distributed homogeneously to RPV and the injection is stopped. This leads to 9.4 % sodium pentaborate solution in the boron tank, clearly less than the planned 13 %. In the TRAB-3D transient calculations, RPV was safely borated at the end of the injection after 150 seconds. Figure 5 shows the calculated fission power for the first 40 seconds of a turbine trip transient. In the Case 1, FABIS was activated immediately after the scram. In the Case 2, a delay of about 10 s was assumed. The analyses were made assuming the pumps are kept running at the minimum speed. If the pumps are stopped, the flow in the core by-pass stops almost totally. In this case, more studies are needed to confirm the function of the system.

Tests of the Flow between the Boron Tank and the RPV

Figure 2 shows the principle view of the test rig at LUT for the experiments of WP4. The rig consists of a boron tank, RPV, three electric heaters, piping, two fast opening valves, an orifice device, measurement instrumentation and data acquisition system. The instrumentation included two differential and three absolute pressure sensors, temperature measurements, valve position sensors and three strain gauges. WP4 included a series of pre-tests for testing and practicing the operation of the rig, and 7 final tests. The tests followed the actual operation of the full-scale FABIS system. The initial parameters were 65-80 bar, 15-180 °C (280-295 °C at the top) in the boron tank and 5-15 bar, 152-198 °C in RPV. The opening of the valves in the blowdown line actuated water injection from the boron tank. The time difference for opening the valves in the blowdown line was 0.3 s. Before each test, the tanks

were filled with water. The blowdown line was full of water at atmospheric pressure. The water in the boron tank was heated to the desired temperature with the lower heater. Electrical heaters were also used to pressurize the boron tank and RPV. Opening the valves in the blowdown line actuated the water injection. During the tests, the whole water inventory of the boron tank was injected. The initial volume fraction of saturated water in the boron tank varied between 21-31 %. See Figure 6 for the measured pressure in the tests with different initial pressures, boron tank water levels and mass of saturated water in the boron tank.

After opening the first valve, a pressure wave propagated between the valves. When the initial pressure in the boron tank was 65 bar, a 30 MPa tension stress on the outer wall of the blowdown pipe in circumferential direction was observed. Initial pressure of 80 bar caused a 40 MPa tension stress. When the fluid started to flow in the pipe, the inner wall temperature changed faster than at the temperature at the outer wall. This caused thermal stresses. When the inner wall temperature was below the outer wall temperature, a tensile stress occurred on the outer wall. The maximum tension stress was 75 MPa. When the temperature on the inner wall was lower than on the outer wall, compression stress occurred. The maximum value for compression stress of - 130 MPa was measured after the second valve. These stress values didn't risk the integrity of the blowdown pipe.

Transformation of the Test Results to the Actual Plant

WP5 of the FABIS project included analyses to transfer the test results to the real plant conditions. Two different investigations were done, since the forces induced by the pressure waves and thermal shock do not appear simultaneously. The first analyses assessed the effects of the propagating pressure waves on the piping system between the boron tank and RPV. The second assessed the effects due to the thermal shock by injecting the hot boron solution to the cold pipes. The pressure wave analysis showed higher pressures in the piping system than in the tests of WP4. The reason was the too rough time step of the data acquisition in the tests. A check analysis using the same integration time step showed a good agreement between the tests and analysis. In this way the test results, the analysis method and the transferability to the real plant were validated. A further investigation concerning fatigue due to the thermal shock and maximum operating conditions was done showing that all loads on the real system are within allowable limits.

DISSEMINATION AND EXPLOITATION OF THE RESULTS

The FABIS system is a part of a new generation nuclear power plant. It provides a cost-effective way to improve safety of the existing and new nuclear power plants. FABIS system is a part of the safety systems of the SWR 1000 nuclear power plant, one of the plants offered to TVO in Finland as an alternative for the fifth Finnish NPP.

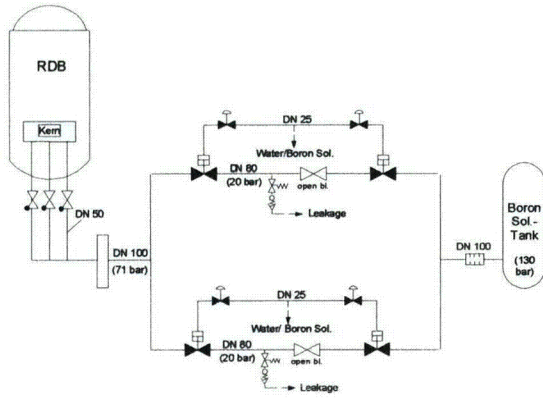


Figure 1: Principle flow diagram of the Fast-Acting Boron Injection System, FABIS

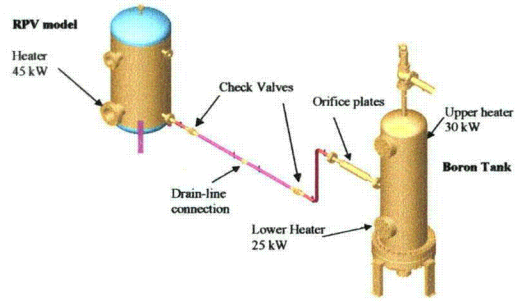


Figure 2: Principle view of the test rig of WP 4

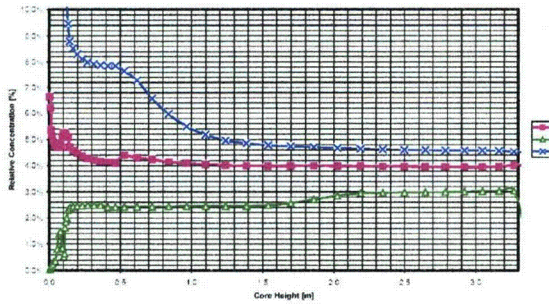


Figure 3: Relative boron concentration (mean, min., max.) across core height. Case I: injection/bypass ratio 4 %, inj. veloc./angle: 20 m/s, 40 deg.

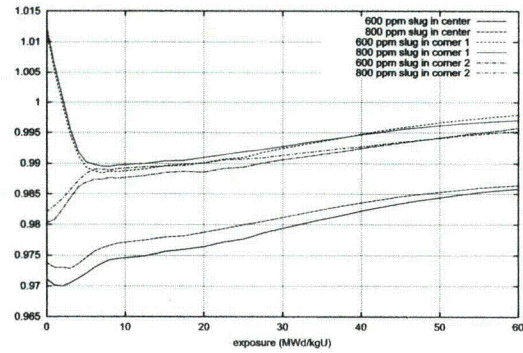


Figure 4: Boron heterogeneity weight factor for a 3 cm slug of 600 and 800 ppm boron concentration

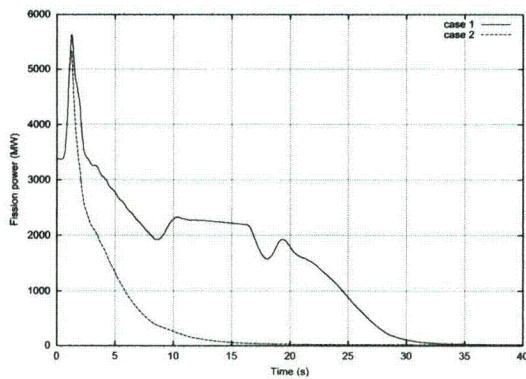


Figure 5: Fission power for the first 40 seconds in the TRAB-3D calculations

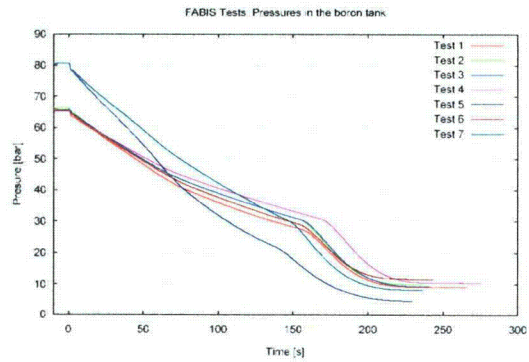


Figure 6: Depressurization of the boron tank in the experiments of WP4

Monitoring the Thermal Power of Nuclear Reactors with a Prototype Cubic Meter Antineutrino Detector

A. Bernstein

Lawrence Livermore National Laboratory, 7000 East Ave., Livermore, CA 94550

N. S. Bowden

Sandia National Laboratories, 7011 East Ave, Livermore, CA 94550

A. Misner and T. Palmer

Department of Nuclear Engineering, Oregon State University, Corvallis, OR 97331

(Dated: April 30, 2008)

In this paper, we estimate how quickly and how precisely a reactor's operational status and thermal power can be monitored over hour to month time scales, using the antineutrino rate as measured by a cubic meter scale detector. Our results are obtained from a detector we have deployed and operated at 25 meter standoff from a reactor core. This prototype can detect a prompt reactor shutdown within five hours, and monitor relative thermal power to 3% within 7 days. Monitoring of short-term power changes in this way may be useful in the context of International Atomic Energy Agency's (IAEA) Reactor Safeguards Regime, or other cooperative monitoring regimes.

I. INTRODUCTION

The International Atomic Energy Agency uses an ensemble of procedures and technologies, collectively referred to as the Safeguards Regime, to detect diversion of fissile materials from civil nuclear fuel cycle facilities into weapons programs. Nuclear reactors are a central element of the nuclear fuel cycle and of the Safeguards Regime. As we show here, it is possible and practical to monitor the operational status and thermal power of reactors with an antineutrino detector.

In the context of cooperative monitoring, an independent measure of the reactor power can allow confirmation of normal operation of the reactor without a physical inspection, and places a constraint on the total amount of fissile material generated in a given period. The measurement can also be used to verify the operator's own declarations of the reactor power and fuel burnup.

In an earlier paper [1], we presented a general method for exploiting the high rate of antineutrinos emitted by fission reactors to track the power and plutonium content of the reactor core in real time. Such monitoring was first performed by a Russian group at a reactor in Ukraine [2]. Recently, we presented first results from a detector, "SONGS1", developed to demonstrate this method as a possible non-intrusive, remotely operated safeguards tool [3]. SONGS1 has been acquiring data at the San Onofre Nuclear Generating Station (SONGS) in Southern California over the past two years. With it, we have been able to confirm many of the important claims made in [1]: non-intrusiveness with regard to core and site operations; continuous, remote and automatic data collection and calibration; sensitivity to both short term

(several hour) and medium term (daily or weekly) reactor power excursions; and sensitivity to changes in the reactor fissile isotopic content.

In this paper, we quantify sensitivity of our prototype to relative changes in the reactor power over hourly to monthly time scales, using only the antineutrino signal. Over these time scales, we show this sensitivity is limited primarily by counting statistics even with a detector of quite simple design.

The relevance of the measurement for reactor safeguards depends on the period over which the antineutrino data is acquired. One can monitor the relative power on an hourly basis and look for sudden outages or other short-term anomalies in reactor operations. This type of monitoring may be of interest for off-line refueled reactors, since a reactor outage allows the operator direct access to the weaponizable fissile material in the core. Alternatively, one can acquire data for week or month long periods, and measure the average power in this period with the higher precision afforded by the longer integration time. This more precise measurement can be used to verify stable operations. For continuous monitoring throughout a typical 12-24 month reactor cycle, the month-to-month antineutrino rates must be corrected to account for the influence of variations in the isotopic content of the reactor fuel. This effect is analyzed in a forthcoming companion paper.

It is important to emphasize that antineutrino-based monitoring need not depend on operator declarations - the detector can be kept under the control of the safeguards agency, providing a wholly independent measurement of reactor status. The non-intrusive and continuous nature of the antineutrino signal, the fact that it provides quantitative information about the reactor thermal power and burnup, is under control of the safeguards agency, and does not require frequent site visits, all point to its potential utility for cooperative monitoring.

*Electronic address: bernstein3@llnl.gov

II. ANTINEUTRINO EMISSION FROM NUCLEAR REACTORS

Antineutrino emission in nuclear reactors arises from the beta decay of neutron-rich fragments produced by heavy element fissions, and is thereby linked to the fissile isotope production and consumption processes of interest for reactor safeguards. On average, a fission is followed by the production of approximately six antineutrinos. The antineutrinos emerge from the core isotropically, and effectively without attenuation. Over the few MeV energy range within which reactor antineutrinos are typically detected, the average number of antineutrinos produced per fission is significantly different for the two major fissile elements, ^{235}U and ^{239}Pu . Hence, as the core evolves and the relative mass fractions and fission rates of these two elements change, the measured antineutrino flux in this energy range will also change. This relation between the fissile mass fractions and antineutrino flux, known as the burnup effect, has been observed consistently in previous experiments, e.g. [4].

For our present purpose it is useful to express the relation between fuel isotopics and the antineutrino count rate explicitly in terms of the reactor thermal power, P_{th} . The thermal power is defined as

$$P_{th} = \sum_i N_i^f \cdot E_i^f, \quad (1)$$

where N_i^f is the number of fissions per unit time for isotope i , and E_i^f is the thermal energy released per fission for this isotope. The sum runs over all fissioning isotopes, with ^{235}U , ^{238}U , ^{239}Pu , and ^{241}Pu accounting for more than 99% of all fissions.

For reactor power monitoring applications, it is important to note that the thermal energy release per fission E_i^f differs from the *total* energy release per fission, which includes contributions E_ν from the antineutrinos themselves, from neutron capture on fission products E_{nc} , and a time dependent term $\Delta E_{\beta\gamma}$ arising from beta and gamma decays which have not completed by a given instant in time. Fortunately, the neutron capture component is readily calculable from instantaneous fission product inventories, and the relative contribution from decaying betas and gammas is small. As a result, the thermal power is nearly proportional to the fission rate as defined in equation 1. [5] calculates the ratio of these terms to be $E_i^f : E_\nu : \Delta E_{\beta\gamma} : E_{nc} \simeq 200 : 9 : 0.3 : 10$

Following the formulation in [6], we define the power fractions $f_i(t)$ contributed by each isotope as

$$f_i(t) = \frac{N_i^f(t) \cdot E_i^f}{P_{th}}. \quad (2)$$

The antineutrino emission rate $n_{\bar{\nu}}(t)$ can then be expressed in terms of the power fractions and the total thermal power as:

$$n_{\bar{\nu}}(t) = P_{th}(t) \sum_i \frac{f_i(t)}{E_i^f} \int dE_{\bar{\nu}} \phi_i(E_{\bar{\nu}}), \quad (3)$$

where the explicit time dependence of the fission fractions and, possibly, the thermal power are noted. $\phi(E_{\bar{\nu}})$, is the energy dependent antineutrino number density per MeV and fission for the i th isotope. $\phi(E_{\bar{\nu}})$ has been measured and tabulated by various authors, with recent summary tables available in [6].

Equation 3 defines the burnup effect. The fission rates $N_i^f(t)$ and power fractions $f_i(t)$ change by several tens of percent throughout a typical reactor cycle as ^{235}U is consumed and ^{239}Pu produced and consumed in the core. These changes directly affect the antineutrino emission rate $n_{\bar{\nu}}(t)$.

III. ANTINEUTRINO DETECTION THROUGH INVERSE BETA DECAY INTERACTIONS

Reactor antineutrinos are normally detected via the inverse beta decay process on quasi-free protons in hydrogenous scintillator. In this charged current interaction, the antineutrino $\bar{\nu}$ converts the proton into a neutron and a positron: $\bar{\nu} + p \rightarrow e^+ + n$. For this process, the cross section σ is small, with a numerical value of only $\sim 10^{-43} \text{cm}^2$. The small cross section can be compensated for with an intense source such as a nuclear reactor. For example, cubic meter scale hydrogenous scintillator detectors, containing $\sim 10^{28}$ target protons N_p , will register thousands of interactions per day at standoff distances of 10-50 meters from typical commercial nuclear reactors.

In a measurement time T , the number of antineutrinos detected via the inverse beta decay process is:

$$N_{\bar{\nu}}(t) = \left(\frac{TN_p}{4\pi D^2} \right) P_{th}(t) \sum_i \frac{f_i(t)}{E_i^f} \int dE_{\bar{\nu}} \sigma \phi_i \epsilon. \quad (4)$$

In the above equation, σ is the energy-dependent cross-section for the inverse beta decay interaction, N_p is the number of target protons in the active volume of the detector, and D is the distance from the detector to the center of the reactor core. ϵ is the intrinsic detection efficiency, which may depend on both energy and time. The antineutrino energy density and the detection efficiency are folded with the cross-section σ , integrated over all antineutrino energies, and summed over all isotopes i to yield the antineutrino detection rate.

To further clarify the relation between the thermal power, the fuel burnup, and the antineutrino detection rate, it is useful rewrite this equation as:

$$N_{\bar{\nu}}(t) = \gamma (1 + k(t)) P_{th}(t), \quad (5)$$

where γ is a constant encompassing all non-varying terms, including the number of target protons, the detector standoff distance, and the detection efficiency. $k(t)$ describes the change in the antineutrino flux due to changes in the reactor fuel composition. γ is chosen so that the value of k at the beginning of a reactor fuel cycle is zero.

Typically, commercial reactors are operated at constant thermal power. In this mode, k decreases by ≈ 0.1 over the course of a reactor fuel cycle, depending on the initial fuel loading and operating history, i.e. the antineutrino detection rate decreases by $\approx 10\%$. The magnitude of this effect can be predicted at the few percent level in an absolute sense, if the reactor fuel loading and power history are known. Much of the uncertainty arises from systematic shifts in measured antineutrino energy densities $\phi_i(E_{\bar{\nu}})$, so that the relative uncertainty in the predicted burnup rate can be considerably smaller.

IV. REACTOR SIMULATION

In order to study the relation between the reactor thermal power and the measured antineutrino rate, we must quantify the distorting effect of fuel burnup on the antineutrino rate. For this purpose, we simulated the isotopic evolution of the SONGS core through a single fueling cycle of the reactor, using the ORIGEN simulation package [7]. ORIGEN benchmarking studies against assayed fuel assemblies have shown that the package predicts the fissile isotopic content of Low Enriched Uranium (LEU) fuel with 1-2% accuracy [8].

The input fuel loading per fuel assembly, the fuel assembly power densities, and nominal cycle time were obtained from the reactor operator. The assemblies were simulated in ORIGEN and the fission rates, and mass and number densities of the main fissile isotopes tracked through a 590 full power day evolution, corresponding to the length of Cycle 13 of the SONGS Unit 2 reactor. The fission rates predicted by the simulation, folded with the antineutrino spectral densities [6], allow us to estimate the emitted antineutrino rate at any time during the cycle. (Fig. 1a).

For the long cycles typical of the San Onofre plant, the burnup effect causes a 10% decrease in detectable antineutrinos by end of cycle. Cycle times have lengthened over the last two decades as plant operations have improved, with the result that the cumulative effect of burnup on the antineutrino count rate is larger. However, the relevant point for the current analysis is that the effect is small over the hour to month time scales of interest for safeguards-related thermal power monitoring. The effect of burnup is never greater than 0.62% over any thirty day period (Fig. 1b). Provided that the detection efficiency, target mass and distance are constant, this figure demonstrates that the change in the quantity $k(t)$ in Equation 5 is small over month or shorter time scales, so that the detected antineutrino rate is nearly proportional

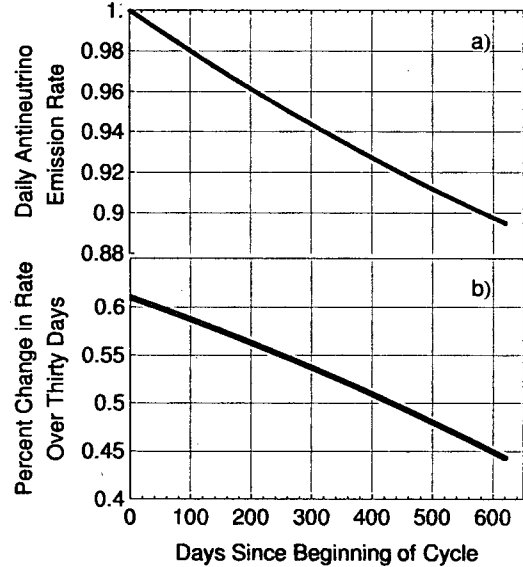


FIG. 1: a) The predicted relative daily antineutrino emission rate versus cycle day. The rate is normalized to its value at the beginning of the cycle. b) The percent change in the instantaneous antineutrino emission rate over the previous thirty day period, versus cycle day.

to reactor power over these time intervals.

V. THE SONGS REACTOR

The SONGS1 detector is deployed at Unit 2 of SONGS. There are two operational reactors at this station; both are pressurized water reactors designed by Combustion Engineering in the 1970s and have maximum thermal (electric) power of 3.4 GWt (1.1 GWe). The detector is located in the tendon gallery of Unit 2. A feature of many commercial reactors, the tendon gallery is an annular concrete hall that lies beneath the walls of the reactor containment structure. It is used to inspect and adjust the tension in reinforcing steel cables known as tendons, which extend throughout the concrete of the containment structure. At SONGS these inspections occur every several years, and involve the examination of only a handful of representative tendons. Apart from these inspections, the placement of the detector in the tendon gallery has little or no impact on regular plant operations, and vice-versa.

SONGS1 is located 24.5 ± 1.0 m from the Unit 2 reactor core and 149 ± 3 m from that of Unit 3. The physical core is well approximated by a 4 m tall cylinder with a 3.5 m diameter. Compared with a point source, its finite size has a less than 1% effect on the measured rate at the 24.5 m standoff distance of the SONGS1 detector.

Since the antineutrino flux generated by each core is isotropic, 97% of the reactor antineutrinos reaching the

SONGS1 detector originate from Unit 2. With Unit 2 at full power the antineutrino flux at the SONGS1 location is $10^{17} m^{-2} s^{-1}$.

VI. THE SONGS1 DETECTOR

As described in detail elsewhere [3], the SONGS1 detector consists of three subsystems; a central detector, a passive shield, and a muon veto system. The central detector consists of four identical stainless steel cells filled with a total of 0.64 ± 0.06 tons of liquid scintillator. A passive water/polyethylene shield for gamma rays and neutrons surrounds the detector on six sides, with an average thickness of 0.5 m. A 2 cm thick plastic scintillator envelope read out by PMTs covers five sides of the detector and identifies cosmic ray muons.

In the central detector, positrons created by the inverse beta process deposit energy via Bethe-Bloch ionization as they slow in the scintillator. Annihilation with an electron yields two gamma rays which can deposit up to an additional 1.022 MeV of energy in the detector. This set of interactions, occurring within about 1 ns, is referred to as the "prompt" energy deposition. The neutron carries away a few keV of energy from the antineutrino interaction. After thermalization, this neutron can be detected by capture on a gadolinium (Gd) dopant. A concentration of 0.1% Gd by weight yields a neutron capture time of 28 μs , and an 8 MeV energy release via a gamma ray cascade resulting from the capture. The measured response of the detector to this 8 MeV cascade is referred to as the "delayed" energy deposition.

The time separation between prompt and delayed energy depositions follows an exponential distribution with time constant equal to the 28 μs neutron capture time in the Gd doped scintillator. Taken together, the prompt and delayed energy depositions are referred to as a *correlated* event. This refers to the fact that the same underlying physical process generates both interactions, and that they occur close in time relative to most other pairs of interactions taking place in the detector.

Correlated events can be created by mechanisms other than inverse beta decay. For example, fast muogenic neutrons can scatter off protons in the scintillator, giving a prompt energy deposition, and then be captured on Gd with the same time distribution as occurs for inverse beta events. Such events, which mimic the time structure of the antineutrino events, are referred to as correlated backgrounds. The detector also registers uncorrelated backgrounds - random coincidences between two energy depositions from natural radionuclide decays and other sources. Since the occurrence of such uncorrelated backgrounds is governed by Poisson statistics, the time separation between these events will also follow an exponential distribution, with a time constant equal to the inverse of the single event rate (effectively the detector trigger rate).

The detector trigger rate above a 1 MeV threshold, and

the trigger rate for the muon veto system are both ~ 500 Hz. Data is acquired through a NIM/VME-based Data Acquisition System and an on-site computer automatically performs the data analysis. A telephone modem is used to automatically retrieve the results of this analysis, as well as detector state of health indicators, allowing for the remote monitoring of detector operation, and, through the antineutrino signal, of reactor operation. The prototype SONGS1 system (which is not a highly engineered design) operates unattended for months at a time.

A. Expected Antineutrino Interaction Rate

With our current 0.64 ton liquid scintillator detector at a standoff of 24.5 ± 1 m from the reactor core, and with the reactor parameters defined in Sec. V, the rate predicted by Eqn. 5 at the beginning of the reactor fuel cycle ($k(t) = 0$) is 3800 ± 440 antineutrino interactions per day for 100% detection efficiency. The uncertainty in the absolute antineutrino rate arises primarily from the uncertainty in our knowledge of the amount of scintillator in the detector. This uncertainty is a systematic shift in the absolute rate that has no effect on the relative power measurements of interest in the analysis presented below.

VII. THE SELECTION PROCEDURE FOR ANTINEUTRINO EVENTS

To isolate antineutrino events, we form candidate event pairs from the raw data. For each pair of sequential events meeting the hardware trigger criteria, the first is labeled prompt or positron-like, and the second delayed or neutron-like. Two time intervals are also defined: the interval between the prompt event and the most recent muon trigger or central detector trigger, and the time between the prompt and delayed events (interevent time). To select antineutrino candidates we apply several cuts to the sequential pairs. To exclude events with highly non-uniform light collection, a cut is applied to ensure that each PMT observing a particular cell sees a similar amount of light per event. For two PMTs observing a given cell, a and b, the cut is applied to the ratio z , defined as:

$$z = \frac{a - b}{a + b} < 0.4. \quad (6)$$

This selection criterion is referred to as the ratio cut. In practice, it determines which interaction locations in the scintillator are accepted by the selection process, thereby defining a fiducial volume.

Next, we apply cuts on the amount of energy recorded in each cell. For simplicity and flexibility in our analysis, we have chosen to consider each cell as an independent detector.

TABLE I: The Antineutrino Event Selection Criteria

Quantity	Criterion
Prompt Energy	$2.39 \text{ MeV} < E_{\text{positron}} < 9 \text{ MeV}$
Delayed Energy	$3.5 \text{ MeV} < E_{\text{neutron}} < 10 \text{ MeV}$
PMT Ratio Cut	$ z < 0.4$
Interevent Time	$t_{\text{min}} = 10 \mu\text{s}$
Muon Veto	$t_{\text{mu}} > 100 \mu\text{s}$

Hardware limitations impose a cut of $10 \mu\text{s}$ on the minimum time between any event pair. Finally, we accept only those events that occur at least $100 \mu\text{s}$ after the last muon hit/acquisition trigger. This final cut significantly reduces the number of contaminating antineutrino-like event pairs in the data set caused by muon interactions. From the empirically measured time constant of the muon correlated events ($20 \mu\text{s}$), we calculate that this cut excludes all but 0.7% of antineutrino-like backgrounds correlated with a muon recorded in the veto.

Table I summarizes our event selection criteria. The predicted rate of antineutrinos at beginning of cycle based on these criteria is 407 ± 75 /day. As mentioned earlier, this error includes the large absolute uncertainty in the number of target atoms. As shown below, a relative measurement has a considerably smaller uncertainty.

VIII. THE ANTINEUTRINO-LIKE EVENT SAMPLE

After applying these selection criteria, we examine the spectrum of time intervals between pairs of successive energy depositions (Fig. 2). Two clear exponential features are visible. The faster and more prominent of these arises from a prompt, positron-like, energy deposition followed a characteristic time later by a delayed, neutron capture-like energy deposition. The second, slower exponential is due to the random coincidence of two sequential background events both of which exceed the relevant thresholds. As would be expected for such coincidences, the time constant of this slow exponential is equal to the inverse of the acquisition trigger rate.

To further select antineutrino events we integrate the interevent time distribution from $10 \mu\text{s}$ to $100 \mu\text{s}$. Beyond the upper time limit of $100 \mu\text{s}$, the event sample is dominated by uncorrelated backgrounds. This integral defines the total number of events prior to any background subtraction, and includes contributions from true antineutrino interactions as well as both correlated and uncorrelated backgrounds. We refer to these as antineutrino-like events.

It is impossible in this detector to distinguish backgrounds from true antineutrino interactions on an event-by-event basis. For the analysis below, when a net number of antineutrino events is required, we perform a statistical subtraction of the same definite integral determined over a reactor off period. We use this procedure to estimate the net daily or weekly number of antineutrinos.

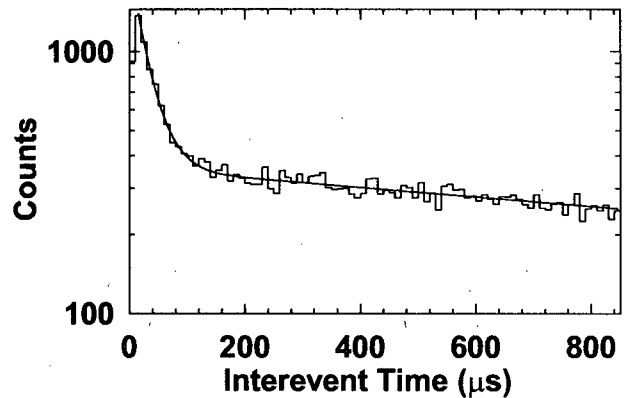


FIG. 2: A representative interevent time spectrum of event pairs that pass all selection cuts acquired during 7 days of data taking. The fit to the data has four parameters: an exponent and amplitude each for the fast and slow exponentials describing respectively the correlated signal and coincident singles background.

For integration times less than 24 hours, unacceptably large uncertainties are introduced by such a procedure due to limited counting statistics. Instead, we apply a standard hypothesis test to the total (non-background-subtracted) antineutrino-like event rate to look for significant changes.

IX. HOURLY MONITORING OF THE REACTOR OPERATIONAL STATUS

In the off-line refueled reactors which constitute the majority of the world's reactor stock under safeguards, fissile materials can only be accessed during shutdowns. Thus, it is of potential interest for safeguards to estimate how quickly a shutdown or a large change in the reactor thermal power can be identified using the antineutrino signal.

For a quantitative estimate of the statistical significance of such changes, the Sequential Probability Ratio Test (SPRT) [9] can be used to estimate the amount of time required to conclude, with a given level of confidence, that the reactor thermal power has changed based on a change in the antineutrino signal. The SPRT is based on a log-likelihood ratio, defined as

$$r_{SPRT} = \log \frac{P(\mu_1, nevents)}{P(\mu_2, nevents)}. \quad (7)$$

$P(\mu, nevents)$ is the probability that the measured number of events $nevents$ is drawn from a parent distribution with mean μ . μ_1 and μ_2 are the expected mean values of the number of events in a fixed time interval during periods at two different power levels - for example, 100% power and zero power. In the examples discussed below, the expected mean values are derived from data taken

during periods in which the thermal power was known by independent means to be at the level being tested for (zero power, full power, or some intermediate value). In a real regime, a set of calibrations between thermal power and antineutrino rate would be established in an initial cycle, and used at later times to specify mean values μ which would serve as inputs for the test statistic. Using the test, measured mean values at any given time would be tested against a set of possible expected values derived from the earlier calibration. The length of the calibration periods would be optimized based on the detected antineutrino event rate, and the size of the burnup effect for a given reactor and fuel type. With the configuration discussed here, we used a calibration period of one month, which gives $\sim 1\%$ statistical accuracy on the rate, compared with a $< 0.65\%$ systematic error induced by burnup, as described earlier.

To apply the test, one calculates the cumulative sum of the logarithmic quantity r_{SPRT} , with the sum updated at fixed intervals. Once this sum exceeds an upper or lower bound a and b , the test has confirmed that the reactor is in one and only one of the two possible states, with a specified level of confidence. The statistic is then reset and the testing process continues anew until a conclusion is reached. This is referred to as ‘online’ testing, since the test is constantly being updated with new data until a decision is made, at which point the statistic is reset.

The probability for change detection can be directly quantified in terms of a change in the test statistic. The upper and lower thresholds are defined in terms of the probability α of a false alarm, and probability β of a false negative (i.e. failing to recognize the change of state when it has occurred). The equations relating the thresholds for the test statistic to the probabilities of detection or non-detection are:

$$a = \log \frac{1 - \beta}{\alpha} \text{ and } b = \log \frac{1 - \alpha}{\beta}.$$

The thresholds can be selected to balance the need for timely detection with the need for high confidence in the result. For the analysis below, we demand 1% probability of either a false alarm or false negative.

Under a broad range of conditions, this method allows one to detect a change in the status of a time-varying process within the minimum possible time [9]. With the SPRT method, one can also explicitly quantify the probability of false alarms (changes being detected where none existed) and misses (undetected changes in operational status) [10].

A simple implementation of the test assumes Poisson distributed signal and background. We first confirm that our data meet this criterion. Fig. 3 shows the histograms of the number of detected antineutrino-like events in one hour intervals for equal amounts of reactor on and reactor off data. Both distributions are reasonably well fit by a Gaussian distribution, a good approximation for the Poisson distribution even with these low counting statis-

tics. The chi-squared per degree of freedom values for the Gaussian fits are 0.9 and 1.1 for the on and off data respectively. As seen in the figure, there is significant overlap in the distributions, so that a single measurement is insufficient to determine the operational status.

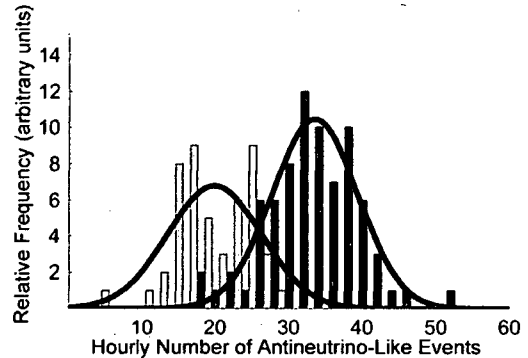


FIG. 3: A histogram of the number of antineutrino-like events per hour interval before (black) and during (light gray) the reactor outage.

In our first example, the outage occurs within one hour (Fig. 4a), and the test requires about 5 hours of data to determine that the reactor has turned off, with 1% probability of either a false alarm or false negative (missed alarm) (Fig. 4b). This condition is satisfied when the value of the test statistic is smaller than $b = -4.59$.

In another excursion, the reactor was ramped from zero to 80% power over an ~ 14 hour period, and held at this level for 3 days (Fig. 5a). In this case, the test requires 2 hours to determine that the reactor is in fact in the 80% power state, with 99% confidence. (Fig. 5b).

A somewhat more challenging circumstance is presented by a subsequent transition from 80% to 100% thermal power. In this case, it is difficult to see the power step by direct inspection of the change in the number of antineutrino-like events (Fig. 6a). However, the SPRT is able to detect the change with 99% confidence, albeit with a longer time to detect due to the closer proximity of the mean number of antineutrino-like events in the 80% and 100% power states. The test is able to detect the 20% power shift in approximately twelve hours. (Fig. 6b).

X. DAILY AND WEEKLY MONITORING OF RELATIVE THERMAL POWER

Hourly monitoring can quickly detect gross changes in the operational state of the reactor, such as the 20% power shift just described. For more precise measurements, longer integration times are required. We define a relative thermal power estimator by forming the ratio of the daily or weekly average antineutrino detection rate (after background subtraction) to the prior month

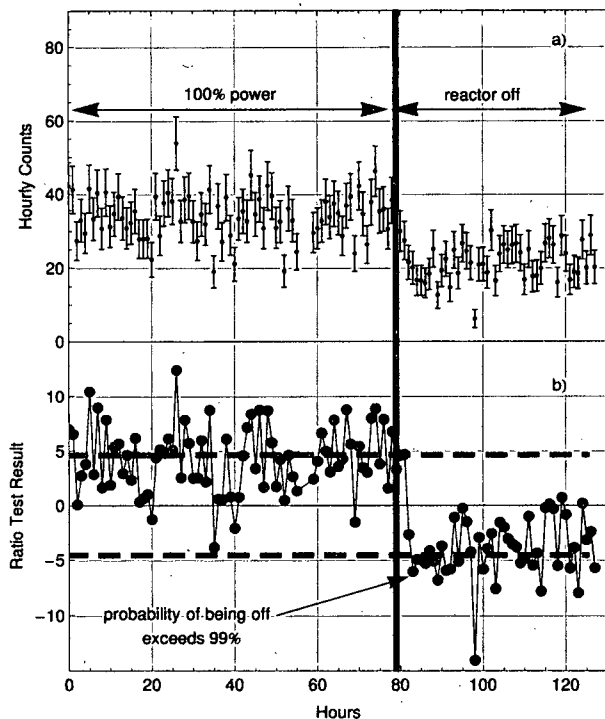


FIG. 4: (a): the hourly number of antineutrino-like events, plotted versus hour, through a reactor outage. (b): the value of the SPRT statistic plotted versus hour over the same time range. The dashed lines in this figure are the 99 % confidence level values of the test statistic. In both plots, the vertical line indicates the hour in which the reactor shutdown occurred. Values of the statistic above the upper dashed indicate that the reactor is in the on state. For this data set, these values are obtained only during the reactor on period, meaning that no false positives or negatives occurred.

background-subtracted average rate. This ratio is proportional to the daily or weekly average of the thermal power, with an accuracy to be calculated below. Assuming the thermal power of the reactor to be known by independent means at the start of a month-long measurement period, the antineutrino rate can thereby be directly associated with a particular power level, and excursions from this level can be detected by changes in the daily or weekly average

Month-long periods of comparison form a natural break point for the analysis presented here. This is due to the fact that the effect of burnup on the detected (and emitted) antineutrino rate never exceeds 0.65% over one month, as demonstrated in section IV, while statistical uncertainty is at the 1% level for this averaging period. As long as the period of comparison is no longer than one month, we will show that the variation in the ratio just defined will be dominated by counting statistics, and not by burnup-induced changes or other systematic effects. For longer comparison periods, the effect of bur-

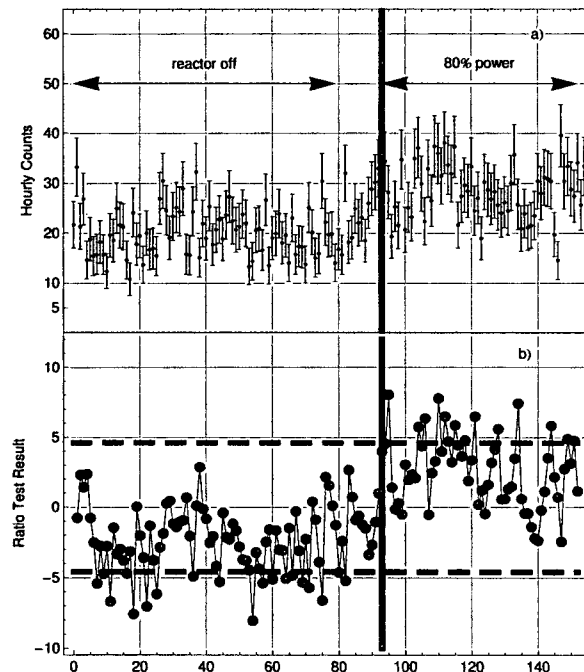


FIG. 5: (a): the hourly number of antineutrino-like events, plotted versus hour, through a reactor ramp from zero to 80% power. (b): the value of the SPRT statistic plotted versus hour over the same time range. The dashed lines have significance analogous to those in Fig. 4.

nup on the relative power estimate grows, and we must explicitly introduce our burnup model. This analysis is performed separately in a forthcoming paper.

The precision of the daily or weekly estimator is determined by counting statistics, and by any time-dependent systematic effects (other than burnup) which can alter the detection efficiency. By making the measurement relative to an initial monthly average value, time independent corrections to the detection rate - such as those caused by an incorrect estimate of the number of targets or of the overall detection efficiency - only induce an overall shift in the constant of proportionality between reactor power and the absolute antineutrino detection rate. This shift has no effect on the stability or precision of our relative power estimator.

To analyze the correlation between the daily and weekly average antineutrino detection rate and the thermal power, we must subtract the background, which is measured during reactor off periods.

A. Reactor Off Data

During a 63 day period with Unit 2 (the near reactor) at 0% power, the average daily rate of events passing all antineutrino selection criteria was 441 (Fig. 7). This rate is primarily comprised of uncorrelated non-antineutrino

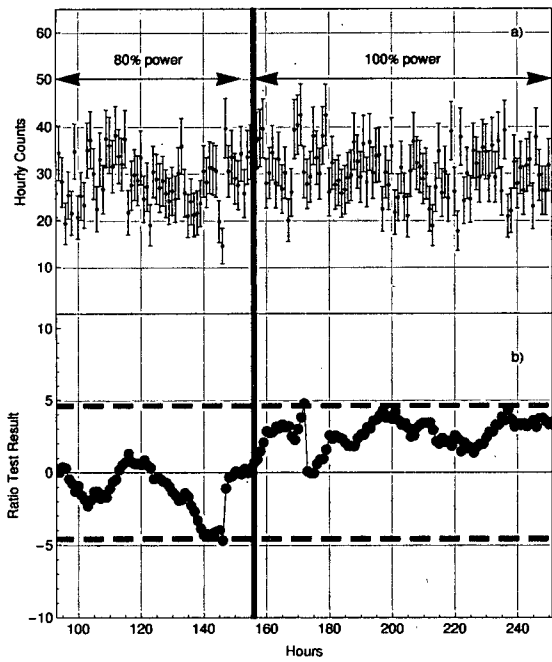


FIG. 6: (a): the hourly number of antineutrino-like events, plotted versus hour, through a reactor ramp from 80% to 100% power. (b): the value of the SPRT statistic plotted versus hour over the same time range. The dashed horizontal lines have significance analogous to those in the lower plot in Fig. 4. The solid vertical line shows the hour in which 100% thermal power was obtained.

backgrounds (as well as an ~ 10 count per day contribution of real antineutrinos from the distant reactor). The measured standard deviation for the reactor off data sample is 22.3 events, or 5%, (with an uncertainty in this standard deviation value of 0.5%). The predicted uncertainty due to Poisson counting statistics alone is 4.7%, consistent with the measured standard deviation value. We also performed a Gaussian fit to the data as a check on the measured sample mean and standard deviation. The value of the Gaussian mean is 435 events, close to the sample mean, and the Gaussian sigma is 20 events, close to the sample standard deviation value of 22.3 events.

Over the same 63 day (reactor off) interval, the average weekly rate of events passing all antineutrino selection criteria was 3088, with a measured standard deviation of 88 events, or $2.6 \pm 0.5\%$. The predicted Poisson uncertainty based on counting statistics in this case is 1.9%, close to the sample standard deviation, but indicative of a possible small additional uncertainty not accounted for by counting statistics. The Gaussian mean (3088) and standard deviation (87) are also close to the sample mean and standard deviation.

For both daily and weekly integration times, the mean value of the background is subtracted from the signal during reactor on periods to obtain the net antineutrino

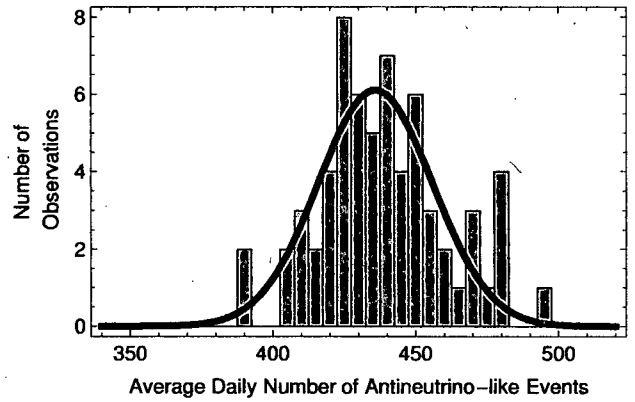


FIG. 7: A histogram of events passing all antineutrino selection cuts during a 63 day long reactor off period.

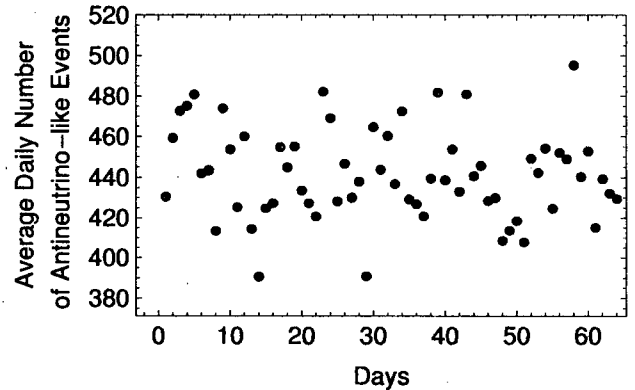


FIG. 8: Events per day passing all antineutrino selection cuts during a 63 day long reactor off period, plotted versus day.

detection rate.

A linear fit to reactor off daily antineutrino-like detection rate plotted versus day (Figure 8) has a slope of 0.13 ± 0.15 , consistent with a constant background.

B. The Stability of the Antineutrino-Based Power Estimate

Next we consider the stability of a relative power measurements based on the daily and weekly average background-subtracted antineutrino detection rate. According to operator records, the reactor power in our analysis period is constant to within 0.5%, at 99.5% of full power.

Rearranging Equation 3 it can be seen that the thermal power depends on the measured number of antineutrino events per unit of time, divided by the detector related constant γ :

$$P_{th} = \frac{N_{\bar{\nu}}}{\gamma(1+k(t))} \quad (8)$$

We define a relative power measurement r as

$$r = \frac{\langle P_{th} \rangle_{day,week}}{\langle P_{th} \rangle_{month}} \quad (9)$$

The brackets and subscript indicate averaging for the previous day, week or month. The small systematic variation between the daily or weekly value of k and its monthly average can be neglected, and the term γ , depending on the detector mass and distance, is assumed constant. With better than 1% precision, the variation in the ratio now depends only on the statistical variations in the count rates, averaged over the periods in question. However, this neglects possible time variations in the detection efficiencies over the relevant time interval. If these variations are large, the measured standard deviation of the data will be larger than the $\sqrt{\text{nevents}}$ spread expected from Poisson counting statistics alone. We consider this possibility directly.

With the above assumptions, the ratio r can be expressed in terms of the ratio of average detected antineutrino rates as:

$$r = \frac{\langle N_{\bar{\nu}} \rangle_{day,week}}{\langle N_{\bar{\nu}} \rangle_{month}}, \quad (10)$$

where the subscripted brackets again signify averaging over the indicated time periods.

Fig. 9 shows the spread in this ratio for daily and weekly averaging. By examining the standard deviation of r , we can quantify the degree to which the ratio obeys Poisson statistics, and estimate the contribution of non-Poisson, time-varying systematic drifts on the relative power estimate.

For the daily averaged data, the measured standard deviation in the ratio r is $8.3 \pm 0.5\%$, while the spread based on a gaussian fit is $8.0 \pm 0.5\%$. These values are within error of the 7.8% expected spread in the ratio r due to Poisson statistics alone. For the weekly data, the measured standard deviation in r is $3.0 \pm 0.3\%$ - again consistent with the expected 3% variation due to Poisson statistics.

For both daily and weekly averaging, statistical uncertainty fully accounts for the total observed spread in the ratio. Aside from the known $\leq 0.65\%$ systematic contribution to the spread due to burnup, such small additional effects as are present may come from periodic drifts in the gain scale, or other efficiency changes that are not fully accounted for in the calibration procedure.

XI. CONCLUSIONS

The above analysis demonstrates that our current prototype detector can monitor changes in reactor status (on versus off) in five hours with greater than 99% confidence, and can directly measure power levels over month

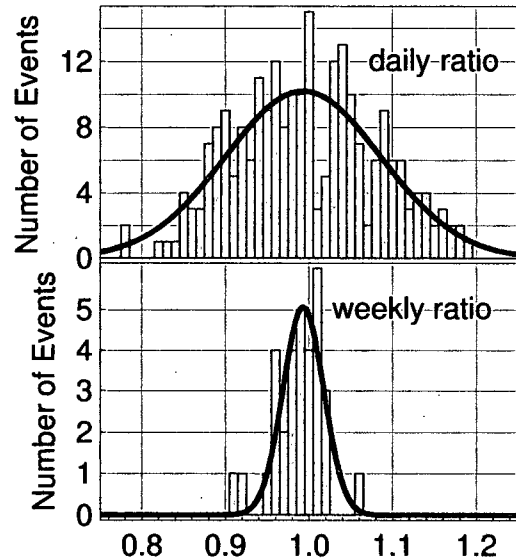


FIG. 9: The histograms of the ratio of r , defined as the net daily or weekly average detected antineutrino rate to the net detected antineutrino rate averaged over the 28 days prior to the measurement. Both the daily and weekly data sets extend over the same 33 week period.

long time scales with an estimated 8.3% precision using a daily background subtracted number of detected antineutrinos, or 3% using a weekly number, limited almost entirely by statistics. By construction, this estimate is independent of the long term $\approx 12\%$ systematic trend induced by the changing core isotopics. It provides a measure of the precision of the detector itself, including all statistical and systematic effects occurring over periods of days to months. Slightly longer integration times, or improvements in the detection efficiency would further reduce this uncertainty. Ultimately, however, the effect of burnup must be fully accounted to extract a stable long term power or burnup measurement beyond one month. This analysis is the subject of a separate article.

The fact that our current detector approaches the Poisson limit for a relative power measurement on day to week time scales has further significance. It implies that even a simple detector design can suffice for the relative thermal power monitoring approach envisioned here. Our experience is that the simplicity of the detector design will play a key, even decisive role in determining whether this technology is adopted by the IAEA or other safeguards regimes.

Acknowledgements

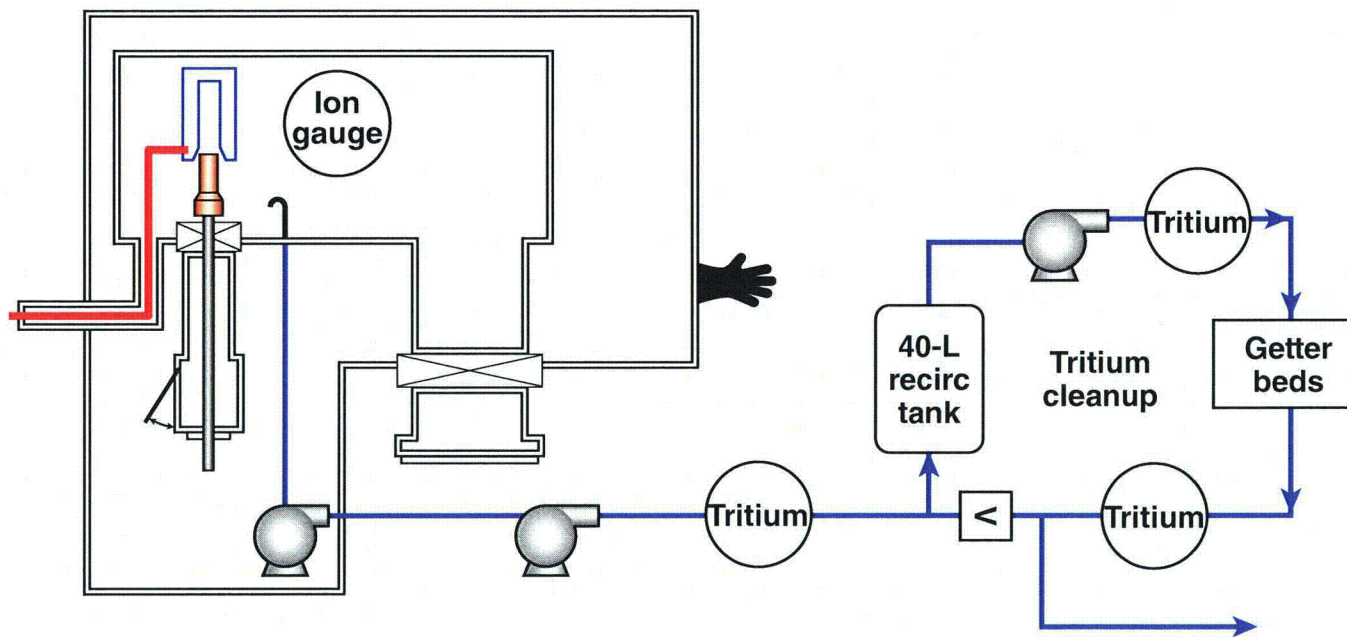
We thank DOE Office of Nonproliferation Research and Engineering for their sustained support of this project. We are indebted to the management and staff of

the San Onofre Nuclear Generating Station for allowing us to deploy our detector at their site. We thank Norman Madden, Dennis Carr, Alan Salmi, and James Brennan for invaluable technical assistance and advice. We are

grateful to Felix Boehm for donation of the liquid scintillator used in our detector, and Giorgio Gratta for his early contributions to this project.

-
- [1] A. Bernstein, et. al., J. Appl. Phys. 91 (2002) 4672
 - [2] Y.V.Klimov, et. al., Atomnaya Energiya, 76 (1994) 130
 - [3] N. Bowden, et. al., NIM A 572 (2007) 985-998
 - [4] Eguchi et al., Phys. Rev. Lett. 90, 021802 (2003)
 - [5] Phys.Atom.Nucl. 67 (2004) 1892-1899; Yad.Fiz. 67 (2004) 1916-1922
 - [6] Patrick Huber, Thomas Schwetz, Phys. Rev. D 70 (2004) 053011
 - [7] Gauld, I. C., etal "ORIGEN-ARP: Automatic Rapid Processing for Spent Fuel Depletion, Decay, and Source Term Analysis," ORNL/TM-2005/39 (2005)
 - [8] O.W. Hermann and M.D. DeHart. Validation of SCALE (SAS2H) Isotopic Predictions for BWR Spent Fuel. ORNL/TM-13315, Lockheed Martin, Oak Ridge National Laboratory, 1998.
 - [9] Wald, A. Sequential Analysis. John Wiley & Sons, New York, 1947.
 - [10] Jarman, K.D., Smith, L.E., Carlson, D.K., IEEE Transactions on Nuclear Science, Vol.51, No.4, (2004) 1662-1666

Tritium Handling During LLE's Cryogenic Target Filling Operation



R. Janezic
University of Rochester
Laboratory for Laser Energetics

8th International Conference on
Tritium Science and Technology
Rochester, NY
16-21 September 2007

Collaborators



W. T. Shmayda

G. P. Wainwright

P. Regan

K. J. Lintz

D. R. Harding

S. J. Loucks

T. Duffy

Summary

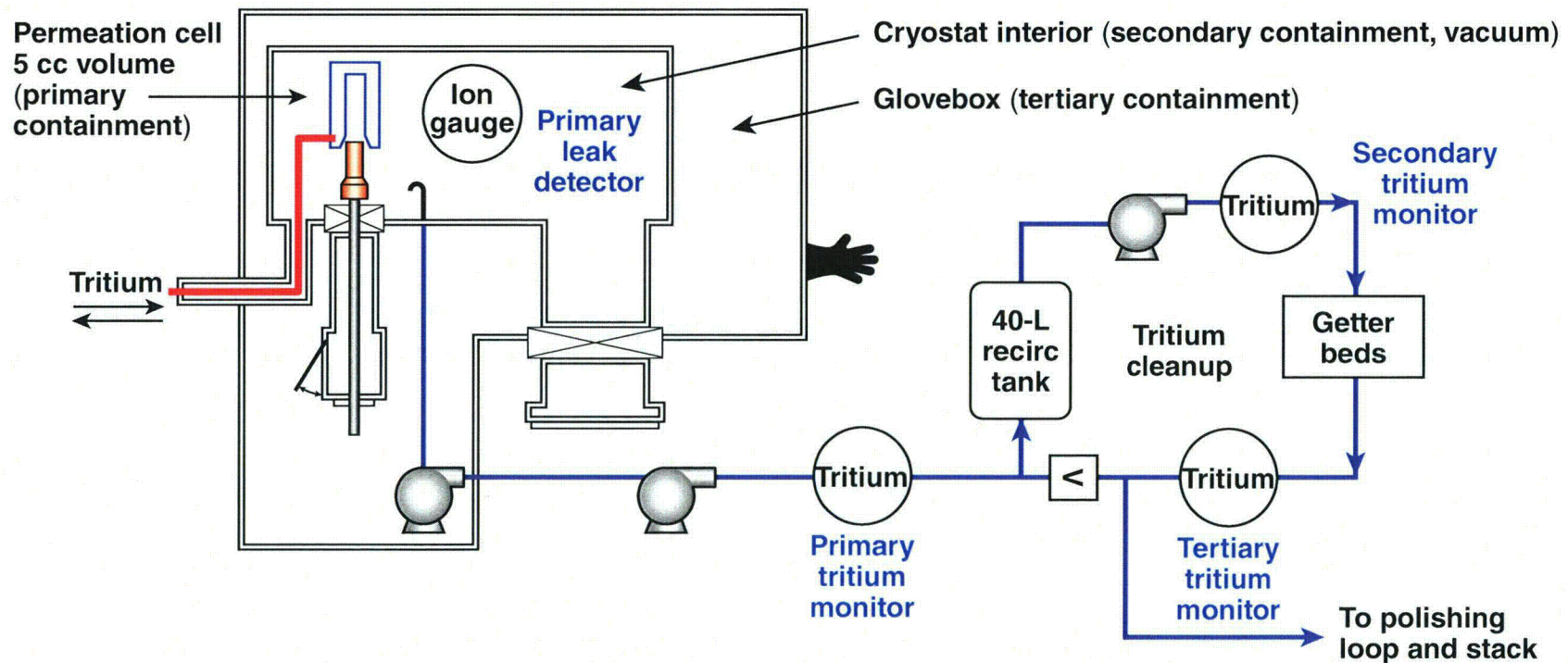
Tritium leakage from the cryogenic DT-filling operation is contained and abated with no loss to the environment



- LLE has conducted 20 fills employing 50:50 D:T at 1000 atm since June 2006
- Routine leakage from the filling operation is measurable and controlled
- The tritium cleanup system exhibits high efficiency

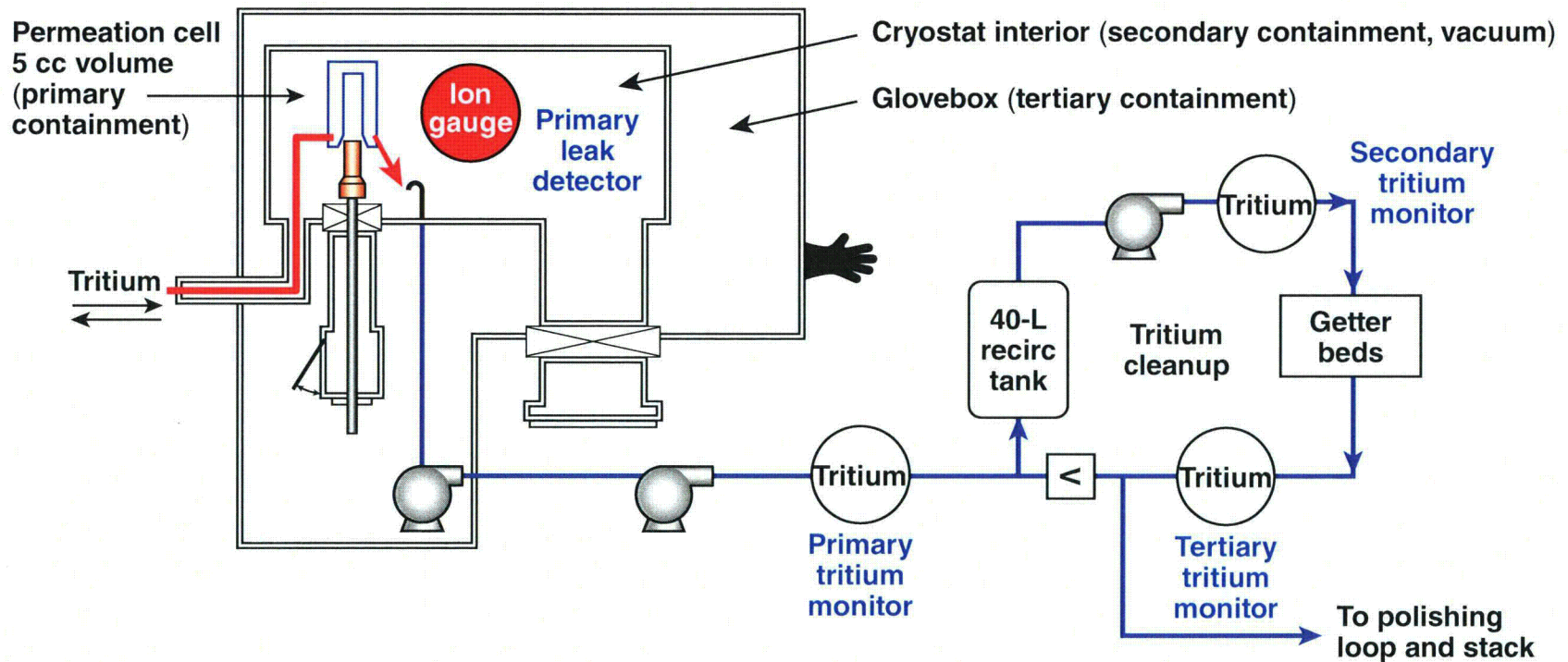
Stack readings indicate only small releases (<10 mCi/week) during filling operations.

Tritium leakage from the filling operation is mitigated by the tritium-cleanup subsystem



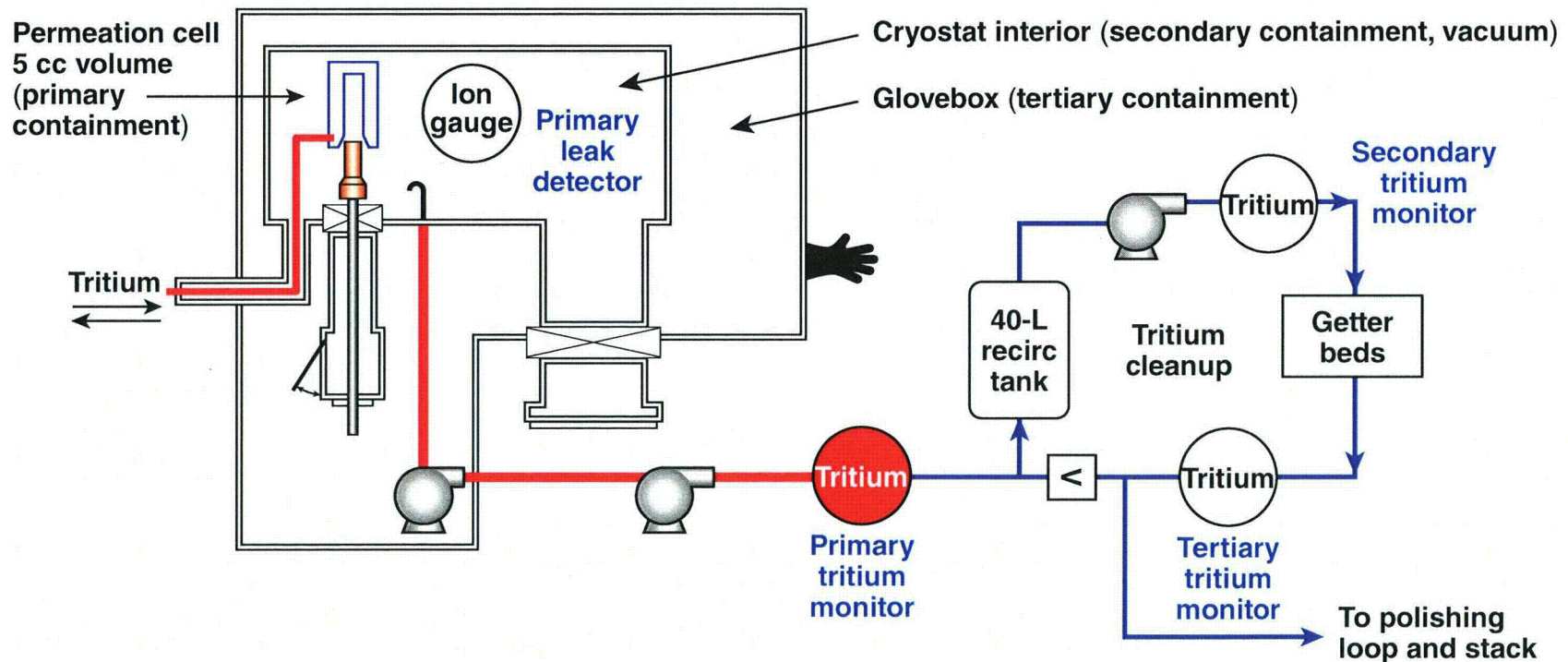
- ~3000 Ci in permeation cell
- ~2 days to fill targets
- The permeation cell = most significant source of tritium leakage

Tritium leakage from the filling operation is mitigated by the tritium-cleanup subsystem



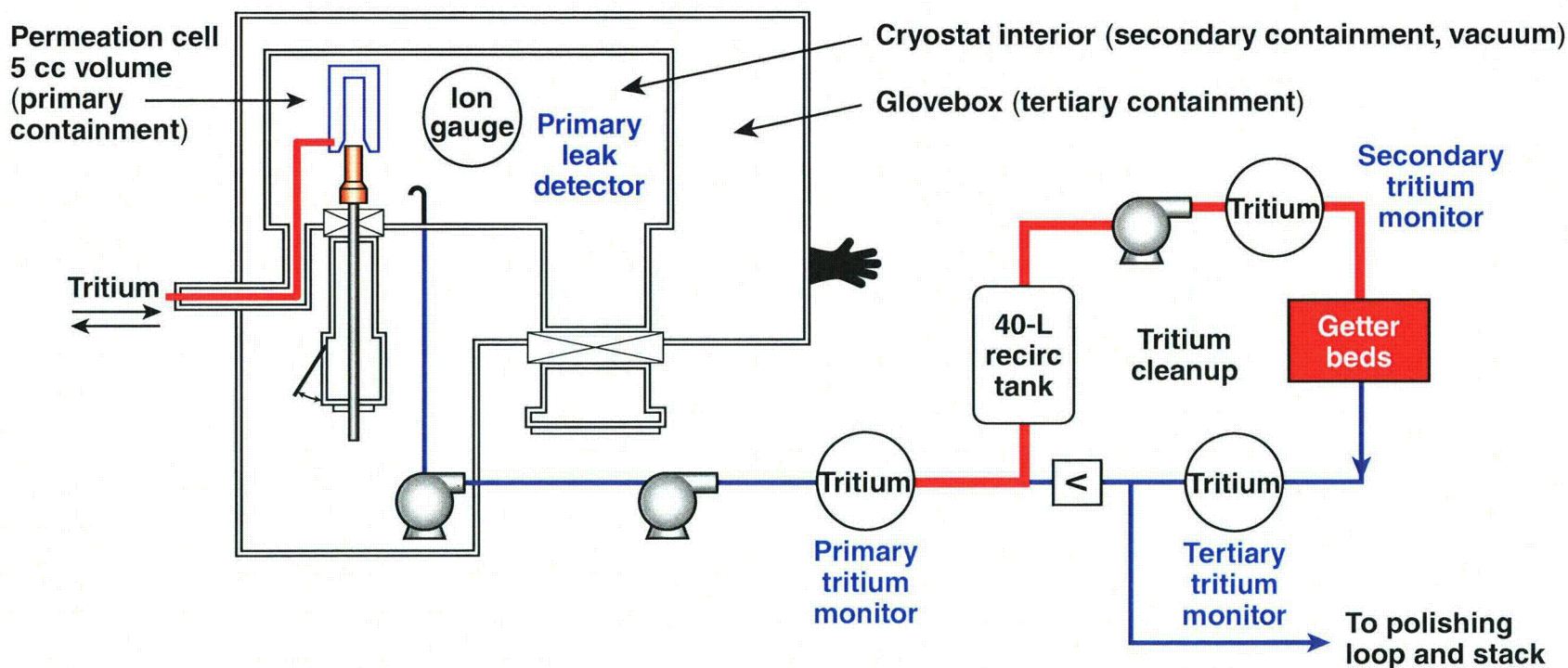
- ~3000 Ci in permeation cell
- ~2 days to fill targets
- The permeation cell = most significant source of tritium leakage

Tritium leakage from the filling operation is mitigated by the tritium-cleanup subsystem



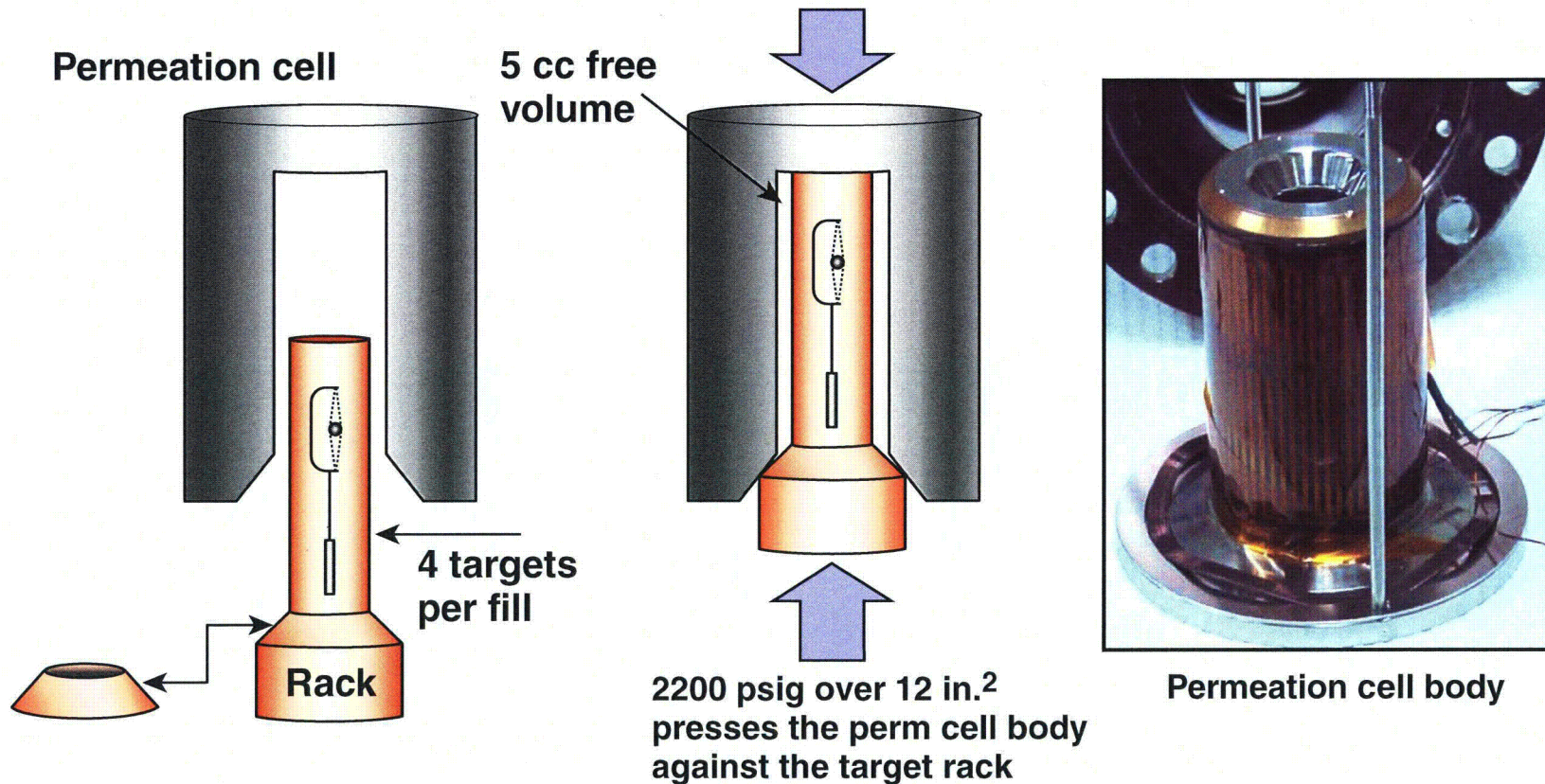
- ~3000 Ci in permeation cell
- ~2 days to fill targets
- The permeation cell = most significant source of tritium leakage

Tritium leakage from the filling operation is mitigated by the tritium-cleanup subsystem



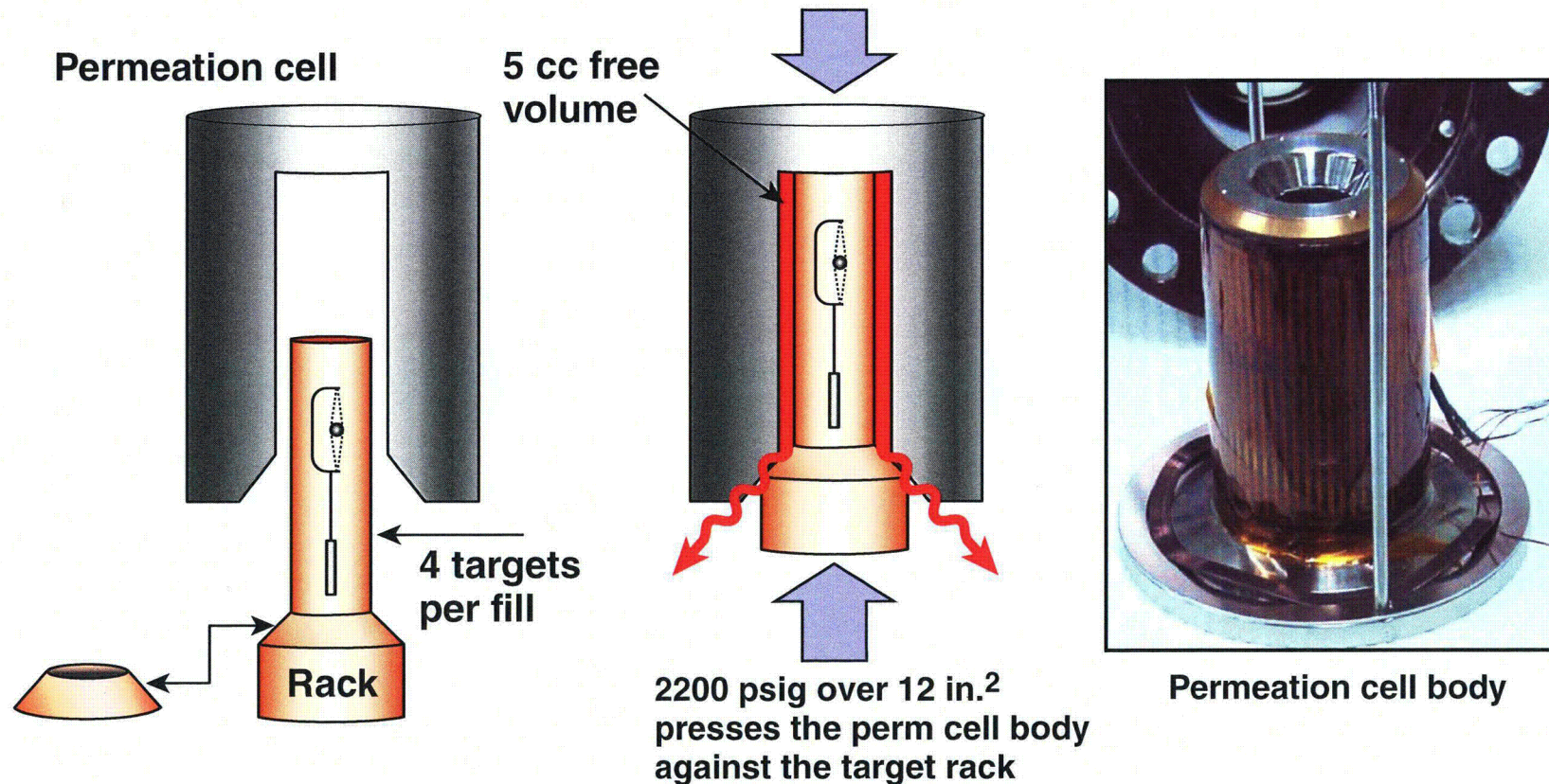
- ~3000 Ci in permeation cell
- ~2 days to fill targets
- The permeation cell = most significant source of tritium leakage

The permeation cell is a high-pressure vessel with a metal-metal seal using a soft copper gasket



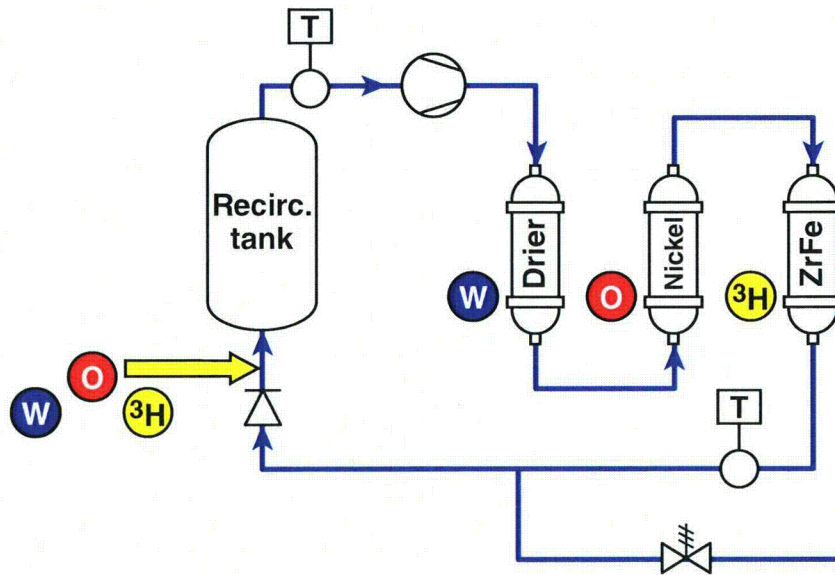
- Up to 30 Ci leaks occasionally observed (1%)
- Normally leakage <0.2% (within experimental error)
- New gasket each fill

The permeation cell is a high-pressure vessel with a metal-metal seal using a soft copper gasket



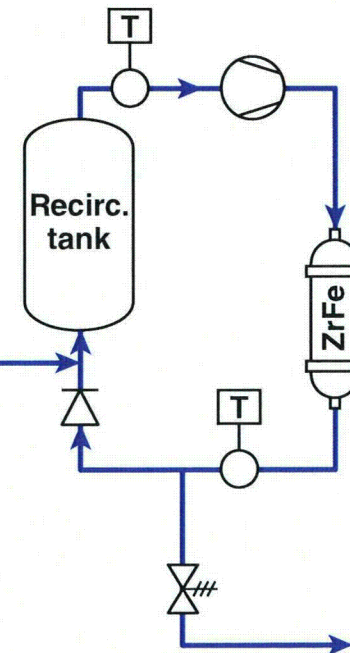
- Up to 30 Ci leaks occasionally observed (1%)
- Normally leakage <0.2% (within experimental error)
- New gasket each fill

The tritium-cleanup subsystem employs ZrFe getters to remove tritium from helium gas volumes



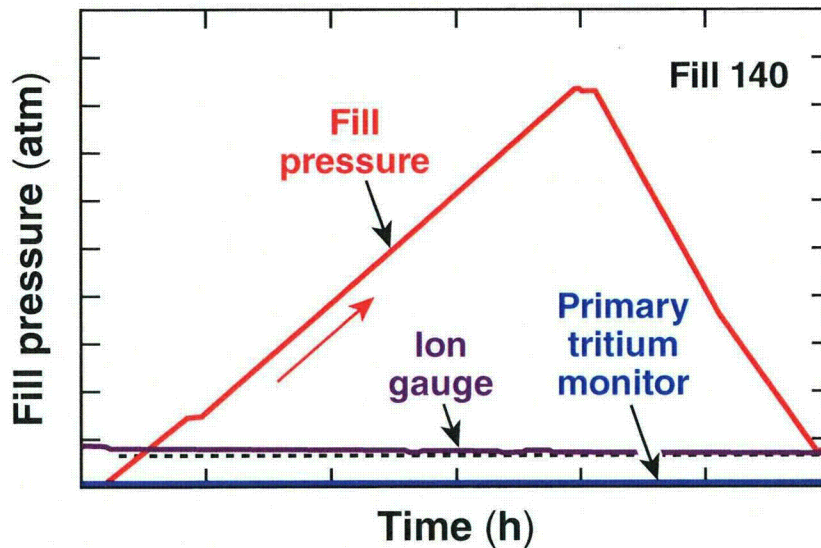
The PRIMARY LOOP removes the majority of the tritium and all of the measurable water/O² and organic molecules from the helium stream.

The SECONDARY LOOP polishes the helium stream, reducing the tritium concentration down to releasable limits.



- System runs continuously at temp and flow
- Beds reversibly adsorb species

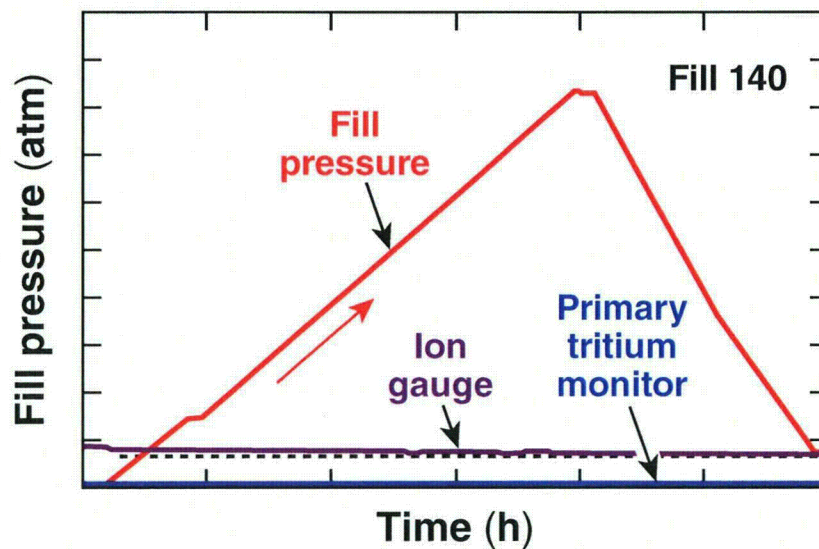
Tritium leakage is monitored by instrumentation as the fill proceeds



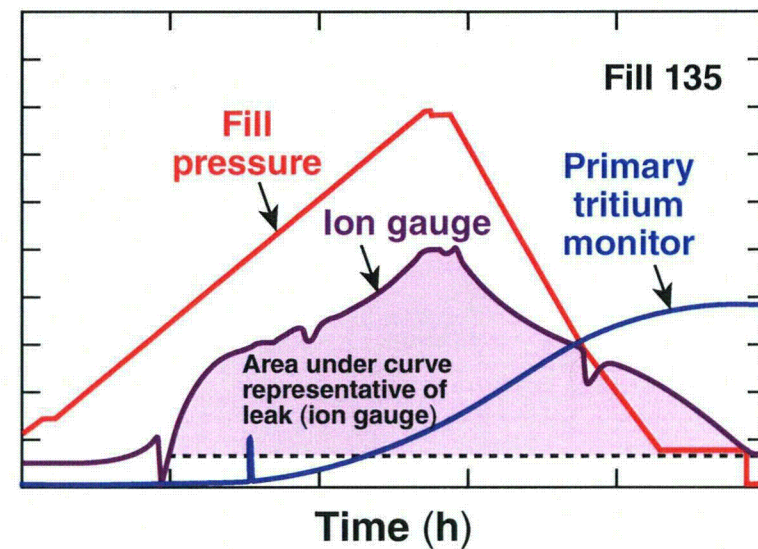
Typical response during most fills

- Interior ion gauge – real-time leakage
- Primary tritium monitor – aggregated leak
- Good agreement – assays and calcs from tritium monitor

Tritium leakage is monitored by instrumentation as the fill proceeds



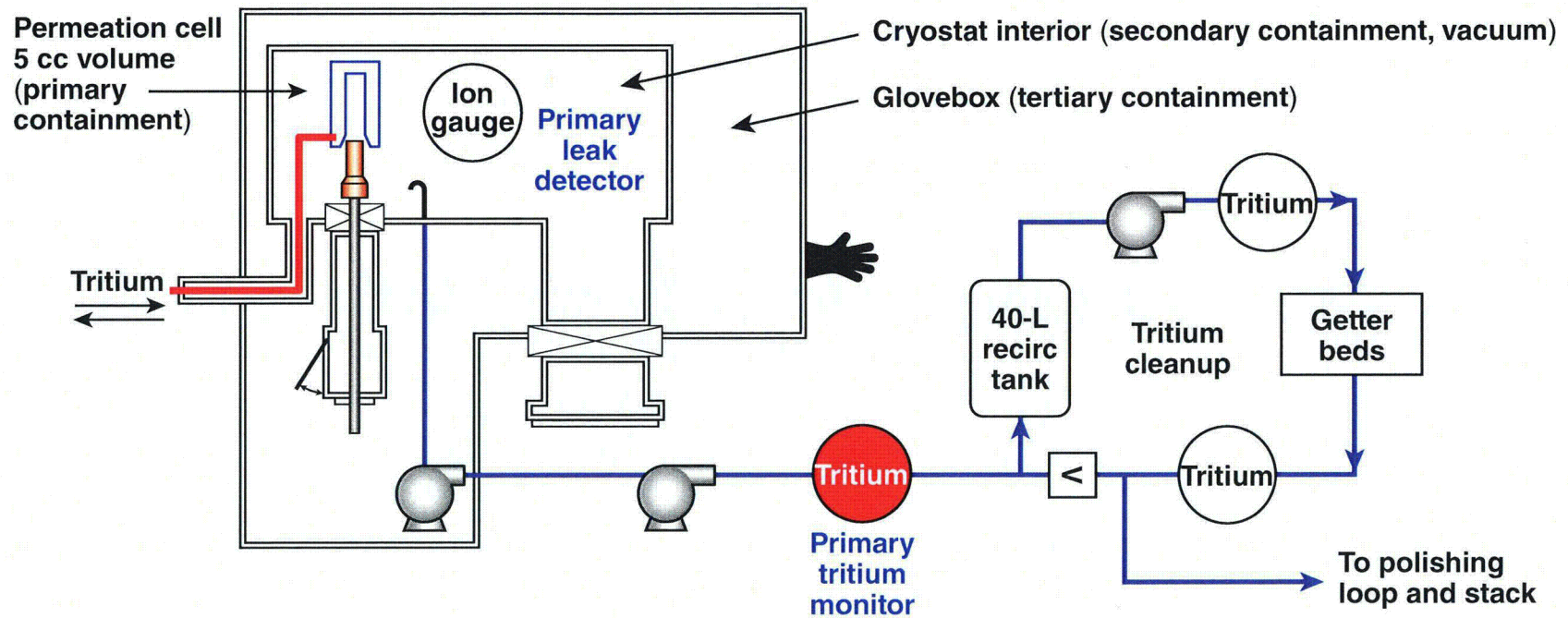
Typical response during most fills



A large leak occurred in Fill 135 corresponding to ~30 Ci lost to the cryostat

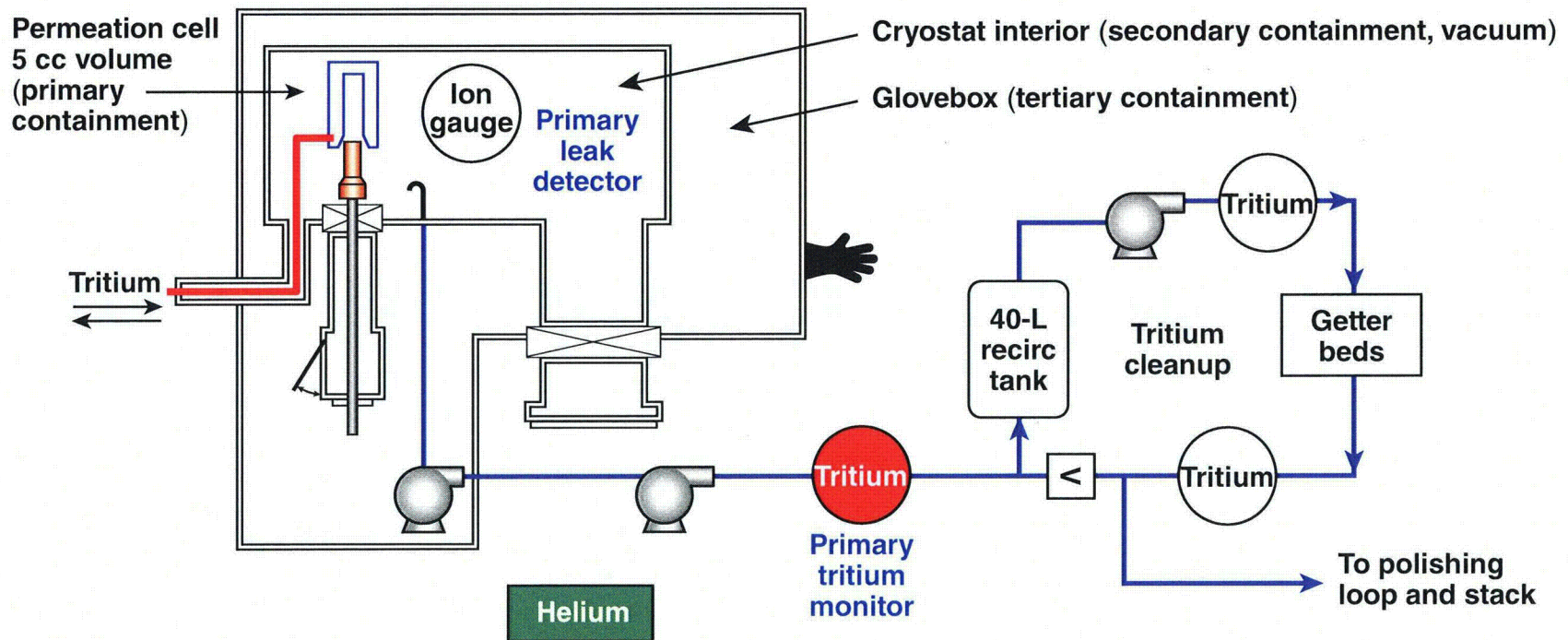
- Interior ion gauge – real-time leakage
- Primary tritium monitor – aggregated leak
- Good agreement – assays and calcs from tritium monitor

Tritium is observed to concentrate at the primary tritium monitor



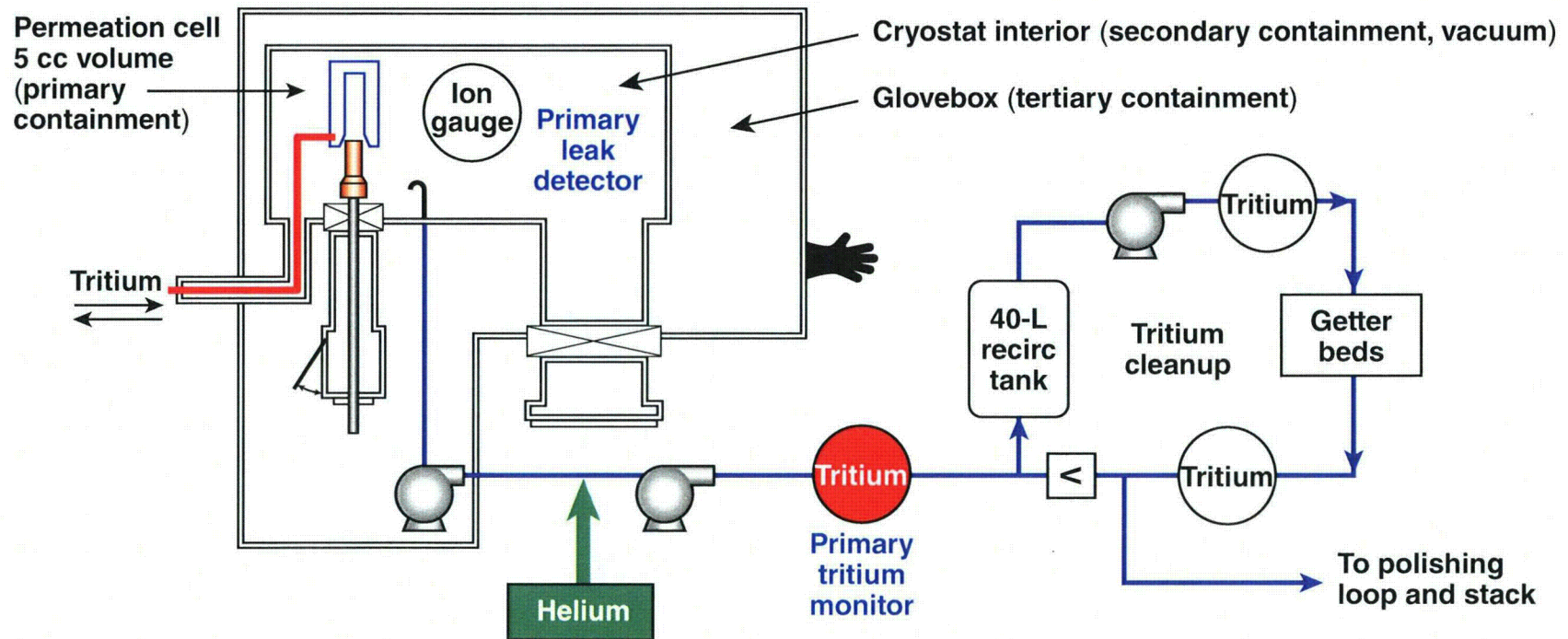
- Helium purge sweeps tritium downstream

Tritium is observed to concentrate at the primary tritium monitor



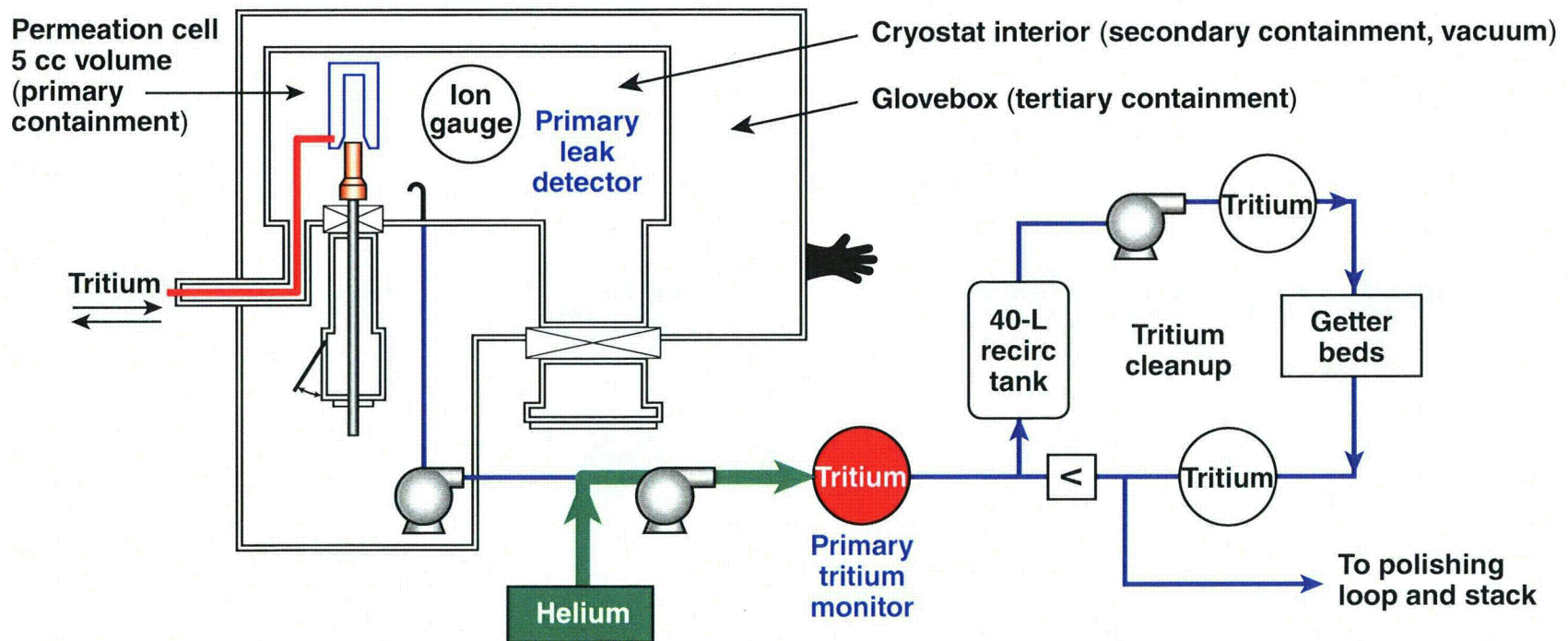
- Helium purge sweeps tritium downstream

Tritium is observed to concentrate at the primary tritium monitor



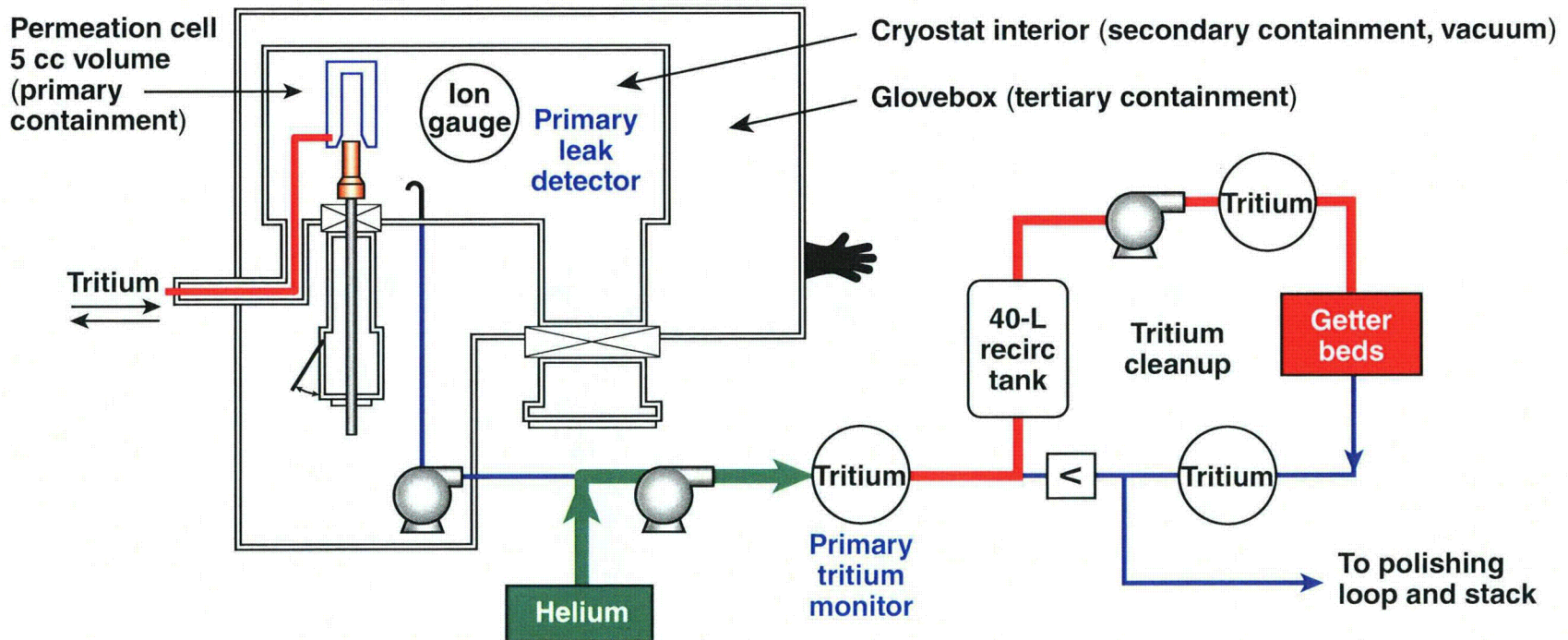
- Helium purge sweeps tritium downstream

Tritium is observed to concentrate at the primary tritium monitor



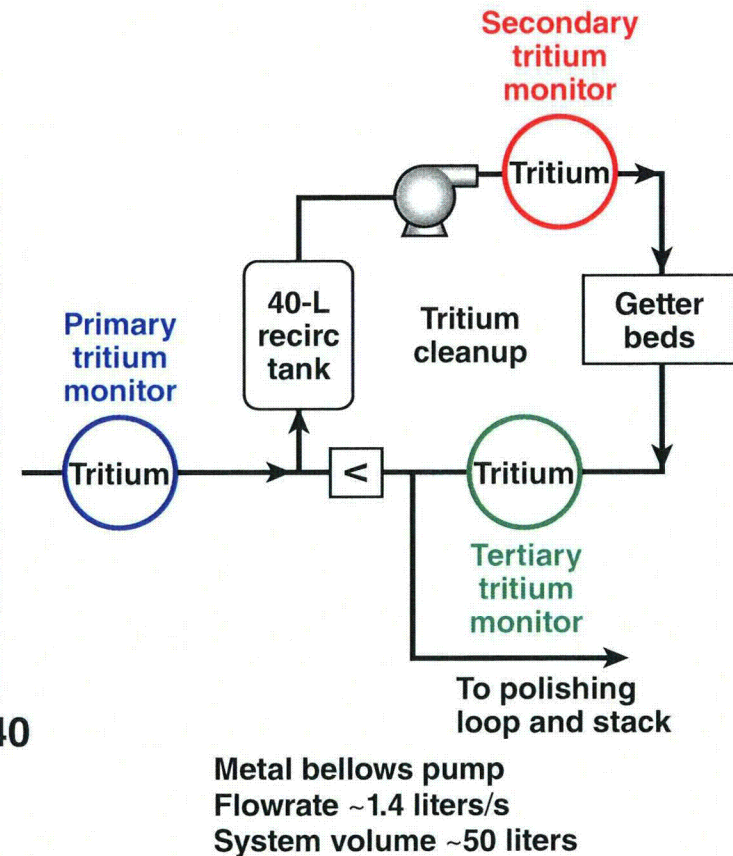
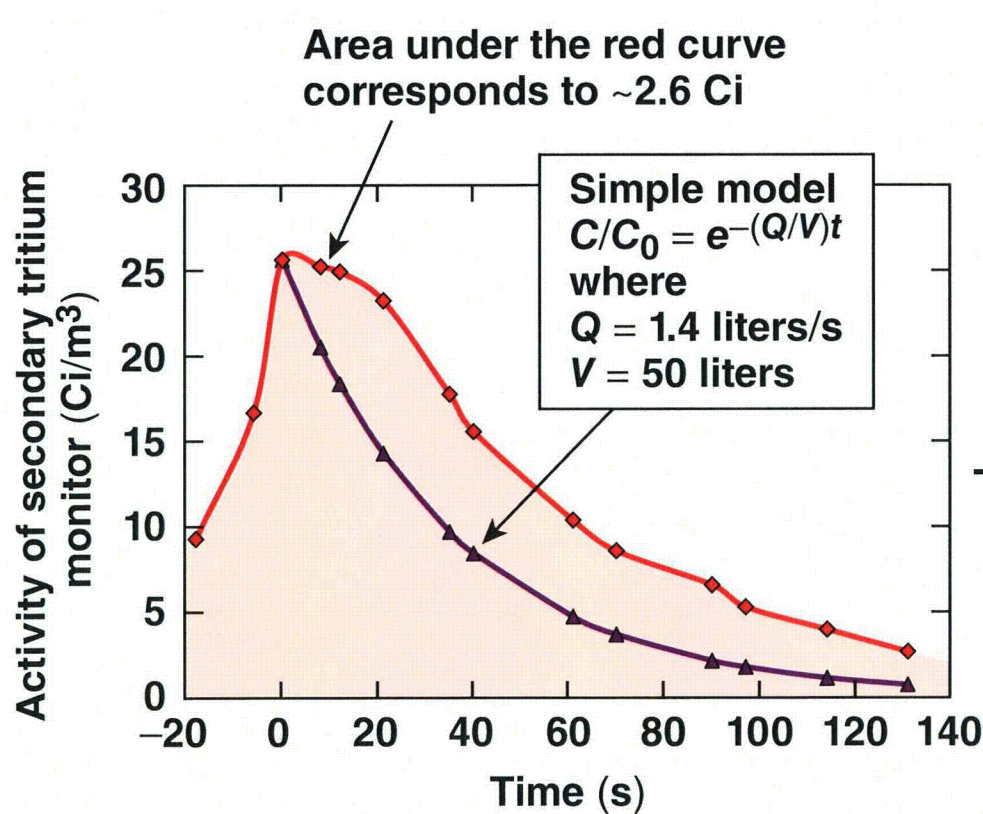
- Helium purge sweeps tritium downstream

Tritium is observed to concentrate at the primary tritium monitor



- Helium purge sweeps tritium downstream

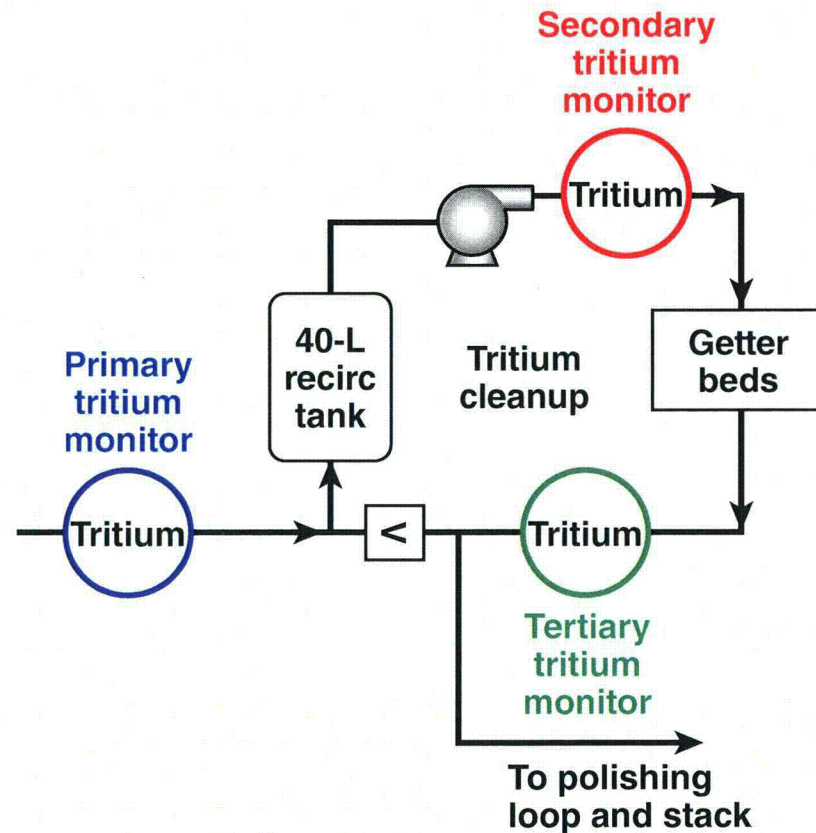
The abatement of tritium in the first loop is efficient and appears to agree with a simple decay model



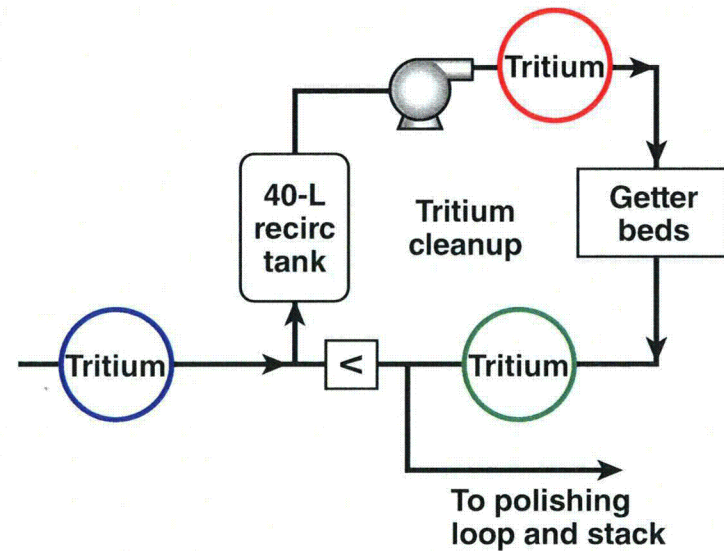
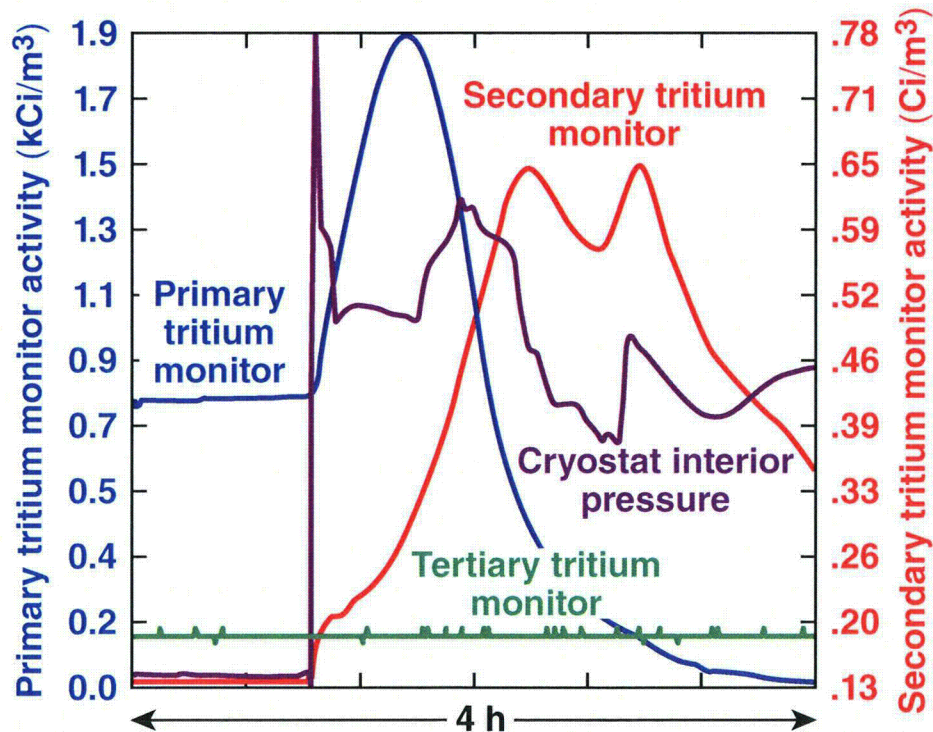
- Behavior consistent with other ZrFe systems
- Tertiary tritium monitor typically <1 mCi/m³

Recently, the use of a continuous purge of helium has further improved the tritium-removal performance

- Abrupt additions of helium can overwhelm getters
- Secondary tritium monitors can reach 40 Ci/m^3 and tertiary 30 mCi/m^3
- Continuous purge of helium reduces pressure and tritium spikes
- Helium is added to maintain the cryostat interior at 5 mtorr



A continuous purge of helium can efficiently sweep tritium downstream



- Secondary tritium monitor concentration is 10× lower
- Tritium gradually swept out of piping
- No downstream (green) tritium observed

Summary/Conclusions

Tritium leakage from the cryogenic DT-filling operation is contained and abated with no loss to the environment



- LLE has conducted 20 fills employing 50:50 D:T at 1000 atm since June 2006
- Routine leakage from the filling operation is measurable and controlled
- The tritium cleanup system exhibits high efficiency

Routinely observe <10 mCi stack releases per week during filling operations.

DEVELOPMENT AND VALIDATION OF FISSION PRODUCT RELEASE MODELS AND SOFTWARE AT PBMR

Jacobus Johannes van der Merwe

PBMR (Pty) Ltd, Lake Buena Vista Building, Gordon Hood Avenue, Centurion 1267;
PO Box 9396, Centurion 0046, South Africa; hanno.vdmerwe@pbmr.co.za

ABSTRACT: A brief overview of PBMR's fission product release model and software development is presented. Gaseous and metallic fission product release from spherical fuel elements into the coolant gas is calculated by the steady state code NOBLEG and the dynamic code GETTER respectively. NOBLEG calculates short-lived fission gas release based on the Booth model and GETTER metallic fission product release based on Fick's laws of diffusion under normal and accident conditions. Both codes are used extensively in the design and safety analyses of the Pebble Bed Modular Reactor (PBMR). An overview of the models used is presented, including the development of new models to calculate the oxidation effect water ingress have on gaseous fission product release, and loss of forced coolant heat-up effects on metallic and halogen release. For loss of forced coolant events, the software FIPREX was developed as a post-calculation data reduction application for GETTER's accident calculations. Calculated results for a sample PBMR core design are presented as well as design factors derived by sensitivity analyses. The PBMR models and their application in NOBLEG are validated in part with the irradiation data from fuel irradiation tests HFR-K5 and -K6, and in GETTER with HFR-K3. A brief overview of these benchmarking calculations is presented.

KEYWORDS: Fission products release, GETTER, models, NOBLEG, PBMR, spherical fuel elements, verification, validation.

0. INTRODUCTION

The current Pebble Bed Modular Reactor (PBMR) design [1] allows for thermal power output of up to 400 MW, or $\sim 1.25 \times 10^{19}$ fissions per second. Large numbers of fission products are created in the process that pose a considerable risk to operating personnel and the general public if not contained. Central to high-temperature pebble fuel reactor design is the concept that no significant fission product activities are released from the fuel elements [2] and therefore from the closed coolant gas circuit. The safety of a high-temperature gas-cooled nuclear power plant therefore stands and falls with its fuel elements' ability to retain fission products under all expected reactor conditions. The reactor design must therefore be such that fuel elements are never exposed to conditions in excess of their design qualification. Similarly, fuel design must be such that fuel elements can be manufactured economically at large volumes, while maintaining fuel quality and integrity during manufacture and subsequent irradiation. Even under the best manufacturing conditions a small fraction of Coated Fuel Particles (CFPs) will be defective, which together with contamination in the fuel materials, source fission product release into the coolant gas. Furthermore, under abnormally high temperatures and power surges, CFP's may start to fail and increase the release of fission products. These releases cause radiation dangers to operating personnel, and if released from the closed coolant circuit, also to the public. It is therefore imperative to predict, with a reasonable level of certainty, the fission product release from the fuel elements and the plant under any expected operation or accident conditions.

Fission product release analysis at PBMR is divided into relatively short-lived gaseous and long-lived metallic fission products. Both groups' release model and software development and validation are presented in this paper. The software is described briefly, followed by each group's model description with some sample core design calculation results for normal operating and abnormal event conditions. Some benchmarking calculations to verify and validate the main models conclude this presentation.

0. 1. Fission Product Release Calculations at PBMR

Fission product release analyses at PBMR are presented in *FIGURE 1*. The reactor design is analysed by the core neutronics codes, VSOP [3] for normal operation and TINTE [4] for accident conditions. These codes supply the necessary input parameters (temperatures, cross sections, neutron fluxes, power densities, residence times, etc.) for the fission product release codes NOBLEG [5] (gases) and GETTER [6] (metals) to calculate the fission product releases from the PBMR core [7].

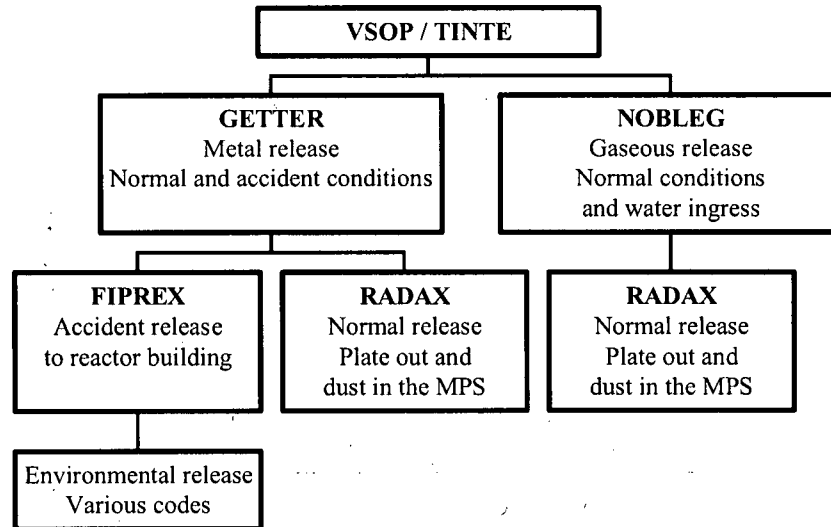


FIGURE 1. Fission product release analyses at PBMR.

These fission product release values are used by the dust and plate out simulation code RADAX [8] to calculate the fission product concentration in the Main Power System (MPS). These fission product concentrations are then used to determine the radiological doses that operational personnel might experience during maintenance work and accidents at the PBMR. The fission products released from the core cavern into the containment building during accidental leaking or pipe breaks are modelled by FIPREX [9]. The final release into the environment is modelled by various software that incorporate plant containment design and meteorological parameters.

0. 2. Fission Product Release Software

The fission product release from coated fuel particles and the spherical fuel elements used in modern high-temperature gas-cooled reactors is one of the first source terms used in describing the safety of planned nuclear plants during normal and accident conditions. Several software products that cover the range of fission products and operational conditions expected are currently employed at PBMR.

0. 2. 1. NOBLEG

The activity of gaseous fission product release is a direct indicator of fuel performance and is calculated with the code NOBLEG. In NOBLEG, the main sources contributing to gaseous fission product release are the heavy metal contamination in the fuel graphite and defective/failed coated particles. Standard particles within the specification limits are not expected to contribute to the release of gaseous fission products under normal operating conditions [10]. NOBLEG is a steady state fission product release code using Booth equations to solve short-lived gaseous fission product diffusion behaviour under normal operating conditions. NOBLEG calculates the temperature distribution in fuel elements to determine diffusion rates in each fuel component according to relations dependent on fast neutron fluence and gas temperatures. NOBLEG is a legacy code from the German High Temperature Reactor (HTR) programme, bought and further developed by PBMR, for PBMR specific parameters and conditions. The code is versatile though, and can be easily applied to any other high-temperature pebble bed type reactor design.

0. 2. 2. GETTER

The transient release behaviour of long-lived metallic fission products can be predicted by using diffusion models. An intact TRISO particle coating presents an effective barrier against fission product release at normal operation temperatures (except for silver [11]). Therefore the most important input data for coated particle performance during normal operation will be the fraction of failed/defective particles and the fraction of heavy metal contamination in the fuel element graphite in combination with the transport data of coated particle materials and fuel element graphite. In addition to diffusion, other release mechanisms during normal operation are the recoil effect and the knockout effect [11]. Both present a geometrical problem and are not dependent on temperature, making them significantly more important at lower temperatures. The computer code GETTER based on Fick's laws of diffusion, was developed to model experimental (irradiation tests) and operational (normal and accident) conditions. The code solves the differential equations of Fick's laws with numerical techniques. GETTER includes subroutines, which calculate the burn-up and the power history of a fuel sphere in the core and the temperature distribution in the spheres on the basis of given neutron cross sections, thermal and fast neutron fluxes, and gas temperatures. GETTER is a legacy code from the German HTR programme, bought and further developed by PBMR, to include PBMR specific requirements such as iodine release determination under accident conditions. GETTER is a multipurpose tool and found use in diverse applications at PBMR such as spent fuel tank contamination calculations, temperature transients and accident event investigations, and evaluation of irradiation tests and Post Irradiation Examinations (PIE).

0. 2. 3. FIPREX

FIPREX is a specially developed EXCEL application to do post-calculation data manipulation of GETTER output in calculating fission product release from the PBMR core under accident conditions. FIPREX stands for FISSION PPRODUCT RELEASE under accident (X) conditions. The software makes corrections for decay of short-lived nuclides and calculates the gas expansion curve during a loss of forced coolant event, which determines the fraction coolant of gas escaping the core cavern during heat up. FIPREX is currently able to calculate depressurised and pressurised loss of forced coolant events. More applications are continuously being developed for FIPREX at PBMR, including core shutdown and reactivity insertion events. FIPREX is an adaptable tool and may be used on any high-temperature gas-cooled reactor type to calculate any required fission products.

0. 3. PBMR Core Design

A sample PBMR core design was used to explain the basic calculation and input models that the software applies to determine fission product release from the fuel elements and the core cavern during normal operating and expected abnormal event conditions. The core geometry is presented in *FIGURE 2*. The results presented in this paper refer to this sample core design. This design has a fixed central reflector with a diameter of 2 m, which is surrounded by a fuel annulus of 85 cm. The core volume of $\sim 83.7 \text{ m}^3$ is divided into 93 equivalent-sized partial volumes, each of which contains a mixture of six different fuel element loads. These loads represent the various passes through the core, i.e. from the fresh state to a total of six times through the core. The burn-up of each of these fuel element loads is followed individually. Note that the inner channel contains 20 layers, the second channel 18 layers, etc. The ratios 20/18/18/18/19 are used to model the different flow rates in the channels and, since the layers are defined to have the same volume, this results in approximately 18.6 effective layers (or time steps) per pass for the fuel. The residence time in each layer is 8.4 days, which gives on average a total fuel spheres residence time of 938 days in the core (accumulative over the average of six passes as calculated for the equilibrium core in VSOP). PBMR fission product release codes use this core layout, with the gas temperatures, fast and thermal neutron fluences, absorption and fission cross sections, fission power outputs and residence times to calculate fission product behaviour in the fuel elements.

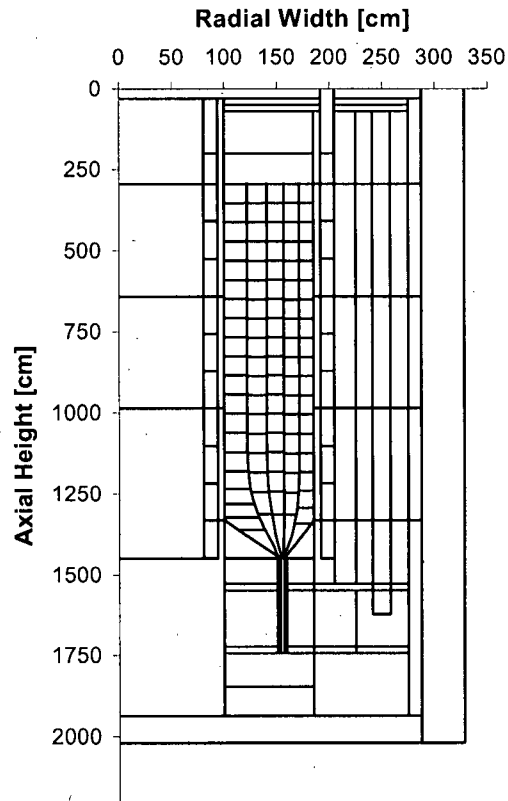


FIGURE 2. PBMR VSOP calculational model layout.

1. GASEOUS FISSION PRODUCT RELEASE

The steady state release from the fuel elements and consequent coolant gas activities of all relevant krypton, bromine, iodine and xenon nuclides are calculated. The primary importance of the released noble gases (key nuclide: ^{88}Kr) and halogens (key nuclide: ^{131}I) is their environmental radiological impact under the conditions of normal reactor operation (leakage from the primary circuit) and loss of coolant accidents. Gaseous fission product releases under normal operating conditions as well as low vapour pressure water ingress incidents are calculated by NOBLEG. NOBLEG calculates the release over birth (R/B) values from contamination and failed coated particles separately and estimates the expected fission product release from the core and the coolant gas activities. Halogen (^{131}I) release during loss of forced coolant conditions is calculated by GETTER and FIPREX, and is discussed in paragraph 0. The code and the models used are being verified and validated with code-to-code comparisons, sample calculations and benchmarking with the irradiation fuel tests HFR-K5 and -K6 [12].

1. 1. Gaseous Fission Product Release under Normal Operating Conditions

The theory behind noble gas and halogen release from spherical HTR fuel elements is well understood. The mechanisms of halogen and noble gas transport through the layers of the coated particle were investigated in many countries, in the United States, Japan, Russia and Germany in particular [13]. The Booth equation forms the basis for most models created over the world and is described in brief. There are three potential sources for fission gas release: intact particles, failed particles and the heavy metal (uranium and thorium) contamination of the matrix material. Due to the extremely low diffusion constants for xenon and krypton in pyrolytic carbon and the relative short half-lives of the gas isotopes, the transport from the fuel kernel through intact coatings can be neglected. The two remaining sources of the noble gas/halogen release, the finely distributed uranium and thorium contamination of the

graphite matrix material and failed coated particles are treated separately, but use similar equations. Because of the short half-lives (compared with fuel sphere residence time in the core) of the nuclides considered (except ^{85}Kr), steady state conditions prevail, so that no numerical methods are needed to solve time-dependent diffusion equations [10].

The model used to describe gaseous fission product release from contamination is shown in *FIGURE 3*. The graphitic matrix material is treated as a three-component system: 1) the graphite grains, 2) binder material and 3) open pores in the matrix material. Fission products recoil from the fission sites into the three components and slowly diffuse through to the matrix pores. In the matrix pores the fission products diffuse through to the surface of the fuel element and desorb into the coolant stream.

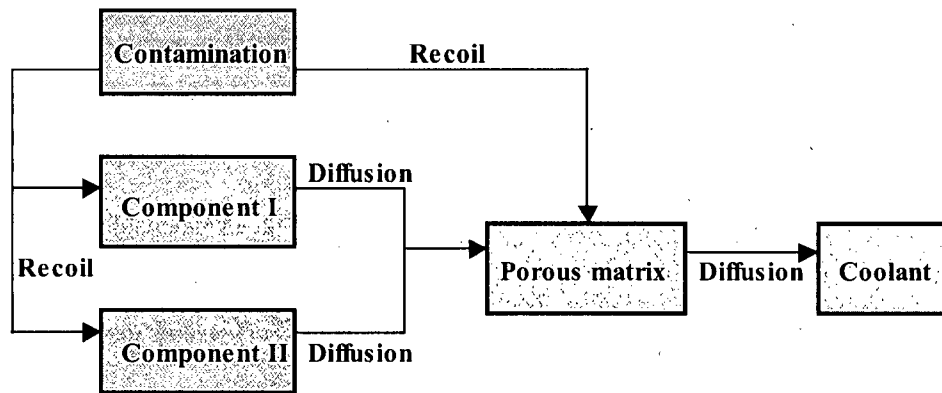


FIGURE 3. Transport model: release from the contamination of the matrix material.

FIGURE 4 shows the flow scheme for the release of fission gases from fuel particles, which failed either during manufacture or during reactor operation. Failed fuel particles embedded in the matrix are described by a four-component system consisting of kernel 'grains', two material components of the buffer layer ('grains' and 'amorphous constituents') and helium filled open pores in the kernel and in the porous buffer layer. The birth rates of primary fission products in the four components are calculated with the known relations for the recoil stopping ranges in different materials. The release from the three solid components is treated in the same way as the contamination-induced release.

These models are used by NOBLEG to calculate expected gaseous fission product release from the PBMR core. The analysis of a sample 400 MW core design is presented in [14]. The out of core activity is the steady state activity of the fission products releases from the fuel elements and released into the Power Conversion Unit (PCU), and the coolant gas activity is the steady state activity of fission products in the total MPS gas inventory, after taking plate out and radioactive decay into consideration. Whereas the contamination amounts only to 7% of the failed particle fraction, the corresponding R/B increases from 8% to 16% of the failed particle contribution from top to bottom of the core. This is due to the rather effective retention capability of the particle kernels. Failed particles cause local R/B values of ^{88}Kr in the core between 1.0×10^{-7} and 2.5×10^{-7} , and contamination between 8.0×10^{-9} and 4.4×10^{-8} . Thus, less than 1% of the ^{88}Kr atoms produced by the uncontained uranium (3×10^{-5}) is released.

From sensitivity analyses performed on all the important fuel transport parameters, a design factor of four for gaseous fission product release is recommended [14]. The sensitivity analyses are based on German HTR experience, PBMR thermohydraulic uncertainties, fuel design specifications and limitations caused by manufacture processes and can be summarized as follows:

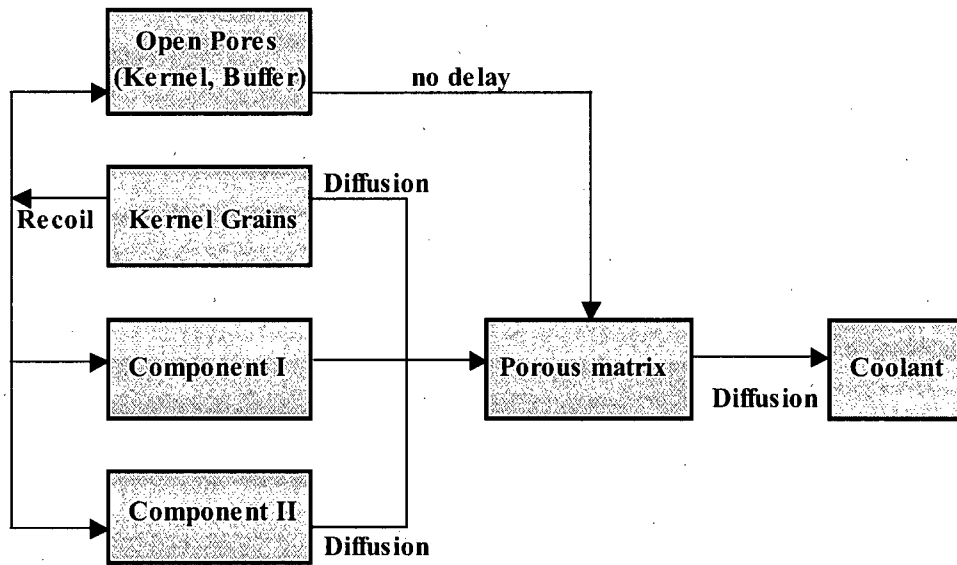


FIGURE 4. Transport model: release from failed fuel particles.

The fuel specification allows maximum values for the uncontained uranium fraction of 6×10^{-5} and the thorium contamination of 0.4 mg Th/FS. This defines upper limits for the failed particle fraction, the uranium contamination and the thorium contamination of 5.6×10^{-5} , 4.0×10^{-6} and 6.0×10^{-6} (effective), respectively. With these source values, the R/B of ^{88}Kr and ^{131}I increases by a factor of 2.1 compared to the expected result. The uncertainties of the diffusion constants and of the fractions of highly releasing components are covered by factors 4 and 2, respectively. The higher diffusion constants cause a 41% increase in the ^{88}Kr R/B, and a 54% increase in ^{131}I . The higher amorphous component fractions increase the R/B by 37% (^{88}Kr) and 14% (^{131}I). The statistical uncertainties of the fuel sphere temperatures are tentatively described by a global reduction of the thermal conductivities of the matrix and a reduction of the heat transfer coefficient both by 20%. Increasing all gas temperatures by 50 K pessimistically covers these uncertainties of the core layout. Both effects together increase the ^{88}Kr release by 10% and the ^{131}I by 6%. The expected release values are calculated with a constant failed particle fraction of 2.8×10^{-5} . The statistical evaluation of German irradiation experiments with TRISO UO_2 particles [11] showed that due to the restricted sample size (Poisson distribution), growing failure fractions cannot be excluded at burn-ups above 5% Fissions per Initial Metal Atoms (FIMA). To simulate these statistical phenomena, the failure fraction in NOBLEG was increased linearly with the fast fluence (\sim residence time) starting at $1.0 \times 10^{21} \text{ cm}^{-2}$ with 2.8×10^{-5} up to 2.8×10^{-4} at $3.0 \times 10^{21} \text{ cm}^{-2}$. This increased failure fractions enhance gaseous fission product release increases by 60%. All other systematic errors (thickness of fuel free zone, uncertainties in the calculation model, chemical interactions etc.) and statistical errors amount to 50% increase in the expected release rate. The total error for noble gases is 3.5 and 4.0 for halogens. These total errors were rounded to a factor 4 for calculation of design values.

In FIGURE 5, R/B values are plotted vs the half-lives of the listed nuclides in a log-log diagram (Channel 1 axial layer 11, first pass). The heavy (Xe, I) and the lighter, more mobile (Kr, Br) nuclides are clearly distinguishable. The Kr/Br points can well be approximated by a straight line with a slope of approximately 1/3 ($R/B \approx t/21/3$). For half-lives above 0.5 hours, the Xe/I results follow a straight line with a slope of $\sim 1/4$ ($R/B \approx t/21/4$). For shorter half-lives, the slope becomes steeper due to the growing retention effect of the porous matrix.

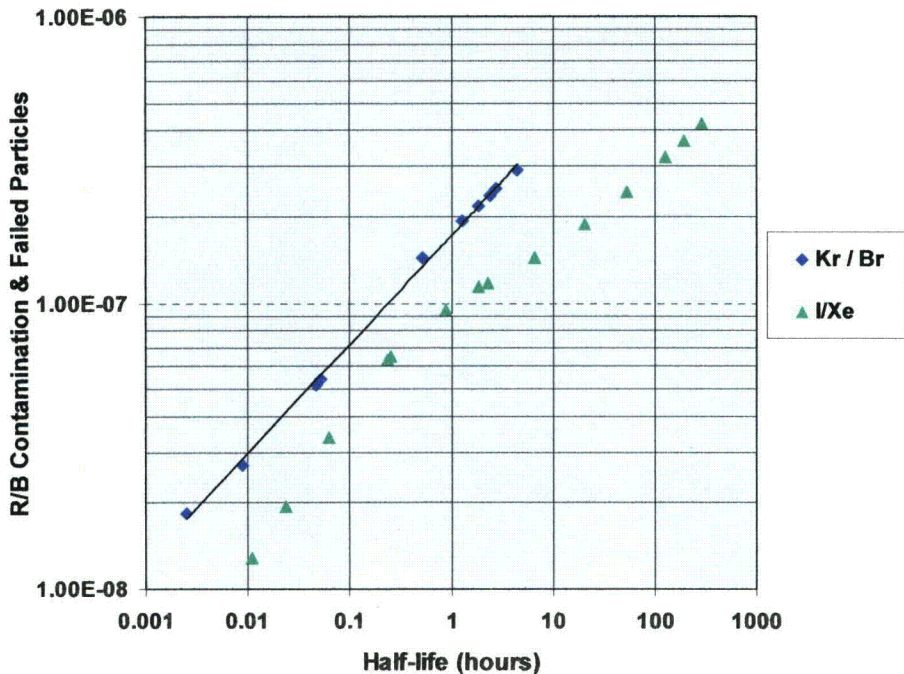


FIGURE 5. Total R/B at 1 003 °C fuel temperature, 89 bar helium pressure.

1. 2. Gaseous Fission Product Release under Abnormal Event Conditions

Gaseous fission product releases during loss of forced coolant conditions are calculated with GETTER and FIPREX, and are described in paragraph 0. The effect water vapour has on fuel material diffusion properties is modelled with NOBLEG. Due to high coolant gas operating pressures, no major water ingress incidents are expected. Low water vapour pressures have however been foreseen as a possible event, and a model to determine the effect on fission gas release was developed [15]. This model is incorporated into NOBLEG's calculation scheme. Observations made during the water vapour injection tests performed during the irradiation experiment HFR-K6 [16], were used to determine simple relations that can be used to determine gaseous fission product release from spherical fuel elements under oxidizing conditions caused by water ingress events. By comparing fission product release profiles from test elements containing no failed particles and test elements containing two failed particles, it is suggested that water vapour has an important effect on fuel kernel diffusion rates, and to a lesser extent on matrix material graphite diffusion rates. The relationship between fission product release and partial water vapour pressure was determined by comparing the Increase Factors (IF) of the R/B release with different partial water pressures. At fuel temperatures in the region of 680 °C, fission product release under oxidizing conditions from water ingress events, exhibits a square root dependence on the partial pressure of the water vapour. This dependence further decreases linearly for increasing partial water pressures. A relation was derived to describe the increase in gaseous fission product release. There is little variation between the measured increase factors between noble gases and halogens of different half-lives. The relationship is therefore applicable for the whole range of both halogens and noble gases.

$$IF = k_1 (pH_2O)^{3/2} + k_2 (pH_2O)^{1/2}$$

Where IF is the increase factor, or the increase in fission product release rate due to water vapour,

pH_2O is the partial water vapour pressure and

k_1, k_2 are constants dependent on the specific temperature range.

The model suggests that the square root dependence of fission product release increase on partial water pressure is linearly dependent on the partial water pressure. The constants k_1 and k_2 were derived for the test temperatures (~ 680 °C), where the linear increase factor was plotted against the partial water vapour pressure. In *TABLE 1* the derived relationship for different experimental partial pressures of water vapour is listed, and shows a conservative estimate of the measured increase in R/B from failed particles in the 100 Pa to 2 000 Pa partial water vapour pressure range.

TABLE 1. Measured and calculated R/B increase values during water injection tests, period 25, HFR-K6.

Vapour partial pressure p _{H₂O} in Pa	Relation with fitted constants k_1 and k_2	Measured increase factor	
		⁸⁸ Kr	¹³⁸ Xe
0	-	1	1
200	1.59	1.59	1.53
500	2.37	2.33	2.37
2 000	3.23	3.23	3.16

2. METALLIC FISSION PRODUCT RELEASE

The activity of the released and subsequent deposited nuclides ¹³⁷Cs, ¹³⁴Cs, ⁹⁰Sr, ^{110m}Ag and ¹¹¹Ag, and their radiation field near primary circuit components during maintenance and repair work are of primary importance for long-lived metallic release from spherical fuel element calculations. At PBMR these releases are calculated with the software code GETTER, which is based on Fick's second law of diffusion. It determines the important dynamic caesium, silver and strontium nuclide releases for both normal and postulated event conditions (e.g. loss of forced coolant event). Furthermore it estimates the halogen ¹³¹I release under loss of forced coolant event conditions and the noble gas ⁸⁵Kr release from spent fuel elements under long-term storage conditions. The code and the models used are being verified and validated with code-to-code comparisons, sample calculations and benchmarking with the irradiation fuel tests HFR-K3 [17].

2. 1. Metallic Fission Product Release under Normal Conditions

The large number of structural entities the core is made up of complicates the description of fission product behaviour in a PBMR core, and therefore the many parallel pathways that have to be considered. The variety of phenomena the fission product is subjected to further complicates the model that describes its migration from its site of production to the primary coolant. Therefore the release of metallic fission products from spherical fuel elements has been investigated in a great number of irradiation and laboratory experiments [13]. The transient release behaviour of long-lived metallic fission products can be predicted by using diffusion models based on these experimental results and phenomenological derived formulae. The diffusion code GETTER uses these mathematical models from phenomenological approximations and experimentally derived parameters.

The following transport processes control the release of long-lived metallic fission products from the fuel spheres [6]:

- direct recoil from fission sites;
- solid state diffusion in the various components of the fuel sphere;
- steady state diffusion of gaseous precursors;
- temperature activated desorption from the fuel sphere surface;
- convective mass transfer to the coolant gas.

The sources of fission products are nuclear fission, radioactive decay of precursors and activation of mother products. Radioactive decay of fission products and neutron absorption act as sinks. In

GETTER, each transport processes' equations are solved numerically for fuel kernels, coated particles and fuel spheres separately. The source term in the fuel sphere consists of [6]:

- diffusion release from failed particles;
- diffusion release from coated particles;
- release from coated particles by direct recoil;
- direct recoil from bare kernels (failed particles) and from the contamination of the outer pyrocarbon layer;
- uranium and thorium contamination of the matrix material;
- decay of gaseous precursors.

GETTER applies these transport processes and source terms to calculate the long-lived metallic fission product release from spherical fuel elements from high-temperature gas-cooled reactor cores. In case of activation products (e.g. ^{134}Cs , $^{110\text{m}}\text{Ag}$) GETTER is run twice: first for the release of the parent nuclide (^{133}Cs , ^{109}Ag) and afterwards for the activation product whereby the time-dependent concentration profiles of the parent nuclides define the source term for the second run. The sphere pass history through the different channels in the core is modelled by selecting a specific sphere pass history as a reference case. Calculating the ^{137}Cs release for various core pass histories that represent all the channels weighted by the probability that a fuel sphere will travel in a channel, defines a reference history. For a sample six-channel core design history 6/5/4/3/2/1 was chosen with the highest release rates for the sake of conservatism, and where all the channels are represented. The expected metal release data from the 400 MW PBMR core are given in TABLE 2 [18], the design factors were derived from a sensitivity analysis done on all the fission product release parameters.

TABLE 2. Expected metal release data.

	^{137}Cs	^{134}Cs	$^{110\text{m}}\text{Ag}$	^{90}Sr
Release Rate (atoms/s)	6.53×10^{12}	1.92×10^{11}	1.08×10^{11}	1.83×10^8
Activity Release Rate (Bq/s)	4 750	2 050	3 470	0.138
Design Factor	5	5	20	10

In FIGURE 6, the release rates from the fuel sphere during pass 1 (channel 6), 2 (channel 5), 3 (channel 4), 4 (channel 3), 5 (channel 2) and 6 (channel 1) are plotted vs the residence time in the respective channel (viz. logarithmic scale). The figure reveals that only after about 60 Full Power Days (FPD), appreciable rates (> 106 atoms/s) are released.

Design factors were derived from sensitivity analysis of the important transport and core parameters. The sensitivity of the input parameters on calculated releases was studied for ^{137}Cs , ^{136}Cs , ^{134}Cs , ^{111}Ag , $^{110\text{m}}\text{Ag}$ and ^{90}Sr for metal release, but for the sake of brevity only ^{137}Cs and $^{110\text{m}}\text{Ag}$ will be discussed. With the sensitivity analysis, the influences of uncertain input parameters and limitations of the applied methods are assessed. A distinction is made between systematic and random effects. Systematic errors are predominantly caused by the calculation method and by restrictions and simplifications of the underlying physical transport models. In this context, random effects are not due to the statistical distribution of material parameters within a population of items (e.g. diffusion constants of single coated particles), but they are related to uncertainties of the average value of an input parameter. Known systematic errors of the computational method (discretization error, homogeneously distributed direct recoils in the SiC layer, thorium and uranium contaminations equally distributed, neglect of fission product back pressure from the coolant) influence the results only moderately. The larger mean fuel free shell thickness of the spheres compared with the nominal thickness increases the metal release by less than 50%.

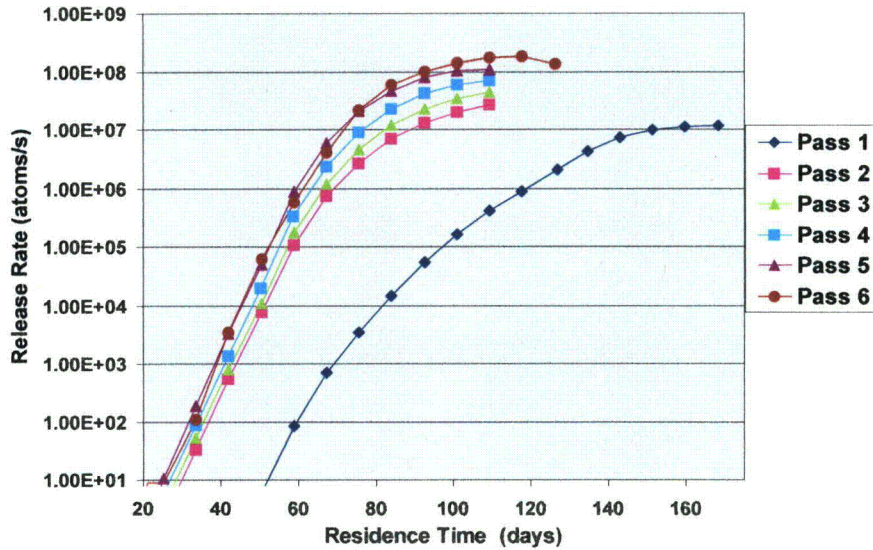


FIGURE 6. Expected ^{137}Cs release from a fuel sphere (sequence 6/5/4/3/2/1).

For conservatism sake, unknown, however conceivable shortcomings of the underlying transport model (e.g. concentration dependent diffusion coefficients, intrinsic variability of the diffusion coefficients (in contrast to random uncertainty), temperature activated trapping processes, non-diffusional transport processes, chemical interactions, fuel free shell thickness) are accounted for by a factor 2 to be equally applied to the expected result. Expecting the same design contamination uncertainties as for the gaseous fission product release design factor derivation in paragraph 0, increases in ^{137}Cs and $^{110\text{m}}\text{Ag}$ releases of 38% and 1% are achieved respectively. This large difference is due to the fact that silver is predominantly released from intact-coated fuel particles and caesium from contamination and failed fuel particles. Silver is also very sensitive to temperature and accounting for the temperature uncertainties increase the $^{110\text{m}}\text{Ag}$ release by 570% compared to 69% for ^{137}Cs . The uncertainty of the applied solid-state diffusion constants is estimated to be covered by a factor 2 and the operation-related failure fractions are multiplied by 3 and added to the base value of 2.8×10^{-5} based on German Thorium High Temperature Reactor (THTR) experience [11]. Statistical errors (95% confidence level) of the thermo-hydraulic core layout are derived provisionally also in accordance with THTR practice: Statistical errors in the radial (3.5%) and axial (7%) power distributions and 5% core bypass coolant gas flow cover thermo-hydraulic layout uncertainties. The residence time of the fuel spheres in the core is a statistically defined quantity. A longer fuel sphere history increases the release rate but correspondingly shorter sequences counteract this effect. The reference history 6/5/4/3/2/1 (732 days) has the nominal residence time. Moreover, longer residence times do not necessarily increase the release. Sphere histories 4/2/3/4/5/5/2 (765 days) and 6/5/4/3/2/6 (774 days) days reduce the ^{137}Cs release by 25% and 30% respectively. No adjustments to the design values are therefore necessary from a sphere residence time point of view. All statistical errors σ_i ($i = 1, 2, \dots, n$) of input parameters x_i are assumed to be independent of each other, thus enabling application of the statistical error propagation for the total error Δr of the result $r = r(x_i)$ as convenient first order approximation (exact for small relative σ_i/x_i , only) of the total error with identical confidence level as used for σ_i :

$$\Delta r(x_i, \sigma_i) = \left(\sum (\sigma_i \delta r / \delta x_i)^2 \right)^{1/2}.$$

For $^{110\text{m}}\text{Ag}$ the uncertainty of the SiC diffusion parameters cause the largest errors (880%) followed by temperature and thermohydraulic layout uncertainties. The $^{110\text{m}}\text{Ag}$ total design factor is a factor 20 compared to caesium (factor 5 for ^{137}Cs and ^{134}Cs). For caesium, the coated particle failure fractions from both manufacture and operation are the dominant uncertainties followed by temperature effects.

2. 2. Metallic Fission Product Release under Abnormal Event Conditions

At PBMR the GETTER code is applied to calculate metal and halogen fission product release from spherical fuel elements under accident conditions. Typical accident conditions include loss of forced coolant either from large or small breaks. A model was developed to calculate fission product release from spherical fuel elements during loss of forced coolant events for PBMR [19]. This model is used to determine GETTER calculation sequences and input parameters. The GETTER output is used as input for FIPREX [9], a post-calculation reduction software developed at PBMR. The FIPREX data reduction yields the fission product release from the fuel elements and from the PBMR core. The three radiological dominant nuclides identified; ^{131}I , ^{137}Cs and ^{111}Ag are calculated. These three selected fission products presents more than 80% of the radiological impact of a DLOFC event [20]. For a typical PBMR design, a DLOFC presents a 65 mm connection pipe break directly connected to the Reactor Pressure Vessel (RPV) [21]. It is assumed that all reactor neutron activity is stopped by control rod or Small Absorber Sphere (SAS) action. After pressure balance is achieved, the core heats up due to radioactive decay of the fission products contained in the fuel sphere. The helium gas volume in the core expands due to increased temperatures at constant pressure whereby the released fission products are transported from the core cavern into the depressurized MPS circuit. After approximately 36 hours, the maximum average core temperature is reached and the gas expansion reverses. Thus after 36 hours, no more fission products released from the fuel spheres are released from the core cavern [22].

A typical PBMR core is modelled with several (four to six) fuel sphere flow channels, each channel divided into axial layers (10 to 20), to yield 70 to 120 core regions. These core regions are used by core neutronics, thermo-hydraulic and fission product release codes to model the core parameters. To reduce the number of GETTER calculations performed, up to nineteen core regions can be selected, each region presenting a number of regions in the core. Time steps after event initiation are chosen to show the event progression. The GETTER code is then executed under normal operation conditions for sphere histories adjusted for the final axial positions, followed by the LOFC event for each chosen core position. The resulting release rates are corrected to take into account excess inventory for fuel with different burn-up histories. The corrected DLOFC release rates per fuel sphere are weighted with the number of core regions represented by the selected core regions. The sum of the weighted release rates multiplied with the number of fuel spheres per core region equals the total release rate from all fuel spheres into the gas volume of the core cavern. For the gaseous fission products a 1% burst release is added as observed in irradiation testing [23]. It is assumed that the released fission products are homogeneously distributed in the gas volume of the core cavern (pebble bed porosity + upper plenum) and that the release from the core cavern (core release) is driven by the thermal expansion of the remaining helium in the core cavern under ambient pressure. Thus, the core release rate is determined by the inventory of released gaseous fission products in the core cavern multiplied by the fractional expansion rate of the remaining helium mass. Finally the radioactive decay is taken into account for calculating the release rates and the accumulated release. Results for a sample 400 MWt PBMR design after a large break DLOFC event are presented in TABLE 4 [22]. The release from the core cavern provides an upper limit to the accident induced radiological load of the environment because the filter efficiencies of the core structure and of the metal surfaces along the way to the MPS break were not considered.

TABLE 3. Expected fission product release data.

	Units	^{137}Cs	^{131}I
Maximum release rate from fuel spheres	atoms/s	1.02×10^{15}	1.48×10^{13}
	MBq/s	0.743	14.8
Maximum release rate from core cavern	atoms/s	1.57×10^{13}	4.90×10^{11}
	MBq/s	0.0114	0.489
Maximum released inventory in core cavern	Atoms	2.18×10^{20}	2.13×10^{18}
	GBq	159	2 130
Maximum release from core cavern	atoms	1.44×10^{18}	4.15×10^{16}
	GBq	1.05	41.4

3. VERIFICATION AND VALIDATION

The function of the fission product release analyses group at PBMR is to ensure that fuel performance and fission product release analyses are performed in a correct manner that is reliable, accurate and repeatable. This is achieved by employing only qualified analysts to perform reactor and radiation analyses, using only verified and validated material, thermohydraulic and neutronic parameters, and applying only verified and validated models, methods and software. This is achieved by creating proper training and development assignments for candidate analysts, and formal verification and validation programs. The verification and validation of all parameters, models and software are conducted through the following process:

- Classification: Definition of the V&V requirements and development of a V&V plan.
- Identification: A study of the major fission product release experiments done in the history of HTR, to determine the best experimental data to be used for the validation of PBMR fission product release models and codes [24].
- Description: The theories behind fission product behaviour and release from spherical fuel elements as well as the thermohydraulic model was established from existing knowledge, and compared with the models developed and applied in the software [25].
- Analysis: Full code analysis, followed by assessments of code outputs compared to hand calculations of the models to mathematically verify the software [25].
- Comparison, models: Model to model calculations comparing the Booth model with Fick's laws of diffusion, and the theoretical model describing the breakthrough case [17].
- Comparison, codes: Code to code comparisons between fission product release, thermohydraulic and neutronic software to verify application of thermohydraulic models [26] and the numerical methods used to solve diffusion equations.
- Benchmarking: The selected irradiation experiments HFR-K3, -K5 and -K6, as well as the post-irradiation examinations completed were evaluated with the software [12].

3.1. Verification and Validation of Gaseous Fission Product Models and Software

The Verification and Validation (V&V) of gaseous fission product release models and the PBMR code NOBLEG is described in detail in [12], [17], [25] and [26]. This paper only highlights the important results of the benchmarking evaluation of irradiation test HFR-K6. The fuel proof test HFR-K6 was originally designed to test the fuel elements for the planned HTR-MODUL and was the final proof tests of the German HTR-fuel development [27]. Four 60 mm reference fuel elements (from AVR-21 reload batch) with LEU-TRISO coated particles were selected and inserted into a three-capsule BEST-rig for irradiation in the High Flux Reactor (HFR) at Petten, the Netherlands [28]. Capsule A contained the test element A1K6, capsule B the test elements B1K6 and B2K6, and capsule C test element C1K6. The fuel test conditions and experimental setup is available in [12] and [28]. No

particle failure occurred during irradiation. Unfortunately no post-irradiation examinations were conducted on the test elements. The irradiation load of the test elements of HFR-K6; the fast neutron fluence, burn-up and power output exceeds those that are expected from the PBMR design fuel. The PBMR fuel specification is based on the AVR-21 batch standards so that HFR-K6 can be used as a conservative irradiation test for PBMR quality fuel.

3. 1. 1. Contamination caused release

The noble gas fission products ^{88}Kr and $^{135\text{m}}\text{Xe}$ were selected for in-depth analyses, as their measurements during irradiation were the most consistently available. During irradiation the fertile ^{238}U and ^{232}Th in the matrix material capture neutrons to breed fissile ^{239}Pu , ^{241}Pu and ^{233}U . Therefore the effective uranium contamination increases with burn-up, and the release of fission gases from the fuel elements increases as well. The effective uranium contamination is therefore defined as the total fission power of the fissile nuclides ^{233}U , ^{235}U , ^{239}Pu and ^{241}Pu in the contamination of the fuel sphere divided by the total fission output from the fuel element. Using the known (50 ng uranium and 250 ng thorium per gram carbon) heavy metal contaminations in the fuel elements the effective contamination for the HFR-K6 irradiation periods were calculated with the burn-up routine of GETTER. The total effective uranium contamination that starts off at 7.2×10^{-8} (0.72% ^{235}U in natural uranium) increases to 1.66×10^{-6} at the end of irradiation. The increase in effective contamination explains the general tendency of fission product release to increase over irradiation time, and is therefore not necessarily a function of fuel integrity degradation.

The expected calculated release from a single failed particle exceeds the measured release from test elements A1K6, B1K6 and B2K6 significantly, and therefore it can be deduced that no particle failure, whether from manufacture caused or operationally induced, occurred. Fission product releases for these test elements are therefore determined by the uranium and thorium contamination of the outer pyrocarbon layers of the coated particles and the graphitic matrix material of the fuel element. For well-measured irradiation periods the NOBLEG calculated R/B values were compared with measured values for all the available krypton nuclides. In *FIGURE 7* an example of such a comparison is shown. This graph shows that the fission product release from contamination model (paragraph 0) is applicable for a large range of fission product half-lives.

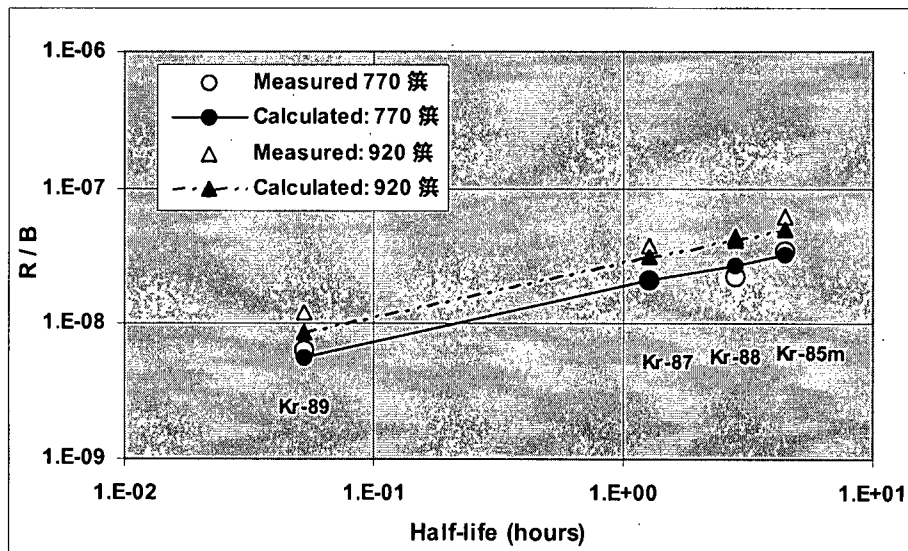


FIGURE 7. Krypton release from capsule A. HFR cycle 91.01. R/B vs half-life.

The full irradiation experiment's ^{88}Kr release, simulated with NOBLEG for test element B1K6, is presented in *FIGURE 8*. Test element B1K6 was chosen for presentation as its irradiation history had the most consistently available and coherent measurements. The NOBLEG simulation matches the measured release excellently with a correlation of 0.936, and the largest difference between the

measured and calculated values is a factor 2.0, which is well below the accepted PBMR design factor of 5. The surface fuel temperatures range from 546 °C to 820 °C, with an average temperature of 702 °C. The noble gas fission product ^{135m}Xe was selected to represent the xenon and iodine gas release from spherical fuel elements. It is also a conservative approach to determine iodine release by assuming that xenon release behaviour is similar to iodine release behaviour [10]. The full irradiation experiment ^{135m}Xe release simulated with NOBLEG for test element B1K6 is presented in *FIGURE 9*.

The NOBLEG simulation matches the measured releases excellently with a correlation of 0.960. The largest difference between the measured and calculated value is a factor 1.5, which is again well below the accepted PBMR design factor of 5 [14]. These results support the validation of the fission product release code NOBLEG for the use of noble gas and halogen release from contamination calculations for PBMR reference fuel.

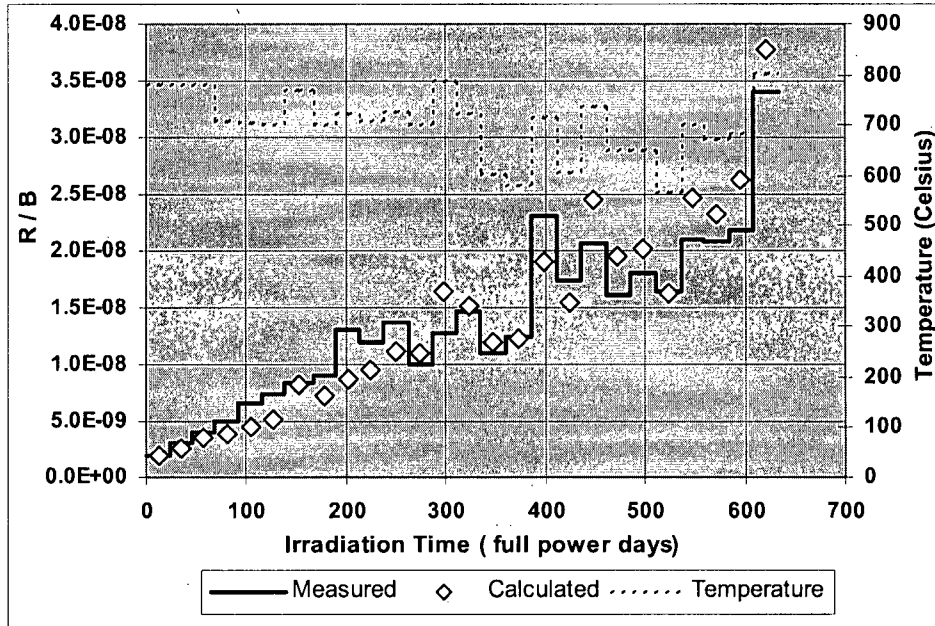


FIGURE 8. Measured and calculated ^{88}Kr R/B comparison for test element B1K6 (contamination release)

3. 1. 2. Failed coated particle caused release

After investigating the fission gas release during irradiation, it was concluded that test element C1K6 had two failed particles. No particle failure occurred during irradiation. The defective particles in test element C1K6 are equal to a manufacture-caused defective particle content of $2/14\ 600 = 1.4 \times 10^{-4}$. The releases from these two elements are thus dominated by defective particle release as the free uranium from one failed particle exceeds the free uranium in the matrix material by a factor of 35. The measured fission gas release from capsule C1K6 is compared with the calculated values in *FIGURE 10* for ^{88}Kr and *FIGURE 11* for ^{135m}Xe respectively for selected temperature regions in the 26 irradiation periods.

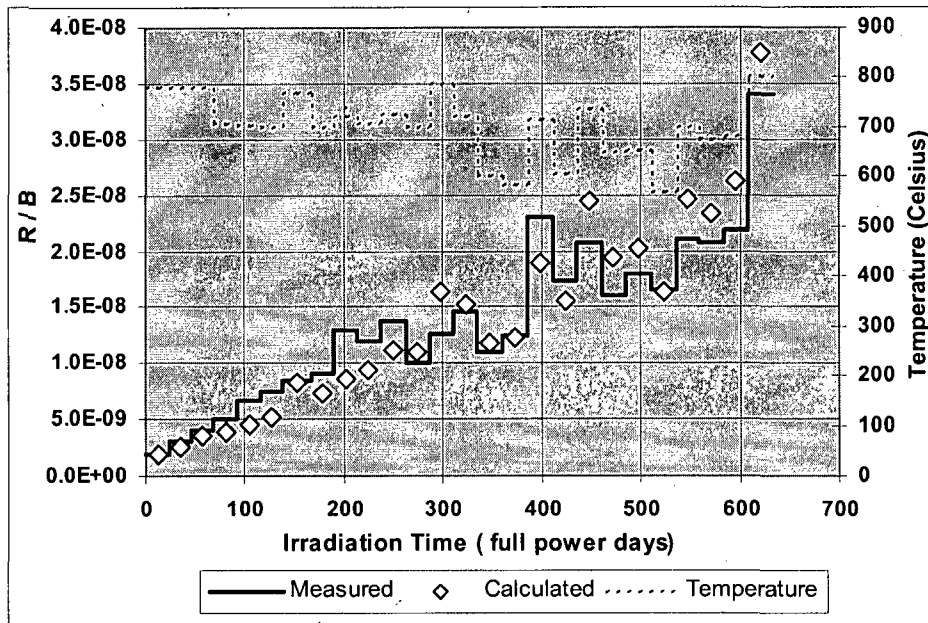


FIGURE 9. Measured and calculated ^{135m}Xe R/B comparison for element B1K6 (contamination release).

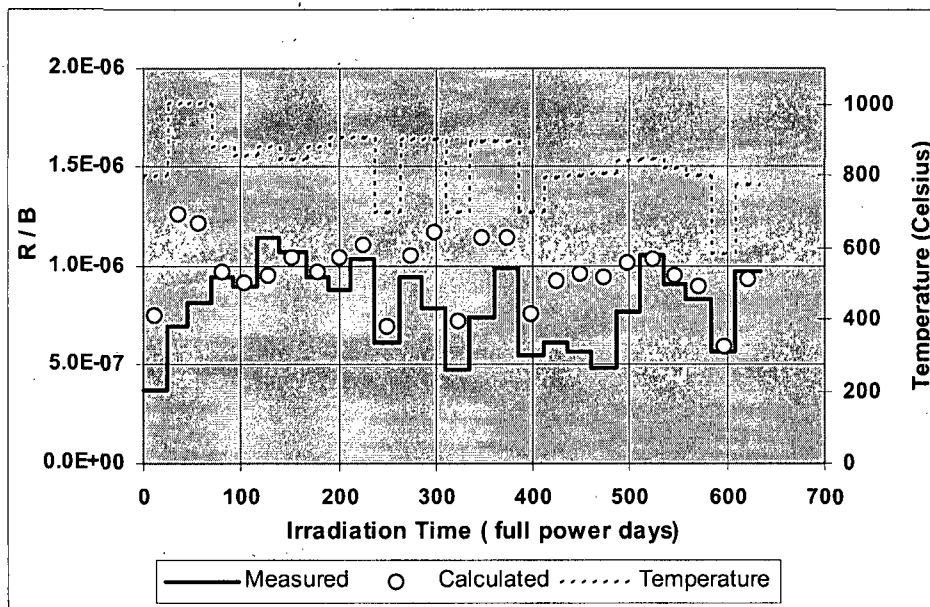


FIGURE 10. Measured and calculated ^{88}Kr R/B comparison for test element C1K6.

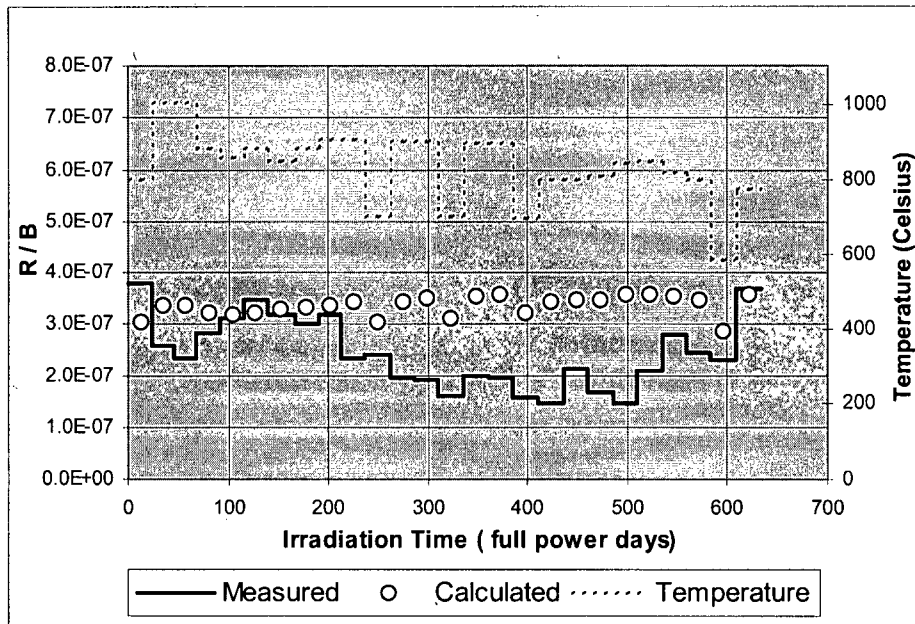


FIGURE 11. Measured and calculated ^{135m}Xe R/B comparison for test element CIK6.

Considering the measurement uncertainties, the agreement between the measured and code calculated values is very good. For ^{88}Kr , the calculated values are within a factor 2 of the measured values and for ^{135m}Xe within a factor 3, with correlations of 0.950 and 0.950 respectively. This is within the design factors calculated and used by PBMR of 3 for noble gases and halogens [14]. It can be seen in FIGURE 11 that the larger xenon atoms' release over the irradiation time decreases relative to the calculated values. This is also noted for ^{88}Kr to a lesser extent from 300 full power days (fpd) to 500 fpd. This is due to the fact that the composition of the two-component system buffer layer in the coated particles changes during irradiation. The buffer layer consists of two components, a low diffusive 'grains' fraction (90%) and a highly diffusive 'amorphous' fraction (10%), representing the graphite buffer material and binder coke used, respectively. During irradiation, the highly diffusive component is compacted by primary fission products, and thus transformed into a less diffusive phase (either by decrease in size of the highly diffusive component or the decrease in diffusion coefficients of the component). This causes the relative release to be decreased as irradiation increases. For the sake of conservatism the current PBMR fission gas release model ignores this uncertain and yet unverified mechanism. After 500 fpd, the release of ^{88}Kr and ^{135m}Xe drastically increases from well below to very close to the calculated values. This rapid increase at the end of the irradiation experiment is most likely caused by the formation of microscopic cracks in the highly compacted and stressed buffer material. The measured fission product release however still does not exceed the calculated values.

3. 2. V&V of Metallic Fission Product Models and Software

The verification and validation of metallic fission product release models and the PBMR code GETTER is described in detail in [17]. This presentation only highlights the important results of the benchmarking evaluation of irradiation test HFR-K3 and its post-irradiation examination [29].

The irradiation test HFR-K3 was part of the High Temperature Reactor Fuel Programme, employed to test fuel systems and to validate the design and production of low enriched fuel spheres and is described in [30]. The test elements were exposed to similar conditions as would be expected for PBMR fuel. After considering all the available experimental results and irradiation conditions the test elements A5K3 and B6K3 were chosen for validation of the fission product release code GETTER. GETTER uses the thermal neutron capture and fission cross-sections calculated at HFR to calculate burn-up and plutonium power fractions. The plutonium power fractions were not measured in the

post-irradiation examination of the test elements and could not be compared with GETTER calculated values. The measured and GETTER calculated burn-up values in Fissions per Initial Metal Atom (FIMA) of the four test elements are listed in TABLE 4. Calculations done by HFR [31] and KFA [32] are included for comparison. These calculations were performed directly after completion of irradiation and before the detectors were analysed to correct measured results. The GETTER calculations were performed with corrected final measured values. GETTER's ability to determine neutronic functions is further verified by these results.

TABLE 4. Irradiation data: burn-up measured and calculated, HFR-K3, all in FIMA.

Fuel element	Measured (Cs-137)	Calculated GETTER	Calculated HFR	Calculated KFA
A5K3	7.53%	7.64%	7.85%	7.65%
B5K3	10.02%	9.96%	9.94%	10.09%
B6K3	10.57%	10.43%	10.11%	10.21%
C1K3	8.97%	8.85%	8.44%	9.07%

The post-irradiation examination was conducted at the Harwell Laboratory at Didcot, England [29]. Test elements A5K3 and B6K3 underwent post-irradiation heat-up tests. Test element A5K3 was heated for 500 hours at 1 600 °C and test element B6K3 for 100 hours at 1 800 °C. Fractional releases of the major fission products were measured during the heat-up tests. The burn-up was determined from the ^{137}Cs content. The fuel free zone was investigated and the fission product content measured as well as the total fuel element fission product inventory. The R/B values for released fission gases during irradiation were below 1×10^{-6} for all capsules, so that the possibility of failed particles could be neglected. The GETTER calculation was therefore done with the assumption that no particle failure, either manufacture caused or operational induced, occurred. Results, however suggest that some particle failure occurred during heat treatments of the post-irradiation examination [32]. The fractional releases over the irradiation period were calculated for the fission product ^{137}Cs and the activation product $^{110\text{m}}\text{Ag}$ and are presented in FIGURE 12.

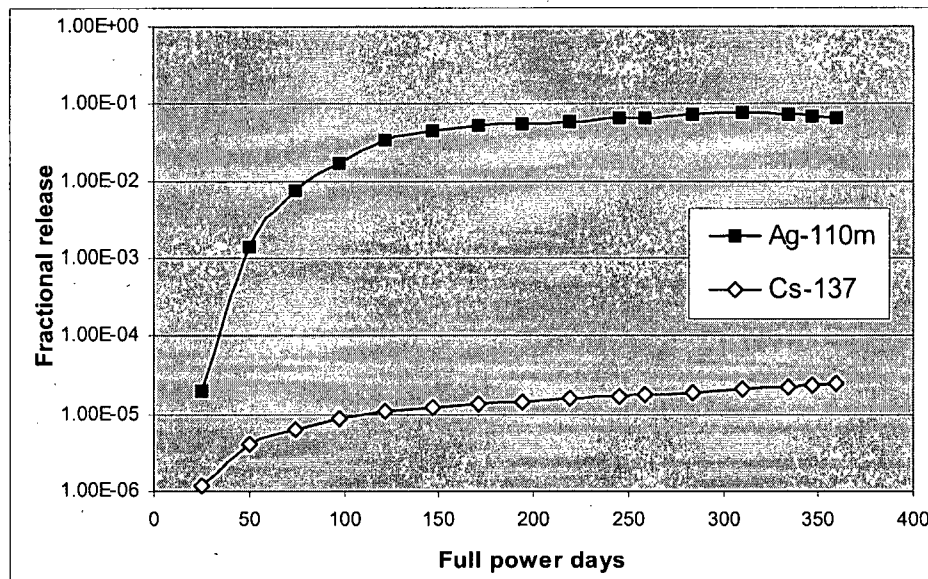


FIGURE 12. Fractional release of test element A5K3 for ^{137}Cs and $^{110\text{m}}\text{Ag}$ calculated by GETTER.

The final fractional release values for the two test elements were measured together with detailed analysis of the sphere component activity contents [29]. The comparison between the measured values and the GETTER calculated results for ^{137}Cs and $^{110\text{m}}\text{Ag}$ is presented in TABLE 5. The original calculations made by HRB [31] are also listed. For test element A5K3 the GETTER calculated values show a conservative estimate of the expected fission and activation product release. The ^{137}Cs calculated release is only a factor 2.7 higher than the measured release, which is well below the uncertainties accepted at PBMR design analyses. The $^{110\text{m}}\text{Ag}$ calculated release is a factor 30 too high, which suggests that the current transport parameters used are too high. Further study in silver transport behaviour is suggested. The calculation is however, still conservative. The fractional releases from test element B6K3 are not compared at this stage, as scanning electron microscopy [32] revealed that several of the particles in test element B6K3 formed hairline cracks in their SiC layers, which would influence fission product release appreciably.

TABLE 5. Fractional release comparison for test element A5K3: measured vs calculated.

Fission Product	Measured	Calculated	
		GETTER	HRB
^{137}Cs	9.1×10^{-6}	2.42×10^{-5}	6.1×10^{-5}
$^{110\text{m}}\text{Ag}$	2.2×10^{-3}	6.71×10^{-2}	5.2×10^{-2}

The fission product inventories calculated by GETTER were compared with the fission product concentrations measured during the post-irradiation fuel sphere deconsolidation in the test element [29]. TABLE 6 presents the test element inventory comparison. This comparison proves that the base source term for fission product release, the production of fission products in the fuel materials, is calculated correctly by GETTER.

TABLE 6. Fission product inventories: A5K3 and B6K3.

Test element	Measured (atoms)		Calculated (atoms)	
	^{137}Cs	$^{110\text{m}}\text{Ag}$	^{137}Cs	$^{110\text{m}}\text{Ag}$
A5K3	1.21×10^{20}	3.56×10^{16}	1.22×10^{20}	3.58×10^{16}
B6K3	1.63×10^{16}	9.29×10^{16}	1.63×10^{16}	9.10×10^{16}

The fission product concentration profiles in the fuel free zone measured during the post-irradiation examination were compared with the GETTER calculated values in

TABLE 7.

TABLE 7. Fission product concentration in the fuel free zone: A5K3.

Nuclide	Measured (Bq/g)	Calculated (Bq/g)
^{137}Cs	789	3 170
$^{110\text{m}}\text{Ag}$	6 113	21 700

The ^{137}Cs fuel free zone concentration is overestimated by a factor 4 and for $^{110\text{m}}\text{Ag}$ by a factor 3.5 by GETTER. This is reasonable, as it is still inside the accepted factor 5 commonly accepted for calculation-measurement comparisons [33]. Furthermore, it proves GETTER's conservative estimation of experimental and operational conditions.

Fission product concentration profiles for ^{137}Cs and $^{110\text{m}}\text{Ag}$ are presented in *FIGURE 13* and *FIGURE 14*. Nearer to the surface of the fuel element, the ^{137}Cs concentration increases contrary to what is to be expected. Similar curves were observed for ^{134}Cs and ^{90}Sr during the post-irradiation examination. This could be because the helium gas mass flow is significantly lower than the planned gas flow in a high-temperature reactor. This causes some fission product backpressure on the sphere surface that will increase the fission product concentrations near the surface of the test element. The backpressure effect in gas-cooled reactors under normal operating conditions is negligible.

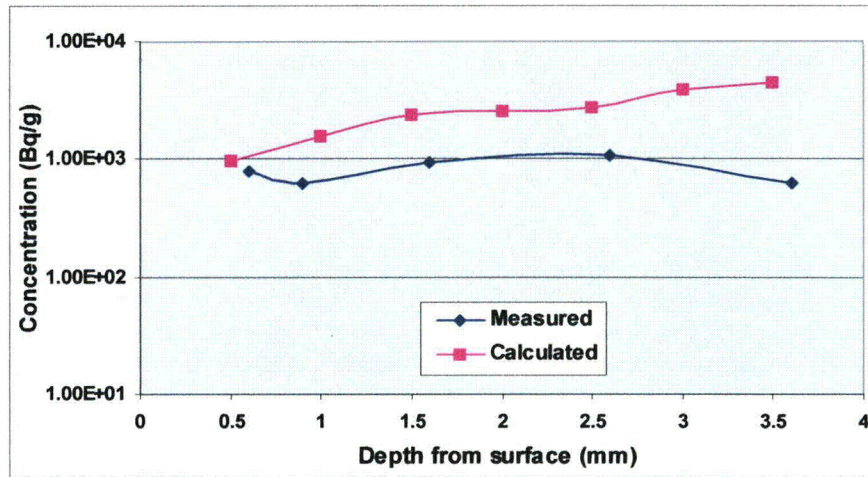


FIGURE 13. ^{137}Cs concentration profile in the fuel free zone for A5K3.

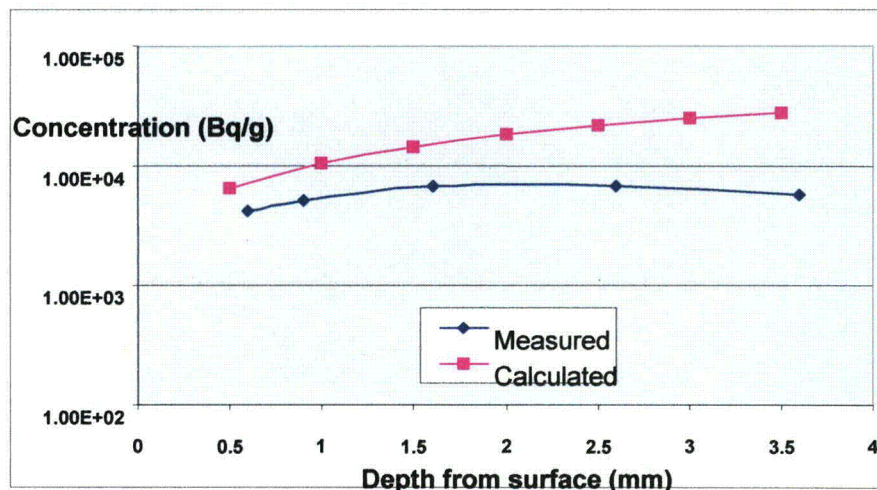


FIGURE 14. $^{110\text{m}}\text{Ag}$ concentration profile in the fuel free zone for A5K3.

4. CONCLUSION

This paper attempts to present only a bird's eye view of fission product release modelling and software development at PBMR. At PBMR, fission products released from coated particles and spherical fuel elements are divided into two groups: Short-lived gaseous fission products and long-lived metallic fission and activation products. Each group is being developed at PBMR for all possible operational and accident events. A set of software and methods is available for design and safety analysis, and the

principles on which they are based are verified and validated. Models and transport parameters are continuously being developed, refined and applied in software products for PBMR reactor and fuel analysis. The verification and validation of the current set of models and codes used to predict the fission product behaviour from spherical fuel elements is approximately 60% complete. New models and software are verified and validated as developed. All models, transport parameters and software were developed on German reference fuel. Any high-temperature reactor design analysed with the software and methods described, must utilize fuel manufactured and tested under the same rigorous conditions as German reference fuel to ensure design and safety analyses credibility.

5. ACKNOWLEDGEMENT

The author wishes to thank the PBMR Company for funding this work as well as the late Dr Klaus Röllig for his technical assistance.

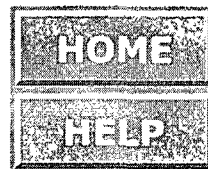
REFERENCES

- [1] D R Nicholls: The Pebble Bed Modular Reactor. South African Journal of science 98, 2002.
- [2] G H Lohnert, H Nabielek and W Schenk: The fuel element of the HTR-Module, a prerequisite of an inherently safe reactor. Nuclear engineering design 109, 1988.
- [3] E Teuchert: VSOP. Computer code system for reactor physics and fuel cycle simulation. KFA, Jülich. March 1980.
- [4] H Gerwin: Daz zweidimensionale Reaktor dynamic programm TINTE. Jül-spez. 2167-987.
- [5] K Röllig: Description of the Computer Code NOBLEG, WER Report GBRA 054 350, 2001.
- [6] K Röllig: Rechenprogramm GETTER, WER Report GBRA 052 477, 2001.
- [7] F Reitsma: Neutronic and other data interface for fission product release analyses. PBMR report number 015669-3240. August 2003.
- [8] H Haas: Beschreibung RADAX 3, WER report EA GHRA 001347. 1984.
- [9] J J vd Merwe: FIPREX software description, PBMR report 024028, 2004.
- [10] K Röllig: Release of Rare Fission Gases from Spherical Elements with Coated Fuel Particles. Nuclear Technology 35, 1977.
- [11] K Röllig: Release of Metallic Fission Products from the PBMR Core, WER Report GBRA 052 341, 2001.
- [12] J J vd Merwe, K Röllig, PP Coetzee: Validation of the PBMR Model Used to Predict Gaseous Fission Product Releases from Spherical Fuel Elements. Submitted to Nuclear Technology, March 2004.
- [13] K Verfondern: Fuel Performance and Fission Product Behaviour in Gas Cooled Reactors IAEA-TECDOC-978, 1997.
- [14] J J van der Merwe: Halogen and Noble Gas Release from the 400 MW PBMR Core. PBMR report 015804-334, 2003.
- [15] J J vd Merwe: Verification and validation of the PBMR models and codes used to predict gaseous fission product releases from spherical fuel elements. MSc Thesis, RAU 2004.
- [16] R Conrad, R van Ulft, L Coutinho: Irradiation progress report no. 25, HFR-Cycle 93.02. Project D138.05, HFR-K6, Petten, 1993.
- [17] J J vd Merwe: Development and validation of fission product release models and software at PBMR. Unpublished work, PBMR.

- [18] J J van der Merwe: Metal, Halogen and Noble Gas Release from the 400 MW PBMR Core. PBMR report 012313-334, 2002.
- [19] J J vd Merwe, K Röllig, PP Coetzee: Development of the Model to Determine Fission Product Release from the PBMR during DLOFC events. Unpublished paper.
- [20] P J Fourie: Selection of Radionuclides to study radionuclide behaviour in the PBMR. PBMR Report 015429, 2003.
- [21] S Struth: Thermal-Hydraulic Analysis on Rupture of connecting pipes to the main system. Forschungszentrum Jülich, ISR report on PBMR working package 2, 2002.
- [22] J J vd Merwe: Preliminary Getter Calculated Caesium and Iodine Release from the PBMR Core During a DLOFC Accident. PBMR Report 015395-334, 2002
- [23] K Röllig: Transiente Edelgasfreisetzung, HRB report BG GHRA 006 904, 1992.
- [24] J J vd Merwe: Selection of applicable fuel irradiation tests for PBMR fission product release validation. PBMR Report 023432-459, 2004
- [25] J J vd Merwe: Verification and validation of the fission product release code NOBLEG. PBMR Report 018776-404, 2004
- [26] J J vd Merwe: Verification of the thermo hydraulic model used in fission product release codes. PBMR Report 023595-459, 2004
- [27] H Ragoss: Development of advanced HTR fuel elements. Nuclear Engineering Design 121. 1990.
- [28] R Conrad: Irradiation of high temperature fuel elements for the HTR module in the HFR Petten. Design and safety report, 1990.
- [29] P E Brown: Post-irradiation examination of HTR fuel elements. Final report to KFA, Jülich, Germany from Harwell Laboratory, Didcot, Oxon, England. 1988.
- [30] RWA Kraakman, WP Voorbraak: Neutron metrology in the HFR. D138-03: Irradiation of fuel spheres. Energy Council of the Netherlands report ECN 84-122, 1984.
- [31] R Christ: Spaltproduktfreisetzung bei HFR-K3. HRB report HTR-5125-1343, 1985.
- [32] P R Kasten, DA Smith, JJ Lichtenwalter, H Nabielek, K Verfondern: Fuel performance in modular high temperature gas-cooled reactors. KFA internal report, ISR-IB-12/94, 1994.
- [33] P R Kasten, DA Smith, JJ Lichtenwalter, H Nabielek, K Verfondern: Development of correlations between fuel performance and test parameters in modular high temperature gas cooled reactors. KFA internal report, ISR-IB-9/94, 1994.

AUTHOR INTRODUCTION

J J vd Merwe, born in Pretoria, South Africa in 1973, is a fission product release and core design analyst at the South African Nuclear Energy Corporation and the PBMR Company. He obtained his Bachelors degree (hons) in 1996 at the University of Pretoria and his Masters degree in chemistry at the Rand Afrikaans University in 2004. He is currently enrolled as a doctoral student at the Rand Afrikaans University. His research interests include nuclear chemistry, fission product transport modelling and analyses, accident analysis as well as fuel element design and development.



ORNL/TM-5253
UC-76

Contract No. W-7405-eng-26

CHEMICAL TECHNOLOGY DIVISION

NOTICE
This report was prepared as an account of work sponsored by the United States Government. Neither the United States nor the United States Energy Research and Development Administration, nor any of their employees, nor any of their contractors, subcontractors, or their employees, makes any warranty, express or implied, or assumes any legal liability or responsibility for the accuracy, completeness or usefulness of any information, apparatus, product or process disclosed, or represents that its use would not infringe privately owned rights.

CONCEPTUAL DESIGN OF A CONTINUOUS FLUORINATOR
EXPERIMENTAL FACILITY (CFEF)

R. B. Lindauer
J. R. Hightower, Jr.

JULY 1976

NOTICE This document contains information of a preliminary nature and was prepared primarily for internal use at the Oak Ridge National Laboratory. It is subject to revision or correction and therefore does not represent a final report.

OAK RIDGE NATIONAL LABORATORY
Oak Ridge, Tennessee 37830
operated by
UNION CARBIDE CORPORATION
for the
ENERGY RESEARCH AND DEVELOPMENT ADMINISTRATION

DISTRIBUTION OF THIS DOCUMENT IS UNLIMITED ²⁶

CONTENTS

	<u>Page</u>
ABSTRACT	1
1. INTRODUCTION	1
2. SUMMARY	2
3. DESIGN DESCRIPTION	3
3.1 Fluorine Supply System	10
3.2 Fluorine Disposal System	12
4. OPERATING PROCEDURE	12
5. MAINTENANCE	15
5.1 Maintenance Philosophy	15
5.2 Preventive Maintenance	15
6. STANDARDS AND QUALITY ASSURANCE	15
6.1 Codes and Standards	15
6.2 Quality Assurance	16
7. REFERENCES	16

CONCEPTUAL DESIGN OF A CONTINUOUS FLUORINATOR
EXPERIMENTAL FACILITY (CFEF)

R. B. Lindauer
J. R. Hightower, Jr.

ABSTRACT

A conceptual design has been made of a circulating salt system, consisting principally of a fluorinator and reduction column, to demonstrate uranium removal from the salt by fluorination. The fluorinator vessel wall will be protected from fluorine corrosion by a frozen salt film. The circulating salt in the fluorinator will be kept molten by electrical heating that simulates fission product heating in an actual MSBR system.

1. INTRODUCTION

The present flowsheet for processing a single-fluid MSBR includes a fluorination step for continuously removing 99% of the uranium from a salt stream coming from the reactor at the rate of 3.3 liters/min. The salt stream passes through a reductive-extraction step for protactinium removal, and a metal-transfer step for rare-earth removal before being returned to the reactor. Two smaller fluorination operations are also required for removing uranium from the secondary salt stream that flows to the protactinium decay tank, and for the periodic recovery of uranium from the protactinium decay tank.

Operability of a frozen wall fluorinator using autoresistance power to simulate fission product heating has been tested in three experiments: AHT-2, AHT-3, and AHT-4.¹⁻⁴ In experiment AHT-2, LiF-BeF₂ salt (67-33 mole %) was used in a simple, vertical test vessel with satisfactory results.² In AHT-3, successful runs were made using MSBR fuel carrier salt with the electrode in the vertical test section.⁵ In AHT-4, MSBR

fuel carrier salt was circulated through the test vessel, which was similar to a proposed fluorinator.⁶ The electrode was placed in a side arm that was connected to the vessel near the top of the vertical fluorination section. No fluorine was used in any of these experiments.

The objective of the continuous fluorinator experimental facility (CFEF) is to demonstrate the actual fluorination of uranium in a circulating salt system that is similar to AHT-4. The uranium that is not volatilized, but which is partially oxidized to UF_5 , will be reduced back to UF_4 in a hydrogen reduction column. This demonstration is expected to provide information about corrosion protection by the frozen salt film, and operating experience and process data, including fluorine utilization, reaction rate, and flow rate effects.

2. SUMMARY

The continuous fluorinator experimental facility will be installed in a cell in Building 7503 to provide beryllium containment. The system will contain 8 to 9 ft³ (0.23 to 0.25 m³) of MSBR fuel-carrier salt (72-16-12 mole % LiF-BeF₂-ThF₄) containing an initial quantity of 0.35 mole % of uranium. The salt will be circulated at up to 100% of MSBR flow rate (3.3 liters/min). Because of the short fluorination height and depending on operating conditions, the uranium that is volatilized will range between 80% and 95%. The variables of salt flow rate, fluorine flow rate, and fluorine concentration will be studied by measuring the UF_6 concentration in the fluorinator off-gas stream, and by sampling the salt stream after reduction of UF_5 to UF_4 . Mass flowmeters in the fluorinator off-gas stream before and after the NaF traps will provide a continuous indication of the uranium volatilization rate.

Fluorine utilization can be calculated from the final mass flowmeter reading and the fluorine feed rate. The amount of UF_5 in the stream going to the reduction column can be determined from the fluorine utilization and UF_6 volatilization rates. Another mass flowmeter in the gas stream coming from the reduction column will indicate the unreacted

hydrogen plus the HF which is formed. The reduction efficiency can be calculated from this reading. The fluorinator will have two fluorine inlets to provide data for determining the column end effects. Reduction of UF_5 will be carried out in a gas lift in which hydrogen will be used as the driving gas and also as the reductant. If additional reduction is required, it can be done in the salt surge tank. The surge tank is designed to provide sufficient salt inventory for about 4 hr of fluorination under operating conditions which result in 80% uranium volatilization per pass, and 11 hr of fluorination under conditions which result in 95% uranium volatilization per pass. About 99% of the uranium should have been removed from the salt batch after these periods of time.

3. DESIGN DESCRIPTION

The flowsheet is shown in Fig. 1. Salt will enter the fluorinator through the electrode in a side arm. The electrode flange will be insulated electrically from the rest of the fluorinator, and the autoresistance power will be connected to a lug on the flange. The salt will leave at the bottom of the fluorinator below the fluorine inlet side arm. The fluorinator pipe wall will be cooled by external air-water coils to form the frozen salt film, which serves the dual purpose of preventing nickel corrosion and autoresistance current shorting. Below the fluorine inlet, the fluorinator wall will not be cooled and the molten salt will complete the electrical circuit to the vessel wall. Since all of the uranium will not be volatilized, some partially oxidized uranium will be found as UF_5 at the bottom of the fluorinator. The fluorinator bottom, exit line, and reduction column will be protected from the highly corrosive UF_5 by gold lining (or plating). The molten salt containing UF_5 will enter at the bottom of the column where it will be contacted with hydrogen. The hydrogen will be introduced into the column through a palladium tube; this will result in the formation of atomic hydrogen, which greatly increases the reduction rate of UF_5 to UF_4 . The hydrogen reduction column will also act as a gas lift to raise the salt to a gas-liquid separator. The salt will then flow by gravity to the fluorinator through a salt sampler,

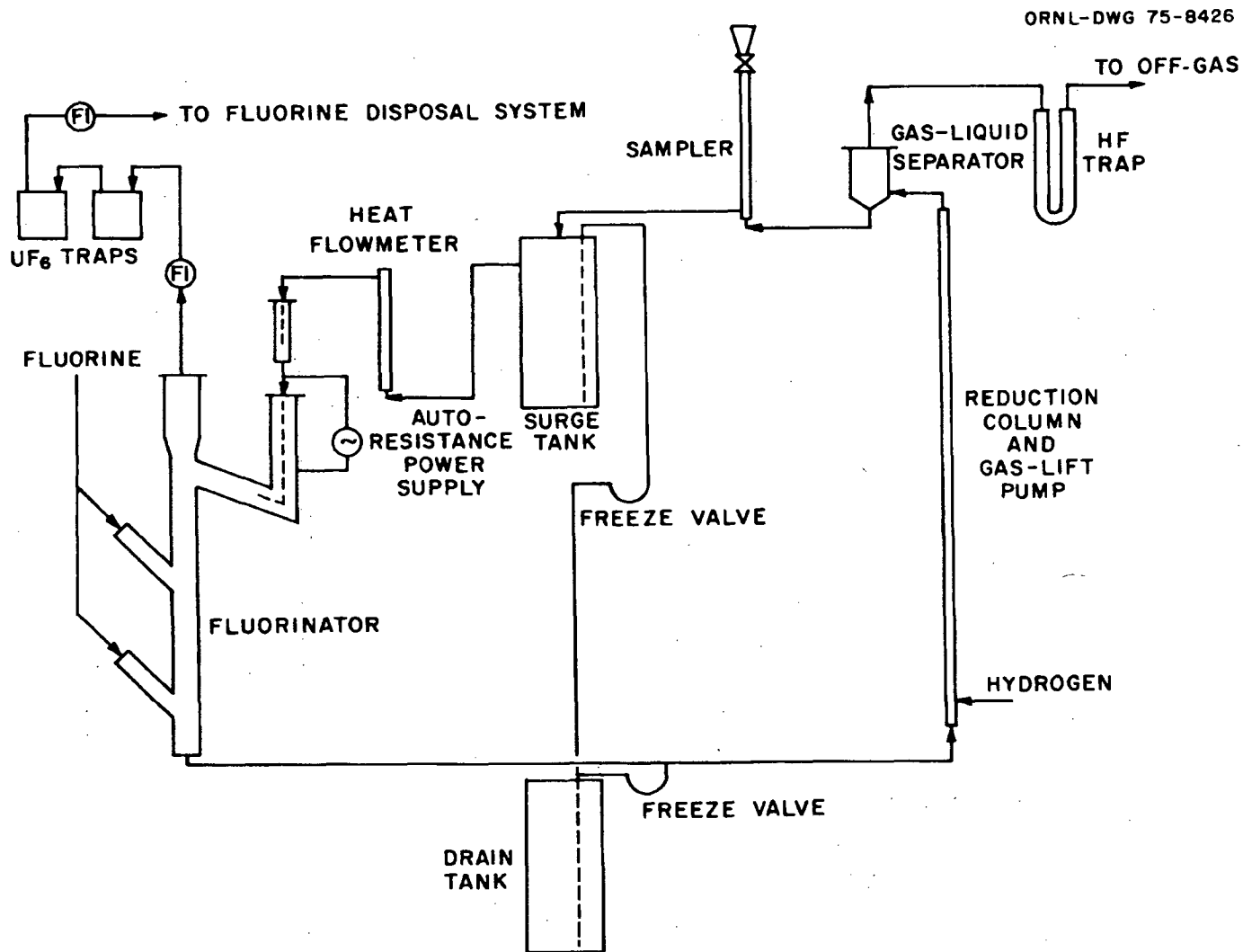


Fig. 1. Continuous Fluorinator Experimental Facility flowsheet.

surge tank, heat flowmeter, and electrical circuit-breaking pot. The surge tank will have a working volume of 5 ft³ (0.14 m³), and a dip tube through which hydrogen can be introduced if further uranium reduction is required. Reduction off-gas from the separator and surge tank that contains HF and excess hydrogen will pass through a NaF bed for removal of the HF. The excess hydrogen will be diluted below the explosive limit before being discharged to the cell off-gas.

Off-gas from the fluorinator will contain UF₆ and excess fluorine; argon will also be in the off-gas if it is used to dilute the fluorine. The gas will pass through two sodium fluoride beds for uranium removal. Hastings mass flowmeters will be installed upstream and downstream from the beds. The difference between the two readings is a measure of the UF₆ flow rate. This provides an instantaneous and reasonably accurate means for determining the fluorine utilization and reaction rate. An engineering layout of the equipment to be installed in the spare equipment cell in Building 7503 is shown in ref. 7. A description of the individual equipment items follows.

Fluorinator. This vessel (Fig. 2) is similar to the test vessel used in experiments AHT-3 and AHT-4; however, several changes have been made based on operating experience. The diameter of the entire vessel was increased from 6 to 8 in. (0.15 to 0.20 m) to simplify frozen-film formation and to provide space for a thicker film, thus minimizing the effect of nonuniform film thickness. The heated jacket over the electrode was lengthened to reduce the danger of the salt freezing in the unheated end. Fluorination zones of 3 and 6 ft (0.9 and 1.8 m) are provided by having two fluorine inlets. Since complete fluorination is not expected, and UF₅ (which is very corrosive) will be present in the salt below the fluorine inlet, it will be necessary to cool all five jackets regardless of whether the 3-ft or 6-ft (0.9 or 1.8 m) fluorinator is being used. The bottom of the fluorinator and the line to the reduction column will be protected from corrosion by a gold lining. Contact between the molten salt and this lining will complete the electrical circuit for autoresistance heating.

Alternative fluorinator designs (to the autoresistance heated unit shown) are being considered for the CFEF. The salt core could be kept

ORNL DWG 76-128

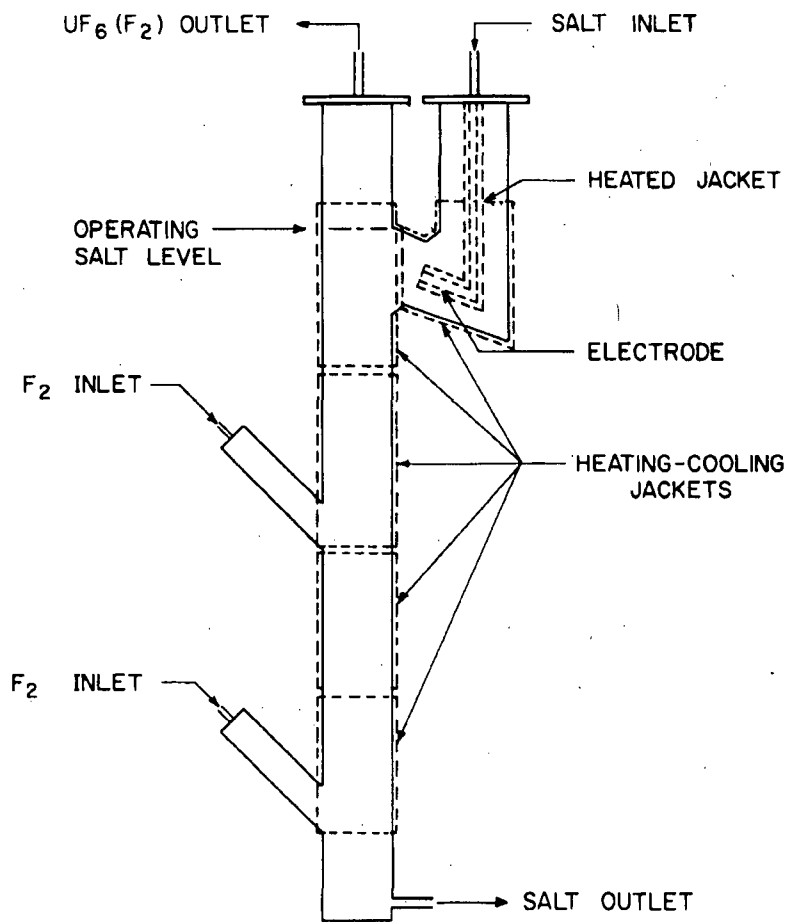


Fig. 2. Continuous fluorinator.

molten by the use of a jacketed axial heater in the center of the fluorinator. Although corrosion would be severe (probably ~ 0.03 mm/hr), at least 100 hr of fluorination should be possible before the jacket fails and/or the salt is saturated with NiF_2 (~ 0.9 wt %). It would also be possible to supply sufficient heat in the entering salt so that the salt leaving the bottom of the fluorinator will not be cooled below the liquidus temperature. Figure 3 shows, for example, that the heat loss through a 1-in.- (25-mm) thick salt film could be compensated by a salt temperature drop of 40°C (inlet-exit) at one-half the MSBR salt flow rate if a 400°C -pipe wall temperature is desired.

There are disadvantages to these two alternative designs. Corrosion of the axial heater jacket would consume fluorine and prevent the accurate calculation of fluorine utilization in the uranium-fluorine reaction. Without knowing the fluorine consumption in the oxidation of uranium it would not be possible to calculate the amount of UF_5 formed. If no internal salt heating is used, the high inlet salt temperature that is required could cause difficulty in forming and maintaining a salt film near the electrode. In any case, the salt film would probably be less uniform than with internal heating, because the film would be thinner near the salt inlet and thicker near the salt outlet.

Reduction column. Since the reduction column also functions as a gas-lift to provide salt circulation, the diameter, height, and elevation will be determined primarily by the gas-lift design. The salt head in the fluorinator will determine the gas-lift submergence (about 50%), and the salt circulation rate (1 to 3 liters/min) will determine the column diameter. The entire column height will probably not be required to accomplish complete reduction of UF_5 . The palladium catalyst at the hydrogen inlet should provide adequate reduction with a small contact height. The column will be lined or plated with gold to prevent corrosive attack by the UF_5 . If additional reduction is required, hydrogen could be supplied easily through a dip tube in the surge tank to complete the reaction there; however, corrosion from UF_5 could be a problem since there are no plans to gold line this tank.

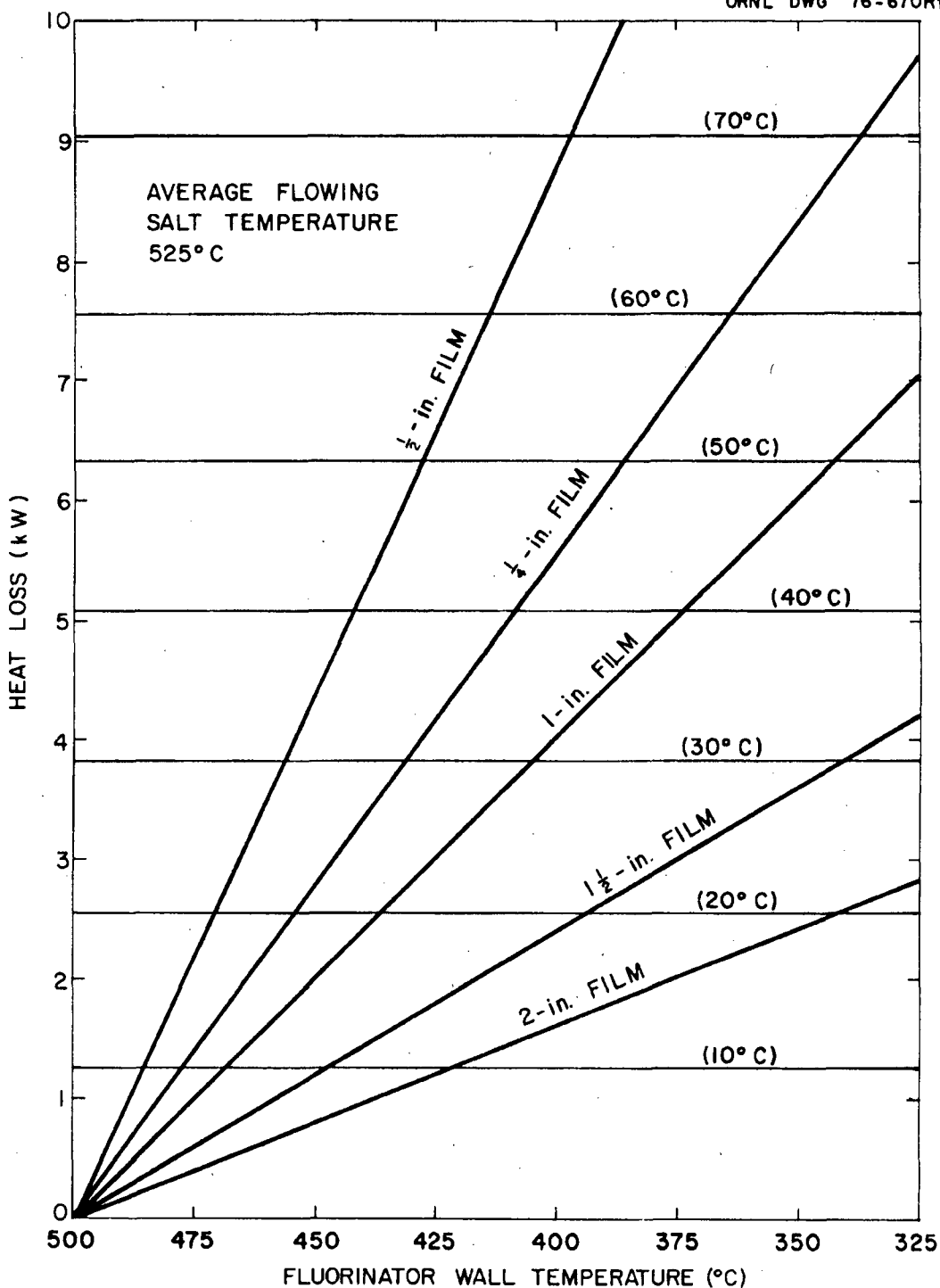


Fig. 3. Heat loss from a fluorinator through several thicknesses of frozen salt film as a function of fluorinator wall temperature. Horizontal lines show heat removal from salt flowing through the fluorinator at 1.7 liters per minute [1/2 the processing rate for a 1000-MW(e) MSBR] for the indicated salt temperature change.

Surge and drain tanks. Before being returned to the fluorinator, the salt will pass through a 5-ft³ (0.14-m³) surge tank to provide salt inventory. This tank will have a baffle to prevent short circuiting of salt flow from inlet to outlet. Salt overflows from a side outlet, the level of which determines the tank capacity.

The drain tank is similar to the surge tank in size and design and has sufficient capacity to contain the salt volume of the test vessel and reduction column. It will be necessary to drain these vessels periodically for inspection and possible maintenance. The drain tank will be subjected to the greatest pressure in the entire system when salt is transferred back to the circulating system. Design of this vessel must therefore be approved by the ORNL Pressure Vessel Review Committee.

HF trap. The off-gas from the gas-liquid separator and the surge tank will contain HF and excess hydrogen from the UF₅ reduction step. This gas is passed through a NaF bed. The bed depth is 3.3 ft (1.0 m), and has a calculated pressure drop of 0.15 psi (1034 kPa) with a gas flow rate of 1 cfm (4.7 x 10⁻⁴ m³/sec). The bed has the capacity to absorb the HF evolved from 1.3-fuel salt batches containing 0.35 mole % uranium, assuming no UF₆ evolution (all UF₄ is converted to UF₅, and is reduced by hydrogen to UF₄). Since absorption is poor at high temperatures, the gas from the reduction step is cooled to 100°C before it enters the trap. Cooling the gas to below 100°C at the inlet would result in a high partial pressure of HF (probably ~ 20%), which would form the higher HF complexes (NaF·2HF, NaF·3HF, etc.) and cause plugging. A cooler is provided on the bed exit to improve absorption at that point and prevent HF release.

UF₆ traps. The absorbers for collecting the UF₆ on NaF pellets are made of carbon steel that is sufficiently resistant to fluorine corrosion at low temperatures. Surplus absorbers from the MSRE fuel processing will be used.⁸ One of these absorbers, having a bed depth of 10 in. (0.25 m), contains 24 kg of NaF and has a capacity of about 15 kg of uranium. Less than 10 kg of uranium is contained in 8 ft³ (0.23 m³) of fuel salt. The absorbers are designed with an open 2-in. (51-mm) center pipe for air

cooling, although this was not found to be necessary in MSRE operation. The UF_6 flow rate is expected to be much lower in the CFEF.

Sampler. The salt will be sampled after it leaves the reduction column and the gas-liquid separator, and before it enters the surge tank. The sample will be analyzed for total uranium and the oxidation state will not affect the results. The sampler is of the same design that has been used successfully for many years. It is the only piece of equipment extending through the containment cover over the cell. Local ventilation will be required to prevent spread of beryllium contamination.

Circuit-breaking pot. In order to minimize the equipment operating at the autoresistance potential (up to 200 V), a pot will be inserted between the heat flowmeter and the electrode-salt inlet pipe in the fluorinator. In this pot, the salt stream will impinge on a horizontal disk causing a salt spray that breaks the electrical circuit. As shown on the flowsheet (Fig. 1), the pot and fluorinator both have insulated flanges so that only the pot and fluorinator top flange will be at high potential.

Heat flowmeter. The salt leaving the surge tank will pass through a 28-in. (0.71-m) section of 2-in. nickel pipe containing a cartridge heater. Heat loss from the flowmeter will be balanced by external heaters. The salt flow rate can be calculated from the temperature rise of the salt as it passes through the flowmeter and the known power input of the cartridge heater.

3.1 Fluorine Supply System

The fluorine supply system that was used in processing the MSRE fuel salt will be reactivated for use with the CFEF.⁹ The system (Fig. 4) has provisions for the connection of two 18-std-m³ fluorine trailers with safety controls to limit the maximum flow rate and to remotely stop the flow in case of a leak. A NaF trap is available to remove HF from the fluorine. The HF could cause plugging of the UF_6 absorbers by formation of complexes of NaF with two or more molecules of HF. The bed inlet is heated to prevent the formation of these complexes in the trap. Fluorine flow is controlled by means of a control valve and an orifice flowmeter.

ORNL DWG. 76-127

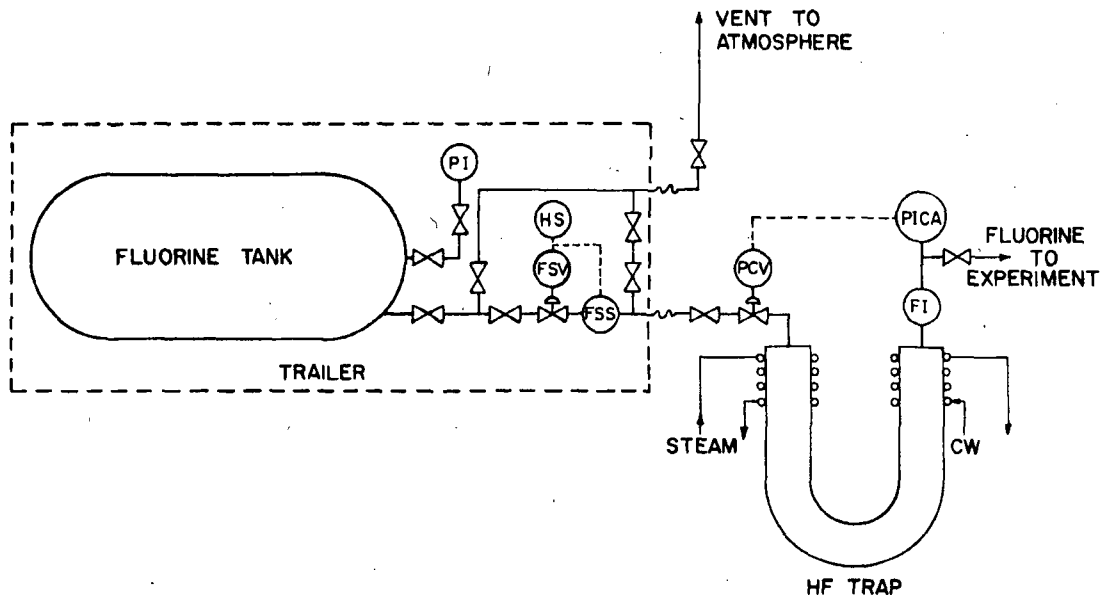


Fig. 4. Fluorine supply system.

3.2 Fluorine Disposal System

The CFEF will be the first test of the frozen-wall fluorinator using fluorine. A vertical scrubber is being installed in Building 7503 for the disposal of the excess fluorine. A flow diagram of the system is shown in Fig. 5. The scrubber is a 6-in., 8-ft- (2.4-m) high Monel pipe with three spray nozzles in the upper half of the vessel. The surge tank contains 200 gal (0.76 m^3) of an aqueous solution containing 15 wt % KOH and 5 wt % KI. This equipment is designed to be able to dispose of one trailer of fluorine (18 std m^3) at a flow rate of 30 slm. The KOH solution will be circulated through the spray nozzles at a maximum total flow rate of 15 gpm ($9.5 \times 10^{-4} \text{ m}^3/\text{sec}$). The fluorinator off-gas stream will flow cocurrent to this stream. The scrubber exit stream will pass through a photometric analyzer for monitoring the efficiency of the scrubber.

4. OPERATING PROCEDURE

After the system has been leak tested, all salt-containing equipment and piping will be purged with argon and heated to 600°C . All heaters and thermocouples will be checked after the system has been held at this temperature for several hours. MSBR fuel salt will then be charged to the surge tank. Approximately 65 liters will overflow through the flowmeter and circuit-breaking pot to the fluorinator. After the level is equalized in the reduction column, the salt will fill the fluorinator to several inches above normal operating level. The liquid-level recorders in the fluorinator and surge tank can be checked for operability during this operation.

Argon will be introduced to the bottom of the reduction column at a low rate; the rate will be increased until the salt begins to circulate as indicated by a drop in the fluorinator liquid level, an increase in the gas-liquid separator liquid level, and a temperature difference across the heat flowmeter. The argon flow will be increased stepwise to obtain data of salt flow rate vs argon flow rate. The liquid level in the fluorinator and separator will be observed during this test. If the

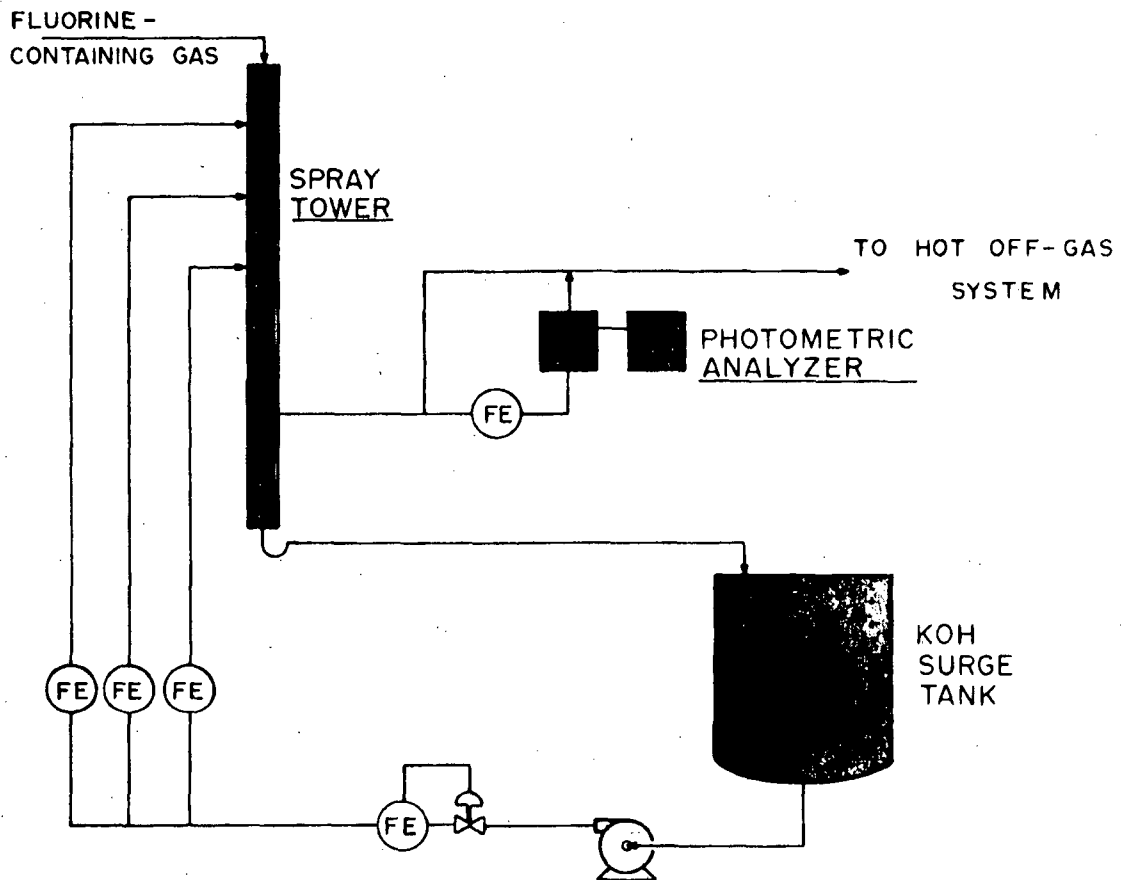


Fig. 5. Fluorine disposal system.

fluorinator liquid level is too high at the normal salt flow rate, some salt will be removed to the drain tank. This can be done by thawing the freeze valve below the surge tank, closing the system vent valve, and opening the drain-tank vent valve to the cell. The system will be pressurized by the purge rotameters to transfer the required amount of salt from the surge tank to the drain tank.

After adjusting the salt inventory, salt circulation will be started again, and temperatures in the fluorinator will be adjusted to 530°C. Lines and other equipment can be maintained between 530°C and 600°C. Heat to the test section of the fluorinator will be turned off and cooling air and water turned on. The autoresistance power will be turned on at very low voltage (less than 1 V) and the resistance can be calculated periodically from the current measurement as the cooling proceeds. Coolant rates to the different zones will be adjusted to keep pipe wall temperatures as uniform as possible. When all pipe wall temperatures are less than 350°C, the resistance of the salt from the electrode to the bottom of the fluorinator will have increased considerably. The autoresistance power will be increased until the resistance of the salt and the wall temperatures become steady.

Following this step, the autoresistance power will be changed, and equilibrium resistance and temperature will be determined for a range of powers to determine the operating range of the system. The argon flow rate to the fluorinator gas inlet (normally the fluorine flow) will be varied to determine the effect on operability and film thickness, as indicated by wall temperature and salt resistance. In addition, the salt flow rate will be varied to determine the operable range, and the sampler will be inspected before fluorine is used.

After the system has operated reliably at various salt and argon flow rates and the operable autoresistance power range has been ascertained, the argon to the column will be replaced with hydrogen to determine what effect, if any, the gas density has on the operability of the gas lift. Argon to the fluorinator will then be replaced by fluorine. Mass flow-meter readings taken upstream and downstream from the NaF traps will

indicate the evolution of UF_6 ; salt samples will be taken periodically for additional data on the fluorination reaction rate. Runs will be made at various fluorine flow rates, fluorine concentrations, and salt flow rates. After good operation has been demonstrated under different conditions, the salt film thickness will be checked by radiography. The freeze valve below the fluorinator will be thawed and salt circulation and autoresistance power stopped as soon as flow to the drain tank begins. Heat will be turned off the fluorinator and radiographs will be taken of the cooled zones.

5. MAINTENANCE

5.1 Maintenance Philosophy

Most components of the system such as the salt storage and drain tanks, separator, sampler, and traps will be designed and constructed for a long, maintenance-free service life. The fluorinator and reduction column may be replaced with equipment of alternate design depending on operating performance. All components of the system will be accessible for possible repair or replacement.

5.2 Preventive Maintenance

The operating temperature of the system will be closely controlled to prevent hot spots that could cause heater burnout. Resistance heaters are to be operated at one-half the design voltage to prolong their usage. Chemical analyses will be made of the salt (especially for NiF_2) to detect unusual corrosion. The facility will be checked regularly to detect incipient failure of parts of the system, and appropriate maintenance measures will be taken.

6. STANDARDS AND QUALITY ASSURANCE

6.1 Codes and Standards

The vessels and piping will be fabricated in accordance with the requirements specified in Sect. VIII of the ASME Boiler and Pressure Vessel

Code and Pressure Piping Code. ORNL MET material specifications and ORNL Weld Procedure Specifications will be used for construction of the vessels and piping. Because of its location at the bottom of the cell, it will be subjected to the highest pressures in the system; therefore, the design must be reviewed by the ORNL Pressure Vessel Review Committee. Details of this vessel are shown in ref. 10.

6.2 Quality Assurance

Quality level III and IV (QL-3) quality assurance standards as outlined in "Quality Assurance Program Planning for Small Research and Development Projects," QA-CT-1-109, will be applied in constructing the facility.

7. REFERENCES

1. J. R. Hightower, Jr., MSR Program Semiannu. Progr. Rep. Feb. 29, 1972, ORNL-4782, p. 230.
2. J. R. Hightower, Jr., MSR Program Semiannu. Progr. Rep. Aug. 31, 1972, ORNL-4832, p. 180.
3. J. R. Hightower, Jr. and R. M. Counce, MSR Program Semiannu. Progr. Rep. Aug. 31, 1974, ORNL-5011, p. 122.
4. R. B. Lindauer in Engineering Development Studies for Molten-Salt Breeder Reactor Processing No. 21, ORNL/TM-4894 (March 1976).
5. R. B. Lindauer in Engineering Development Studies for Molten-Salt Breeder Reactor Processing No. 20, ORNL/TM-4870 (January 1976).
6. R. B. Lindauer in Engineering Development Studies for Molten-Salt Breeder Reactor Processing No. 23, ORNL/TM-5252 (in preparation).
7. "Drain Tank (Continuous Fluorinator Experimental Facility)," ORNL DWG. M 12296 CD 002 ERI.
8. R. B. Lindauer, Processing of the MSRE Flush and Fuel Salts, ORNL/TM-2578 (August 1969) p. 22.
9. Ibid., p. 20.
10. "Continuous Fluorinator Experimental Facility Flowsheet," ORNL DWG. M 12296 CD 003 E.

INTERNAL DISTRIBUTION

1. M. Bender
2. M. R. Bennett
3. R. M. Counce
4. F. L. Culler
5. J. M. Dale
6. J. R. Engel
7. G. G. Fee
8. D. E. Ferguson
9. L. M. Ferris
10. W. S. Groenier
11. R. H. Guymon
12. J. R. Hightower, Jr.
13. R. W. Horton
14. O. L. Keller
15. A. D. Kelmers
16. R. B. Lindauer
17. R. E. MacPherson
18. C. L. Matthews
19. H. E. McCoy
- 20-22. L. E. McNeese
23. H. Postma
24. M. W. Rosenthal
25. H. C. Savage
26. C. D. Scott
27. M. J. Skinner
28. I. Spiewak
29. D. B. Trauger
30. J. R. Weir
31. M. K. Wilkinson
32. J. C. White
33. R. G. Wymer
34. E. L. Youngblood
- 35-36. Central Research Library
37. Document Reference Section
- 38-40. Laboratory Records
41. Laboratory Records (LRD-RC)

CONSULTANTS AND SUBCONTRACTORS

- 42. J. C. Frye
- 43. C. H. Ice
- 44. J. J. Katz
- 45. E. A. Mason
- 46. Ken Davis
- 47. R. B. Richards

EXTERNAL DISTRIBUTION

- 48. Research and Technical Support Division, ERDA, Oak Ridge Operations Office, P. O. Box E, Oak Ridge, Tenn. 37830
- 49. Director, Reactor Division, ERDA, Oak Ridge Operations Office, P. O. Box E, Oak Ridge, Tenn. 37830
- 50-51. Director, ERDA Division of Reactor Research and Development, Washington, D. C. 20545
- 52-155. For distribution as shown in TID-4500 under UC-76, Molten Salt Reactor Technology

Nuclear Detection: Fixed detectors, portals, and NEST teams won't work for shielded HEU on a national scale; a distributed network of in-vehicle detectors is also necessary to deter nuclear terrorism

Nationwide nuclear detection systems consisting exclusively of portals at borders (drive-thru scanning at borders, container screening) and fixed or handheld detectors in the interior (customs agents, NEST teams) will not suffice to deter nuclear terrorists who are attempting to trade, assemble, or transport highly enriched uranium (HEU) in the worldwide transportation system. Calculations of a link budget for passive detection of HEU and Plutonium (Pu) show that using emitted gamma rays and neutrons is physically limited by the sharp attenuation of its radioactivity with distance/shielding (2-4 feet or less)¹ and the time required to count a sufficient number of particles (several minutes to hours), although Pu may be easier to detect than HEU.

Even if the national border was completely covered with detectors, there is not enough time for passive detection of shielded HEU. Once across the border, terrorist vehicles carrying HEU can circumvent or pass by a network of fixed detectors in the interior for the same reasons. Transport carrying people or livestock can't be subject to active neutron or x-ray interrogation like cargo containers can be, and all types of vehicles can't be searched like air passengers are today. Many kinds of vehicles from light road vehicles to private jets to oil tankers are not screened for HEU,² analogous to locking the front door of a house while leaving the garage door wide open. To lock all doors of the house, available detection techniques need to be applied and combined in such a manner that they ensure uniform detection coverage across every transportation mode accessible to terrorists, thereby raising the risk that terrorists transporting HEU and Pu will be detected.

For the vast number of small vehicles (autos, boats, small planes), neutron and gamma detectors located inside the target transport are perhaps the only way that both shielded HEU and Pu detection can be detected. This ensures enough time to record any radioactivity coming from inside the vehicle before securely reporting their readings to a network of check-points (for example, in the same way E-Z pass collects highway tolls).

Today's detection efforts involving fixed/handheld detectors would be useful primarily for detecting unshielded HEU carried by people or animals; active neutron scanning or X-ray portals checking cargo containers may find reasonable quantities (Kgs) of unshielded or shielded HEU depending on the circumstances. In addition to bolstering and expanding these programs, commercially available detector technology should be directly integrated into smaller vehicles and used in conjunction with direct inspection or surveillance schemes for the smaller number of extremely large vehicles not amenable to detection (oil tankers, jumbo-jets).

Besides several hundred thousand casualties and injuries likely, the loss from a terrorist nuclear attack is estimated up to \$1 trillion.³ Back of the envelope estimates of costs for the US to implement an in-vehicle detector program are within \$75 billion and possibly much less.

¹ attenuation of radioactivity with distance is subject to an inverse-square law in free-space and is exponential with shielding

² Medalia, J., 2005, "Nuclear Terrorism: A Brief Review of Threats and Responses," CRS Report for Congress, The Library of Congress
<http://fpc.state.gov/documents/organization/43399.pdf>

³ See [p. 7, O'Hanlon, 2002]

Nuclear Detection: Fixed detectors, portals, and NEST teams won't work for shielded HEU on a national scale; a distributed network of in-vehicle detectors is also necessary to deter nuclear terrorism..... 1

The Problem..... 3

Detection of Shielded HEU (passively) —just how hard? 6

 Gamma Emissions of U-238, U-235, and U-232..... 8

 Neutron Emissions of U-238, U-235, and U-234 9

 Self-Shielding 10

 External Shielding..... 10

 Path Loss..... 10

 Background and Detector Efficiency..... 10

 Detector Area, Detection Time, Detection Distance 10

 Nuclear Detection Link Budget 11

 Detecting HEU with U-238 signal: Dependence on Detector Size 13

 Detection times of a day at a half meter distance are required for ten centimeters shielding..... 13

 U-232 makes detection easy, but is not always present..... 15

 A few centimeters of lead shielding put detection times into minutes at distances of a meter 15

 Fixed detectors on streets don't make sense, but in-vehicle detectors are useful..... 16

Plutonium Detection—easier than HEU? 16

 Neutron Detection..... 17

 Gamma Detection 18

Detector System Manufacturers..... 21

DISARM: Detect and Intercept Shipments of Articles with Radioactive Material..... 22

How good does the detection system have to be?..... 25

What is required to secure each transportation mode? 30

 Water..... 30

 Air 31

 Ground 31

Operational Requirements For Assuring Compliance With DISARM..... 31

How could DISARM be defeated? 34

Economics of Industry Participation and Public Adoption of DISARM..... 36

Conclusion 39

References..... 41

Appendix A: Representative Detector and System Suppliers..... 46

Appendix B: How do we track trends in worldwide terrorism? 51

The Problem

Access to a sufficient amount of highly enriched uranium (HEU) is the only barrier preventing a determined terrorist group from building an atomic bomb, since the know-how to build a gun-type HEU-based bomb has been in the public domain for several decades [p. 28, Campbell, 2004], [p. 97, Falkernrath, 1998].⁴ Improvised nuclear weapons (based on either HEU or Plutonium) are easier to build than military grade weapons, and they can be delivered to populated areas by modes of civilian transport such as road or sea which militaries are not equipped to defend [p. 100, Falkernrath, 1998], including cars, containers, trucks, boats, trains, helicopters, planes, or ships. A black market of procurement networks and easily concealable nuclear enrichment facilities is being formed [Reuters, 2004], [p. 326, Campbell, 2004]. If the security of HEU and Pu stockpiles cannot be guaranteed, then the second line of defense against nuclear terrorism is to deter would-be nuclear terrorists attempting to pursue construction and deployment of a nuclear weapon and to detect or discover special nuclear material (SNM) in transit through the civilian transportation infrastructure.

If nuclear detection has the potential to deter nuclear terrorism by increasing risk of failure of a nuclear terrorism plot, then the question becomes how do detection systems have to be designed in order to be effective? Today's approaches to nuclear detection rely primarily on fixed inspection portals at national borders⁵ and sea-ports through which shipping containers or vehicles pass, fixed radiation detectors positioned at traffic choke-points within the national interior, or handheld detectors used by government agents or nuclear emergency search teams⁶ (NEST) when specific intelligence is available. In FY 2006, \$125 million or over half of the requested budget for the new Domestic Nuclear Detection Office was proposed for next generation detection portals [Chertoff, 2005]. The U.S. Department of Defense has speculated that at an estimated cost of a few billion to a few tens of billions of dollars, roughly 100,000-400,000 fixed detectors strategically placed in the interior both in and around cities along roads, ports, airports would be necessary to secure the US against a "clandestine nuclear attack" between 2004 and 2015 [p. 10, Defense Science Board, 2004].

The first problem with the DHS, DoD, and DoE initiatives involving portals, fixed detectors, and handhelds is that on a national scale there are many loopholes for terrorists to circumvent these systems including private jets, drug shipments, or oil tankers, etc. as described by a Congressional Research Report titled "Nuclear Terrorism: A Brief Review of Threats and Responses" (See [Medalia, 2005] and [p. 26, Bunn, 2004]). Today's radiation portals situated at ports and border crossings will only result in displacement of nuclear transport into many other sea, air, or ground transport mechanisms that avoid the portals. It is not enough to selectively inspect incoming cargo and vehicles at selected

⁴ For varying assessments of the risk of nuclear terrorism, see [Ferguson, 2004], [Allison, 2004], [National Intelligence Council, 2005], [Linzer, 2004], [Medalia, 2005], and [Howe, 2004]

⁵ As part of its Second Line of Defense Program, the Department of Energy has targeted 330 high priority sites Russia and 21 neighboring countries for nuclear detection equipment. These include border crossings and high transit sites, only a small fraction of which (roughly 25%) have been installed and staffed with trained personnel. See [p. 45-46, Bunn, 2005].

⁶ see [Nuclear Threat Initiative, 2005], [Kimery, 1995], and [The Week, 2002]

border checkpoints—the capability to detect nuclear materials *anywhere* within the transportation infrastructure is necessary to detect nuclear smuggling and transport.

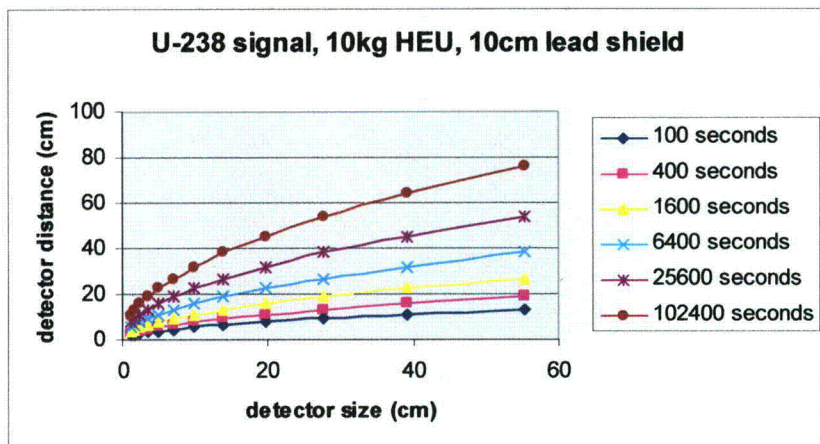


Figure 1 Time and distance required to detect a shielded HEU sample (10kg) using gamma rays

Second, a terrorist could surround HEU with shielding such as lead, concrete, or steel and render passive detection impossible beyond the range of 1 meter using gamma and neutron detection equipment. Shielding all but eliminates the low energy gamma rays (< 200 KeV) and also cuts down the rate of higher energy gamma and neutron emissions so much so that detection times for shielded HEU will necessarily be in the range of many minutes to hours, certainly not seconds. Shielding represents a challenge for detecting HEU with portals or handheld detectors even under ideal detector designs, with 100% detection efficiency, the use of collimation, or even the most advanced gamma detection technologies such as Compton gamma ray imaging⁷ that are still under research (and therefore very costly and bulky).

An alternative to passive detection is to pass the target through a portal that uses highly penetrating active neutron interrogation⁸ (or experimental muon detection⁹ techniques). Active scanning may be suitable for some larger vehicles that carry cargo containers and do not transport living beings, but it is not suitable for the vast majority of vehicles which carry passengers, for which passive scanning or visual inspection are the only remaining options.

Finally, the Department of Homeland Security outlines the need for sensor technology and networks that reliably detect shielded HEU as it crosses national borders and travels within the interior [Kammeraad, 2004], and they indicate that they are funding research into new detection technologies to extend HEU detection to 100 m [see slide 11, Kammeraad, 2004]. Except possibly for very specific nuclear search applications where detection time is not a constraint, detection of shielded HEU based on its radioactivity is

⁷ For an overview of Compton gamma ray imaging, see [Vetter, 2005]

⁸ See [Slaughter, 2003]

⁹ See [Borozdin, 2003]

unlikely to reach ranges of 100m with acceptably low false-positive rates even with any sort of R&D breakthroughs in detector or portal technology. The constraints on detection have to do with the rate and energy of the natural radioactivity of HEU, its attenuation through shielding, its path loss due to the solid-angle subtended by the detector, and the presence of background radiation at the detector. The constraints on detection ranges and detection times stem from physics and it doesn't make sense to look to technological breakthroughs to deliver detection at distances of hundreds of meters.

*Reliable detection of shielded HEU on a national scale will require a completely new nuclear detection architecture and system design that complements portals, fixed detectors, or handheld devices.*¹⁰

We analyze what it would take to design a comprehensive detection system that applies today's portfolio of evolving detection technologies and assembles them into a system that is capable of reliably detecting even small amounts (few kilograms) of shielded HEU and Pu in transit. If the system is to retain enough flexibility to be engineered to deliver any desired level of security where cost and investment replaces physical limits as the determinant of the level of security, then it is not sufficient to simply expand and bolster today's initiatives involving fixed/handheld detectors and portals. We conclude that they will need to be complemented with new approaches involving in-vehicle detectors and inspection or surveillance.

We begin with the assumption that since nuclear terrorists are non-state actors, they won't have access to the weapons delivery vehicles of choice, namely the inter-continental ballistic missiles and air-force jets. In order to deliver a weapon into a city or populated area, terrorists would need to assemble or steal a nuclear weapon in a manner that exploits conventional transportation modes, analogous to how Al-Qaeda attacked the US with commercial airplanes on 9/11 and how they drove a rental truck full of explosives into the World Trade Center in 1993. Assembling or delivering the fissile nuclear material would necessarily involve use of private or government vehicles at multiple points during the development of the terrorist plot, including cars, containers, trucks, boats, trains, helicopters, planes, or ships. Therefore the likelihood of success of a terrorist nuclear plot is directly dependent on the ease with which they can transport nuclear materials without interception by law enforcement and military. Conversely, an increase in the cost and complexity of undetected transportation of fissile nuclear material will serve to dissuade terrorists from pursuing nuclear terrorism plots due to the increased risk of failure they would face. Securing the entire transportation infrastructure against being used to transport nuclear materials is, therefore, key to deterring nuclear terrorism.

Physical constraints of passive detectors are eased with proximity as well as prolonged exposure to the source. For the vast majority of vehicles which are small enough, it is possible to directly integrate emerging and commercially available radiation detector technology into each vehicle such that these detectors travel with vehicles and benefit from having enough time to record radioactivity before reporting their readings to a network of check-points (analogous to how E-Z pass collects highway tolls). One or more

¹⁰ See [Doyle, 2003] for a motivation of the need for a "nuclear dragnet for homeland security."

passive detectors can be mounted on or inside each vehicle, rather than exclusively at fixed locations or check-points (traffic lights, street lamps, or embedded in roads) where the opportunity for sufficient exposure at short enough distance is extremely limited. . We use DISARM to refer to a system designed to **Detect and Intercept Shipments of Articles with Radioactive Materials** by placing detectors inside the vehicles that might be used to transport nuclear materials leverages the close proximity as well as prolonged exposure to the radioactive source in transit.

Under plausible shielding scenarios for HEU, the most effective solution involves energy-selective detectors mounted inside vehicles so that radiation coming from *inside* the vehicle is recognized and detected. These in-vehicle detectors would need to be deployed in all types of vehicles that cannot be actively screened: automobiles, trucks, commercial airplanes, trains, private jets, boats and ships, etc. In addition, these same detectors could also be deployed on shipping containers.¹¹ The larger the vehicle the more shielding it can contain. The smaller subset of vehicles which are too large for passive detection to ever work will need to be dealt with on a case-by-case basis either by requiring them to be screened using fixed portals or through other inspection and surveillance programs.

Detectors used in DISARM can be equipped with tamper-detection circuitry to prevent them from being disabled. Detector readings can be conveyed from the vehicle to a dispersed network of checkpoints (or queried on demand by law enforcement authorities). Checkpoints can be interspersed throughout the interior and around the periphery of the nation as well as around the perimeters of large populated areas. The checkpoints can be designed so that there is no ambiguity about which vehicle transmitted its detector reading. This could be achieved either by using commercially available short-range wireless communication technology between the detector and checkpoint or by designing the checkpoints to be pass-through like toll booths. By programming the checkpoints to discard the readings if the detector does not report anything suspicious, this would also respect personal privacy. One way to ensure deployment in all vehicles of a class is for federal regulations to mandate that all vehicles built after a to-be-determined model year have built-in radiation detectors, with a similar requirement applying to shipping containers as well as commercial and civil aviation airplanes. While it is unusual to call for new federal regulations, the seriousness of the threat and the technical difficulty of otherwise effectively detecting shielded HEU may well warrant this step.

Detection of Shielded HEU (passively) —just how hard?

Short of manual searching or active scanning with neutrons, the only option available for detecting shielded HEU in smaller vehicles, especially those with passengers, is passive detection which utilizes natural radioactivity of HEU as a signal to detect shielded nuclear materials or weapons.

¹¹ For a detailed analysis of various passive and active monitoring schemes for cargo containers at seaports, see [Wein, 2005].

We analyze the fundamental physical constraints on passive detection of shielded HEU, and conclude that a fixed infrastructure-based architecture is all but hopeless. The conclusions discussed below are:

1. The useful radioactive emissions for passively detecting shielded HEU are gamma rays at 1MeV from decay of U-238, although neutrons may offer better or complementary detection options.¹² The gamma rays with energy below 200 KeV are practical for detecting only unshielded HEU since these are too easily attenuated with shielding.
2. The most effective detection solutions will place detectors with the largest possible area and most energy-specificity as close as possible and for as long a time as possible since
 - a. At distances 10 meters or more, the solid angle subtended by the detector (\sim detector area/distance²) from a 50kg HEU source is likely to reduce the signal as much as any reasonable size shielding.
 - b. With sufficient time for the detector to integrate photon counts within a narrow enough photon energy range, even signals below the background can be detected.
3. Due to limitations on both distance and time, a fixed detector infrastructure monitoring vehicles as they pass by can easily be overcome with sufficient shielding.

Advances in detection *technology* cannot alter the fundamental limits on detection that stem from the laws of physics governing attenuation (through shielding) and path loss. Increases in R&D spending aimed at better and more sensitive radiation technology are unlikely to lead to solutions that can detect SNM radiation sources from a great distance (hundreds or thousands of feet) or with short exposure times (seconds or minutes). In characterizing the ultimate limits of passively detecting shielded highly enriched uranium (HEU), distance of the detector, integration time required, and area of detector can all be traded off against each other while energy-discrimination of the detector allows for precise identification the target material (HEU) in the presence of other benign radioactive sources. Throughout this entire section, our estimation methodology and approximations are based on the development in [Fetter, 1990a, 1990b]. An overview of nuclear detection techniques for homeland security is given in [McDonald, 2004]. For a highly engaging introduction to nuclear science, see [Shultis, 2002].

In our model, we assume the HEU core is shielded externally by lead. The linear attenuation coefficient, defined as the probability per unit distance that a gamma ray is scattered by a material, is a function of both the material and the energy of the gamma ray. Steel and concrete have linear attenuation coefficients at 1 MeV that are not all that different from lead, so the conclusions will be roughly similar even with other typical shielding materials. In addition to the external shield, the mass of HEU itself acts to shield gamma rays (self-shielding). The number of gamma rays that reach the detector is limited by the solid angle subtended by the detector from the source. Finally, detection

¹² Although highly penetrating neutrons from HEU can be detected, current technology offers limited options for sufficiently small detectors that are also energy selective enough to rule out false positives from other benign neutron sources. Trace quantities of U-232 can sometimes be present, resulting in more penetrating gamma rays of up to 2.4MeV, but they cannot be relied upon to be present in all HEU samples.

involves reading enough counts of gamma rays to be able to ascertain a significant deviation from the background and the detector only detects a fraction of those gamma rays that are emitted due to detection inefficiencies. Each of these factors when put together forms a “link budget” and is explained below.

We use nuclear theory to estimate the maximum distance possible for passive detection of a lead-shielded HEU spherical core using both U-238 and U-232 signals. The distance is graphed against variables of interest including detector area, detection time, shield thickness, and mass of the HEU core. Detection distance depends on amount of HEU and its surface area, shielding, detector area, distance, and time available to detect the emissions. Maximum detection distance is dependent on these factors. Larger detectors might seem to yield better results. They will not be as portable as smaller ones that can be placed closer to the target. When the increased background radiation of larger detectors is also taken into consideration, the increase in solid angle subtended by the detector will only result in detection distances growing in proportion to the square root of detector size.

Although we also explore neutron emissions of HEU, for our detailed analysis, we focus on the 1 MeV gamma emissions of U-238 for two reasons. First it is technologically feasible to implement portable gamma detectors of sufficient energy selectivity. Second it is analytically tractable to analyze gamma detection under different masses and shielding scenarios, and this helps expose the factors that matter most when designing a system. Further investigation could reveal that there are more optimal detection solutions under these constraints (possibly even a combination of neutron and gamma detection), but our survey of gamma and neutron techniques shows that the basic conclusions are unlikely to change regardless: *detection probability is sensitive to proximity and duration of exposure of the detector to the source requiring distance of not more than a few meters and detection times in the minutes to hours.* The problem of effectively detecting highly enriched nuclear materials whether through neutron- or gamma-detection is a hard one.

Gamma Emissions of U-238, U-235, and U-232

Uranium consists of multiple isotopes. By definition highly enriched Uranium (HEU) has more than 20%¹³ of the isotope U-235 which is fissile, and weapons grade Uranium contains over 90%¹⁴ U-235. Radioactive decay of U-235 results in gamma rays at 185 KeV, but shielding too easily attenuates these and so they are not useful for detecting shielded HEU. HEU also contains the isotope U-238—the more highly enriched, the less the percentage of U-238. A conservative assumption for detection using U-238 emissions is that HEU or weapons grade Uranium contains at least 5% U-238 by weight. U-232 may also be present in trace quantities (parts per trillion).¹⁵

According to [Fetter, 1990a], U-238 emits 81 gammas per second per gram at 1.001MeV, and we use that value denoted by **N**. This number can also be derived using first principles and nuclear data, but results in only a slightly higher value based on data from

¹³ See [p. 107, Ferguson]

¹⁴ [p. 255, Fetter, 1990b]

¹⁵ [p: 256, Fetter, 1990b]

[National Nuclear Data Center, 2004]. Radioactive decay of U-238, which has a half-life of 4.47 billion years, will result in Thorium-234 which in-turn decays to a meta-stable (excited) state of Protactinium-234. Meta-stable Protactinium (half life of 1.17 minutes) quickly decays to U-234 most of the time, but 0.16% of the time it relaxes to a more stable state of Protactinium-234 (half-life of 6.75 hours) before eventually decaying to U-234. Gamma rays at 1.001MeV will be emitted due to the transition of meta-stable Protactinium to Protactinium with a probability of 0.837%. Therefore an estimate of the number of 1.001MeV gamma rays emitted by U-238 is $104 \text{ per gram per second} (= 1 \text{ mole / AMU of U-238}) \times (\ln 2 / \text{half-life of U-238}) \times 0.837\%$.

U-232's decay chain produces even more penetrating gamma rays than U-238. The most important gamma emitter in the U-232 decay chain is Tl-208 which emits a 2.6 MeV gamma ray when it decays. These gamma rays can be effectively used to detect the presence of HEU if U-232 is known to be a contaminant, even to the effect of a few hundred parts per trillion [Gosnell, 2000]. We can similarly arrive at the rates for U-232, the most penetrating of which has emissions at 2.614MeV at a rate of 2.68×10^{11} gammas per gram per second also as reported by [Fetter, 1990a].

Neutron Emissions of U-238, U-235, and U-234

The neutron "link budget" is not easily amenable to analytical approximation as it is for gammas. For a comparison with gammas, we present the basics of neutron emissions and attenuation here in the specific case of weapons grade Uranium (WgU). The lack of energy specific neutron detectors with sufficient portability is currently a technological limitation [McDonald, 2004].

- Weapons grade Uranium (WgU) emits neutrons at the rate of roughly 1/s/kg with an energy distribution centered around 1 MeV—primarily due to spontaneous fission of Uranium isotopes, with each of 234, 235, and 238 contributing roughly equal numbers of neutrons given their relative composition in WgU (see Table 2, Fetter, 1990b).
- These energetic neutrons also have mean free path lengths of 2-6 cm in most shielding materials (tungsten, lead, etc.) whereas 1 MeV gammas are only ~1cm by comparison (Tables B-2/B-3, Fetter, 1990b).
- A 12 kg WgU sample with tungsten tamper emits 30 neutrons per second in addition to 30 1 MeV gamma rays per second at the surface of the sample. The path loss through free space is equivalent for both forms of radiation.
- The background rate of neutrons (per meter-squared per second) is about 50 (for hand-held or portable detectors) whereas the background rate for 1 MeV gamma rays (per meter-squared per second) is cited as being between 17 (for hand-held) and 860 (for portable detectors).

Although neutrons may pass through shielding further than 1MeV gammas, the difference is small enough that detection of shielded WGU using neutrons is likely to be subject to comparable constraints of short distance (2-4 feet) and long observation times (several minutes to hours) like gammas.

Self-Shielding

Gamma rays may be scattered as they escape from the HEU core, losing some fraction of their energy and making them less useful for detection. Fundamentally, the more surface area per gram of material, the more gammas escape. The number of gammas that escape without scattering can be calculated precisely with radiation shielding theory and depends on the geometry of the core. But for a sphere of radius r and linear attenuation coefficient μ , it can be approximated by the self-shielding attenuation coefficient G that describes the fraction of gammas emerging without scattering,

$$G = (1 - e^{-4\mu r/3}) / (4\mu r/3).$$

External Shielding

Our model of the shield is a spherical shell of thickness x surrounding the HEU core, whose effects we approximate as being the same as a sheet of the same thickness. For an external shield material of thickness x and linear attenuation coefficient λ , the well known formula for the fraction of gammas emerging without scattering is

$$F = e^{-\lambda x}$$

Path Loss

The solid angle subtended by a detector of area A at a distance d from the center of the Uranium core is approximately

$$P = A/4\pi d^2$$

Background and Detector Efficiency

Some fraction of the received gamma rays will not be counted due to inefficiencies in the detector. The efficiency is denoted by ϵ . The detector will also receive gamma rays from both its surroundings and the cosmic rays collectively termed "background" and denoted by b , which is dependent on the bandwidth of the channel in which the detector measures counts. Therefore, a high-resolution detector with a large number of channels will have a small value of b . As a result, the average rate of background will be

$$B = Ab$$

and $B\epsilon$ counts will be registered by the detector due to background. In our calculation, we assume a high-purity Germanium detector with a 2keV bandwidth. Other types of detectors may have a higher bandwidth that would result in a greater background rate.

Detector Area, Detection Time, Detection Distance

The total signal received at the detector is therefore given by

$$S = NGFP$$

Signals below the background can be detected when the total counts due to the signal exceeds the fluctuations in the background. If a source is present, the former grows linearly with time while the latter is proportional to the square root of time. If S is the signal received at the detector and t is the time over which counts are integrated, then the $S\epsilon t$ will be the counts due to the signal, while the standard deviation of fluctuations in the background will be proportional to $(Ab\epsilon t)^{1/2}$. Therefore the signal can be detected after the following criterion when the average signal exceeds a multiple, m , of standard deviations of the background

$$S\epsilon t > m (Ab\epsilon t)^{1/2}$$

Solving for t , we arrive at the time required for detection is

$$t > m^2 Ab / (S^2 \epsilon)$$

In our calculations below, we use $m=5$.

Nuclear Detection Link Budget

To illustrate these calculations, an example is shown in the following table for the detection of roughly 50kg of HEU with 10cm lead shielding assuming a detection distance of 100cm. The third column presents a link budget through detection of the 1 MeV gamma ray emitted by U-238 showing that detection of the core under these conditions would require nearly three hours assuming a gigantic 1 square meter solid-state detector (if one existed). The fourth column presents a similar link budget for detection using the 2.6 MeV gamma ray emitted by U-232 (a trace contaminant that may or may not be present in HEU) that requires just 31 seconds to detect the core using a much smaller 30 square centimeter detector.

CORE	Symbol	HEU U-238	HEU U-232
Detectable Isotope			
Gamma Energy (MeV)		1.00	2.6
Production Rate (per gram per second)	N	81.00	2.68E+11
Density (grams per cubic centimeter)		19.00	19
Weight fraction of isotope		0.06	1.00E-10
Inner Radius (cm)		0.00	0.00
Outer Radius (cm)	r	8.50	8.50
Linear Attenuation Coefficient (per centimeter)	μ	1.41	0.87
Thickness (cm)		8.50	8.50
Weight (grams)		48851.60	48851.60
Weight (kg)		48.85	48.85
Total Gamma Rate		217633.86	1309222.79
Beta		1.33	1.33
Self-Shielding Attenuation (dB)	G	-12.04	-9.94
		Lead	Lead
SHIELD			
Density (grams per cubic centimeter)		11.35	11.35
Linear Attenuation Coefficient (per centimeter)	λ	0.77	0.50
Inner Radius (cm)		8.50	8.50
Outer Radius (cm)		18.50	18.50
Thickness (cm)	x	10.00	10.00
Weight (kilograms)		271.69	271.69
Shielding Attenuation (dB)	F	-33.44	-21.71
		Handheld HPGe	Handheld HPGe
DETECTOR			
Area (square cm)	A	10000.00	30.00
Efficiency	ε	0.16	0.16
Bandwidth (KeV)		2	2
Background at this Bandwidth (per sq. cm per sec.)	b	0.0017	0.0003
Background detected (per second)	Aεb	2.72	0.00
Detection threshold (number of standard deviations)	m	5.00	5.00
TIME TO DETECTION			
Distance (cm)	d	100.00	100.00
Path Attenuation (dB)	P	-10.99	-36.22
Total Attenuation: self + shield + path (dB)	G + F + P	-56.47	-67.87
Total Gammas at Detector (per second)		0.49	0.21
Gammas detected (per second)		0.08	0.03
Time to detection (seconds)	t	11017.52	30.80
Time to detection (minutes)		183.63	0.51
Time to detection (hours)		3.06	0.01
DISTANCE TO DETECTION			
Detection time (seconds)		11017.00	30.80
Self + Shield Attenuation		-45.48	-31.65
Total Gammas outside (per second)		6.17	894.63
Detection distance (cm)		100.00	100.00

Detecting HEU with U-238 signal: Dependence on Detector Size

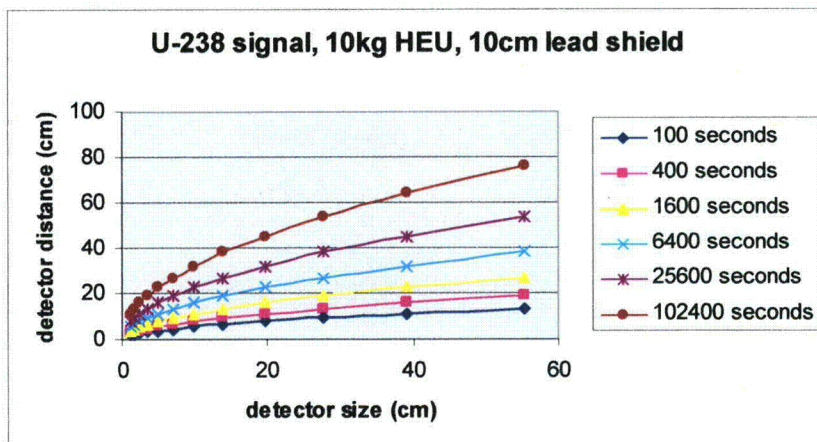


Figure 2

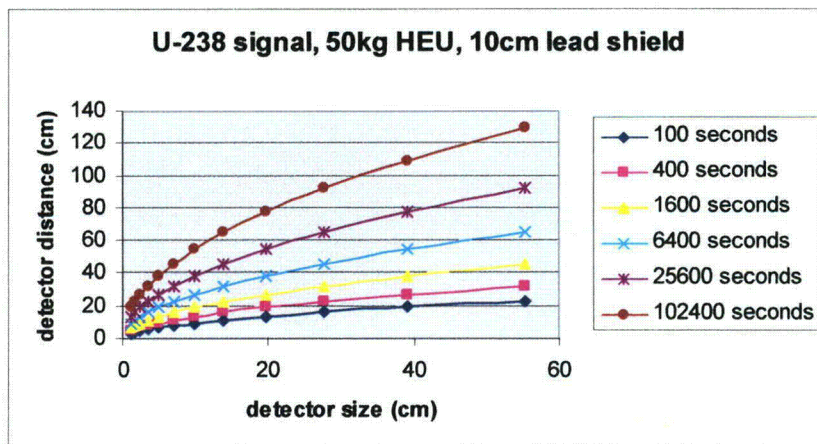


Figure 3

Detection times of a day at a half meter distance are required for ten centimeters shielding

The graphs in this section indicate that 7-10cm of lead shielding requires on the order of a day using U-238 based detection even at distances of 0.5-1m. So detection of heavily shielded HEU looks hopeless at distances greater than 1 meter, and only begins to become feasible below 1m.

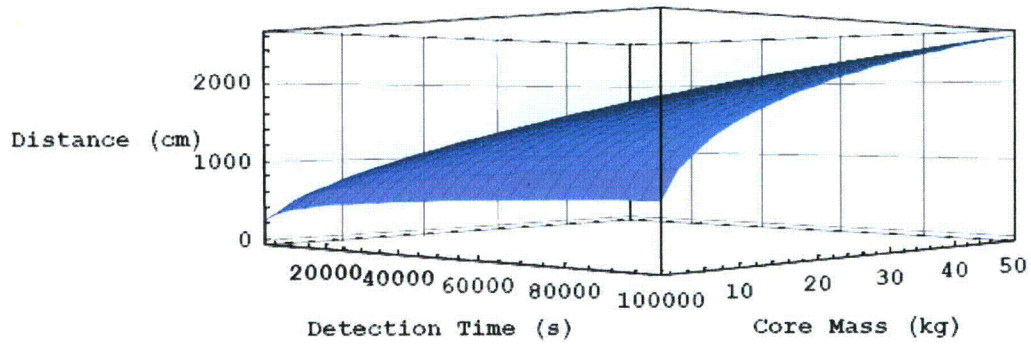


Figure 4 Detection Distance For No Lead Shielding, 1800-100000 seconds of HEU using U-238 signal, 100 sq. cm. detector area (10cm x 10cm). Mass of core varies from 1-50 kg

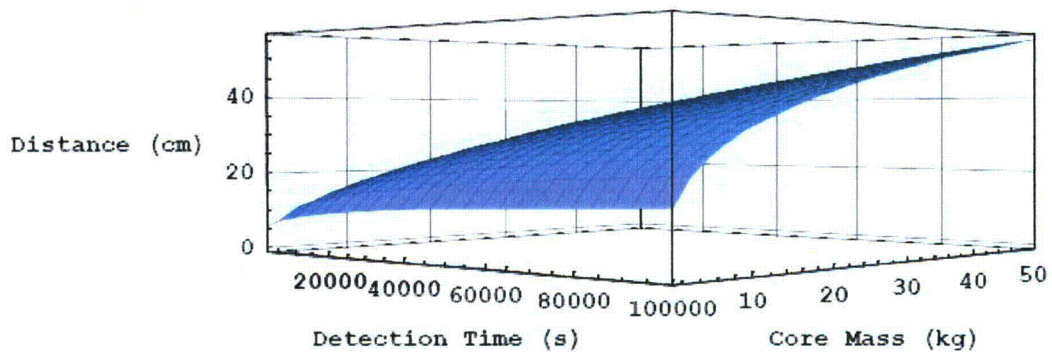


Figure 5 Detection Distance For 10cm Lead Shielding, 1800-100000 seconds of HEU using U-238 signal, 100 sq. cm. detector area (10cm x 10cm). Mass of core varies from 1-50 kg

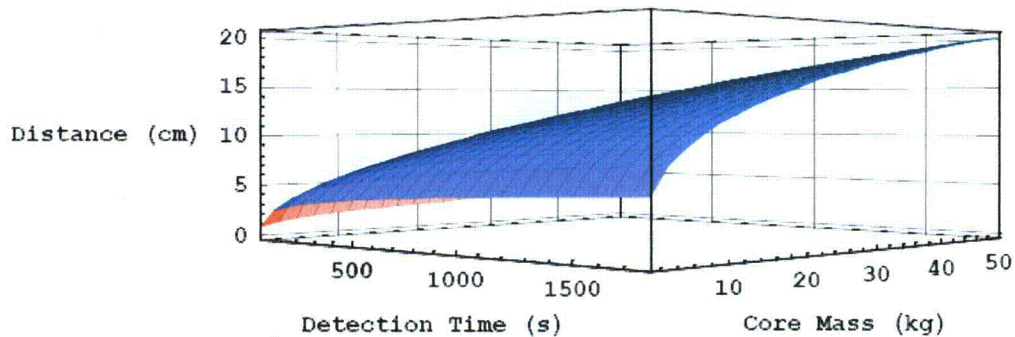


Figure 6 Detection Distance For 10cm Lead Shielding, 1-1800 seconds of HEU using U-238 signal, 100 sq. cm. detector area (10cm x 10cm). Mass of core varies from 1-50 kg

U-232 makes detection easy, but is not always present

If trace quantities of U-232 are present, detection is much easier and can be achieved at several meters distance even with 10cm of lead shielding and for a few kilograms of HEU. The catch is that U-232 is not guaranteed to be present in HEU. From here onwards, we refer to detection with U-238 only.

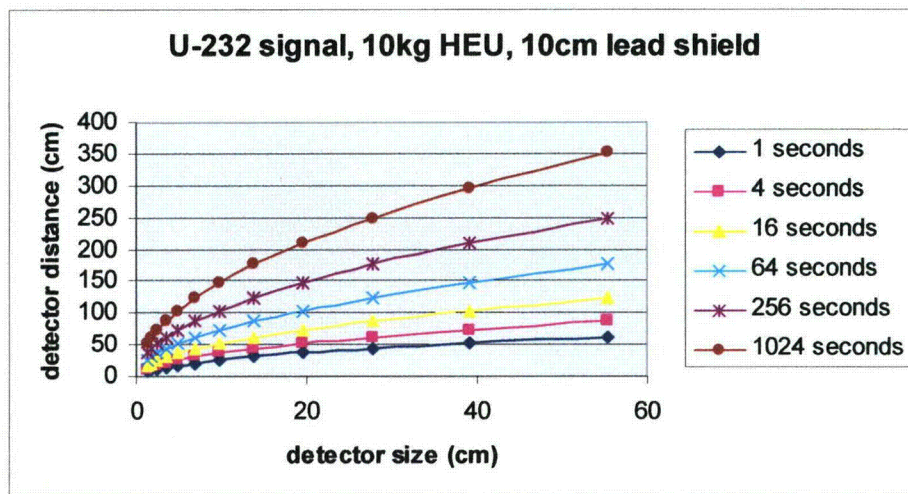


Figure 7

A few centimeters of lead shielding put detection times into minutes at distances of a meter

Detection times on the order of minutes can be achieved at distances of a meter or more only when shielding is less than a 2-3 centimeters. Beyond that, detection times need to be taken to tens, hundreds, or thousands of minutes depending on the shielding and size of the core

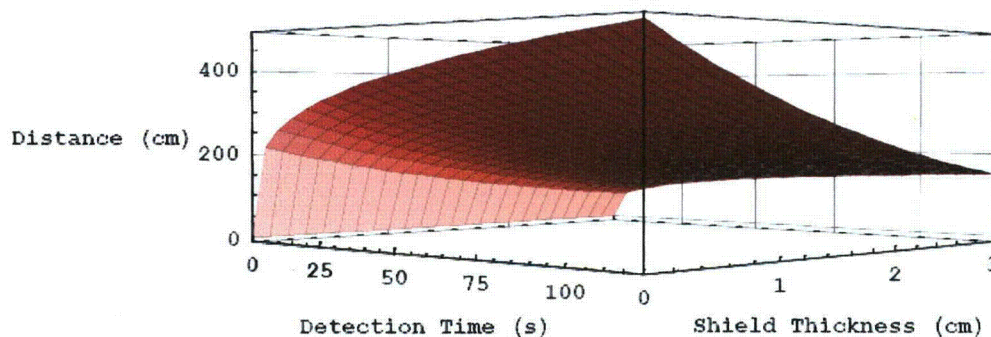


Figure 8 Detection Distance for 0-120s, 0-3 cm lead shielding of 48kg HEU using U-238 signal, 100 sq. cm. detector area (10cm x 10cm)

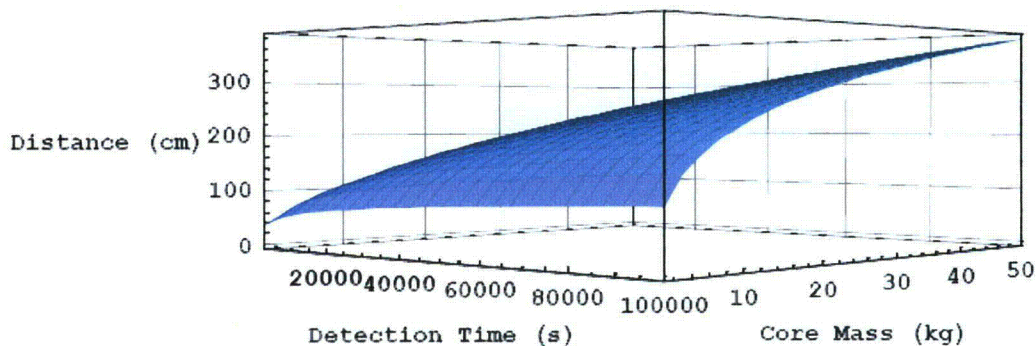


Figure 9 Detection Distance For 5cm Lead Shielding, 1800-100000 seconds of HEU using U-238 signal, 100 sq. cm. detector area (10cm x 10cm). Mass of core varies from 1-50 kg

Fixed detectors on streets don't make sense, but in-vehicle detectors are useful

If either the U-238 signal or neutrons or both are to be relied upon, we conclude that any practical and robust detection scheme is going to require detection times in the range of several tens of minutes to hours. This immediately rules out the use of fixed detector infrastructure to look for signals in vehicles passing by—there will not be enough time to integrate the signal from signals from a moving vehicle. Improving detector efficiency from 16% to 100% would not even double the detection distance since the detection distance is proportional to the fourth root of the efficiency—improvements in detector efficiency result in more background radioactivity counts and because activity from the source has an inverse square law falloff with distance from the source.

Requiring operation of one or more detectors continuously inside the vehicle that ensure proximity and sufficient photon integration time will serve to raise the risk of detection for a terrorist transporting HEU. If an in-vehicle detector were present, hundreds of kilograms of shielding would be required to evade detection, which would make it more likely that the terrorist would have to use a heavier vehicle to transport the HEU. If these larger vehicles are then screened with more invasive (active) techniques that amplify the U-238 signal, the terrorist would probably give up trying.

Plutonium Detection—easier than HEU?

Even reactor-grade (i.e., not weapons-grade) plutonium can be used to achieve a yield of a few kilotons. More generally, plutonium of any isotopic composition can be used to construct an implosion assembly with kiloton yield. The bare critical mass is a function of the isotopic composition. Also, the probability of pre-detonation (resulting in a fizzle)

varies depending on the composition. Furthermore, "the technical problems confronting a terrorist organization considering the use of reactor-grade plutonium are not different in kind from those involved in using weapons-grade plutonium, but only in degree." [Mark 1990]

Since reactor-grade plutonium might be more readily available, it might represent a material of choice for would-be nuclear terrorists. However, they would still be faced with the technical difficulty of constructing an implosion system. Below we consider the limits of detection of plutonium of various grades (from super-grade with 98% Pu-239 through MOX-grade with only 40% Pu-239) based on the natural neutron and gamma ray emissions.

The isotopic compositions of different grades of plutonium are as listed in the table below [Mark 1993]:

	Super-grade	Weapons-grade	Reactor-grade	MOX-grade	FBR Blanket
Pu-238 (%)	0	0.012	1.3	1.9	0
Pu-239 (%)	98	93.8	60.3	40.4	96
Pu-240 (%)	2	5.8	24.3	32.1	4
Pu-241 (%)	0	0.35	9.1	17.8	0
Pu-242 (%)	0	0.022	5	7.8	0

Neutron Detection

In general, isotopes of plutonium undergo spontaneous fission far more readily than uranium isotopes, resulting in much higher rates of neutron emission. The table below lists the approximate number of neutrons per second per kilogram generated due to spontaneous fission for each grade of plutonium. These numbers are can be readily derived from the isotopic composition of each grade of plutonium, the half life of each isotope, the branching ratio for spontaneous fission, and the number of neutrons produced per fission.

Super-grade Pu	Weapons-grade Pu	Reactor-grade Pu	MOX-grade Pu
18400	54000	349000	487000

The dominant contribution to the neutrons for all of the grades comes from the spontaneous fission of Pu-240. Reactor-grade and MOX-grade plutonium have an order of magnitude higher percentage of Pu-240 compared to weapons-grade plutonium, and their neutron emissions are larger by a corresponding factor. Regardless of the grade of plutonium under consideration, the production rate of neutrons from spontaneous fission is about 4 orders of magnitude greater than for weapons-grade uranium (of the order of 1 per second per kilogram).

The mean energy of the neutrons produced by fission is about 2 MeV (just as for weapons-grade uranium). Mean interaction-free paths for common shielding materials are

in the 2-6 cm range and materials containing lighter elements such as boron or lithium can have much shorter mean-free paths. The mean free path for absorption of neutrons is much larger than the mean interaction-free path. The neutron background is about 50 per meter-squared per second, just as for neutrons from weapons-grade uranium.

In comparing neutron detection of weapons-grade uranium versus neutron detection of any grade of plutonium, we can conclude that any grade of plutonium is several times easier to detect than weapons-grade uranium for the following reasons:

- The rate of neutron production is 4 orders of magnitude higher for any grade of plutonium
- The energies of the neutrons produced are identical
- The path loss through shielding and through free space are identical
- The background rates of neutrons at the detector are identical

As noted earlier, the dominant contribution to the neutrons for all of the grades comes from the spontaneous fission of Pu-240. It is possible to reduce the Pu-240 content by a factor of 400-4000 resulting in a corresponding reduction in the neutron emission rate. This purification of plutonium can be achieved through multi-stage atomic-vapor laser isotope separation techniques. This would have the effect of reducing the neutron emissions. It has been estimated [Fetter 1990c] that this would add a cost of \$5MM for 4 kg of weapons-grade plutonium.

Gamma Detection

Plutonium has several gamma ray emissions, notably those at 645.98 KeV and 769 KeV (from the Pu-239 decay chain) and those at 662 KeV and 722.47 KeV (from the Pu-241 decay chain). In addition, there is an energetic neutron-induced 1.597 MeV gamma ray that may be useful for detection. We focus here on the detection of the 769 KeV gamma ray from the Pu-239 decay chain and present a side-by side comparison of detection of plutonium of various grades and the detection of weapons-grade uranium based on the 1.001 MeV gamma ray from the U-238 decay chain. We conservatively assume that for detection of WgU, the 1.001 MeV gamma ray from U-238 is the most useful emission for detection purposes – if trace U-232 contaminants are present, there may be a more penetrating 2.6 MeV gamma emission. Since U-232 contaminants may not be present, we focus on the 1 MeV gamma emission for the purpose of reliable detection.

CORE	Weapons-grade Pu	Reactor-grade Pu	MOX-grade Pu	Weapons-grade U
Detectable Isotope	Pu-239	Pu-239	Pu-239	U-238
Gamma Energy (MeV)	0.769	0.769	0.769	1.001
Production Rate (per gram per second)	252	252	252	81
Density (grams per cubic centimeter)	19.84	19.84	19.84	19
Weight fraction of isotope	0.933	0.603	0.404	0.055
Inner Radius (cm)	0	0	0	0

Outer Radius (cm)	4	4	4	4
Linear Attenuation Coefficient (per centimeter)	2.07584	2.07584	2.07584	1.41
Thickness (cm)	4	4	4	4
Weight (grams)	5316.061867	5316.061867	5316.061867	5090.986667
Weight (kg)	5.316061867	5.316061867	5.316061867	5.090986667
Total Gamma Rate	1249891.202	807807.497	541217.6265	22680.3456
Beta	1.333333333	1.333333333	1.333333333	1.333333333
Self-Shielding Attenuation (dB)	-10.4419936	-10.4419936	-10.4419936	-8.764533496
SHIELD	Lead	Lead	Lead	Lead
Density (grams per cubic centimeter)	11.35	11.35	11.35	11.35
Linear Attenuation Coefficient (per centimeter)	1.012	1.012	1.012	0.77
Inner Radius (cm)	4	4	4	4
Outer Radius (cm)	14	14	14	14
Thickness (cm)	10	10	10	10
Weight (kilograms)	127.3500267	127.3500267	127.3500267	127.3500267
Shielding Attenuation (dB)	-43.95060157	43.95060157	43.95060157	-33.44067511
DETECTOR	Handheld HPGe	Handheld HPGe	Handheld HPGe	Handheld HPGe
Area (square cm)	10000	10000	10000	10000
Efficiency	0.16	0.16	0.16	0.16
Background (per square centimeter per second)	0.00734	0.00734	0.00734	0.0017
Background detected (per second)	11.744	11.744	11.744	2.72
Detection threshold (number of standard deviations)	5	5	5	5
TIME TO DETECTION				
Distance (cm)	100	100	100	100
Path Attenuation (dB)	-10.98989639	10.98989639	10.98989639	-10.98989639
Total Attenuation: self + shield + path (dB)	-65.38249156	65.38249156	65.38249156	-53.195105
Total Gammas at Detector (per second)	0.361928727	0.233915351	0.156719406	0.108677382
Gammas detected (per second)	0.057908596	0.037426456	0.025075105	0.017388381
Time to detection (seconds)	87552.78707	209603.5524	466950.1646	224900.5983
Time to detection (minutes)	1459.213118	2493.392539	7782.502744	3748.343305
Time to detection (hours)	24.32021863	58.22320899	129.708391	62.47238841

**DISTANCE TO
 DETECTION**

Detection time (seconds)	300	300	300	300
Self + Shield	-	-	-	-
Attenuation	-54.39259516	54.39259516	54.39259516	-42.2052086
Total Gammas outside (per second)	4.54582481	2.937976806	1.968395738	1.364987919
Detection distance (cm)	24.19428654	19.45049481	15.92071912	19.11096693

This analysis shows that even at 10cm lead shielding both weapons-grade and reactor-detection of any of the grades of plutonium considered above using only the 769 KeV gamma emission from the Pu-239 decay chain is easier than detection of WgU using the 1.001 MeV gamma ray from the U-238 decay chain. This may be attributed to the following observations:

1. U-238 comprises only about 5% of WgU, whereas Pu-239 comprises anywhere from 40% to 93%, depending on the grade of plutonium. As a consequence, plutonium generates 1 to 2 orders of magnitude (10-13 dB) more gammas (per kg per second) at 769 KeV than WgU generates at 1 MeV
2. The 769 KeV gamma rays have a higher linear attenuation coefficient and are more strongly attenuated than the 1 MeV gamma rays. As a result, the shielding attenuation is about 12 dB greater for the plutonium emissions.
3. The background count of gamma rays is about 5 times higher at the lower energy (769 KeV) compared to 1 MeV.

These two effects counteract each other, the former favoring easier detection of plutonium, the latter favoring easier detection of uranium, with the end result that of either weapons-grade or reactor-plutonium considered is slightly more detectable than weapons-grade uranium, while MOX-grade plutonium is a little harder to detect than WgU.

Note that we assumed that trace quantities of U-232 are absent in the uranium sample and that the most useful emission for reliable detection is the 1 MeV gamma ray from the U-238 decay chain. If trace quantities (ppb) of U-232 were present, the detection problem would be much easier for uranium, since the 2.6 MeV gamma ray is very penetrating. This analysis also only considers plutonium detection using the 769 KeV gamma emission from the Pu-239 decay chain. Including the other gamma ray emissions for plutonium listed previously will only make the plutonium detection problem easier. From this analysis we conclude that any grade of plutonium will be no harder to detect (and perhaps easier to detect) than weapons-grade uranium, based on gamma ray emissions alone. We conclude that a national detection system that is capable of detecting weapons-grade uranium in transit through the transportation system will be capable of also detecting similar quantities of plutonium.

Detector System Manufacturers

Well over 50 companies and laboratories--systems, instrument and technology developers—are involved in producing nuclear detectors worldwide as listed in “Appendix A: Representative Detector and System Manufacturers.” The market has been estimated by some manufacturers at around \$500M/ year. Current offerings can be broadly summarized in the following table:

	Broadband Detection	SNM Discrimination
Portal Type [moving target or scanner]	<ul style="list-style-type: none"> - Large Detector areas/volumes -- Typically designed to work at 5-10m distances - Rapid detection of high activity sources - Slow speed detection of low activity sources - Specs typically 8Km/hr max speed through portal - Price \$10K-\$50K (low range or personal portals); much higher for large vehicle portals 	<ul style="list-style-type: none"> - Higher Sensitivity - Add SNM specificity or spectrum analysis - Otherwise same as broadband - Computational systems and other automation - Mobile Scanners fit in this category; some with GPS location and wireless communications - \$ 50K +
Hand-held [Stationery Target]	<ul style="list-style-type: none"> -Typically High Activity Sources [e.g. Cs, Co] - Small detector volumes/areas - Some designed for permanent placement (e.g. in-container, some with wireless) - Some meet IAEA specs for SNM detection - Work at < 1-2 m range - 30KeV – 1.5MeV range - Price \$1-\$2K 	<ul style="list-style-type: none"> - Higher Sensitivity - Add SNM specificity or spectrum analysis - Otherwise same as broadband - Price \$5- \$15K

As detector volumes reach into the millions or tens of millions of units a year, we can reasonably expect that the detector performance will improve and costs and prices will come down dramatically. Progress in detector technology is likely to result in improvements in cost, form factor, sensitivity, and discrimination. For example, room temperature Cadmium-zinc-telluride gamma detectors have recently been developed [Physorg.com, 2005] and semiconductor neutron detectors are described in US Patent 6,075,261.

DISARM: Detect and Intercept Shipments of Articles with Radioactive Material

Today's nuclear detection systems consist primarily of scans at borders and ports for a small fraction of cargo containers and vehicles. Maintaining the status quo implies a reliance on intelligence and military to catch nuclear terrorists and smugglers in the act. One option is to bolster existing container security schemes to include 100% of all cargo and equip customs/border patrol with energy selective detectors that can reduce false-positive rates—those improvements are likely to deter some attempts and probably not others due to the vast majority of loopholes across the borders. Another option is to distribute a network of fixed detectors with the possibility of detecting fissile material that is contaminated with U-232 using its highly penetrating gamma rays—this approach is like probabilistic insurance because some but not all HEU contains U-232.

How do we create a comprehensive deterrent to smuggling fissile nuclear materials? We propose an in-vehicle detector architecture that we refer to as DISARM (**D**etect and **I**ntercept **S**hipments of **A**rticles with **R**adioactive **M**aterial) which can be used to offer greater likelihood of detecting shielded HEU traveling uniformly through the transportation system, when used in conjunction with expanded initiatives for fixed/handheld detectors, portals, as well as inspection or surveillance schemes for the largest vehicles not amenable to detection. The goal is to interdict smuggling of all or part of an HEU device to defend against both trafficking and delivery to substantially increase the risk for terrorists building and deploying a nuclear weapon.

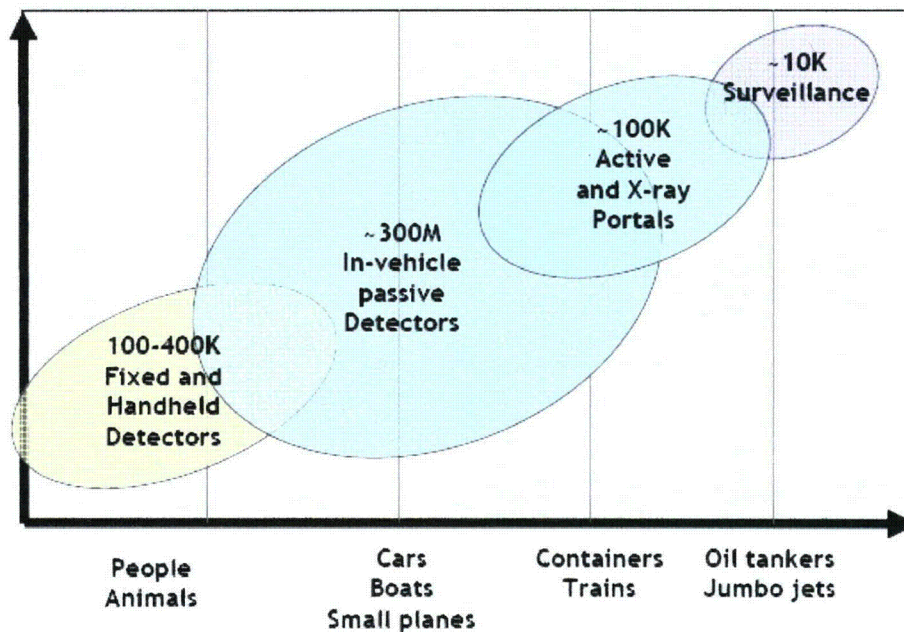


Figure 10 Achieving uniform coverage for nuclear detection across transportation modes

The salient aspects of the DISARM proposal are as follows:

- *In-vehicle detectors:* Nuclear detectors passively searching for the characteristic radioactivity need to be co-located inside any moving vehicle that is capable of transporting shielded HEU and that is either not inspected or actively screened with neutrons. These would include automobiles, trucks, trains, planes, boats, shipping containers, etc. as well as smaller trailers that may be towed by these vehicles. These detectors can be small, mass-produced, and built from the same commercially available and emerging technologies that can be used for handheld and portable detectors, but will be capable of reliable detection of nuclear contraband by virtue of both extremely close proximity and prolonged exposure (minutes to hours to weeks) to the radiation source. A sufficient number of detectors per vehicle continuously powered by the vehicle's batteries or power supply are necessary in order to ensure time to enough count particles from nuclear materials inside the vehicle.
- *Fixed and mobile infrastructure:* A network of detector-readout checkpoints can be deployed liberally throughout highly populated areas [including at transportation chokepoints, around critical infrastructure such as government buildings and bridges, as well as around the perimeters of major metros]. The checkpoints would employ short-range wireless communications to remotely query vehicles and cargo approaching the checkpoint and determine its detector readings. The checkpoints need to be designed such that the received detector reading can be unambiguously associated with the correct vehicle. This is achieved either by using wireless technology whose range is short enough to remove ambiguity of which vehicle originated the reading or by designing the check-point to have the vehicle pass through like a toll-booth or with sufficient proximity to the vehicle. The checkpoints could be designed to generate alarms for further inspection if either the detector reading is reported to be above a threshold, or if the detector fails to report a reading.
- *Incentives to participation:*
 - *Expedited passage:* Vehicles and cargo that can be verified to be carrying on-board detectors would be granted rights to expedited passage while those not similarly equipped might be subjected to manual search, which might be time-consuming and intrusive.
 - *Driver-warnings:*¹⁶ A secondary benefit of in-vehicle detectors for drivers and owners of vehicles can be achieved if detector readings are designed to be conveyed to the driver on their dashboard such that they warn of any radioactive material that has been planted inside the vehicle by a potential terrorist or smuggler or picked up unknowingly contaminated material. This provides an incentive for the driver or owner to ensure that detectors are functioning.
 - *Subsidies:* To promote detector installation, the federal government should provide powerful financial incentives to corporations and private parties to participate in the program and install detectors in their vehicles and containers.
- *Federal regulations for vehicles and containers:*

¹⁶ This idea was suggested to the authors by Michael May when this material was presented at the Center for International Security and Cooperation, Stanford University on October 11, 2005.

- *New vehicles*: Federal regulations should mandate that all motor vehicles after a to-be-determined model year be required to ship with an embedded radiation detector equipped with short-range wireless communications capabilities. Similar regulations should apply to shipping containers [Wein et al, 2005].
- *Old vehicles*: Federal regulations should mandate that older vehicles and containers be retrofitted (through after-market installation) to carry on-board detectors.
- *Vehicle Licensing*: Routine inspections of vehicles for licensing purposes would be expanded to encompass radiation detector functioning (similar to smog certification).
- *To achieve uniform detection coverage, the above proposals complement today's initiatives in perimeter screening systems:*
 - *Portals*: Portals employing active scanning technology can be useful to screen larger heavily shielded containers (in airplanes, trains, trucks) for which use the number of passive detectors required would become too large. These can be located at seaports, truck weigh-stations, rail-stations, and airports to screen cargo.
 - *Fixed and handheld detectors*: SNM carried by people or animals is unlikely to be shielded heavily if at all due to constraints on weight, hence fixed and handheld detectors at border crossings and within the interior are likely to be useful.
 - *Inspections & surveillance*: Securing against transport of nuclear weapons inside large vessels such as oil tankers or jumbo jets (outside cargo containers) is an important aspect of the detection problem not likely to be amenable solely to detector approaches. Due to the combination of their potential for shielding of radiation as well as the proximity of airports and harbors to populated centers, these larger vessels must be safeguarded by monitoring and controlling access through inspection and video surveillance so that terrorists simply can't use them to deliver nuclear weapons.

Stephen Flynn [Flynn, 2004] offers a promising (and similar) proposal aimed at container security. The DISARM proposal generalizes Flynn's basic model. Flynn suggests that containers could be outfitted with internal sensors that detect gamma and neutron emissions from a nuclear weapon or dirty bomb. When the container arrives at a terminal, an inspection unit would interrogate sensors inside the container and the sensor data would be securely transmitted over a secure Internet link to customs authorities along the route. Flynn's in-container approach effectively exploits proximity and prolonged exposure of the detector to the container contents. It is likely to be capable of detecting the presence of even shielded HEU or other radioactive materials. We believe this idea can be extended to all modes of transport as envisioned in our DISARM proposal. Along the lines of Flynn's proposal, two companies have introduced radiation detection systems that place detectors inside shipping containers and in conjunction with communication systems. RAE Systems of San Jose, CA has a case study discussing their results

deploying an in-container solution [RAE Systems, 2005]. RFTrax of Allyn, WA discusses a battery powered radiation sensor [RFTrax, 2005a] and a remote monitoring communication system that integrates GPS, Internet, RFID, and GSM wireless communication technologies [RFTrax, 2005b].

How good does the detection system have to be?

To make it difficult to dissuade the terrorist from trying to transport SNM, there needs to be uniformly high risk of failure in transporting SNM across all transportation modes available to the terrorist. Securing only a subset of accessible transportation modes will result in terrorists resorting to the next available alternative, like locking some doors of a house and leaving other doors open. For instance, preventing the movement of HEU through US ports will not necessarily make it more difficult to transport HEU if it remains easy to use airplanes or ground transport instead. Even if land border crossings and airports were secured from HEU, terrorists could simply bring nuclear materials into a neighboring country's ports and then smuggle it into the US in the same way tons of drugs cross international boundaries every year.

Today's radiation portals situated at ports and border crossings will only result in displacement into many other sea, air, or ground transport mechanisms that avoid the portals. For completeness, we both list and analyze below the set of possible classes of vehicles spanning 2-3 orders of magnitude in their physical dimensions:

1. Water:
 - a. oil tankers
 - b. cargo vessels
 - c. cruise ships
 - d. yachts
 - e. sail boats
 - f. motor boats
 - g. canoes
2. Air:
 - a. jumbo jets (passenger and cargo)
 - b. private jets
 - c. propeller planes
 - d. helicopters
3. Ground:
 - a. trains (passenger and cargo)
 - b. trailer-trucks (oil tankers, trailers, flatbeds)
 - c. four-wheelers (trucks, cars)
 - d. three-wheelers (automated or manual rickshaws)
 - e. two-wheelers (motorcycles, scooters)
 - f. trailers in tow by two, three, or four wheelers.
 - g. anything carried by people on foot or animals (horses, cows, camels, elephants, etc.), or even carts pulled/pushed by them.

Even with an effective nuclear detection network in place, skeptics might contend that a terrorist could remain undeterred by accepting even heavy risk detection in transport of HEU. While that is a possibility, we believe it is unlikely. In its report, the 9/11 Commission points out that,

“Just increasing the attacker’s odds of failure may make the difference between a plan attempted, or a plan discarded. The enemy also may have to develop more elaborate plans, thereby increasing the danger of exposure or defeat.” [p. 383, Kean, 2004].

The basis of this statement is that terrorists¹⁷, just like their target nation-states, are subject to limited resources. When terrorists consider a particular mode of attack, accessibility of the required resources, and likelihood of a successful attack, and the cost of discovery in light of counter-measures will be primary considerations. Studies in behavioral psychology have further established that when making economic tradeoffs “people have a tendency to overweight outcomes that are considered certain, relative to outcomes which are merely probable.”¹⁸ Since terrorists are people making economic tradeoffs, increasing the risk of failure from zero to non-zero across every option available to terrorists will bring about a disproportionately large deterrence effect compared to an approach that improves any one option but does nothing to introduce any risk in other options.

The degree of deterrence that could potentially be achieved by efforts to increase the risk of failure for terrorists is illustrated by examining terrorist use of conventional explosives and the role that screening of passengers and luggage for conventional explosives has played. Critiques of airport screening measures have primarily focused on less than perfect detection probability, i.e. whether or not a weapon or explosive will pass through the screening process at the airport. For instance, [p. 52, Szyliowicz, 2004] remarks on the “porousness” of airport screening by citing the United States GAO finding (July 2002) that fake weapons and explosives had passed through airport screeners a quarter of the time at 32 major airports [p. 2, Dillingham, 2002].

Contrary to popular disbelief, the deterrence effect resulting from “annoying” airport screening procedures has likely turned out to be much greater than would have been predicted simply by a multiplication of the detection probability by the rate of incidents prior to introduction of these measures. Commercial passenger airplanes have historically been a high-visibility target for terrorists, yet statistics indicate that the incidence of aircraft bombings have all but ceased over the past decade. We employ data from the RAND-MIPT database ([MIPT, 2002], [RAND, 2003]) of worldwide terrorism incidents from January 1, 1968 until March 12, 2003.¹⁹ In the figure below, we chart the time series of cumulative fatalities and incidents across four decreasingly inclusive categories,

¹⁷ See [Enders, 1993] for a seminal analysis of terrorists as rational actors in the economic sense.

¹⁸ See [p. 20, Kahneman, 2000]. This work is based on Prospect Theory by Daniel Kahneman and Amos Tversky—Kahneman was awarded the Nobel Prize in Economics for this discovery. See [Kahneman, 2002]

¹⁹ In “Appendix B: How do we track trends in worldwide terrorism?,” we survey the publicly available databases that track terrorism incidents including the RAND-MIPT database from which the data in this study was drawn.

1. ALL: all terrorist incidents
2. EXPLOSIVES: explosives were used or detonated
3. AIRPORT/PLANE: explosives in an airport or onboard an airplane
4. AIRPLANE: explosives onboard an airplane.

From 1989 onwards, ALL fatalities and fatalities from EXPLOSIVES not only increase, but so does their rate as shown by the increasing steepness of the slope (the apparent discontinuity on the ALL graph represents the deaths of nearly 3000 victims on September 11, 2001). In contrast, we observe that fatalities for AIRPORT/PLANE and AIRPLANE remain nearly constant after 1989, with AIRPLANE fatalities rising by only 14 over the course of 14 years.

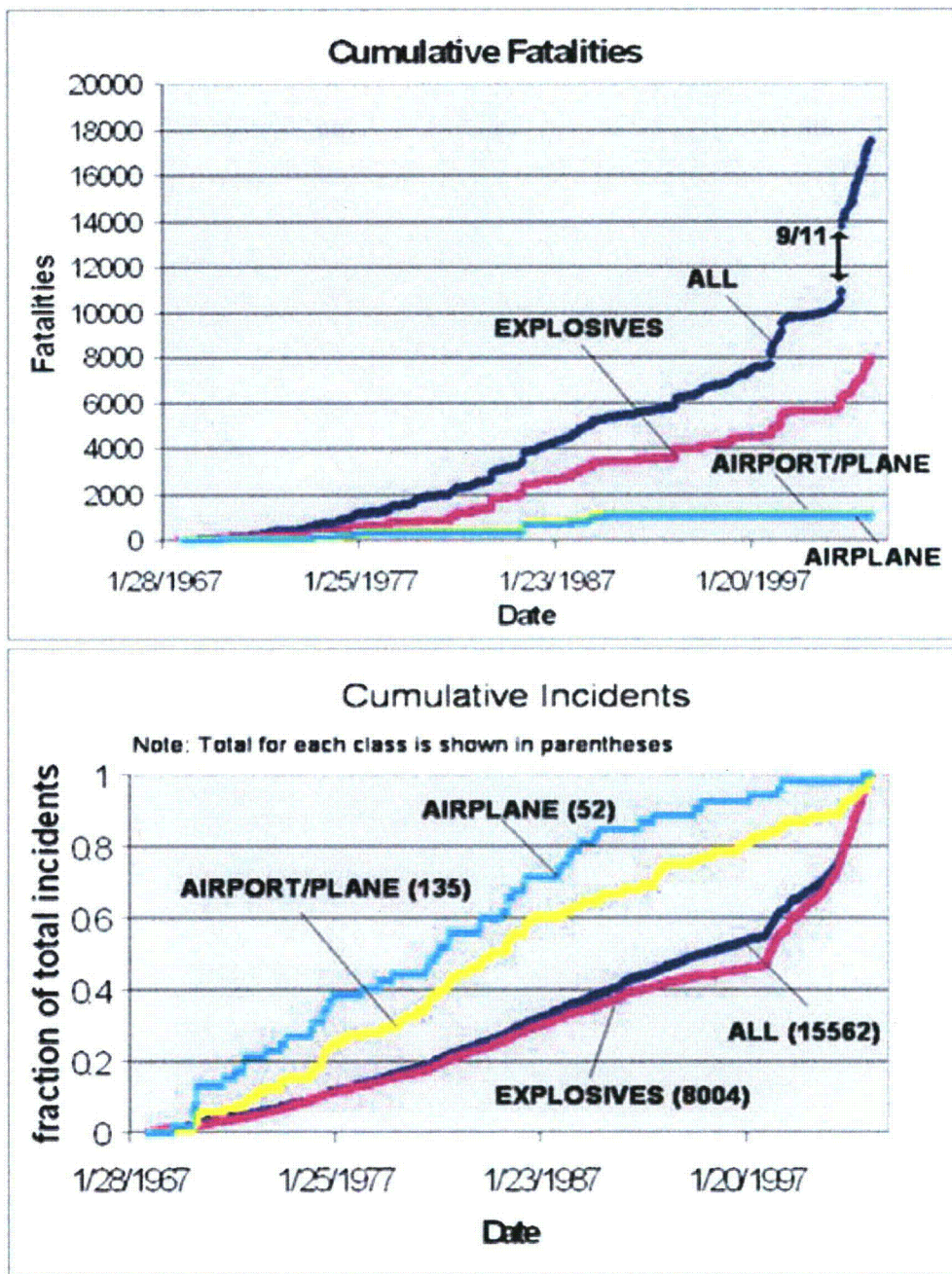


Figure 11

Upon a closer examination of the data for categories AIRPORT/PLANE and AIRPLANE, we find two extended periods of comparatively low fatalities preceded by periods of much greater intensity. In the table below, we show these periods along with the fatalities for each category. Periods II and IV have much smaller fatalities for AIRPORT/PLANE and AIRPLANE when compared to the corresponding statistics

during periods I and III. However, during all periods, including I and II, the number of fatalities in EXPLOSIVES or ALL showed no signs of slowing down. We conclude that during periods II and IV, there was a “displacement²⁰” from airplanes as terrorist bombing targets onto other environments.

Period	Dates	Length (years)	ALL	EXPLOSIVES	AIRPORT/PLANE	AIRPLANE
I	09/02/1974 to 03/27/1977	2.5	593	391	296	283
II	03/28/1977 to 08/07/1984	7.5	2027	1250	51	7
III	08/07/1984 to 03/10/1989	4.5	2050	1520	708	700
IV	03/10/1989 to 03/12/2003	14	12302	4492	26	14

Table 1: Fatalities for each category and time period

Despite continuous increase in fatalities for ALL and EXPLOSIVES, the presence of two periods of accelerated fatalities followed by extremely low fatalities for AIRPORT/PLANE and AIRPORT is telling. We attribute this trend to expansion of airport screening programs,

- First, following frequent hijackings beginning in the late 1960s, a variety of security measures including metal-detectors and X-Ray machines to screen carry-on baggage were introduced in the United States as part of the Air Transportation Security Act of 1974 [Malotky, 1998]. Indeed, a reduction in skyjackings in the United States could be attributed to the introduction of metal detectors in 1973, while also increasing incidents not protected by the detectors such as those involving hostages [Enders, 1993]. In light of the trends in the graph and table, it is likely that introduction of airport security measures worldwide contributed primarily to the reduced number of fatalities in period II.
- Second, following an intense wave of fatalities during period III primarily due to use of explosives in airports/airplanes culminating in the Pan Am airliner explosion over Scotland²¹, increased vigilance and better procedures to sniff and screen for explosives in airports appears to be directly responsible for the period of low fatalities beginning in 1989 and continuing on into the present era. The end of this period was also marked by the United States Aviation Security Improvement Act of 1990 [Bush, 1990].
- Finally, over the 1990s, increasingly better detection techniques and a greater degree of automation to screen for explosives were introduced at airports worldwide [Malotky, 1998] thereby continuing to raise the bar for terrorists who sought to employ explosives aboard airplanes.

²⁰ for more on the use of the term “displacement” in the terrorism context, see [p. 2, O’Hanlon, 2002]

²¹ The bombing killed 259 people on board and 11 people on the ground [MIPT, 2002]

As shown in the graph, during periods II and IV, there was also a significant reduction, but not elimination, in terrorist attempts to deploy explosives in airports and airplanes, even though overall terrorist incidents using explosives continued to rise at an accelerated pace. These data suggest two important conclusions: 1) airport screening of explosives, although imperfect, has successfully prevented fatalities despite a significant number of continued attempted attacks at airports. 2) The screening measures have been successful in deterring a much greater number of attempts that would have taken place had the screening not been present.

Lessons learnt about deterring terrorism from the case of conventional explosives are all the more valuable in light of the fact that terrorist incidents involving alternate modes of attack (without explosives) that were not fully appreciated by aviation authorities have become responsible for much greater fatalities, as had happened with the attacks of September 11, 2001. We conclude that deterring transport of HEU requires a uniform increase in the risk/cost/difficulty of transporting these materials across *all* accessible transportation modes, both across borders and inside the interior.

What is required to secure each transportation mode?

Securing each form of transport from transport of nuclear materials (HEU) poses a unique set of challenges, which we touch upon in this section. We also discuss special challenges posed by larger vehicles and vessels and suggest ways to monitor their contents. Large vessels would need to either be certified as free of HEU, or they must maintain a safe distance from populated areas to provide sufficient isolation from a nuclear blast on the vessel. This is analogous to how the US military closely monitors and disallows the approach of foreign military vehicles (submarines, ships, airplanes, missiles) around national borders. See the section on "Weapon Delivery" in [Medalia, 2005] for a discussion of the ways a terrorist nuclear weapon could be imported into the United States.

Water

Cities have historically been built around ports. Ships of all sizes routinely sail into harbors that are close by. Ships can easily carry a nuclear weapon or nuclear contraband. Screening of cargo for nuclear materials (active and passive) has had its own set of challenges (see [Hecker, 2002]). Large vessels like oil tankers are more difficult, since it is likely to be physically impossible to screen for something inside due to the attenuation of the surrounding oil, see [pp. 7-8, Medalia, 2005]. Such large, thick vessels may need to be certified through initial inspection at the embarkation point followed by constant surveillance while in transit. Otherwise they would be forbidden from approaching populated cities altogether in case they cannot be certified as being free of nuclear materials. For all other types of ships, one or more on-board radiation detectors (matched to on physical dimensions of the yacht) and remote check points located at sea (as described in DISARM) would be the ideal approach to certify them as free of radiation at check points at sufficient distance from the city. If all "floating" vessels were successfully secured, the only remaining option for delivery of nuclear material would be

underwater using submarines, which certainly raises the cost and complexity of HEU transport.

Air

In several respects, airplanes pose an even greater challenge than ships since they can rapidly approach any target, see [p. 6, Medalia, 2005]. It is important to ensure that airplanes can't get close to populated areas, and for the ones that do it is necessary to certify that they are free of nuclear materials. Just like oil tankers, jumbo jets can be initially certified and constantly monitored to prevent nuclear material from being loaded onboard or otherwise disallowed from approaching within the distance of populated areas. Just like container screening at sea ports, air cargo screening for nuclear material (active and passive) is an important step in this direction but to our knowledge is not being pursued aggressively. Just like yachts, private jets and helicopters also would need to implement DISARM with a sufficient number of detectors per aircraft. A mechanism for preventing aircraft that have not been certified as free of nuclear materials from landing near populated areas must be put in place.

Ground

Perhaps the biggest challenge with ground transport is the sheer numbers of vehicles that must be dealt with. Trains, being the largest, require inspection and surveillance to ensure they are free of nuclear materials just like oil tankers and jumbo jets. Rail cargo would have to be screened (actively and passively), and even entire train cars may have to be screened regularly. The same holds for trailers on large trucks and 18-wheelers, just like how trucks with trailers are weighed at weigh stations along the highways. Otherwise they would need to participate in a DISARM program with a number of detectors sufficient to cover the length, width, and height of the trailer. Smaller trailers towed by cars would need their own detectors to participate in the DISARM program, and would likely need to be powered by the towing vehicle to ensure operation of the detector. Just as with water-borne transport, if all ground transport was secured the only option left for terrorists to transport HEU would be underground tunnels which significantly raises the cost and complexity, and would still have to surface at some point near the target.

In theory, people on foot or animals (horses, cows, camels, etc.) can carry unshielded or lightly shielded HEU through forests and other areas. If the only alternative left to the attacker is to use people or animals for transport, the primary purpose of increasing the cost/complexity of transporting shielded HEU to a sufficiently high level would have been served. Even HEU-laden people and animals could be made susceptible to detection by using a sufficiently ubiquitous fixed infrastructure. Carts capable of carrying shielded HEU would still have to be screened.

Operational Requirements For Assuring Compliance With DISARM

One of the key questions in mandating uniform adoption of an in-vehicle detector system is ensuring that all vehicles are compliant. A disabled detector would produce no communication with a checkpoint, and raises suspicions prompting further manual

inspection. What if an attacker tries to tamper with or reprogram the built-in detector? To prevent this, we propose that

- The detector would have to be powered by either a self-contained battery or input power supplied from the vehicle itself.
- In-vehicle detectors would contain a radio to enable them to transmit their readings as they pass by specially designed checkpoints or on-demand to specially equipped law-enforcement vehicles.
- The detector is authenticated from its point of manufacture and public-key infrastructure (PKI) can be used to authenticate the detector's readings.
- The detector housing would be tamper-proof conforming to standards such as FIPS 140-2 [National Institute of Standards, 2005]. The FIPS standard includes requirements on tamper detection (physical evidence of tampering), as well as requirements on tamper mitigation circuitry.

These four concepts permit law-enforcement officials to determine whether the detector readings indicate that a bomb could be present, or to further investigate if the detector is not readable. This can help ensure compliance with the in-vehicle detector program.

Securely transmit detector readings on-demand to law-enforcement (mobile readers or readers at checkpoints)

We envision that mobile or fixed readers will be used to remotely read in-vehicle detectors at borders and checkpoints. The reading could be triggered either manually or automatically, and there would have to be no ambiguity of which vehicle originated the reading. The in-vehicle detector can be equipped with a short-range wireless network interface card using commercial off-the-shelf radio technologies (e.g., Wi-Fi or other), whose range is short enough to eliminate the ambiguity. When the reader chooses to interrogate the detector, it sends a signal to the detector querying its readings. The detector can respond with the current reading, the background and, perhaps, the readings history over the last 24 hours. This will allow the reader to assess the likelihood of presence of HEU aboard the vehicle. Data transfer between reader and detector can be authenticated using public-private keys and encrypted using a suitably robust encryption scheme, such as AES.

Location of checkpoints

Checkpoints, fixed or mobile, will need to be installed at vehicle intersections and traffic choke-points and other places to ensure each vehicle can be queried often enough. This would include, but not be limited to:

- Perimeters of major metros and highway toll booths
- National borders (sea and land)
- Major ports
- Airports
- Train stations
- Other elements of the transportation infrastructure (subway stations, bus stations, etc.)

- Randomly located checkpoints or reading areas should be thrown in from the start as they substantially increase the uncertainty of detection points and therefore deterrence

False Positives and False Negatives

Reducing false positives in nuclear detection has become a national research priority for the DNDO.²² Numerous reports in the media have highlighted false positives and negatives in nuclear detection on those systems deployed in major metros like Washington D.C. and New York.²³ In 2001 just after the 9/11 attack, the Bush Administration ordered a large-scale operational trial of nuclear sensors around a perimeter of Washington DC [see Gellman, 2002b and Crowley, 2005] to detect and intercept a nuclear weapon entering the area through roads and rivers. However the US government apparently gave up on this “Ring Around Washington” as it was eventually shut down due to a large number of false positives (detection of benign radioactive sources) and false negatives (failure to detect real signatures). While it represented a haphazard attempt to secure the nation’s capitol and perhaps sent a signal to would-be attackers, the incremental security it provided is questionable given all the alternative routes such as by all the airplanes entering Dulles National Airport or nearby sea ports. Similarly, according to one New York official, the city employs over 20,000 handheld and stationary nuclear detectors which go off all the time due to transport of medical isotopes [Ruppe, 2005].

In general, detectors may produce misleading readings due to a number of causes including

1. fluctuations in the natural radioactive background
2. the presence of other radioactive isotopes whose radiation cannot be distinguished from that being detected whose radiation lies within the discrimination band of the detector.
3. equipment malfunction

In the case of positive readings, where the detector detects a threat, further inspection will necessarily be called for. The cost of this inspection is directly tied to the feasibility of the DISARM program. The frequency of false positives experienced multiplied by the average cost of inspection is the total cost of dealing with false positives. Each factor in this product needs to be kept in check to make a feasible solution—the lower the better.

In accordance with the program outlined by the DNDO, we expect that acceptable levels of false positives can be achieved through judicious detector design and energy-specific detectors that can discriminate various radioactive signatures. By training local law enforcement in inspection, further reductions in cost due to false positives may also be achieved since federal agents or NEST team members will not be required to inspect suspicious detector readings.

²² See [Oxford, 2005] for the Advanced Spectroscopic Program to create more accurate energy discrimination of nuclear materials

²³ See [Gellman 2002a, 2002b], [Ruppe, 2005], and [Associated Press, 2005].

When operating within the physical limits of passive detection, false negatives may also arise due to equipment malfunction or when high background levels mask the signal. Like false positives, we expect false negatives can be overcome in with judicious detector design.

How could DISARM be defeated?

Just about any security scheme can be circumvented with enough ingenuity, money, and effort, so the security scheme fulfills its role if it increases the attacker's risk of failure. In this section we analyze the "loopholes" that a terrorist might try to use to work around DISARM, and how by doing so that increases their risk of failure. Each of these "loopholes" can be countered by additional engineering to achieve the desired level of security for some cost.

Decoy Vehicles (Binding of Detector Reading)

Binding a detector reading received at the checkpoint to the right vehicle is a key problem that needs to be systematically addressed, and DISARM security is dependent on how well binding can be implemented. If the vehicle transmitting the short-range wireless signal cannot be uniquely determined, then an attacker can simply destroy the detector inside the vehicle carrying the nuclear material and leverage a nearby vehicle's reading to pass through a checkpoint unnoticed. Alternatively, if the detector reading can be authenticated digitally and bound to the vehicle itself rather than the detector, then this is not a problem. Hence security of DISARM is tied directly to how well the reading can be physically localized or authenticated.

For road vehicles, one way to ensure that the readings are bound directly to the vehicle being read is to use something similar to an E-Z pass tollbooth. Using a suitably designed short-range wireless communications system, a check-point that permits fast reading can be incorporated into streets beneath the vehicle or on the side of the road, such that the reading the vehicle providing the reading can be uniquely identified.

Destroy, Tamper With, or Relocate the In-Vehicle Detector (Tamper Resistance)

The checkpoint recognizes non-compliance with DISARM through the absence of a response from the detector, eliciting a more detailed inspection. Implementation of a tamper-detection standard (like Federal Information Processing Standard 140-2) to detect either tampering or removal/relocation of the detector would allow it to immediately shut down. Therefore the security offered by DISARM is dependent on the integrity of the tamper detection standard.

Shielding the Detector (Placement, Solid-Angle, and Number)

Rather than shield the nuclear material, an in-vehicle detector itself can be shielded directly from the interior of the vehicle. The difficulty with which the attacker can effectively shield the detector is dependent on the attacker's knowledge of the detector

locations, the amount of shielding required, the number of detectors in the vehicle, the size of the detector, and ultimately the solid angle cross section the detectors subtend with the interior of the vehicle. The tradeoff is one of cost and form factor. If detector technology becomes cheap and easily integrated, multiple detectors or even detector strips along the length of the vehicle can make it hard to shield.

Divide and Conquer (Minimum Detectible Quantity)

Buy a detector or a car with a detector, then work to optimize the amount of material and shielding such that it is the most material that does not set off the detector. Then transport it in these quantities and collect it at some final destination where it could be assembled into a WMD and never ship the assembled WMD or assembled SNM package.

Splitting up the nuclear material and transporting it multiple times increases the odds of being caught by that factor, and complicates the operation and its logistics. Therefore, the smallest amount of nuclear material that can be carried in any detector-equipped vehicle determines how effective DISARM can be.

Switch Vehicles (Minimum Detection Time)

An idea related to divide and conquer is to overcome DISARM by switching vehicles before the detection time of the detector is reached. This also complicates the operation by necessitating the use of shielding to increase the detection time up to the point where the switch can be made. Hence detection time becomes a key limit to DISARM security. Increasing the detector's solid angle around the vehicle decreases the minimum detectable quantity.

Avoid or Disable Checkpoints (Number, Predictability, and Security)

Naturally, if a path can be charted to avoid checkpoints then DISARM can be circumvented. So the security of DISARM is limited by the distribution of check points that query the in-vehicle detector. The quality of the physical and digital security for the information gathered by checkpoints determines the security of DISARM. One way to further increase security is to make the checkpoints effectively mobile and thereby increase uncertainty as to their whereabouts.

Power-down the In-Vehicle Detector prior to approaching the check-point (Uptime of detector)

If the detector could be disconnected from its power source prior to approaching a check-point for the minimum duration required to detect the nuclear material travelling in the vehicle, then the vehicle can pass through a DISARM check-points circumventing detection. Therefore each check point needs to verify that the detector has been operational for a sufficiently long time prior to reporting its reading, and violation of this condition should raise suspicion. It would also be useful to if the check-point can

determine during what time intervals, if at all, the detector has been powered down through lack of a power source during the past several days or weeks.

Economics of Industry Participation and Public Adoption of DISARM

The E-Z Pass electronic toll-collection system [E-ZPass] offers an example of incentives to spur participation and adoption.

When you establish an E-ZPass prepaid account, you receive a small electronic tag that attaches to the windshield inside your car. Within the tag is an electronic chip that contains information about your account. Each time you use a toll facility where E-ZPass is offered, an antenna at the toll plaza reads the vehicle and account information contained in your tag. The appropriate toll is then electronically debited from your prepaid account. A record of your transactions will be included in your periodic statement.

E-Z Pass customers enjoy the benefit of expedited passage through toll-collection booths. If the inspections process is slow and time-consuming as it might be at border checkpoints, the ease and speed of an E-Z Pass-like system would act as a powerful incentive to adoption and installation of detectors, whether by automotive manufacturers or by the after-market.

Stephen Flynn [Flynn 2004] suggested a similar incentives-based scheme in connection with speeding the adoption of container security initiatives by shipping companies and seaports. Two other examples of relevant programs are the CBP's NEXUS and FAST (Fast and Secure Trade) initiatives [Bonner 2003]. Participation in these programs is voluntary and the incentive for participation is expedited clearance through border checkpoints for individuals (NEXUS) and cargo (FAST). Individuals choosing to participate in NEXUS voluntarily provide background information and biometrics that are used to screen against international crime and terrorist databases. They are provided with a SMART card that can be waved through a border checkpoint.

Proposed incentives and regulatory framework

With DISARM, a network of checkpoints would be established within the transportation infrastructure as well throughout the perimeters of the major metros. Vehicles passing these checkpoints would be either automatically read using a combination of readers and detectors or would be subject to manual inspection, perhaps using a man-portable radiation detector. Vehicle manufacturers would be required to install detectors in all vehicles, beginning in a particular model year, to achieve the radiation safety benefits.

After-market installation of detectors in older model vehicles would be required, but as an interim measure could be facilitated by the incentives to speed passage through checkpoints. Owners of older vehicles would be given the incentive to install detectors since vehicles not equipped with detectors would be subject to a more time-consuming manual inspection, resulting in longer delays. After-market installation of detectors could

be monetarily subsidized by the DoT or through tax incentives. The Transportation Security Administration within the Department of Transportation could administer the regulatory framework. Identification and maintenance of malfunctioning in-vehicle detectors will be a necessary component of a DISARM program—therefore detector design that minimizes maintenance (both frequency and costs) is desirable.

Drivers and owners of vehicles can benefit from in-vehicle detectors whose readings are designed to be appropriately summarized and conveyed to the driver on their dashboard.²⁴ Driver-readable detectors inside vehicles can warn of any highly radioactive material such as Cesium-137 or Cobalt-60 that has been maliciously planted inside the vehicle by a potential terrorist in order to contaminate the occupants, which is a possible way for terrorists to create public panic by inflicting harm, see [p. 783, Steinhausler]. These detectors might also catch unintentionally or unknowingly contaminated normal materials. They can also be used to detect of fissile material such as HEU being smuggled in the vehicle without the driver's knowledge, especially in delivery or cargo vehicles. The information provided by these detectors is likely to be valuable enough that there is an incentive for the driver or owner to ensure that detectors are functioning properly.

In addition, the President's budget request for FY 2006 includes the establishment of a Domestic Nuclear Detection Office (DNDO) within the Department of Homeland Security [DHSFY06]. Coordination between these agencies as well as CBP (Customs and Border Protection) would be necessary.

Precedents for regulation

There are several precedents for mandating the installation of detectors in vehicles and requiring the inspection of vehicles at major transportation choke-points. Some examples:

- To prevent automotive accident deaths due to tread separation and under-inflation, tire pressure sensors in all four wheels of light vehicles will be required in the US by 2007, see [Crawley, 2005] and [Plungis, 2005]. At a cost of \$40-\$70 per vehicle, 100 lives are expected to be saved annually.
- DoT regulations on the installation of seat-belts in the context of Federal Motor Vehicle Safety Standards [FMVSS].
- The Clean Air Act of 1970 that led to the introduction of catalytic converters and the phase-out of tetra-ethyl lead (TEL) [CAA1970]
- EPA's regulations on vehicle emissions testing
- The proposed Vehicle Infrastructure Integration initiative by the DoT [VII]

Respecting Personal Privacy

Unlike E-Z Pass which uniquely identifies the driver/vehicle but is also opt-in from the driver's perspective and can even be disabled, the mandatory inclusion of an always-on device inside each vehicle that will communicate to a state-controlled infrastructure can

²⁴ This idea was suggested to the authors by Michael May when this material was presented at the Center for International Security and Cooperation, Stanford University on October 11, 2005.

raise personal privacy concerns. If privacy is made an important consideration in system design, the DISARM checkpoints can be designed to respect privacy by discarding information about vehicles that do not set off the in-vehicle detector. Compare this to the extent that other security measures have already intruded on people's privacy.

- The FAA requires the inspection of bags as well as passengers at airports through manual procedures as well as through x-ray inspections.
- Video surveillance systems are pervasive on America's streets and highways for traffic monitoring, citations, public safety, and other applications. For example, see [New Orleans, 2005].
- Cell phones are required (under E-911 provisions [E911]) to be able to maintain and transmit location information.
- More than 65% of 2004 model year cars in the US were equipped with "black boxes" that record events. Privacy advocates fear that in the future these devices could be used to record location information and vehicle trajectories [Jones, 2004].

By comparison, the commonplace security measures listed here, a DISARM program explicitly designed to discard information about vehicles which do not set off the in-vehicle nuclear detector would be respectful of personal privacy.

DISARM Startup Costs

Given that the economic losses due a nuclear attack could spiral easily well into the trillions of US dollars, at what cost would it be appropriate to startup a DISARM program? To help gain a preliminary understanding of the most important cost drivers, we develop back-of-the-envelope estimates based of overall system cost to deploy a DISARM-based solution. An in-container detector capable of detecting nuclear (gamma and neutron) radiation as well as other kinds of (conventional) explosives would cost an estimated \$250 [Flynn, 2004], which is comparable (three to four times) the cost of tire sensors that will be mandatory in all light vehicles in the US by 2007 and are expected to save 100 lives annually, see [Crawley, 2005] and [Plungis, 2005]. We use \$250 as a conservative estimate – when dealing with the volumes relevant to the DISARM proposal, the costs are expected be much lower due to volume manufacturing and design, perhaps even approaching the cost comparable to the tire air pressure sensors. At the conservative price of \$250 per detector system, to equip roughly 50 million containers worldwide plus 250 million vehicles in the US with these detectors would cost about \$75 billion.

The next major component of the system cost is the cost of deploying checkpoints, but this turns out to be much less in comparison to the cost of detectors. Since the checkpoints incorporate communications technology, but not detectors, once again we conservatively approximate the cost of deploying a checkpoint by of the order of the cost of a Wi-Fi base-station (< \$10,000 today), and the number of checkpoints based on an assumption of 10 base-stations per square mile. If we were to secure the 100 most densely populated areas, each with an area of 50 square miles, the total number of base-stations required is $100 * 10 * 50 = 50,000$. The total cost to deploy these checkpoints is

therefore \$500 million = \$0.50 billion, which is insignificant compared to the cost of the in-vehicle detectors.

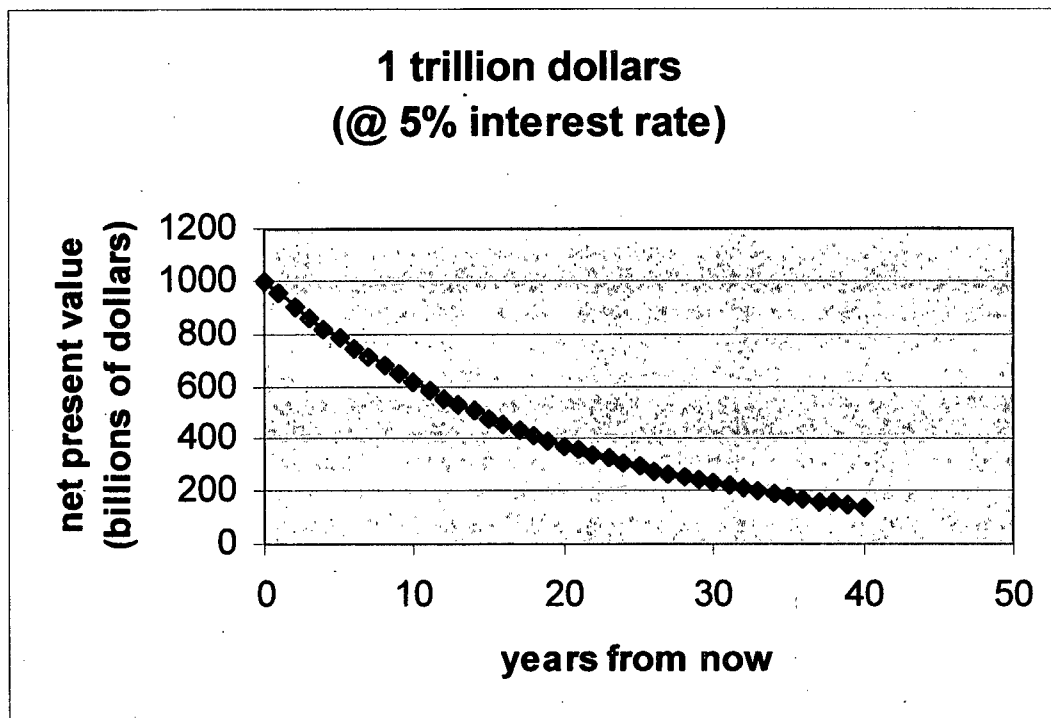


Figure 12 A future loss of \$1 trillion in today's dollars

Our rough analysis suggests that in-vehicle detectors will comprise the bulk of the costs of the system, to be borne by vehicle owners and users and probably with some government subsidies or tax incentives. In either case, the startup cost involved (about \$75 billion) is easily justifiable given the substantial risks and the trillion dollar economic impact that would be caused by a future US \$1 trillion terrorist nuclear attack even in terms of today's dollars. For comparison, the new NHTSA rules on tire pressure sensors would add an additional \$40-70 to the cost of a car (compared to about \$250 for a radiation sensor with DISARM) and are expected to save about 100 lives annually.

Conclusion

Detecting and intercepting terrorist nuclear weapons is a challenging problem, especially on a national and worldwide scale. Our analysis shows that although current and planned architectures represent positive steps and may offer some short-term deterrent value, they are unlikely to be perceived as credible. New architectures involving in-vehicle detection (DISARM) will most likely be required to overcome the problems with current architectures. DISARM programs using existing technology to screen smaller vehicles in conjunction with active screening and inspection of larger vehicles will likely create a strong deterrent for potential nuclear terrorists by uniformly raising the cost and risk of

transporting shielded HEU. Broad adoption of a DISARM architecture will drive down the program's costs over time.

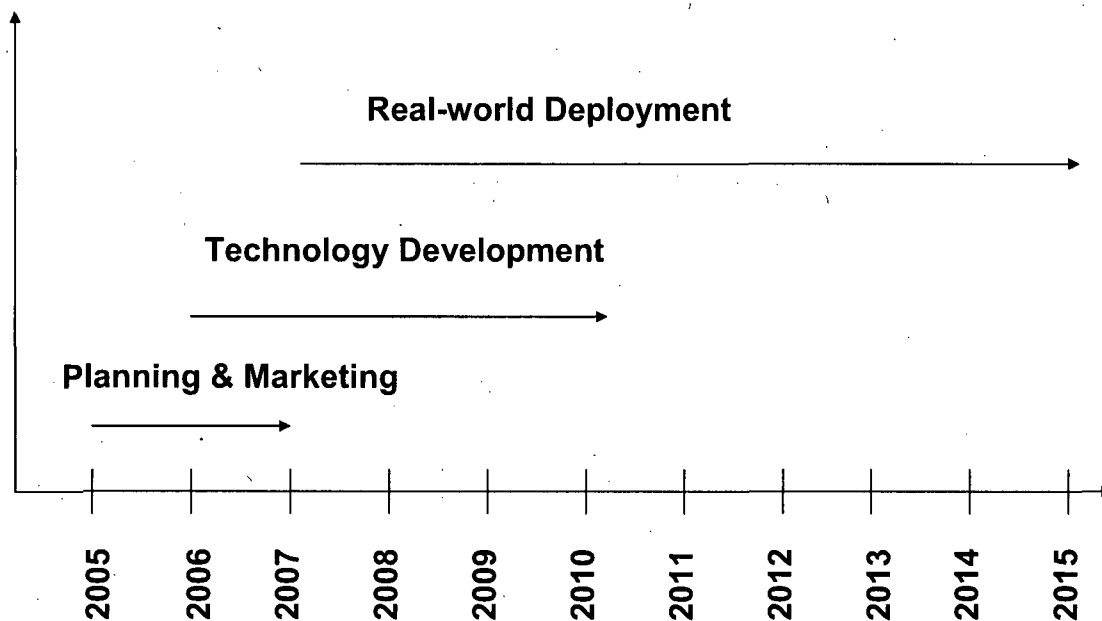


Figure 13 Estimated Timeline for DISARM

At the time of this writing, we are aware of no organization (public or private) that is committed to making a DISARM-like system a reality. We envision a three-stage approach to deployment of DISARM as illustrated in the timeline below. The first stage is to plan and market the DISARM program in consultation with key stakeholders. Within government this includes municipal, state, and national governments, specifically law enforcement, military, coast guard, and transportation authorities such as the DoT/FAA. In private industry this includes shipping and transportation companies, auto and vehicle manufacturers.

Second, a parallel effort in system and technology design & development against specified goals to achieve:

1. Detectors designed to be capable of detecting sufficiently small quantities of HEU & Pu when used inside vehicles such as cargo containers (ship/rail/road), automobiles, boats, and airplanes and can also be manufactured cost-effectively in large volumes.
2. System design to assure infrastructure and security can be designed to work with sufficient coverage and frequency of data collection to be useful to law enforcement.
3. Projected manufacturing and installation costs meet targeted goals over time.
4. False positives, equipment failure rates, labor or cost, and other operational concerns are manageable.
5. The DISARM program costs can be estimated and fall within a budget that is justified by the value-added.

6. Last but not least, the DISARM program in conjunction with complementary initiatives involving fixed/handheld detectors, portals, and inspection/surveillance together create enough risk of interception of nuclear materials to deter nuclear terrorists.

Integration of the technology into the real-world will likely to begin with shipping containers (land/sea/air) initially. It might subsequently be rolled out in the freight and package/mail delivery and public sector transportation system, and then be introduced into other transportation sectors such as automobiles through legislative mandate. The system can eventually be deployed worldwide.

References

- The Week, 2002, "Stopping nuclear terror," The Week, July 5, 2002
<http://www.theweekmagazine.com/article.asp?id=33>
- Kahneman, D., et. Al., 2000, "Choices, Values, and Frames," Cambridge, UK: Cambridge University Press
- Kahneman, D., 2002, "Maps of bounded rationality: a perspective on intuitive judgment and choice." Nobel Prize Lecture, December 8, 2002.
<http://nobelprize.org/economics/laureates/2002/kahnemann-lecture.pdf>
- J. Carson Mark, August 1990, 'Reactor-grade Plutonium's Explosive Properties', www.nci.org/NEW/NT/rgpu-mark-90.pdf
- J. Carson Mark, 1993, 'Explosive Properties of Reactor-Grade Plutonium', Science and Global Security, 1993, Vol. 4, pp. 111-128, www.princeton.edu/~globsec/publications/pdf/4_1Mark.pdf
- Oxford, V., 2005. "Detecting Nuclear Weapons and Radiological Materials: How Effective Is Available Technology?," Testimony to U.S. Congress, June 21, 2005. <http://hsc.house.gov/files/TestimonyOxford.pdf>
- Physorg.com, 2005. "R&D 100 Award for Developing a Novel Radiation Detector"
<http://www.physorg.com/news5282.html>
- Falkernrath, R.A., et. al. 1998. "America's Achilles Heel," Cambridge, MA: The MIT Press.
- Kean, T. H., et. al. 2004. "The 9/11 Commission Report," New York: W. W. Norton & Company.
- RAND. 2003. "The RAND-MIPT Terrorism Incident Database," 16 September. <http://www.rand.org/psj/rand-mipt.html>
- MIPT. 2002. "MIPT Terrorism Database System," 27 August. <http://db.mipt.org>
- Dillingham, G. L. 2002. "AVIATION SECURITY: Transportation Security Administration Faces Immediate and Long- Term Challenges," United States General Accounting Office, GAO-02-971T, 25 July. <http://www.gao.gov/new.items/d02971t.pdf>
- Enders, W., T. Sandler. 1993. "The effectiveness of antiterrorism policies: a vector-autoregression-intervention analysis," American Political Science Review, 87(4): 829-844.

- Malotky, L., S. Hyland. 1998. "Preventing Aircraft Bombings," The Bridge, 28 (3), Fall, 1998. <<http://www.nae.edu/nae/naehome.nsf/weblinks/NAEW-4NHMHC?opendocument>>
- Medalia, J. 2003. "Terrorist Nuclear Attacks on Seaports: Threat and Response," Congressional Research Service, Order Code RS21293, 13 August. <<http://www.fas.org/irp/crs/RS21293.pdf>>
- MIPT. 2002. "MIPT Terrorism Database System," 27 August. <<http://db.mipt.org>>
- O'Hanlon, M. E., et. al. 2002. Protecting the American Homeland: A Preliminary Analysis, Washington D.C.: Brookings Institution Press, an updated version (March 2003) is available online at <<http://www.brookings.edu/dybdocroot/fp/projects/homeland/newpreface.pdf>>
- Szyliowicz, J. 2004. "Aviation Security: Promise or Reality?" Studies in Conflict and Terrorism, 27:47-63.
- Defense Science Board, 2004, "Preventing and Defending Against Clandestine Nuclear Attack," June 2004, Office of the Under Secretary of Defense For Acquisition, Technology, and Logistics Washington, D.C. http://www.acq.osd.mil/dsb/reports/2004-06-Clandestine_Nuclear_Attack.pdf
- Ferguson, C. D. et. al., 2004. "The Four Faces of Nuclear Terrorism," Center for Nonproliferation Studies, Monterey, CA.
- Campbell, 2004. "The Nuclear Tipping Point"
- Allison, G., 2004. "Nuclear Terrorism : The Ultimate Preventable Catastrophe," Times Books
- Steinhausler, F, 'What It Takes To Become A Nuclear Terrorist', American Behavioral Scientist, Vol. 46, No.6, pp 782-795, February 2003
- Flynn, S., 2004, "America the Vulnerable", Harper Collins
- Bonner, Robert C., 2003 "Securing America's Borders While Safeguarding Commerce", Heritage Lecture, <http://www.heritage.org/Research/HomelandDefense/HL796.cfm>
- National Intelligence Council, 2005. "MAPPING THE GLOBAL FUTURE: REPORT OF THE NATIONAL INTELLIGENCE COUNCIL'S 2020 PROJECT," http://www.cia.gov/nic/NIC_2020_project.html
- Linzer, D., 2004. "Nuclear Capabilities May Elude Terrorists, Experts Say," Washington Post, Wednesday, December 29, 2004; Page A01
- Morrison, J., 2004. "Shipping Safety," Washington Post, Embassy Row, November 26, 2004.
- Slaughter, D., et. al., 2003. "Detection of special nuclear material in cargo containers using neutron interrogation," Lawrence Livermore National Laboratory, UCRL-ID-155315, <http://www.llnl.gov/tid/lof/documents/pdf/244044.pdf>
- Fetter, S., et. al., 1990a. "Gamma-Ray Measurements of a Soviet Cruise-Missile Warhead," Science, Volume 248, Issue 4957 (May 18, 1990), 828-834.
- Fetter, S., et. al., 1990b. "Detecting Nuclear Warheads," Science & Global Security, Volume 1, pp. 225-302.

- Steve Fetter et al, 1990c, 'Fissile Materials and Weapons Design', www.princeton.edu/~globsec/publications/pdf/1_3-4FetterA.pdf
- National Nuclear Data Center, 2004. "ENSDF Decay Data in the MIRD format," Brookhaven National Laboratory, Upton, N.Y, <http://www.nndc.bnl.gov/mird/index.html>
- National Institute of Standards, 2005. "FIPS PUB 140-2: Security Requirements for Cryptographic Modules," Computer Security Division, National Institute of Standards and Technology, <http://csrc.nist.gov/cryptval/140-2.htm>
- Wein, L.M., et. al., 2005. "Preventing the Importation of Illicit Nuclear Materials in Shipping Containers," <http://faculty-gsb.stanford.edu/wein/personal/container.pdf>
- Shultis, J. K. and Faw, R. E., 2002. "Fundamentals of Nuclear Science and Engineering," Marcel Dekker.
- Gosnell, T. B., 2000. "Uranium Measurements and Attributes," 41st Annual Meeting of the Institute of Nuclear Materials Management, New Orleans, LA, July 15-20, 2000.
- Kammeraad, J., 2004, "Radiological and Nuclear Counter-Measures", <http://www.ctc.org/DHSIF/Bowyer%20Panel.pdf>
- EZPass: <http://www.ezpass.com/>
- DHSFY06: <http://www.dhs.gov/dhspublic/display?content=4337>
- E911: <http://www.fcc.gov/911/enhanced/>
- FMVSS: <http://www.nhtsa.dot.gov/cars/rules/import/FMVSS/>
- VII: <http://www.its.dot.gov/initiatives/initiative9.htm>
- CAA1970: <http://www.epa.gov/region5/defs/html/caa.htm>
- New Orleans, 2005: 'Cameras eyeball streets in New Orleans for crime', MSNBC, March 8, 2005
- Reuters, November 8, 2004. "Race Against Time to Prevent Nuclear Terror – IAEA"
- Reuters, March 15, 2005, "Pakistan Reviving Nuclear Black Market, Experts Say"
- Howe, D. July, 2004. "Planning Scenarios, Executive Summaries, Created for Use in National, Federal, State, and Local Homeland Security Preparedness Activities," The Homeland Security Council
- Hecker, J. Z., November 18, 2002, "Container Security: Current Efforts to Detect Nuclear Materials, New Initiatives, and Challenges," Testimony before the Subcommittee on National Security, Veterans Affairs, and International Relations, House Committee on Government Reform, GAO-03-297T <http://www.gao.gov/cgi-bin/getrpt?GAO-03-297T>
- McDonald, J. C., et. al., 2004, "Detecting Illicit Radioactive Sources," Physics Today, November 2004, p. 36-41.
- Gellman, B., 2002a. "Fears Prompt U.S. to Beef Up Nuclear Terror Detection Sensors Deployed Near D.C., Borders; Delta Force on Standby," Washington Post, March 3, 2002; Page A01 <http://www.washingtonpost.com/ac2/wp-dyn?pagename=article&node=&contentId=A29406-2002Mar2¬Found=true>

- Gellman, B., 2002b. "In U.S., Terrorism's Peril Undiminished, Nation Struggles on Offense and Defense, and Officials Still Expect New Attacks," Washington Post, December 24, 2002; Page A01
<http://www.washingtonpost.com/ac2/wp-dyn?pagename=article&node=&contentId=A31589-2002Dec23¬Found=true>
- Crowley, M., 2005. "Can Terrorists Build the Bomb?," Popular Science, February 1, 2005.
<http://www.popsci.com/popsci/generaltech/article/0,20967,1017201,00.html>
- Ruppe, D., 2005. "Radiation Detectors Inadequate, New York Official Says," Global Security Newswire, March 18, 2005.
- Campbell, K. M., 2004. "The Nuclear Tipping Point, Why States Reconsider Their Nuclear Choices," Brookings Institution Press, 2004.
- O'Hanlon, et. al., 2002. "Protecting the American Homeland: A Preliminary Analysis," Brookings Institution Press, Washington D.C.
- Crawley, J., 2005, "US to Order Tire Pressure Monitors on New Vehicles," Reuters, April 6, 2005.
<http://www.reuters.com/newsArticle.jhtml?type=domesticNews&storyID=8106919>
- Plungis, J., 2005, "Highway safety agency estimates the new systems will save 120 lives a year," Detroit News Washington Bureau, April 8, 2005.
<http://www.detnews.com/2005/autosinsider/0504/08/C03-143935.htm>
- Jones, W. D., 2004, "Black Boxes Get Green Light," IEEE Spectrum, December 2004, "News" Section, pages 14-16.
<http://www.spectrum.ieee.org/WEBONLY/resource/dec04/1204nbox.html>
- Medalia, J., 2005, "Nuclear Terrorism: A Brief Review of Threats and Responses," CRS Report for Congress, The Library of Congress
<http://fpc.state.gov/documents/organization/43399.pdf>
- Chertoff, M., 2005, "Statement for the Record Before the United States Senate Committee on Homeland Security and Governmental Affairs," March 9, 2005.
<http://hsgac.senate.gov/files/SecChertoffStatement.pdf>
- Borozdin, K. N., 2003, "Radiographic imaging with cosmic-ray muons," Nature, Vol. 422, 20 March 2003, p. 277.
- Kimery, A. L., "NUCLEAR TERRORISM - Your Life May Depend on The Woman from NEST," October 23, 1995
<http://www.insightmag.com/news/1995/10/23/Nation/Nuclear.Terrorism.Your.Life.May.Depend.On.The.Woman.From.Nest-210124.shtml>
- Nuclear Threat Initiative, 2005, "A Tutorial on Nuclear Weapons and Nuclear-Explosive Materials - Part Five: Detecting Nuclear Materials and Nuclear Weapons"
http://www.nti.org/e_research/cnwm/overview/technical5.asp
- Vetter, K., 2004, "High-Sensitivity Gamma-Ray Imaging," Lawrence Livermore National Laboratory, April 2004
http://www-cms.llnl.gov/s-t/gamma_rays_ar.html
- Associated Press, 2005, "Calif. Man Sets Off Nuclear Alert Detector," March 2, 2005.
<http://abcnews.go.com/US/wireStory?id=545809>

- Bunn, M., 2004, "Securing the Bomb: An Agenda for Action," Nuclear Threat Initiative, May, 2004.
<http://www.nti.org/cnwm>
- Bunn, M., 2005, "Securing the Bomb: The New Global Imperatives," Nuclear Threat Initiative, May, 2005.
<http://www.nti.org/cnwm>
- Doyle, J. E., 2003, "Needed: A Nuclear Dragnet for Homeland Security?," The Nonproliferation Review/Fall-Winter 2003.
<http://cns.miis.edu/pubs/npr/vol10/103/103doyle.pdf>
- RAE Systems, 2005, "Securing the Supply Chain: Container Security and Sea Trial Demonstration Results," RAE Systems, January 2005
http://www.raesystems.com/~raedocs/Securing_the_Supply_Chain_011205.pdf
- RFTrax, 2005a, "RAD-CZT Radiation Sensor," RFTrax Inc, September, 2005.
http://www.rftrax.com/radiation_sensor.xml
- RFTrax, 2005b, "Flexible communications for critical sensor data," RFTrax Inc., September 2005,
<http://www.rftrax.com/communication.xml>

Appendix A: Representative Detector and System Suppliers

	Name	Offerings	Products
1	Alrad Instruments Berkshire, UK http://www.alrad.co.uk	Detectors	Distributor of others' products
2	American Science and Engineering, Inc.[AS&E] Billerica, MA www.as-e.com	Detectors, Instruments & Systems	Xray inspection systems
3	Applied Scintillation Technologies Harlow, UK www.appscintech.com	Scintillation Detectors	
4	Aracor Sunnyvale, CA http://www.aracor.com/	Xray Inspection systems	Xray inspect., industrial CT scan
5	Atlantic Nuclear Corp. Canton, MA USA www.atnuke.com	Nuclear material safety	Distributor of others' products
6	BAE SYSTEMS plc London, UK www.baesystems.com	Systems supplier & Integrator	
7	BIL Solutions (formerly BNFL Instrument, Ltd.) www.bilsolutions.co.uk BIL, Inc. [USA Head Office] Santa Fe, NM	System Integrator	Vehicle Portal Systems etc
8	Berkeley Nucleonics, Inc. San Rafael, CA www.berkeleynucleonics.com	Radiation Instruments & systems	Radionuclide Detection & Identification
9	Bruker Daltonik GmbH 04318 Leipzig, Germany www.bdal.de	Chem & Rad Instruments	NBC instruments Handheld detectors SVG2
10	Canberra Industries Meridien, CT USA CANBERRA Industries (Canberra EURISYS) Saint Quentin En Yvelines Cedex, France http://www.canberra-hs.com	Detectors, instruments & systems	Portal Monitors, Handheld units, other
11	Centronic Croydon, UK www.centronic.co.uk	Detectors and sensors	Semiconductor detectors & others
12	EADS - European Aeronautic Defence & Space Co. Defence Electronics Division Ryle, Netherlands www.eads.net	System integrator	

13	Exploranium [SAIC acquired December, 2003-see SAIC] Operated as SAIC Canada Missisagua, Ontario Canada		See SAIC
14	Fluke Biomedical Radiation Management Services (acquired Cardinal Health/Victoreen) Cleveland, OH USA www.flukebiomedical.com/rms	Worker health monitoring	Detectors, Instruments & Services
15	GammaSight Technologies, Inc. Newport News, VA, USA http://www.gammasight.com/	Nonintrusive inspection of closed spaces	pulsed gamma ray system to find NBC material
16	Hopewell Designs, Inc. Alpharetta, GA USA http://www.hopewelldesigns.com/	Detector test irradiation standards	
17	Innovative Survivability Technologies Goleta, CA www.istsurvive.com	LLNL licensee for ARAM	Area radiation monitoring
18	L.Q.C. s.I. La Escala, Spain http://www.radal.com/	Radiation detectors & alarms	Wall-mount radiation alarms
19	Lockheed Martin Company Maritime Systems and Sensors Manassas, VA USA www.lmco.com	NBC detection systems	Metroguard™ system
20	Ludlum Measurements Inc. Sweetwater, TX www.ludlums.com	Radiation Instruments and systems	-portal monitor -Conveyor monitors
21	MGP Instruments (part of Synodys group) www.mgpi.com	Radiation Instruments & systems	-Monitoring -Dosimetry -Surface Contamination
22	Nucsafe, Inc. Oak Ridge, TN www.nucsafe.com	Detectors & systems	Neutron & γ detecting panels & instr.
22	Nuctech Company Limited Haidian District, Beijing , China PRC http://www.nuctech.com/en/index.php	Instruments & systems	Xray Container & vehicle scan -Rad monitor
24	Orobotech Yavney, Israel [Billerica, MA in US] www.orbotech.com	Detector technology	CZT detectors for medical imaging, other
25	Passport Systems Acton, MA www.passportsystems.com	Detector technology & systems	Nuclear Resonance Fluorescence

26	Polimaster Ltd. Minsk, Belarus www.polimaster.com	Radiation Instruments & systems	-Polismart γ and n detectors
27	Quintell of Ohio LLC Beachwood OH [no website]	Patent owner- cfTannenbaum 6/21/05 remrk	Possibly developing system
28	Rados (part of Synodys group) D22761 Hamburg, Germany www.rados.com	Systems	RTM910 Gamma Scan Vehicle Portal System
29	RAE Systems Sunnyvale, CA www.raesystems.com	Instruments & systems [see also Polismart].	-Rad detector -Hand Held - In-container (remote readout)
30	Rapiscan Systems (combining Aracor, Ancor, Metor) Hawthorne, CA www.rapiscansystems.com	Systems	-Portal, fixed & mobile systems -active & passive methods
31	RFTrax, Inc. Allyn, WA USA www.rftrax.com	RF interrogated sensors	RAD-CZT sensor remote readout (containers)
32	S.E.A. GmbH Dülmen, Germany www.sea-duelman.de	Instruments & systems	
33	SAPHYMO Massy, France www.saphymo.com	Instruments & systems	Vehicle, package & container scanning
34	Science Application International Corp. [SAIC] San Diego, CA http://www.saic.com/products/security	Instruments & systems	Exploranium™ portals, detectors, mobile units
35	Target Systemelectronic GmbH Solingen, Germany www.target-systems-gmbh.de/	Instruments & systems	Handheld & integrated γ & n detectors
36	Technical Associates Canoga Park, CA www.tech-associates.com	Instruments and systems	
37	Thales Security Systems UK Ltd. Chessington, Surrey, United Kingdom www.thales-security.com	System Integrator	

38	Thermo Electron Radiation Measurement and Protection Erlangen, Germany www.thermo.com	Instruments & Systems	"Safety-guard" Portal Radiation Monitor
	Thermo Electron Corporation Franklin, NJ Radiation Measurement Div, Albuquerque, NM http://www.thermo.com	Instruments & systems	Matrix Mobile Radiation Detection System (Matrix MRDS)
39	Transgalactic Instruments 1000 Sofia, Bulgaria www.tgi-sci.com	Instruments	γ radiation spectrometer
40	TSA Systems, Ltd. Longmont, Colorado, USA http://www.tsasystems.com/	Instruments & Systems	Vehicle Portal Monitors
Some Detector Material Developers and Manufacturers			
1	Argonne Nat'l Lab Argonne, IL USA www.anl.gov	Detector Technologies	
2	Brookhaven Nat'l Laboratory Nonproliferation and National Security Dept (N&NS) www.bnl.gov		CZT, Xenon, other sensors
3	Brookhaven Nat'l Laboratory Nonproliferation and National Security Dept (N&NS) www.bnl.gov/nns		RADTEC detection test facility
4	EV Products Saxonburg, PA USA www.evproducts.com	Radiation detectors	CZT semi-conductor materials, products
5	Imarad [Israel] – See Orbotech Above		
6	LND, Inc. Oceanside [Long Island], NY www.lndinc.com	Custom nuclear detectors	Ionization chambers, GM Tubes, neutron detectors
7	ORTEC (a brand of AMETEK, formerly an EGG sub) Oak Ridge, TN http://www.ortec-online.com	Detectors & instruments	
8	Radiation Monitoring Devices, Inc. (RMD, Inc.) Watertown, MA www.rmdinc.com	Detectors & Instrument Research	

9	Sandia National Labs Albuquerque, NM USA www.sandia.gov		Neutron & γ detection microsystems
10	Scientific Production Center ASPECT 141980 Dubna, Moscow Region, Russia http://aspect.dubna.ru/english	Detector Materials	Plastic scintillators
11	Yinnel Tech, Inc. South Bend, IN	Detector Materials	CdZnTe
12	Non-Proliferation and Arms Control (NPAC) Technology Working Group (TWG) Fieldable Nuclear Detectors [FND] Focus Group	Facilitate R&D to improve FND	
13	Princeton Plasmas Physics Lab (US DOE) PPPL Tritium Systems Group www.pppl.gov	Detection subsystem	

Appendix B: How do we track trends in worldwide terrorism?

The United States State Department chronicles terrorist incidents annually in its publication, Patterns of Global Terrorism [US Department of State]. According to this chronology, international terrorists conducted 199 incidents in 2002, a drop of 44% from the previous year. However, analysis based on the RAND-MIPT terrorism incident database [MIPT, 2002] shows the total number of incidents in year 2001 as 1532 and year 2002 as 2631, thus representing an increase of over 70%. In each instance, they employ their chosen criteria decide what incidents are recorded as terrorism as shown in Table 1.

United States State Department (Incident Review Panel's definition)	RAND (Research Team's definition)
"An International Terrorist Incident is judged significant if it results in loss of life or serious injury to persons, abduction or kidnapping of persons, major property damage, and/or is an act or attempted act that could reasonably be expected to create the conditions noted." [p. 83, US Department of State, 2002]	"For the purpose of this database, terrorism is defined by the nature of the act, not by the identity of the perpetrators. Terrorism is violence calculated to create an atmosphere of fear and alarm to coerce others into actions they would not otherwise undertake, or refrain from actions they desired to take. Acts of terrorism are generally directed against civilian targets. The motives of all terrorists are political, and terrorist actions are generally carried out in a way that will achieve maximum publicity. [RAND, 2003]"

Table 2 Definitions of what constitutes a terrorist incident

It appears that an order of magnitude more incidents were tracked by RAND when compared to the State Department in 2001/2002, and these definitions alone offer little insight into the cause of this discrepancy between the two databases. In addition to RAND and the US State Department, other public databases for terrorist incidents exist within government and academia. One such database is ITERATE [Vinyard Software, 2003] that chronicles terrorism incidents from 1978 onwards²⁵. However, we found that the RAND-MIPT database represents the most comprehensive, longest running, publicly available database of worldwide terrorist incidents, and provides a detailed summary of the incident in a format that is uniform across all incidents including description, fatalities, injuries, location, type of weapon used, terrorist organization responsible, to name a few.

In this paper, we employed²⁶ data from the database of terrorism incidents that has been kept by RAND and later MIPT continuously since January 1, 1968²⁷. Current until March

²⁵ Available for a fee

²⁶ With the aid of purpose-written automated (Perl) scripts, the entire contents of the RAND-MIPT database was downloaded, parsed, and arranged in a tabular spreadsheet (MS Excel). Having the incident data in this format enabled generation of charts and tables shown in this paper.

12, 2003, the contents of the RAND database have been made available by the MIPT on their website [MIPT, 2002]. In Figure 1, we chart the growth of terrorism incidents according to the RAND-MIPT database.

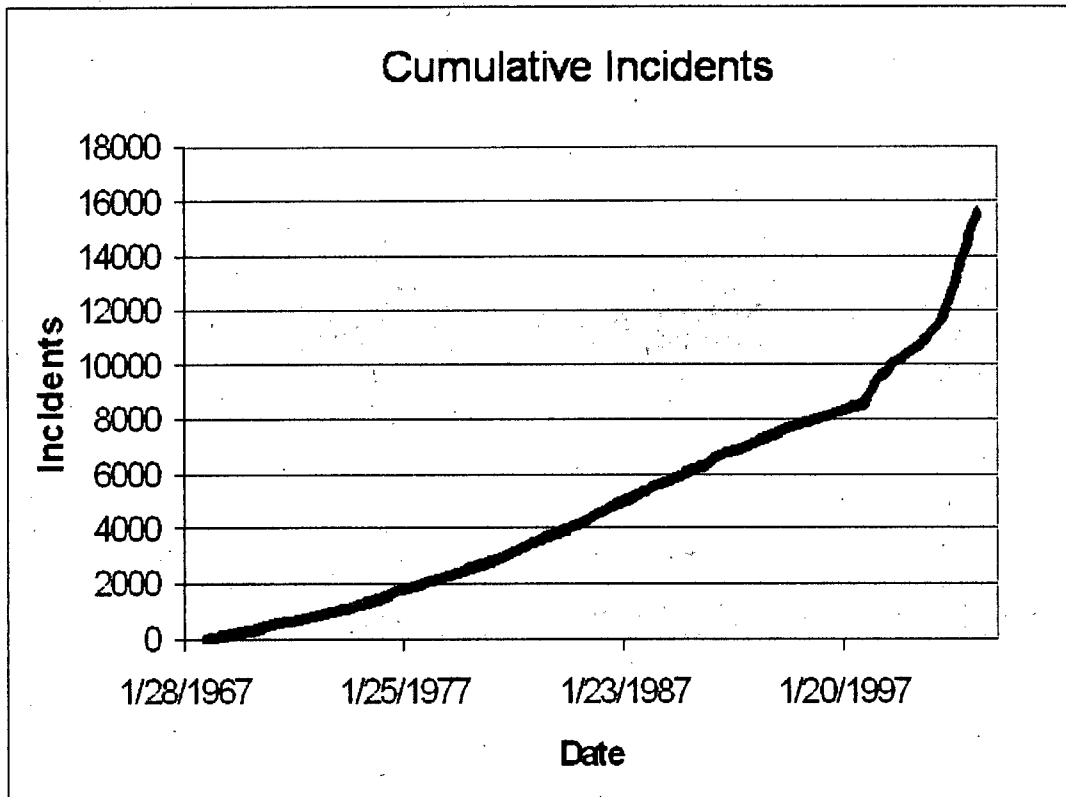


Figure 14

At the time of writing, this site was still a beta version. With over 15,000 incidents recorded, the database system is not yet absolutely perfect. For instance, at least two well-known incidents appeared to be missing in the RAND database that can be attributed either to bugs in the web-based software system²⁸ or simply delayed in their process of tracking and following up on incidents²⁹. These bugs are being fixed. Nevertheless, the RAND-MIPT database of incidents remains a useful chronology upon which we can draw reasonably accurate conclusions.

Terrorism is frightening for several reasons, perhaps in large part due to the uncertainty inherent in the terms we use to describe it such as its causes, its perpetrators, the methods they employ, their targets, etc. To place terrorism in context, consider that the total number of terrorism fatalities worldwide from January 1, 1968 through March 12, 2003

²⁷ Through 1997, only international terrorist incidents were recorded by RAND. From 1998 onwards, both domestic and international incidents were recorded.

²⁸ bombing of the USS Cole on October 12, 2000 [RAND, 2003]

²⁹ bombing of Indian Parliament on December 12, 2001 [BBC News, 2001]

as calculated from the RAND Terrorism database [RAND, 2003] were less than half of total automotive accident-related fatalities that occur in the United States every year [NHTSA, 2003]. However, in contrast to automotive accidents, terrorism is rising rapidly and there are no actuarial tables upon which uncertainty can be managed or mitigated. Furthermore, when gaming out plausible scenarios for terrorist incidents, the fatalities and cost could potentially skyrocket beyond anything witnessed to date [Associated Press, 2002].

U-232 and the Proliferation-Resistance of U-233 in Spent Fuel

Jungmin Kang^a and Frank N. von Hippel^b

The factors influencing the level of U-232 contamination in U-233 are examined for heavy-water-moderated, light-water-moderated and liquid-metal cooled fast breeder reactors fueled with natural or low-enriched uranium and containing thorium mixed with the uranium or in separate target channels. U-232 decays with a 69-year half-life through 1.9-year half-life Th-228 to Tl-208, which emits a 2.6 MeV gamma ray upon decay.

We find that pressurized light-water-reactors fueled with LEU-thorium fuel at high burnup (70 MWd/kg) produce U-233 with U-232 contamination levels of about 0.4 percent. At this contamination level, a 5 kg sphere of U-233 would produce a gamma-ray dose rate of 13 and 38 rem/hr at 1 meter one and ten years after chemical purification respectively. The associated plutonium contains 7.5 percent of the undesirable heat-generating 88-year half-life isotope Pu-238.

However, just as it is possible to produce weapon-grade plutonium in low-burnup fuel, it is also practical to use heavy-water reactors to produce U-233 containing only a few ppm of U-232 if the thorium is segregated in "target" channels and discharged a few times more frequently than the natural-uranium "driver" fuel. The dose rate from a 5-kg solid sphere of U-233 containing 5 ppm U-232 could be reduced by a further factor of 30, to about 2 mrem/hr, with a close-fitting lead sphere weighing about 100 kg.

Thus the proliferation resistance of thorium fuel cycles depends very much upon how they are implemented.

The original version of this manuscript was received by *Science & Global Security* on 15 March, 2001.

a Jungmin Kang (jmkang55@hotmail.com) will be working this coming year, in collaboration with the Nautilus Institute, on establishing a Center for Nuclear Policy at Seoul National University.

b Frank N. von Hippel (fvhippel@princeton.edu) is a Professor of Public and International Affairs at Princeton University, Princeton, NJ 08544.

INTRODUCTION

Uranium-233 is, like plutonium-239, a long-lived fissile isotope produced in reactors by single-neutron capture in a naturally-occurring abundant fertile isotope (see Figure 1). The fast critical mass of U-233 is almost identical to that for Pu-239 and the spontaneous fission rate is much lower, reducing to negligible levels the problem of a spontaneous fission neutron prematurely initiating the chain reaction -- even in a "gun-type" design such as used for the U-235 Hiroshima bomb (see Table 1). Why then has plutonium been used as the standard fissile material in the "pits" of modern nuclear weapons while U-233 has not? This question is not just of historical interest, since there is increasing interest in U-233-thorium fuel cycles.

Table 1: Comparison of some nuclear characteristics of U-233, U-235, and Pu-239

Property	Uranium-233	Uranium-235	Plutonium-239
Half-life (years)	1.6×10^5	7.0×10^8	2.4×10^4
Fertile isotope (continental crust mass abundance ^a) and thermal neutron absorption cross-section	Th-232 (9.6ppm) 7.4 barns (10^{-24} cm ²)	U ²³⁵ is derived from natural uranium.	U-238 (2.7 ppm) (99.3% in U _N) 2.7 barns
Critical Mass (kg) (reflector) ^b	8.4 (98.3% U ²³³) (3.7 cm Be)	21 (93.5% U ²³⁵) (5.1 cm Be)	7.5 (4.9% Pu ²⁴⁰) (4.2 cm Be)
Neutrons released per neutron absorbed (energy of neutron causing fission) ^c	2.5 (1 MeV) 2.28 (0.025 eV)	2.3 2.07	2.9 2.11
Spontaneous fission rate (sec·kg) ⁻¹	0.5	0.6 (for 1% U ²³⁴ and 5.5% U ²³⁸)	2.5×10^4 (for 6% Pu ²⁴⁰)
Decay heat (W/kg)	0.3	10^{-4}	2.4 (6% Pu ²⁴⁰)
Delayed neutron fraction ^d	0.00266	0.0065	0.00212

a. *Handbook of Chemistry and Physics*, 76th edition (1995-6): 14-11.

b. *Critical Dimensions of Systems Containing U-235, Pu-239, and U-233* (LA-10860-MS, Los Alamos National Laboratory, 1986 revision). Plutonium, 15.6 gm/cc; U-233, 18.6 gm/cc.

c. A.M. Perry and A.M. Weinberg, "Thermal Breeder Reactors," *Annual Review of Nuclear and Particle Science*, 22 (1972): 317-354.

d. *Thorium based fuel options for the generation of electricity: Developments in the 1990s* (Vienna, IAEA-TECDOC-1155, May 2000): 9.

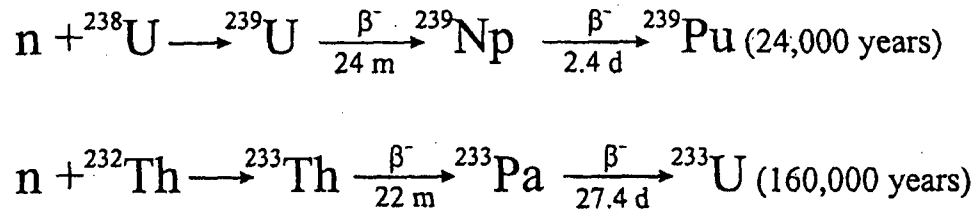


Figure 1: Production of Pu-239 and U-233.

In this paper we examine: how U-233 can be produced in existing reactor types; its attractions as a reactor fuel; the determinants of the co-production of U²³², one of whose decay products emits hard gamma rays; and the influence of that isotope at various contamination levels on the weapons-usability of U-233. Our findings are summarized in the body of the paper. The calculational tools are described in the Appendices.

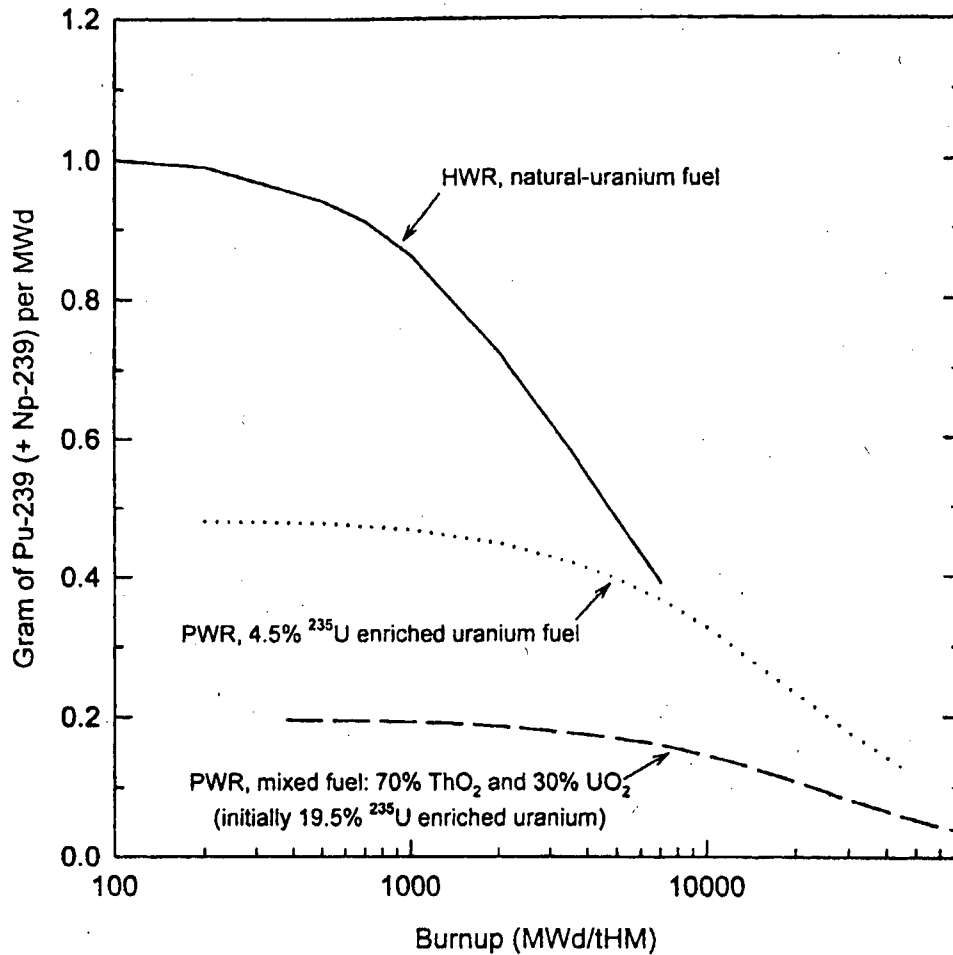


Figure 2: Net production rate of Pu-239 per Megawatt-day (MWd) of fission energy released as a function of burnup in HWR and pressurized light-water reactor (PWR) fuel.

U-233 Production

One of the most important reasons why plutonium was chosen over U-233 as a weapons material is that first-generation plutonium-production reactors were fueled by natural uranium, which contains almost as large a fraction of neutron-absorbing fertile material (U-238) as is possible consistent with a reactor achieving criticality. In a natural-uranium fueled reactor, such as the Canadian heavy-water-moderated (HWR) reactor type, Pu-239 is produced by neutron absorption in U-238 at a rate of about one gram of plutonium per thermal

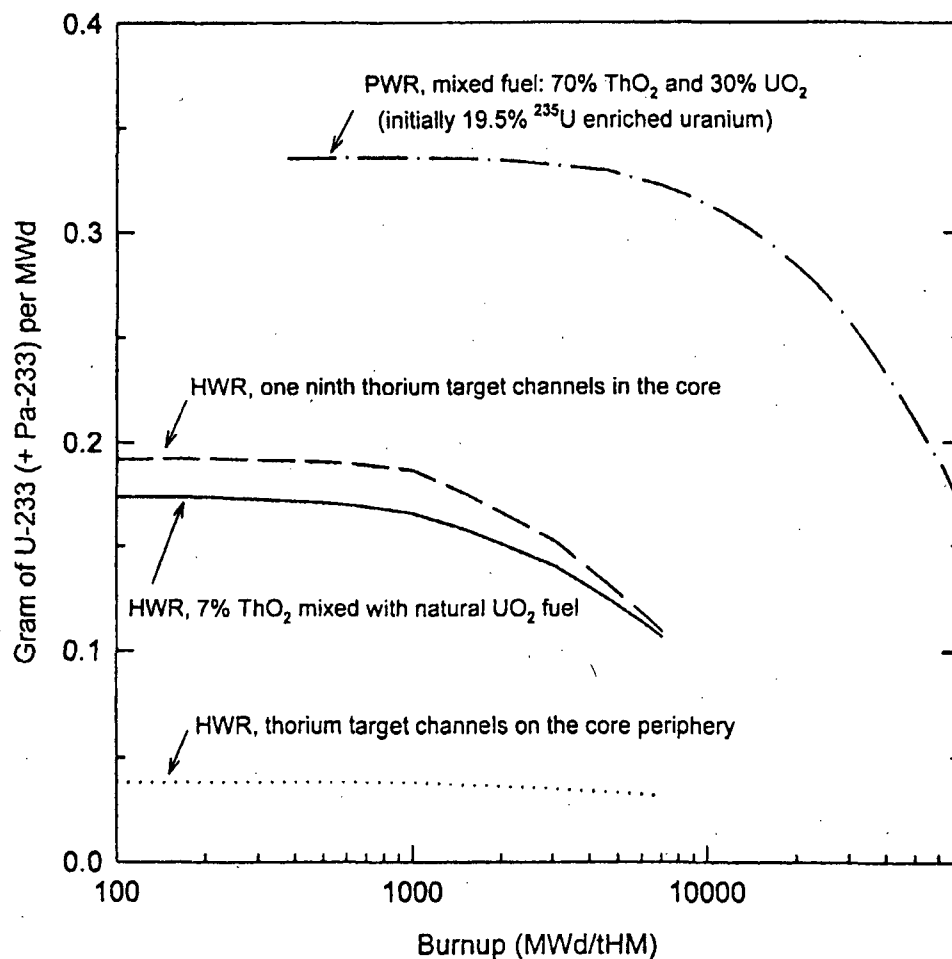


Figure 3: Net production rate of U-233 as a function of burnup of driver fuel per MWd in a PWR and in a natural-uranium-fueled HWR for thorium mixed in the fuel, or in separate channels (one out of nine), or in channels on the periphery of the core.

megawatt-day (MWd) of fission energy release at low U-235 "burnups," (see Figure 2).¹ Approximately one MWd is released by the fission of one gram of fissile material. After taking into account the neutron requirements for maintaining a steady chain reaction, there is about one excess neutron available per fission and virtually all of these neutrons are absorbed by U-238.²

Production of U-233 requires the addition of the fertile material Th-232. If the fuel is natural uranium, only a relatively small percentage of thorium can be added before it becomes impossible to sustain a chain reaction. We estimate that about 7 percent thorium oxide can be added to HWR fuel before the

achievable burnup is reduced from 7000 to 1000 MWd/t (thermal megawatt-days per ton-heavy metal). Because the thermal-neutron absorption cross-section of Th-232 is almost 3 times larger than that of U-238, this concentration of thorium would yield about 0.2 grams of U-233 per MWd at burnups lower than 1000 MWd/t (see Figure 3). Thus most of the fissile material produced in the core would still be plutonium.

In all the figures in this article, we include in the production of Pu-239 and U-233, the production of their short-lived precursors, Np-239 (2.4-day half-life) and Pa-233 (27-day half-life) respectively.

For a country with uranium-enrichment capabilities, the balance between plutonium and U-233 production could be shifted almost all the way toward U-233 by fueling production reactors with highly-enriched uranium. Indeed the U.S. produced much of its weapons plutonium in the Savannah River heavy-water-moderated production reactors, using highly-enriched uranium fuel and depleted uranium targets in mixed-lattice arrangements.³

U-232 Radiation Hazard

A second problem with U-233 as a fissile material for either weapons or reactor fuel is that it contains an admixture of U-232, whose decay chain produces penetrating gamma rays. The decay chain of U-232 is shown in Figure 4. The most important gamma emitter, accounting for about 85 percent of the total dose from U-232 after 2 years, is Tl-208, which emits a 2.6-MeV gamma ray when it decays (see Appendix C). For plutonium containing a significant admixture of 14.4-year half-life Pu-241, the most important source of gamma-ray irradiation from is its 433-year half-life decay product, Am-241, which emits low-energy (< 0.1 MeV) gamma rays. These gamma rays do not represent a significant occupational hazard for weapon-grade plutonium (0.36% Pu-241) but their dose becomes more significant for "reactor-grade" plutonium, which contains on the order of 10 percent Pu-241. Thus both U-233 contaminated with U-232 and reactor-grade plutonium are made less desirable as weapons materials by virtue of the fact that their gamma emissions bring with them the potential for significant radiation doses or shielding requirements for workers involved in nuclear weapons production and for military personnel handling nuclear weapons.

Figure 5a shows the calculated buildup with time of the gamma dose rate 0.5 meters (a typical working distance for glove-box operations) from 5-kg spheres of freshly separated U-233 containing 0, 1 and 5 ppm of U-232. It will be seen that the dose rate from pure U-233 is of the same order as that from

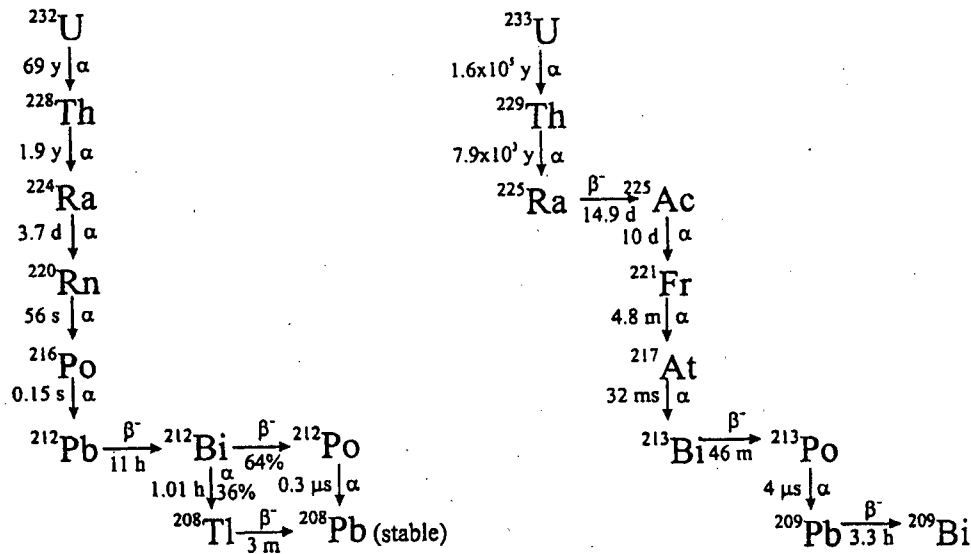


Figure 4: Decay chains of U-232 and U-233.

weapon-grade plutonium. For U-233 containing U-232, the buildup in dose rate with time reflects the in-growth of Th-228, which has a half-life of 1.9 years. After this in-growth, the dose rate from U-233 containing 1 ppm U-232 is about the same as reactor-grade plutonium after a large fraction of its 14.1-year half-life. Pu-241 (initially 9.1 % of the plutonium)⁴ has decayed to Am-241.

Figure 5b shows the effectiveness of lead shielding in reducing the dose from 5 kg spheres of reactor-grade plutonium and U-233 as a function of the weight of lead in a close-fitting shell. It will be seen that the lower-energy

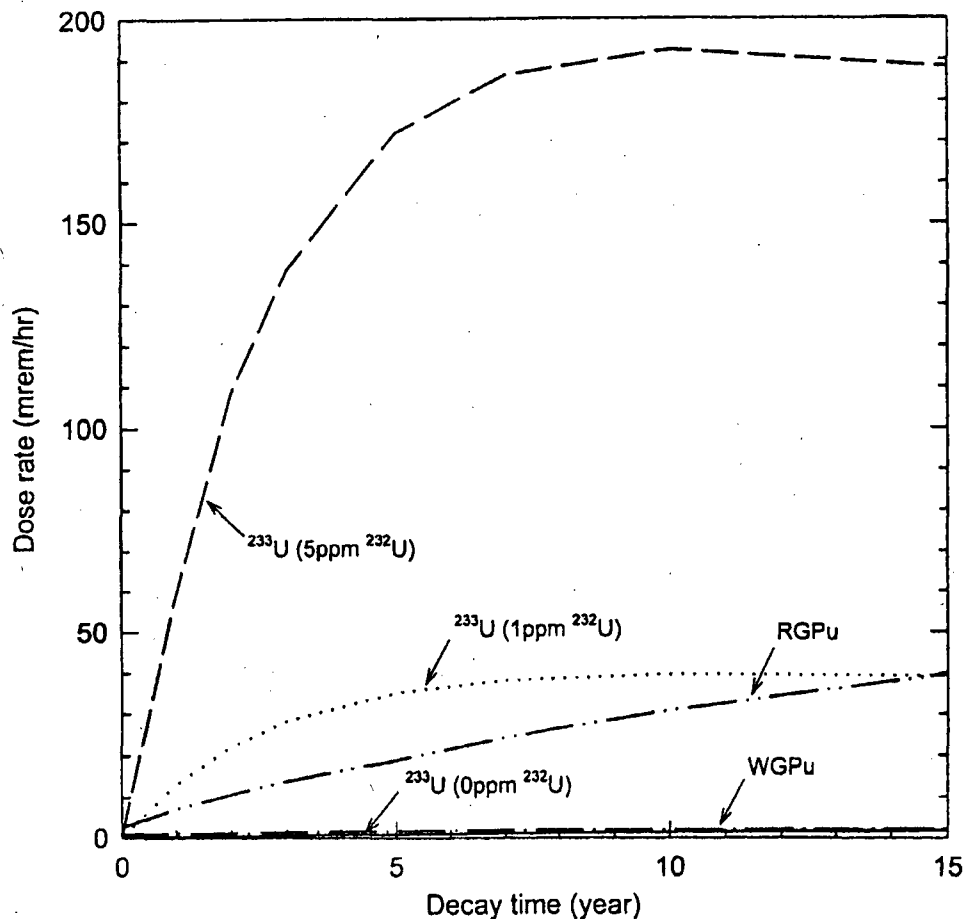


Figure 5a: Radiation-dose-rate buildup at 0.5 m from 5-kg spheres of U-233 and Pu-239 for different admixtures of U-232 and higher plutonium isotopes, respectively.

gamma rays from the plutonium are easily shielded. Shielding the neutron dose from spontaneous fission of the even-numbered plutonium isotopes in reactor-grade plutonium would require a relatively thick layer of neutron moderator containing hydrogen (e.g. plastic) followed by a layer of neutron absorbing material and then additional shielding from the gamma-rays produced when the neutrons are captured.

Occupational radiation doses are currently limited to 5 rem/yr in the US.⁵ A worker could be 0.5 meters from an unshielded 5-kg sphere of 1-year-separated weapon-grade plutonium (dose rate, 1.3 mrem/hr) for almost 3800 hours

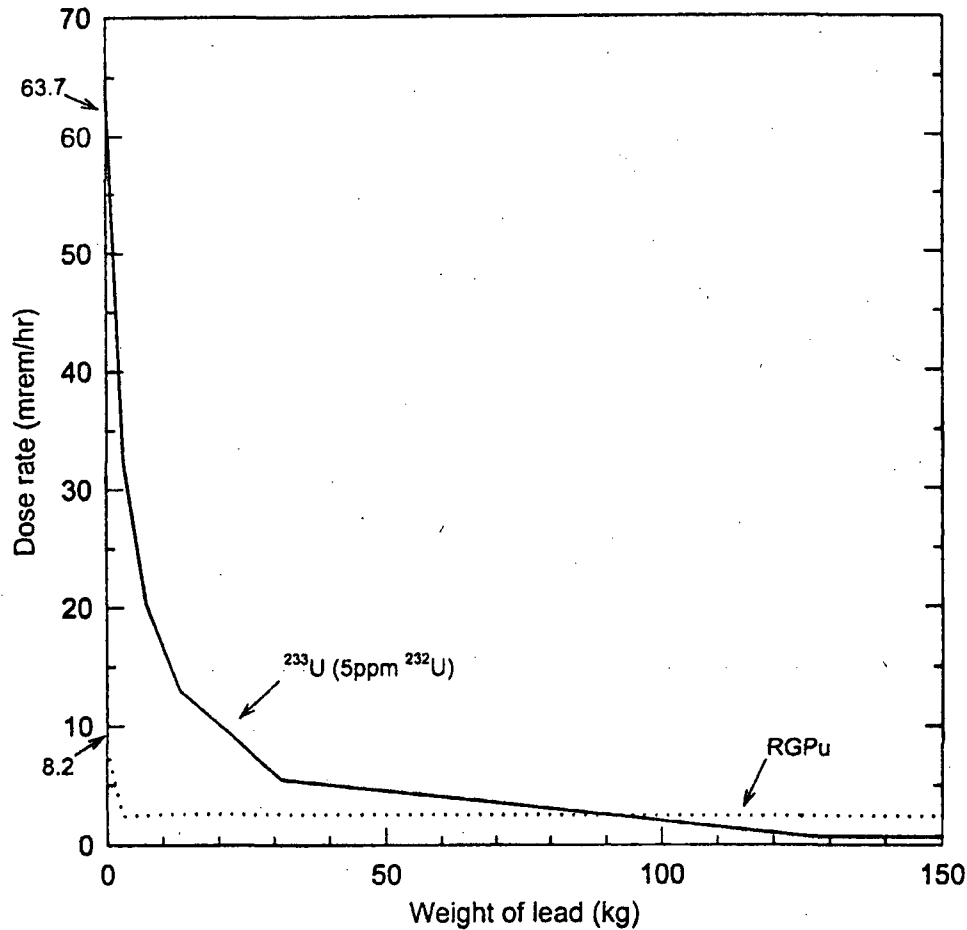


Figure 5b: Radiation-dose-rate attenuation for one-year-old separated reactor-grade plutonium and U-233 containing 5 ppm U-232 as a function of the weight of a close-fitting hollow-sphere lead shield.

before reaching that dose limit. After in-growth of Am-241, the dose rate from a sphere of reactor-grade plutonium one year after separation would be about 8.2 mrem/hr, limiting the worker to about 610 contact hours per year. The situation is about the same with U-233 containing 1 ppm U-232 after in-growth of Tl-208. For 1-year-separated U-233 containing 5 ppm U-232, a worker could only be allowed about 80 contact hours. Thus maximizing the contamination level of U-232 in U-233 would make it both significantly more difficult to fabricate and make it more detectable because of the difficulty of shielding the 2.6 MeV gamma ray. However, it would require a level of 2.4 percent U-

232 before the U-233 would satisfy the IAEA's standard for reduced physical-protection requirements (>100 rem/hr at 1 meter).⁶

Table 2: Unshielded working hours required to accumulate a 5 rem dose (5 kg sphere of metal at 0.5 m one year after separation)

Metal	Dose Rate (rem/hr)	Hours
Weapon-grade plutonium	0.0013	3800
Reactor-grade plutonium	0.0082	610
U-233 containing 1ppm U-232	0.013	380
U-233 containing 5ppm U-232	0.059	80
U-233 containing 100 ppm U-232	1.27	4
U-233 containing 1 percent U-232	127	0.04

India's Department of Atomic Energy (DAE) has been concerned about the occupational hazards associated with the fabrication of fuel containing U-233. Its long-term ambition is to cleanse U-233 down to "a few ppm" U-232 using laser isotope purification.⁷ In the meantime, a 1993 article from the Bhabha Atomic Research Center in Bombay reported a 6.7 person-rem summed dose incurred by workers fabricating a research-reactor core containing 0.6 kg "clean" U-233 containing 3 ppm U-232.⁸

Interest in U-233 as a Reactor Fuel

One reason for interest in U-233 as a reactor fuel is the superior conversion ratios C_R that can be achieved with it in slow-neutron reactors.⁹ It will be seen from Table 1 that about 0.2 more neutrons are produced on average per "thermal" (20 °C or 0.025 eV) neutron absorbed on U-233 than for absorption in Pu-239. This difference increases with neutron energy to about 0.4 at 0.1 eV neutron energy and to about 0.6 at 0.3 eV. These are important differences because the amount of fissile material required per megawatt-day of fission energy released from closed fuel cycles is proportional to $1-C_R$. In fact, the Th-232/U-233 fuel cycle can have $C_R > 1$, i.e. be a net "breeder" of fissile material in thermal-neutron reactors if the use of neutron "poisons" to control excess reactivity is minimized by use of continuous fueling or geometry control of reactivity.

There was a great deal of interest in breeder reactors from the 1940s through the 1970s. During this period it was believed that world nuclear-power capacity would rapidly outgrow the ability of the world's high-grade

capacity is an order of magnitude lower than projected in the mid-1970s; reprocessing and plutonium fuel fabrication costs are an order of magnitude higher; and uranium costs are an order of magnitude lower. However, interest in the thorium fuel cycle continues in India, because of its relatively small uranium reserves, large thorium resources, and the unwillingness of uranium exporters to sell it uranium because it is not a party to the Nonproliferation Treaty. Indeed, India's nuclear establishment continues to adhere to the 3-stage plan of nuclear-energy development laid out in the 1950s by its founder, Homi Bhabha. The first stage involves the use of HWRs fueled by natural uranium and light-water reactors fueled by low-enriched uranium. In the second stage, plutonium extracted from the spent fuel of these reactors is to be used as startup fuel for liquid-sodium-cooled fast breeder reactors. In the third stage, U-233 produced by neutron capture in the thorium blankets of these breeder reactors would be mixed with thorium and used to start up heavy-water and perhaps also high-temperature gas-cooled reactors operating on a closed Th-232/U-233 fuel cycle.¹³

Recently, there has also been a revival of interest in thorium in the U.S. and Western Europe because it can be used to increase the achievable burn-ups in light-water-reactors operating on a once-through fuel cycle and also reduce the quantity of weapons-usable transuranic elements in radioactive waste.¹⁴ Five successive neutron captures are required before Np-237 is produced from Th-232 whereas a single neutron capture on U-238 produces Pu-239 (see Figure 6).¹⁵ Proposals have therefore been brought forward for light-water-reactor designs in which thorium largely replaces U-238¹⁶ and for accelerator-driven fast-neutron sub-critical reactors that would produce U-233 out of thorium.¹⁷

Isotopic "Denaturing" of U-233 for weapons use

According to the IAEA, the enrichment boundary below which enriched uranium is not directly usable to make fission explosives is 20 percent U-235. Thus dilution by U-238 "denatures" U-235 for weapons purposes. There is no comparable isotopic dilutant for plutonium.¹⁸ However, U-238 is available in abundance in natural and depleted uranium to denature U-233. Figure 7 shows the reflected critical mass of U-233 and U-235 mixtures with U-238 as a function of percentage of the fissile isotope.¹⁹ It will be seen that the critical mass of a sphere of uranium 20-percent enriched in U-235 and surrounded by a 4-cm thick layer of beryllium is about 400 kg. A U-233/U-238 mixture has a corresponding critical mass when the U-233 percentage is approximately 12

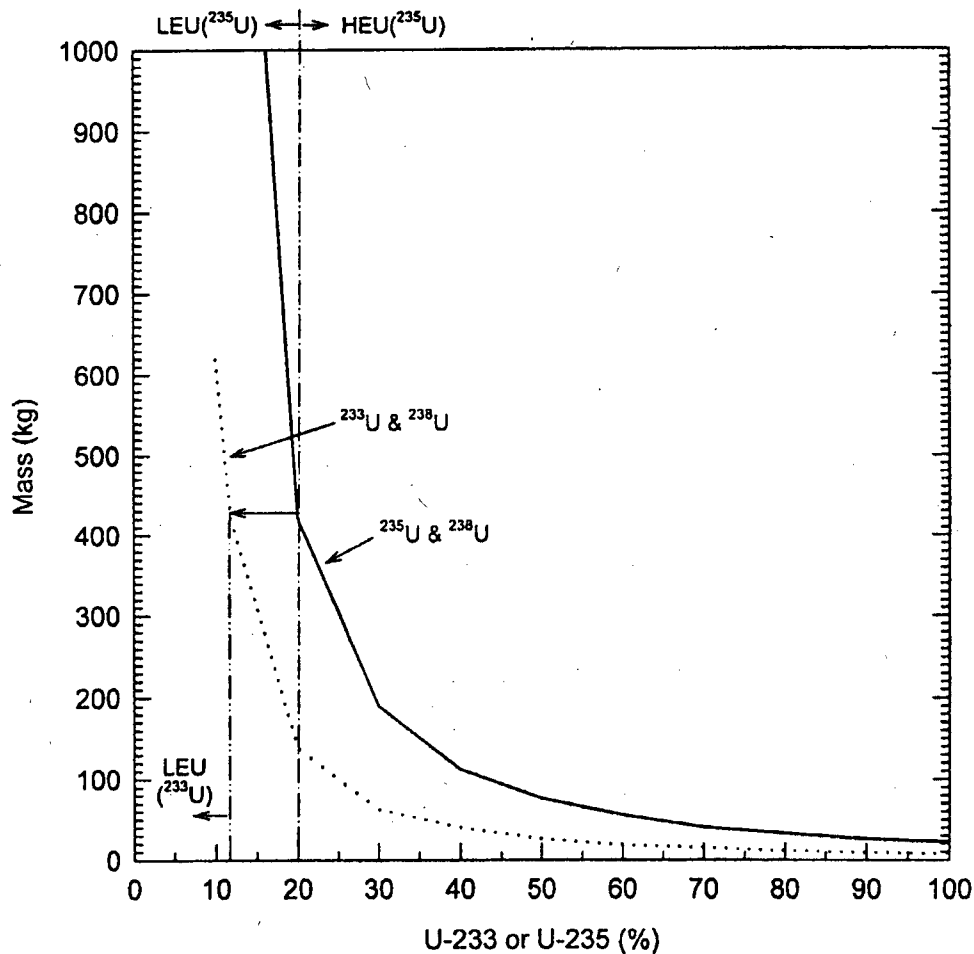


Figure 7: Reflected critical masses as a function of percentage of U-233 or U-235 in isotopic mixture with U-238.

percent.

Uranium enriched to just under 20 percent in U-235 may not be directly useable to make a nuclear explosive. However, it requires only about one quarter as much enrichment work to enrich to weapon grade (90 percent U-235) as from 4.5% enriched uranium.²⁰

Determinants of U-232 concentration in U-233. U-232 is produced from Th-232 via two of the reaction chains shown in Figure 6. Each of these chains involves a neutron-absorption (n, γ) reaction and a reaction in which an incoming neutron knocks two neutrons out of a target nucleus [($n, 2n$) reac-

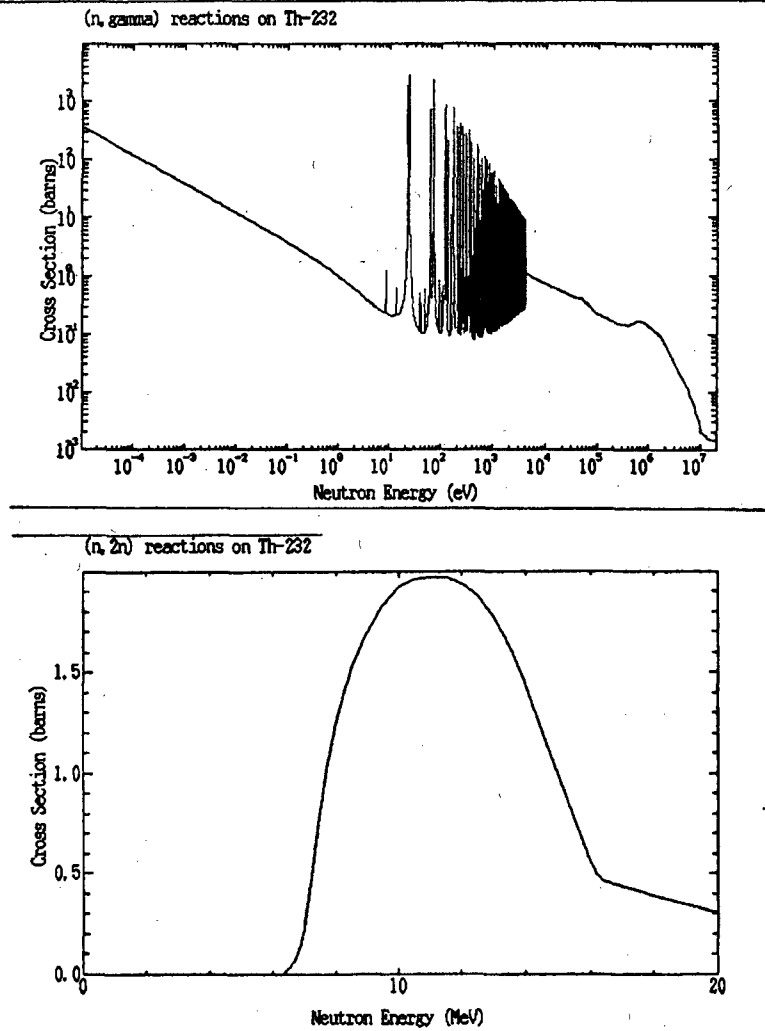


Figure 8: Cross-sections for neutron absorption: a) (n, gamma) and b) (n,2n) reactions on Th-232.

tion]. U-232 can also be produced by two successive single neutron captures starting with naturally-occurring Th-230. Thorium-230 is a decay product of U-234, which is in turn a decay product of U-238, is in secular equilibrium at a concentration of about 17 ppm in natural uranium. Minimizing U-232 production therefore requires naturally thorium that is minimally contaminated with Th-230 from intermixed or nearby natural uranium. In the calculations described below, we have assumed zero Th-230 contamination and have tested the sensitivity of the results to a contamination level of 1 ppm.

The threshold neutron energy required for the (n,2n) reactions involved in

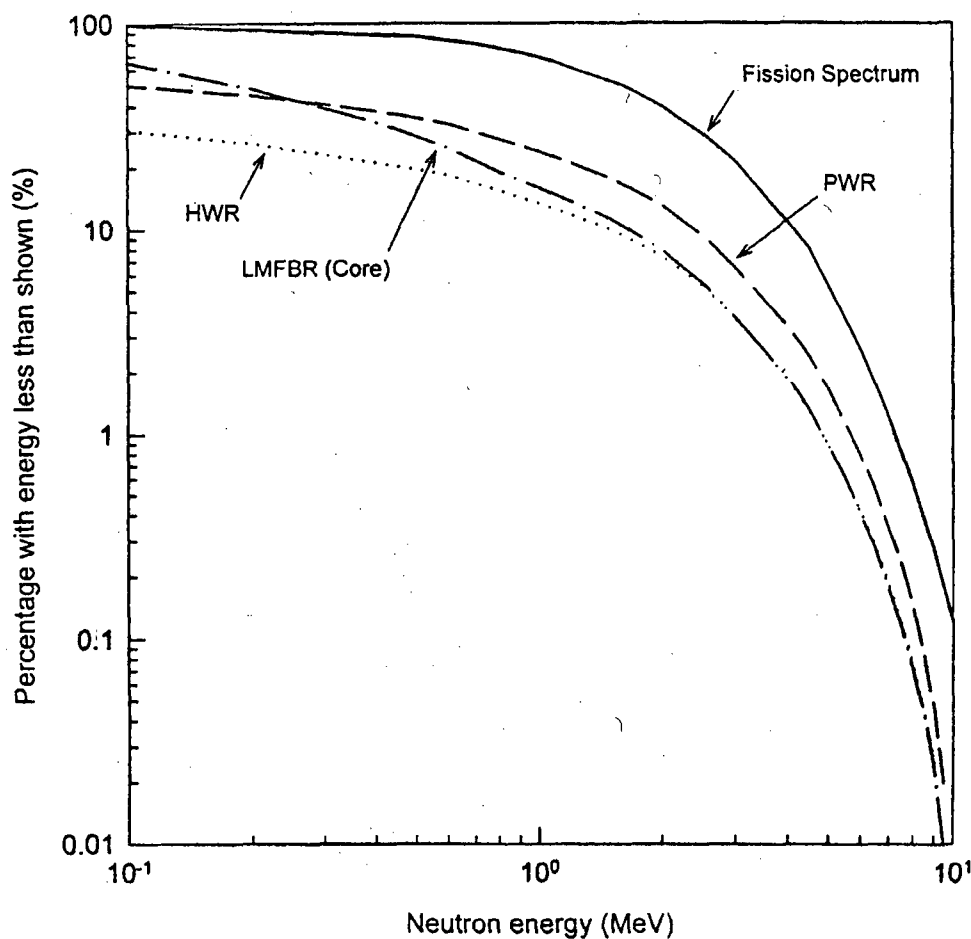


Figure 9a: Neutron-energy spectra: a) Fission spectrum compared with spectra in fuel of an HWR and cores of an LMFBR and PWR.

U-232 production is around 6 MeV.²¹ Such energies are found only in the high-energy tail of the fission spectrum. (Figure 8 shows the cross-section for neutron-capture $[n, \gamma]$ and $[n, 2n]$ reactions on Th-232.²²) The fission-spectrum average cross-sections are 14.46 mb for the reaction $n + Th232 \rightarrow Th231 + 2n$ and 4.08 mb for the reaction $n + U233 \rightarrow U232 + 2n$.²³ The development of the U-232/ U-233 concentration ratio in thorium therefore depends upon the fraction of the neutron fluence above 6 MeV in the thorium target material.

Figure 9a and Table 3 show a fission neutron-energy spectrum and compare it with the neutron energy spectra in the fuel of HWR, PWR and LMFBR

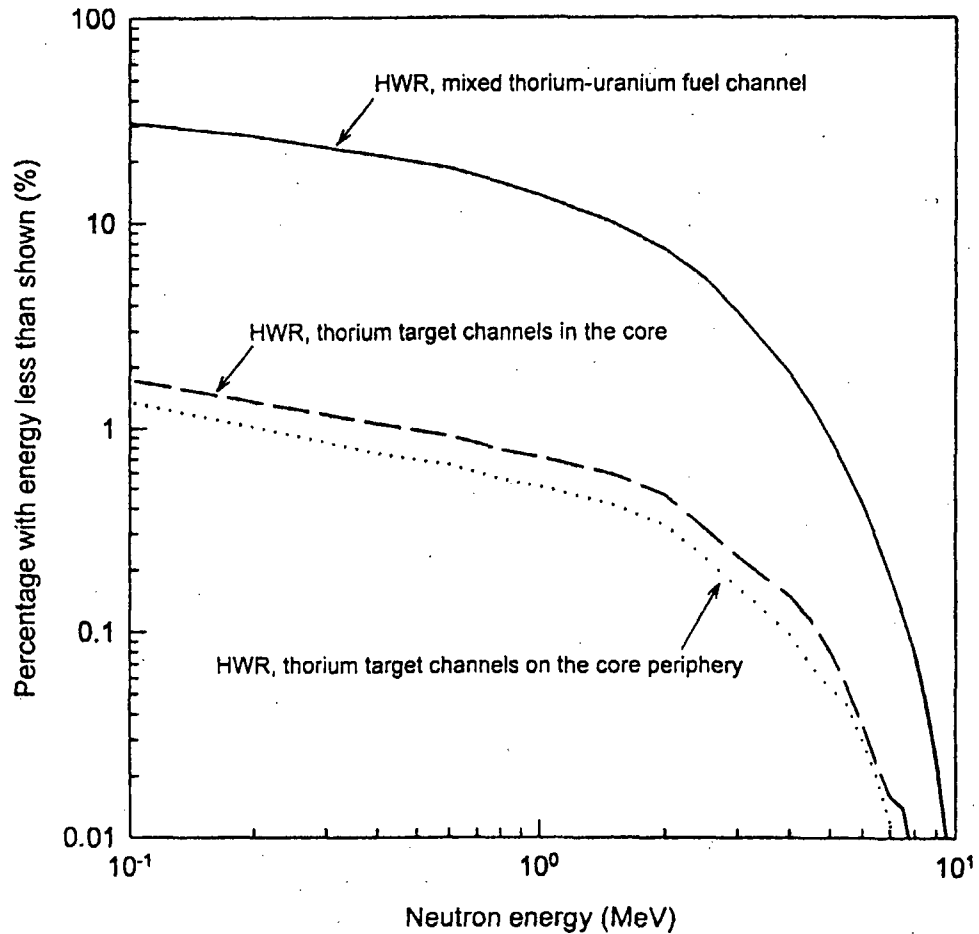


Figure 9b: Neutron-energy spectrum in HWR fuel compared with those in mixed thorium-uranium fuel channel and thorium "target" channels in the core and on the core periphery.

reactors.²⁴ The portions of the neutron fluence above 6 MeV are reduced respectively by factors of about 0.15, 0.3 and 0.15 relative to the fission spectrum. The high-energy fluence is still less in a core location away from the fuel. Figure 9b shows the neutron spectrum in HWR channels filled with thorium "target" assemblies inside and in the periphery of an HWR core compared with the neutron spectrum in a fuel channel. In both cases, the flux in the high-energy tail is reduced by a factor of about 0.01 relative to the fission spectrum. Figure 9c shows the neutron spectrum in an LMFBR radial tho-

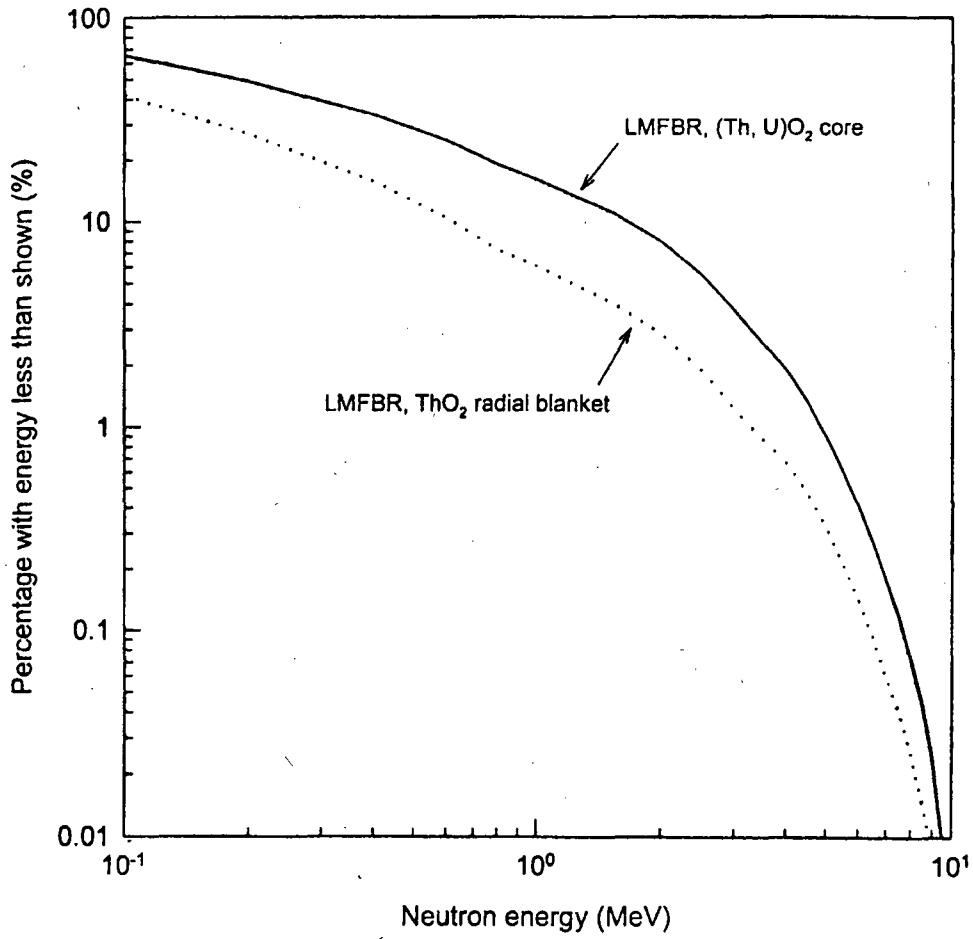


Figure 9c: Neutron-energy spectrum in LMFBR core and radial blanket.

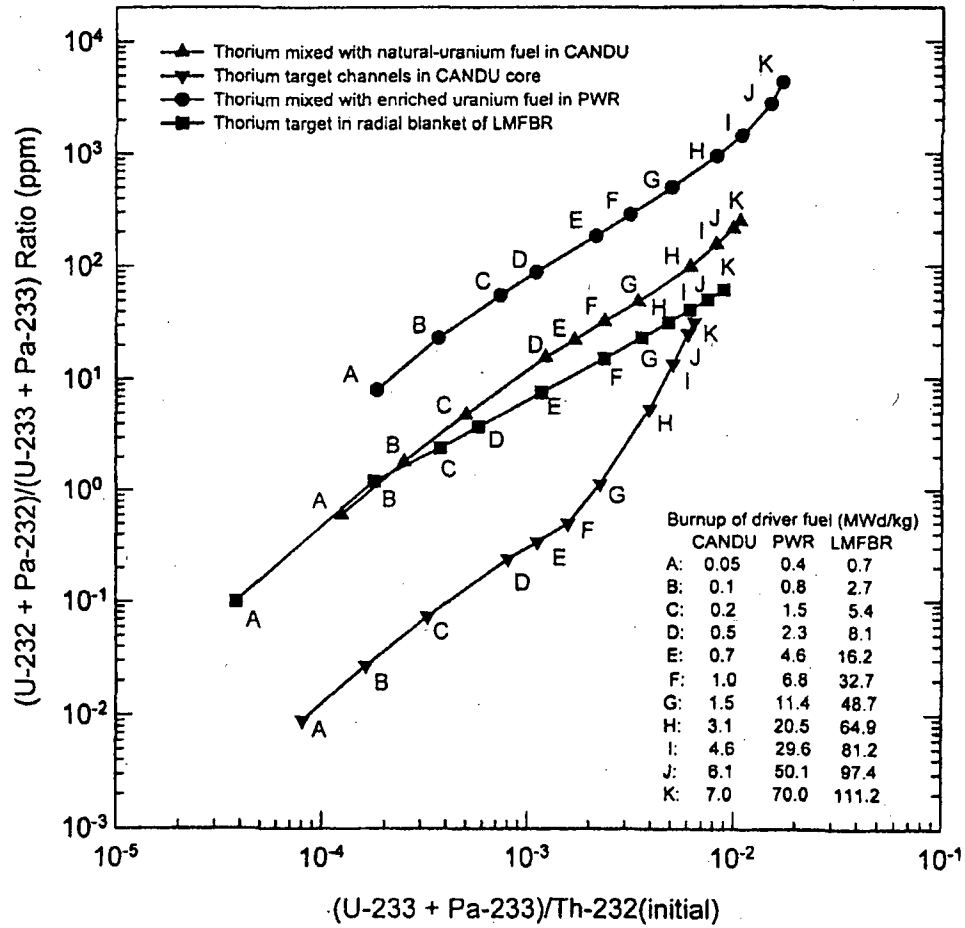


Figure 10: U-232/U-233 ratio as a function of U-233/Th-232 ratio in HWR, PWR, and LMFBFR.

rium blanket compared to that in the core.

Table 3: Percentage of neutron flux in different energy intervals for fission spectrum and in HWR, PWR, and LMFBR fuel and target channels (percent).

Energy interval (in electron Volts [eV], and millions of eV [MeV])	$E \leq 1 \text{ eV}$	$1 \text{ eV} < E \leq 6 \text{ MeV}$	$E > 6 \text{ MeV}$
Fission Spectrum	-	97.4	2.6
HWR			
Mixed Fuel (7% ThO ₂)	41.0	58.0	0.4
Target channel	81.5	18.5	0.02
PWR			
Fuel (70% ThO ₂ , 30% UO ₂)	8.4	90.8	0.8
LMFBR			
Core Fuel (ThO ₂ , UO ₂)	-	99.6	0.4
Radial blanket (ThO ₂)	-	99.9	0.1

Figure 10 shows the U-232/U-233 ratio as a function of the U-233/Th-232 concentration ratio for: U-233 production in: thorium mixed with natural-uranium fuel and in a separate thorium target channel in a HWR; a mixture of 19.5% enriched uranium and thorium in a homogenous PWR core; and in an LMFBR thorium blanket.²⁵

It will be seen that, in general, U-232 contamination of the U-233 increases with burnup, reflecting the fact that two successive neutron captures are required to produce U-232. It will also be seen that contamination levels at comparable U-233/Th-232 ratios are higher for PWR's than in homogeneously fueled HWRs and lower for HWRs in which the thorium is segregated into separate "target" channels and in LMFBR blankets. To first order, these differences are explainable by differences in the presence of high-energy neutrons in the corresponding neutron spectra, as shown in Table 3.

"Clean" U-233 with a low (< 1 ppm) U-232 contamination can be produced in heavy-water reactors in mass fractions up to 0.2 percent in thorium "targets" (see Figure 10). The corresponding mass fraction in which "weapon-grade" (< 6% Pu-240 plutonium) is produced in natural uranium is 0.12 percent (see Figures 11a and 2). However, for a natural-uranium-fuel reactor, the production rate would be limited to about one quarter of that feasible for weapon-grade plutonium (see Figures 2 and 3). Plutonium containing less than 6-percent Pu-240 is considered weapon-grade, although plutonium con-

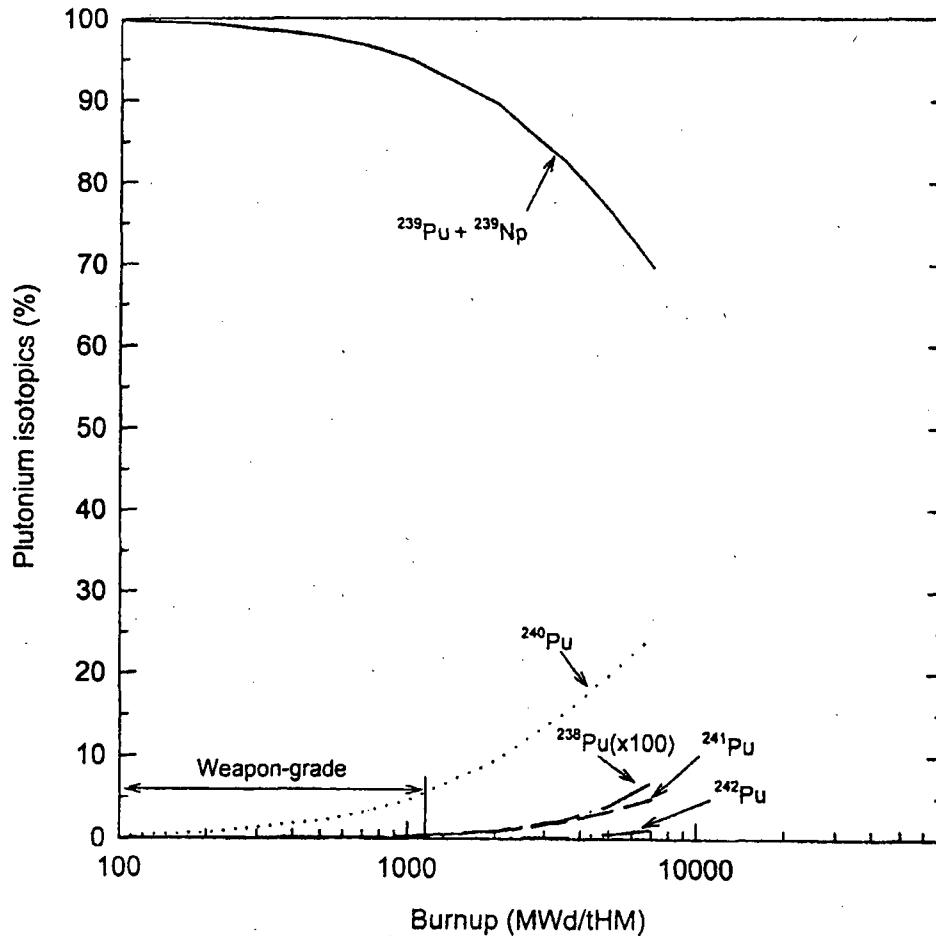


Figure 11a: Plutonium isotopics as a function of burnup in a natural-uranium fueled heavy-water reactor.

taining more Pu-240 is weapons-usable.

For LWRs with feasible target replacement schedules (on the order of ten times the frequency for maximum driver-fuel burnup) the concentration of U-232 will be above 100 ppm. At such contamination levels, remote production operations would be required to produce fuel or weapons on a large scale without incurring large occupational doses. However, it could still be feasible for a highly motivated group to make a few nuclear weapons with this material without remote processing facilities.

The U-232 contamination level in U-233 would reach about 2000 ppm in

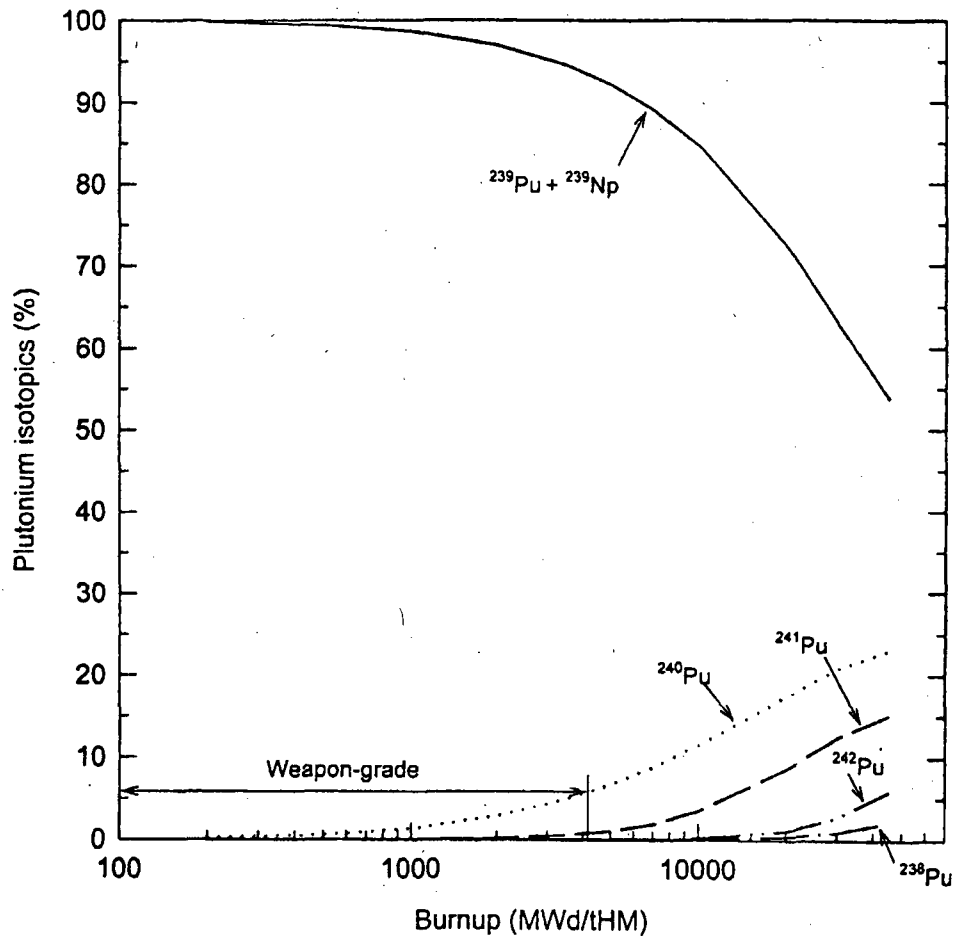


Figure 11b: Plutonium isotopics as a function of burnup in a pressurized light-water reactor (PWR) fueled with 4.5-percent enriched uranium.

LMFBR core fuel in equilibrium recycle.²⁶ The contamination level of the U-233 produced in LWRs fueled with mixtures of enriched uranium and thorium would be still higher but, even at several thousand ppm, the dose rate from a 5-kg sphere of U-233 would be still about an order-of-magnitude lower than that required to achieve the IAEA criterion for self-protection of 100-rem per hour at 1 meter (see Table 2).

For "fresh" U-233, i.e. U-233 cleansed of the U-232 decay product Th-228, more recently than one year, the dose rates would be proportionately smaller. Furthermore, after a U-233 "pit" for a nuclear weapon had been fabricated, it

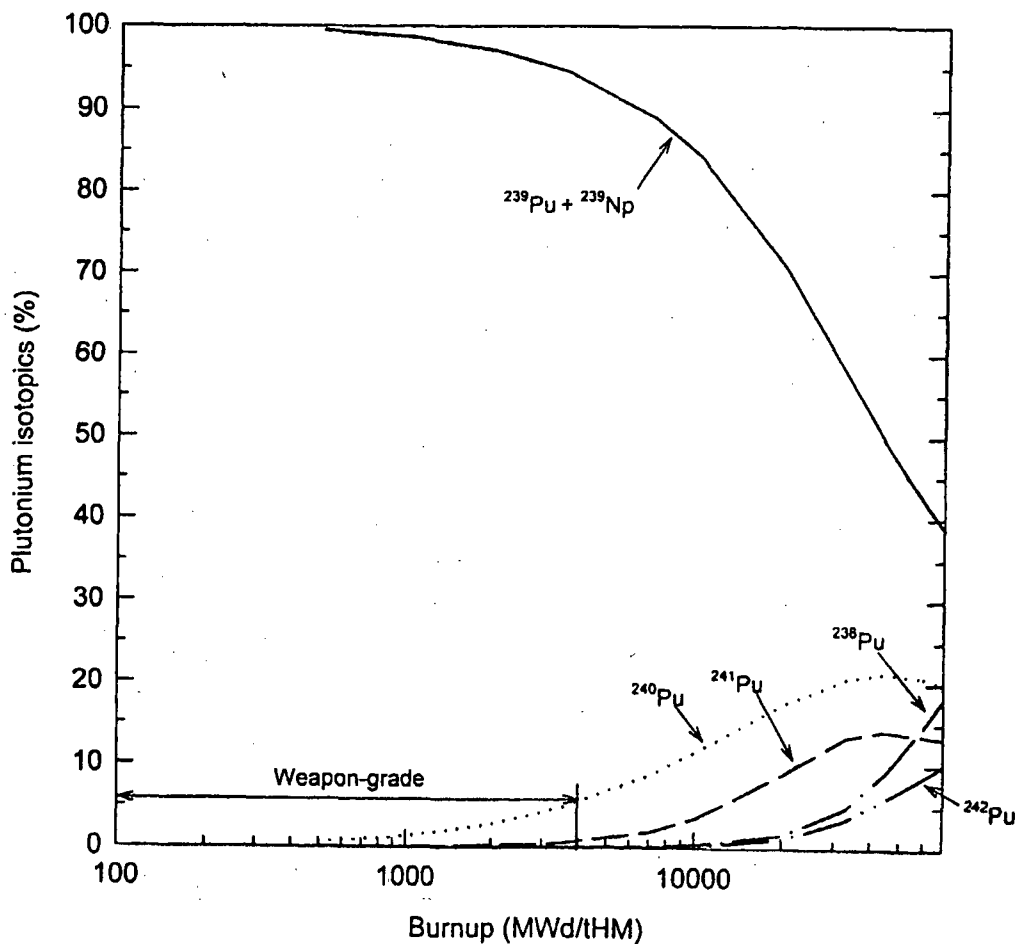


Figure 11c: Plutonium isotopics as a function of burnup in a PWR fueled with a 1:3 mixture of 19.5-percent enriched uranium and thorium.

would be practical to reduce the radiation levels to nearby personnel by an order of magnitude with a portable lead shield if the warhead design were such that the pit was solid and insertable shortly before use. Such designs were standard for safety reasons in early U.S. nuclear bombs.²⁷

Conclusions

On the one hand, gamma radiation from U-232 makes the U-233 from high-burnup U-233-thorium fuel cycles more of a radiation hazard than plutonium. On the other hand, because of its low rate of spontaneous-neutron emission, U-233 can, unlike plutonium, be used in simple "gun-type" fission-weapon designs without significant danger of the yield being reduced by premature initiation of the fission chain reaction.

The necessity for remote handling of heavily U-232 contaminated U-233 in a closed fuel cycle provides a strong incentive for integration of reprocessing and fuel-fabrication. Such integration was envisioned for plutonium breeder reactors in the integral fast reactor proposal.²⁸ In the case of the molten-salt U-233 breeder reactor, it was proposed to have continual chemical processing of a stream of liquid fuel. Such an arrangement also offers a way to completely bypass the U-232 contamination problem because 27-day half-life Pa-233 could be separated out before it decays into U-233.²⁹

In any case, no fuel cycle involving the separation and recycle of U-233 would approach the proliferation resistance of unprocessed spent fuel from which the radiation dose rate is on the order of one thousand rem per hour at one meter for decades after discharge.³⁰

Appendix A: Calculation of U-233, U232 and Plutonium Production using ORIGEN2 and MCNP

The Oak Ridge Isotope Generation and Depletion Code (ORIGEN 2.1) was used to calculate the buildup and depletion of isotopes in reactor fuel and fertile materials. ORIGEN2 is a depletion code using a matrix exponential method to calculate the production, transmutation and decay of nuclides. It is a one-group code, i.e. it comes with nuclear cross-sections which have already been convoluted with the neutron energy spectra of different reactors. A starting mix of isotopes is exposed to this neutron flux and the buildup and depletion of different species is calculated in steps of total fluence corresponding to 60-day time-steps. Many of the plots shown in this paper are obtained from correlations of isotope ratios calculated in this way.

In calculating the production rates of actinides in the fuel of natural-uranium-fueled HWRs and LEU-fueled PWRs, we used the CANDUNAU.LIB and PWRU50.LIB respectively in the ORIGEN2 cross section library. However, for production rates of actinides in thorium bearing fuels and targets in HWRs, PWRs, and LMFBRs, we modified the cross section libraries of CANDUNAU.LIB, PWRD5D35.LIB, and AMO0TTTR.LIB respectively, using set of accurate neutron fluences and one-group cross sections using the MCNP code.

MCNP is a Monte Carlo code that can calculate the transport and interaction of neutrons, photons and electrons in a three dimensional system.

ORIGEN2 was then used to do the buildup and depletion calculations for the isotopes in the fuel. The resultant ORIGEN2 output composition is then incorporated into a new MCNP input and a new set of fluxes and cross sections calculated. The entire cycle is repeated for each time-step.

Appendix B: Calculating one-group transmutation cross-sections using MCNP

MCNP. The neutron energy spectra in different core regions were calculated using simplified core models in MCNP. In this code, a cycle of calculations is initiated by introducing an initial number of neutrons into the reactor fuel with a fission-spectrum energy distribution. The code then follows the trajectory of each neutron, selecting on a random probabilistic basis in steps along the trajectory one of all the possible interactions (including none) that the neutron could have had.

Each neutron is followed until lost by absorption or leakage. Then a new set of neutrons is generated probabilistically at sources determined by reactions [fission or (n, 2n)] associated with the absorption of the first set. Thus the calculation follows the neutrons generation by generation. After a number of generations, the neutron energy and spatial distributions become insensitive to the starting distribution. Output results are then calculated by averaging the results of subsequent generations. We end the calculations when the standard deviations of the statistical fluctuation in the averages being calculated have been reduced to less than 5 percent.

The neutron multiplication factor of an assembly (k_{eff}) is calculated from the average number of neutrons produced per neutron absorbed. The production of specific isotopes per neutron absorbed in, for example, Th-232 is calculated by taking the average of the ratio of the number of atoms of that isotope produced divided by the number of neutrons absorbed in Th-232. Neutron energy spectra are calculated by adding the total path lengths of neutrons in a particular energy interval and dividing by the total neutron path-length. Neutron cross sections are calculated from the number of reactions of a specified type per unit volume (R_i) in a homogeneous region divided by the concentration of the target species (N_t) and by the total neutron path-length L_n per unit volume in that region.

$$\sigma_i = R_i / (N_t L_n)$$

HWR core models. In CANDU HWR cores the fuel is placed in "pressure tubes" carrying pressurized high-temperature heavy water coolant. A 600-MWe CANDU HWR contains 380 fuel channels (see Figure B-1³¹). The pressure tube is surrounded by an insulating, gas-filled gap and "calandria" tube. The calandria tubes are submerged in a large tank (the calandria) of cooled low-pressure heavy water moderator. Each channel contains twelve 50-cm-long fuel bundles.³² Each fuel bundle contains 37 fuel rods, approximately 1.2 cm in diameter. Table B-1 gives the tube and fuel-element dimensions, materials and material densities.

In the MCNP calculations whose results are presented here, the fuel bundle and pressurized heavy water are treated as a homogeneous mix inside the tube and the pressure and calandria tube materials are mixed with the moderator heavy-water outside. The cross-section of the calandria is divided into square cells, as shown in Figure B-1, each of which contains one calandria tube.

In all HWR calculations, the amount of thorium added was limited by the requirement that $k_{\text{eff}} = 1.01$ at a core fuel burnup of 1000 MWd/ton-U. This is one seventh of the typical burnup in HWRs fueled with natural uranium but typical of the burnups used to produce weapon-grade plutonium from natural uranium fuel.³³

Homogeneous-core calculations were done in single-cell approximation (see Figure B-2a). The effect of the surrounding core was simulated by imposing reflecting boundary conditions (i.e. any neutron leaving the cell was replaced by a neutron of the same energy entering at the same point from the adjoining cell with the component of its velocity vector perpendicular to the cell wall reversed). This is a reasonable approximation when the core radius is large measured in cell diameters.

For heterogeneous cores, partial-core models involving multiple cells were used. For cases where fuel and thorium target assemblies were in separate pressure tubes, we did a 3x3 "super-cell" calculation with the thorium cell in the center (see Figure B-2b). The presence of channels surrounding the super-cell was again simulated by making the outer boundaries of the super-cell neutron reflecting.

For the case with thorium channels on the periphery of the reactor, a 95-cell super-cell was used (see Figure B-2c). Here the boundaries adjoining other parts of the core were made reflecting. The boundaries that were outside of the reactor, including, the ends of the cells, were made absorbing, reflecting the neutron leakage from the core.

Table B-1: Heavy-water reactor (CANDU 600) fuel, tube and cell dimensions, materials and densities³⁴

Fuel rods per bundle	37
Uranium enrichment	0.711 w/o (natural)
Fuel pellet diameter	1.217 cm
Cladding thickness	0.041 cm
Cladding and tube material	Zircalloy-4
Pressure tube inside diameter	10.363 cm
Pressure tube thickness	0.419 cm
Calandria tube inside diameter	12.878 cm
Calandria tube thickness	0.156 cm
Tube spacing (square array)	28.575 cm
Length of fuel channel	600 cm
UO ₂ density	10.36 g/cm ³
ThO ₂ density	9.45 g/cm ³
Zircalloy density	6.50 g/cm ³
Coolant (D ₂ O, 561 °K) density	0.81 g/cm ³
Moderator (D ₂ O, 346 °K) density	1.11 g/cm ³

Table B-2: PWR fuel pin and cell dimensions, materials and densities³⁵

Fuel pellet diameter	0.819 cm
Active fuel length	365.8 cm
Uranium enrichment	4.5 w/o
Cladding thickness	0.057 cm
Cladding material	Zircalloy-4
Cell dimension	1.26 x 1.26 cm
UO ₂ density	10.36 g/cm ³
ThO ₂ density	9.45 g/cm ³
Zircalloy density	6.50 g/cm ³
Coolant (H ₂ O, 605 °K) density	0.64 g/cm ³

PWR and LMFBR Core Models

Since fuel pins are closely spaced with no major gaps in PWR (and LMFBR) cores, homogeneous-core calculations were done with a cell including a single fuel pin with its share of surrounding light-water (or sodium) coolant/moderator with a reflecting boundary. The specifications for the pin and cell are shown in Table B-2 (B-3).

Table B-3: 1GWe LMFBR core dimensions, materials and densities³⁶

Radii	
Core	162.2 cm
Radial blanket outer edge	202.5 cm
Shield inner edge	254.6 cm
Heights	
Core	50 cm
Axial blanket	35 cm
Volume ratio (Fuel or target material/ Structure/Coolant)	
Core	40.5/22.4/37.1
Radial blanket	50.5/18.4/37.1
Material	
Fuel	(U,Th)O ₂
Radial and axial blanket	ThO ₂
Heavy metal isotopic ratio of core	
Th-232/U-232/U-233/U-234/U-235	79.31/0.04/17.22/2.98/0.45
(U,Th)O₂ density	9.64 g/cm ³
ThO₂ density	9.45 g/cm ³
Stainless steel (SS-304) density	0.97 g/cm ³
Coolant (Na, 823 °K) density	0.84 g/cm ³

Appendix C : Calculating dose rates using ORIGEN2 and MCNP

We calculated the radiation doses from 5-kg spheres of uranium and plutonium metal of varying isotopic composition (see Table C-1). Given a specified initial mix of radioisotopes, ORIGEN2 calculates, as a function of decay time, the source intensities of spontaneous neutron emissions and gamma-ray emissions – the latter grouped in 18 energy intervals.

This radiation-source data is then used as input to MCNP which performs radiation transport calculations throughout the material yielding the intensities and energy spectra of the gamma-rays and neutrons leaving the sphere. Self-shielding by the human body is simulated by assuming a 10-cm-thick water shield around the sphere. The dose rate at a point 0.5 m from the

sphere surface is then calculated using ANSI/ANS-1991 fluence-to-dose factors.³⁸ Statistics are accumulated until the standard-deviation uncertainty is less than 5 percent. Figure 5a and Table C-2 show the calculated buildup of the dose rates from the 5-kg spheres as a function of time.

Table C-1: Composition of 5-kg U and Pu spherical radiation sources

	Pure U-233	U-233 +1 ppm U-232	Plutonium ³⁹	
			Weapon-grade	Reactor-grade
Density (g/cm ³)	19.05	19.05	19.86	19.86
Sphere radius (cm)	3.97	3.97	3.92	3.92
Isotopic %				
U-232	0.0	0.0001		
U-233	100.0	99.9999		
Pu-238			0.01	1.3
Pu-239			93.80	60.3
Pu-240			5.80	24.3
Pu-241			0.35	9.1
Pu-242			0.02	5.0

Table C-2: Dose rates 0.5 m from surface of 5-kg spheres of U and Pu (mrem/hr)

Source Material	Radiation Type	0 yr	1 yr	5 yr	10 yr	15 yr
U-233 + 0 ppm U-232	Gamma	0.32	0.42	0.84	1.35	1.89
U-233 + 1 ppm U-232	Gamma (from TI-208)	0.32 (0.00)	13.08 (11.12)	35.10 (29.96)	39.57 (33.48)	39.17 (32.64)
Weapon-grade Plutonium	Gamma	0.49	0.71	1.16	1.57	1.84
	Neutron	0.56	0.56	0.56	0.56	0.56
	Total	1.05	1.27	1.71	2.13	2.40
Reactor-grade Plutonium	Gamma (from Am-241)	0.49 (0.00)	5.54 (3.24)	16.72 (14.60)	28.64 (26.00)	37.54 (34.80)
	Neutron	2.66	2.66	2.65	2.64	2.63
	Total	3.16	8.20	19.37	31.28	40.17

NOTES AND REFERENCES

1. Calculations are done with ORIGEN2 (ORIGEN 2.1: "Isotope Generation and Depletion Code Matrix Exponential Method," [Oak Ridge National Laboratory, Radiation Safety Information Computational Center, August 1996]).
2. There are approximately 2.42 neutrons released per thermal-neutron induced fission of U-235. Of these, an average of 1.22 must be absorbed by U-235 to induce a follow-on fission, leaving 1.2 for absorption in U-238, fission products, actinides, structural, moderator and reactivity-control materials, and leakage out of the core. The relatively low light-water reactor (LWR) conversion ratio shown in Figure 2 (i.e. its delivery of a smaller fraction of excess neutrons to U-238) at low burnups reflects the facts that there is a large net flow of neutrons from fresh LWR fuel to fuel assemblies with higher burnups and the greater use of neutron absorbers in PWRs to even out swings in reactivity because they are refueled at annual or longer periods, versus continuous refueling for the HWRs. It also reflects the fact that the neutrons in HWRs are absorbed at lower energies where the fissile material capture cross sections are very high and therefore the competition from absorption on fission products is reduced (0.3 neutrons lost in the PWR vs. 0.08 in the HWR). This is partially offset by the greater absorption in HWR structural materials (0.12 neutrons vs. 0.02 in the PWR), although the absorption is less in the HWR coolant (0.03 vs 0.07 for the LWR). At higher burnups the net production of plutonium falls primarily because a significant fraction of the fissions are in plutonium.
3. Thomas Cochran et al, *U.S. Nuclear Warhead Production* (Ballinger, 1987) pp. 67-70.
4. Plutonium recovered from low-enriched pressurized-water-reactor fuel with a burnup of 33 MWd/kg and stored for 10 years before reprocessing ("Plutonium Fuel: An Assessment" (Paris: OECD/NEA, 1989), Table 9.
5. US Nuclear Regulatory Commission, "NRC Dose Limits" (<http://www.nrc.gov/NRC/EDUCATE/REACTOR/09-DOSESTANDARD/index>).
6. International Atomic Energy Agency, "The Physical Protection of Nuclear Material and Nuclear Facilities," INFCIRC/225/Rev.4 (<http://www.iaea.org/worldatom/program/protection/index.html>). Vomiting would begin within a few hours and a short-term dose of ionizing radiation could be lethal at a whole-body dose of 200 rems. Lethality within 10 days would be virtually certain above 1000 rems (*The Effects of Nuclear Weapons, 3rd edition*, Samuel Glasstone and Philip J. Dolan, eds [US Departments of Defense and Energy, 1977], Table 12.108).
7. R. Chidambaram and C. Ganguly, "Plutonium and thorium in the Indian nuclear programme," *Current Science* 70, January 10, 1996, pp. 21-35.
8. A.M. Bhagwat, K.V. Kamath, K.N. Kutty, G.R. Naik, K.K. Narayan, P.R. Pillai, G.J. Prasad, and C. Ganguly, "Radiological Safety Experience in the Fabrication of Alloy Plate Fuels Bearing ²³³U/Pu," *Nuclear Technology* 103 (August 1993): 246-256. Unfortunately the time since separation of the U-233 was not reported. "Person-rem" denotes the sum of the individual doses incurred by the workers.
9. A.M. Perry and A.M. Weinberg, "Thermal Breeder Reactors," *Annual Review of Nuclear and Particle Science*, 22 (1972): 317-354.
10. See, e.g., J.B. Slater, "An Overview of the Potential of the CANDU Reactor as a Thermal Breeder," (*Atomic Energy of Canada Limited, AECL-5679, 1977*).

11. See, e.g. "Final Environmental Statement, Light Water Breeder Program," (U.S. Energy Research and Development Administration, ERDA-1541, 1976).
12. See e.g. Perry and Weinberg, "Thermal Breeder Reactors."
13. R. Chidambaram and C. Ganguly, "Plutonium and thorium in the Indian nuclear programme."
14. "Thorium based fuel options for the generation of electricity: Developments in the 1990s" (Vienna, IAEA-TECDOC-1155, May 2000).
15. Manson Benedict, Thomas Pigford and Hans Wolfgang Levi, *Nuclear Chemical Engineering*, McGraw-Hill (1981): 367, 377.
16. See e.g. Alex Galperin, Paul Reichert and Alvin Radkowsky, "Thorium Fuel for Light Water Reactors – Reducing Proliferation Potential of Nuclear Power Fuel Cycle," *Science & Global Security* 6 (1997), pp. 265-290 [heterogeneous core]; J. Stephen Herring and Phillip E. MacDonald, "Characteristics of Mixed Thorium-Uranium Dioxide High Burnup Fuel" (Idaho National Engineering and Environmental Laboratory, INEEL/CON-99-00141 preprint, Nov. 13, 1998).
17. C. Rubbia et al, "Conceptual Design of a Fast Neutron Operated High Power Energy Amplifier," CERN/AT/95-44 (ET), 1995 (<http://preprints.cern.ch/cgi-bin/tiff2ps?archive/electronic/cern/preprints/at/at-95-044>); C. Roche and C. Rubbia, "Some Preliminary Considerations on the Economical Issues of the Energy Amplifier," CERN/AT/95-45 (ET) (<http://preprints.cern.ch/cgi-bin/setlink?base=preprint&categ=cern&id=lhc-98-012>).
18. The IAEA considers plutonium containing more than 80 percent Pu-238 to be not weapons usable because of the high heat output of the short-lived (88-year half-life) Pu-238 (560 Watts/kg). However, Pu-238 is produced by neutron capture on Np-237, which is itself produced by two successive neutron captures on U-235 and then U-236. It is therefore impractical to produce Pu-238 in sufficient quantities to denature a significant fraction of the hundreds of tons of currently separated weapon- and reactor-grade plutonium.
19. Calculated using MCNP (MCNP4B2: "Monte Carlo N-Particle Transport Code System," (CCC-660 MCNP4B2, Radiation Safety Information Computational Center, January 1998).
20. For tails assay one quarter to one half of the feed assay. For a common tails assay of 0.3 percent, the ratio is about 0.3.
21. 5.7 MeV for $n + U-233 \rightarrow U-232 + 2n$; 6.3 MeV for $n + Th-232 \rightarrow Th-231 + 2n$.
22. ENDF/B-6.0: <http://hpngp01.kaeri.re.kr/cgi-bin/w3endf/?lab=aa&mt=Th-232%3D102&ax=auto&e0=&e1=&ay=auto&y0=&y1=&sx=&sy=>>, <http://hpngp01.kaeri.re.kr/cgi-bin/w3endf/?lab=aa&mt=Th-232%3D16&ax=auto&e0=&e1=&ay=auto&y0=&y1=&sx=&sy=>>.
23. ENDF/B-6.0: <http://hpngp01.kaeri.re.kr/cgi-bin/CoNquery?nuc=U233>, <http://hpngp01.kaeri.re.kr/cgi-bin/CoNquery?nuc=Th232>.
24. Examples of average neutron-flux levels in the different reactors (in units of 1014 neutrons cm⁻² sec⁻¹) are: CANDU: 2.35, PWR: 3.25, and LMFBR core ((Th,U)O₂): 40.1 and radial blanket (ThO₂): 5.1. (A.G. Croff and M.A. Bjerke, "Once-Through CANDU Reactor Models for the ORIGEN2 Computer Code" [Oak Ridge National Laboratory, ORNL/TM-7177, November 1980]. A.G. Croff et al., "Revised Uranium-Plutonium

Cycle PWR and BWR Models for the ORIGEN Computer Code" [Oak Ridge National Laboratory, ORNL/TM-6051, September 1978]; and A.G. Croff et al., "LMFBR Models for the ORIGEN2 Computer Code" [Oak Ridge National Laboratory, ORNL/TM-7176, October 1981].)

25. The U-232 and U-233 concentrations include respectively the U-232 precursor, Pa-232 (1.3 day half-life), and the U-233 precursor, Pa-233 (27 day half-life). Adding 1 ppm Th-230 to pure Th-232 increases the U-232/U-233 ratios compared to those without Th-230 by 0.04%, 3.5%, 3.3%, and 0.00% respectively, for thorium mixed with HWR natural-uranium fuel, a thorium target in a HWR core, thorium mixed with LEU fuel in a PWR, and thorium in the radial blanket of an LMFBR. In the case of the thorium target and blanket elements, we have assumed residence times in the reactor equal to those of the driver fuels.

26. Croff et al., "LMFBR Models for the ORIGEN2 Computer Code"

27. R.E. Kidder, "Report to Congress: Assessment of the Safety of U.S. Nuclear Weapons and Related Nuclear Test Requirements" (Lawrence Livermore National Laboratory, UCRL-LR-107454, 1991): 6.

28. See e.g. "The Design Rationale of the IFR," D. C. Wade and R. N. Hill, *Progress in Nuclear Energy*, 31, 13 (1997).

29. The designers of the molten-salt breeder reactor planned to do this so as not to lose Pa-233 to neutron capture before it decays into fissile U-233.

30. At 50 years, the dose rate is about 1000 rem/hr 1 meter from the mid-point of a spent PWR assembly and about 400 rem/hr 1 meter from the end (Dose Rate Estimates from W.R. Lloyd, M.K. Sheaffer and W.G. Sutcliffe "Irradiated Light-Water-Reactor Fuel Assemblies in Air" [Lawrence Livermore National Lab, UCRL-ID-115199, 1994]).

31. "A Study on the Direct Use of Spent PWR Fuel in CANDU Reactors: Fuel Management and Safety Analysis," (Korea Atomic Energy Research Institute, KAERI/RR-1345/93, 1994).

32. K.M. Wasywich, "Characteristics of Used CANDU Fuel Relevant to the Canadian Nuclear Fuel Waste Management Program," AECL-10463, COG-91-340, May 1993.

33. Because a CANDU can be refueled during operation, an average burnup of 1000 MWd/t-U would correspond to a discharge burnup of 2000 MWd/t-U.

34. C.E. Till and Y.I. Chang, "CANDU Physics and Fuel Cycle Analysis," (Argonne National Laboratory, RSS-TM-2, May 1977); C.A. Bollmann et al., "Environmental and Economic Performance of Direct Use of PWR Spent Fuel in CANDU Reactors," (Department of Nuclear Engineering, MIT, MIT-NFC-TR-014, June 1998).

35. J.W. Roddy et al., "Physical and Decay Characteristics of Commercial LWR Spent Fuel," (Oak Ridge National Laboratory, ORNL/TM-9591/V1, October 1985); J.S. Herring and P.E. MacDonald, "Characteristics of Mixed Thorium-Uranium Dioxide High-Burnup Fuel," June 1999 (Idaho National Engineering Laboratory, INEEL/CON-99-00141).

36. H. Matsumoto et al., "Improvement of the Prediction Accuracy of LMFBR Burnup Properties," Proceedings of International Conference on Fast Reactors and Related Fuel Cycles; FR'91, October 28 – November 1, 1991, Kyoto, Japan; A.G. Croff et al., "LMFBR Models for the ORIGEN2 Computer Code" (Oak Ridge National Laboratory, ORNL/TM-7176, October 1981).

37. H. Matsumoto et al., "Improvement of the Prediction Accuracy of LMFBR Burnup Properties," *Proceedings of International Conference on Fast Reactors and Related Fuel Cycles, FR'91*, October 28 – November 1, 1991, Kyoto, Japan.
38. "American National Standard for Neutron and Gamma-Ray Fluence-to-Dose Factors" (American Nuclear Society, ANSI/ANS-6.1.1, 1991).
39. The isotopic compositions of WGPu and RGPu are before the decay of 14-year half-life Pu241 to Am241 begins, "Management and Disposition of Excess Weapons Plutonium: Reactor-Related Options" (Academy Press, Washington, D.C., 1995), Table 2.2.

Rulemaking Comments

From: elling@torium.se
Sent: Thursday, July 03, 2008 12:34 PM
To: Rulemaking Comments
Subject: DCThMSR 2/3
Attachments: Appendices-2_5_18_19.zip

Dear Sir,

referring to the NRC-2008-0237, Thorium ElectroNuclear AB, based in Stockholm Sweden, submits comments for the Double Cylinder Thorium Molten Salt Reactor.

The DCThMSR is protected by Patent Pending. The patent text is not enclosed but scientific publications would describe it adequately.

This is email 2 of 3.

Pls acknowledge.

Kind regards
Elling Disen
elling@torium.se
Founder
Thorium ElectroNuclear AB
www.torium.se

Received: from mail1.nrc.gov (148.184.176.41) by TWMS01.nrc.gov
(148.184.200.145) with Microsoft SMTP Server id 8.0.751.0; Thu, 3 Jul 2008
12:37:55 -0400

X-Ironport-ID: mail1

X-SBRS: 1.6

X-MID: 27110647

X-IronPort-AV: E=Sophos;i="4.27,742,1204520400";
d="pdf?zip'48?scan'48,208,48";a="27110647"

Received: from pne-smtpout1-sn1.fre.skanova.net ([81.228.11.98]) by
mail1.nrc.gov with ESMTP; 03 Jul 2008 12:35:51 -0400

Received: from [192.168.1.113] (81.233.0.25) by
pne-smtpout1-sn1.fre.skanova.net (7.3.129) id 47A9795002AA3A6D for
Rulemaking.Comments@nrc.gov; Thu, 3 Jul 2008 18:35:45 +0200

Message-ID: <486CFF5C.7050000@torium.se>

Date: Thu, 3 Jul 2008 18:33:32 +0200

From: "elling@torium.se" <elling@torium.se>

User-Agent: Thunderbird 2.0.0.14 (Windows/20080421)

MIME-Version: 1.0

To: Rulemaking.Comments@nrc.gov

Subject: DCThMSR 2/3

Content-Type: multipart/mixed;

boundary="-----000805030205070609070000"

Return-Path: elling@torium.se

: Materials Issues for Generation IV Systems: Status, Open Questions and Challenges

Editor(s): (a) Véronique GHETTA, (b) Dominique GORSE, (c) Dominique MAZIERE, (d) Vassilis PONTIKIS

Publisher : SPRINGER

Date of Publication : 2008, April

**COMBINED EFFECT OF MOLTEN FLUORIDE SALT AND
IRRADIATION ON NI-BASED ALLOYS**

SHORT TITLE: EFFECT OF MOLTEN SALT AND IRRADIATION

A.S. BAKAI*

*Kharkiv Institute of Physics and Technology,
61108, Kharkiv, Ukraine**Tel./fax: +380 57 3350854. e-mail: bakai@kipt.kharkov.ua.

Abstract. Results of investigations of combined effect of molten fluoride salt and electron irradiation on structure, mechanical properties and corrosion of Ni-based alloys are reviewed.

Keywords: molten salt reactor; Ni-based alloys; electron irradiation test facility; microstructure; corrosion; mechanical properties

1. Introduction

Fluoride molten salts (MS) are considered as means of heat and/or fuel transport in Generation IV (G-IV) nuclear reactors. Fluid fuel in form of fissile and fertile materials dissolved in MS is promising fuel for both MS reactors and subcritical accelerator driven systems. MS also can serve as a coolant of high-temperature low pressure systems.

It is commonly believed that Ni-Mo alloys (the Hastelloys) are proper construction materials for MS transportation pipes. The Hastelloy N (see Table 1) was successfully used in the molten salt reactor experiment (Haubereich and Engel, 1970) but the experiment duration time was in order of magnitude less than a reasonable time of G-IV reactor operation. Since that time corrosion tests of Ni-Mo alloys of different compositions were performed in loops without irradiation (DeVan, 1969, Ignatiev et al., 2006). These tests were focused on investigation of role of different dopants on the corrosion rate. In part, it was revealed that small amount of Nb (0.5÷2wt%) depresses the corrosion of alloys in fluoride MS.

Since corrosion is result of transport and dissolution of the alloy components in MS, impact of irradiation on the corrosion is considerable for two reasons. First, irradiation increases the chemical reaction rates within

the salt-alloy interface. Second, irradiation accelerates the bulk diffusion due to generation of point defects. Therefore one can expect that corrosion of alloys under irradiation can dramatically differ from those without irradiation. It has to be noted that microscopic mechanisms of the structural and compositional changes of Ni-Mo alloys in the molten salts under and without irradiation were never studied in detail. Very scant information about precipitations and heterogeneities of these alloys is available.

Experiments using reactor irradiation are rather expensive. For this reason the idea to simulate the reactor irradiation by accelerated electrons or ions is in use for a long time. Evidently, the electron (e) irradiation is an efficient tool to impact the corrosion process due to enhancement of the interface corrosion kinetics. But it is less efficient in simulation of the bulk effects of reactor irradiation. Therefore an important issue is corresponding data of the simulative tests under e -irradiation to the results of reactor irradiation. To solve this problem both reactor tests and computer simulations can be used.

In this lecture I present a review of results of the corrosion tests of Ni-Mo alloys of two compositions (with and without Nb) under and without electron irradiation at $T = 660^\circ\text{C}$. Partially the results obtained were published in the special issue¹ "Materials for molten salt reactors" (Guest eds. A.S. Bakai and F.A. Garner) and reviewed by Azhazha et al. (2005a).

Results of extensive simulations determining quantitative irradiation characteristics of both 10 MeV electrons and MS reactors (MSR) with different neutron spectra are given, too. These results allow to judge about suitability of the simulation experiment data.

2. Methodology

2.1. ELECTRON IRRADIATION TEST FACILITY (EITF)

Specific features of the electron irradiation which are relevant to these investigations are the following:

1. Because energetic thresholds of nuclear reactions induced by electrons and γ -quanta are ~ 10 MeV, use of the electron beams of 10 MeV energy does not induce considerable radioactivity in the irradiated materials. For this reason hot cells are not needed in post-irradiation investigations.

¹ *Problems of Atomic Science and Technology. Ser.: Radiation Damage Physics and Radiation Materials Science*, No. 4(87), 2005, available online at <http://vant.kipt.kharkov.ua>.

2. The penetration depth of electrons with 10 MeV energy is of the order of several centimeters. On this length scale the electron energy decreases from 10 to ~1 MeV or less due to bremsstrahlung and other inelastic energy-loss processes. Therefore, on one hand, the test ampoules can have reasonable sizes to mimic large scale experiments and, on the other hand, the irradiation conditions change strongly over a comparatively small length. Therefore we can use many specimens of sub millimeter thickness within one ampoule to investigate the dependence of corrosion and radiation damage processes versus energy deposited by e^- and γ fields.
3. The electron beam can be used as an efficient heater of the irradiated target, to maintain a desired temperature if the electron beam power, target geometry and construction are chosen properly.

The EITF test bench construction (Azhazha et al., 2005b) is shown in Fig. 1. It was designed taking into account calculations of the e^- and γ fields as well as calculations of the thermal balance and temperature field (Bakai et al., 2005a, 2005b).

2.2. SIMULATIONS OF THE ELECTRONS AND GAMMA FIELDS AND DEPOSITED ENERGY DISTRIBUTION.

The e^- and γ radiation fields, the profiles of deposited energy E_{dep} in salt and samples, as well as the point defect generation in alloy have been calculated by using radiation transport codes in the test bench geometry (Bakai et al., 2004, 2005a, 2007). A novel computer code RaT (Dyuldya et al., 2006) based on the CERN GEANT4 Monte Carlo toolkit (Agostinelli et al., 2003) was used for this simulation. The results of simulations are needed for optimization of the ampoule construction, as well as for obtaining quantitative dependencies of the specimen properties on the dose.

2.3. TEMPERATURE DISTRIBUTION

Equations of the heat balance, taking into account the integral deposited energy and the radiant heat from the surface, is the basis for estimation of the temperature balance of the total irradiated target. To calculate the temperature field within an ampoule the deposited energy distribution and heat transport equations have to be deduced and solved (Bakai et al., 2005b). The temperature distribution is an important characteristic of the irradiated target. In our experiments the goal was to make this distribution as homogeneous as possible.

2.4. MECHANICAL TESTS

Macroscopic mechanical properties are changing due to the influence of the molten fluoride salts and irradiation. These changes are caused by microstructural alternations, primarily by alternations of the grain boundaries and dislocation system, as well as by compositional heterogeneities induced by radiation. Along with the standard mechanical tests (Azhazha et al., 2005c), microindentations and nanoindentations of the materials in the vicinity of surface and in bulk were performed. Nanoindentation allows to measure the local value of Young modulus which is sensitive to local compositional and microstructural changes (Azhazha et al., 2005d).

2.5. STRUCTURE AND COMPOSITION INVESTIGATIONS

Compositional and phase changes in specimens are responsible for changes of mechanical properties and corrosion. The microstructure was characterized by high resolution TEM in a Philips CM30 microscope operating at 300 kV. For microchemical analysis, a 3D LEAP3000 (Imago Scientific Instruments) and 3DAP tomograph (APT, Cameca) were employed. The atomic absorption analysis was performed on a Pionicum SP-9 spectrophotometer. The IR spectroscopic investigations were made on a Specord 80M instrument, while X-ray microanalysis and visual control of the state of the sample surface was determined on a REM-101M scanning electron microscope-microanalyzer. Secondary ion mass spectrometry (SIMS) also was used to detect compositional changes in surface layers of tested samples (Azhazha et al., 2005e, 2005f).

2.6. CORROSION TESTS

The corrosion of alloys and in the molten eutectic sodium fluoride-zirconium fluoride mixture without and under irradiation has been studied by cyclic voltammetry, X-ray analysis, scanning electron microscopy and metallography. Impact of small addition of La in the molten salt on the alloy corrosion was investigated, too. The corrosion rates of the samples exposed in salt at 650°C for different times and deposited energy doses were measured afterward in fresh molten salt by the voltammetric method (Azhazha et al., 2005d; Bakai et al., 2005c).

2.7. ROENTGEN SPECTROSCOPY

After irradiation by 10 MeV electrons a small amount of nuclear reactions happens, leading to formation of γ -active nuclei. Therefore a possibility ex-

ists to reveal products of alloy corrosion in molten salt under irradiation. In spite of the fact that this method does not produce a proper quantitative compositional analysis it does provide both semiquantitative and qualitative information (Bakai et al., 2005d).

2.8. THEORETICAL MODELS

For quantitative analysis of the experimental data theoretical models developed to describe corrosion kinetics and phase transformation kinetics (Bakai et al., 2005e; Bakai et al., 2005f).

3. Materials and Electron Irradiation Test Facility

3.1. TESTED MATERIALS

3.1.1. Fluoride salts.

Purified ZrF_4 (51mol%)- NaF (49mol%) mixture which is molten at 650°C was used in experiments. To investigate impact of the lanthanide impurities on the alloy corrosion, La additions were used in one of the experiments.

3.1.2. Ni-Mo alloys

Ni-Mo alloys showed a satisfactory corrosion resistance in contact with molten fluoride salts and ZrF_4 - LiF - BeF at temperatures 600÷800°C (DeVan, 1969; Haubereich and Engel; 1970; Novikov et al., 1990). It was revealed that comparatively small compositional changes of alloys can lead

Table 1. Compositions (wt%) of Hastelloy type Ni-Mo alloys for G-IV MSR applications.

	ORNL Hastelloy N		IAE	SKODA	KIPT fabricated alloys	
	standard	modified	HN80MTY	MONICR	alloy A	alloy B
Ni	base	base	base	base	78.15	78.10
Mo	15÷17	12	11÷12	15.8	11.70	11.70
Cr	6÷8	7	5÷7	6.85	6.70	6.20
Fe	4÷6	0.5	1.5	2.27	1.50	1.50
Al	—	—	0.8÷1.2	0.02	0.83	0.83
Mn	0.5	0.2	0.5	0.037	0.50	0.50
Nb	—	1÷2 ¹	—	<0.01	—	0.50
Ti	—	≤2 ¹	0.5÷1	0.026	0.47	0.47
Si	0.05	0.1	0.1	0.13	0.15	0.15
Y	—	—	—	—	—	0.05
C	0.05	0.05	0.04	0.014	—	—

¹ different Nb-to-Ti ratios are considered having the total (Nb+Ti) share less then 2wt%.

to considerable decrease or increase of the corrosion resistance. For example alloying with a few percent of Nb improves the corrosion resistance of the alloy. Taking these results as a starting point and background, two compositions the Hastelloy type (alloy A and alloy B, see Table 1) were designed from components of high purity (Azhazha et al., 2005g).

Purification of the components allows to exclude impact of uncontrolled impurities. Composition of prototype alloys of Hastelloy family investigated earlier are also presented in Table 1. The alloys were homogenized at 1100°C for 1 h and aged at 675°C for 50 h. One can see that alloy B differs from alloy A only by additions of Nb (0.5wt%) and Y (0.05wt%). Comparatively small amounts of these additions allows to judge the sensitivity of the alloy properties to dopants.

3.2. ELECTRON IRRADIATION TEST FACILITY.

EITF has been constructed and built at Linac-10 electron linear accelerator in NSC-KIPT (see Fig. 1). Schematically construction of the ampoule containing specimens in fluoride salt is shown in Fig. 2.

A container assembly consists of 16 ampoules made of the C-C composite. Ampoules hold specimens embedded in fluoride salt. The assembly was disposed in a water cooled chamber in Ar atmosphere.

Electron beam of 10 MeV energy and up to 1 mA of average current (up to 1 kW of power) was in use. The electron beam was scanning over the chamber inlet window. The container assembly temperature was monitored with three thermocouples. The temperature is kept to be $(660 \pm 20)^\circ\text{C}$ and controlled by the beam current.

4. Results

4.1. COMPUTER SIMULATIONS

Geant4.8.0 based code RaT (Dyuldya et al., 2006) was developed and systematically used for these purposes. The code inherits a Geant4 framework for 3D Monte Carlo modeling of radiation (e^\pm , γ , n , p , d , t , α , ^3He , heavy ions) transport in multicomponent heterogeneous media, and extends Geant4 with problem-oriented physical models and methods of scoring of the derived physical quantities relevant to nuclear engineering and materials science calculations. Particularly, it implements the methods of nuclear heating and primary radiation damage rates calculations as well as the reactor neutronics specific methods based on the evaluated nuclear data driven

models. The RaT code is continuously benchmarking against the state-of-the-art nuclear codes such as MCNP(X), TART, and KENO.

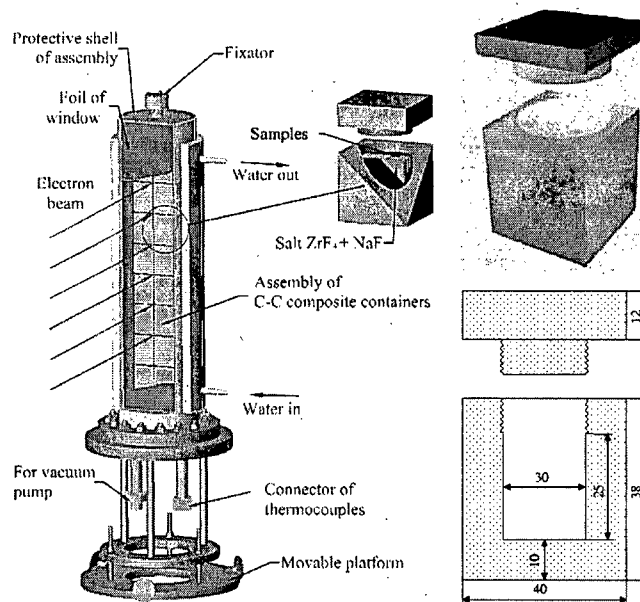


Fig. 1. Construction of the EITF-KIPT container assembly (CA) and ampoules.

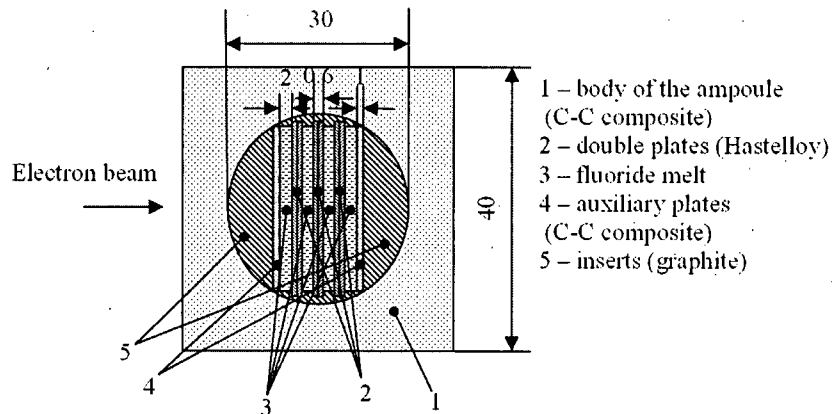


Fig. 2. Top view of the filled ampoule loaded with Ni-Mo alloy specimens.

4.1.1. EITF experiment simulation

The specific requirement of the EITF experiment consisted in total utilization of the linac beam power and in obtaining of substantially different irradiation loads at successive MS–alloy interfaces concerning both energy deposition and point defects production rates. Various ampoule designs and arrangements of specimens were simulated to optimize the experimental setup (Bakai et al., 2004, 2005a) exactly reproduced by the RaT 3D computer models. Depth profiles of (e^\pm, γ) fluxes, energy deposition and alloy dpa rates were built with 50 μm resolution over a beam penetration path.

Preliminary optimization calculations were carried out for nominal EITF beam parameters, a monoenergetic 10 MeV, $i=1.25 \mu\text{A}/\text{cm}^2$ e -beam, and for $\sim 2 \cdot 10^{19} e^-/\text{cm}^2$ projected fluence. It has been shown that at optimal setup the specific deposited energy at different MS–alloy interfaces varies from 5066 down to 64 eV/atom while the point defects concentration decreases from $2.12 \cdot 10^{-3}$ to $4.42 \cdot 10^{-6}$ dpa (Bakai et al., 2005a).

Monitored in course of the EITF experiment e -beam parameters differ from the nominal ones. The Linac-10 irradiation mode (Azhazha et al., 2005b) kept the average beam current $i = 520 \mu\text{A}$ resulted in $1.625 \mu\text{A}/\text{cm}^2$ target front face current density; the total fluence over a 700 h long irradiation reached $2.56 \cdot 10^{19} e^-/\text{cm}^2$; the beam energy spectrum had a sharp peak at 9.6 MeV, and a tail spreading up to 12 MeV. These parameters were applied (Bakai et al., 2007) to get the revised EITF irradiation environment.

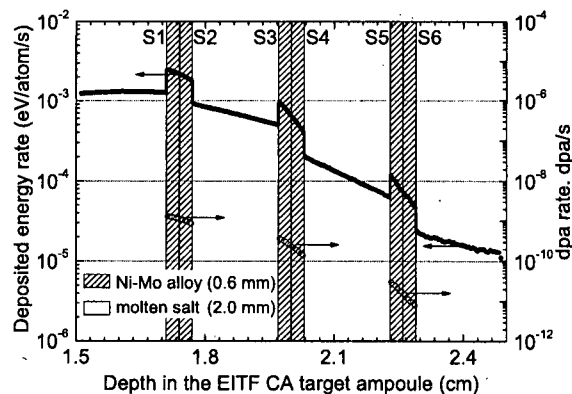


Fig. 3. Depths dependencies of the deposited power (close markers) and the Ni–Mo alloy A dpa rate (open markers) in the vicinity of the loaded EITF target ampoule. The positions S1–S6 enumerate the successive interfaces of alloy specimens with molten fluorides.

Results of the EITF irradiation environment simulations using the monitored parameters of irradiation are shown in Fig. 3. From front (S1) to the last (S6) MS–alloy interface the deposited energy decreases by 51 times

(from 6192 down to 121 eV/atom), the absorbed dose falls from ≈ 10 GGy down to ≈ 0.2 GGy in both alloy and melt, and the primary damage decreases by 165 times from $3.31 \cdot 10^{-3}$ dpa down to $2.01 \cdot 10^{-5}$ dpa.

The deposited energy and dpa profiles calculated for Ni–Mo alloys A and B agree within the limits of the Monte Carlo statistical error ($\leq 0.5\%$). Therefore, the difference of alloys compositions (see Table 1) is too weak to affect the electron beam energy deposition and displacement of atoms.

In the front specimens the irradiation effects are due to energy losses of primary beam electrons while in the last samples the contribution of secondary bremsstrahlung γ -quanta dominates. The contribution of photonuclear reactions into the energy deposition and damage is found as marginal ($< 0.1\%$ of totals) though the alloy and salt γ -activation mainly with the long-lived ^{57}Co and ^{95}Zr radionuclides, respectively, was revealed by the Roentgen spectroscopy (Bakai et al., 2005d), and accounted in simulations.

As a whole, the computer simulation results show that the strongly variable rates of major factor controlling the alloys corrosion, the energy deposition and primary damage, have been achieved in the EITF experiment. The data are useful for quantitative investigation of the Ni–Mo alloy structure and properties evolution under irradiation. Besides, it allows to expect the EITF irradiation capability to simulate different conditions of irradiation of alloys in molten salt reactors.

4.1.2. Correlation with MSR irradiation environment conditions

Obviously the irradiation environments of MS reactors are essentially differing from electron beam irradiation both in nature and intensity. In MSR Ni–Mo alloys are exposed to coupled (n, γ) irradiation, for alloys contacted with fissile MS fuel the impact of fission fragments on surface layers is significant (McCoy, 1978). An issue of big importance is the investigation of applicability of the EITF test data for prognoses of alloys behavior in MSR.

To simulate reactor radiation fields the “effective medium” model with homogeneously mixed MS fuel and graphite moderator was used (Bakai et al., 2007). The fuel enrichment was systematically adjusted to make a system critical. It ensures the correct ratio of correlated (n, γ) fluxes as well as the appropriate fission density. The MSR radiations source strength scales with its power, and was normalized to the realistic estimate of a total neutron flux $\phi_0 = 10^{15} \text{ cm}^{-2} \cdot \text{s}^{-1}$ in a core.

Calculations have shown that the neutron and photon energy spectra in MSR are sensitive to the “moderator-to-fuel” ratio C/MS used as a core design parameter. As C/MS increases, the successive transition from the unmoderated (mainly epithermal) neutronics toward that of highly moderated thermal MSRs is observed (see Fig. 4). In line with the results of the MCNP

code simulations of MSR cores (Merle-Lucotte et al., 2007), it is peculiar to various concepts of Uranium and Thorium based molten salt reactors.

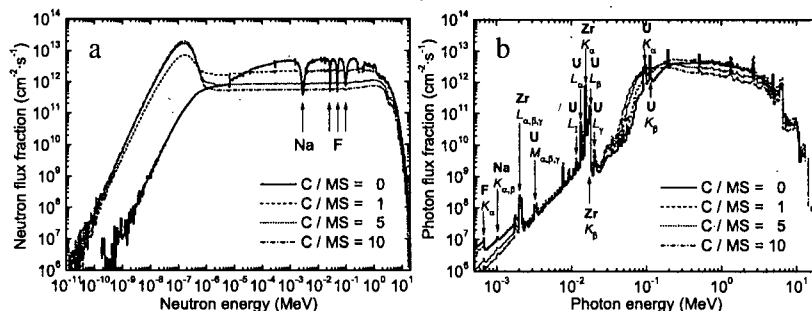


Fig. 4. Energy-weighted neutron (a) and photon (b) spectra (normalized to the total neutron flux $\phi_n = 10^{15} \text{ cm}^{-2} \cdot \text{s}^{-1}$) of critical MSR cores with different moderator-to-fuel (C/MS) ratios.

Effect of the alloy on the (n, γ) fluxes was neglected. The calculations of the Ni–Mo alloys engineering responses were performed within the kerma approximation (Abdou et al., 1975) for energy deposition (nuclear heating), and the NRT standard (Norgett et al., 1975) damage energy model for radiation damage of alloys. Kerma factors $k_{n, \gamma}(E_{n, \gamma})$ and damage-energy cross sections σ_D (the material dependent parameters that correlate nuclear responses to fluxes) were calculated using the RaT code. It has been found that the energy dependencies of these parameters of KIPT fabricated alloys A and B in average differ not more than by 0.6%, and small doping by Nb and Y is insignificant in respect to alloys nuclear responses.

The code also calculated optional contributions of fission fragments using the simulation of depth profiles of energy deposition and damage produced in the vicinity of the MS–alloy interface by heavy ions from MS fuel.

The simulation results depicted in Fig. 5 show that for alloy–fuel interfaces fission fragments make major contributions to both energy deposition and damage of thin ($\sim 1 \mu\text{m}$) surface layers. For interfaces with non-fissile salts (coolants), gamma heating and neutron damage are predominant.

Generally, the EITF related energy deposition rates correspond to MSR irradiation environments with neutron fluxes $\phi_n \sim 10^{14} \div 10^{15} \text{ cm}^{-2} \cdot \text{s}^{-1}$ (see Fig. 5a). One can conclude that the EITF is capable to simulate the energy deposition in Ni–Mo alloys embedded into the MS media for wide range of irradiation conditions they would experience in MSRs. The damage rates at EITF amount only to $10^{-2} \div 10^{-4}$ of those of MSR environments (see Fig. 5b), and are comparable only with MSR related gamma damage that is marginal ($\leq 0.01\%$) as compared with the neutron induced dpa rates. The EITF experiments can reproduce the alloy damage rates for low ($\sim 10^{10 \div 12} \text{ cm}^{-2} \cdot \text{s}^{-1}$)

neutron fluxes unrealistic for core devices but more relevant to MSR vessel and piping.

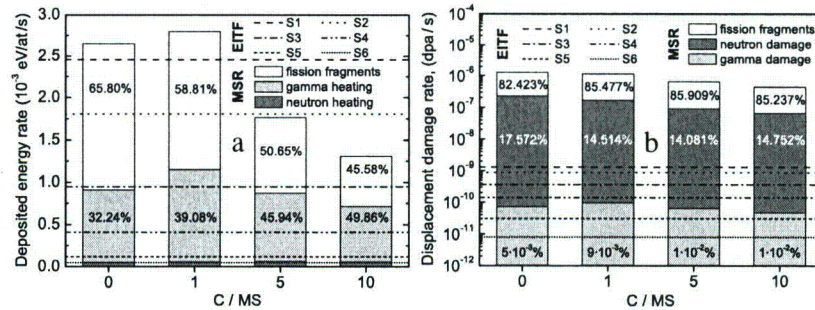


Fig. 5. The rates of the energy deposition (a) and the point defects (NRT dpa) production (b) in the Ni-Mo alloy A calculated for 10^{15} $\text{cm}^{-2}\cdot\text{s}^{-1}$ neutron irradiation in MSRs with different moderator-to-fuel (C/MS) ratios in comparison with the EITF electron beam deposited energy and damage rates at different MS-alloy interfaces S1÷S6 (see Fig. 3).

4.1.3. Temperature field

Equation of the heat balance taking into account the integral deposited energy (see Section 4.1.1), and the heat irradiation from the surface is a base for estimation of the temperature balance of irradiated target in total. To calculate temperature field within an ampoule, the deposited energy distribution and heat transport equations were deduced and solved (Bakai et al., 2005b). The temperature distribution is an important characteristic of the irradiated target. In our experiments the goal was to make this distribution as homogeneous as possible. The calculations performed show that the temperature variance within the ampoule core is really small (660 ± 20)°C.

4.2. ALLOYS: STRUCTURE, COMPOSITION, PRECIPITATES

4.2.1. Metallography

Metallography and scanning electron microscopy (SEM) was used to reveal macroscopic structural changes of the tested specimens in molten salt under irradiation.

Unirradiated specimens of alloy A show no noticeable changes of the surface layer while some compositional changes up to 2 μm depth were revealed (Azhazha et al., 2005e; Bakai et al., 2005c). As the measurement of the corrosion rate of this alloy show (see Sec. 4.4.1) that after 700 h of exposure it becomes rather low ($\sim 2 \times 10^{-4}$ mm/yr). Thus the alloy A possesses

an excellent corrosion resistance in fluoride MS without irradiation. It is believed that the alloy has the same corrosion rate with irradiation.

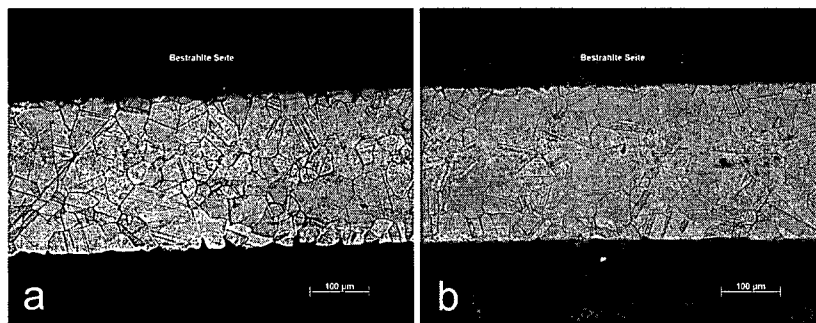


Fig. 6. Structure of the alloy A after 700 hr exposure in the molten salt under irradiation at $T = 650^{\circ}\text{C}$ with the deposited energy $E_{\text{dep}} = 6192 \text{ eV/atom}$ (a) and $E_{\text{dep}} = 121 \text{ eV/atom}$ (b). Corrosion and precipitates within boundaries are larger at $E_{\text{dep}} = 6192 \text{ eV/atom}$.

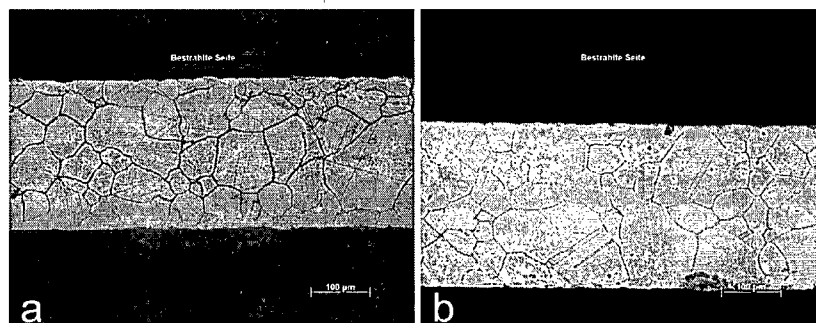


Fig. 7. Structure of the alloy B after 700 hr exposure in the molten salt under irradiation at $T = 650^{\circ}\text{C}$ with the deposited energy $E_{\text{dep}} = 6192 \text{ eV/at}$ (a) and $E_{\text{dep}} = 121 \text{ eV/at}$ (b). No considerable corrosion is seen.

Metallography of irradiated specimens in salt are shown in Fig. 6 and Fig. 7 (Azhazha et al., 2005a; Wanderka et al., 2005). It is seen that the surface layer of specimens of the alloy A irradiated in the molten salt for 700 h at $T = 650^{\circ}\text{C}$ (Fig. 6) are corroded. The depth of intercrystalline corrosion essentially depends on the deposited energy. The depth is $25\div 30 \mu\text{m}$ at $E_{\text{dep}} = 6192 \text{ eV/atom}$ and $5\div 10 \mu\text{m}$ at $E_{\text{dep}} = 121 \text{ eV/atom}$.

No considerable intercrystalline corrosion of specimens of alloy B is visible at high and smaller values of the deposited energy (see Fig. 3) in spite the corrosion rate at $E_{\text{dep}} = 6192 \text{ eV/atom}$ is larger than that at $E_{\text{dep}} = 121 \text{ eV/atom}$ by two orders of magnitude. One can see that the mode of corrosion and the irradiation dose dependence of the alloy A differs considerably from that of the alloy B.

The morphology, microstructure and compositions of the macroscopic precipitates indicate inclination of alloy to phase decomposition. The macroscopic precipitation is developed in both alloys after 700 h irradiation in molten salt at $T = 650^\circ\text{C}$. The irradiated in molten salt alloy B shows much larger grain boundary precipitation as compare to that of alloy A (see Fig. 8). Not only density but also sizes of precipitates in grain boundaries of alloy A are considerably less than in alloy B. In alloy A precipitates have mainly Ni–Ti–Si composition. The grain boundaries of alloy B are decorated by precipitates of $2\div 7\ \mu\text{m}$ in size and many of them include high content of Y (up to 30 at%).

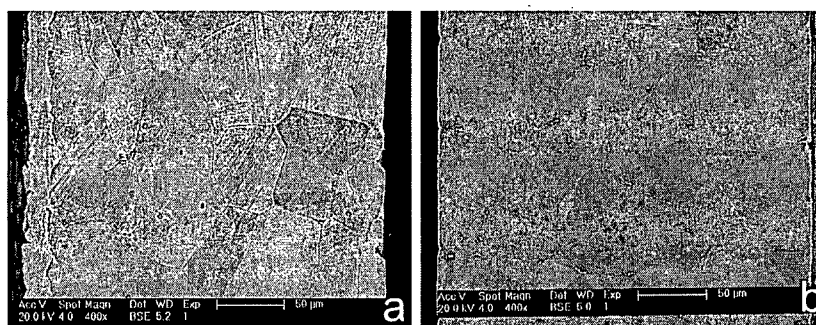


Fig. 8. (a) Irradiated in molten salt alloy A. Macroscopic precipitates in grains and grain boundaries are seen. (b) Irradiated in molten salt alloy B. Much more than in alloy A precipitates in grain boundaries are seen.

Precipitate formation in the unirradiated alloy A is similar to that in irradiated specimens but the X-ray phase analysis performed on a DRON-UM diffractometer (CuK_α radiation) reveals stronger reflections belonged to precipitates in the irradiated specimens (Azhazha et al., 2005c).

4.2.2. Micro- and nano-structure of the tested specimens

Since the alloy B shows more attractive corrosion behavior, its microstructure and compositional heterogeneities were investigated first (Wanderka et al., 2007a). Microstructure of alloy B was investigated by means of TEM, TEM/SAED, TEM/EDX and by means of 3D atom probe tomography (APT). The data obtained allow to connect the results of mechanical and corrosion tests with the structural properties.

Fig. 9a shows a bright field TEM image obtained from the non-irradiated alloy B. The grain boundaries are decorated by up to $2\ \mu\text{m}$ large precipitates, indicated in Fig. 9a by arrows, with varying compositions of the main elements Ni, Ti, Mo and Y; e.g. $\text{Mo}_{19}\text{Ni}_{26}\text{Ti}_{44}$, $\text{Mo}_{31}\text{Ni}_{51}\text{Cr}_{10}$ and $\text{Mo}_{16}\text{Ni}_{19}\text{Y}_{31}$ as measured by EDX analysis in the TEM. Besides the large precipitates, the small spherical precipitates are formed in grains of the non-

irradiated alloy, as it is seen in dark field image, Fig. 9b. These last small precipitates with a bright contrast and a mean diameter of 22 nm are

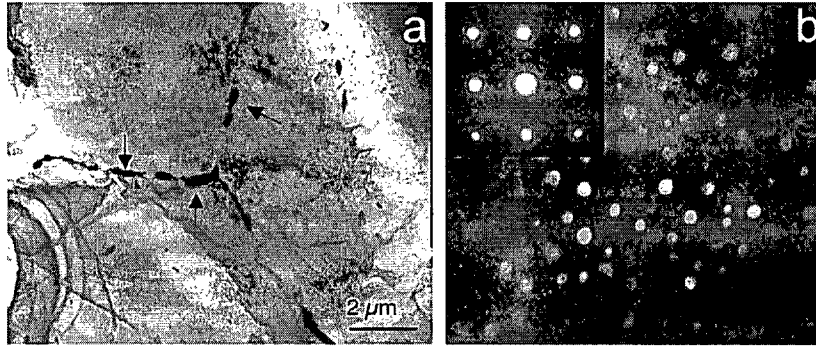


Fig. 9. (a) Bright field TEM image, large Ni-Ti-Mo-Y precipitates have formed at grain boundaries; (b) Dark field TEM image of homogeneously distributed small precipitates which have been formed in the interior of the grains. The [001] zone-axis electron-diffraction pattern (inset) exhibits L_{12} -type superlattice reflections.

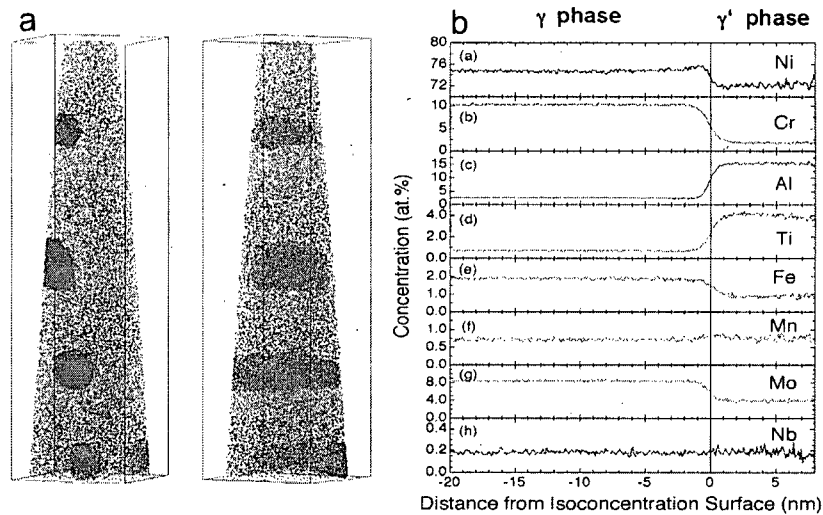


Fig. 10. (a) Distribution of Al atoms in non-irradiated alloy B after homogenizing at 1100°C for 1 h and aging at 675°C for 50 h. Investigated by 3D APT volume is $63 \times 62 \times 268 \text{ nm}^3$. Precipitates of L-12 structure in the matrix are clearly seen. (b) Concentration profiles of the main components obtained by the proxigram method. Precipitates possess composition $(\text{Ni}+\text{Fe}+\text{Mn})_{0.753}(\text{Al}+\text{Ti}+\text{Mo}+\text{Nb}+\text{Cr}+\text{Si})_{0.247}$.

homogeneously distributed throughout in the matrix without any obvious correlation with extended microstructural elements such as defect clusters,

dislocations, or grain boundaries. The corresponding selected-area electron-diffraction (SAED) pattern of a region containing matrix with these small precipitates is shown in the inset of Fig. 9b. The [001] zone-axis electron diffraction pattern exhibits superlattice reflections, which are generated by the small precipitates embedded in the matrix. The superlattice reflections correspond to the ordered $L1_2$ (γ') structure.

The chemical composition of the γ' -precipitates is measured by APT with nanometer spatial resolution. The rectangular parallelepiped analyzed by atom probe tomography (APT) has the dimensions $63 \times 62 \times 268 \text{ nm}^3$ and contains $\sim 2 \times 10^7$ atoms. Two phases appear in the investigated volume: the matrix phase depleted in Al and an Al-rich precipitate phase.

Fig. 10 displays a 3D reconstruction of the analyzed volume. Just the Al atoms are shown for clarity. The precipitates have ordered structure of (Ni_3Al) -type with composition $(\text{Ni}+\text{Fe}+\text{Mn})_{0.753}(\text{Al}+\text{Ti}+\text{Mo}+\text{Nb}+\text{Cr}+\text{Si})_{0.247}$.

One can see that the content of Nb within the matrix and $L1_2$ precipitates is almost the same. Therefore similar precipitates are expected to be formed in the alloy A also

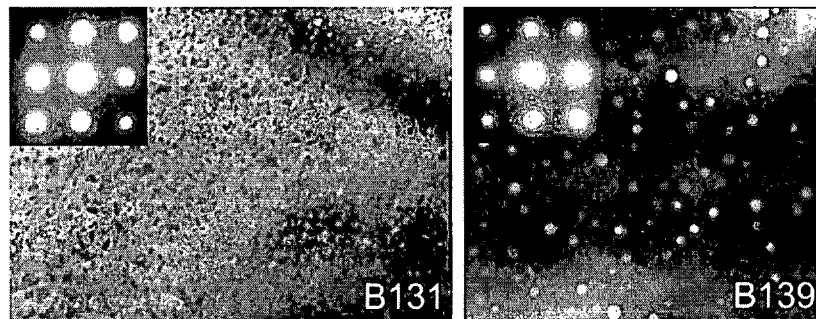


Fig. 111. TEM bright-field image and selected-area electron-diffraction patterns with [001] zone axis exhibiting diffuse SRO diffraction spots for the alloy B after electron irradiation to $E_{\text{dep}} \approx 6 \text{ keV/at}$ (B131) and $\approx 100 \text{ eV/at}$ (B139). SAED pattern of the unirradiated alloy is shown in the upper left corner. The $L1_2$ ordered spherical γ -precipitates and smaller γ -precipitates of irregular shape and the $\langle 1/2 0 \rangle_{\text{fcc}}$ reflections are seen at $E_{\text{dep}} \approx 100 \text{ eV/at}$.

In Fig. 11 TEM bright-field images and selected-area electron-diffraction (SAED) patterns with [001] zone axis exhibiting diffuse SRO diffraction spots for the alloy B after electron irradiation to $E_{\text{dep}} \approx 6 \text{ keV/at}$ (B131) and $E_{\text{dep}} \approx 100 \text{ eV/at}$ (B139) are shown. The most dramatic changes of the microstructure appears at $E_{\text{dep}} \approx 6 \text{ keV/at}$. The spherical $L1_2$ precipitates disappeared completely. This result is confirmed also by APT. From the other hand, the precipitates of Ni_4Mo type were coarse graining in the course of the irradiation. At $E_{\text{dep}} \approx 6 \text{ keV/at}$ their mean size is $\approx 10 \text{ nm}$.

For the specimen B139 deposited energy was much smaller, $E_{\text{dep}} \approx 100 \text{ eV/atom}$. As it is seen in Fig. 111, both γ ($L1_2$) and smaller

γ'' precipitates of irregular shape ($\langle 1 \frac{1}{2} 0 \rangle_{fcc}$) exist in this specimen. One can conclude that the microstructure of the alloy B is rather sensitive to the electron irradiation of doses in the range $E_{dep} = 10^4 \div 10^2$ eV/atom.

In spite the diffuse diffraction spots are not observed at the $\langle 1 \frac{1}{2} 0 \rangle_{fcc}$ positions in unirradiated specimens, thorough APT investigation of the composition heterogeneities of the unirradiated alloy B was performed looking for small clusters of Ni₄Mo composition which have this type of the short range ordered (SRO). The result is shown in Fig. 2. It occurs that Ni–Mo clusters of Ni₄Mo SRO ($\langle 1 \frac{1}{2} 0 \rangle_{fcc}$) exist in unirradiated alloy B. Composition of the clusters is given in Table 2. They have irregular shapes and diameters of 1–3 nm. It is worth to note that Ni–Mo ratio within the clusters is 80Ni – 20Mo. Thus really Ni₄Mo SRO cluster formation started in the initial alloy.

Table 2. Composition of clusters, (at.%)

Ni	Mo	Al	Cr	Ti
67.18	17.6	2.37	8.4	0.72

Growth of these clusters along with dissolution of γ' precipitates occurs under irradiation.

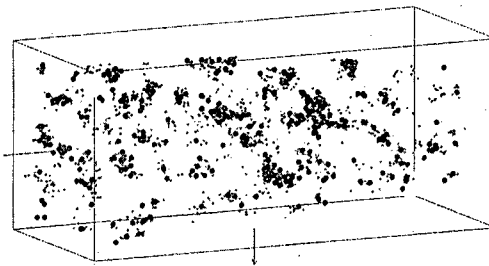


Fig. 12. APT image of the Mo enriched (with Mo content larger than 16 at%) clusters in volume $6 \times 6 \times 29$ nm³.

4.3. ALLOYS: MECHANICAL PROPERTIES

Mechanical properties of the tested alloys are tightly connected with their structural peculiarities. Impact of irradiation on the mechanical properties is an issue of a special interest because it reflects changes of microscopic and macroscopic structural elements of the alloys. Results of the mechanical tests of initial and exposed in molten salt without and under irradiation specimens of the alloys A and B are given in Table 3 (Azhazha et al., 2005c). One can see that the initial mechanical properties of both alloys are rather

similar. The yield strength, $\sigma_{0.2}$, and ultimate tensile stress, σ_B , are depending on the deposited energy, E_{dep} . This dependence is clearly seen from

Table 3. Mechanical properties of irradiated and unirradiated alloys.

Sample condition	T_{test} (°C)	σ_B (MPa)	$\sigma_{0.2}$ (MPa)	δ , %
E_{dep} (eV/atom)		Alloy A		
6192 (sample #1)	20	626	333	35
121 (sample #3)		848	576	54
6192 (sample #2)	650	276	213	15
121 (sample #4)		362	255	15
Initial non-irradiated	20	900	395	63
	600	397	288	14
Post-corrosion test	20	1070	875	43
(650°C, 700 h, non-irradiated)	650	510	440	9
E_{dep} (eV/atom)		Alloy B		
6192 (sample #5)	20	876	412	50
121 (sample #7)		851	415	48
6192 (sample #6)	650	293	214	15
121 (sample #8)		350	318	15
Initial non-irradiated	20	845	397	53
	600	443	310	19

comparison of parameters $\sigma_{0.2}$ and σ_B of irradiated to 6192 and 121 eV/at and unirradiated but also exposed in molten salt alloy A for 700 h at 650°C. The alloy A becomes softer due to irradiation. The plasticity of the irradiated alloy (15%) is considerably larger than that of the unirradiated specimen (9%) but not different from its plasticity in the initial state (14%). It is clearly seen that $\sigma_{0.2}$ is the most sensitive to the irradiation feature. For example, at $T = 20^\circ\text{C}$ $\sigma_{0.2}$ of the alloy A at $E_{dep} = 121$ eV/at is 1.8 times larger than that at 6192 eV/at. Both these values are considerably less than that of unirradiated alloy (875 MPa). Dependence of $\sigma_{0.2}$ on E_{dep} is less pronounced at 650°C.

Unlike to alloy A, for alloy B the $\sigma_{0.2}$ dependence on E_{dep} is small at $T = 20^\circ\text{C}$ and appears to be considerable at $T = 650^\circ\text{C}$. (Unfortunately the corrosion tests of this alloy without e -irradiation was not completed and impact of e -irradiation can not be separated from the annealing effect).

Since $\sigma_{0.2}$ depends of the initial structure of the specimen and σ_B in addition depends on the structure evolution in the course of deformation, one can conclude that microstructure including composition heterogeneities and precipitates is sensitive to the irradiation. Confirmation of this conclusion one can find in Sect. 4.2.

4.4. CORROSION RATES

4.4.1. Corrosion in ZrF_4 -NaF salt

The corrosion rates of the alloys A and B after exposure in molten salt for 700 h at $T = 650^\circ\text{C}$ without and under irradiation are presented in Table 4.

It is seen that without irradiation the corrosion rate saturates on a rather low level $\sim 2 \times 10^{-4}$ mm/yr. Due to irradiation the corrosion rates considerably increase. The corrosion rates of both alloys are ~ 0.2 mm/yr at $E_{\text{dep}} = 6192$ eV/at. At much smaller deposited energy, $E_{\text{dep}} = 121$ eV/at, the corrosion rate of alloy A is twice smaller but alloy B has the corrosion rate smaller in two orders in magnitude.

It is seen that Nb and Y additions not only depress the intergranular corrosion but also make the corrosion rate sensitive to the deposited energy.

Table 4. Corrosion rates of alloys A and B.

Sample	Corrosion current density i_c , mA/cm ²	Corrosion rate		Conditions
		K_m , g/m ² -h	K_k , mm/yr	
Alloy A	0.00002	0.0002	0.0002	700 h of isothermal soaking in a fluoride melt at 650°C without irradiation
Alloy A	0.018	0.20	0.19	700 h of isothermal soaking in a fluoride melt at 650°C under electron irradiation $E_{\text{dep}} = 6192$ eV/atom
Alloy A	0.0074	0.081	0.080	—«»— $E_{\text{dep}} = 121$ eV/atom
Alloy B	0.02	0.22	0.22	—«»— $E_{\text{dep}} = 6192$ eV/atom
Alloy B	0.0004	0.0044	0.0043	—«»— $E_{\text{dep}} = 121$ eV/atom

4.4.2. Corrosion in salt with La addition

It occurs that small addition of La (10.8 wt%) in salt considerably changes the corrosion rate and nanohardness of the alloy A (Bakai et al., 2005c). In this case the nanoindentations allows determine the width of corroded layer very well.

Investigation of the surface layer of the alloy A after exposure in molten salt with La impurities for 500 h at $T = 600^\circ\text{C}$ shows that the corrosion damaged the sample on depth $20 \div 25$ μm . The nanohardness of the corroded layer of 20nm in thickness is poor.

5. Discussion

The data reviewed show that

- irradiation considerably impacts microstructure, mechanical properties and the corrosion of Ni-Mo alloys;
- corrosion resistivity is sensitive to small compositional changes. The alloys A and B have minor composition difference but their corrosion resistivity without and under irradiation are considerably different. The corrosion rate of alloy B is more sensitive to the deposited energy E_{dep} ;
- impurities of La in the $\text{ZrF}_4\text{-NaF}$ molten salt dramatically enhance the corrosion of the alloy A even without irradiation.

Evidently, systematic investigations of corrosion of Ni-Mo alloys of different compositions in molten salts containing fluorides of actinides, lanthanides and other impurities expected to appear in blanket of MSR is severely needed. Since the role of the irradiation and dopants is so essential, it has to be investigated in much more detail.

Theoretical models of the corrosion kinetics under irradiation have to be more developed. Since all of them include phenomenological coefficients like diffusion coefficients and chemical reaction rates, extensive empirical data are needed to identify them.

A correlation of the nanohardness and yield stress of the irradiated specimens is revealed in our measurements. Similar correlation of microhardness and yield stress of irradiated alloys was demonstrated by Busby et al. (2005). Despite that a poor data base on this correlation is stored, it is believed that the nanoindentations can be used for semi-quantitative estimations of the macroscopic mechanical properties of irradiated materials.

Direct reactor tests of the alloys are desirable to make clear availability of the test devices like EITF.

6. Conclusions

- EITF is an efficient device for corrosion tests of G-IV candidate construction materials.
- EITF electron beam irradiation is capable to reproduce realistic irradiation conditions of G-IV molten salts reactor concerning the major factor affecting the Ni-Mo alloys corrosion, the energy deposition in surface layers of alloys.
- Ni-Mo alloys A and B have acceptable corrosion resistance in molten salt at 650°C. After electron irradiation in EITF for 700 h the voltamperic data provide estimation of the corrosion rate to be ~0.1 mm/year.
- The corrosion mode and resistance is rather sensitive to Nb and Y and presumably to other dopants. The alloy doped with Nb (0.5%) and Y

(0.05%) does not show considerable intercrystalline corrosion, but its corrosion rate is sensitive to the deposited energy dose.

- Compositional optimization is needed to minimize the corrosion rate.
- Precipitates located in grain boundaries contain a lot of Y and apparently work as getters mitigating the intercrystalline corrosion attack.
- Structure, composition and SRO of nano-scale precipitates in Ni–Mo alloys is evolving under irradiation. This fact has to be taken into account at R&D of advanced materials for G-IV reactors.

ACKNOWLEDGMENTS.

Collaboration and fruitful discussion with V.G. Baryakhtar, I.M. Neklyudov, V.M. Azhazha, V.F. Zelenskii, A.M. Dovbnya, V.A. Gurin, A.A. Omel'chuk, S.V. Dyuldya, B.M. Shirokov, N. Wanderka, F.A. Garner, and S.J. Zinkle are acknowledged very much.

This research was partially supported by Science & Technology Center in Ukraine (STCU) within the framework of Project #294.

References

- Abdou, M. A., and Maynard, C. W., 1975, Calculation methods for nuclear heating — Part I: Theoretical and computational algorithms, *Nucl. Sci. Eng.* **56**:360–380.
- Agostinelli, S., Allison, J., Amako, K., Apostolakis, J., et al., 2003, Geant4 — a simulation toolkit, *Nucl. Instr. and Meth. in Phys. Res. Sec. A: Accelerators, Spectrometers, Detectors and Associated Equipment.* **22**(3):250–303.
- Andriiko, A. A., Omelchuk, A. A., and Bakai, A. S. 2005, Reaction of zirconium with alkali halide melts, *Problems of Atomic Science and Technology. Ser.: Radiat. Damage Phys. and Radiat. Mater. Sci.* No. 4(87):90–96.
- Azhazha, V. M., Bakai, A. S., Gurin, I. V., Neklyudov, I. M., et al., 2005a, Study of materials for reactors employing molten fluoride salts or Pb–Bi coolant using an Electron Irradiation Test Facility, *Problems of Atomic Science and Technology. Ser.: Radiat. Damage Phys. and Radiat. Mater. Sci.* No. 4(87):3–19.
- Azhazha V. M., Bakai, A. S., Gurin, I. V., Dovbnya, A. N., et al., 2005b, Electron Irradiation Test Facility for irradiation of structural materials in conditions of molten salt reactor, *Problems of Atomic Science and Technology. Ser.: Radiat. Damage Phys. and Radiat. Mater. Sci.* No. 4(87):20–23.
- Azhazha V. M., Bakai, A. S., Dovbnya, A. N., Kovtun, K. N. et al., 2005c, The effects of electron irradiation and fluoride melt ZrF_4 –NaF on mechanical properties of Hastelloy N type alloys, *Problems of Atomic Science and Technology. Ser.: Radiat. Damage Phys. and Radiat. Mater. Sci.* No. 4(87):53–61.
- Azhazha, V. M., Andriiko, A. A. Bakai, A. S., Volkov, S. V., et al., 2005d, Corrosion of irradiated Ni–Mo alloys in Sodium Fluoride – Zirconium Fluoride melt, *Problems of Atomic Science and Technology. Ser.: Radiat. Damage Phys. and Radiat. Mater. Sci.* No. 4(87):67–73.

- Azhazha V. M., Bakai, A. S., Bobrov, Yu. P., Virich, V. D., et al., 2005e, The corrosion resistabce of heatproof nickel alloy in molten fluoride salts, *Problems of Atomic Science and Technology. Ser.: Radiat. Damage Phys. and Radiat. Mater. Sci.* No. 4(87):74–81.
- Azhazha V. M., Bakai, A. S., Bobrov, Yu. P., Dovbnya, A. N., et al., 2005f, Variation of compositional content in subsurface layers of Hestelloy N type alloys as caused by melt of fluorides ZrF_4 -NaF and electron irradiation, *Problems of Atomic Science and Technology. Ser.: Radiat. Damage Phys. and Radiat. Mater. Sci.* No. 4(87):82–88.
- Azhazha, V. M., Bakai, A. S., Lavrinenko, S. D. Bobrov, Yu. P., et al., 2005g, Alloys for molten-salt reactors, *Problems of Atomic Science and Technology. Ser.: Radiat. Damage Phys. and Radiat. Mater. Sci.* No. 4(87):40–47.
- Azhazha, V. M., Bakai, A. S., Glushko, P. I., Kovtun, K. V., et al., 2005h, Corrosion stability of molybdenum and tungsten coating in lead-bismuth eutectic, *Problems of Atomic Science and Technology. Ser.: Radiat. Damage Phys. and Radiat. Mater. Sci.* No. 4(87):100–103.
- Bakai, A. S., Bratchenko, M. I., and Dyuldy, S. V., 2004, Modeling of electron beams energy deposition profiles in imitation experiments on the investigations of radiation stability of Hastelloy in a molten fluorides medium, in: *Proc. of 16th Int. Conf. on Physics of Radiation Phenomena and Radiation Material Science (ICPRP2004)*, NSC KIPT, Alushta, Crimea, Ukraine, 2004, pp. 274–275, in Russian.
- Bakai, A. S., Bratchenko, M. I., and Dyuldy, S. V., 2005a, Electron beams transport and energy deposition in heterogeneous assemblies of the Hastelloy samples embedded into the molten fluorides mix, *Problems of Atomic Science and Technology. Ser.: Radiat. Damage Phys. and Radiat. Mater. Sci.* No. 4(87):24–31.
- Bakai, A. S., Tanatarov, L. V. Gonchar, V. Y., and Sergiyeva, G. G., 2005b, Calculation of temperature fields in ampoules under the radiation treatment by electrons with energy 10 MeV, *Problems of Atomic Science and Technology. Ser.: Radiat. Damage Phys. and Radiat. Mater. Sci.* No. 4(87):32–39.
- Bakai, A. S., Volkov, S. V., Azhazha, V. M., Andriiko, A. A., et al., 2005c, Corrosion processes in Zirconium Fluoride – Sodium Fluoride melts. Study of shortcut cell $C/(Zr_4-NaF)_{EUT}/Hastelloy$, *Problems of Atomic Science and Technology. Ser.: Radiat. Damage Phys. and Radiat. Mater. Sci.* No. 4(87):62–66.
- Bakai, A. S., Dovbnya, A. N., Zykov, A. I., Lavrinenko, S. D., et al., 2005d, Nuclide control of structural materials tested in Electron Irradiation Test Facility, *Problems of Atomic Science and Technology. Ser.: Radiat. Damage Phys. and Radiat. Mater. Sci.* No. 4(87):97–99.
- Bakai, A. S., Borisenko, A. A., Russel, K., 2005e, Amorphization kinetics under electron irradiation, *Problems of Atomic Science and Technology. Ser.: Radiat. Damage Phys. and Radiat. Mater. Sci.* No. 4(87):108–113
- Bakai A.S., Tanatarov L.V., 2005f, Corrosion kinetics of an alloy immersed into a liquid metal melt containing oxygen, *Problems of Atomic Science and Technology. Ser.: Radiat. Damage Phys. and Radiat. Mater. Sci.* No. 4(87):114–119
- Bakai, A. S., Bratchenko, M. I., and Dyuldy, S.V., 2007, to be published.
- Busby, J. T., Hash, M. C., and Was, G. S. 2005, The relationship between hardness and yield stress in irradiated austenitic and ferritic steels, *J. Nucl. Mater.* **336**:267–278.
- DeVan, J. H., 1969, Effect of alloying additions on corrosion behaviour of nickel-molybdenum alloys in fused fluoride mixtures, Report ORNL-TM-2021, Oak Ridge National Laboratory, Oak Ridge, Tennessee 37830.
- Dyuldy, S. V., Bratchenko, M. I., and Skorobogatov, M.A., 2006, Novel methods and software tools of statistic modeling in physics of radiation phenomena and technologies, in:

- Proc. of 17th Int. Conf. on Physics of Radiation Phenomena and Radiation Material Science. (ICPRP2006)*, NSC KIPT, Alushta, Crimea, Ukraine, pp. 30–31, in Russian.
- Haubereich, P. N., and Engel, J. R., 1970, Experience with molten salt reactor experiment, *Nucl. Appl. Technol.* **8**:118–136.
- Ignatiev, V. V. Surenkov, A. I., Gnidoi, I. P., et al., 2006, Investigation of the corrosion resistance of nickel-based alloys in fluoride melts, *Atomic Energy.* **101**:(4)730–738.
- McCoy, H. E., Jr., 1978, Status of materials development for molten salt reactors, Report ORNL/TM-5920, Oak Ridge National Laboratory, Oak Ridge, Tennessee 37830.
- Merle-Lucotte, E., Heuer, D., Allibert, M., Ghetta, V., Le Brune, C., 2007, Introduction to the Physics of Molten Salt Reactors, This book, XXX–XXX.
- Norgett, M. J., Robinson, M. T., and Torrens, I. M., 1975, A proposed method of calculating displacement dose rates, *Nucl. Eng. and Design.* **33**:(1)50–54.
- Novikov, V. M., Ignat'ev, V. V., Fedulov, V. I., Cherednikov, V. N., 1990, *Molten Salt Nuclear Energy Systems — Perspective and Problems*, Energoatomizdat, Moscow, in Russian.
- Wanderka, N., Bakai, A., Kropf, H., et al., 2005, unpublished.
- Wanderka, N., Bakai, A., Abromeit, C., Laheim, D., and Seidman, D.N., 2007a, Effects of 10 MeV electron irradiation at high temperature of a Ni–Mo-based Hastelloy, *Ultramicroscopy.* **107**:786–790.
- Wanderka, N., 2007b, Atom probe and new results in material research, *Int. Young Scientists School on Nuclear Physics and Energy*, June 11–16, Alushta, Ukraine, unpublished.

Rulemaking Comments

From: elling@torium.se
Sent: Thursday, July 03, 2008 11:51 AM
To: Rulemaking Comments
Subject: DCThMSR 3/3
Attachments: Appendices5.zip

Dear Sir,

referring to the NRC-2008-0237, Thorium ElectroNuclear AB, based in Stockholm Sweden, submits comments for the Double Cylinder Thorium Molten Salt Reactor.

The DCThMSR is protected by Patent Pending. The patent text is not enclosed but scientific publications would describe it adequately.

This is email 3 of 3.

Pls acknowledge.

Kind regards
Elling Disen
elling@torium.se
Founder
Thorium ElectroNuclear AB
www.torium.se

Received: from mail1.nrc.gov (148.184.176.41) by TWMS01.nrc.gov
(148.184.200.145) with Microsoft SMTP Server id 8.0.751.0; Thu, 3 Jul 2008
11:54:19 -0400

X-Ironport-ID: mail1

X-SBRS: 1.9

X-MID: 27103926

X-IronPort-AV: E=Sophos;i="4.27,742,1204520400";
d="pdf?zip'48?scan'48,48,208";a="27103926"

Received: from pne-smtpout2-sn1.fre.skanova.net ([81.228.11.159]) by
mail1.nrc.gov with ESMTP; 03 Jul 2008 11:52:50 -0400

Received: from [192.168.1.113] (81.233.0.25) by
pne-smtpout2-sn1.fre.skanova.net (7.3.129) id 4843FAEB00630450 for
Rulemaking.Comments@nrc.gov; Thu, 3 Jul 2008 17:52:41 +0200

Message-ID: <486CF552.70200@torium.se>

Date: Thu, 3 Jul 2008 17:50:42 +0200

From: "elling@torium.se" <elling@torium.se>

User-Agent: Thunderbird 2.0.0.14 (Windows/20080421)

MIME-Version: 1.0

To: Rulemaking.Comments@nrc.gov

Subject: DCThMSR 3/3

Content-Type: multipart/mixed;

boundary="-----030506070208080609080407"

Return-Path: elling@torium.se